DESIGN, SIMULATION AND OPTIMISATION OF A CHIMNEY-DEPENDENT DIRECT-MODE SOLAR CROP DRYER (CDSCD)

JOHN KWASI AFRIYIE, MSc. (Stuttgart), BSc. (Kumasi)

A thesis submitted in partial fulfilment for the degree of

Doctor of Philosophy

to De Montfort University, Leicester – England

School of Engineering and Technology

Faculty of Computing Sciences and Engineering

August 2007

ABSTRACT OF THE RESEARCH

The thesis describes the design, simulation and optimisation processes performed on a Chimney-dependent Direct-mode Solar Crop Dryer (CDSCD). The programme is aimed at the development of mathematical models and computer codes as design tools to help standardise the design of direct-mode solar crop dryers that depend on the chimney for ventilation.

Physical trials were carried out on a small-scale laboratory model of the CDSCD designed and built in De Montfort University, Leicester – England. The tests were conducted for different roof angles and inlet openings of the drying chamber. Two sets of laboratory trials were performed. The no-load trials were conducted to investigate the effects of roof angle and inlet gap on the ventilation in the dryer. The under-load trials were performed to examine the mutual effects of the airflow rate and the drying process. Also, different loading arrangements inside the drying chamber were experimented on. Field trials were also performed on a large-scale dryer in Ghana. The no-load and the under-load trials each had eighteen tests in the laboratory. Five tests were done with the field dryer in Ghana.

Mathematical models were developed to predict the performances of the CDSCD. These were used together with the experimental results to develop a well-validated simulation code. The results of the no-load parametric studies performed with the simulation code indicate the following:

- The optimum drying-chamber roof-angle for maximum airflow lies between 50^0 and 60^0 with respect to the vertical plane; locations that are far away from the equator may have an optimum angle of around 50^0, and those close to the equator may have around 60^0.
- Maximum air velocities through the dryer are attained within the inlet-exit area ratios of 4.8:1 to 5.9:1.
- Relying on one particular feature of the CDSCD for airflow improvement may render the dryer uneconomical or unstable; reasonably moderate changes in two or more features may be the best way to improve the performance of the CDSCD.
- A high drying chamber with a short solar chimney is favoured in areas close to the equator, whereas a short drying chamber with a high solar chimney is suitable for areas far away from the equator.

On the whole, the research has shown the usefulness of modelling and simulation procedures for optimising the design of the CDSCD. The simulation code will help in avoiding the emergence of inefficient and inappropriate structures of the CDSCD. It will also set the criteria by which present or future standards-enforcing agencies will operate.

ABSTRACT OF THE RESEARCH

The thesis describes the design, simulation and optimisation processes performed on a Chimney-dependent Direct-mode Solar Crop Dryer (CDSCD). The programme is aimed at the development of mathematical models and computer codes as design tools to help standardise the design of direct-mode solar crop dryers that depend on the chimney for ventilation.

Physical trials were carried out on a small-scale laboratory model of the CDSCD designed and built in De Montfort University, Leicester – England. The tests were conducted for different roof angles and inlet openings of the drying chamber. Two sets of laboratory trials were performed. The no-load trials were conducted to investigate the effects of roof angle and inlet gap on the ventilation in the dryer. The under-load trials were performed to examine the mutual effects of the airflow rate and the drying process. Also, different loading arrangements inside the drying chamber were experimented on. Field trials were also performed on a large-scale dryer in Ghana. The no-load and the under-load trials each had eighteen tests in the laboratory. Five tests were done with the field dryer in Ghana.

Mathematical models were developed to predict the performances of the CDSCD. These were used together with the experimental results to develop a well-validated simulation code. The results of the no-load parametric studies performed with the simulation code indicate the following:

- The optimum drying-chamber roof-angle for maximum airflow lies between 50^0 and 60^0 with respect to the vertical plane; locations that are far away from the equator may have an optimum angle of around 50^0, and those close to the equator may have around 60^0.
- Maximum air velocities through the dryer are attained within the inlet-exit area ratios of 4.8:1 to 5.9:1.
- Relying on one particular feature of the CDSCD for airflow improvement may render the dryer uneconomical or unstable; reasonably moderate changes in two or more features may be the best way to improve the performance of the CDSCD.
- A high drying chamber with a short solar chimney is favoured in areas close to the equator, whereas a short drying chamber with a high solar chimney is suitable for areas far away from the equator.

On the whole, the research has shown the usefulness of modelling and simulation procedures for optimising the design of the CDSCD. The simulation code will help in avoiding the emergence of inefficient and inappropriate structures of the CDSCD. It will also set the criteria by which present or future standards-enforcing agencies will operate.

4.2 The drying model 85
4.2.1 The drying equation 87
4.2.2 The mass balance of the drying air 88
4.2.3 Energy balance of air in the drying chamber 89
4.2.4 Energy balance on the wet crop 92
4.2.5 Energy balance on the base of drying chamber 94
4.2.6 Energy balance on the walls of the drying chamber 94
4.2.7 Using two layers of crops 95
4.2.8 Factors and coefficients of the drying model 99
4.3 Solution methods to the models 103
4.3.1 Modelling the no-load process 103
4.3.2 Modelling the under-load process 105
Chapter 5 Experimental results 112
5.1 No-load trials 112
5.1.1 Test-set 1: No-load results with the normal chimney 116
5.1.2 Test-set 2: No-load results with the solar chimney and the various configurations of the drying chamber 117
5.1.3 Test-set 3: No load with different angles of incidence 121
5.1.4 Test-set 4: The temperature profile of the drying chamber 122
5.2 Under load trials 123
5.2.1 Test-set 5: Drying with normal chimney 124
5.2.2 Effects of the solar chimney, roof angle and inlet gap on drying; test-set 6 140
5.2.3 Test-set 7: The mutual effects of crop size and air flow 155
5.2.4 Test-set 8: Drying with higher crop mass (1.4 kg cassava) 157
5.2.5 Test-sets 9 and 10: Lower crop mass and the effect shelf height 162
5.2.6 Test-sets 11 and 12: Using different loading arrangements 165
5.3 Field Work results 171
5.3.1 Field-trial 1 172
5.3.2 Field-trial 2 175
5.3.3 Field-trial 3 177
5.3.4 Field-trial 4 179
5.3.5 Field-trial 5 180
5.4 Summary observations, discussions and recommendations 182
5.4.1 The laboratory model 182
5.4.2 The field model 183
5.4.3 Comparing the CDSCD with other natural-convection solar crop dryers 187
5.4.4 Ways of improving the CDSCD 187
Chapter 6 Development of the simulation code 189
6.1 Empirical relations and other data 189
6.1.1 The air bulk temperatures and mean temperature approximations 189
6.1.2 Determining the Pressure coefficients 192
6.1.3 Irradiation 194
6.2 Components of the simulation code 197
6.2.1 The program FLODRY 197
6.2.2 Subroutines 199
6.2.3 The flow chart for the simulation code 202
6.3 Validation of the simulation code 214
6.3.1 The no-load validation 214

6.3.2 The under-load validation 223
6.4 Parametric studies 245
6.4.1 Varying the drying-chamber roof angles.....245
6.4.2 Effect of inlet-exit area ratio of the CDSCD.....247
6.4.3 Varying the chimney height for a given height of drying chamber 248
6.4.4 Varying the heights of chimney and the drying chamber for a given total height. 249
6.5 Summary observations, discussions and recommendations.....251
Chapter 7 Conclusions and suggestions for further work.....253
List of references.....256

LIST OF TABLES.....

Table 2.1	Moisture contents	10
Table 2.2	Minimum required airflow rates for wheat and shelled maize	13
Table 2.3	Advantages and disadvantages of direct-mode, indirect-mode, mixed-mode and hybrid types of the solar dryer	23
Table 2.4	Comparison of the performance against cost of a PGCP solar coconut dryer (direct-mode type), the Kenya Black Box Solar Dryer (mixed- mode natural convection)	24
Table 2.5	Models for analysing M_e in relation to H_R and T	34
Table 2.6	Mathematic models applied to the drying curves.	35
Table 3.1	Dimensions of dryer used for the field trials	55
Table 4.1	The diffusion coefficient D of cassava in relation to the absolute temperature T.	87
Table 5. 1	Overview of ambient, inlet and exit conditions of dryer trials with various configurations	113
Table 5. 2	Overview of ambient, inlet and exit conditions of dryer trials with different angles of incidence	121
Table 5.3	The temperature profile of the drying chamber	123
Table 5.4	Field-work data symbols and the meanings	172
Table 5.5	Field-trial 1; Daily Moisture Contents (Inlet was left open at night)	173
Table 5.6	Field-trial 1; Data Overview	174
Table 5.7	Field-trial 2; Daily Moisture Contents	175
Table 5.8	Field-trial 2; Data Overview	175
Table 5.9	Field-trial 3; Daily Moisture Contents	178
Table 5.10	Field-trial 3; Data Overview	179
Table 5.11	Field-trial 4; Daily Moisture Contents	180

Table 5.12	Field-trial 4; Data Overview	180
Table 5.13	Field-trial 5; Daily Moisture Contents	181
Table 5.14	Field-trial 5; Data Overview	182
Table 5.15	Average Drying Efficiencies of the Field Dryer for various trials	185
Table 6.1	Air bulk temperature relations in the chimney	190
Table 6.2	Air bulk temperature relations in the drying chamber	191
Table 6.3	Determining the values of K_{roof} for each roof angle	193
Table 6.4	Determining the value of K_{out}	193
Table 6.5	Exit velocities for different angles of drying chamber roof with respect to the vertical plane (with higher irradiation into the chimney than into the drying chamber)	246
Table 6.6	Exit velocities for different angles of drying chamber roof with respect to the vertical plane (with higher irradiation into the drying chamber than into the chimney)	246
Table 6.7	Exit velocities for different inlet-exit area ratios of the CDSCD (with higher irradiation into the chimney than into the drying chamber)	247
Table 6.8	Exit velocities for different inlet-exit area ratios of the CDSCD (with higher irradiation into the drying chamber than into the chimney)	248
Table 6.9	Exit velocities for a given height of drying chamber with varying heights of chimney (with higher irradiation into the chimney than into the drying chamber).	249
Table 6.10	Exit velocities for a given height of drying chamber with varying heights of chimney (with higher irradiation into the drying chamber than into the chimney).	249
Table 6.11	Exit velocities for a given total height with varying heights of chimney and drying chamber (with higher irradiation into the chimney than into the drying chamber)	250
Table 6.12	Exit velocities for a given total height with varying heights of chimney and drying chamber (with higher irradiation into the drying chamber than into the chimney)	250

LIST OF FIGURES

Figure 2.1	Schematic diagram of a direct-mode cabinet dryer	20
Figure 2.2	Schematic diagram of an indirect-mode cabinet dryer	21
Figure 2.3	Schematic diagram of a mixed-mode cabinet dryer	22
Figure 3.1	Functional Architecture of the Chimney-dependent Direct-mode Solar Crop Dryer	52
Figure 3.2	Sketch of dryer arrangements (side view)	55
Figure 3.3	The pictorial view of field model	57
Figure 3.4	A Setup of the CDSCD model for the laboratory trials	58
Figure 3.5	Schematic diagram of positions of temperature-measuring sensors	59
Figure 4.1	Schematic diagram of a Chimney-dependent Direct-mode Solar Crop Dryer	67
Figure 4.2	Diagram showing the pressure loss at the roof	69
Figure 4.3:	Elemental layer of crop bed	86
Figure 5.1	Air temperature above ambient vs. Height, for Roof 81^0 with different inlet gaps; No Load	114
Figure 5.2	Air temperature above ambient vs. Height, for Roof 51^0 with different inlet gaps; No Load	114
Figure 5.3	Air temperature above ambient vs. Height, for Roof 64^0 with different inlet gaps; No Load	115
Figure 5.4	Air temperature above ambient vs. Height, for Inlet 70 mm with different roof angles; No Load	115
Figure 5.5	Air temperature above ambient vs. Height, for Inlet 50 mm with different roof angles; No Load	116
Figure 5.6	Air temperature above ambient vs. Height, for Inlet 30 mm with different roof angles; No Load	116

Figure 5.7	Air temperature above ambient vs. Height for different angles of incidence; No Load	122
Figure 5.8	Inlet velocity vs. drying time, for a given Inlet Gap; Under load	125
Figure 5.9	Ambient RH vs. Drying time for, a given Inlet Gap; Under load	126
Figure 5.10	Ambient RH vs. Drying Time, for a given Roof Angle; Under load	127
Figure 5.11	Moisture Content vs. Drying Time, for a given Inlet Gap; Under load	128
Figure 5.12	Moisture Content vs. Drying Time, for a given Roof Angle; Under load	129
Figure 5.13	Drying Rate vs. Drying Time, for a given Inlet Gap; Under load	130
Figure 5.14	Drying Rate vs. Drying Time, for a given Roof Angle; Under load	131
Figure 5.15	Temperature Above Ambient vs. Height; Under load, Inlet Gap 70 mm	132
Figure 5.16	Temperature Above Ambient vs. Height; Under load, Inlet Gap 50 mm	133
Figure 5.17	Temperature Above Ambient vs. Height; Under load, Inlet Gap 30 mm	134
Figure 5.18	Temperature Above Ambient vs. Height; Under load, Roof Angle 81^0	135
Figure 5.19	Temperature Above Ambient vs. Height; Under load, Roof Angle 64^0	136
Figure 5.20	Temperature Above Ambient vs. Height; Under load, Roof Angle 51^0	137
Figure 5.21a	Ambient RH vs. Drying Time; Standard and Half Sizes	158
Figure 5.21b	Inlet Velocity vs. Drying Time; Standard and Half Sizes	158
Figure 5.21c	Dying Rate vs. Drying Time; Standard and Half Sizes	159
Figure 5.21d	Moisture Content vs. Drying Time; Standard and Half Sizes	159
Figure 5.22a	Moisture Content vs. Drying Time; crop masses of 1 kg and 1.4 kg	160

Figure 5.22b	Ambient RH vs. Drying Time; crop masses of 1 kg and 1.4 kg	160
Figure 5.22c	Drying Rate vs. Drying Time; crop masses of 1 kg and 1.4 kg	161
Figure 5.22 d)	Inlet Velocity vs. Drying Time; crop masses of 1 kg and 1.4 kg	161
Figure 5.23	The performances on Half mass, Standard mass and Control	164
Figure 5.24	The performances of the two half loads being dried together at different height (without interchange), with Standard and Control	167
Figure 5.25	The performances of the two half loads being dried together at different height (with interchange on Day 2), with Standard and Control	168
Figure 5.26	Ambient RH vs. Drying Time; The Half Loads together (with and without interchange), Standard and Control Loads	169
Figure 6.1	Flow chart for determining the Glazing Radiative Properties and the Irradiations into the Chimney and the Drying Chamber of the Laboratory Model	196
Figure 6.2	Coordination between the main program FLODRY and the various subroutines	198
Figure 6.3	Flow chart for the Simulation Code	203
Figure 6.4	Air Temperature vs. Height: Simulation and Lab Results; Roof 81^0 Inlet 70mm, No Load	215
Figure 6.5	Air Temperature vs. Height: Simulation and Lab Results; Roof 81^0 Inlet 50mm, No Load.	216
Figure 6.6	Air Temperature vs. Height: Simulation and Lab Results; Roof 81^0 Inlet 30mm, No Load	217
Figure 6.7	Air Temperature vs. Height: Simulation and Lab Results; Roof 64^0 Inlet 70mm, No Load	218
Figure 6.8	Air Temperature vs. Height: Simulation and Lab Results; Roof 64^0 Inlet 50mm, No Load	219
Figure 6.9	Air Temperature vs. Height: Simulation and Lab Results; Roof 64^0 Inlet 30mm, No Load	220

Figure 6.10	Air Temperature vs. Height: Simulation and Lab Results; Roof 51^0 Inlet 70mm	221
Figure 6.11	Air Temperature vs. Height: Simulation and Lab Results; Roof 51^0 Inlet 50mm	222
Figure 6.12	Air Temperature vs. Height: Simulation and Lab Results; Roof 51^0 Inlet 30mm	223
Figure 6.13	Moisture Content vs. Drying Time: Simulation and Lab Results; Roof 81^0 Inlet 70mm	226
Figure 6.14	Air Temperature vs. Height: Simulation and Lab Results; Roof 81^0 Inlet 70mm	228
Figure 6.15	Moisture Content vs. Drying Time: Simulation and Lab Results; Roof 81^0 Inlet 50mm	229
Figure 6.16	Air Temperature vs. Height: Simulation and Lab Results; Roof 81^0 Inlet 50mm	230
Figure 6.17	Moisture Content vs. Drying Time: Simulation and Lab Results; Roof 81^0 Inlet 30mm	231
Figure 6.18	Air Temperature vs. Height: Simulation and Lab Results; Roof 81^0 Inlet 30mm	232
Figure 6.19	Moisture Content vs. Drying Time: Simulation and Lab Results; Roof 64^0 Inlet 70mm	233
Figure 6.20	Air Temperature vs. Height: Simulation and Lab Results; Roof 64^0 Inlet 70mm	234
Figure 6.21	Moisture Content vs. Drying Time: Simulation and Lab Results; Roof 64^0 Inlet 50mm	235
Figure 6.22	Air Temperature vs. Height: Simulation and Lab Results; Roof 64^0 Inlet 50mm	236
Figure 6.23	Moisture Content vs. Drying Time: Simulation and Lab Results; Roof 64^0 Inlet 30mm	237
Figure 6.24	Air Temperature vs. Height: Simulation and Lab Results; Roof 64^0 Inlet 30mm	238
Figure 6.25	Moisture Content vs. Drying Time: Simulation and Lab Results; Roof 51^0 Inlet 70mm	239

Figure 6.26 Air Temperature vs. Height: Simulation and Lab Results; Roof 51^0 Inlet 70mm 240

Figure 6.27 Moisture Content vs. Drying Time: Simulation and Lab Results; Roof 51^0 Inlet 50mm 241

Figure 6.28 Air Temperature vs. Height: Simulation and Lab Results; Roof 51^0 Inlet 50mm 242

Figure 6.29 Moisture Content vs. Drying Time: Simulation and Lab Results; Roof 51^0 Inlet 30mm 243

Figure 6.30 Air Temperature vs. Height: Simulation and Lab Results; Roof 51^0 Inlet 30mm 244

NOMENCLATURE

A characteristic area (m^2)

A_b base area of drying chamber (m^2)

A_{dc} total area of drying chamber walls (m^2)

A_{in} inlet area of dryer (m^2)

A_{out} outlet area of dryer (m^2)

c_p specific heat capacity of air (J/kg.K)

$C_{p,a}$ specific heat capacity of air (J/kg.K)

$C_{p,g}$ specific heat capacity of water vapour (J/kg.K)

C_M specific heat capacity of moisture (J/kg.K)

C_{ss} specific heat capacity of support structures (trays etc) in the drying chamber (J/kg.K)

D crop diffusivity (m^2/s)

D_0 crop specific pre-exponential factor (m^2/s)

f friction coefficient

g acceleration due to gravity (m/s^2)

G_a Grashof number

G_a air mass flux ($kg/m^2.s$)

h_{ba} convective heat transfer coefficient from the bottom of drying-chamber base to environment ($W/m^2.K$)

h_{bf} convective heat transfer coefficient between air and drying-chamber base ($W/m^2.K$)

h_{ca} convective heat transfer coefficient from chimney glazing to environment ($W/m^2.K$)

h_{dca} convective heat transfer coefficient from drying-chamber glazing to environment ($W/m^2.K$)

h_{fc} convective heat transfer coefficient from air in the chimney to the cover ($W/m^2.K$)

$h_{f,dc}$ convective heat transfer coefficient from air to the drying-chamber walls ($W/m^2.K$)

h_{pa} convective heat transfer coefficient from chimney absorber wall to the environment ($W/m^2.K$)

h_{pf} convective heat transfer coefficient between air and the absorber plate ($W/m^2.K$)

$h_{r,bcr}$ radiation heat transfer coefficient from drying-chamber base to the crop ($W/m^2.K$)

$h_{r,bdc}$ radiation heat transfer coefficient from drying-chamber base to the walls ($W/m^2.K$)

$h_{r,ca}$ radiation heat transfer coefficient from chimney glazing to the environment ($W/m^2.K$)

$h_{r,cs}$ radiation heat transfer coefficient between the cover and the sky ($W/m^2.K$)

$h_{r,dca}$ radiation heat transfer coefficient from drying-chamber glazing to the environment ($W/m^2.K$)

$h_{r,pc}$ radiation heat transfer coefficient between chimney plate and the cover ($W/m^2.K$)

$h_{r,z}$ radiation heat transfer coefficient from crop bed perimeter to the drying chamber walls ($W/m^2.K$)

h_v volumetric heat transfer coefficient ($W/m^3.K$)

H characteristic height (m)

H Absolute humidity (decimal)

H_{ch} height of chimney (m)

I_{chm} irradiation on the chimney glazing (W/m^2)

I_{dc} irradiation on the drying-chamber glazing (W/m^2)

k_b thermal conductivity of drying-chamber base (W/m.K)

k_p thermal conductivity of chimney absorber wall (W/m.K)

K_{in} pressure coefficient at dryer inlet

K_{out} pressure coefficient at dryer exit (or outlet)

$K_{roof,}$, $K_{obs,}$ pressure coefficient at the drying-chamber roof (or obstacle)

L characteristic length (m)

L latent heat of vaporisation of moisture (J/kg)

m_{ss} total mass of support structures in the drying chamber (kg)

$\dot{m}$ mass flow rate (kg/s)

M moisture content (dry basis) of material (kg_w/kg_s)

M_0	moisture content (dry basis) of material at time t=0 (kg_w/kg_s)
M_e	equilibrium moisture content (dry basis) of crop (kg_w/kg_s)
M_1	Moisture content of wet grain (%)
M_2	Moisture content of dried grain (%)
Nu	Nusselt number
p_{cr}	partial pressure of water vapour in the grain
p_a	partial pressure of water vapour in drying air
Pr	Prandtl number
Q_{12}	heat flow by radiation between surface 1 and surface 2 (W)
Ra	Rayleigh number
RH_{dcin}	Relative humidity of air at inlet of dryer (decimal)
$RH_{f,cr}$	Relative humidity of air in the crop zone (decimal)
S_b	radiation heat flux absorbed by the drying-chamber base (W/m^2)
S_c	radiation heat flux absorbed by the chimney glazing (W/m^2)
S_{cr}	radiation heat flux absorbed by the crop (W/m^2)
S_{dc}	radiation heat flux absorbed by the drying-chamber glazing (W/m^2)
S_p	radiation heat flux absorbed by the chimney absorber (W/m^2)
t	drying time (s)
T	absolute temperature of air (K)
T	temperature of air in the drying zone of the drying chamber (K)
T_{dcair}	temperature of air in the drying chamber during the no-load process (K)
T_a	temperature of the atmosphere (K)
T_{bot}	air temperature at the bottom of crop bed (K)
T_c	temperature of chimney glazing (K)
$T_{ch,i}$	air temperature at chimney inlet (K)
T_{cr}	crop temperature (K)
T_{dc}	temperature of drying chamber walls (K)
T_{in}	air temperature at dryer inlet (K)
T_{out}	air temperature at dryer outlet (K)
T_{pf}	mean film temperature at between absorber plate and air (K)
T_s	temperature of the sky (K)
T_{top}	air temperature at the top of crop bed (K)

U_{ba} overall heat transfer coefficient through the drying-chamber base to the environment ($W/m^2.K$)

U_{ca} resultant heat transfer coefficient from glazing to the environment ($W/m^2.K$)

$U_{dc,a}$ resultant heat transfer coefficient from drying-chamber glazing to the environment ($W/m^2.K$)

U_{pa} overall heat transfer coefficient from chimney absorber plate through absorber wall to the environment ($W/m^2.K$)

v_{in} air velocity at dryer inlet (m/s)

v_{out} air velocity at dryer outlet (m/s)

v_{cr} velocity of air across the crop bed (m/s)

V wind velocity of the local geographical area (m/s)

V_{cr} bulk volume of drying crop (m^3)

W width of the chimney, width of the dryer (m)

W_1 Weight of wet grain (kg)

W_2 Weight of dried grain (kg)

dz thickness of crop layer

α_{cr} absorptivity of crop

α_1 absorptivity of cover (glazing)

α_2 absorptivity of absorber

β air thermal expansion coefficient = $1/T$ (1/K)

γ_{chm} a constant for determining the fluid mean temperature in the chimney

γ_{dc} a constant for determining the fluid mean temperature in the drying chamber

ε_b emittance of drying-chamber base

ε_c emittance of chimney glazing

ε_{dc} emittance of drying-chamber glazing

ε_p emittance of chimney absorber plate

θ roof tilt angle to the vertical plane

ρ density of air

σ Stefan-Boltzman constant

τ_c transmittance of glazing

Subscripts

b	drying-chamber base
bf	the air film between the drying-chamber base and the main air stream
chm	chimney
cr	crop
dc	drying chamber
f	air (fluid)
p	chimney absorber
pf	the air film between the chimney absorber and the main air stream
r	radiation
roof	roof of drying-chamber
vw	vertical wall of drying chamber

Others

$\frac{\partial H}{\partial z}$	change of absolute humidity per unit height ($kg_w/kg_{air}.s$)
$\frac{\partial M}{\partial t}$	rate of change of moisture content ($kg_w/kg_s.s$)
ΔP_{cr}	pressure resistance of the crop bed (N/m^2)
Δw_b	thickness of drying-chamber base (m)
Δw_p	thickness of chimney absorber (m)

ACKNOWLEDGEMENTS

I would like to express deep appreciation to my supervisors Professor M. A. A. Nazha and Dr. Hobina Rajakaruna, whose invaluable support and guidance carried me through the research. Thanks are also due to the late Mr. Bob Burdett and Messrs John Maginty, Paul Dean and Keith Harrop, technicians in the School of Engineering and Technology, De Montfort University (DMU), for the help in the construction and testing of the laboratory model of the dryer. I also wish to extend my thanks to Mr. Andy Rylott, and Mr. Mambir Sambhi and other technical staff of the Faculty of Computing Sciences and Engineering in DMU, for their assistance on the computer network of the university.

My next thanks go to Dr. Francis K. Forson, the supervisor of the field work in Ghana for his good-natured advice and suggestions, not forgetting Robert Kyere, the technician and entire staff of the Mechanical Engineering Department of the Kwame Nkrumah University of Science and Technology (KNUST), for their immense help during the field work in Ghana. Also, the assistance of Ing. Ato Bart-Plange and the staff of the Agric. Engineering Department of KNUST, who allowed me to use the facilities of the department for testing the crop moisture contents, is very much appreciated.

I also express my sincere thanks to the Government of Ghana, without whose financial support the programme would have been impossible, and also the Kumasi Polytechnic (Ghana) for granting me a study leave to pursue the programme.

Great thanks go to my wife, Mrs Augustina Afriyie for all the support throughout my stay in Leicester for the research.

Most of all, I thank the Almighty God for the strength, courage, wisdom, protection and direction which enabled me to work, sometimes through extreme pressures, to bring the programme to completion.

August 2007 **JOHN KWASI AFRIYIE**

CHAPTER 1 INTRODUCTION

1.1 Background

A high percentage of the population of developing countries is made up of rural-based farmers. In Ghana, the figure is about 65 %[1]. In spite of this high percentage the food in the Ghanaian markets is generally not enough. This is partly caused by post-harvest losses, which is between 20 and 30 %[2]. This problem is being compounded by the fact that the population of Ghana keeps increasing.

A lot of crops produced in developing countries during the harvesting periods are left to go waste within a short period of the year. As a result, there is always an over-abundance of particular farm produce during its harvest season and scarcity of the same produce in the other periods within the year. Rural farmers are therefore normally compelled to sell their produce at very cheap prices, during the harvesting season. For instance, in September 2002, a bag of maize (about 100kg) was selling at ¢60 000 (about US$7)[3] in the Techiman District of the Brong-Ahafo Region of Ghana. This price had doubled (to ¢120 000) in that same district as at the beginning of December the same year, after the farmers had sold all their produce. Such a development does not make farming attractive enough, and it discourages the farmers from toiling to produce the same quantities or more in the following year. Food then has to be imported into the country[4]. The rural farmers are increasingly being forced out of job, and the youth keep on drifting into the cities for non-existent jobs. One adverse effect of this is already being felt in slum development with increased crime rate etc. in the

---

[1] This estimate was given by the Ministry of Agriculture on the Farmers' Day, 6th December 2002 in Takoradi, Ghana, and was reported in the Daily Graphic (a national news paper) on 7th December 2002

[2] This value was obtained from the report by Christine Asser on Field Testing of Natural Convection Solar Driers; http://www.kenes.com/Ises.Abstracts/Htm/0012.htm

[3] Facts were obtained from the daily announcements of prices of foodstuffs by the Garden City Radio (a state-owned radio station in Kumasi, Ghana). The exchange rate was around ¢8500 to $1.

[4] This importation of food was attested to by the international pop star, Ronan Keating, on the Channel 1 BBC-Breakfast Show on Thursday, 10 June 2004 after a trip to Ghana with the Christian Aid (a charity organisation). The interview was also published on the same day at the website; http://www.bbc.co.uk/breakfast

cities. Furthermore, the problem of food insecurity affects the economy of Ghana to a large extent, as the nation depends so much on agriculture[5].

Among the methods of finding ways of meeting the present and future demand for food, which also has the benefit of generating income in the rural communities of a developing country like Ghana is the use of solar crop drying. The absence of electricity from the national grid and also the high cost of fossil fuel make this option a feasible one not only from environmental but also from economic point of view (Sharma *et al.* 1995). Solar crop drying could provide ways of equipping rural farmers in Ghana to prepare their produce well for storage and add value to the food so that they may receive remunerative prices at the appropriate time of sale. The produce must be dried to the right moisture content before storage. Surplus crops could then be preserved for sale in their prime marketable condition.

Solar drying uses the sun as direct source of energy to dry the crops thermally. A traditional method of 'open-sun' drying has been used by the rural farmers since time immemorial. This entails the spreading of the crops on mats in the open sun and turning them occasionally for effective drying. This method, normally used to dry about 90 % of the crops in Ghana, is cheap and environmental friendly but inefficient and labour intensive. Also, the drying commodity is normally exposed to rain and other unhygienic conditions. A more appropriate method expected to suit the rural farmer is a method of solar drying which works by natural (or free) convection (Singh *et. al*, 2004).

The use of the natural convection (or natural ventilation) solar crop dryer is normally seen as an improvement of the traditional open-sun drying. It is normally one of 3 main types; the direct-, the indirect- or the mixed-mode type. However, according to some earlier reports, natural ventilation solar crop dryers are characterised by poor air circulation which, in most cases, results in excessive temperatures within the drying chamber (Bassey *et al*, 1994; Green and Schwarz, August 2001). Products dried with

---

[5] At a Workshop on ECOWAS agricultural policy, Mr. Kwaku Owusu-Baah (the Chief Director of Ministry of Food and Agriculture) gave the following figures: agriculture accounts for 65% of the workforce and 35% of the total export earnings in Ghana. Yet 36% of the population leave in extreme poverty. 50% of the poor are in agricultural sector. (Accessed from the Ghana Homepage: **http://www.ghaweb.com** on 30/11/2004)

these dryers, especially the direct-mode cabinet types, are at times partially cooked instead of being well dried. The quality of such products can sometimes be below that of the crops dried in the open air, unless the dryer is very well designed (Ekechukwu and Norton, 1997; Jain and Tiwari, 2004).

Despite the problems associated with the direct-mode solar crop dryer, it is still the simplest and not so expensive to construct. The economic base, the level of awareness, the low science culture and the socio-cultural practices of the target group (e.g. the rural farmers in Ghana) are such that this group can only patronise the direct-mode dryers, at least for a start. A lot of interests have been expressed in such dryers, even in the Ghana Parliament[6]. The need to house the farm produce and protect it during drying is increasingly raising the demand for simple structures like direct-mode natural convection solar crop dryers.

It has therefore become more necessary to find ways of improving the natural ventilation in the direct-mode dryer. The development of the direct-mode dryers will:

1 Provide services that are more responsive to the needs and circumstances of a wide range of farmers in rural areas.
2 Provide jobs for the local artisans and employable skills for most of the young graduates, who are normally produced from the third-cycle institutions in excess of what the existing industries can absorb.
3 Reduce poverty and the rural-urban drift which poses problems for the town and city planners
4 Ensure food security and promote the growth of the Ghanaian agricultural-based economy.

A solar chimney has been identified as a structure that improves the ventilation through a room. However, with most practical natural-circulation dryers, very little attention has been paid to the efficient design of chimneys. (Ekechukwu and Norton, 1997).

---

[6] This was from the parliamentary discussion on Friday, 13 June 2003 (Reported by the Daily Graphic in Ghana on Saturday, 14 June 2003). Comment was made by Mrs Cecilia Gyan Amoah (a Member of Parliament of NPP – the governing party) as she spoke about the health hazards associated with the methods of open sun drying. Her voice was added to by Alhaji Ali Amadu (a Member of Parliament of NDC - the main opposition party).

There is the need to verify this expected performance of the solar chimney on natural convection solar crop dryers (especially the direct-mode type). A solar chimney uses the radiant energy from the sun to heat up the air in the chimney to become less dense than the surrounding air. This causes the cold, dense air from the surroundings to rush into the chimney to displace the warm, less dense air, and so a continuous air circulation ensues. Also, the tent dryer (with inclined roof) is reported to perform better than the cabinet dryer, which has a nearly horizontal roof (Ekecukwu and Norton, 1999). Therefore the angle to which the dryer roof is positioned is also to be considered in the investigations

A number of vocation centres are being set up in Ghana to train the unemployed youth to enable them to produce some simple equipment as a means of livelihood. The high demand of the direct-mode dryer and the simplicity of its construction could drive a number of local artisans, including those trained from the various vocation centres, to go into mass production of the dryers. This may give rise to the emergence of inefficient and inappropriate structures, which would tend to compromise the integrity of solar drying, unless the right standards are established for future designers, consultants and the various standards-enforcing agencies to use as guidelines.

Establishing the various performance criteria through manual designing, constructing and testing of solar dryers of many different dimensions in all the farming communities under varying climatic conditions would be very tedious, expensive and daunting. So, modelling and simulation procedures are used to determine the performance of a solar chimney of identified design and operating configurations on the direct-mode dryer in relation to environmental conditions. Modelling is a very important step for refining an identified concept of an engineering structure for optimisation. It normally results in the development of a simulation code for possible modification and standardisation of the design (Dally *et al,* 1993). Modelling is generally of 2 kinds; 1) the analytical type, which is a mathematical approximation of the product and 2) the physical type, which consists of the experimental testing of a physical model (or copy) of the structure to verify the mathematical model and also to exhibit any possible phenomena that was not anticipated by the mathematical model. As Ulrich and Eppinger (1995) put it, the

mathematical model normally focuses on a few selected phenomena, with a number of assumptions, and the results are not so accurate. It is however flexible in the demonstration of options in the dimensions and conditions of those selected events. The physical model is more comprehensive, as it is able to demonstrate more physical events accurately for some chosen conditions and dimensions. It is therefore used to verify the mathematical model for a valid simulation code. The physical model is however not so flexible, since the construction and testing of physical structures for all the intended dimensions and conditions would be very costly and tiresome.

In the case of the dryers, the air that circulates to keep the temperature low (as in buildings) has an additional role of absorbing more moisture from the wet crops in a drying chamber. Investigations are necessary to find out the extent to which the solar chimney can help in achieving this dual function of the drying air.

1.2 Objectives of the programme

The main task is to develop a simulation code to be used as a design tool to help standardise the design of a solar crop dryer that depends on a chimney for effective natural ventilation. The title of this programme is the Design, Simulation and Optimisation of a Chimney-dependent Direct-mode Solar Crop Dryer (CDSCD). The main aims of the programme are to;

1. develop a procedure for the design of a CDSCD.
2. design, construct and test a laboratory model of CDSCD.
3. formulate a mathematical model capable of describing the behaviour of a CDSCD and validate it against the laboratory model.
4. carry out field trials on a full-scale CDSCD, designed, constructed and modified according to the findings obtained from the laboratory model.
5. compare the performance of a CDSCD against other forms of solar crop dryers.

1.3 Methodology

The methods proposed to accomplish the above objectives are the following;

1. A critical review of the literature on natural ventilation solar crop dryers and solar chimneys, in order to come out with clear steps for the design of the chimney-dependent direct-mode solar dryer.
2. Design and construction of a small-scale laboratory model of CDSCD with adjustable roof-tilt angle and inlet openings, for experimentations in the laboratory.
3. Formulation of a mathematical model to be used to simulate the behaviour of the laboratory model and to investigate the various design possibilities.
4. The use of the laboratory model to test the different roofing angles, chimney design and drying shelves arrangement within the drying chamber.
5. Analysis of the coefficients and factors of heat and mass transfers with the help the experimental work and the simulation code.
6. Testing and refinement of the mathematical model and the simulation code through validation against experimental results.
7. Design and construction of a full-scale model based on the findings of the studies so far.
8. Execution of field trials on the full-scale model and comparison of results with those predicted from simulation.
9. Comparison of the results of investigations on the CDSCD with those of other crop dryers.
10. A parametric study to predict the performance of CDSCDs under given conditions.
11. Documentation of the whole project.

1.4 Structure of the thesis

The thesis is arranged in seven chapters. The first chapter explains the background and motivation for the subject area chosen for the programme. It also defines the title and spells out the objectives of the programme and the methods for accomplishing the objectives. This chapter ends with the description of the thesis structure. Chapter 2

presents a literature review on crop drying and natural ventilation operations and their systems. Modelling and simulation studies on crop drying and heated chimneys are described. The availability of insolation from the sun in a given geographical area is also considered. The chapter ends with a brief description of the architectural concept of the CDSCD and the type of investigations proposed for the current programme. Chapter 3 describes the physical models with their instrumentations set-up. The various physical trials are also described in this chapter. In chapter 4, the mathematical models formulated for simulating the behaviour of the physical models are explained. The results of the trials conducted on the physical models are presented and discussed in chapter 5. The development of the simulation code from the mathematical models and the experimental results are demonstrated in chapter 6, with some parametric studies. Chapter 7 concludes the thesis, with some suggestions for further work.

CHAPTER 2 LITERATURE REVIEW

This chapter presents a report of the literature review which was conducted for an insight into the process of designing and optimising the Chimney-dependent Direct-mode Solar Crop Dryer. The first two subsections in this chapter report on crop drying and natural ventilation operations and their systems. These are followed by a sub-section on the availability of insolation from the sun in a given geographical area. The next sub-section reports on the methods and findings of some modelling studies (both analytical and experimental) performed earlier on solar dryers and solar chimneys. Finally, a summary is presented on the findings from the whole literature review, with a subsequent description of the selected architectural concept of the CDSCD and the type of investigations decided on.

2.1 Crop drying

Crop drying is the removal of moisture from the crop to a level where the crop can be stored for an appreciable length of time in its safe and marketable condition. Mujumdar (1997) defines drying as the operation which converts a liquid, solid or semi-solid material into a solid product of significantly lower moisture content. The drying process occurs with the moisture leaving the crop into the surrounding air. This section describes the properties of the crop and air which steer the crop drying process. The drying process, the general components and classifications of a crop dryer are also discussed. The subchapter ends with the description of solar crop drying and the main types of natural ventilation solar crop dryers.

2.1.1 Crop properties

2.1.1.1 Moisture content

The moisture content (or moisture fraction) of the crop is the proportion by mass of the moisture in the crop. It can be defined on wet basis M_w and on dry basis M_d as follows (ASHRAE Handbook, 2001):

$$M_w = \frac{100\,W_w}{W_w + W_d} \tag{2.1}$$

$$M_d = \frac{100\,W_w}{W_d} \tag{2.2}$$

where W_w is the mass of water (moisture) and W_d is the mass of dry matter (dry crop), and

$$M_d = \frac{100 M_w}{100 - M_w} \tag{2.3}$$

$$M_w = \frac{100 M_d}{100 + M_d}. \tag{2.4}$$

The moisture is normally present in the crop in a particular form, depending on the level of the moisture content, some of which are (Mujumdar, 1997):

1. Bound moisture: the moisture that is physically and/or chemically bound to the solid crop matrix with a vapour pressure lower than that of pure water at the same temperature.
2. Unbound moisture: the moisture that exerts a vapour pressure equal to that of pure water at the same temperature.
3. The equilibrium moisture content: the moisture content of the crop in equilibrium with the surrounding air at a given temperature and pressure. The moisture at this stage is not free to be removed in the drying process. The equilibrium moisture content decreases with increase in temperature (at a given relative humidity) and increases with increase in relative humidity (at a given temperature).
4. Free moisture: the moisture content in excess of the equilibrium moisture content at a given air temperature and humidity. This moisture is free to be removed.
5. The critical moisture content: the moisture content at which the drying rate starts falling.

Every crop has a desired level of moisture content for storage. The moisture content on wet basis of fresh foods ranges between 20% and 90%. Fruits, in general, need to be stored with moisture content below 20%. For vegetables, the moisture content should

be below 10% and that for grains should be between 10% and 15%. (Green and Schwarz, August 2001). Table 2.1 shows the moisture content values of some food items at the time of harvest and also those values desired for storage.

	Moisture Content (Wet Basis)	
Food	**Initial**	**Desired**
Rice	24%	14%
Maize	35%	15%
Potatoes	75%	13%
Apricots	85%	18%
Coffee	50%	11%

Table 2.1: Moisture contents (source: Green and Schwarz, August 2001)

2.1.1.2 Water activity

The water activity a_w is defined as the ratio of the partial pressure of water over the wet food system to the equilibrium vapour pressure of pure water at the same temperature (Mujumdar, 1997). It is equal to the decimal value of the relative humidity of the surrounding air. As noted by Okos et al (1992), the higher the water activity of a crop, the faster the deterioration of the crop quality. At a given temperature, a crop of high moisture content has higher water activity than the same crop with low moisture content. Thus, the quality of the crop reduces only slightly when it is properly dried. The quality can however degrade dramatically when the drying is not well done. The chances of quality degradation are very much reduced by fast drying.

Also, for constant moisture contents, water activity increases with rising temperatures, according to Okos et al (1992). Therefore high drying temperatures should be matched by fast drying to reduce the rate of quality deterioration. Quality reduction manifests itself among others in the change in colour of the crop.

2.1.1.3 Other properties of the crop

Moisture diffusivity describes the ease of moisture transfer in foods. It depends on the permeability of the crop, the amount of moisture in the crop and the temperature of the surrounding air (Okos et al, 1992).

The binding energy, also known as the enthalpy of wetting, is the energy required to remove the bound moisture from the crop. This energy adds to the latent heat of vaporisation of water to form the total energy required to remove a unit mass of moisture from the crop. The binding energy is positive for most crops, and it generally decreases with increase in moisture content, with a value of zero for unbound moisture. The value can however be negative for materials like peanut oil and starches at low temperatures (Mujumdar, 1997).

2.1.2 Psychometrics

This section describes some properties of the air (or air-vapour mixture) in relation to crop drying. These are:

1. Dry-bulb temperature: the air temperature measured by the dry bulb of a thermometer immersed in the air.
2. Wet-bulb temperature: the temperature that is measured by passing the air rapidly over a wet thermometer bulb. This is used along with the dry-bulb temperature to determine the relative humidity of the air.
3. Dew point: the temperature at which unsaturated air becomes saturated with the vapour. The vapour is then about to start condensing out of the air at this temperature. The dry-bulb temperature is equal to the wet-bulb temperature at this point.
4. Absolute humidity: mass of water vapour per unit mass of air.
5. Relative humidity: ratio of the partial pressure of water vapour in the air to the equilibrium vapour pressure (i.e. the partial pressure of the vapour when the air is saturated) at the same temperature. The decimal value is equal to the water activity of the crop.

As noted earlier, the lower the relative humidity of the drying air, the higher the rate of drying. For a given absolute humidity of the air, the relative humidity decreases with increase in temperature. When the air is not warm and dry enough, the drying commodity becomes partially cooked, rather than being dried. But when the temperature gets too high while the air is too humid, hard coats are formed at the surfaces of certain crops which then inhibit the drying process.

2.1.3 The drying process

In the process of drying, moisture evaporates out of the crop into the surrounding air. The drying time depends on how quickly the moisture evaporates. Generally, moisture evaporates from a porous material (e.g. crop material) into the air whenever the vapour pressure of the moisture in the crop is higher than the partial pressure of the vapour in the drying air. The rate of evaporation is proportional to the pressure difference. The higher the relative humidity of the drying air the less the pressure difference and, therefore, the less the rate of evaporation (Rogers and Mayhew, 1993; Jain and Tiwari, 2004). The drying process continues until the partial pressure of the vapour in the air is equal to the crop vapour pressure. At this stage, equilibrium is established between the moisture in the crop and the vapour in the air. The moisture content at this point is known as the equilibrium moisture content, and the vapour pressure and the air relative humidity are known as equilibrium vapour pressure and equilibrium relative humidity respectively.

Thus, for an enhanced drying process, there must be proper ventilation to ensure fast replacement of the drying air that becomes humid as a result of moisture absorption by less humid air. However, as noted by Bengtsson and Whitaker (1986) the air becomes under-utilised when the airflow through the dryer is too high. On the other hand, certain minimum airflow rates are necessary to prevent mould formation during drying. In general, the drying air should be appreciably warm, dry and moving. Table 2.2 gives values of required minimum rates for wheat and maize as against their initial moisture contents

	Moisture content (%, w.b.)	Airflow / (m^3/ m^2 s)
Wheat	20	0.06
	18	0.04
	16	0.02
Maize	25	0.10
	20	0.06
	18	0.04
	16	0.02

Table 2.2 Minimum required airflow rates for wheat and shelled maize (source; Bengtsson and Whitaker, 1986)

The rate of drying depends on the rate of diffusion of moisture through the crops to the surface, the temperatures of the crop and drying air and the mass flow rate of the drying air (Mujumdar, 1997). The rate of diffusion, in turn, depends on the type of crop, crop size, the temperatures of crop and drying air, and the airflow rate. The crop must also be permeable enough to allow easy diffusion of moisture.

The crop loses weight and shrinks, as it releases moisture into the drying air. The loss of weight may be found as follows (Bengtsson and Whitaker, 1986);

$$W_2 = W_1 - \frac{W_1(M_1 - M_2)}{100 - M_2} \tag{2.5}$$

where

W_1 = mass of wet grain (kg)

W_2 = mass of dried grain (kg)

M_1 = moisture content of crop before drying (%)

M_2 = moisture content of crop after drying (%)

For a given crop, drying is fastest at the beginning when the moisture content is high. The drying rate reduces as the moisture content becomes lower, with lower vapour pressure in the crop.

Two periods are identified in the drying process; Constant-rate and Falling-rate periods. During the constant rate period, which is normally at the beginning of the drying process, the evaporation rate per unit drying area is constant. Unbound water is removed from the surface. Water evaporates as if there is no solid present, and the rate of diffusion is not dependent on the solid. The water moves at the same rate to the crop surface as the rate of evaporation. This continues until the water from the interior is no longer available at the surface. The critical moisture content is then reached, after which the falling rate period begins.

The falling-rate period begins when the rate at which the water moves from the interior to the crop surface is lower than the rate of evaporation at the surface. When the surface becomes completely dry, the evaporation front moves towards the centre of the crop. The moisture that is then removed from the interior then moves to the surface as vapour. Although the amount of moisture removed during the falling-rate period is relatively small, it normally takes a significantly longer time than during the constant rate periods.

At times only the falling-rate period is observed in practice, and the drying time is modelled on the falling-rate period (Forson, 1999). The drying rate at this stage decreases with time, and the process is controlled by the internal mass transfer of moisture to the crop surface. This internal mass transfer or moisture diffusion process is analysed by Fick's law as

$$\frac{\partial m}{\partial t} = D_{eff} \frac{\partial^2 m}{\partial x^2} \tag{2.6}$$

where m is the local moisture content on dry basis, t the time, and x the spatial coordinate. In applying this law, the crop is usually assumed to be unidimensional with uniform initial moisture content. Also, the main resistance to moisture transfer is assumed to be due to internal moisture movement. The solution to the differential

equation (2.6) is used to determine the moisture content in relation to the drying time, depending on the shape of the crop or crop bed (Okos et al, 1992; Crank, 1975).

2.1.4 General components of a crop dryer

For given range of crops and environmental conditions, crop dryers are designed to achieve the required airflow and drying temperature for the desired product quality. The main components of a crop dryer are;

- A drying chamber, in which the drying commodity is placed for drying
- An air-heating chamber for heating the drying air
- An air-flow device, for generating air current through the dryer as in forced-convection dryers. Some dryers are designed without any air-flow device, and these rely on natural ventilation, as described in the next section.

2.1.5 Classification of crop dryers

Crop dryers are classified according to a number of criteria some of which are described in the following sections.

2.1.5.1 Classification by means of ventilation

The dryer may operate by forced ventilation. An air flow device (e.g. blower) is normally needed in the case of forced convection. This could be powered by electricity from the grid, solar electricity or by a fuelled engine, as noted by Ekechukwu and Norton (1999). On the other hand, the system can be designed for air circulation by natural convection through buoyancy.

2.1.5.2 Classification by source of power

The power supplied directly to the dryer is normally for heating. Heating can be done through the burning of fuel (e.g. oil, wood), using electricity or solar energy. The mode of energy input can also one of conduction, convection, radiation, dielectric heating or a combination of two or more of them.

2.1.5.3 Mode of loading

A crop dryer can be classified according to how the crop is loaded into the dryer. A deep-layer dryer has the crop arranged on beds, in bins, silos or even warehouses in layers of 30 cm to 350 cm deep (Bengtsson and Whitaker, 1986). The dryer normally works by forced convection with the drying air driven through some ducting at the base into the drying commodity to exit at the top. The crop dries first at the point of air entry (the base), and a drying front is created at the tip of a drying zone which advances through the crops in the direction of air flow. The thickness and rate of progress of the drying zone depends mainly on the moisture content and the air speed. In practice, air speed of 0.10 – 0.15m/s is used, as suggested by Bengtsson and Whitaker (1986).

With a shallow-layer dryer, the farm produce is spread in layers of depth up to 30 cm. Dryers can also be classified as batch or continuous. In a batch dryer, the crops are arranged on a number of trays, one on top of the other, with gaps between them. The dryer can function by forced or natural ventilation, depending on the depth and the desired rate of drying. Batch drying can be for several hours or a few days. A continuous-flow dryer has the crop passing through the dryer at a controlled rate. The depth is normally 15 cm or less, and the drying air is forced through the crop as it passes through the dryer. Continuous drying is normally for several minutes or a few hours, as noted by Mujumdar (1997).

The dryer can be semi-continuous, where the crops at the hottest part of the dryer dry fast and are taken out. Partially dried crops are shifted to the hottest part and their places are occupied by fresh crops.

2.1.5.4 Classification by the design of the drying chamber

A dryer can be classified according to its design. A cabinet dryer has a near-cubical-shaped drying chamber with the roof slightly tilted to the horizontal. It has an opening for air inlet at the base and an exit opening in or near the roofing. It operates either by forced convection through the use of a blower or by natural ventilation where buoyancy forces are employed with the height of the dryer. The drying air encounters the dryer roof almost perpendicular to the flow before exit into the atmosphere. Thus the

resistance offered by the roof to the flow of air is high (Widden, 1996; Young et al, 1997). This aggravates the problem of poor air circulation and excessive temperature rise in the chamber during natural convection.

A tent dryer has a horizontal base (normally rectangular) and a triangular side view with the maximum height at the centre of the base (like a tent). This dryer is at times also referred to as green house dryer (Ekechukwu and Norton, 1999). Like the cabinet dryer, this can also work by forced or natural ventilation, but with the drying air meeting the roof of the dryer at an angle far less than 90^0. The roof therefore offers less resistance to the air flow than the cabinet type, so that the air circulation is improved, thereby reducing the excessive temperature rise.

Another type of dryer is the tunnel dryer, in which the crop is spread in a long horizontal tunnel. It normally operates by forced convection, as no room is allowed for buoyancy flow in a horizontal tunnel. As with all forced convection dryers, the air circulation is better than the above two when they work by natural convection. Some researches have though included the solar tunnel dryer that has been tilted for natural ventilation (Garg and Kumar, 2000).

2.1.6 Solar crop drying

The oldest method of crop drying is the Open-sun drying, where the crops are spread on a flat surface and solar energy is directly absorbed. In the process of solar drying the energy is also supplied by the sun. A solar dryer consists mainly of a drying chamber and a solar collector with or without a system to propel the air through the dryer. Solar drying process is much faster, with better quality of dried product than the open sun drying, when the solar dryer is well constructed. As Bala and Woods (1994) put it, the process is an elaboration of open-sun drying for higher efficiency and better quality of end product.

Solar dryers work without emissions or noise. They require less space than open sun drying, although this space is higher than that required for convectional drying (Reuss et al, 1997). In dealing with solar drying, environmental factors such as the intensity of

local solar radiation (dependent of the sun's position) and the temperature and relative humidity of ambient air are taken into account.

Solar crop dryers are generally designed and constructed to use the prevailing environmental conditions to dry the goods to the desired quality in minimum time with maximum efficiency. Table 2.2 compares the use of solar dryer with open-air drying and with fuelled dryer:

Type of drying	**Benefits (+) & Disadvantage (-) of solar dryers**
Solar vs. open-air	+ Can lead to better quality dried products and better market prices + Reduces loses and contamination from insects, dust and animals + Reduces land required (by roughly 1/3) + Some dryers protect food from sunlight, give better nutrition and colour + May reduce the labour required + Faster drying time reduces the chances of spoilage + More complete drying allows longer storage + Crops are better controlled (e.g. sheltered from rain) - More expensive, materials may need to be imported - In some cases, food quality is not significantly improved - In some cases, market value of food will not be increased
Solar vs. fuelled	+ Avoids the dependence on fuel + Often less expensive + Reduces environmental impact (consumption of non-renewables) - Hot & dry climates preferred (usually RH below 60 %) - Requires more time - Greater difficulty in controlling the process, may result in lower quality product.

Table 2.2: Comparing the use of solar dryers with open-air drying and with the use of fuelled dryers (source: Green and Schwarz, August 2001)

The drying chamber keeps and protects the drying commodity from animals, insects, dust and rain. Local materials like sawdust may be used to reduce energy losses and

increase the efficiency. The crop is normally dried on trays in the chamber. The crop trays may be coated with plastic for safe contact with the food and also to avoid harmful residues in the food (Green and Schwarz, August 2001).

An air heater generally has the following:

1. 1. UV-stabilised glazing, which allows sunlight to be transmitted through it and prevent the energy emitted from the absorber from escaping. Glass is normally recommended for glazing, although it is very expensive and very delicate to use (Singh *et. al*, 2004). Plastic may be accepted if it is firm or can be supported by a rib to avoid sagging and collection of rain water (Green and Schwarz, July 2001; Vanderhulst, 1990).
2. The absorber absorbs the light from the sun and emits heat energy as its temperature rises.
3. Side and back cover materials – preventing energy losses.

The air heater can be supported on wood or bamboo frame etc.

Airflow device can be a mechanically-powered blower (as in forced convection dryers). Natural ventilation dryers rely on the dryer design in relation to the environmental conditions for ventilation (e.g. solar chimney, tilted roof). Natural circulation (or ventilation) can be more effective with a multiple small dryers than with one large unit, as the simple construction of small dryers and their independent mode of operation allow more flexibility. However, where there should be forced convection, then economics of scale favour large centralised dryers, so that there could be maximum use of the ventilation equipment (Green and Schwarz, August 2001).

There are 3 main types of natural ventilation dryers; the direct-mode, the indirect-mode and the mixed-mode types (Ekechukwu and Norton, 1999). These are described in the following sections.

2.1.6.1 Direct-mode dryer

Figure 2.1 shows a schematic diagram of a direct-mode cabinet dryer. With direct-mode dryers, there is no separate air pre-heater and the dryer contents serve simultaneously as the radiant energy absorber. Solar energy passes through a transparent cover and is absorbed by the crops. Around the base of the dryer are inlet openings for entry of fresh air into the cabinet dryer. During operation, the air temperature inside the dryer rises, creating a less dense and low pressure area in the dryer. Air rushes in from the atmosphere through the inlet opening to displace the warm air which exits at the top. A continuous flow of air is thus created through the drying material placed on perforated trays in the dryer. The use of the direct-mode dryer is generally more effective and more hygienic than open-sun drying but it has been observed not to perform so well, particularly as compared to the performance of the mixed-mode dryer. As Jain and Tiwari (2004) put it, the poor performance of direct-mode dryers is due to ineffective ventilation. Singh et al (2004) however declared that the direct-mode dryer can be more efficient than the indirect-mode dryer; the only problem at times is the poor quality of the produce, especially those that are sensitive to sunlight. The direct-mode dryer may either be of the cabinet or the tent type. There are some modified forms of the direct-mode type like the staircase solar dryer (Hallak et al, 1996), the multi-shelf dryer (Singh et al, 2004). In this dryer, the shelves are displaced both vertically and horizontally like a staircase, and the air is heated in between the shelves for effective drying.

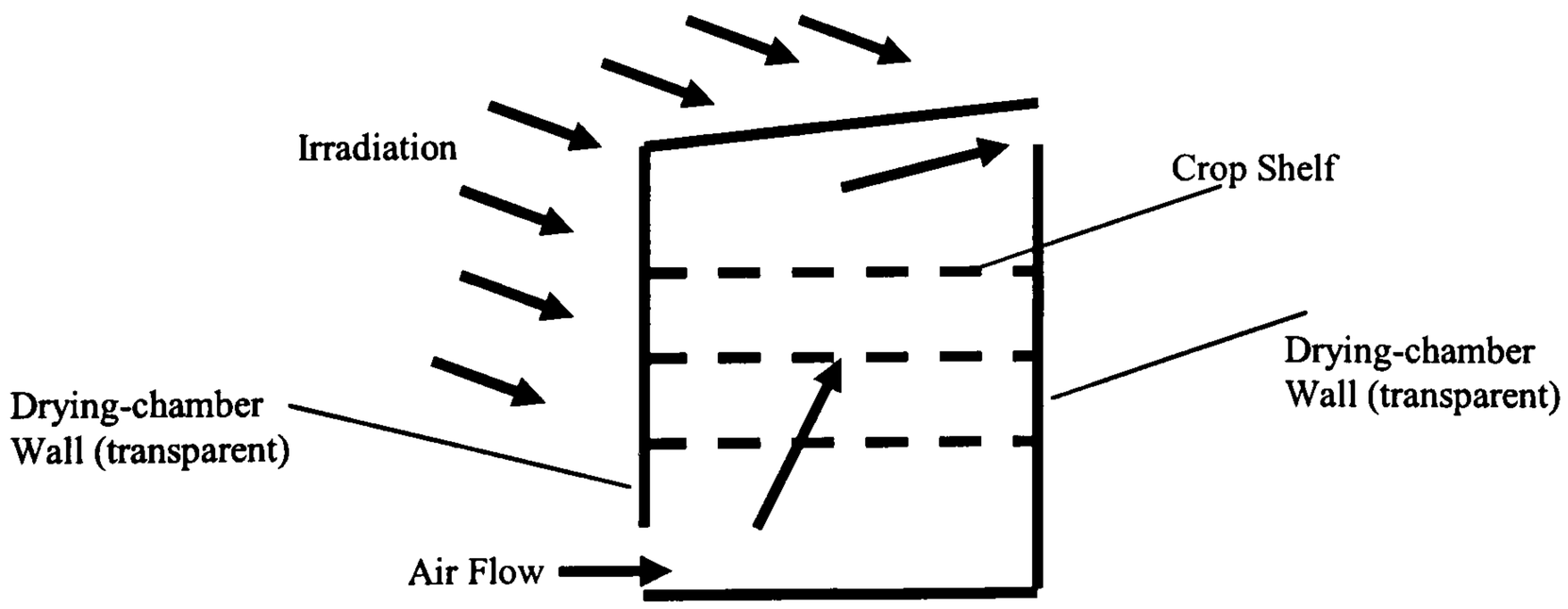

Figure 2.1 Schematic diagram of a direct-mode cabinet dryer

2.1.6.2 Indirect-mode dryer

The indirect-mode dryer has an air pre-heating device, but the drying commodity has no direct contact with the light rays for heat transfer. As shown in figure 2.2, the drying chamber walls are opaque. Convection heat is transferred to the crops by the pre-heated air for moisture evaporation (Reuss et al, 1997).

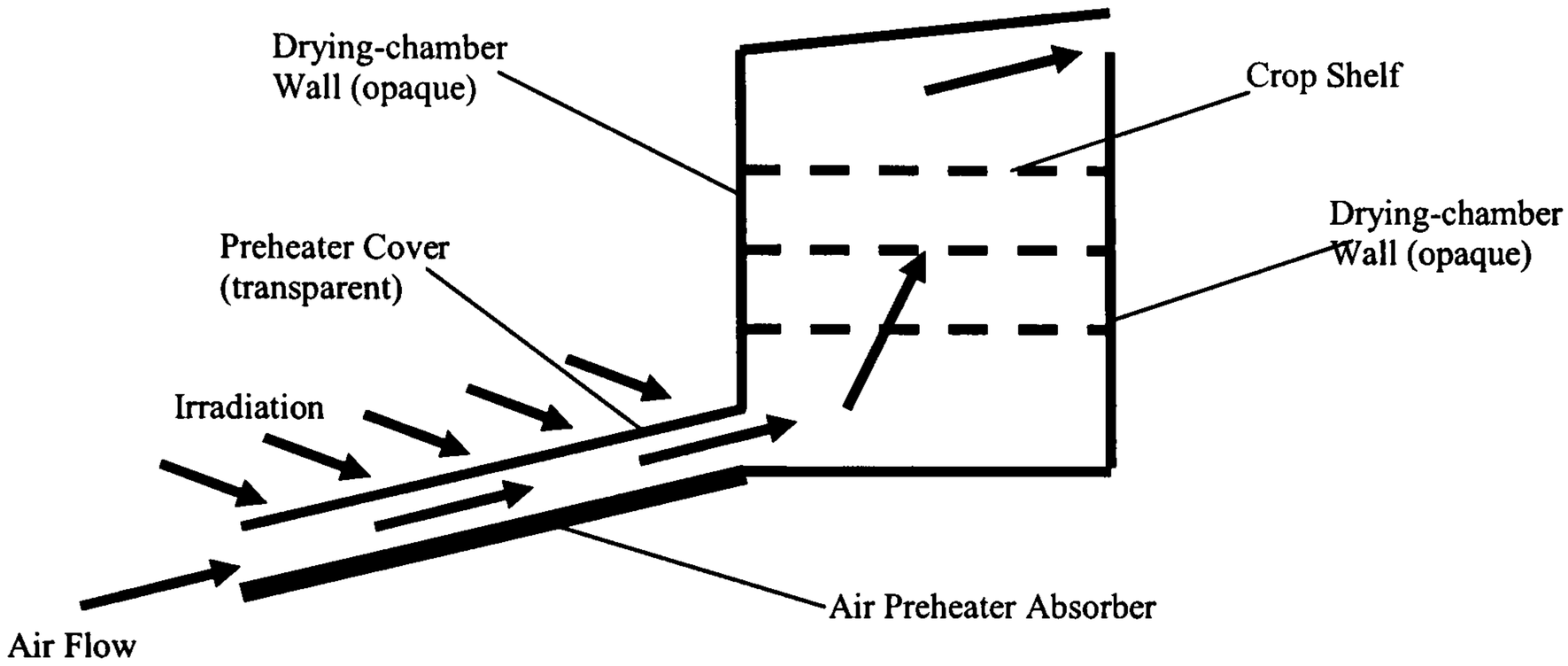

Figure 2.2 Schematic diagram of an indirect-mode cabinet dryer

2.1.6.3 Mixed-mode dryer

As shown in figure 2.3, the mixed-mode dryer has an air pre-heater, and the drying commodity is also exposed to the radiant energy, during operation (offering a combination of the direct- and indirect-mode operations). Thus, the crop is dried simultaneously by both irradiation and the convective transfer of heat from the air entering the drying chamber from the air preheater. This dryer has been found to have the most effective performance of all the three types (Bala and Woods, 1994), though there could be discoloration of crops from direct irradiation, as in the direct-mode operation.

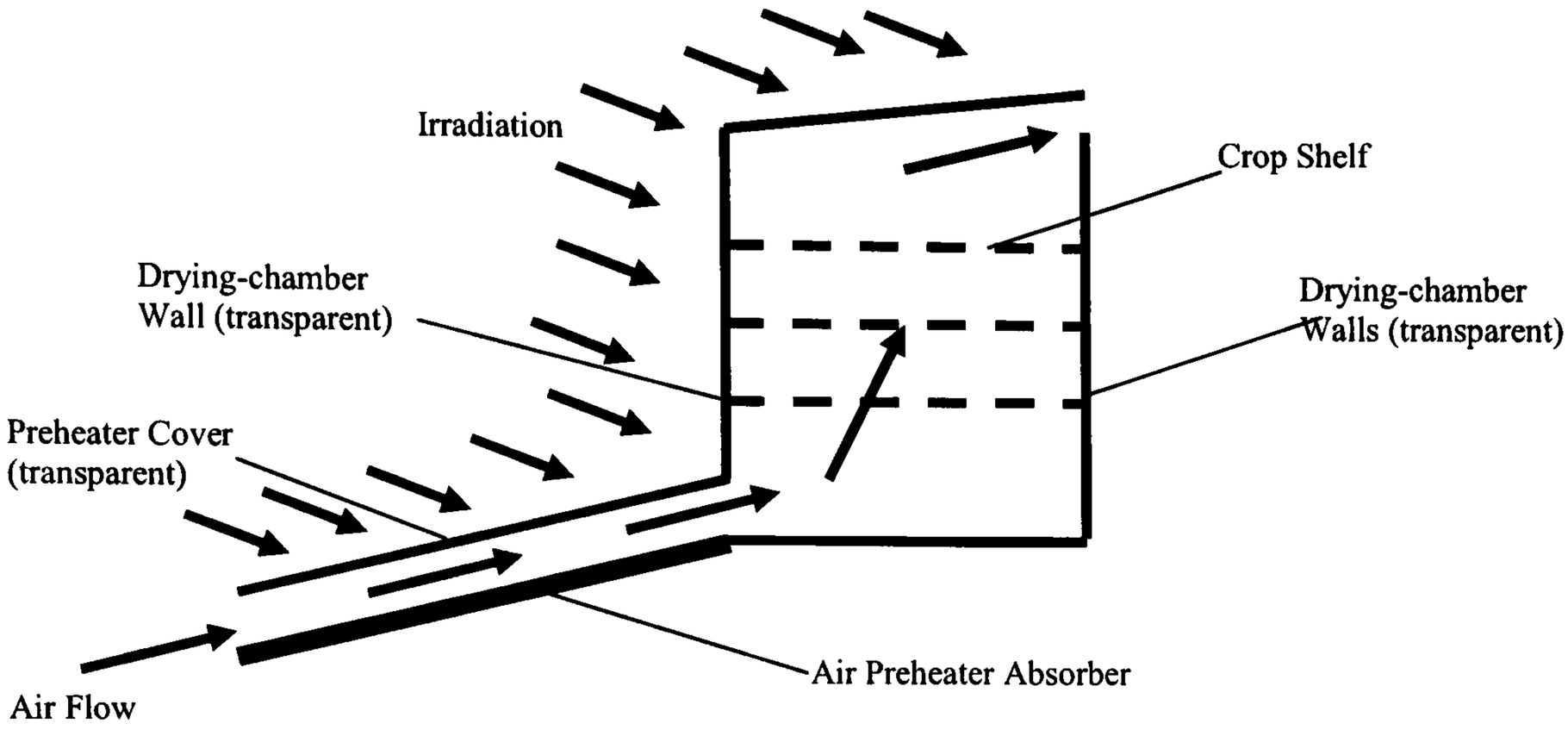

Figure 2.3 Schematic diagram of a mixed-mode cabinet dryer

In all the 3 main types, extreme care must be taken against non-uniform drying, when a number of shelves are been dried in layers in the drying chamber. There could be over-drying in the bottom tray for the indirect type, where the air meets the crops at its highest temperature (Singh et. al, 2004) and the top layer may not be well dried. The direct-mode type could have the problem of improper drying for trays below the topmost tray, unless proper exposure of all shelves to the sun is ensured. Similarly, the design of the mixed-mode dryer should guard against improper drying of the middle shelves and also against under-utilisation of the heat transferred from the air preheater as observed by Forson (1999).

The dryer can also be of the hybrid type where the energy supply for heating and air circulation is subsidised by other conventional means (Green and Schwarz, August 2001). Table 2.3 shows some advantages and disadvantages of the various classifications of solar dryers. Table 2.4 gives a summary comparison of the performance against cost of a PGCP[7] solar coconut dryer (direct-mode type), the Kenya Black Box Solar Dryer (mixed- mode natural convection) and the Hohenheim Solar Tunnel Dryer (mixed mode forced convection).

---

[7] PGCP is a GTZ project in Philippine; Philippine German Coconut Project

Classification	Advantages	Disadvantages
Direct-mode	1. Least expensive 2. Simple	1. UV radiation can damage food
Indirect-mode	1. Products are protected from UV radiation 2. Less damage from excessive temperatures	1. More expensive and complex to build than direct-mode type
Mixed-mode	1. Less damage from excessive temperatures	1. UV radiation can damage food 2. More expensive and complex to build than direct-mode type
Hybrid	1. Ability to operate without sun reduces the chance of food loss 2. Allows better control of drying 3. Fuel-mode may be up to 40x faster than exclusive solar drying	1. Very Expensive 2. Dependent on fuel.

Table 2.3: Advantages and disadvantages of direct-mode, indirect-mode, mixed-mode and hybrid types of the solar dryer. Source: Green and Schwarz, August 2001.

Name & type	Design dimensions and features	Performance	Cost
PGCP Coconut dryer; direct-mode (natural convection)	Drying area; $7m^2$ Size; 4.5m x 1.6m x 0.3m	Dries 200-300 coconuts within 4-5 days	$15 (manufacture) + $3 every 2 to 3 years
Kenya Black Box Solar Dryer; mixed-mode (natural convection)	Drying area; 5 x $1m^2$ Length x width; 2m x 0.8m	Dries 1mm-thick mango slices (under Kenyan climate) in 1 day	$340 (local manufacture)
Hohenheim Solar Tunnel Dryer mixed-mode (forced-convection)	Drying area; $20m^2$ Size; 18m x 2m x ≈1m high 3 fans; PV or mains powered	One day set-up time under arid and humid conditions	$5,500

Table 2.4; Comparison of the performance against cost of a PGCP solar coconut dryer (direct-mode type), the Kenya Black Box Solar Dryer (mixed- mode natural convection) and the Hohenheim Solar Tunnel Dryer (mixed mode forced convection). Source; Green and Schwarz, July 2001.

2.2 Natural ventilation through a chimney

Natural ventilation is an air-exchange process where the air inside a structure is continuously replaced by ambient air as a result of lower pressure inside the structure than ambient air pressure. As Cook (2002) puts it, natural ventilation can be brought about by buoyancy forces caused by temperature differences, or by wind pressure, or both. It has of late become widely spread due to its simplicity and lower cost.

A natural ventilation block, such as the chimney, creates a natural draft by building an internal stack pressure along its height and thereby causes the flow of air through the chimney channel. Ekechukwu and Norton (1997) relate the buoyancy force required to generate the air flow through the chimney as being directly proportional to the difference between the mean air density within the chimney and the density of the ambient air as

$$\Delta P_b = gH(\rho_a - \rho_{ch}), \qquad 2.7$$

where ΔP_b is the pressure drop due to buoyancy, g is the acceleration due to gravity, H the chimney height, ρ_a the ambient air density, ρ_{ch} the mean chimney air density. Thus air circulation through the chimney is assured, so long as the mean air density in the chimney remains lower than that of ambient air.

As the air moves up the chimney, its temperature falls, causing an increase in the average density inside the chimney. At some point when the conditions in the chamber become similar to those outside, the air flow stops or even a reverse stack flow can ensue, unless the wind is strong enough to produce the Bernoulli Effect (Lowndes, 2004). According to Ekechukwu and Norton (1997), the air temperature in the chimney, if saturated, may sometimes be close to the wet bulb temperature of the drying chamber, during the process of crop drying. The temperature then becomes lower than the ambient temperature, and the contribution of the buoyancy force becomes negligible.

Heating the air in the chimney can help to prevent the problems described above and ensure that the air density inside the chimney is always lower than outside it,

irrespective of the chimney's height. Bassey (1994) remarked that the performance of indirect passive dryers is not necessarily improved by the addition of chimneys, unless the chimneys are sufficiently heated. Forson (1999) also indicated the need for the chimney to be heated to improve the air flow, since the temperature of the air inside the chimney fell below that in the drying chamber during the laboratory experimentation, as a result of heat transfer (losses) through the walls of the chimney. The heated chimney operates on the basic principle of replacement of warmer air in the chimney by cooler air from outside the chimney, so that there is a continuous flow of displaced, warm and less-dense air from the chimney through the opening at the top to the atmosphere and a flow of cold and dense air from the atmosphere into the chimney (Reuss et al, 1997; Afonso and Oliveira, 2000).

The airflow is generally determined by the inlet area and the square root of the product of chimney height and the average temperature difference between the air inside the chimney and ambient air (Hinrulabh et al, 1999). Also, the wind plays an important role in the flow by producing suction as it blows over the chimney at the top and also by aiding the flow through the system when the inlet faces its direction (Awbi, 1994; Reuss et al, 1997; Green and Schwarz, 2001).

2.2.1 Chimney design considerations and airflow analyses

Chimneys must be designed with much energy gain, for enough temperature difference between the chimney air and ambient air. As noted by Lowndes (2004), the principal aim is to maximise the air temperature within the chimney, thereby minimising air density and pressure in relation to that of the air outside the chimney, in order to drive the "stack effect" air flow. From Ekechukwu and Norton (1997), heated chimneys normally have to be designed in such a way that the differential buoyancy head is far greater than the pressure losses. These pressure losses are generally due to friction at the walls of the chimney, and they are generally negligible in natural flow systems. Therefore the main emphasis on solar chimney designs should be to minimise the rate at which the air temperature cools relative to ambient temperature. Chen et al (2003) however indicated that the pressure losses at inlet and outlet of the chimney are also very significant and so must be considered. Upward flow occurs through the system,

when the stack pressure is able to overcome all the pressure losses (Afonso and Oliveira, 2000; Flourentzou et al, 1998)

As deduced by Rogers and Mayhew (1993), for a reduction in pressure to cause an upward increase in velocity in a heated vertical chimney, the chimney must either be of constant cross section or convergent, as long as the flow remains subsonic (i.e. fluid velocity remains lower than the velocity of sound in the fluid). The airflow is further enhanced, when the inlet cross-sectional area is increased, for a given exit area, to allow more air into the system. However, Zambrano and Alvarado (1984) indicate that under non-lamina conditions, the chimney should have lowest diameter at the base for improved airflow. The report by Chen et al (2003) indicates that, for a chimney of a given height and uniform heat flux, there exists an optimum chimney gap for maximum air flow (i.e. an optimum gap-to-height ratio). This optimum gap-to-height ratio depends on the chimney inlet design.

Generally, for a heated chimney to function effectively by natural ventilation, the ambient air must enter through the bottom opening, get heated inside the chimney and then exit through the vent at the top. Thus the density at the top must always be lower than at the bottom. Therefore in analysing the airflow in a heated chimney, equation (2.7) is applied for the buoyancy pressure head from the chimney inlet to the outlet as

$$\Delta P_b = g\Delta H(\rho_{in} - \rho_{out}) \tag{2.8}$$

From Incropera and DeWitt (1996), an approximate relation between the air density and temperature is given as

$$\beta = \frac{1}{\rho}\frac{(\rho_{in} - \rho_{out})}{(T_{out} - T_{in})} \tag{2.9}$$

Equations (2.8) and (2.9) are combined to give

$$\Delta P_b = g\rho\beta\Delta H(T_{out} - T_{in}) \tag{2.10}$$

From the basic principle that the increase in buoyancy pressure must be equal to the sum of all flow pressure losses (or resistances) between inlet and outlet, the underlying equation for the airflow is obtained as

$$g\rho\beta(T_{out} - T_{in})\Delta H = \sum_i K_i \rho \frac{v^2}{2} + \sum_j f_j \frac{L_j}{D_j} \rho \frac{v^2}{2} \qquad (2.11)$$

The first term on the right-hand side of equation (2.11) denotes the sum of all local pressure losses or resistances (from expansion, contraction and bending, including those at entry and exit). The second term is the sum of all losses due to friction at surfaces along the airflow direction. Heating the air in the chimney can ensure that the air exits at a higher temperature than that of the ambient air that enters the system. The temperature difference must be high enough to provide the pressure head required to overcome the pressure resistances.

2.2.2 Solar chimney

A solar chimney is a heated chimney that receives radiant energy from the sun to heat up the air. It has one or more transparent wall(s). An absorber is positioned inside the chimney to absorb radiant energy from the sun that enters the chimney through the transparent wall(s). The absorber produces thermal energy which increases the internal energy of the air, thereby converting solar energy into kinetic energy (Bernardes et al, 2003; Chen et al, 2003).

As noted by Bansal et al (1994) and Hamdy and Fikry (1998), one advantage of solar chimney is that it is self regulatory; the hotter the day (i.e. the higher the insolation) the higher the temperature of the chimney absorber and, therefore, the faster the air circulation to avoid excessive temperature rise in the chimney. The solar chimney is normally designed to provide ventilation during the day, although some energy could be stored in the walls of the chimney during the day (as heat inertia) to be released at night

to prolong the ventilation. Thick chimney walls store more energy and reduce the flow rate during the peak period of sunshine (Afonso and Oliveira, 2000). As noted by Bassey (1994), the gap between the chimney absorber and transparent cover should be close enough for effective heat transfer between the fluid and chimney absorber.

2.3 Availability of solar radiation

Solar radiation is a key factor that is considered in the design of solar dryers and solar chimneys. As noted by Duffie and Beckman (1991), the most common measurements of solar radiation are total radiation on a horizontal surface, which is often referred to as global radiation. Radiations onto other surfaces are then deduced in relation to that on the horizontal surface, using the angles between those surfaces and the horizontal surface. The following angles are used to describe the relationships between a plane and the incoming solar radiation:

- Latitude φ: This is the angular location north or south of the equator (north is positive); $-90^0 \leq \varphi \leq 90^0$.
- Surface azimuth angle γ: The angle between the projection of the normal to the surface onto the horizontal plane and the local meridian; the angle is zero when the projection is towards south, towards east is negative and towards west is positive ($-180^0 \leq \gamma \leq 180^0$).
- Slope β: The angle between the plane of a given surface and the horizontal such that $0 \leq \beta \leq 180^0$. The surface faces downward when $\beta > 90$.
- Angle of incidence θ: The angle between the beam radiation on a surface and the normal to that surface.
- Zenith angle θ_z: The angle between the vertical plane and the line to the sun. This is the angle of incidence of beam radiation on a horizontal surface.
- Solar altitude angle α_s: The angle between the horizontal and the line to the sun. This is the complement of the zenith angle.
- Solar azimuth angle γ_s: The deviation of the projection of beam radiation on the horizontal plane from south; east is negative and west is positive

The solar radiation G_o incident on a horizontal plane outside of the atmosphere is given by (Duffie and Beckman, 1991)

$$G_o = G_{sc}\left(1+0.033\cos\frac{360n}{365}\right)\cos\theta_z \tag{2.12}$$

where G_{sc} is the solar constant and n is the day of the year ($1 \leq n \leq 365$)

The global radiation consists mainly in two parts; beam (or direct) radiation and diffuse radiation. These are described below.

2.3.1 Beam radiation

Beam radiation is that part of solar radiation received directly from the sun without being scattered by the atmosphere. For the estimation of the beam proportion of the total radiation, the clearness index of the particular geographical area must be known. The higher the clearness index the higher the beam proportion of the global irradiation. A number of studies have been done, relating the clearness index to the average daily proportion of diffuse radiation, as reported by Duffie and Beckman, 1991).

2.3.1.1 Direction of beam radiation on a given surface

The angle of incidence θ of beam radiation on a given surface is given by

$$\cos\theta = \cos\theta_z\cos\beta + \sin\theta_z\sin\beta\cos(\gamma_s - \gamma) \tag{2.13}$$

For a horizontal surface, $\beta = 0$, so that equation 2.13 becomes

$$\cos\theta = \cos\theta_z \tag{2.14}$$

Thus on a horizontal surface, the angle of incidence becomes the Zenith angle.

For a vertical surface, $\beta = 90^0$ and equation (2.13) becomes

$$\cos\theta = \sin\theta_z\cos(\gamma_s - \gamma) \tag{2.15}$$

The ratio R_b of beam radiation on tilted surface to that on horizontal surface is given by

$$R_b = \frac{\cos\theta}{\cos\theta_z} \tag{2.16}$$

2.3.2 Diffuse, reflected and total radiations

Diffuse radiation (sometimes known as sky radiation or solar sky radiation) is the part of radiation that is received after being scattered by the atmosphere. The higher the clearness index the lower the diffuse proportion of the total radiation in a geographical location.

The diffuse radiation consists in three parts. The isotropic part is received on a surface uniformly from all parts of the sky dome. The circumsolar diffuse is from the forward scattering of solar radiation and it is concentrated around the part of the beam radiation. The third part is the horizon brightening, which is concentrated near the horizon, and is most prominent in clear skies.

There are also radiations which are reflected from other surfaces around the surface under consideration. Thus the total radiation incident on a unit area of a given surface is

$$G_T = G_{T,b} + G_{T,d,iso} + G_{T,d,cs} + G_{T,d,hz} + G_{T,refl} \tag{2.17}$$

where the subscript b denotes beam radiation and the subscripts *iso*, *cs*, *hz* and *refl* refer to isotropic, circumsolar, horizon and reflected radiations respectively.

From equation 2.12, the lower the Zenith angle the higher the insolation on a horizontal plane outside the atmosphere. The Zenith angles in the tropics (geographical areas of low latitudes) are lower than those of areas far away from the equator. Thus, as noted by Alexander and Boyle (2004) sunlight falls in a more perpendicular direction onto the horizontal surface in tropical regions and more obliquely in areas of high latitudes. It has been argued before that due to its vertical orientation, a solar chimney must be far away from the equator to be able to receive enough radiation from the sun. But there is also a counter argument that in areas near the equator, there is a fairly high proportion of diffuse radiation, and a solar chimney can be effectively designed to make use of this diffuse radiation for air heating (Ekechukwu and Norton, 1997).

2.3.3 Other terms

Some terms are used to describe the rate and intensity of solar radiation reaching a surface. The rate at which the radiant energy is incident on a unit area of surface is

termed irradiance (normally inW/m^2). Irradiation or radiation exposure (J/m^2) is the total energy incident on a unit surface over a specified time, usually an hour or a day. This term can refer to radiation from any source of light. Insolation is a term applied specifically to solar irradiation. The terms are at times used interchangeably.

The solar time is the time that is based on the apparent angular motion of the sun across the sky. The solar noon is then the time when the sun crosses the meridian of the observer. The difference in minutes between solar time and standard time is (Duffie and Beckman, 1991)

$$\text{Solar time} - \text{standard time} = 4\,(L_{st} - L_{loc}) + E \tag{2.18}$$

where L_{st} is the standard meridian for the local time zone, L_{loc} is the longitude of the location in question (in degrees west) and E is the equation of time given as

$$E = 229.2\,(0.000075 + 0.001868\cos B - 0.032077\sin B - 0.014615\cos 2B - 0.04089\sin 2B)$$

where

$B = (n-1)\frac{360}{365}$, and n is the day of the year; $1 \leq n \leq 365$.

2.4 Studies on crop drying and heated chimneys

Some available studies on crop drying and heated chimneys are reviewed in this section.

2.4.1 Studies in crop drying

2.4.1.1 Modelling and simulation methods in drying

As noted in ASHRAE (2001), the drying rate or time is the most important criteria in crop drying. This is predicted through a drying model. The drying model is normally developed for thin-layer drying, where the crop properties are assumed to be uniform across the thickness. Methods of thin-layer modelling can then be extended to cover deep-bed drying by considering the thin layers in series.

Some models develop a solution out of the Fick's law introduced earlier (equation 2.6). A solution is deduced for a slab-shaped crop as (Crank, 1975; Okos et al 1992)

$$\frac{M - M_e}{M_o - M_e} = \frac{8}{\pi^2} \sum_{n=0}^{\infty} \frac{1}{(2n+1)^2} \exp\left[-(2n+1)^2 \frac{\pi^2}{4} \frac{D_{eff} t}{L^2} \right] \tag{2.19}$$

where M_0 is the moisture content at time zero, M is the moisture content at time t, L is half thickness of the slab.

The effective diffusivity (diffusion coefficient) D_{eff} is determined as

$$D_{eff} = D_0 \exp\left(-\frac{E_a}{RT} \right) \tag{2.20}$$

where T is the absolute temperature, E_a is activation energy, R is the universal gas constant and D_0 is a product-dependent parameter (Mujumdar, 1997: Okos et al, 1992).

A number of studies have been performed on the equilibrium moisture content M_e. Table 2.5 gives some of the studies relating the M_e, the temperature T and relative humidity H_R.

Other models are deduced from the maximum rate (dM/dt) at which a thin layer of crop kernel loses moisture to the air. This can be approximated as (ASHRAE, 2001);

$$\frac{dM}{dt} = -C(p_{cr} - p_a). \tag{2.21}$$

where C = constant representing vapour conductivity of kernel and surround air film

p_{cr} = partial pressure of water vapour in the crop

p_a = partial pressure of water vapour in the drying air

Thus if $p_{cr} > p_a$, drying occurs. If $p_{cr} = p_a$, moisture equilibrium exists and no drying takes place. Rewetting occurs, if $p_{cr} < p_a$.

Model	Equation
Modified Henderson equation	$H_R = 1 - \exp(-A(T+C)M_e{}^B)$
Chung-Pfost equation	$H_R = \exp\left[\frac{-A}{T+C}\exp(-BM_e)\right]$
Modified Halsey equation	$H_R = \exp[\exp(A+BT)M_e{}^{-C}]$
Modified Oswin equation	$H_R = \frac{1}{\left(\frac{A+BT}{M_e}\right)^C + 1}$
Guggenheim-Anderson-de Boer (GAB)	$M_e = \frac{ABCH_R}{(1-BH_R)(1-BH_R+BCH_R)}$

Table 2.5 Models for analysing M_e (%, d.b.) in relation to H_R (decimal) and T (^{0}C). A, B and C are product dependent constants. Source; Chen (2002).

In thin-layer drying, linear relationships are assumed between the water vapour pressure and equilibrium relative humidity and also between the equilibrium relative humidity and moisture content. Equation 2.21 is then transformed into

$$\frac{dM}{dt} = -k(M - M_e) \tag{2.22}$$

where k is a product-dependent constant.

Solution to equation (2.22) is obtained in the form

$$M_R = \exp(-kt) \tag{2.23}$$

where

$$M_R = \frac{M - M_e}{M_0 - M_e}$$

This equation is modified further for more promising results, according to ASHRAE, (2001) into;

$$M_R = \exp(-Kt^N) \tag{2.24}$$

K is function of air temperature and velocity, and N is a function of the relative humidity of the drying air and the initial crop moisture content. Other forms of the equations have been developed and used. Some of them are summarised in table 2.6

Model number	Model name	Model expression
1	Newton	$M_R = \exp(-kt)$
2	Page	$M_R = \exp(-kt^n)$
3	Modified Page	$M_R = \exp((-kt)^n)$
4	Modified Page II	$M_R = \exp(-(kt)^n)$
5	Henderson and Pabis	$M_R = a \exp(-kt)$
6	Logarithmic	$M_R = a \exp(-kt) + c$
7	Two term	$M_R = a \exp(-k_0t) + b \exp(-k_1t)$
8	Two term exponential	$M_R = a \exp(-kt) + (1\text{-a}) \exp(-kat)$
9	Wang and Singh	$M_R = 1 + at + bt^2$
10	Approximation of diffusion	$M_R = a \exp(-kt) + (1\text{-a}) \exp(-kbt)$
11	Modified Henderson and Pabis	$M_R = a \exp(-kt) + b \exp(-gt) + c \exp(-ht)$
12	Verma et al.	$M_R = a \exp(-kt) + (1\text{-a}) \exp(-gt)$
13	Midilli-**Kucuk**	$M_R = a \exp(-kt^n) + bt$

Table 2.6 Mathematic models applied to the drying curves. The parameters *a*, *b*, *k* and *n* are dependent on type of product, temperature and relative humidity. Sources; Lahsasni et al (2004); Togrul and Pehlivan (2004).

2.4.1.2 Reports of some modelling and simulation trials on crop drying

Forson (1999) used the solution for a slab-shaped crop in modelling the performance of a mixed-mode dryer and validated the model successfully with experimental results. It was observed that the air temperature in the chimney reduced, as the air moved up through the chimney. It was then recommended that the chimney be heated, in order to improve the airflow.

Yaldiz et al (2001) performed thin-layer drying experiments for sultana grapes with an indirect forced convection solar dryer (cabinet type). According to their results, the thin layer solar drying behaviour of sultana grapes could adequately be described by the two term model.

Jain and Tiwari (2004, I) investigated the convective mass transfer coefficients *hc* and rates of moisture removal in open sun drying and in greenhouse drying, using cabbage and peas. They performed a regression analysis with the two-term model, using *hc* as a function of the drying time;

$$hc = A_1 \exp(k_1 T) + A_2 \exp(k_2 T). \tag{2.25}$$

They observed that the two-term model can only be applied within certain limits of the drying time (independent variable) for predicting the convective mass transfer. Jain and Tiwari (2004) however observed that, at the initial stage of drying, the convective mass transfer coefficient was lower for the drying inside the greenhouse with natural convection than for open sun drying. The value obtained from forced convection drying was double that of greenhouse drying under natural convection at the initial stage. This was attributed to the fact that, without the forced convection, there was always poor ventilation in the greenhouse.

Jain and Tiwari (2004, II) used the mass transfer model of equation (2.25) in the modelling of the thermal behaviour of cabbage and peas. The observed a fair agreement between the models and experimental values.

In developing a mathematical model for the drying of prickly pear peel, Lahsasni et al (2004) applied all the 13 models in table 2.6 to thin-layer forced-convection solar drying processes. The model that gave the best results and showed good agreement with their experimental data was that of Midilli-Kucuk.

Schoenau et al (1995) used the Page model to perform the simulation and optimisation of energy systems for in-bin drying of canola grain. They concluded that solar heating could be more cost effective than other supplemental heating systems provided a well designed flat-plat collector could be found for use in locations of good solar availability.

In order to investigate the drying of fruits under natural conditions, Togrul and Pehlivan (2004) performed open-sun drying experiments on apricots (pre-sulphured with SO_2 or $NaHSO_3$, grapes, peaches, figs and plums in ambient temperature ranges of 27 – 43^0C

and solar radiations of 0.72 – 2.93 MJ/m^2h. No constant-rate periods were observed. The results were fitted to the first twelve of the models shown in table 2.6. They observed that for one-layer drying processes, the approximation of diffusion model was the best fit for apricots (non-pre-treated or SO_2-sulphured) and figs, the modified Henderson and Pabis model was found to be the best for apricot ($NaHSO_3$-sulphured), grape and plum, and the model by Verma et al was the best for peaches.

Bala and Woods (1994) investigated the indirect natural convection of rough rice. From their observations, the drying wave moved slowly due to the low airflow rates produced by natural convection, and the drying layer was not uniform within the grain. Serious over-drying took place in the bottom layer. They therefore used equation 2.21 to develop a mathematical model for simulating the indirect natural convection of rough rice. They incorporated the temperatures in the collector and across the air-bed to predict the thermal buoyancy effect. The need for tempering the bed through regular turning was also stressed. Regular turning, however, did not increase the drying rate, though it reduced significantly the over-drying at the bottom of the bed. The normal chimney on the dryer offered no significant contribution to the flow, because of the temperature drop across the indirect dryer.

This model developed by Bala and Woods (1994) was later combined with a cost prediction method by Bala and Woods (1995) to find the optimum design with minimum cost per unit moisture removal. The results of their findings indicate that the optimum design for typical conditions of Bangladesh is a relatively long collector, a thin grain bed and negligible chimney height. The greater the grain capacity, the longer the collector needed.

A lot more modelling and simulation investigations have been reviewed. All of them used one or more of the studies described in subsection 2.4.1.1 or their derivatives. The reports point to the fact that the best fit for a particular physical trial depends on the crop type and experimental conditions.

2.4.1.3 Comparative and other trials

In their experiment to find an appropriate design of a solar dryer on a household, farm or industrial scale, Sharma et al (1995) performed outdoor experiments to investigate the following dryers

1. a cabinet-type natural convection solar dryer,
2. a multistacked natural convection solar dryer and
3. an indirect multi-shelf forced convection solar dryer

For all the three experiments, it was observed that the moisture content decreased exponentially with the drying time. Drying was fastest in the indirect forced convection dryer, especially on cloudy days. However, on clear sunny days, the total drying times were almost the same for all the dryers, with no significant difference in the quality of dried product. The most important points for choosing a dryer were therefore narrowed down to

1. quantity of material to be dried,
2. time available for the drying operation and
3. availability of resources, technical skill and power.

The conclusion drawn was that, the solar cabinet dryer is most suited to household purposes. The multistacked dryer, which is seen as a modified form of the cabinet dryer for large quantities of crop is best suited for on-the-farm applications with limited crop volumes. The indirect multi-shelf forced convection dryer is very efficient and can be used for large quantities of crop, but its use is associated with problems of high capital cost, the need for technical know-how, electric power requirement and the need for trained man power. This dryer is suitable for use in industries on a large scale. Sharma et al (1995) however suggested that the dryers could perform better, with slight modification to their designs.

Singh et. al, 2004 designed and built a multi-shelf dryer in the form of a rack inclined at an angle of 45^0 to the horizontal, for drying fenugreek leaves. It consisted basically of a multi-rack frame with four layers of black high-density plastic wrapped around it. A movable UV-stabilised glazing was placed over the structure. The design was such that

the drying air was heated in-between the trays for uniform drying. The dryer could function as direct-mode, indirect-mode or mixed-mode dryer. According to Singh et. al (2004), light-sensitive crops could be dried under indirect-mode conditions with the crops under shade. The dryer was made portable and moveable so that it could always be moved to an area where crop drying is needed. During a no-load test at Ludhiana (31 ^{0}N) with all the outlets closed, a maximum stagnation temperature of 75 ^{0}C was attained at a corresponding solar radiation of 750W/m^2 and an ambient temperature of 30 ^{0}C.

When the multi-shelf dryer was tested under load in the batch mode for 3 days, the thermal efficiencies of the dryer were 28.55%, 16.2% and 8.6% on the first, second and third days respectively. For these same days, the solar energy needed to remove 1 kg moisture from the product was 8.83, 15.4 and 29.09 MJ/kg. A semi-continues mode was adopted in which the fully-dried product in the lower tray(s) was taken and the partially dried product was transferred from the upper tray(s) to the lower tray(s). Fresh product was then loaded in the upper tray(s). For four consecutive days, the thermal efficiencies were 28.96%, 27.6%, 23.4% and 25.3%. The solar energy input per kg moisture removal for each of those days was 8.6, 9.06, 10.7 and 9.88 MJ/kg. Thus, with the batch mode there was a significant decrease in performance on each consecutive day, whereas the performance remained almost the same in the semi-continuous mode of drying.

Hallak et al (1996) designed and tested a modified direct-mode solar dryer in the form of a staircase. The drying air passes through the vertical mesh of the staircase and gets heated before it gets into contact with the crop on the next horizontal mesh. The dryer was used to dry Apricots ($NaHSO_3$), Apricots (sugar solution), Figs, Grapes, Prunes, Okra and Tomatoes. Hallak et al (1996) observed that the crops dried within 2.5 to 3.5 days and concluded that the drying rates were very competitive with published experimental results for other types of dryers; such as those used by Sharma et al (1995).

2.4.2 Studies on heated chimneys

2.4.2.1 Modelling and simulation methods on heated chimneys

Equation 2.11 is generally used as the basis for developing a velocity model in terms of the design dimensions of the chimney, the pressure (or airflow resistance) coefficients and the temperature difference between the outlet and inlet of the chimney. The equation is used together with the principle of flow continuity; constant airflow rate through the chimney. The average air density is used as a constant density in these equations (AboulNaga, 1998). The air velocity at one section normal to the airflow direction is deduced in terms of the other sections which are also normal to the airflow. Uniform air temperatures are assumed at all points of the same height inside the chimney. Smooth wall surfaces are also assumed, and the wall friction effect is normally considered negligible, compared to the other local losses (Afonso and Oliveira, 2000; Ekechukwu and Norton, 1997). So equation 2.11 becomes

$$g\rho\beta(T_{out} - T_{in})\Delta H = \sum_i K_i \rho \frac{v^2}{2} \tag{2.26}$$

Other models are developed as mass or volume flow models in the from

$$Q = a\mathrm{T}^b \tag{2.27}$$

where Q is either the mass flow rate or volume flow rate, and a and b are process-dependent constants (Ekechukwu and Norton, 1997; Sandberg and Moshberg, 1996; Gan, 1998). The air and wall temperatures are normally analysed through the energy balances of the air and the walls concerned. Some models also consider the effects of turbulence (Sandberg and Moshfegh, 1996). However, most studies on heated chimneys neglect the effects in the direction of the airflow. The next section describes some trials on natural ventilation in a heated chimney.

2.4.2.2 Modelling and simulation trials on heated chimneys

In comparing the performance of a solar chimney with a conventional one, Afonso and Oliveira (2000) combined the equations for heat transfer and natural ventilation flow in the solar chimney. Equation (2.26) was used together with the principle of continuity, and a model was developed for the volumetric flow rate V with reference to the outlet velocity as

$$V = \frac{1}{\sqrt{K_{in}\left(\frac{A_{out}}{A_{in}}\right)^2 + K_{out} + f_{out}\frac{H}{D_{out}}}} A_{out}\sqrt{2\beta g \Delta T \Delta H}\ . \qquad (2.28)$$

A is the flow sectional area, D is the hydraulic diameter of a section and H is the height of the chimney.

To take the wind effect into account, the above equation was modified as

$$V = \frac{1}{\sqrt{K_{in}\left(\frac{A_{out}}{A_{in}}\right)^2 + K_{out} + f_{out}\frac{H}{D_{out}}}} A_{out}\sqrt{2\beta g \Delta T \Delta H + C_p {v_w}^2} \qquad (2.29)$$

where C_p is the pressure coefficient and v_w is the velocity of the wind.

In the simulation procedure, Afonso and Oliveira assumed the value of $K = 3$ for both inlet and outlet, a chimney of uniform cross-section ($A_{in} = A_{out}$), with $\Delta H = H$. Heat transfer coefficients in the chimney were allowed to vary throughout the day from the varying temperature, as solar radiation was absorbed. In validating the model, the tracer gas technique was used to measure the airflow rates in both chimneys. Using climatic data of Lisbon and an initial temperature of 20 ^{0}C in the chamber for the simulation, they obtained the heat transfer coefficients, heat transfer to the air and the air flow rate as functions of time.

Better performance was achieved with the solar chimney than with the convectional chimney (about 10 – 20 % more airflow). From their observations, the simulation results indicated a negligible friction coefficient (always less than 0.01). A brick wall of 5 cm thick was enough to provide the necessary insulation to avoid the loss of solar-assistance efficiency (this loss could otherwise be up to 60 %). Thick walls could store enough energy as heat inertia whilst reducing the peak temperature to moderate the air flow. Also, the performance of larger chimney width (which increases the flow cross section) was better than a chimney of greater height for the same chimney absorber area. Moreover, the experimental results validated more closely the model that incorporates the wind effect, and so they concluded that the wind effect should not be neglected in the model. However, as the nature of the wind varies greatly with time,

Afonso and Oliveira (2000) noted that the solar chimney may be designed without consideration of the wind, so that the wind effect becomes a bonus for performance enhancement.

Ekechukwu and Norton (1997) conducted a study on an experimental solar chimney of uniform cross-sectional area of height 5.3m and outer diameter 1.64m, with a selectively absorbing surface in the middle. A flow model was derived to determine the velocity v of air through the chimney as

$$v = f(\Delta T_{ch})^{1/2} \tag{2.30}$$

where = $f = 0.453\left[\frac{Dg}{\overline{\rho}}\right]^{1/2}$, with D = chimney diameter in m, $\overline{\rho}$ = mean density of air (kgm^{-3}) and g = acceleration due to gravity. This model was deduced from the buoyancy pressure head and the relation between the density and temperature of dry air for a natural-circulation solar energy dryer operating in the temperature range 25-90^{0}C. The derivation was based on the fact that the pressure drops in the chimney of uniform cross-sectional area are mainly due to friction. A turbulent coefficient of 0.03 was used (Ekechukwu and Norton, 1997). The experiment was performed to measure the temperature difference ΔT_{ch} between the air inside chimney and ambient air to be used in the model as an index for the chimney's performance, since the accurate monitoring of velocities was difficult. Peak chimney temperature elevations of 6^{0}C to 15^{0}C above ambient were observed.

The flow model of Ekechukwu and Norton (1997) did not take into account the increased humidity of air stream (especially when the chimney is used on a crop dryer). Also, the pressure drop that would be caused by the crops in the dryer was not considered. It was therefore suggested that the model would predict a much higher value of airflow than the measured one when it is used to predict the performance on a solar crop dryer. An assumption is therefore required to correspond with the pressure drop and the added moisture to the air stream, if the model is to be used with a dryer. This would only alter the value of f in the flow model for the same functional relationship of v and ΔT_{ch}. Ekechukwu and Norton (1997) then concluded that the results were satisfactory and that solar chimneys, if properly designed, can maintain a

chimney air temperature consistently above that of ambient. This would enhance the desired buoyancy-induced airflow through the chimney.

In their studies, Sandberg and Moshfegh (1996) investigated the heat transfer and fluid flow created between two parallel walls, with one wall heated. An analytical study was first conducted (in Part I) in which they considered the fact that both convection and radiation form the mechanisms of heat transfer to the air. A steady-state two-dimensional model was used for the study. Balances of momentum and turbulence were also used in the model.

The analytical study was verified (in Part II) by an experimental one in which one wall was heated by a PV element. Surface temperatures were recorded, and the flow rate was determined by tracer gas technique. The whole set up formed a chimney configuration of width 1.64 m, breadth 0.23 m and height 6.5 m. The test was first performed with both ends of chimney open (i.e. gap = 23 cm). This was followed by another one with rain protection at the top, which constrained the air to pass through an opening of only 1 cm (a reduction of exit gap to only 4 %).

With the constrained flow, the velocity was below 0.1m/s, and laminar relations were used along the whole length of the chimney. For the open ended chimney, the flow was deemed transitional, starting as laminar at the bottom and gradually changing to become turbulent. A power relationship was found between the volumetric flow rate Q (m^3/s) and the heat flow q (W/m^2) as $Q = q^{\gamma}$ where $\gamma = 0.407$ (for the 1 cm slot) and 0.438 (with both ends open). According to Sandberg and Moshfegh (1996), the exponent agreed with the theoretical exponent which lies between 1/3 and 1/2. They also found that 40 % of the heat was transferred by radiation from the heated surface to the unheated surface, thus verifying the importance of radiation exchanges between the heated and unheated walls.

Gan (1998) predicted the mass flow rate with the methods of computational fluid dynamics (CFD). Good agreement was obtained, when the CFD program was validated against experimental data from the literature. The flow rate was predicted as

$$\dot{m} = 0.0197\Delta T^{0.4015} \tag{2.31}$$

where $\dot{m}$ is the mass flow rate per unit length (kg/ms) and ΔT is the temperature difference between the wall surface and inlet air (K). According to Gan's report, the prediction confirmed the findings of Sandberg and Moshberg (1996).

Chen et al, 2003 carried out an experimental investigation using a solar chimney model with uniform heat flux (through electric heating) on one chimney wall, for different chimney gap-to-height ratios between 1:15 and 2:5 and different heat flux values and inclination angles of the chimney. The model had a height of 1.5 m, with variable chimney gap from 0.1 to 0.6 m. Their experiment sought to validate the flow model developed from the energy balance and normal pressure loss equations. The deductions are demonstrated below.

The energy balance for the airflow for a chimney of small cross-sectional area is;

$$qhw = Q\rho C_p(T_{average} - T_{amb}), \tag{2.32}$$

where h is the height along the chimney, w is the width of chimney, q is the heat flux, Q is the air flow rate in the chimney, ρ and C_p are the air density and specific heat capacity at ambient temperature (T_{amb}) respectively and $T_{average}$ is the average temperature in the chimney at the height h.

The stack pressure ΔP_S is given by:

$$\begin{aligned}\Delta P_S &= \int_0^H \frac{(T_{average} - T_{amb})\rho g\cos\alpha}{T_{amb}} dh \\ &= \int_0^H \frac{qhwg\cos\alpha}{QC_P T_{amb}} dh = \frac{qwgH^2\cos\alpha}{2QC_P T_{amb}} \\ &= \frac{\rho BH\cos\alpha}{2Q},\end{aligned} \tag{2.33}$$

where H is the height of the chimney and α is the angle of inclination of the chimney to the vertical plane. The buoyancy flux B is given by:

$$B = \frac{gqwH}{\rho C_P T_{amb}}.$$

Also, along the flow path is a pressure loss ΔP_L which may be expressed as:

$$\Delta P_L = c_{in}\frac{\rho(Q/A_{in})^2}{2} + c_{out}\frac{\rho(Q/A_{out})^2}{2} + f\frac{H}{D_h}\frac{\rho(Q/A)^2}{2}, \tag{2.34}$$

where A is the area of channel cross section, A_{in} and A_{out} are inlet and outlet areas, f is the channel wall friction factor, c_{in} and c_{out} are the inlet and outlet pressure loss coefficients and D_h is the hydraulic diameter of the chimney channel.

The ventilation flow rate Q for the chimney with uniform wall heat flux was obtained by balancing equation (2.33) and equation (2.34) to get

$$Q = A\left(\frac{B\cos\alpha}{2\psi}\right)^{1/3}, \tag{2.35}$$

where

$$\psi = \frac{A}{H}\left[f\frac{H}{2D_h} + \frac{1}{2}\left[c_{in}\left(\frac{A}{A_{in}}\right)^2 + c_{out}\left(\frac{A}{A_{out}}\right)^2\right]\right].$$

Chen et al (2003) used the same data by Sandberg (1999) to the validate the model for a rectangular channel with both ends open, a uniform heat flux to a single wall and a chimney gap-to-height ratio of 1:28; with $f = 0.056$, $c_{in} = 1.5$ and $c_{out} = 1.0$.

Chen et al (2003) found that the available methods of prediction in the literature over-predicted the flow rate for their chimney geometry, especially vertical chimneys with large gaps. This over-prediction was attributed to the underestimation of the pressure losses at the chimney outlet through the use of loss coefficients obtained for normal forced flows (i.e. inaccurate estimation of the outlet loss coefficient) and the assumption of uniform temperature and air velocity across the same vertical height.

It was concluded that the above methods of using the energy balance and normal pressure loss to predict the flow rate was valid only for narrow chimneys (up to a gap of about 100 cm or slightly higher) when the velocity and temperature of the air are

reasonably uniform across both the width and gap of the chimney. For wider, vertical chimneys (particularly those with small inlets and large outlets), there was significant variation across the gap, with reverse flow under extreme conditions. Suggestion was therefore made for further investigations, to develop a model that could take care of wider chimneys. There was a continuous increase in airflow rate with chimney gap, and no optimum gap was found. Also, it was noted that though there are no clear lines for separating narrow chimneys from wide chimneys, single-wall-heated solar chimneys of 1:10 gap-to-height ratio (or smaller) may be considered narrow whilst the limit for the two-wall-heated solar chimneys is 1:5.

Chen et al (2003) further observed a maximum air flow at an angle around 45^{0} for a gap of 200 mm and a height of 1.5 m. According to them, the air flow rate at this chimney configuration was 45 % higher than that of a vertical chimney under identical conditions, and this was attributed to even air speed which reduced the pressure losses at the inlet and outlet of the chimney.

The work of Bansal et al (1993) was the development of a steady state mathematical model for a solar chimney system. The system consisted of a solar air heater connected to a conventional (normal) chimney. The equations for the energy balance of the absorber and chimney were combined to derive a temperature distribution equation for the air. With a collector area of $2.25m^2$, airflow rates of 140 to $330m^3/h$ were calculated for solar radiations of 200 to $1000W/m^2$.

A spread-sheet computer program was used by AboulNaga (1998) for an analytical study of a roof solar chimney coupled with wind cooled cavity. The program used the balance between the buoyancy and pressure resistance (equation 2.26). An inclined roof chimney of uniform cross-section on a house was studied. The results indicated that the best performance of the chimney could be attained at a chimney gap of 0.2m and a ratio of inlet area to chimney cross sectional area (or exit area) of 2.5.

AboulNaga and Abdrabboth, (2000) combined the model of AboulNaga (1998) with that of a wall chimney for the investigation of a wall-roof solar chimney. The model

was developed to predict the induced air flow rate and to find the best height of the system in relation to the height of chimney inlet. Tests were done for varying chimney heights of 1.95 to 3.45m. The results gave values of airflow rates (0.81 to 2.3m^3/s) which are three times more than that of the roof solar chimney alone. The maximum of 2.3m^3/s was obtained for a chimney height of 3.45m and an inlet height of 0.15m.

Ong (2003) proposed a mathematical model to simulate the thermal performance of a rectangular-channelled solar chimney under varying ambient and geometrical features. Steady state conditions were assumed, and energy balance equations were deduced for the chimney absorber, the glazing and the air in the chimney to predict the temperatures of the chimney glazing, absorber and the air flowing through the chimney. Also the airflow rate, for the chimney of uniform cross-section, was estimated from an air flow model used earlier by Bansal (1993) as a function of the discharge coefficient, fluid density, inlet and outlet areas, temperatures of fluid inside and outside the chimney and length (height) of the chimney wall. Energy balance equations were formulated for the chimney glazing, absorber and the flowing fluid. The equations were solved simultaneously through the method of matrix inversion to obtain the temperatures of the glazing, absorber and fluid. The results were further used to determine the instantaneous efficiency of energy collection as the ratio of energy absorbed by the fluid to the incident radiation on the chimney absorber.

Ong and Chow (2003) carried outdoor experimentations to check the validity of the mathematical model proposed by Ong (2003). Tests were conducted on a physical model that was 2m high and 0.45m wide, with chimney gaps of 0.1, 0.2 and 0.3m. Air velocities of 0.25 to 0.39m/s were measured for radiation intensity up to 650W/m^2 with no reverse air circulation. The difference between the predicted instantaneous efficiency and that obtained for the experiment was always about 10 %. For all the incident solar radiations encountered, the mean air temperature in the chimney was lower than the mean temperature of the glazing, but all the parameters increased with incident solar radiation. Larger air gaps (i.e. larger inlet openings) caused more airflow through the chimney, so that the absorber wall and glazing cooled faster. Also, the higher airflow caused a lowering of the mean air temperature rise, as more air was

heated by the chimney at a time. However, the higher airflow rate caused an increase in instantaneous efficiency.

Hirunlabh et al (1999) had earlier performed an experimental verification of a model similar to that by Ong (2003) to study the energy removal from habitation, with a metallic solar wall (MSW). Four different combinations of height and air gap were used. Highest airflow rates of about 0.01-0.02kg/s were produced with 14.5cm air gap and $2m^2$ surface area. Good accord was shown between the simulated and experimental results; there were similar trends, with variations of around 10%. The slight discrepancies in their results were attributed by Ong (2003) to the assumption of different physical values and ambient conditions. Also, disturbances at chimney outlet, which the mathematical model was not able to handle, also caused the exit temperature to be slightly lower than the predicted value. Their experimental results however showed similar performance trends to those estimated by the model.

Bansal et al (2004) developed a mathematical model for air velocity in a solar chimney of uniform cross-section. The mass flow was first determined through the mass model of Bansal et al (1993) and related to the sectional area to get the velocity of the section concerned. The model was applied to a small-sized solar chimney (of absorber length less than 1 m) to verify it experimentally. Three different air gap and inlet openings were used for the experimentations. The model was said to slightly under-predict the temperature of glass and the air in the flow channel, whilst the temperature of the absorber was slightly over-predicted. The model was nevertheless found to be applicable to small-sized solar chimneys. A highest flow velocity of 0.24m/s was attained.

Similar modelling and simulation principles to those used in the above reports were also used by Awbi and Gan, 1992; Awbi, 1994; Bansal et al, 1994 and lot others.

2.4.2.3 Some other trials on heated chimneys

In an experimental study of the performance of a heated chimney on an indirect passive cabinet dryer, Bassey et al (1994) performed tests on 4 chimneys on the dryer. The

chimneys were always heated at the base with sawdust. They concluded that heated chimneys should be at least 2 m high for drying rates to be significantly improved.

Hamdy and Fikry (1998) investigated the performance of a chimney connected to a tilted air heater to find the optimum tilt angle. They used a relation of the flow rate with the temperatures and chimney dimensions from Bansal et al (1994) to determine the Solar Heat Gain Factor (SHGF) of the solar chimney. The air heating was done in the roof before the air got into the vertical chimney. Their study showed the best performance at 60^0 for that study area (latitude 32^0 North).

An experimental study was conducted by Khedari et al (2000) to investigate the feasibility of heat gain reduction by a solar chimney through natural ventilation and also to examine the effects of openings (door, window and inlet of solar chimney) on the airflow through the building. With the use of the windows and doors, the temperature difference between the room and ambient was around 4 ^{0}C. This difference dropped to 2-3 ^{0}C, when the chimneys were used.

Zambrano and Alvarado (1984) in their studies compared the behaviours of a cylindrical chimney to a truncated conical chimney (shortest diameter at the base). The chimneys were of the same height with no absorber, but they were connected to a mixed mode dryer. Turbulent conditions were assumed and verified. The results indicate, the air velocity at the base of the inverted conical chimney is higher (by a factor of 2-3) than that of the cylindrical chimney of equal diameter, while the temperature in the dryer was lower (by about 10 ^{0}C).

Das and Kumar (1989) designed, constructed and tested experimentally a solar chimney on a batch dryer equipped with an inclined air heater for drying high moisture paddy. The unit consisted of an inclined air preheater, a cabinet batch dryer and a vertical solar chimney in series. The system dried the paddy in 9 hours, representing a saving of 7 hours, compared with open sun drying.

2.5 Summary observations and selected aspects for investigation

The review confirmed that solar crop drying is a complex problem involving simultaneous physical processes of heat and mass transfers in and around the crop. The physical processes and crop properties may change during the course of the drying process.

A solar crop dryer (especially the direct-mode natural ventilation type) can be very simple and inexpensive to construct. However, they could do more harm than good when they are not properly designed. The direct-mode natural convection solar crop dryer is reported to be the least effective of all crop dryers in terms of performance. The poor performance is generally attributed to poor ventilation through the dryer, with excessively high temperatures so that the drying process in some cases ends with the crop partially cooked rather than properly dried.

The use of a solar chimney has been identified as an antidote to the ventilation problem in the natural ventilation dryers. The solar chimney can utilise the beam radiation when it is far away from the equator. It can also make use of the high proportion of the diffuse light in areas near the equator to provide the adequate air heating needed to enhance the airflow through a chamber. It is self regulatory and is able to maintain a constant temperature in a room.

A number of simulation models have been developed for both the drying process and the natural ventilation through a solar chimney. However, a number of areas require attention for further research and development, as explained below:

1. The tent dryer is reported to perform better than the cabinet dryer. There is therefore the need to investigate the tent-dryer effect on the performance of the dryer
2. Solar crop drying generally takes more than a day. It is therefore necessary to develop a model that predicts the performance of a solar dryer over a period spanning more than a day to examine how the 'insolation breaks' in the night (periods with little or no insolation) affect the predictions of the simulation program.

3. The models on solar chimneys are mainly for room ventilation. A simulation model is required that incorporates the effect of the drying process on the chimney performance and the other way round.
4. Without any air preheater, a direct-mode dryer has to depend on the drying-chamber base and walls and the content of the crops for air heating, air flow and crop drying. Therefore the design of the drying chamber and also the loading arrangement in the direct-mode dryer are critical for optimum performance. Investigations are needed on these aspects.

A simulation code is therefore proposed to examine a solar crop dryer designed to make simultaneous use of the solar chimney and the tent-dryer effect to achieve the required ventilation needed for optimum performance. This chimney-dependent direct-mode solar crop dryer (CDSCD) is to consist of a drying chamber with tilted roof on which a solar chimney is positioned. The simulation code is to be capable of investigating the effects of the following aspects on the performance of the CDSCD with respect to the ventilation, air temperatures and crop drying:

1. The design of the solar chimney
2. The roof angles of the drying chamber with respect to the vertical plane
3. The ratio of inlet area to the exit area
4. The loading arrangements in the dryer
5. Insolation

The simulation process is to cover two or more days, to take into account how the absence of insolation at night affects the drying predictions by the simulation code.

CHAPTER 3 EXPERIMENTAL WORKS

Experiments were performed to investigate the effects of solar chimney, the roof angle and the inlet gap on the performance of the CDSCD and also to acquire some data for validation of the simulation code (see chapter 6). Figure 3.1 shows the functional architecture of the direct-mode dryer. Air enters through the bottom inlet, absorbs heat from the base and walls of the drying chamber and moisture from the crop. The air then enters the chimney where it is heated again before it exits into the environment.

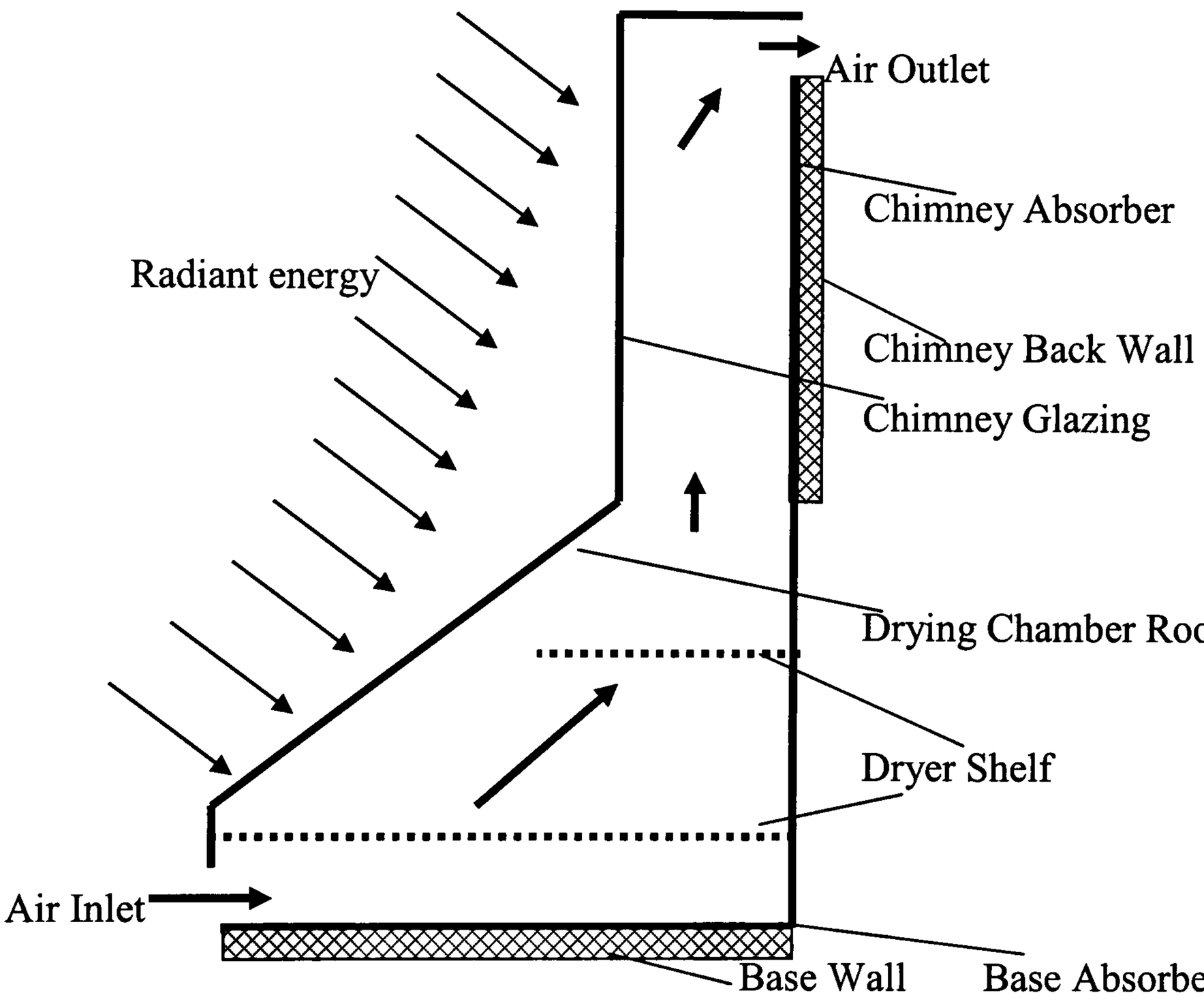

Figure 3.1 Functional Architecture of the Chimney-dependent Direct-mode Solar Crop Dryer

The heat in the dryer is principally transferred from the absorbers, after the absorbers have absorbed part of radiant energy that enters the dryer through the walls (glazing) of the dryer.

3.1 The Physical models of the solar dryer

Trials were performed on a laboratory-scale model of the dryer designed and constructed in the Mechanical Engineering Workshop of De Montfort University (DMU), Leicester – England. This was followed by trials on a large-scale model on the field behind the Mechanical Engineering Workshop of Kwame Nkrumah University of Science and Technology, Kumasi – Ghana.

3.1.1 The laboratory model

The laboratory model had three replaceable roofs for the drying chamber, each with a different roof angle with respect to the vertical plane. Three separate doors ware also built to match the various roofs. Roof angles 81^0 (close to that of a cabinet dryer), 64^0 and 51^0 were used. The walls of drying chamber consisted of a glazing material (Lexan sheet). The width of drying chamber was 440 mm (normal to the airflow) and the length was 420 mm in the airflow direction. The total height of the drying chamber was 530 mm. The base of the chamber was made of wood (40 mm thick) with the top surface painted black to serve as absorber in the drying chamber. The inlet width was 390 mm.

Three plates were prepared from the Lexan sheet, each with length covering the width of the dryer, to be placed at inlet to set the inlet gaps at 30, 50 and 70 mm during the trials. A steel mesh (width = 400 mm; length = 370 mm) was prepared to be positioned 150 mm above the base of drying chamber to serve as drying shelf, as shown in figure 3.1. Two other meshes, each with about half the length of the first mesh, were also provided to be used for different shelf arrangements in some of the drying processes.

The chimney was of rectangular cross-section of width 440 mm, uniform gap 80 mm and height 625 mm. The dryer exit, which was at right angles to the chimney cross-section at the top, had a gap of 30 mm, a straight width of 335mm, and it is curved at the ends with radius of 15 mm. The chimney was all-round glazed with Lexan sheet, as with the drying chamber. An additional replaceable back wall was also constructed of wood with the inner surface painted black to serve as chimney absorber. This was to

replace the transparent back wall to transform the chimney into a solar chimney to be used in most of the trials.

3.1.2 The field model of dryer

In order to save time and cost, an existing tent dryer was reconstructed in a form suitable for the field trials. The framework of the tent dryer was divided along the vertical plane through the heights of the side triangles of the dryer, to get each half similar to that of the laboratory model, and one of them was used, as shown in figure 3.2. Across the width of the half being used, a vertical chimney with a metallic absorber was constructed at the top. Thus the exit vents were converted from the vertices of the triangular side walls to the top of the chimney (above the absorber), so that both the inlet and exit vents cover the whole width of dryer, to enhance the airflow.

As suggested after the laboratory trials (see chapter 5), the chimney was made much shorter in relation to the drying chamber, to reduce the impedance to night drying. Also, the low chimney height was necessary to reduce vulnerability of the dryer to draft in stormy conditions. Moreover, cost benefits prompted the need to avoid much hotter air of high moisture-carrying capacity at chimney exit which would just be wasted in the atmosphere, as was found in the laboratory trials. The purpose of the solar chimney was to maintain an air temperature higher enough in the chimney than in the drying chamber, to facilitate an improved airflow. The chimney dimensions were arrived at, with guidelines from published reports on solar chimneys (Afonso and Oliveira, 2000; Ong and Chow, 2003; Chen et al, 2003). These reports favoured wide chimneys over high chimneys.

The drying shelves of the original tent dryer were moved higher up (lower trays of the old tent dryer were changed from height of 40 to 62 cm) in the drying chamber to get them in the hotter zones of the chamber. This height also allowed some more irradiation and air-heating at the base and lower section of the drying chamber. A roof was constructed at the top to prevent rain from entering the chimney through the exit. The dimensions of the final structure are given in table 3.1. To prevent insects and

rodents from entering the dryer, mosquito nets and wire mesh were used to cover the inlet and outlet.

Drying chamber base	Width = 392 cm; length in airflow direction = 255 cm
Height of drying chamber	= 243 cm
Thickness (depth) below the base with gravel (chippings)	= 40 cm
Roof angle to the vertical plane	= 44^0
Dryer Inlet	Width = 245 cm; gap = 50 cm
Height of chimney walls (glazing)	= 33 cm
Height of chimney roof (glazing)	= 24 cm
Height of chimney absorber	= 40 cm
Chimney gap	= 23 cm
Chimney roof angle to horizontal	= 28^0
Exit gap	= 15 cm
Height of lower shelf from base	= 62 cm
Height of upper shelf from base	= 117 cm

Table 3.1 Dimensions of dryer used for the field trials

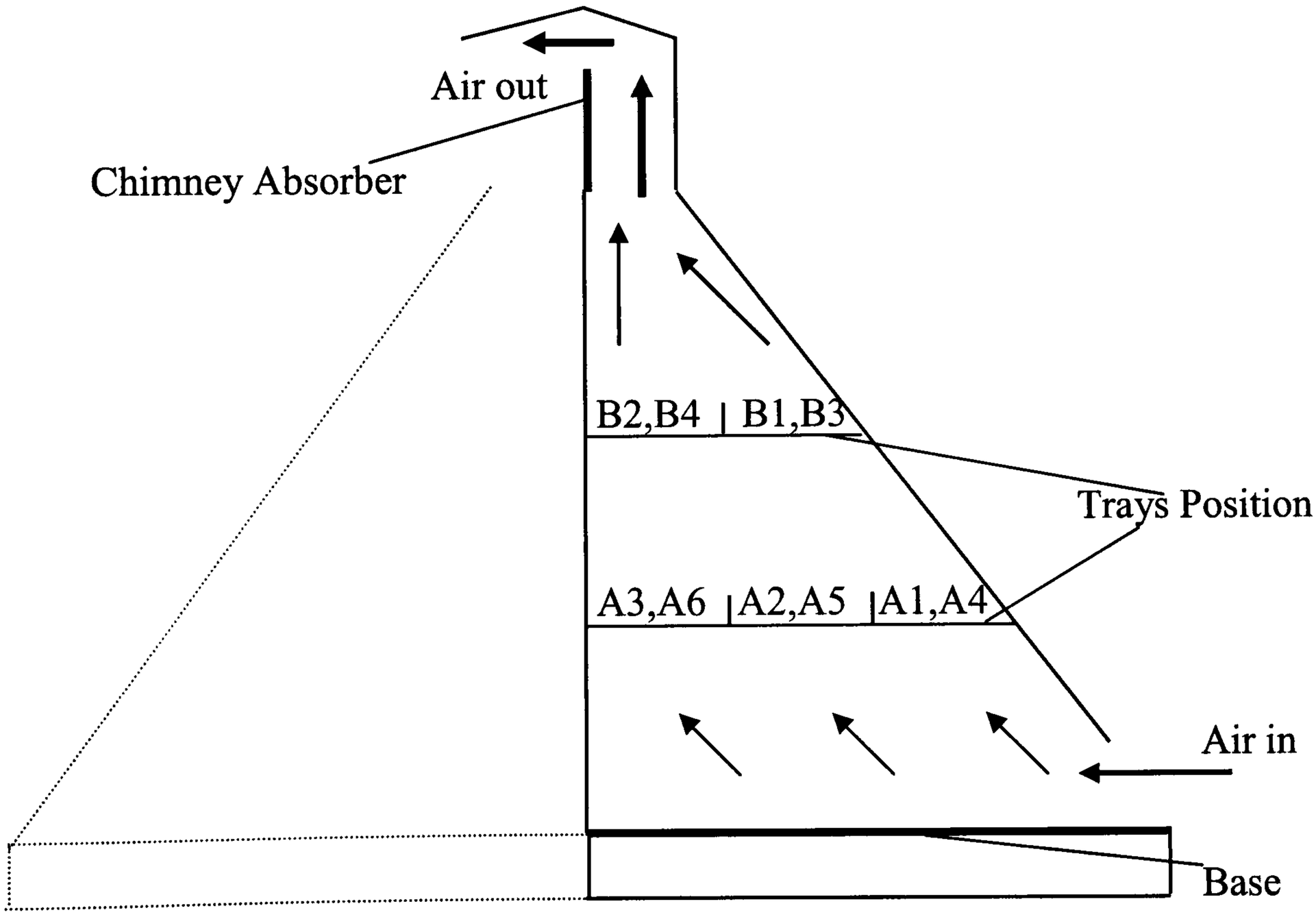

Figure 3.2 Sketch of dryer arrangements (side view)

Figure 3.2 shows a sketch of the side view of the final arrangement. There were 6 trays on the lower shelf; arranged as A1, A2 and A3 on one side and A4, A5 and A6 on the other side. Thus along the width of the dryer, A1 was in line with A4, A2 in line with A5 and A3 in line with A6. Four additional trays were similarly arranged on the upper shelf, with B1 and B2 on one side, and B3 and B4 on the other side along the width. The pictorial view of field model is shown in Figure 3.3.

Each tray was of rectangular cross section with mosquito net at the bottom to support the cassava, whilst allowing the air to flow through the system. The ground of the drying chamber was filled with stone chippings, and these were covered with a black sheet of polythene to form the base of chamber. Initially, a roof was constructed over the inlet to prevent direct precipitation from the atmosphere into the dryer, as with the exit. But after the first trial, this roof was replaced with a polythene sheet which was rolled over the inlet to prevent the direct precipitation and also for covering the inlet at each night.

3.2 Experimental arrangements

3.2.1 Arrangement of dryer model and equipment in the laboratory

Figure 3.4 shows the pictorial view of the set up of the physical laboratory model together with the instrumentations for the trials. A structure was constructed of wood to support the model. As shown in this figure, the model was placed in a wooden structure which had an adjustable framework at the top for holding eight 100W infrared lamps between 15^0 and 30^0 (in steps of 2.5^0) to the horizontal. These lamps were for sending radiation energy onto the dryer model, thus simulating the sun.

Fifteen thermocouples (type K; range 0 to 200 ^{0}C) were positioned at various heights of the dryer. Each one was centrally placed, so that the recorded temperature represents the temperature of the air at that height (see figure 3.5). The thermocouples were connected to a meter which was installed for temperature reading and recording.

Figure 3.3 The pictorial view of field model

Along the main chimney height, three thermocouples were attached to the inner surface of the absorber wall; one couple at height 0 (chimney inlet), another at a height of 350 and the third at 600 mm (chimney exit). At heights corresponding to those of the absorber, three other thermocouples were attached to the inner surface and three others at the outer surface of the glazing which was facing the lamps. In the air stream, one thermocouple was positioned at chimney inlet and another at height 350 mm of the chimney. The inlet of the chimney (the summit of the drying-chamber roof) was at 490 mm above the base of the drying chamber.

In the drying chamber, a thermocouple was attached to the base, and the last three thermocouples were positioned each at heights of 60, 160 and 260 mm respectively in the air above the base. All the thermocouples in the air stream were inserted into the dryer through holes in the glazing, held in place with corks to avoid air leakage. A hand-held liquid-in-glass thermometer was used to measure the air temperatures of the environment, dryer inlet and chimney exit. Also, all velocity readings were taken with a

hand-held anemometer (Hot Wire Thermistor Bead Type: TA 400; range 0 to 2 m/s). A thermo-hygrometer (also hand-held; type HANNA HI 8564 with relative humidity range of 10-95 % and temperature range of 0-60 ^{0}C) was used for measuring the relative humidity.

To facilitate the weighing of the crop without having to remove it from the dryer during a trial, a cantilever beam was fixed in the top of drying chamber for the tray to be suspended on. The cantilever beam was then connected through a Whetstone-Bridge arrangement to a microstrain gauge (Digital Strain Indicator; type 5792). This whole arrangement was calibrated, using known weights, in steps of 100 g up to around 1.4 kg, together with an electronic weighing scale. The instrument could display microstrain of up to 3 digits. A linear relation was found between the weight and microstrain as

$$weight = 1.5 \bullet microstrain\ .$$

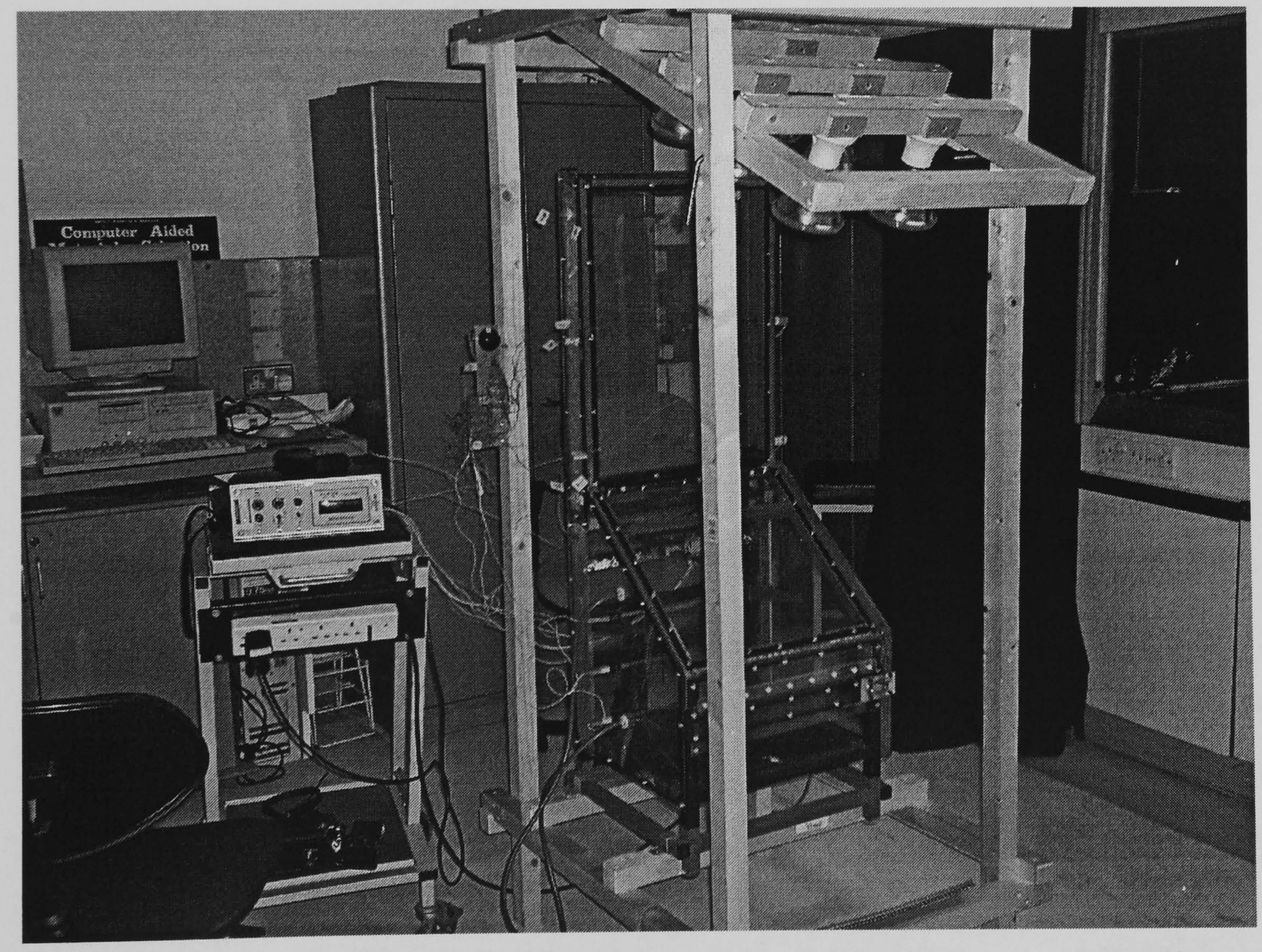

Figure 3.4 A Setup of the CDSCD model for the laboratory trials

However, where the weights of two different shelves needed to be determined in a recording process, the electronic weighing scale was used in addition to the microstrain indicator.

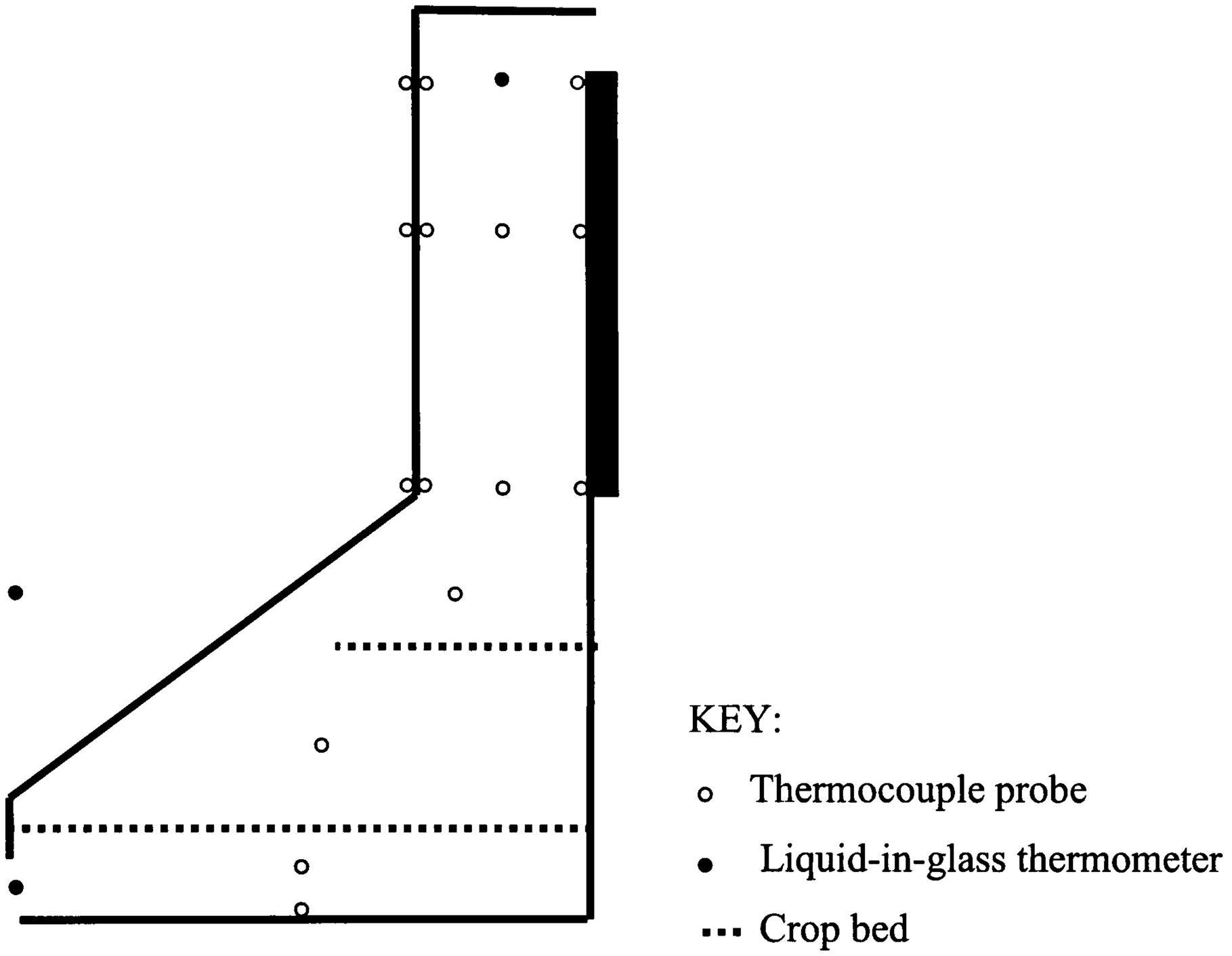

Figure 3.5 Schematic diagram of positions of temperature-measuring sensors

3.2.2 Instrumentations for the field trials

On the field, a data logger 21X MICROLOGGER, SM192 STORAGE MODULE S/N 11486 (CAMPBELL SCIENTIFIC INC.) was installed and connected to various points of the field dryer to record the temperatures at various points. In the drying chamber, air temperatures were recorded at midpoints between the drying-chamber base and lower shelf, between the lower and upper shelves and between the upper shelf and chimney inlet. Air temperatures were also recorded at dryer inlet, chimney inlet, chimney exit and the environment. Also recorded were temperatures of the drying-

chamber base and walls (glazed all round) and the chimney absorber and glazing. Insolation and other environmental data were also gathered from another system installed on the rooftop of the Mechanical Engineering Workshop of Kwame Nkrumah University of Science and Technology (KNUST), which was very close to the site of the field trials. These systems processed and stored the data at hourly intervals. A hand-held solarimeter and a thermo-hygrometer were also used to further check the insolation, the temperature and relative humidity of environment, of the dryer inlet and the dryer exit at intervals of two hours.

3.3 Tests overview

3.3.1 Laboratory trials

Two main groups of trials were conducted in the laboratory; one group with no load (i.e. with no crop in the dryer), and the other with a predetermined load of cassava in the dryer (under-load trials). The infrared lamps were used to simulate the irradiation from the sun. The laboratory tests started on 29th July 2005 and ended on 4th November 2005. In the following sections, the laboratory trials are grouped into Test-sets for easy description. The no-load trials are described in test-sets 1 to 4, whilst test-sets 5 to 12 describe the under-load tests.

3.3.1.1 The no load trials

To examine and verify the expected air temperature profile and airflow characteristics of the CDSCD model, a total of 18 no-load tests were performed, using different roof and inlet configurations. Each no-load test was performed for 6½ hours during the day, with the infrared lamps switched on. The first 3 data sets were taken at 30-minute intervals to establish a steady state, and the rest of the data were recorded at hourly intervals for the next 5 hours. Among the data recorded in these sets were temperatures in and around the dryer. Also recorded were the air velocities and relative humidity at inlet and exit of dryer and the environment. To ensure simultaneous irradiation on both the chimney and the drying chamber, the lamps were fixed at an angle of 22½^0 to the horizontal as standard angle, except for trials in which the incident angle was being investigated in relation to the performance of the system.

Test-set 1: Using the normal chimney

A no-load test was done on the near cabinet dryer (with the drying-chamber roof positioned at 81^0 with respect to the vertical plane), using a normal chimney with all the walls glazed. This was followed by another test with the roof at 51^0 to the vertical plane. These trials served for investigating the performance of the normal chimney with regard to air circulation through the dryer. An inlet gap of 70 mm was used for both trials.

Test-set 2: Investigating the effects of chimney-heating, roof angle and inlet area on airflow.

This set of trials was done to examine the effects of chimney heating, roof angle and inlet area on airflow through the dryer. The chimney was transformed into a solar chimney by replacing the back wall of the chimney with a wooden wall having its inner surface blackened to serve as an absorber, for heating the air in the chimney. The roof of angle 81^0 to the vertical plane was placed again on the drying chamber. A trial was done with the inlet gap set at 70 mm. This was repeated with inlet gaps of 50 and 30 mm respectively. The trials were repeated with the roofs of angle 64^0 and 51^0, each with the 3 inlet gaps, as with the first. There was a total 9 trials in this test-set.

Test-set 3: Testing the angle of incidence of irradiation

In the third test-set, the effect of angle of incidence of irradiation on the airflow was examined. The roof was at angle 51^0 and the inlet gap was 70 mm. Six different tests were performed, with the lamps set at 15^0, $17½^0$, 20^0, 25^0, $27½^0$, and 30^0 respectively to the horizontal plane.

Test-set 4: The profile of drying chamber walls

Due to the lack of sufficient thermocouples and a pyranometer in the laboratory, this test had to be carried out to examine the temperature profile of drying chamber walls and also to estimate the irradiation onto the drying chamber. Some thermocouples were taken from the chimney walls and attached to the drying chamber walls, and a test was performed with the lamps at $22½^0$, drying-chamber roof at 51^0 and inlet at 70 mm.

3.3.1.2 Trials under load

After the no-load tests, a series of under-load tests (with some crops in the dryer) were conducted, to verify the mutual effects of airflow and drying rate (or drying time) at various design configurations. The dependence of airflow and drying rate on the method of loading, crop size, and crop weight was also observed. The day and night performances of the dryer were also considered. Each under-load test was done for 3 days and 3 nights (the objective was to perform the test until the crop attain the desired moisture content of around 20 % - db, and if this was not attained then the trial was stopped after 3 days and 3 nights).

Cassava was used as crop for the trials, as it was readily available in the market. The crop was always purchased from an open market in Leicester on the eve of the first day of each drying trial and prepared the next morning before the trial began. In total, 18 under-load trials were performed. 1 kg of cassava, cut into quadrants of average radius 30 mm and thickness 15 mm, was used as standard for most trials, except where the size effect was being investigated. Also except where the effect of shelf arrangement was being observed, the drying tray was generally positioned at a height of 150 mm above the base of drying chamber. At the beginning of each trial, some cassava was set aside and the initial moisture content was determined by the oven-dry method.

In each drying process, the lamps were switched on for 7 hours in the day during which data were recorded at hourly intervals. The lamps were then switched off and the dryer was left alone throughout the night till the next morning when the weight of crop was noted before drying resumed. This was to examine the night performance of the dryer without any irradiation. Similar to the no-load trials, temperatures, air velocities and the relative humidity were measured. In addition, the microstrain reading was noted at every hour to determine the weight.

Test-set 5: Drying with the normal chimney

Two drying trials were carried out in the dryer with configurations similar to those of Test-set 1 (i.e. with the normal chimney), with 1 kg of cassava in the dryer. This was to examine the drying performance of the CDSCD with the normal chimney.

Test-set 6: The effects of chimney-heating, roof angle and inlet area on drying.

Test-set 6 was the repetition of the nine trials in test-set 2 (of the no-load trials), each with 1 kg of cassava in the drying chamber. The trials were to provide data for investigating the effects of chimney-heating, roof angle and inlet area on the drying process. The mutual effects of airflow and drying were also examined. This test-set was also to provide the data needed for validating the simulation code.

Test-set 7: Effect of crop size and airflow

This under-load set had two trials, for examining how the crop size affects the airflow and drying rate. With the roof at 51^0 and inlet at 70 mm, 1 kg of cassava with half the standard crop size was used. One trial used half the cross-sectional area (half quadrant), whilst the other trial used half the height ($\approx$ 8mm).

Test-set 8: Effect of higher crop mass

In this set, 1.4 kg of cassava was dried to observe the effect of crop mass **on** airflow and drying rate.

Test-set 9: Effect of lower crop mass

Test-set 9 was a repetition of test-set 8, but with 0.5 kg of cassava. Some crops were also dried outside the dryer at the same height and loading density as the crops in the dryer. The outside drying was to serve as control trial for comparison with the performance inside the dryer.

Test-set 10: Effect of drying height

Test set 10 also had 0.5 kg cassava like set 9, but the tray was moved 100 mm higher up the drying chamber to observe the effect of drying height on the airflow and drying rate. As in set 9, some crops were dried outside the dryer as control trial.

Test-set 11: Loading arrangement

In set 11, two half trays (each with 0.5 kg crop) were dried together, with one tray at the same height as in test-set 9 and the other at the same height as in test-set 10. This was to test the outcome of a different loading arrangement to those in which all the 1 kg cassava was placed at the same height. The two shelves were displaced horizontally to ensure complete exposure to the source of radiation (8 infrared lamps, 100 W each). This test-set also had some crops outside for control drying.

Test-set 12: Loading with interchange on the second day

Test-set 11 was repeated in test-set 12, but the trays were interchanged on the second day of drying. There were some crops outside the dryer for control drying, as in test-sets 9, 10 and 11.

3.3.2 Field trials

With the large-scale model, drying trials were done on the field to obtain the data needed to check the validity of the simulation code on the field. Also, based on the results of the trials on the laboratory model, the field work was needed to try out some of the suggested ways of improving the performance of the Chimney-dependent Direct-mode Solar Crop Dryer on the field.

The field trials were performed in Ghana from the 15th of February up to the 10th of March 2006. Because of the initial preparations of the cassava, drying could only start around midday on the first day of each drying process. As the time was limited, the intended variation of inlet gap had to be abandoned, so only the different arrangement of crop in the dryer was considered in these trials. Five trials were conducted on the field.

As with the laboratory trials, cassava was used as the drying crop. The cassava was either obtained directly from a nearby farm or purchased from the farmers early morning at a lorry park in the city before they could reach the market place. The initial moisture contents were always tested in the Agricultural Engineering Department of KNUST. A loading density of around 12.35 kg/m^2 was used in all the field trials.

Throughout the trials, some cassava was spread on one tray (as control drying) at the same height as the lower trays and with the same loading density as in the dryer. This offered the best way of comparing the relative advantages of using the dryer and open-sun drying, as both processes took place under the same environmental conditions at all times. At the beginning of each drying, the cassava on each tray was weighed in a bucket on an electronic scale. This was repeated at 5.00 p.m. local time, and then at 8.00 a.m. the next morning, continuing until the end of each drying process. The hand-held solarimeter and thermo-hygrometer were also used to check the insolation and the temperature and relative humidity respectively of the environment, dryer inlet and outlet at two-hour intervals. A preinstalled data-logging system was used to record all the other data.

In the first trial on the field, the dryer inlet was left open at night, as in the laboratory. However, due to the poor night performance (as explained in chapter 5) the inlet was covered at each night of the other trials, when it became evident that the dryer performed better at night with the inlet covered. After the laboratory trials, the poor nocturnal drying performance was suspected to be mainly caused by the very high chimney which functioned at night as a normal chimney. This is one of the reasons for using a much shorter chimney in relation to the height of drying chamber of the field model. Some glazing was also taken off the unused half of the tent dryer, to enhance a more effective irradiation through the back wall into the drying chamber.

3.3.2.1 Trial 1

Trial 1 was done from 1:00 p.m. on 15th February to 5:00 p.m. on 19th February 2006, and it later became a test case for setting up the other trials that followed (as explained in chapter 5). On the lower shelf, 9.5 kg of cassava was spread on each tray (A1 to A6).

The control tray had 4.1 kg of crop spread to the same loading density. Like the laboratory trials, both the inlet and outlets of the dryer were left open in the evening. However, the upper part of the control tray was covered with a polythene sheet to protect the crop from possible direct precipitation at night, but the air still had contact with the crop through the net at the bottom.

3.3.2.2 Trial 2

Trial two was done from 12:00 noon, 2nd March to 5:00 p.m., 5th March. This trial had the same loading arrangement as trial 1, with each tray having 10 kg of cassava. But in trial two, the dryer inlet was covered at night. The top part of the control tray was also covered, with the bottom part still in contact with atmospheric air, as in trial 1.

3.3.2.3 Trial 3

For trial three, the upper trays (B1 to B4) were each loaded with 9.6 kg of the crop. The two lower trays not directly below the upper trays were also loaded; A1 with around 9.1 kg and A4 with 9.6 kg. The control tray had 8.0 kg. The relevant points on the tray A1 and control were marked to ensure that their crops were spread to the same loading density as others. This trial started at 1:00 p.m. on 27th February and ended completely at 8:00 a.m. on the 2nd of March.

3.3.2.4 Trial 4

This trial took place from 11:40 a.m. on March 7 to 5:00 p.m. on March 10. Only the top four trays were loaded in the dryer, each with 10.7 kg, whilst the control had 10.6 kg of cassava.

3.3.2.5 Trial 5

This was a full-load trial, with all the ten trays in the dryer as well as the control tray each loaded with 9.8 kg. Trial five was started at 11:30 a.m. on the 21st of February and it ended completely at 8:00 a.m. on 25th February.

CHAPTER 4 THE MATHEMATICAL MODEL

The focus of the mathematical model is on 3 main aspects of the CDSCD; airflow, air heating and crop drying. Figure 4.1 shows a functional model of the system which is used to formulate a preliminary mathematical model.

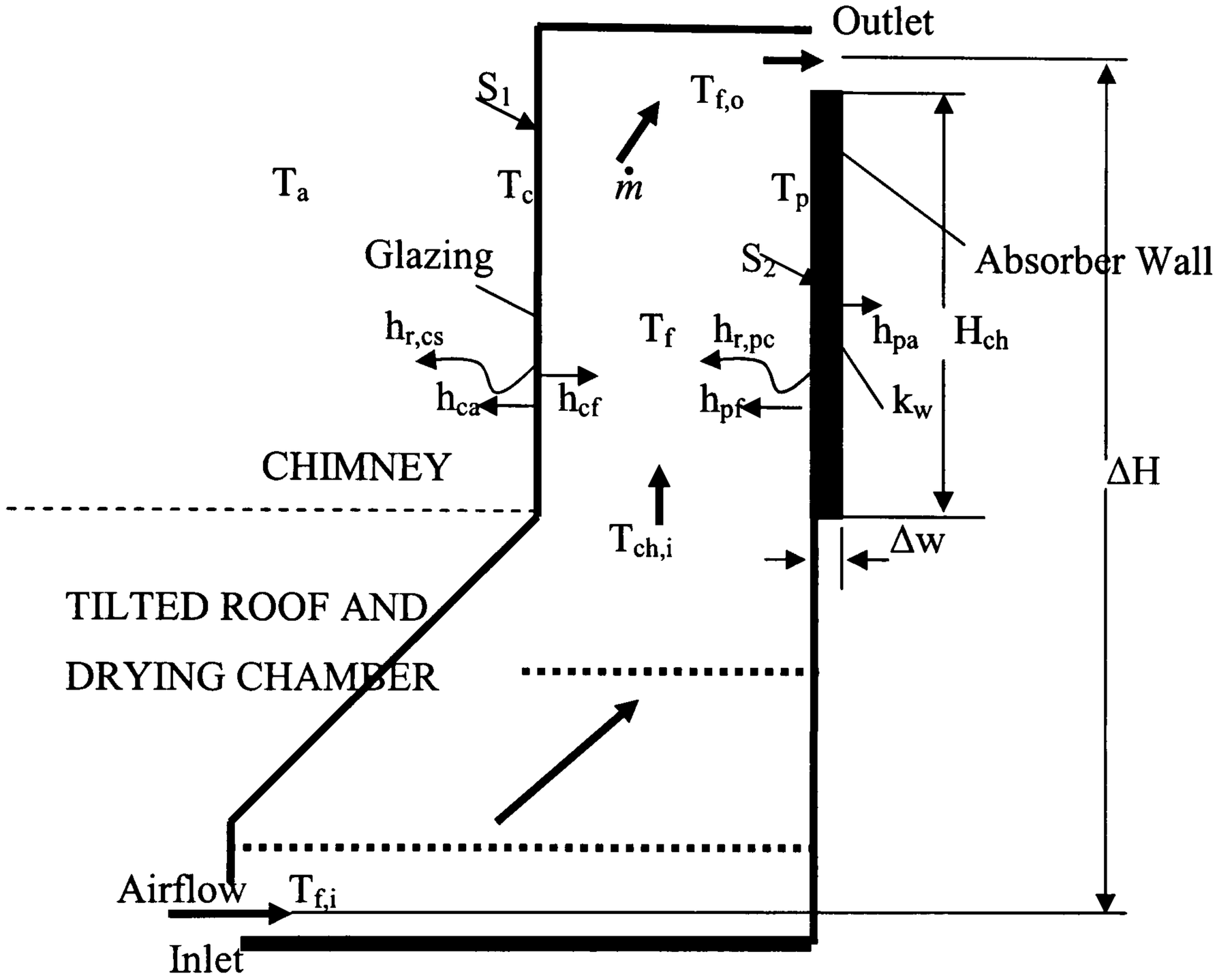

Figure 4.1 Schematic diagram of a Chimney-dependent Direct-mode Solar Crop Dryer

Air enters the dryer at the inlet temperature $T_{f,i}$, gets heated up while it absorbs moisture from the content of the drying chamber, enters the chimney at $T_{ch,i}$ where it is heated further to $T_{f,o}$ before it exits into the environment. The heat in the chimney is transferred by the absorber after it absorbs part of the radiant energy S_2. The radiant energy is reduced from S_1 to S_2 as it enters the chimney through the glazing.

4.1 The airflow model

The following assumptions are made in formulating the various models:

1. Wall surfaces are smooth, so friction resistances to airflow along the surfaces are negligible
2. The air media between these surfaces are non-participating in the radiant energy transmission
3. Properties of air are functions of temperature (assumed linear, because of the low temperature range)
4. There is complete displacement of air in the direction of airflow without any mixing
5. The heat transfer processes in the system occur under steady state conditions and they are one-dimensional
6. The glazings of chimney and drying chamber are opaque to the diffuse radiation from the chimney absorber and drying chamber base.
7. With regard to radiation exchange in the drying chamber, the dryer inlet and chimney inlet gaps are very small compared to other dimensions of the drying chamber, so that the drying-chamber walls together form a complete enclosure over the drying-chamber base.
8. Isothermal walls are assumed
9. Thermal capacitances of the system are neglected.

4.1.1 The airflow model formulation

The airflow model is formulated from the balance of buoyancy stack pressure and losses with friction effects neglected. Thus, equation 2.26 is used as the basis for the velocity model:

$$\rho\beta g\left(T_{out}-T_{in}\right)\Delta H=\sum_{i}K_{i}\rho\frac{v_{i}^{2}}{2} \tag{4.1}$$

The pressure-loss terms on the right-hand side of equation (4.1) represent the drag force per unit projected area perpendicular to the flow at the sections of orientation. These terms, with their various loss coefficients K, depend on the distributions of forces along

the surface and, therefore, the structural orientation (or angle of orientation) of the obstacle to the flow (Widden 1996; Young *et al*, 1997).

The roof of the dryer in Figure 4.1 represents an obstacle oriented to the flow at an angle between 0 and 90^0. Applying equation (4.1) to the various sections of the dryer, including the tilted roof of the chamber, gives

$$\rho\beta g\left(T_{out} - T_{in}\right)\Delta H = K_{in}\rho\frac{v_{in}^{\ 2}}{2} + \Delta \mathrm{P}_{obs} + K_{out}\rho\frac{v_{out}^{\ 2}}{2}, \tag{4.2}$$

where ΔP_{obs} is the total pressure loss at the obstacle (roof). The projected area A_{obs} of the roof is given by

$$A_{obs} = A_1 - A_2 \tag{4.3}$$

where A_1 and A_2 are the airflow cross-sectional areas at sections 1 and 2 (i.e. the start- and end-points of the roof) respectively (see Figure 4.2).

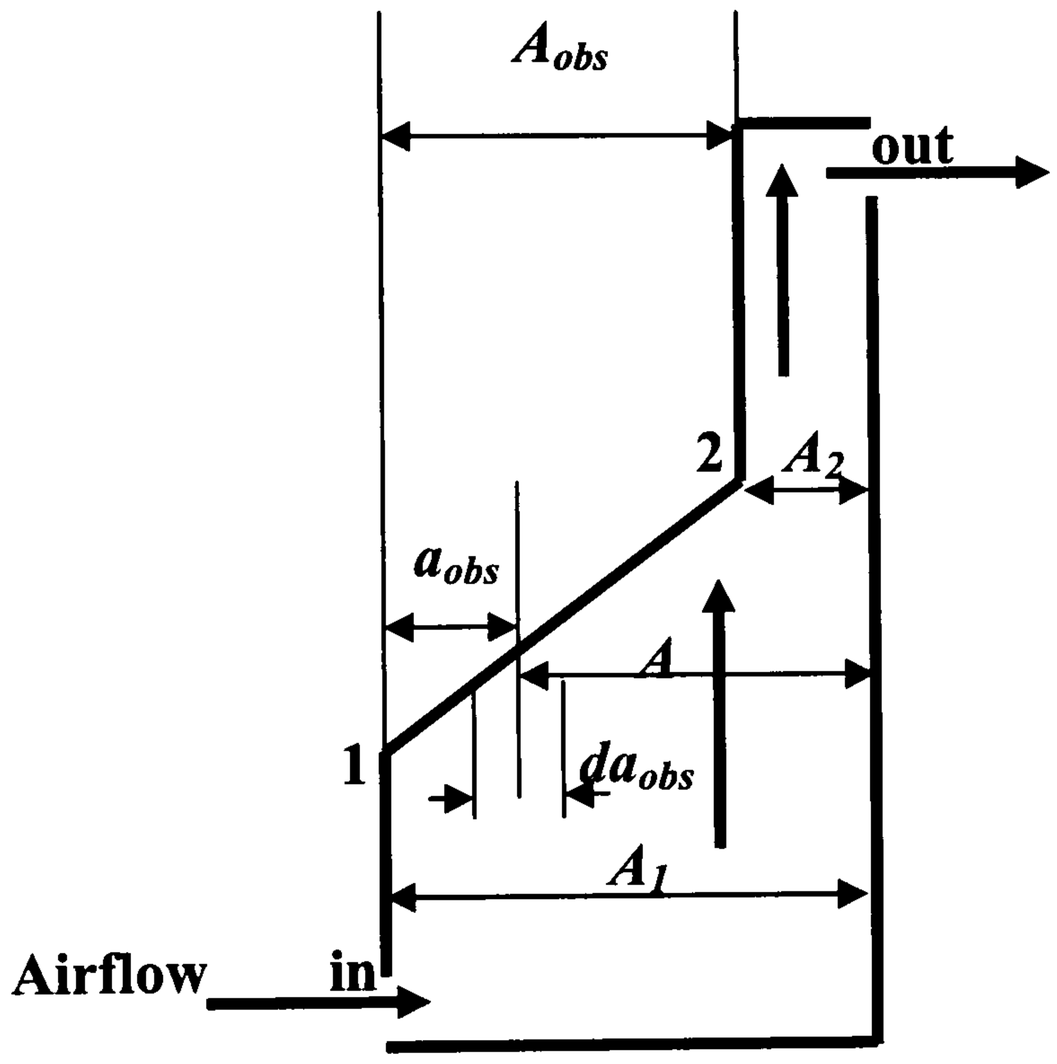

Figure 4.2 Diagram showing the pressure loss at the roof

For a given angle of orientation of the roof with coefficient K_{obs} (or K_{roof}), the local drag force of a fluid of local flow velocity v_{obs} at an arbitrary section (between sections 1 and 2) of the roof with infinitesimal projected area da_{obs} is

$$F_{drag} = K_{obs}\rho\frac{v_{obs}^{\ 2}}{2}da_{obs}\,. \tag{4.4}$$

Thus the pressure drop caused by the whole roof is

$$\Delta P_{obs} = \frac{\int_1^2 K_{obs}\rho\frac{v_{obs}^{\ 2}}{2}da_{obs}}{A_{obs}}, \tag{4.5}$$

a_{obs} is the projected area of obstacle from section 1 to the arbitrary section, and it is given as

$$a_{obs} = A_1 - A, \tag{4.6}$$

where A is the airflow cross-sectional area at the arbitrary section. So

$$da_{obs} = -dA. \tag{4.7}$$

Also, from continuity

$$v_{obs} = \frac{\dot{m}}{\rho A}, \tag{4.8}$$

Combining equations 4.3, 4.5, 4.7 and 4.8, the equation obtained is

$$\Delta P_{obs} = -\frac{\int_1^2 K_{obs}\rho\frac{1}{2}\left(\frac{\dot{m}}{\rho A}\right)^2 dA}{A_1 - A_2} = -\frac{K_{obs}}{A_1 - A_2}\frac{\dot{m}^2}{\rho}\frac{1}{2}\int_1^2\frac{dA}{A^2}$$

$$= -\frac{K_{obs}\,\dot{m}^2}{\rho(A_1 - A_2)}\frac{1}{2}\left[-\left(\frac{1}{A_2} - \frac{1}{A_1}\right)\right] = \frac{K_{obs}\,\dot{m}^2}{\rho(A_1 - A_2)}\frac{1}{2}\left[\frac{(A_1 - A_2)}{A_1 A_2}\right]$$

or

$$\Delta P_{obs} = \frac{1}{2}\frac{K_{obs}\,\dot{m}^2}{\rho A_2 A_1}. \tag{4.9}$$

Using the principle of continuity and assuming a constant average density of air through the dryer (as stated in ASHRAE, 1997), a flow model with reference to outlet conditions is deduced as follows:

$$\dot{m} = \rho v_{out} A_{out} = \rho v_{in} A_{in} = \rho v_1 A_1 = \rho v_2 A_2,$$

or

$$v_{in} = \frac{A_{out}}{A_{in}} v_{out}, \qquad v_1 = \frac{A_{out}}{A_1} v_{out}, \qquad v_2 = \frac{A_{out}}{A_2} v_{out}. \tag{4.9a}$$

and

$$\Delta \mathrm{P}_{obs} = K_{obs} \rho \frac{{A_{out}}^2}{A_2 A_1} \frac{{v_{out}}^2}{2} \tag{4.10}$$

Equations (4.9a) and (4.10) together with equation (4.2) give

$$\rho \beta g \Delta \mathrm{T} \Delta \mathrm{H} = K_{in} \rho \left(\frac{A_{out}}{A_{in}} \right)^2 \frac{{v_{out}}^2}{2} + K_{obs} \rho \frac{{A_{out}}^2}{A_2 A_1} \frac{{v_{out}}^2}{2} + K_{out} \rho \frac{{v_{out}}^2}{2} \tag{4.11}$$

where $\Delta \mathrm{T} = (T_{out} - T_{in})$. K_{in} is determined by the construction at inlet, K_{obs} (or K_{roof}) depends on the roof tilt angle and K_{out} depends on the exit configuration.

The exit velocity may be obtained from equation 4.11 as

$$v_{out} = \frac{1}{\sqrt{K_{in} \left(\frac{A_{out}}{A_{in}} \right)^2 + K_{roof} \frac{{A_{out}}^2}{A_1 A_2} + K_{out}}} \sqrt{2 \beta g \Delta \mathrm{T} \Delta \mathrm{H}} \tag{4.12}$$

or the inlet velocity as

$$v_{in} = \frac{1}{\sqrt{K_{in} + K_{roof} \frac{{A_{in}}^2}{A_1 A_2} + K_{out} \left(\frac{A_{in}}{A_{out}} \right)^2}} \sqrt{2 \beta g \Delta \mathrm{T} \Delta \mathrm{H}} \tag{4.12a}$$

The corresponding mass flow is obtained as

$$\dot{m} = \rho A_{out} v_{out} = \frac{1}{\sqrt{K_{in} \left(\frac{A_{out}}{A_{in}} \right)^2 + K_{roof} \frac{{A_{out}}^2}{A_1 A_2} + K_{out}}} \rho A_{out} \sqrt{2 \beta g \Delta \mathrm{T} \Delta \mathrm{H}} \tag{4.13}$$

or

$$\dot{m} = \rho A_{in} v_{in} = \frac{1}{\sqrt{K_{in} + K_{roof} \frac{{A_{in}}^2}{A_1 A_2} + K_{out} \left(\frac{A_{in}}{A_{out}} \right)^2}} \rho A_{in} \sqrt{2 \beta g \Delta \mathrm{T} \Delta \mathrm{H}} \tag{4.13a}$$

The expression of the mass flow in terms of inlet conditions is normally required during the under-load process to determine the mass flux, which is used in the pressure drop and drying equations (see equation 4.15 and subsection 4.2). Considering the effect of dryer content, the flow model is expanded to include the pressure loss through the crop.

With respect to inlet conditions, equation (4.13a) is modified as

$$\dot{m} = \rho A_{in} v_{in} = \frac{1}{\sqrt{K_{in} + K_{roof}\left(\frac{A_{in}}{A_b A_{ch,i}}\right)^2 + K_{out}\left(\frac{A_{in}}{A_{out}}\right)^2}} \rho A_{in} \sqrt{2\beta g \Delta T \Delta H - \frac{\Delta P_{cr}}{\rho}} \qquad (4.14)$$

The pressure drop ΔP_{cr} is obtained from the general equation recommended for a rectangular crop bed (Duffie and Beckman, 1991) as

$$\Delta P_{cr} = \frac{L G_a^{\,2}}{\rho_{air} D}\left(21 + 1750\frac{\mu}{G_a D}\right) \qquad (4.15)$$

where L is the length (thickness) of the bed in flow direction, G_a (as defined later in equation 4.46) is the mass velocity or mass flux in kg/m^{2}s (air mass flow rate divided by the frontal area), and D is the diameter of spherical particle of equal volume to that of the crop particle. From equation 4.15, an estimation of the mass flow rate is required to estimate ΔP_{cr} for substitution into equation 4.14 for the iterative determination of the mass flow rate. With knowledge of the temperatures across the crop bed, the ideal gas is initially assumed as guide to this estimation. So the pressure drop is initially estimated as

$$\Delta P_{cr} = \rho R\left(T_{bot} - T_{top}\right) \qquad (4.16)$$

where the gas constant R = 287.1 J kg^{-1}K^{-1}. The calculated initial mass flow is used to determine the mass flux G_a which is then used in equation 4.15 for subsequent iterations.

Equation 4.14 may be extended to cover the effect of the wind to give

$$\dot{m} = \rho A_{in} v_{in} = \frac{1}{\sqrt{K_{in} + K_{roof}\left(\frac{A_{in}}{A_b A_{ch,i}}\right)^2 + K_{out}\left(\frac{A_{in}}{A_{out}}\right)^2}} \rho A_{in} \sqrt{2\beta g \Delta T \Delta H - \frac{\Delta P_{cr}}{\rho} - C_p V^2} \qquad (4.14a)$$

where C_p is the wind pressure coefficient (an average value can be obtained from the literature; Afonso and Oliveira, 2000 suggest an average value of 0.25). V is the local wind velocity.

From the above equations, the ventilation flow rate can be predicted as in equation 4.13 or 4.14 for a dryer of known dimensions when ΔT, the pressure loss coefficients K_{in}, K_{roof} and K_{out} and the volumetric coefficient of expansion $\beta = (1/T)$ are known. For ΔT, the exit temperature T_{out} of the chimney needs to be obtained, using the heat transfer balances in the solar chimney. Equations 4.12 to 4.16 have been derived for the whole structure consisting of a drying chamber followed by chimney connected in series. Hence β must be derived for the whole structure. The β equation below (Incropera and De Witt, 1990) is applied between the chimney air and drying-chamber air as:

$$\beta = \frac{1}{T} = -\frac{1}{\rho}\frac{\rho_{chm,a} - \rho_{dc,a}}{T_{chm,a} - T_{dc,a}} \tag{4.17}$$

Considering the fact that the flow process is temperature-driven, the variation of pressure can be assumed negligible, compared with the variation of temperature, from the drying chamber into the chimney. So using the ideal gas relation, equation (4.17) becomes

$$\frac{1}{T} = -\frac{RT}{P}\frac{\frac{P}{RT_{chm,a}} - \frac{P}{RT_{dc,a}}}{T_{chm,a} - T_{dc,a}}$$

or

$$T = \sqrt{T_{chm,a} \cdot T_{dc,a}} \tag{4.18a}$$

When the difference between $T_{chm,a}$ and $T_{dc,a}$ become too small, then their product approaches their simple average, so that

$$T \approx \frac{T_{chm,a} + T_{dc,a}}{2} \tag{4.18b}$$

K_{in} and K_{out} may be established from the reports on similar inlet and outlet configurations or from the results of physical experiments on the laboratory model. The work performed by Flourentzou *et. al* (1998) for examining the discharge coefficients was based on the relationship

$$\Delta p = \sum_i \frac{\rho}{2}\left(\frac{v}{\varphi}\right)^2 \tag{4.19}$$

where Δp is the pressure loss (as shown on the right hand side of equation 4.1) and φ is the velocity coefficient. Comparing equations (4.1) and (4.19), the following relation is deduced

$$K = \frac{1}{\varphi^2}. \tag{4.18}$$

For an inlet configuration similar to that of the CDSCD, an average value of $\varphi = 0.7$ was obtained by Flourentzou *et al* (1998). This, together with equation (4.18), gives an approximate value as $K_{in} = 2.0$. However, as noted by Young *et al* (1997) the theoretical determination of the pressure coefficients K_{roof} at the roof is very difficult. Information was lacking on how the pressure coefficient relates to the tilting angle for the flow of gases through pyramids. Values in relation to the tilt angle may be determined experimentally, as shown in Chapter 6.

4.1.2 The heating models

Analysis of heat transfer into/out of the system is required for calculating the temperature difference which is requested for determining the airflow rate and also for assessing the crop drying process (see 4.2 The drying model).

4.1.2.1 Determining the temperatures in the chimney

The temperatures T_c, T_f and T_p can be determined from the energy balances in terms of the heat flow per unit area of chimney absorber surface (assuming equal areas of absorber and glazing) as follows:

Cover (T_c); $$S_c + h_{fc}(T_f - T_c) + h_{r,pc}(T_p - T_c) = U_{ca}(T_c - T_a) \tag{4.20}$$

Air (T_f); $$h_{pf}(T_p - T_f) = q'' + h_{fc}(T_f - T_c) \tag{4.21}$$

Absorber plate (T_p); $$S_p = h_{pf}(T_p - T_f) + h_{r,pc}(T_p - T_c) + U_{pa}(T_p - T_a) \tag{4.22}$$

where q'' in equation 4.21 is defined from the enthalpy change of the air (i.e. enthalpy change per unit absorber area) as

$$q^{"} W_{ch} H_{ch} = \dot{m} c_f (T_{out} - T_{ch,i}) . \qquad (4.23a)$$

Also

$$T_f = \gamma_{chm} T_{out} + (1 - \gamma_{chm}) T_{ch,i} \quad \text{or} \qquad T_{out} = \frac{T_f - (1 - \gamma_{chm}) T_{ch,i}}{\gamma_{chm}} . \qquad (4.23b)$$

The mean temperature approximation γ_{chm} is a constant used for determining the fluid mean temperature T_f from the chimney inlet and outlet temperatures. A value of γ_{chm} = 0.75 was assumed by Hirunlabh *et al* (1999) in the modelling and physical testing of the natural ventilation of houses by a metallic solar wall. In the experiment by Ong and Chow (2003) on the performance of a solar chimney, γ_{chm} was found to be 0.74.

Combining equations (4.23a) and (4.23b) gives

$$q^{"} = M_{ch} (T_f - T_{ch,i}) \qquad (4.24)$$

where $M_{ch} = \dfrac{\dot{m} c_f}{\gamma_{chm} W_{ch} H_{ch}}$.

The symbols in equations (4.20) to (4.22) may be defined and estimated as follows (also see figure 4.1 for graphical location of the symbols).

The heat radiated from a surface (area A_1, emissivity ε_1) to another surface (area A_2, emissivity ε_2) is given by (Duffie and Beckman, 1991; Incropera and DeWitt, 1990)

$$Q_{12} = -Q_{21} = \frac{\sigma (T_1^4 - T_2^4)}{\dfrac{1 - \varepsilon_1}{A_1 \varepsilon_1} + \dfrac{1}{A_1 F_{12}} + \dfrac{1 - \varepsilon_2}{A_2 \varepsilon_2}} \qquad (4.25)$$

The view factor F_{12} is the fraction of the radiation energy that leaves surface 1 to fall on surface 2.

a) Radiation heat transfer coefficient $h_{r,cs}$ from outer surface of glass cover (glazing) to the sky is obtained from the equation (4.25) as

$$Q_{cs} = \frac{\sigma(T_c^{\,4} - T_s^{\,4})}{\frac{1-\varepsilon_c}{A_c\varepsilon_c} + \frac{1}{A_c F_{cs}} + \frac{1-\varepsilon_s}{A_s\varepsilon_s}}.$$

With $F_{cs} = 1$ and $\frac{A_c}{A_s} \approx 0$, the above equation is simplified to

$$Q_{cs} = \sigma\varepsilon_c A_c (T_c^{\,4} - T_s^{\,4}) = A_c\sigma\varepsilon_c (T_c + T_s)(T_c^{\,2} + T_s^{\,2})(T_c - T_s)$$

so that the radiation heat transfer coefficient from the cover surface is

$$h_{r,cs} = \sigma\varepsilon_c (T_c + T_s)(T_c^{\,2} + T_s^{\,2})$$

and with reference to the environment temperature

$$h_{r,ca} = \sigma\varepsilon_c (T_c + T_s)(T_c^{\,2} + T_s^{\,2})(T_c - T_s)/(T_c - T_a), \qquad (4.26a)$$

where the T_s is the sky temperature given by (Ong, 2003)

$$T_s = 0.0552 T_a^{\,1.5}. \qquad (4.26b)$$

Convective heat transfer coefficient from glazing to the environment

$$h_{ca} = 5.7 + 3.8V, \qquad (4.26c)$$

where V is velocity of surrounding air (Ong, 2003).

Resultant heat transfer coefficient from glazing to the environment

$$U_{ca} = h_{r,ca} + h_{ca}. \qquad (4.26d)$$

But in the lab where the velocity is low enough to assume natural convection, equations 4.26f to 4.26h may be used to calculate the U_{ca}.

b) For the radiation heat transfer coefficient $h_{r,pc}$ between absorber plate and glazing, the two parallel plates are assumed to be infinitely long, compared to the side dimensions, so that

$$F_{pc} = 1 \text{ and } A_p = A_c.$$

Thus, from equation 4.25, radiation heat transfer coefficient between the absorber plate and glass cover is

$$h_{r,pc} = \frac{\sigma(T_p + T_c)(T_p{}^2 + T_c{}^2)}{\frac{1}{\varepsilon_p} + \frac{1}{\varepsilon_c} - 1}. \tag{4.26e}$$

c) The convective heat transfer coefficients from the fluid in the chimney to the glass cover h_{fc} and from the absorber plate to the fluid h_{pf} are determined as

$$h_{fc} = \frac{k_{fc} Nu}{H}; \tag{4.26f}$$

$$h_{pf} = \frac{k_{pf} Nu}{H} \tag{4.26g}$$

$$Nu = 0.68 + \frac{0.67 Ra^{1/4}}{\left[1 + \left(\frac{0.492}{\Pr}\right)^{9/16}\right]^{4/9}}, \text{ for lamina flow } (Ra<10^9) \tag{4.26h}$$

or

$$Nu = \left\{0.825 + \frac{0.387 Ra^{1/6}}{\left[1 + \left(\frac{0.492}{\Pr}\right)^{9/16}\right]^{8/27}}\right\}^2, \text{ for turbulent flow } (\text{Ra}>10^9) \tag{4.26i}$$

where $Ra = Gr \Pr$, $\quad Gr = \frac{g\beta(T_p - T_f)H^3}{\nu^2}$, $\quad \Pr = \frac{c_f \mu_f}{k_f}$

or

$Ra = \frac{g\beta(T_p - T_f)H^3}{\nu\alpha}$ (Incropera and De Witt, 1990).

The physical properties of air are evaluated at the mean film temperature, e.g. $T_{pf} = (T_p+T_f)/2$. The empirical relationships of the fluid properties with temperature were proposed by Ong, 2003 (based on the handbook data range of 300 – 350 K from Incropera and DeWitt, 1996) and verified by Ong and Chow (2003) as;

$$\mu_{pf} = \left[1.846 + 0.00472(T_{pf} - 300)\right] x10^{-5}$$

$$\rho_{pf} = 1.1614 - 0.00353(T_{pf} - 300)$$

$$k_{pf} = 0.0263 + 0.000074(T_{pf} - 300)$$

$$c_{pf} = \left[1.007 + 0.00004(T_{pf} - 300)\right] x10^3$$

$$\beta_{pf} = \frac{1}{T_{pf}}$$

$$\nu_{pf} = \frac{\mu_{pf}}{\rho_{pf}}$$

$$\alpha_{pf} = \frac{k_{pf}}{\rho_{pf} c_{pf}}, \text{ etc.}$$

The above relations have been deduced with 300K as pivot. So, for values just below 300 K like room temperature, the same empirical relationship can be used with the same accuracy as those in the temperature range (300 -350 K) given above.

d) Overall heat transfer coefficient from the absorber wall through the absorber plate is

$$U_{pa} = \frac{1}{\frac{\Delta w_p}{k_p} + \frac{1}{h_{pa}}}, \tag{4.26j}$$

with h_{pa} calculated similar to h_{ca} in equation 4.26c.

e) Radiation heat flux absorbed by the glazing,

$$S_c = \alpha_c I_{chm} \tag{4.26k}$$

and that absorbed by the plate,

$$S_p = \tau_c \alpha_p I_{chm}, \tag{4.26l}$$

where α_c and α_p are the absorptivities of the glazing and absorber respectively.

Equation 4.20 may be rearranged as

$$\left(U_{ca} + h_{r,pc} + h_{fc}\right) T_c - h_{fc} T_f - h_{r,pc} T_p = S_c + U_{ca} T_a \tag{4.20a}$$

Also, when equation (4.24) is substituted into equation (4.21) the result is

$$h_{fc} T_c - \left(h_{pf} + h_{fc} + M_{ch}\right) T_f + h_{pf} T_p = -M_{ch} T_{ch,i}. \tag{4.21a}$$

The energy balance for the absorber plate (4.22) is arranged as

$$-h_{r,pc} T_c - h_{pf} T_f + \left(h_{pf} + h_{r,pc} + U_{pa}\right) T_p = S_p + U_{pa} T_a \tag{4.22a}$$

and with the following substitutions

$$U_{ca} + h_{r,pc} + h_{fc} = C_1,$$

$$h_{pf} + h_{fc} + M_{ch} = C_2 \text{ and}$$

$$h_{pf} + h_{r,pc} + U_{pa} = C_3,$$

equations 4.20a, 4.21a and 4.22a are finally transformed, respectively, into

$$C_1 T_c - h_{fc} T_f - h_{r,pc} T_p = S_c + U_{ca} T_a \qquad (4.20b)$$

$$h_{fc} T_c - C_2 T_f + h_{pf} T_p = -M_{ch} T_{ch,i} \qquad (4.21b)$$

$$-h_{r,pc} T_c - h_{pf} T_f + C_3 T_p = S_p + U_{pa} T_a \qquad (4.22b)$$

Subtracting C_1 x (4.21b) from h_{fc} x (4.20b) gives

$$(C_1 C_2 - h_{fc}^{\ 2}) T_f - (h_{fc} h_{r,pc} + C_1 h_{pf}) T_p = h_{fc} (S_c + U_{ca} T_a) + C_1 M_{ch} T_{ch,i} \qquad (4.27)$$

Also, $h_{r,pc}$ x (4.21b) + h_{fc} x (4.22b) gives

$$-(h_{r,pc} C_2 + h_{fc} h_{pf}) T_f + (h_{r,pc} h_{pf} + h_{fc} C_3) T_p = h_{fc} (S_p + U_{pa} T_a) - h_{r,pc} M_{ch} T_{ch,i} \qquad (4.28)$$

Equations 4.27 and 4.28 may be simplified by the following substitutions

$$C_1 C_2 - h_{fc}^{\ 2} = D_1 \qquad h_{fc} h_{r,pc} + C_1 h_{pf} = D_2$$

$$h_{r,pc} C_2 + h_{fc} h_{pf} = D_3 \qquad h_{r,pc} h_{pf} + h_{fc} C_3 = D_4$$

$$h_{fc} (S_c + U_{ca} T_a) = E_1 \qquad C_1 M_{ch} T_{ch,i} = E_2$$

$$h_{fc} (S_p + U_{pa} T_a) = E_3 \qquad h_{r,pc} M_{ch} T_{ch,i} = E_4$$

to become

$$D_1 T_f - D_2 T_p = E_1 + E_2 \qquad (4.27a)$$

$$-D_3 T_f + D_4 T_p = E_3 - E_4 \qquad (4.28a)$$

Further, D_4 x (4.27a) + D_2 x (4.28a) gives

$$(D_1 D_4 - D_2 D_3) T_f = D_4 (E_1 + E_2) + D_2 (E_3 - E_4)$$

or

$$T_f = \frac{D_4(E_1 + E_2) + D_2(E_3 - E_4)}{D_1 D_4 - D_2 D_3}. \tag{4.29}$$

T_p is then obtained from equation (4.27a) as

$$T_p = \frac{D_1 T_f - E_1 - E_2}{D_2} \tag{4.30}$$

From the equation (4.21b),

$$T_c = \frac{C_2 T_f - h_{pf} T_p - M_{ch} T_{ch,i}}{h_{fc}} \tag{4.31}$$

4.1.2.2 Determining the temperatures of the drying chamber

The drying chamber temperatures are determined for the no-load process. The drying-chamber air temperature T_{dcair}, the wall temperature T_{dc} and the base temperature T_b are determined from the energy balances of the air, the walls and the base of drying chamber respectively. The energy balance for the process when the crop is in the dryer is considered in the drying model under subsection 4.2.

Energy balance of air in the drying chamber:

$$\dot{m} c_p (T_{ch,i} - T_{in}) = h_{f,dc} A_{dc} (T_{dc} - T_{dcair}) + h_{bf} A_b (T_b - T_{dcair}) \tag{4.32}$$

Similar to equation 4.23b, the chimney inlet temperature is obtained from

$$T = \gamma_{dc} T_{ch,i} + (1 - \gamma_{dc}) T_{in} \qquad \text{or} \qquad T_{ch,i} = \frac{T_{dcair} - (1 - \gamma_{dc}) T_{in}}{\gamma_{dc}}. \tag{4.33}$$

Equations (4.32) and (4.33) are combined and rearranged to give

$$h_{f,dc} A_{dc} T_{dc} - \left(\frac{\dot{m} c_p}{\gamma_{dc}} + h_{f,dc} A_{dc} + h_{bf} A_b\right) T_{dcair} + h_{bf} A_b T_b = -\frac{\dot{m} c_p}{\gamma_{dc}} T_{in} \tag{4.34}$$

Energy balance on the walls of drying chamber is

$$A_{dc} S_{dc} + h_{f,dc} A_{dc} (T_{dcair} - T_{dc}) + h_{r,bdc} A_b (T_b - T_{dc}) = U_{dc,a} A_{dc} (T_{dc} - T_a)$$

By arranging the above gives

$$(h_{f,dc} + h_{r,bdc}\frac{A_b}{A_{dc}} + U_{dc,a})T_{dc} - h_{f,dc}T_{dcair} - h_{r,bdc}\frac{A_b}{A_{dc}}T_b = S_{dc} + U_{dc,a}T_a \qquad (4.35)$$

Energy balance of the base of drying chamber is

$$A_b S_b = A_b h_{bf}(T_b - T_{dcair}) + A_b h_{r,bdc}(T_b - T_{dc}) + A_b U_{ba}(T_b - T_a),$$

by arranging gives

$$-h_{r,bdc}T_{dc} - h_{bf}T_{dcair} + (h_{bf} + h_{r,bdc} + U_{ba})T_b = S_b + U_{ba}T_a \qquad (4.36)$$

The radiation heat transfer coefficient from outer surface of drying chamber (glazing) to the sky $h_{r,dca}$ (with reference to the environment temperature) is given by

$$h_{r,dca} = \sigma\varepsilon_c(T_{dc} + T_s)(T_{dc}^{\ 2} + T_s^{\ 2})(T_{dc} - T_s)/(T_{dc} - T_a), \qquad (4.37a)$$

where the T_s is the sky temperature given by (see equation 4.26b)

The convective heat transfer coefficient from drying chamber glazing to the environment is

$$h_{dca} = 5.7 + 3.8V, \qquad (4.37b)$$

The resultant overall heat transfer coefficient from drying chamber glazing to environment is

$$U_{dc,a} = h_{r,dca} + h_{dca}. \qquad (4.37c)$$

Radiation heat transfer coefficient between the base plate and drying chamber walls (from equation 4.25, with $F_{bdc} = 1$) is

$$h_{r,bdc} = \frac{\sigma}{A_b}\frac{(T_b + T_{dc})(T_b^{\ 2} + T_{dc}^{\ 2})}{\frac{1-\varepsilon_b}{\varepsilon_b A_b} + \frac{1}{A_b} + \frac{1-\varepsilon_{dc}}{\varepsilon_{dc}A_{dc}}}. \qquad (4.37d)$$

The convective heat transfer coefficient from the base plate to the air in the drying chamber $h_{f,b}$ is determined as

$$h_{bf} = \frac{k_{f,b} Nu_L}{L}; \tag{4.37e}$$

For the base of the drying chamber

$$\overline{Nu}_L = 0.54 Ra_L^{1/4} \qquad (10^4 \le Ra_L \le 10^7) \tag{4.37f}$$

$$\overline{Nu}_L = 0.15 Ra_L^{1/3} \qquad (10^7 \le Ra_L \le 10^{11}) \tag{4.37g}$$

where $L = \frac{A_b}{P_b}$, $Ra_L = Gr_{bf} \Pr_{bf}$,

$$Gr_{bf} = \frac{g\beta_{bf}(T_b - T_f)L^3}{\nu_{bf}^2}, \qquad \Pr_{bf} = \frac{c_{bf}\mu_{bf}}{k_{bf}}$$

For the vertical walls

$$h_{f,dc} = \frac{k_{f,dc} Nu_{H,dc}}{H_{dc}} \tag{4.37h}$$

$$Nu_{Hdc} = 0.68 + \frac{0.67 Ra_{Hdc}^{1/4}}{\left[1 + \left(\frac{0.492}{\Pr}\right)^{9/16}\right]^{4/9}}, \text{ for lamina flow } (Ra<10^9) \tag{4.37i}$$

or

$$Nu_{Hdc} = \left\{0.825 + \frac{0.387 Ra_{Hdc}^{1/6}}{\left[1 + \left(\frac{0.492}{\Pr}\right)^{9/16}\right]^{8/27}}\right\}^2, \text{ for turbulent flow } (Ra>10^9) \tag{4.37j}$$

where $Ra_{Hdc} = Gr_{Hdc} \Pr_{Hdc}$, $Gr_{Hdc} = \frac{g\beta_{f,dc}(T_{dc} - T_f)H_{dc}^3}{\nu_{f,dc}^2}$ and $\Pr_{Hdc} = \frac{c_{f,dc}\mu_{f,dc}}{k_{f,dc}}$

or

$Ra_{Hdc} = \frac{g\beta_{f,dc}(T_{dc} - T_f)H_{dc}^3}{\nu_{f,dc}\alpha_{f,dc}}$ (Incropera and De Witt, 1990).

The physical properties of air are evaluated at the mean film temperature, as in equations (4.26). For the inclined roof of angle θ from 0 to 60^0, g in equation 4.26 may be replaced by $gcos\theta$ for determining the average Nusselt number at the roof surface facing downwards (Incropera and De Witt, 1990). If θ is greater than 60^0, then the Nusselt number is interpolated between 60^0 and 90^0; as there is no formula for that range, as far as the author is aware. Equation (4.26c) is used to determine the convection heat coefficient from the glazing to the environment.

In determining $h_{f,dc}$ and A_{dc}, the drying-chamber wall and inclined roof may be considered separately. The convective heat transfer coefficient is then obtained as

$$h_{f,dc} = \frac{h_{f,vw}A_{vw} + h_{f,roof}A_{roof}}{A_{dc}} \tag{4.37k}$$

where

$$A_{dc} = A_{vw} + A_{roof}\,.$$

Overall heat transfer coefficient through the base plate to the air underneath is

$$U_{ba} = \frac{1}{\frac{\Delta w_b}{k_b} + \frac{1}{h_{ba}}} \tag{4.37l}$$

with h_{ba} calculated similar to h_{ca} in equation 4.26c. The above coefficient U_{ba} gets to zero, when the ground is used as the base, since Δw_b then gets to infinity.

Radiation heat flux absorbed by the drying chamber glazing,

$$S_{dc} = \alpha_{dc} I_{dc} \tag{4.37m}$$

and that absorbed by the base plate,

$$S_b = \tau_{dc}\alpha_b I_{dc} \tag{4.37n}$$

where α_{dc} and α_b are the absorptivities of the drying chamber glazing and base respectively, and τ_{dc} is the transmissivity of the drying chamber walls .

Equations 4.34 to 4.36 are transformed respectively as

$$F_1 T_{dc} - F_2 T_{dcair} + F_3 T_b = -\frac{\dot{m} c_p}{\gamma_{dc}} T_{in} \tag{4.34a}$$

$$G_1 T_{dc} - h_{f,dc} T_{dcair} - G_2 T_b = S_{dc} + U_{dc,a} T_a \tag{4.35a}$$

$$-h_{r,bdc} T_{dc} - h_{bf} T_{dcair} + H_1 T_b = S_b + U_{ba} T_a \tag{4.36a}$$

where

$$F_1 = h_{f,dc} A_{dc}, \qquad F_2 = \frac{\dot{m} c_p}{\gamma_{dc}} + h_{f,dc} A_{dc} + h_{bf} A_b, \qquad F_3 = h_{bf} A_b$$

$$G_1 = h_{f,dc} + h_{r,bdc} \frac{A_b}{A_{dc}} + U_{dc,a}, \qquad G_2 = h_{r,bdc} \frac{A_b}{A_{dc}}, \qquad H_1 = h_{bf} + h_{r,bdc} + U_{ba}$$

T_{dc} is eliminated between 4.34a and 4.35a to give

$$(G_1 F_2 - F_1 h_{f,dc}) T_{dcair} - (F_1 G_2 + G_1 F_3) T_b = F_1 (S_{dc} + U_{dc,a} T_a) + G_1 \frac{\dot{m} c_p}{\gamma_{dc}} T_{in} \tag{4.38}$$

Similarly, from equations (4.34a) and (4.36a)

$$-(F_1 h_{bf} + F_2 h_{r,bdc}) T_{dcair} + (F_1 H_1 + F_3 h_{r,bdc}) T_b = F_1 (S_b + U_{ba} T_a) - h_{r,bdc} \frac{\dot{m} c_p}{\gamma_{dc}} T_{in} \tag{4.39}$$

With the following substitutions

$$J_1 = G_1 F_2 - F_1 h_{f,dc}, \quad J_2 = F_1 G_2 + G_1 F_3, \quad J_3 = F_1 h_{bf} + F_2 h_{r,bdc}, \quad J_4 = F_1 H_1 + F_3 h_{r,bdc}$$

$$K_1 = F_1 (S_{dc} + U_{dc,a} T_a), \quad K_2 = G_1 \frac{\dot{m} c_p}{\gamma_{dc}} T_{in}, \quad K_3 = F_1 (S_b + U_{ba} T_a), \quad K_4 = h_{r,bdc} \frac{\dot{m} c_p}{\gamma_{dc}} T_{in}$$

(4.38) and (4.39) become, respectively

$$J_1 T_{dcair} - J_2 T_b = K_1 + K_2 \tag{4.38a}$$

$$-J_3 T_{dcair} + J_4 T_b = K_3 - K_4 \tag{4.39a}$$

Combining the above two equations to eliminate T_b, the following is obtained

$$(J_1 J_4 - J_2 J_3) T_{dcair} = J_4 (K_1 + K_2) + J (K_3 - K_4)$$

or

$$T_{dcair} = \frac{J_4(K_1 + K_2) + J_2(K_3 - K_4)}{J_1 J_4 - J_2 J_3} \tag{4.40}$$

From 4.38a

$$T_b = \frac{J_1 T_{dcair} - K_1 - K_2}{J_2} \tag{4.41}$$

T_{dc} is calculated from 4.34a as

$$T_{dc} = \frac{F_2 T_{dcair} - F_3 T_b - \dfrac{\dot{m} c_p}{\gamma_{dc}} T_{in}}{F_1} \tag{4.42}$$

4.2 The drying model

The drying model is formulated for direct-mode dryer in a drying process. The following processes are assumed within a small interval *dt*:

1. Air enters the dryer and is heated up by the drying chamber base as the base absorbs irradiation energy through the walls of the chamber.
2. The heated air then exchanges convection heat with the crops and the walls of the drying chamber and receives mass and energy of evaporation as it passes through the crops above the base.
3. The crops absorb radiant energy from the base and also exchange direct heat with the drying air. Part of the energy absorbed by the crops is used to evaporate the crop moisture into the flowing air, part is transferred to the chamber walls by radiation and the rest causes a change of enthalpy of the crops.
4. The chamber walls absorb part of the irradiation energy falling into the drying chamber, receive radiation energy from the crop and chamber base, emit radiation heat into the sky and exchange heat with both the drying air and the environment air by convection.

The above processes can be analysed through the energy and mass balances of the crops and drying air, and also the energy balances of the drying chamber walls and base. As explained in chapter 2, the formulation is first based on a thin layer and can then be

extended to cover the whole bed, where necessary. An elemental layer of crop bed of height *dz* with the drying air passing through it at a specified flow rate is considered (Figure 4.3).

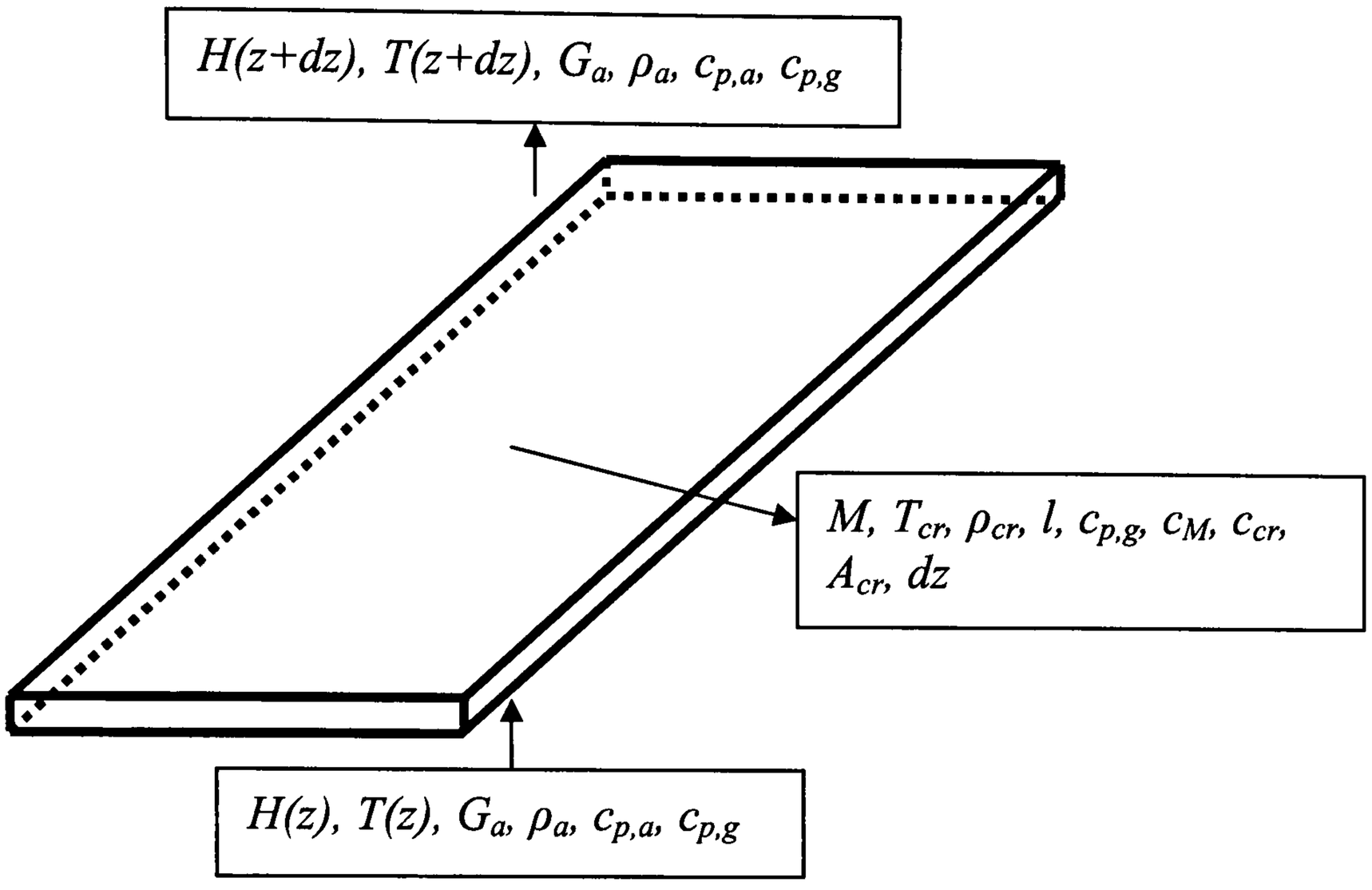

Figure 4.3: Elemental layer of crop bed

The temperature T and absolute Humidity H of drying air and the temperature T_{cr} and the average moisture content M of crop are determined for a short time interval dt, with the following assumptions:

1. there is no temperature gradient within each crop particle;
2. conduction from one crop particle to another is negligible
3. there is uniform air flow rate through the crop
4. within the time interval dt, the heat capacities of the air and the crop remain constant
5. changes in air temperature and humidity within the short time interval dt are negligible compared to the changes over the elemental layer of crop bed (i.e. steady conditions are assumed for the drying air)
6. changes in crop temperature and moisture content are negligible, compared to changes in air temperature, over the elemental layer dz
7. the moisture evaporates at the same temperature as that of the crop
8. the bed is a rectangular slab with void spaces
9. no condensation takes place on the walls of drying chamber

10. the convective film resistance on the outer surface of drying chamber is negligible.
11. Properties of the crop are independent of temperature.
12. Properties of air are functions of temperature (assumed linear, because of the low temperature range)

4.2.1 The drying equation

The drying equation is formulated from the analytical solution of the Fick's law (equation 2.6) for a slab or rectangular crop bed of thickness z as (Crank 1975; Okos et al, 1992):

$$\frac{M - M_e}{M_o - M_e} = \frac{8}{\pi^2} \sum_{n=0}^{\infty} \frac{1}{(2n+1)^2} \exp\left[\frac{-(2n+1)^2 D \pi^2 t}{z^2}\right] \tag{4.43}$$

The diffusion coefficient (or diffusivity) D is obtained from the general equation recommended by Mujumdar (1997) as

$$D = D_0 \exp[-E_a / RT] \tag{4.44a}$$

where D_0 is a crop dependent constant, E_a is the activation energy, R is the universal gas constant (8.314 J/mol.K) and T is the absolute temperature. The values of D for cassava at three different temperatures as obtained from Okos et al (1992) are shown in table 4.1 below.

T / K	D / m^2/s
357	6.7 x 10^{-11}
347	4.8 x 10^{-11}
328	3.5 x 10^{-11}

Table 4.1 The diffusion coefficient *D* of cassava in relation to the absolute temperature *T*. Source: Okos et al (1992)

Substituting the values for the temperatures of 357K and 347K in equation (4.44a) and solving simultaneously gives

$D_0 = 7.11 \times 10^{-6}$ m^2/s and $E_a = 34347.30$ J/mol.

When the same equation is applied between the temperatures of 347K and 328K, the values obtained are

$$D_0 = 1.12 \times 10^{-8}\ \mathrm{m^2/s} \quad \text{and} \quad E_a = 15730.58\ \mathrm{J/mol}$$

According to Okos et al (1992) the D_0 depends only on the pore structure of the food material. So, the different values obtained for different temperature ranges may be due to change in the pore structure of the crop with change in temperature.

The equilibrium moisture constant, M_e is determined from the Modified Oswin Equation as

$$M_e = \frac{A + BT}{\left(\frac{1}{RH_{f,cr}} - 1\right)^{1/C}} \bullet \frac{1}{100} \tag{4.44b}$$

with A= 15.803, B= -0.1101, C = 2.4921 (Chen, 2002).

4.2.2 The mass balance of the drying air

The mass balance of air through the control volume of the crop bed in figure 4.3 is as follows:

Amount of moisture leaving the crops = moisture gained by the air

The moisture gained by the air is related to the rate of change of moisture content:

$$\frac{\partial M}{\partial t} = \frac{M(t+dt) - M(t)}{dt} \tag{4.45}$$

for a very small time interval *dt*.

From equation (4.45), the rate of change gives a negative value, as *M(t+dt)* is less than *M(t)* in the drying process. The moisture gained by the drying air within the time interval *dt* then becomes

$$-\rho_{cr} A_{cr} dz \bullet \left(\frac{\partial M}{\partial t} dt\right).$$

In the same time interval, the amounts of moisture in the air entering at section *z* and leaving at *z+dz* are respectively

$$G_a A_{cr} H(z)dt$$

and

$$G_a A_{cr} H(z+dz)dt = G_a A_{cr}\left(H(z) + \frac{\partial H}{\partial z} dz \right) dt$$

where G_a, the mass-flux (kg/s.m^2) through the crop bed (as defined in the previous section) is given by

$$G_a = \frac{\dot{m}}{A_{cr}} \tag{4.46}$$

From the above analyses, assuming steady state conditions with no condensation on the walls of the drying chamber, the mass balance of air is

$$G_a A_{cr}\left(H + \frac{\partial H}{\partial z} dz \right) dt - G_a A_{cr} H dt = -\rho_{cr} A_{cr} dz \frac{\partial M}{\partial t} dt$$

which is simplified to

$$G_a \frac{\partial H}{\partial z} = -\rho_{cr} \frac{\partial M}{\partial t}. \tag{4.47}$$

4.2.3 Energy balance of air in the drying chamber

The energy balances on air are considered separately for the 3 zones with different temperatures in the drying chamber, namely the drying zone, beneath the drying zone and above the drying zone, within the time interval *dt*.

4.2.3.1 Energy balance of air in the drying zone

The energy balance of the air is used to derive a differential equation involving the change in air temperature with respect to the thin layer crop bed of height *dz*. The formulation is based on the following:

Change of enthalpy of air = heat of evaporation from the crop
– heat transfer to the crop
– heat transfer to the chamber walls

The enthalpy of moist air is given as (ASHRAE Handbook, 2001)

$$h = h_a + H h_g$$

where $h_a = c_{p,a}T$ and $h_g = c_{p,g}T + l$ at temperature T of air. Combining them together, the enthalpy of air entering the control volume at z is

$$G_a A_{cr}\left\{\left(c_{p,a} + H(z)c_{p,g}\right)T(z) + lH(z)\right\}dt$$

and the enthalpy of air leaving at $z+dz$ is

$$G_a A_{cr}\left\{\left(c_{p,a} + H(z+dz)c_{p,g}\right)T(z+dz) + lH(z+dz)\right\}dt$$

$$= G_a A_{cr}\left\{c_{p,a}\left(T(z) + \frac{\partial T}{\partial z}dz\right) + c_{p,g}\left(H(z) + \frac{\partial H}{\partial z}dz\right)\left(T(z) + \frac{\partial T}{\partial z}dz\right) + l\left(H(z) + \frac{\partial H}{\partial z}dz\right)\right\}dt$$

$$= G_a A_{cr}\left\{c_{p,a}\left(T(z) + \frac{\partial T}{\partial z}dz\right) + c_{p,g}\left(H(z)T(z) + H(z)\frac{\partial T}{\partial z}dz + T(z)\frac{\partial H}{\partial z}dz\right)\right.$$

$$\left. + l\left(H(z) + \frac{\partial H}{\partial z}dz\right)\right\}dt$$

On subtracting the enthalpy of air entering from that of the air leaving the control volume, the change in enthalpy of air in the control volume becomes

$$G_a A_{cr}\left\{\left(c_{p,a} + c_{p,g}H\right)\frac{\partial T}{\partial z} + c_{p,g}T\frac{\partial H}{\partial z} + l\frac{\partial H}{\partial z}\right\}dtdz\,.$$

Heat of evaporation from a thin layer of crop bed of height (or thickness) dz is (see sub-section 4.2.2 for the mass transfer derivation)

$$-\rho_{cr}A_{cr}dz\left(c_{p,g}T_{cr} + l\right)\frac{\partial M}{\partial t}dt = -\left(c_{p,g}T_{cr} + l\right)\rho_{cr}A_{cr}\frac{\partial M}{\partial t}dtdz$$

Heat transfer to the crop is

$$h_v A_{cr}dz(T - T_{cr})dt = h_v A_{cr}(T - T_{cr})dtdz\,.$$

Heat lost to the chamber walls is (assuming all-round vertical walls for that thin layer)

$$h_{f,dcz}P_{dcz}dz(T - T_{dc})dt = h_{f,dcz}P_{dcz}(T - T_{dc})dtdz$$

Thus, the energy the balance equation for the air in the drying zone is

$$G_a A_{cr}\left\{\left(c_{p,a} + c_{p,g}H\right)\frac{\partial T}{\partial z} + c_{p,g}T\frac{\partial H}{\partial z} + l\frac{\partial H}{\partial z}\right\}dtdz$$

$$= -\left(c_{p,g}T_{cr} + l\right)\rho_{cr}A_{cr}\frac{\partial M}{\partial t}dtdz - h_v A_{cr}\left(T - T_{cr}\right)dtdz - h_{f,dcz}P_{dcz}\left(T - T_{dc}\right)dtdz$$

or

$$G_a A_{cr}\left\{\left(c_{p,a}+c_{p,g}H\right)\frac{\partial T}{\partial z}+c_{p,g}T\frac{\partial H}{\partial z}+l\frac{\partial H}{\partial z}\right\}$$
$$=h_v A_{cr}\left(T_{cr}-T\right)-\left(c_{p,g}T_{cr}+l\right)\rho_{cr}A_{cr}\frac{\partial M}{\partial t}-h_{f,dcz}P_{dcz}\left(T-T_{dc}\right) \quad (4.48)$$

Equations (4.47) and (4.48) are combined and rearranged to give the final energy balance of air in the drying zone as

$$\frac{\partial T}{\partial z}=\frac{1}{G_a\left(c_{p,a}+c_{p,g}H\right)}\left\{h_v\left(T_{cr}-T\right)+\rho_{cr}c_{p,g}\left(T-T_{cr}\right)\frac{\partial M}{\partial t}-\frac{h_{f,dcz}P_{dcz}}{A_{cr}}\left(T-T_{dc}\right)\right\}. \quad (4.49)$$

4.2.3.2 Energy balance of air beneath the drying zone

Change in enthalpy of air = heat transfer from the lower part of drying chamber walls

+ heat transfer from the drying chamber base

$$\dot{m}c_{pl}\left(T_{bot}-T_{in}\right)=h_{f,dcl}A_{dcl}\left(T_{dc}-T_l\right)+h_{bfl}A_b\left(T_b-T_l\right) \quad (4.50)$$

Also, similar to equations (4.23b) and (4.33)

$$T_l=\gamma_{dc}T_{bot}+\left(1-\gamma_{dc}\right)T_{in} \qquad \text{or} \qquad T_{bot}=\frac{T_l-\left(1-\gamma_{dc}\right)T_{in}}{\gamma_{dc}} \quad (4.51)$$

Substituting for T_{bot} in equation (4.50) gives

$$h_{f,dcl}A_{dcl}T_{dc}-\left(\frac{\dot{m}c_{pl}}{\gamma_{dc}}+h_{f,dcl}A_{dcl}+h_{bfl}A_b\right)T_l+h_{bfl}A_bT_b=-\frac{\dot{m}c_{pl}}{\gamma_{dc}}T_{in}$$

$$T_l=\frac{\frac{\dot{m}c_{pl}}{\gamma_{dc}}T_{in}+h_{f,dcl}A_{dcl}T_{dc}+h_{bfl}A_bT_b}{\frac{\dot{m}c_{pl}}{\gamma_{dc}}+h_{f,dcl}A_{dcl}+h_{bfl}A_b} \quad (4.52)$$

4.2.3.3 Energy balance of air above the drying zone

Change in enthalpy of air = heat transfer from the upper part of drying chamber walls

$$\dot{m}c_{pu}\left(T_{ch,i}-T_{top}\right)=h_{f,dcu}A_{dcu}\left(T_{dc}-T_u\right) \quad (4.53)$$

with

$$T_u = \gamma_{dc} T_{ch,i} + (1-\gamma_{dc}) T_{top} \qquad \text{or} \qquad T_{ch,i} = \frac{T_u - (1-\gamma_{dc}) T_{top}}{\gamma_{dc}} \tag{4.54}$$

Substituting for $T_{ch,i}$ in equation (4.53) gives

$$h_{f,dcu} A_{dcu} T_{dc} - (\frac{\dot{m} c_{pu}}{\gamma_{dc}} + h_{f,dcu} A_{dcu}) T_u = -\frac{\dot{m} c_{pu}}{\gamma_{dc}} T_{top}$$

or

$$T_u = \frac{\frac{\dot{m} c_{pu}}{\gamma_{dc}} T_{top} + h_{f,dcu} A_{dcu} T_{dc}}{\frac{\dot{m} c_{pu}}{\gamma_{dc}} + h_{f,dcu} A_{dcu}} \tag{4.55}$$

4.2.4 Energy balance on the wet crop

The energy balance on the wet crop is used to obtain a differential equation involving the change in temperature of crop (of thin layer; *dz*) per unit time as:

Change in enthalpy of the wet crops

= radiant energy absorbed by crops from irradiation

\+ radiant energy from drying chamber base

\+ heat transfer from air to the crop

– radiant heat exchange with drying chamber walls

– The net heat transfer to other structures (e.g. trays, supports) in the chamber

– heat of evaporation from crop

The various components of the energy balance per unit time are analysed in the following section.

Change in enthalpy of crops (given by the change in enthalpies of both the solid crop mass and the moisture in the crop) = $[\rho_{cr} A_{cr} dz(c_{cr} + c_M M)]\frac{\partial T_{cr}}{\partial t}$.

Irradiation energy absorbed by crops = $A_{cr} S_{cr}$.

Radiant energy from drying chamber base = $A_{cr}h_{r,bcr}(T_b - T_{cr})$.

Heat transfer from air to the crop = $A_{cr}dz \cdot h_v(T - T_{cr})$.

Radiant heat exchange with drying chamber walls consists of exchange of the bottom surface with the part of walls beneath the crop, exchange of the top surface with the part of walls above the crop and the exchange with the part of the wall facing the perimeter surface of the crop bed.

Thus the total exchange with the walls of chamber

$$= A_{cr}h_{r,dcl}(T_{cr} - T_{dc}) + A_{cr}h_{r,dcu}(T_{cr} - T_{dc}) + P_{cr}dz \cdot h_{r,dcz}(T_{cr} - T_{dc})$$

$$= A_{cr}(h_{r,dcl} + h_{r,dcu} + \frac{P_{cr}dz \cdot h_{r,dcz}}{A_{cr}})(T_{cr} - T_{dc})$$

$$= A_{cr}h_{r,crdc}(T_{cr} - T_{dc})$$

where $h_{r,crdc} = h_{r,dcl} + h_{r,dcu} + \frac{P_{cr}dz \cdot h_{r,dcz}}{A_{cr}}$

The net heat supplied to other structures (e.g. trays) = $m_{ss}c_{ss}\frac{\partial T_{cr}}{\partial t}$

Heat of evaporation = $-(c_{pg}T_{cr} + l)\rho_{cr}A_{cr}dz\frac{\partial M}{\partial t}$

$$= G_a A_{cr}dz(c_{pg}T_{cr} + l)\frac{\partial H}{\partial z}$$

Putting all the breakdowns together, the energy balance equation on the wet material becomes

$$[\rho_{cr}A_{cr}dz(c_{cr} + c_M M)]\frac{\partial T_{cr}}{\partial t} = A_{cr}S_{cr} + A_{cr}h_{r,bcr}(T_b - T_{cr}) + A_{cr}dz \cdot h_v(T - T_{cr})$$
$$- A_{cr}h_{r,crdc}(T_{cr} - T_{dc}) - m_{ss}c_{ss}\frac{\partial T_{cr}}{\partial t} - G_a A_{cr}dz(c_{p,g}T_{cr} + l)\frac{\partial H}{\partial z}$$

or

$$\frac{\partial T_{cr}}{\partial t} = \frac{1}{\rho_{cr}(c_{cr} + c_M M) + \dfrac{m_{ss} c_{ss}}{A_{cr} dz}} \left\{ \frac{S_{cr}}{dz} + \frac{h_{r,bcr}}{dz}(T_b - T_{cr}) + h_v (T - T_{cr}) \right.$$

$$\left. - \frac{h_{r,crdc}}{dz}(T_{cr} - T_{dc}) - G_a \left(c_{p,g} T_{cr} + l\right) \frac{\partial H}{\partial z} \right\} \tag{4.56}$$

4.2.5 Energy balance on the base of drying chamber

At steady state (assuming the temperature of the base remains constant):

Irradiation energy absorbed by base

= heat transfer to air in the lower part of the drying chamber

+ radiant heat transfer to the crops

+ radiant heat transfer to the walls of the drying chamber

+ heat transfer through the base to the environment.

Thus

$$A_b S_b = h_{bfl} A_b (T_b - T_l) + A_{cr} h_{r,bcr} (T_b - T_{cr}) + A_b h_{r,bdc} (T_b - T_{dc}) + A_b U_{ba} (T_b - T_a)$$

rearranged as

$$-h_{r,bdc} T_{dc} - h_{bfl} T_l + (h_{r,bdc} + h_{bfl} + \frac{A_{cr}}{A_b} h_{r,bcr} + U_{ba}) T_b - \frac{A_{cr}}{A_b} h_{r,bcr} T_{cr} - U_{ba} T_a = S_b$$

or

$$T_b = \frac{S_b + h_{r,bdc} T_{dc} + h_{bfl} T_l + \dfrac{A_{cr}}{A_b} h_{r,bcr} T_{cr} + U_{ba} T_a}{h_{r,bdc} + h_{bfl} + \dfrac{A_{cr}}{A_b} h_{r,bcr} + U_{ba}} \tag{4.57}$$

4.2.6 Energy balance on the walls of the drying chamber

The wall temperature is also assumed constant, so that in a unit time:

Irradiation energy absorbed by the walls

+ energy received from the air

+ energy received from the crops by radiation + radiant energy received from the base of chamber

= energy lost to the surroundings

The breakdown of the above is as follows:

Irradiation energy absorbed by the walls = $A_{dc}S_{dc}$

Energy received from the drying air = energy from the air beneath the crops
+ energy from the air in the crop zone
+ energy from the air above the crop zone

Thus total energy received from air

$$= A_{dcl}h_{f,dcl}(T_l - T_{dc}) + P_{dcz}dz \cdot h_{f,dcz}(T - T_{dc}) + A_{dcu}h_{f,dcu}(T_u - T_{dc})$$

Energy received from the crop by radiation = $A_{cr}h_{r,crdc}(T_{cr} - T_{dc})$

Energy received from the base of chamber = $A_b h_{r,bdc}(T_b - T_{dc})$

Energy lost to the surroundings = $A_{dc}U_{dc,a}(T_{dc} - T_a)$

The energy balance of the drying chamber walls becomes

$$A_{dc}S_{dc} + A_{dcl}h_{f,dcl}(T_l - T_{dc}) + P_{dcz}dz \cdot h_{f,dcz}(T - T_{dc}) + A_{dcu}h_{f,dcu}(T_u - T_{dc})$$
$$+ A_{cr}h_{r,crdc}(T_{cr} - T_{dc}) + A_b h_{r,bdc}(T_b - T_{dc}) = A_{dc}U_{dc,a}(T_{dc} - T_a)$$

which is rearranged to become

$$A_{dc}S_{dc} = (A_{dcl}h_{f,dcl} + P_{dcz}dz \cdot h_{f,dcz} + A_{dcu}h_{f,dcu} + A_{cr}h_{r,crdc} + A_b h_{r,bdc} + A_{dc}U_{dc,a})T_{dc}$$
$$- A_{dcl}h_{f,dcl}T_l - P_{dcz}dz \cdot h_{f,dcz}T - A_{dcu}h_{f,dcu}T_u - A_{cr}h_{r,crdc}T_{cr} - A_b h_{r,bdc}T_b - A_{dc}U_{dc,a}T_a$$

or

$$T_{dc} = \frac{A_{dc}S_{dc} + A_{dcl}h_{f,dcl}T_l + P_{dcz}dz \cdot h_{f,dcz}T + A_{dcu}h_{f,dcu}T_u + A_{cr}h_{r,crdc}T_{cr} + A_b h_{r,bdc}T_b + A_{dc}U_{dc,a}T_a}{A_{dcl}h_{f,dcl} + P_{dcz}dz \cdot h_{f,dcz} + A_{dcu}h_{f,dcu} + A_{cr}h_{r,crdc} + A_b h_{r,bdc} + A_{dc}U_{dc,a}} \quad (4.58)$$

4.2.7 Using two layers of crops

The energy balances described so far for the drying model are for a dryer with one layer of crops on a shelf. When two shelves are used (one above the other, for the intended full load of the dryer) then the various energy balances are modified to accommodate the additional shelf. All the balances are adjusted accordingly, except that of the drying-chamber base which is not affected by the inclusion of the second shelf.

4.2.7.1 Energy balance on drying air with two shelves

The mass balance remains unchanged but has to be applied to each shelf. The same applies to the balance for the air temperature in the drying zone, so that for the lower shelf (additional subscript 1)

$$\left.\frac{\partial T}{\partial z}\right|_1 = \frac{1}{G_{a,1}(c_{p,a}+c_{p,g}H_1)}\left\{h_{v,1}\left(T_{cr,1}-T_1\right)+\rho_{cr}c_{p,g}\left(T_1-T_{cr,1}\right)\left.\frac{\partial M}{\partial t}\right|_1 - \frac{h_{fdcz,1}P_{dcz,1}}{A_{cr,1}}\left(T_1-T_{dc}\right)\right\} \tag{4.59}$$

and for the upper shelf (additional subscript 2)

$$\left.\frac{\partial T}{\partial z}\right|_2 = \frac{1}{G_{a,2}(c_{p,a}+c_{p,g}H_2)}\left\{h_{v,2}\left(T_{cr,2}-T_2\right)+\rho_{cr}c_{p,g}\left(T_2-T_{cr,2}\right)\left.\frac{\partial M}{\partial t}\right|_2 - \frac{h_{fdcz,2}P_{dcz,2}}{A_{cr,2}}\left(T_2-T_{dc}\right)\right\} \tag{4.60}$$

Also the energy balances remain the same for the air at the start (or bottom) of the lower crop bed (with T_{bot} changed to $T_{bot,1}$) and top end of the upper crop bed (with T_{top} changed to $T_{top,2}$) of drying chamber. However, an additional energy balance is constructed for the temperature T_m between the two shelves as follows:

$$\dot{m}\,c_{pm}(T_{bot,2}-T_{top,1}) = h_{f,dcm}A_{dcm}(T_{dc}-T_m) \tag{4.61}$$

with

$$T_m = \gamma_{dc}T_{bot,2}+(1-\gamma_{dc})T_{top,1} \quad \text{or} \quad T_{bot,2} = \frac{T_m-(1-\gamma_{dc})T_{top,1}}{\gamma_{dc}} \tag{4.62}$$

to get

$$T_m = \frac{\frac{\dot{m}\,c_{pm}}{\gamma_{dc}}T_{top,1}+h_{f,dcm}A_{dcm}T_{dc}}{\frac{\dot{m}\,c_{pm}}{\gamma_{dc}}+h_{f,dcm}A_{dcm}} \tag{4.63}$$

4.2.7.2 Energy balances on crops with two shelves

The energy balance on crops of the lower shelf is as follows:

Change in enthalpy of crops = $\left\{\rho_{cr} A_{cr,1} dz\left(c_{cr} + c_M M_1\right)\right\}\left.\frac{\partial T_{cr}}{\partial t}\right|_1$

Irradiation energy absorbed by crops = $A_{cr,1} S_{cr,1}$

Radiant energy from drying chamber base = $A_{cr,1} h_{rbcr,1}(T_b - T_{cr,1})$

Heat transfer from air to the crop = $A_{cr,1} dz \cdot h_{v,1}\left(T_1 - T_{cr,1}\right)$

Radiant energy exchange with upper layer = $A_{cr,1} h_{rcr,12}(T_{cr,1} - T_{cr,2})$

The total exchange with walls of chamber

$$= A_{cr,1} h_{r1,dcl}(T_{cr,1} - T_{dc}) + A_{cr,1} h_{r1,dcm}(T_{cr,1} - T_{dc}) + P_{cr,1} dz \cdot h_{rdcz,1}(T_{cr,1} - T_{dc})$$

$$= A_{cr,1} h_{rcrdc,1}(T_{cr,1} - T_{dc})$$

where $h_{rcrdc,1} = h_{r1,dcl} + h_{r1,dcm} + \frac{P_{cr,1} dz \cdot h_{rdcz,1}}{A_{cr,1}}$

The net energy supplied from the lower crop to the lower tray = $m_{ss1} c_{ss1} \left.\frac{\partial T_{cr}}{\partial t}\right|_1$

Heat of evaporation = $G_{a,1} A_{cr,1} dz\left(c_{pg} T_{cr,1} + l\right)\left.\frac{\partial H}{\partial z}\right|_1$

The energy balance for the lower crops then becomes

$$\left\{\rho_{cr} A_{cr,1} dz\left(c_{cr} + c_M M_1\right)\right\}\left.\frac{\partial T_{cr}}{\partial t}\right|_1 = A_{cr,1} S_{cr,1} + A_{cr,1} h_{rbcr,1}(T_b - T_{cr,1}) + A_{cr,1} dz \cdot h_{v,1}(T_1 - T_{cr,1})$$

$$- A_{cr,1} h_{rcr,12}(T_{cr,1} - T_{cr,2}) - A_{cr,1} h_{rcrdc,1}(T_{cr,1} - T_{dc}) \qquad \text{o}$$

$$- m_{ss1} c_{ss1} \left.\frac{\partial T_{cr}}{\partial t}\right|_1 - G_{a,1} A_{cr,1} dz (c_{p,g} T_{cr,1} + l) \left.\frac{\partial H}{\partial z}\right|_1$$

r

$$\left.\frac{\partial T_{cr}}{\partial t}\right|_1 = \frac{1}{\rho_{cr}(c_{cr} + c_M M_1) + \frac{m_{ss1} c_{ss1}}{A_{cr,1} dz}} \left\{ \frac{S_{cr,1}}{dz} + \frac{h_{rbcr,1}}{dz}(T_b - T_{cr,1}) + h_{v,l}(T_1 - T_{cr,1}) \right.$$

$$- \frac{h_{rcr,12}}{dz}(T_{cr,1} - T_{cr,2}) - \frac{h_{rcrdc,1}}{dz}(T_{cr,1} - T_{dc}) \qquad (4.64)$$

$$\left. - G_{a,1}\left(c_{p,g} T_{cr,1} + l\right)\left.\frac{\partial H}{\partial z}\right|_1 \right\}$$

Similarly, for the balance of upper layer

Enthalpy change of crops = $\left\{\rho_{cr} A_{cr,2} dz\left(c_{cr} + c_M M_2\right)\right\}\left.\frac{\partial T_{cr}}{\partial t}\right|_2$

Absorbed irradiation = $A_{cr,2} S_{cr,2}$

Radiant energy from lower layer = $A_{cr,1} h_{rcr,12}(T_{cr,1} - T_{cr,2})$ (see balance for lower tray)

Heat transfer from air to the crop = $A_{cr,2} dz \cdot h_{v,2}\left(T_2 - T_{cr,2}\right)$

Thus the total exchange with walls of chamber

$$= A_{cr,2} h_{r2,dcm}(T_{cr,2} - T_{dc}) + A_{cr,2} h_{r2,dcu}(T_{cr,2} - T_{dc}) + P_{cr,u} dz \cdot h_{r,2}(T_{cr,2} - T_{dc})$$

$$= A_{cr,2} h_{rcrdc,2}(T_{cr,2} - T_{dc})$$

where $h_{rcrdc,2} = h_{r2,dcm} + h_{r2,dcu} + \frac{P_{cr,2} dz \cdot h_{rdcz,2}}{A_{cr,2}}$

The net energy supplied from the upper crop to upper tray = $m_{ss2} c_{ss2} \left.\frac{\partial T_{cr}}{\partial t}\right|_2$

Heat of evaporation = $G_{a,2} A_{cr,2} dz\left(c_{pg} T_{cr,2} + l\right)\left.\frac{\partial H}{\partial z}\right|_2$

With all the breakdowns put together, the balance for the upper shelf is

$$\left\{\rho_{cr} A_{cr,2} dz\left(c_{cr} + c_M M_2\right)\right\}\left.\frac{\partial T_{cr}}{\partial t}\right|_2 = A_{cr,2} S_{cr,2} + A_{cr,1} h_{rcr,12}(T_{cr,1} - T_{cr,2}) + A_{cr,2} dz \cdot h_{v,2}(T_2 - T_{cr,2})$$

$$- A_{cr,2} h_{rcrdc,2}(T_{cr,2} - T_{dc}) - m_{ss2} c_{ss2} \left.\frac{\partial T_{cr}}{\partial t}\right|_2$$

$$- G_{a,2} A_{cr,2} dz (c_{p,g} T_{cr,2} + l) \left.\frac{\partial H}{\partial z}\right|_2$$

or

$$\left.\frac{\partial T_{cr}}{\partial t}\right|_2 = \frac{1}{\rho_{cr}(c_{cr} + c_M M_2) + \frac{m_{ss2} c_{ss2}}{A_{cr,2} dz}} \left\{\frac{S_{cr,2}}{dz} + \frac{A_{cr,1}}{A_{cr,2}} \frac{h_{rcr,12}}{dz}(T_{cr,1} - T_{cr,2})\right.$$

$$+ h_{v,2}(T_2 - T_{cr,2}) - \frac{h_{rcrdc,2}}{dz}(T_{cr,2} - T_{dc}) \qquad (4.65)$$

$$\left. - G_{a,2}\left(c_{p,g} T_{cr,2} + l\right)\left.\frac{\partial H}{\partial z}\right|_2\right\}$$

4.2.7.3 Energy balance on drying chamber walls with two shelves

For the drying chamber walls

Total energy received from air

$$= \begin{aligned} &A_{dcl}h_{f,dcl}(T_l - T_{dc}) + P_{dcz,1}dz \cdot h_{fdcz,1}(T_1 - T_{dc}) + A_{dcm}h_{f,dcm}(T_m - T_{dc}) \\ &+ P_{dcz,2}dz \cdot h_{fdcz,2}(T_2 - T_{dc}) + A_{dcu}h_{f,dcu}(T_u - T_{dc}) \end{aligned}$$

Total radiant energy from the crops

$$= A_{cr,1}h_{rcrdc,1}(T_{cr,1} - T_{dc}) + A_{cr,2}h_{rcrdc,2}(T_{cr,2} - T_{dc})$$

Expressions for the energy received from irradiation, that from drying-chamber base and that lost to the surroundings remain the same as with the single layer. So, the balance for the drying chamber walls with two shelves of crops is

$$\begin{aligned} &A_{dc}S_{dc} + A_{dcl}h_{f,dcl}(T_l - T_{dc}) + P_{dcz,1}dz \cdot h_{fdcz,1}(T_1 - T_{dc}) \\ &+ A_{dcm}h_{f,dcm}(T_m - T_{dc}) + P_{dcz,2}dz \cdot h_{fdcz,2}(T_2 - T_{dc}) + A_{dcu}h_{f,dcu}(T_u - T_{dc}) \\ &+ A_{cr,1}h_{rcrdc,1}(T_{cr,1} - T_{dc}) + A_{cr,2}h_{rcrdc,2}(T_{cr,2} - T_{dc}) + A_b h_{r,bdc}(T_b - T_{dc}) \\ &= A_{dc}U_{dc,a}(T_{dc} - T_a) \end{aligned}$$

or

$$A_{dc}S_{dc} + A_{dcl}h_{f,dcl}T_l + P_{dcz,1}dz \cdot h_{fdcz,1}T_1 + A_{dcm}h_{f,dcm}T_m + P_{dcz,2}dz \cdot h_{fdcz,2}T_2$$

$$T_{dc} = \frac{+ A_{dcu}h_{f,dcu}T_u + A_{cr,1}h_{rcrdc,1}T_{cr,1} + A_{cr,2}h_{rcrdc,2}T_{cr,2} + A_b h_{r,bdc}T_b + A_{dc}U_{dc,a}T_a}{\begin{aligned} &A_{dcl}h_{f,dcl} + P_{dcz,1}dz \cdot h_{fdcz,1} + A_{dcm}h_{f,dcm} + P_{dcz,2}dz \cdot h_{fdcz,2} \\ &+ A_{dcu}h_{f,dcu} + A_{cr,1}h_{rcrdc,1} + A_{cr,2}h_{rcrdc,2} + A_b h_{r,bdc} + A_{dc}U_{dc,a} \end{aligned}} \quad (4.66)$$

4.2.8 Factors and coefficients of the drying model

The determination of the heat transfer coefficients used in the calculations of the under-load model are described in this section.

The mass flux G_a is already defined (see equation 4.46). The volumetric heat transfer coefficient is given by

$$h_v = 650\left(\frac{G_a}{D}\right)^{0.7} \qquad h_{v,1} = 650\left(\frac{G_{a,1}}{D}\right)^{0.7} \qquad h_{v,2} = 650\left(\frac{G_{a,2}}{D}\right)^{0.7} \quad (4.67a)$$

where D is the diameter of a sphere having the same volume as the average volume of crop particle (Duffie And Beckman, 1991)

Heat capacities and transfer coefficients of air in the various zones of the drying chamber are obtained through similar procedures to those of equations (4.26f to 4.26i) and (4.37e to 4.37k), using the appropriate characteristic lengths and surface temperatures and areas.

Equation 4.25 is used for deducing the various radiation coefficients. Thus

$$h_{r,bcr} = \frac{\sigma}{A_{cr}} \frac{(T_b + T_{cr})(T_b^{\,2} + T_{cr}^{\,2})}{\dfrac{1-\varepsilon_{cr,bot}}{A_{cr}\varepsilon_{cr,bot}} + \dfrac{1}{A_{cr}F_{cr,b}} + \dfrac{1-\varepsilon_b}{A_b\varepsilon_b}} \tag{4.67b}$$

The view factor from the crop to the base $F_{cr,b}$ is deduced from that in the opposite direction $F_{b,cr}$. With A_{cr} small than A_b and assuming even distribution of views on the surfaces, the view factor $F_{b,cr}$ is given by

$$F_{b,cr} = \frac{A_{cr}}{A_b} F_{eq} \tag{4.67c}$$

where F_{eq}, the view factor from the base to the crop for equal areas of base and crop, separated by a height D_{bcr} is given by (Incropera and DeWitt, 1996)

$$F_{eq} = \frac{2}{\pi XY}\left\{\ln\left[\frac{(1+X^2)(1+Y^2)}{1+X^2+Y^2}\right]^{1/2} + X(1+Y^2)^{1/2}\tan^{-1}\frac{X}{(1+Y^2)^{1/2}} + Y(1+X^2)^{1/2}\tan^{-1}\frac{Y}{(1+X^2)^{1/2}} - X\tan^{-1}X - Y\tan^{-1}Y\right\}$$

with

$$X = \frac{L_b}{D_{bcr}}, \qquad Y = \frac{W}{D_{bcr}}.$$

Also, from the reciprocity relation

$$A_{cr}F_{cr,b} = A_bF_{b,cr}$$

and together with equation (4.67c)

$$F_{cr,b} = \frac{A_b}{A_{cr}} F_{b,cr} = F_{eq} \tag{4.67d}$$

Beneath the drying zone, radiation coefficient $h_{r,dcl}$ from the bottom surface of crops to the lower walls of drying chamber is

$$h_{r,dcl} = \frac{\sigma}{A_{cr}} \frac{(T_{cr} + T_{dc})(T_{cr}^{\ 2} + T_{dc}^{\ 2})}{\dfrac{1-\varepsilon_{cr,bot}}{A_{cr}\varepsilon_{cr,bot}} + \dfrac{1}{A_{cr}F_{cr,dcl}} + \dfrac{1-\varepsilon_{dc}}{A_{dcl}\varepsilon_{dc}}}. \tag{4.67e}$$

Using the summation rule in the enclosure beneath the drying zone

$$F_{cr,dcl} + F_{cr,b} = 1$$

Thus, the view factor from the crop to the lower part of drying chamber walls is

$$F_{cr,dcl} = 1 - F_{cr,b} = 1 - F_{eq} \tag{4.67f}$$

Above the drying zone, the view factor from top surface of crop to the walls is unity. Therefore the radiation coefficient $h_{r,dcu}$

$$h_{r,dcu} = \frac{\sigma}{A_{cr}} \frac{(T_{cr} + T_{dc})(T_{cr}^{\ 2} + T_{dc}^{\ 2})}{\dfrac{1-\varepsilon_{cr,top}}{A_{cr}\varepsilon_{cr,top}} + \dfrac{1}{A_{cr}} + \dfrac{1-\varepsilon_{dc}}{A_{dcu}\varepsilon_{dc}}} \tag{4.67g}$$

From the perimeter surface to chamber walls (view factor = 1)

$$h_{r,dcz} = \frac{\sigma}{P_{cr}dz} \frac{(T_{cr} + T_{dc})(T_{cr}^{\ 2} + T_{dc}^{\ 2})}{\dfrac{1-\varepsilon_{cr,per}}{P_{cr}dz \cdot \varepsilon_{cr,per}} + \dfrac{1}{P_{cr}dz} + \dfrac{1-\varepsilon_{dc}}{P_{dc}dz\varepsilon_{dc}}} \tag{4.67h}$$

The heat transfer coefficient from the base to the walls of drying chamber is

$$h_{r,bdc} = \frac{\sigma}{A_b} \frac{(T_b + T_{dc})(T_b^{\ 2} + T_{dc}^{\ 2})}{\dfrac{1-\varepsilon_b}{A_b\varepsilon_b} + \dfrac{1}{A_bF_{b,dc}} + \dfrac{1-\varepsilon_{dc}}{A_{dc}\varepsilon_{dc}}} \tag{4.67i}$$

with

$$F_{b,dc} = 1 - F_{b,cr} = 1 - \frac{A_{cr}}{A_b} F_{eq}. \tag{4.72j}$$

With two layers, equation 4.67h for the radiation heat coefficient is done for both the lower and upper layers, using their appropriate values. Appropriate equations of (6.67a) are also used for the convection heat coefficients between the layers and the surrounding air. Similar equations to (4.37) are used to determine the convection heat coefficient between the air and the drying-chamber walls. Also, the radiation heat transfer coefficient between the crop layers is

$$h_{rcr,12} = \frac{\sigma}{A_{cr,2}} \frac{(T_{cr,1} + T_{cr,2})({T_{cr,1}}^2 + {T_{cr,2}}^2)}{\frac{1-\varepsilon_{crbot,2}}{A_{cr,2}\varepsilon_{crbot,2}} + \frac{1}{A_{cr,2}F_{cr,21}} + \frac{1-\varepsilon_{crtop,1}}{A_{cr,1}\varepsilon_{crtop,1}}} \tag{4.67k}$$

The view factor $F_{cr,21}$ from the upper crop to the lower crop is obtained from equation (4.67d) with A_b replaced by $A_{cr,1}$, and A_{cr}, L_b and D_{bcr} replaced by $A_{cr,2}$, $L_{cr\,1}$ and D_{12} respectively.

The overall heat transfer coefficient through the drying chamber walls $U_{dc,a}$ and that through base U_{ba} to the surroundings are obtained from equations 4.37c and 4.37*l* respectively.

Rates of absorption of irradiation energies per unit area

$$S_{dc} = \sigma_{dc} I_{dc} \tag{4.67l}$$

$$S_{cr} = \sigma_{cr} \tau_{dc} I_{dc} \tag{4.67m}$$

The crops shade part of the base and therefore reduce the energy of irradiation that is supposed to get to the base. In determining the energy absorbed by the base, beam radiation is separated from diffuse radiation, as the two are affected differently. Thus the energy falling on the base is then given by (Duffie and Beckman, 1991)

$$A_b I_{net} = A_b I_{dir} f_i + A_s F_{sb} I_{dif},$$

and with the reciprocity relation

$$A_s F_{sb} = A_b F_{bs},$$

then

$$A_b I_{net} = A_b I_{dir} f_i + A_b F_{bs} I_{dif}$$

or

$$I_{net} = I_{dir} f_i + F_{bs} I_{dif}. \tag{4.67n}$$

The ratio f_i is the fraction of the base area exposed to direct radiation and is given by

$$f_i = \frac{(A_b - A_{shade})}{A_b} = 1 - \frac{A_{shade}}{A_b} \tag{4.67o}$$

The shaded area A_{shade} of the base depends on the areas of the crop bed and the base and the angle of incidence of direct radiation. The view factor F_{bs} is obtained from

$$F_{bs} = 1 - F_{bcr} \tag{4.67p}$$

So

$$S_b = \alpha_b A_b I_{net} \tag{4.67q}$$

Likewise, the energy per unit area absorbed by the lower crops in the two layer model is

$$I_{net,cr1} = I_{dir} f_{i,cr1} + F_{cr1,s} I_{dif} \tag{4.67r}$$

with

$$f_{i,cr1} = 1 - \frac{A_{shade,cr}}{A_{cr,1}} \tag{4.67s}$$

and

$$F_{cr1,s} = 1 - F_{cr,12} \tag{4.67t}$$

4.3 Solution methods to the models

As already indicated, temperatures at various sections of the system are needed for the prediction of the mass flow rate of air. These can be obtained from the chimney heating model which, in turn, requires knowledge of the airflow for determining the temperatures. Thus the temperatures and the airflow are mutually dependent. This calls for iterative solutions to the problems in the airflow and heating models with initial guesses. The modelling procedure is initially applied to the no-load process and then extended to cover the under-load process.

4.3.1 Modelling the no-load process

The following are the known input variables for modelling the no-load process.

1. Dimensions of dryer
2. Constants and coefficients of mass flow
3. Conditions at inlet of the structure
4. Environment and climate data

The iteration process is as follows

1. Guess (initially) the values of T_c, T_f, and T_p for the chimney and T_{dc}, T_{dcair} and T_b for the drying chamber.
2. Determine the value of K_{roof} from roof angle (see chapter 6)
3. Calculate $T_{ch,i}$ from T_{dcair} and T_{in} (equation 4.33) and T_{out} from T_f and $T_{ch,i}$, (equation 4.23b)
4. Compute v_{out} and $\dot{m}$ (equations 4.12 and 4.13).
5. Determine the coefficients for chimney heating (equations 4.26).
6. Calculate the improved value of T_f as $T_{f,nw}$ (equation 4.29)
7. Compare $T_{f,nw}$ to T_f; if the relative difference (i.e. the difference divided by T_f) is greater than 0.01, replace T_f with $T_{f,nw}$ and repeat the processes from step 3, otherwise continue with the next step, with $T_{f,nw}$ in place of T_f.
8. Calculate the improved value of T_p as $T_{p,nw}$ (equation 4.30)
9. Compare $T_{p,nw}$ to T_p; if the relative difference is greater than 0.01, replace T_p with $T_{p,nw}$ and repeat the processes from step 3, otherwise continue with the next step, with $T_{p,nw}$ in place of T_p.
10. Calculate the improved value of T_c as $T_{c,nw}$ (equation 4.31)
11. Compare $T_{c,nw}$ to T_c; if the relative difference is greater than 0.01, replace T_c with $T_{c,nw}$ and repeat the processes from step 3, otherwise continue with the next step, with $T_{c,nw}$ in place of T_c.
12. Determine the coefficients for drying chamber heating (equations 4.37).
13. Calculate the improved value of T_{dcair} as $T_{dcair,nw}$ (equation 4.40)
14. Compare $T_{dcair,nw}$ to T_{dcair}, if the relative difference is greater than 0.01, replace T_{dcair} with $T_{dcair,nw}$ and repeat the process from step 3, otherwise continue with the next step, with $T_{dcair,nw}$ in place of T_{dcair}.
15. Calculate the improved value of T_b as $T_{b,nw}$ (equation 4.41)
16. Compare $T_{b,nw}$ to T_b; if the relative difference is greater than 0.01, replace T_b with $T_{b,nw}$ and repeat the process from step 3, otherwise continue, with $T_{b,nw}$ in place of T_b.
17. Calculate the improved value of T_{dc} as $T_{dc,nw}$ (equation 4.42)

18. Compare $T_{dc,nw}$ to T_{dc}; if the relative difference is greater than 0.01, replace T_{dc} with $T_{dc,nw}$ and repeat the process from step 3, otherwise continue, with $T_{dc,nw}$ in place of T_{dc}.
19. Output the temperatures and airflow rate.
20. End.

4.3.2 Modelling the under-load process

4.3.2.1 Finite difference methods for the under-load model

In this process, the changes occur both in space and time. Finite difference methods are employed for solutions to the differential equations of air and crop in the drying zone. The continuous changes of air temperature T and humidity H with height are transformed into discrete linear variations along small steps of height dz. The changes of temperature T_{cr} and moisture content M of crop are similarly transformed into linear variations over small steps of time dt.

As noted by Forson (1999), the choice of dt and dz affects the stability of the solution procedure. The solution becomes inaccurate, if one value (e.g. dt) is too high in comparison with the other (dz). On the other hand, the computations take too long to converge, when dt is too small compared to dz. The current model uses a single layer, with dz equal to the crop-bed thickness (0.015 m). Equation 4.47 is employed, in a finite difference form, for deducing dt in terms of dz. For a given airflow rate and crop mass, dH is proportional to $-dM$. Thus

$$-\frac{dH}{dM} = c\,, \tag{4.47a}$$

which transforms equation 4.81a into

$$dt = \frac{1}{c}\frac{\rho_{cr}}{G_a}dz \qquad \text{or} \qquad dt = k\frac{\rho_{cr}}{G_a}dz \tag{4.47b}$$

where c and k are constants of proportionality. The value of k determines the accuracy of the solution and also the converging time. A value of unity is initially assumed in this current model.

As assumed earlier, T_{cr} and M remain uniform across dz, whilst T and H remain constant in the interval dt. Equation (4.49) then becomes

$$\frac{T_{top}-T_{bot}}{dz}=\frac{1}{G_a(c_{p,a}+c_{p,g}H)}\left\{h_v(T_{cr}-T)+\rho_{cr}c_{p,g}(T-T_{cr})\frac{\partial M}{\partial t}-\frac{h_{f,dcz}P_{dcz}}{A_{cr}}(T-T_{dc})\right\}$$

or

$$T_{top}=T_{bot}+\frac{dz}{G_a(c_{p,a}+c_{p,g}H)}\left\{h_v(T_{cr}-T)+\rho_{cr}c_{p,g}(T-T_{cr})\frac{\partial M}{\partial t}-\frac{h_{f,dcz}P_{dcz}}{A_{cr}}(T-T_{dc})\right\} \tag{4.68}$$

and equations (4.56, 4.59, 4.60, 4.64 and 4.65) are similarly transformed as

$$T_{cr,t+dt}=T_{cr,t}+\frac{dt}{\rho_{cr}(c_{cr}+c_M M)+\frac{m_{ss}c_{ss}}{A_{cr}dz}}\left\{\frac{S_{cr}}{dz}+\frac{h_{r,bcr}}{dz}(T_b-T_{cr})+h_v(T-T_{cr})-\frac{h_{r,crdc}}{dz}(T_{cr}-T_{dc})-G_a\left(c_{p,g}T_{cr}+l\right)\frac{\partial H}{\partial z}\right\} \tag{4.69}$$

$$T_{top,1}=T_{bot,1}+\frac{dz}{G_{a,1}(c_{p,a}+c_{p,g}H_1)}\left\{h_{v,1}(T_{cr,1}-T_1)+\rho_{cr}c_{p,g}(T_1-T_{cr,1})\frac{\partial M}{\partial t}\bigg|_1-\frac{h_{fdcz,1}P_{dcz,1}}{A_{cr,1}}(T_1-T_{dc})\right\} \tag{4.70}$$

$$T_{top,2}=T_{bot,2}+\frac{dz}{G_{a,2}(c_{p,a}+c_{p,g}H_2)}\left\{h_{v,2}(T_{cr,2}-T_2)+\rho_{cr}c_{p,g}(T_2-T_{cr,2})\frac{\partial M}{\partial t}\bigg|_2-\frac{h_{fdcz,2}P_{dcz,2}}{A_{cr,2}}(T_2-T_{dc})\right\} \tag{4.71}$$

$$T_{cr1,t+dt}=T_{cr1,t}+\frac{dt}{\rho_{cr}(c_{cr}+c_M M_1)+\frac{m_{ss1}c_{ss1}}{A_{cr,1}dz}}\left\{\frac{S_{cr,1}}{dz}+\frac{h_{rbcr,1}}{dz}(T_b-T_{cr,1})+h_{v,1}(T_1-T_{cr,1})-\frac{h_{rcr,12}}{dz}(T_{cr,1}-T_{cr,2})-\frac{h_{rcrdc,1}}{dz}(T_{cr,1}-T_{dc})-G_{a,1}\left(c_{p,g}T_{cr,1}+l\right)\frac{\partial H}{\partial z}\bigg|_1\right\} \tag{4.72}$$

$$T_{cr2,t+dt} = T_{cr2,t} + \frac{dt}{\rho_{cr}(c_{cr} + c_M M_2) + \frac{m_{ss2}c_{ss2}}{A_{cr,2}dz}} \left\{ \frac{S_{cr,2}}{dz} + \frac{A_{cr,1}}{A_{cr,2}} \frac{h_{rcr,12}}{dz}(T_{cr,1} - T_{cr,2}) \right.$$

$$+ h_{v,2}(T_2 - T_{cr,2}) - \frac{h_{rcrdc,2}}{dz}(T_{cr,2} - T_{dc})$$

$$\left. - G_{a,2}\left(c_{p,g}T_{cr,2} + l\right)\left.\frac{\partial H}{\partial z}\right|_2 \right\} \qquad (4.73)$$

where

$$\frac{\partial M}{\partial t} = \frac{M_{t+dt} - M_t}{dt}, \qquad \left.\frac{\partial M}{\partial t}\right|_1 = \frac{M_{1,t+dt} - M_{1,t}}{dt}, \qquad \left.\frac{\partial M}{\partial t}\right|_2 = \frac{M_{2,t+dt} - M_{2,t}}{dt} \qquad (4.74)$$

$$\frac{\partial H}{\partial z} = \frac{H_{top} - H_{bot}}{dz}, \qquad \left.\frac{\partial H}{\partial z}\right|_1 = \frac{H_{top,1} - H_{bot,1}}{dz}, \qquad \left.\frac{\partial H}{\partial z}\right|_u = \frac{H_{top,2} - H_{bot,2}}{dz} \qquad (4.75)$$

$$T = \frac{T_{top} + T_{bot}}{2}, \qquad T_1 = \frac{T_{top,1} + T_{bot,1}}{2}, \qquad T_2 = \frac{T_{top,2} + T_{bot,2}}{2} \qquad (4.76)$$

$$T_{cr} = \frac{T_{cr,t} + T_{cr,t+dt}}{2}, \qquad T_{cr,1} = \frac{T_{cr1,t} + T_{cr1,t+dt}}{2}, \qquad T_{cr,2} = \frac{T_{cr2,t} + T_{cr2,t+dt}}{2} \qquad (4.77)$$

$$H = \frac{H_{top} + H_{bot}}{2}, \qquad H_1 = \frac{H_{top,1} + H_{bot,1}}{2}, \qquad H_2 = \frac{H_{top,2} + H_{bot,2}}{2} \qquad (4.78)$$

Equations (4.43) is transformed as

$$M = M_e + (M_o - M_e)\frac{8}{\pi^2}\sum_{n=0}^{\infty}\frac{1}{(2n+1)^2}\exp\left[\frac{-(2n+1)^2 D\pi^2 t}{z^2}\right] \qquad (4.79)$$

where, as in equations (4.44a) and (4.44b)

$$D = D_0 \exp[-E_a / RT] \qquad (4.80a)$$

$$\text{and } M_e = \frac{A + BT}{\left(\frac{1}{RH_{f,cr}} - 1\right)^{1/C}} \bullet \frac{1}{100} \qquad (4.80b)$$

Equation (4.47) is transformed into

$$G_a \frac{dH}{dz} = -\rho_{cr} \frac{dM}{dt} \quad \text{or} \quad \frac{dH}{dz} = -\frac{\rho_{cr}}{G_a} \frac{dM}{dt} \tag{4.81a}$$

so that

$$\frac{H_{top} - H_{bot}}{dz} = -\frac{\rho_{cr}}{G_a} \frac{M_{t+dt} - M_t}{dt} = \frac{\rho_{cr}}{G_a} \frac{M_t - M_{t+dt}}{dt}$$

or

$$H_{top} = H_{bot} - dz \frac{\rho_{cr}}{G_a} \left(\frac{M_{t+dt} - M_t}{dt} \right) = H_{bot} + \frac{\rho_{cr}}{G_a} \frac{dz}{dt} \left(M_t - M_{t+dt} \right) \tag{4.81b}$$

H_{bot} is obtained from

$$H_{bot} = H_{dcin} = 0.62198 \frac{p_w}{p - p_w} \tag{4.82}$$

where

$$p_{w,dcin} = p_{ws,dcin} RH_{dcin}$$

with

$$p_{ws,dcin} = \exp\left(C_8 / T_{dcin} + C_9 + C_{10} T_{dcin} + C_{11} {T_{dcin}}^2 + C_{12} {T_{dcin}}^3 + C_{13} \ln T_{dcin} \right)$$

and

$$C_8 = -5.8002206e^3 \quad C_9 = 1.3914993 \quad C_{10} = -4.8640239e^{-2}$$

$$C_{11} = 4.1764768e^{-5} \quad C_{12} = -1.4452093e^{-8} \quad C_{13} = 6.5459673 \text{ (ASHRAE, 2001)}$$

Also, within the crop zone, RH is obtained from

$$RH_{f,cr} = \frac{p_w}{p_{ws}} \tag{4.83}$$

where

$$p_w = \frac{pH}{(0.62198 + H)}$$

and

$$p_{ws} = \exp\left(C_8 / T + C_9 + C_{10} T + C_{11} T^2 + C_{12} T^3 + C_{13} \ln T \right).$$

4.3.2.2 The iteration processes

As in the no-load iteration, the temperatures at various necessary positions in the whole structure are guessed. Confirmation of these guessed values completes the initialisation

process for establishing the flow conditions of drying. Then, T_{cr} and M are calculated in steps of time interval dt. As stated in step 24 of the under-load iteration process described below, each newly calculated moisture content is compared with a set-down desired value. The program terminates when the moisture content is within a certain range of this desired value. Alternatively the program stops when a specified time is reached. The program outputs the newly determined values in either situation. With the two-layer scenario, the average moisture content is used for this check. All the required known variables for the no-load are also needed for the under-load process. In addition, internal positioning of the drying shelves and also the initial crop variables must be known. The following initial conditions apply:

$M_{t=0} = M_0$ (or $M_{1,0} = M_{2,0} = M_0$); $RH_{dcin} = RH_a$;

$T_{dcin} = T_a$; $T_{cr,t=0} = T_a$ (or $T_{cr1,t=0} = T_{cr2,t=0} = T_a$)

The under-load iteration processes are described as follows:

1. Guess (initially; at time $t = 0$) the values of T_c, T_f, and T_p for the chimney, T_{dc}, and T_b for the drying chamber walls and base respectively. T_l, T_{top} and T_u are the guesses for the air temperature in the drying chamber with single layer. With two layers $T_{top,1}$ and $T_{top,2}$ are used instead of T_{top}; T_m is then guessed in addition to T_l and T_u.
2. Determine K_{roof} (the relationship between K_{roof} and the drying-chamber roof aingle is determined empirically, and this is explained in chapter 6) and T_{bot} (equation 4.51), or $T_{bot,1}$ and $T_{bot,2}$ for two layers (equations 4.51 and 4.62)
3. Calculate the following initial values
   - $T_{ch,i}$ (equation 4.54)
   - T_{out} (equation 4.23b)
   - ΔP_{cr} (equation 4.16)
4. Compute v_{dcin} and $\dot{m}$ (4.14)
5. Determine G_a; or $G_{a,1}$ and $G_{a,2}$ for two layers (4.46)
6. Repeat steps 5 to 11 of the no-load iterations for calculations on the chimney (referring to step 3 of the under-load instead of the no-load process).
7. Determine the coefficients for drying chamber heating (4.67)
8. Calculate the improved value of T_l as $T_{l,nw}$ (4.52)

9. Compare $T_{l,nw}$ to T_l; if the relative difference is greater than 0.01, replace T_l with $T_{l,nw}$ and repeat the processes from step 3, otherwise continue with the next step, with $T_{l,nw}$ in place of T_l.
10. Calculate T_{bot}; or $T_{bot,1}$ (4.51)
11. Determine H or H_1 (4.82, 4.81 and 4.78), RH (4.82, 4.81, 4.78, 4.76 and 4.83). Note; H is uniform across the crop bed at the start of the drying process. Also $\frac{\partial M}{\partial t} = 0$ at the start.
12. Calculate the improved value of T_{top} (or $T_{top,1}$) as $T_{top,nw}$ (or $T_{top1,nw}$), using (4.76 and 4.68 or 4.70)
13. Compare $T_{top,nw}$ (or $T_{top1,nw}$) to T_{top} (or $T_{top,1}$); if the relative difference is greater than 0.01, replace T_{top} ($T_{top,1}$) with $T_{top,nw}$ (or $T_{top1,nw}$) and repeat the processes from step 3, otherwise continue with the next step, with $T_{top,nw}$ (or $T_{top1,nw}$) in place of T_{top} (or $T_{top,1}$).
14. If two layers are used, then calculate the improved T_m as $T_{m,nw}$ (4.63), confirm T_m as with steps 8 and 9. and perform similar steps to 10 to 13 for layer 2, using the following equations
    - (4.62) for $T_{bot,2}$
    - (4.81 and 4.78) for H_2; with $H_{bot,2} = H_{top,1}$.
    - (4.74, 4.81, 4.78, 4.71) to calculate and confirm $T_{top,2}$.
15. Calculate the improved T_u as $T_{u,nw}$ (4.55)
16. Compare $T_{u,nw}$ to T_u; if the relative difference is greater than 0.01, replace T_u with $T_{u,nw}$ and repeat the processes from step 3, otherwise continue with the next step, with $T_{u,nw}$ in place of T_u
17. Calculate the improved T_b as $T_{b,nw}$ (4.57)
18. Compare $T_{b,nw}$ to T_b: if the relative difference is greater than 0.01, replace T_b with $T_{b,nw}$ and repeat the processes from step 3, otherwise continue with the next step, with $T_{b,nw}$ in place of T_b
19. Calculate the improved T_{dc} as $T_{dc,nw}$ (4.58); or (4.66) for the two-layer scenario
20. Compare $T_{dc,nw}$ to T_{dc}: if the relative difference is greater than 0.01, replace T_{dc} with $T_{dc,nw}$ and repeat the processes from step 3, otherwise continue with the next step, with $T_{dc,nw}$ in place of T_{dc}

21. Drying conditions are established. Output all the temperature and airflow values
22. Increase the current time by dt.
23. Determine the $RH_{f,cr}$ (4.83), M_e (4.80b), D (4.80a) and M (4.79) at current time for the single layer or two layers.
24. Compare the current M with the desired M: if the desired M is reached, then output the required values and stop. Otherwise compare the current time to the set-down time. Output the values and stop, if the set time is reached, else continue with the next step.
25. Calculate $\frac{\partial M}{\partial t}$ or $\left.\frac{\partial M}{\partial t}\right|_1$ and $\left.\frac{\partial M}{\partial t}\right|_2$ (4.74), $\frac{\partial H}{\partial z}$ or $\left.\frac{\partial H}{\partial z}\right|_1$ and $\left.\frac{\partial H}{\partial z}\right|_2$ (4.81a) and T_{cr} or $T_{cr,1}$ and $T_{cr,2}$ (4.69 or 4.72 and 4.73) at current time.
26. Determine the $T_{top,\ nw}$ or $T_{top1,nw}$ (4.76 and 4.68 or 4.70) and set to $T_{top.}$ For two layers calculate $T_{m,nw}$, T_{bot2} and T_{top2} and set them in place of their old values Determine T in the crop zone(s)
27. Repeat the processes from step 23.

CHAPTER 5 EXPERIMENTAL RESULTS

The results of various trials on the laboratory and field models of the CDSCD are presented and discussed in the following. The outcomes of the no-load and under-load trials (both conducted in the laboratory) are first discussed. This is followed by discussions of tests on the field model.

5.1 No-load trials

Table 5.1 shows an overview of ambient, inlet and exit air conditions of the dryer model in the various no-load trials. The temperature, relative humidity and velocity values shown in the table are the averages of those recorded over a steady-state period of 5 hours. To counteract the effect of the slightly changing external conditions, the rise of air temperature above ambient at various points of the dryer (i.e. the temperature difference between those of the points and the environment) are used for comparing the performance of the different configurations. For clarity of understanding, the figures have been represented in two sections. The air temperatures above ambient at different heights from the base of the dryer are shown in figures 5.1 to 5.3 for different inlet gaps of the same roof angles and in figures 5.4 to 5.6 for different roof angles of the same inlet gaps. Air temperatures in the drying chamber were measured at heights 6, 16, 26 and 49 cm respectively above the base, whilst those at heights 49, 84 and 109 cm represent the measuring points in the chimney. These heights correspond to the positions of the thermocouple probes that measure the air temperature in the CDSCD.

The velocity of air in the laboratory remained low at 0.01 to 0.02 m/s. Exit velocities are used to compare the airflow rates, as the exit areas remained the same for all the trials. The effect of the metal framework of the rig was significant, for the small size of the model. The frames caused shading of the inner surfaces of the dryer and offered additional resistance to the air flow. They also absorbed radiant energy to transfer some extra heat to the air.

	No Absorber		With Absorber								
	Test-set 1		Test-set 2								
	Inlet 70 mm		Roof 81^0			Roof 64^0			Roof 51^0		
	Roof 81^0	Roof 51^0	Inlet 70mm	Inlet 50mm	Inlet 30mm	Inlet 70mm	Inlet 50mm	Inlet 30mm	Inlet 70mm	Inlet 50mm	Inlet 30mm
Ambient air temperature (^{0}C)	21.83	23.50	23.00	22.33	21.00	22.17	23.83	21.67	23.50	24.67	22.17
Dryer exit air temperature (^{0}C)	26.83	29.67	31.33	30.83	31.83	29.50	31.50	31.33	30.83	32.33	31.00
Inlet air relative humidity (%)	57.17	41.50	42.17	49.33	68.67	51.67	50.67	45.00	42.33	32.83	37.00
Dryer exit air relative humidity (%)	38.17	29.67	26.00	29.00	41.50	34.17	34.50	28.83	24.83	19.50	22.83
Ambient air velocity (m/s)	0.02	0.02	0.01	0.01	0.01	0.02	0.02	0.02	0.01	0.03	0.02
Dryer inlet air velocity (m/s)	0.14	0.16	0.18	0.23	0.34	0.19	0.24	0.36	0.20	0.26	0.37
Dryer exit air velocity (m/s)	0.39	0.40	0.45	0.44	0.39	0.49	0.45	0.40	0.52	0.47	0.40

Table 5. 1 Overview of ambient, inlet and exit conditions of dryer trials with various configurations

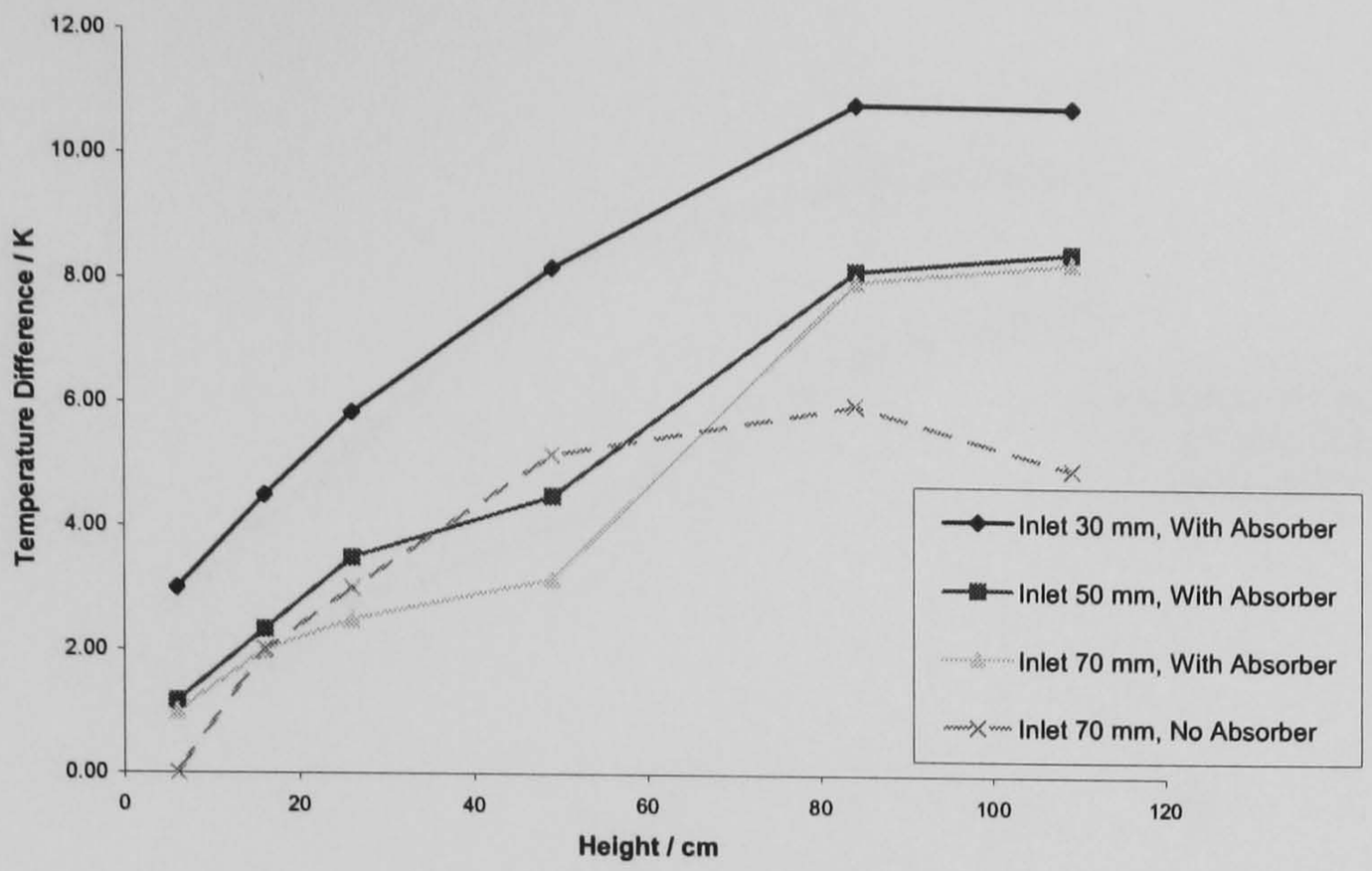

Figure 5.1 **Air temperature above ambient vs. Height, for Roof 81^0 with different inlet gaps; No Load**

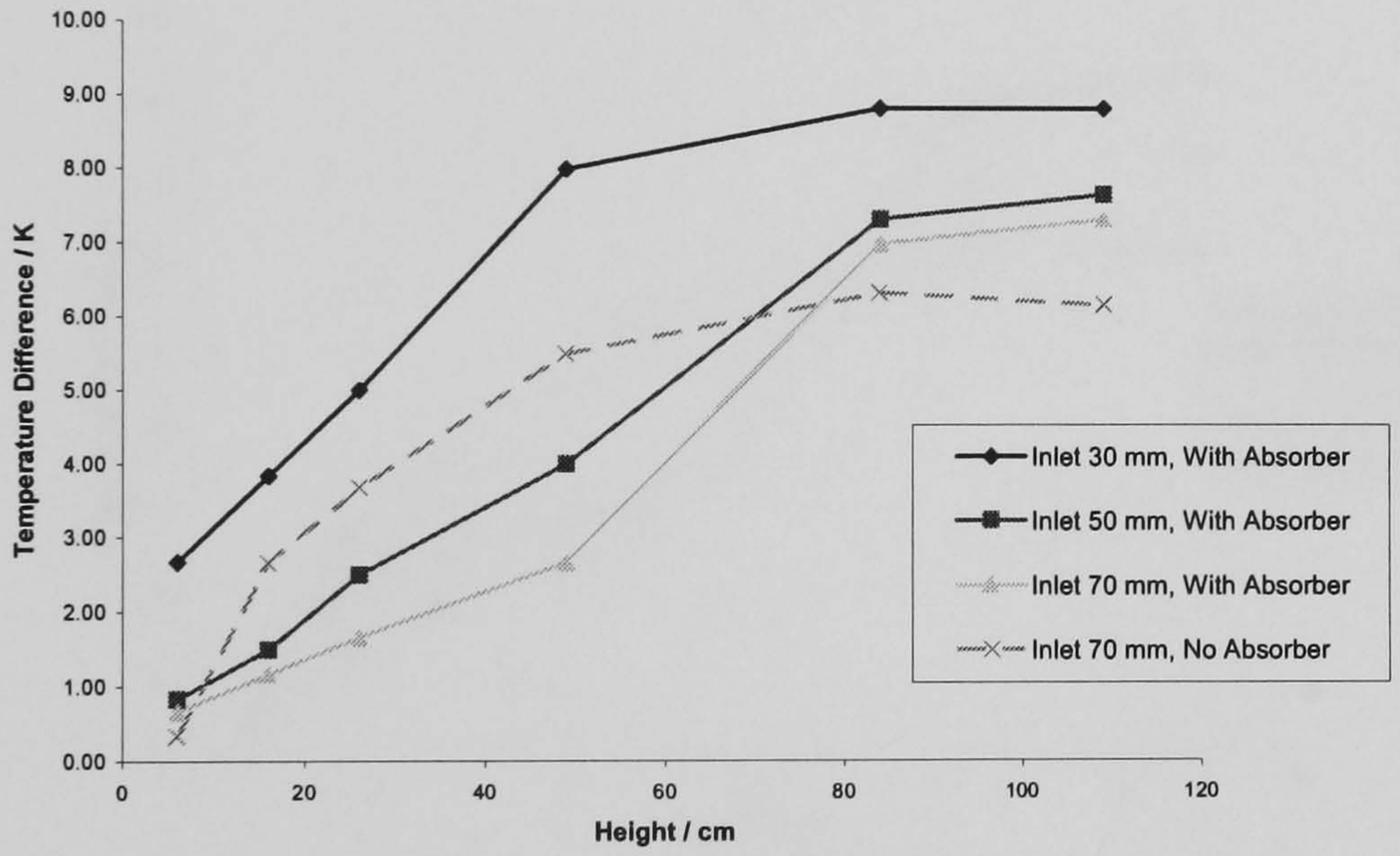

Figure 5.2 **Air temperature above ambient vs. Height, for Roof 51^0 with different inlet gaps; No Load**

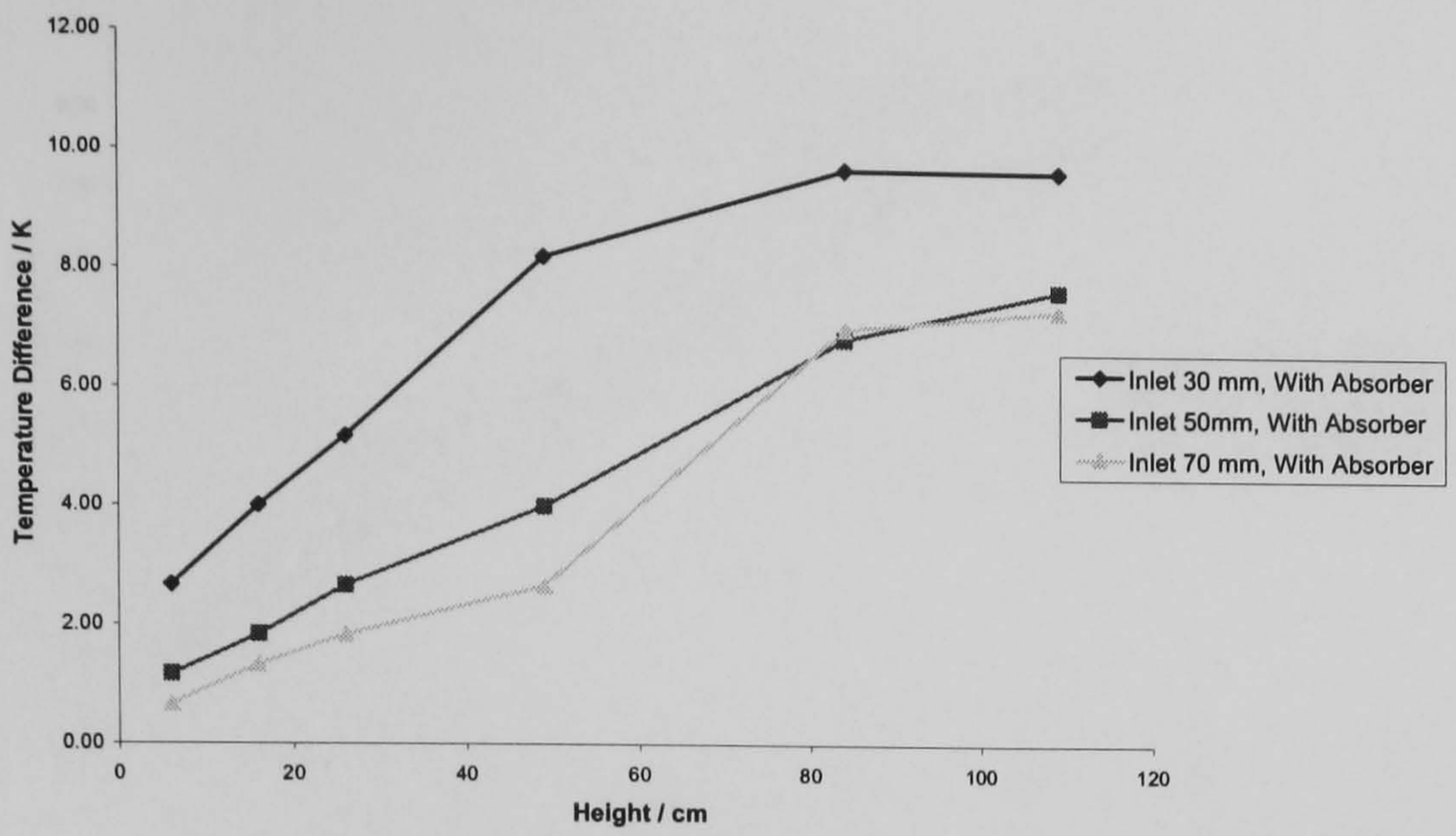

Figure 5.3 **Air temperature above ambient vs. Height, for Roof 64^0 with different inlet gaps; No Load**

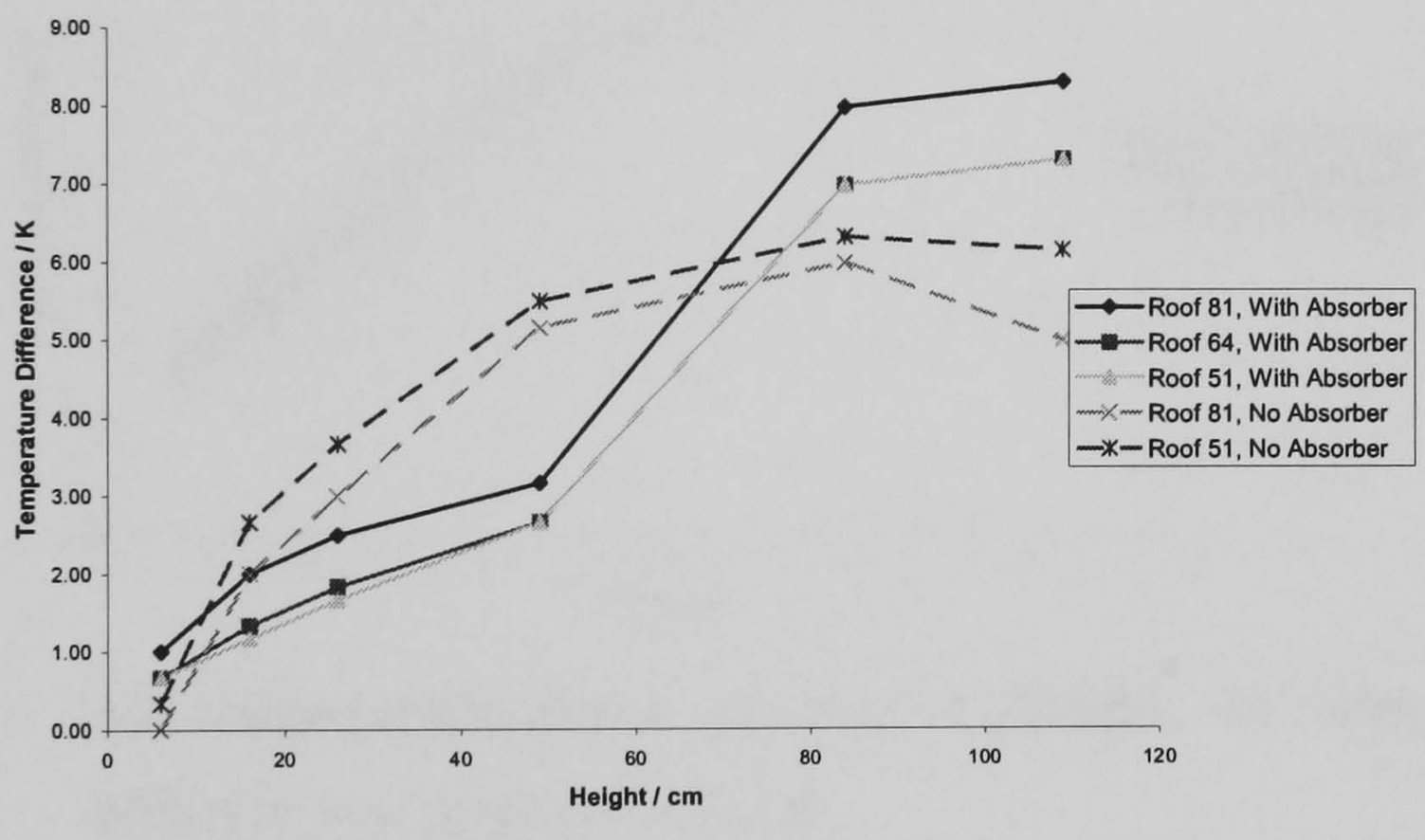

Figure 5.4 **Air temperature above ambient vs. Height, for Inlet 70 mm with different roof angles; No Load**

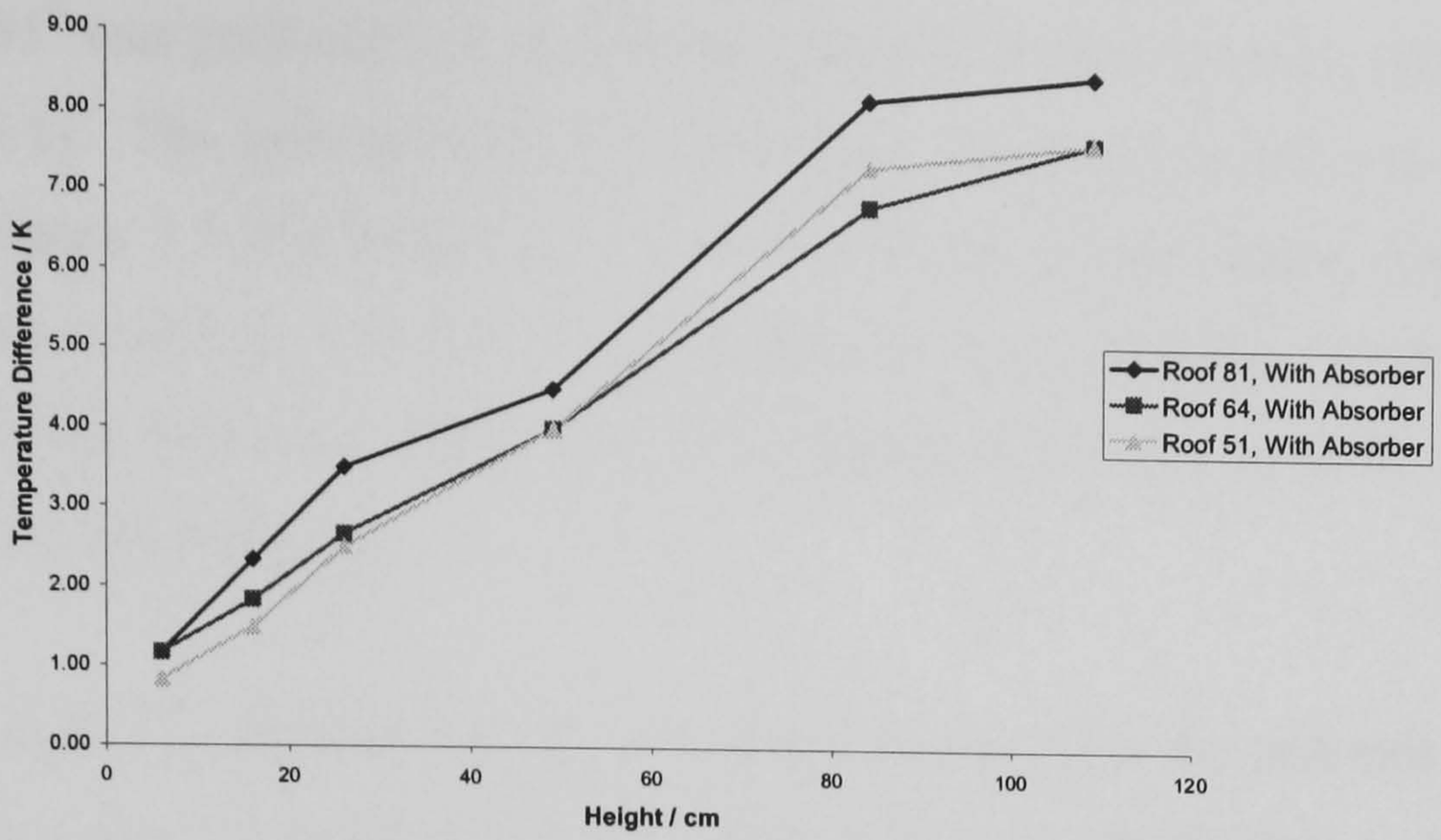

Figure 5.5 **Air temperature above ambient vs. Height, for Inlet 50 mm with different roof angles; No Load**

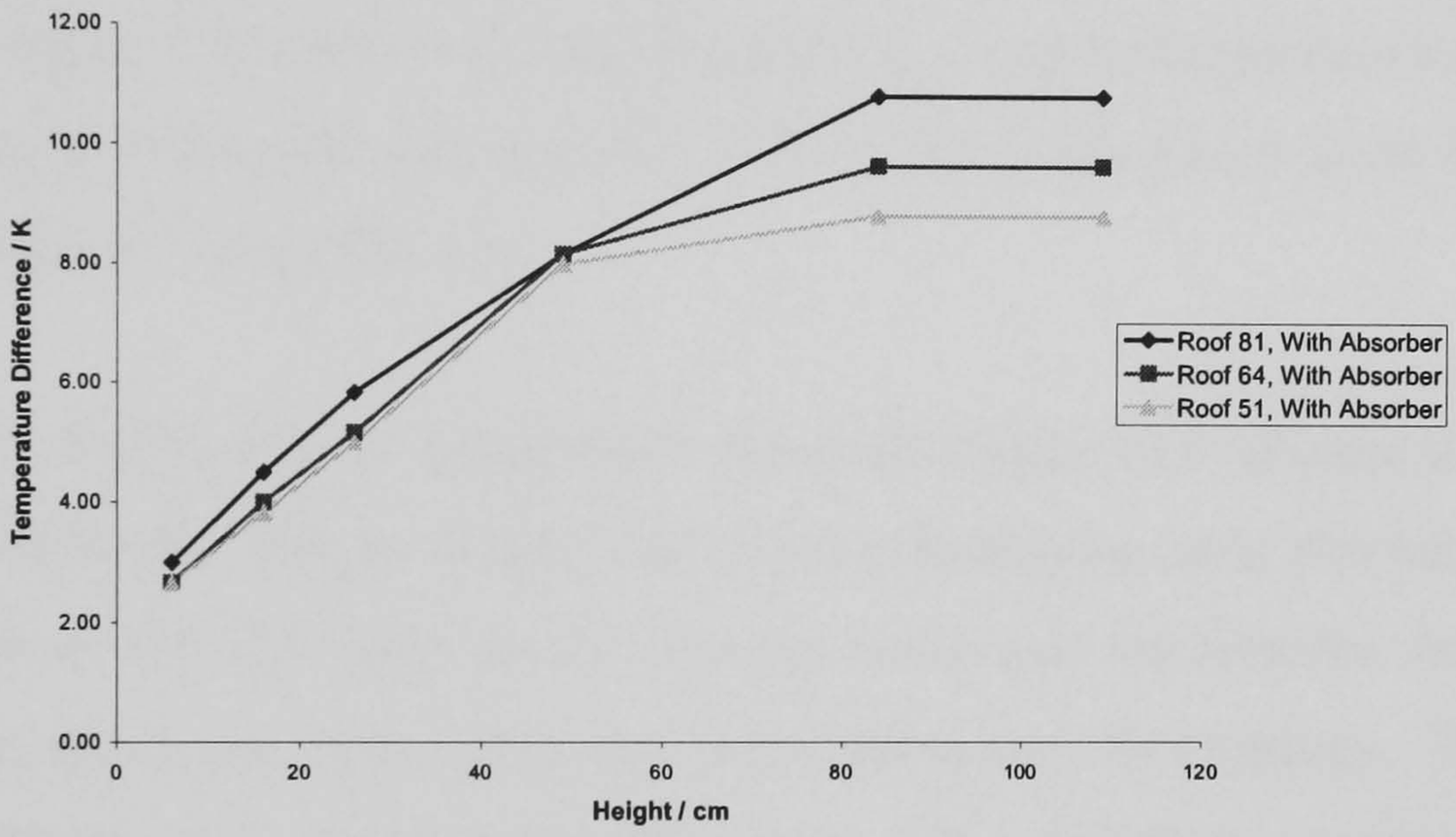

Figure 5.6 **Air temperature above ambient vs. Height, for Inlet 30 mm with different roof angles; No Load**

5.1.1 Test-set 1: No-load results with the normal chimney

As defined in chapter 3, the term 'normal chimney' refers to the chimney with all-round glazed walls (i.e. with no absorber in any wall). It is also recalled, that this trial was just to obtain results for comparison with the performance of the solar chimney (i.e. the chimney with absorber in the back wall). So, two trials were performed in this test-set, both with inlet gap 70 mm. One trial had roof angle of 81^0, whilst the other had 51^0 (see figures 5.1 and 5.2). In the absence of a chimney absorber, there was still a certain

amount of air heating in the chimney by the chimney glazing and frames. The test with roof angle 81^0 was performed in an average ambient relative humidity (RH) of 57.17 % (see table 5.1). The inlet air velocity was 0.14m/s and that of exit was 0.39 m/s. As seen from figure 5.1, the heights 6, 16, 26 and 49 cm (of the drying chamber) had air temperature rise of 0, 2, 3 and 5.17 ^{0}C respectively above ambient. In the chimney, the temperature rise increased from 5.17 ^{0}C at height of 49 cm to 6 ^{0}C at 84 cm and decreased to 5 cm at the exit.

With roof angle 51^0, the RH was 41.5 %, inlet velocity 0.16 m/s and exit velocity 0.40. The slightly higher velocity of the test with roof 51 is attributable to the lower roof angle with respect to the vertical plane. The rise of temperature at various points in the drying chamber were 0.33, 2.67, 3.67 and 5.5 ^{0}C in that order, whilst those in the chimney changed from 5.5 ^{0}C (height 49 cm) to 6.33 ^{0}(height 84 cm) and then reduced to 6.17 ^{0}C (figure 5.2). However, each height had a higher temperature rise than that of a similar height in the trial with roof 81^0. This could be due to the lower RH of the trial with roof angle 51^0 (see table 5.1).

There was an increase in air temperature along the height up to around the midpoint of the normal chimney. The air temperature started decreasing from this height. Thus the heat flow from the all-round glazed chimney walls and the metallic frames was not enough to maintain the temperature rise from midway up the chimney. The inadequate chimney heating gave rise to low airflow rate. The air left the drying chamber (i.e. height 49) with 5.5 ^{0}C of temperature above ambient.

5.1.2 Test-set 2: No-load results with the solar chimney and the various configurations of the drying chamber

As defined earlier the solar chimney refers, in the context of this work, to the chimney with absorber in the back wall with the other walls glazed. Beside the comparison with the performance of the normal chimney, experimental data were also required of the various drying-chamber configurations with the solar chimney for validation of the simulation code. Therefore a total of 9 trials were performed; for 3 different angles, each with 3 different inlet gaps.

5.1.2.1 Roof angle 81^0, with solar chimney

When the normal chimney of roof 81^0 was replaced with a solar chimney with the inlet gap still at 70 mm, there was a much improved chimney air heating, although the height contribution to temperature rise reduced after midway up the chimney. As seen in figure 5.1, the temperatures above ambient in the chimney were 3.17 ^{0}C at the height of 49 cm through 8 ^{0}C at 84 cm to 8.33 ^{0}C at the top. The improved chimney heating gave rise to a higher air flow (with inlet velocity of 0.18 m/s and exit velocity of 0.45 m/s). This higher airflow caused a reduction of temperature in the drying chamber, so that the air left the chamber with reduced rise of 3.17 ^{0}C at height 49 cm (as compared to 5.17 ^{0}C of roof 81^0 with the normal chimney).

When the inlet gap was reduced to 50 mm, less amount of air was allowed into the drying chamber, as observed by Ong and Chow (2003). Then the exit velocity reduced to 0.44 m/s. With a smaller amount of air passing through the system to be heated in a given time by the same irradiation and radiant energy absorbers, the temperatures at various heights were higher than those at the same heights with inlet 70 mm. The temperatures above ambient were 1.17 ^{0}C, 2.33 ^{0}C, 3.50 ^{0}C, 4.50 ^{0}C, 8.17 ^{0}C and 8.50 ^{0}C at heights 6 cm, 16 cm, 26 cm, 49 cm, 84 cm and 109 cm respectively (figure 5.1).

With the inlet gap 30 mm, the inlet air was further restricted and the exit velocity was 0.39 m/s. Hence the temperatures recorded at all the heights in the structure were higher than similar points in those with larger inlet gaps. Temperatures recorded at heights 6 cm, 16 cm, 26 cm, 49 cm, 84 cm and 109 cm were 3.00 ^{0}C, 4.50 ^{0}C, 5.83 ^{0}C, 8.17 ^{0}C, 10.83 ^{0}C, and 10.83 ^{0}C in that order above ambient (figure 5.1). The higher RH of 68.67 % did not seem to have any significant effect on the temperature rise in the dying chamber, due to the reduced quantity of air being heated in the system in a given time.

In all the trials the increase in temperature with height reduced in the upper half of the chimney. With inlet 70 mm there was less temperature rise in the drying chamber (with the air leaving the chamber at 3.17 ^{0}C) in the trials than that with the normal chimney,

due to higher airflow rate. Higher air heating occurred in the chamber when the inlet gap was reduced to limit the amount of air entering the dryer. The air temperatures at exit of the drying chamber were 4.50 ^{0}C and 8.17 ^{0}C for inlet 50 and inlet 30 mm respectively.

5.1.2.2 Roof angle 64^0, with solar chimney

With a lower roof angle (64^0) the flow velocities observed were higher than those of roof angle 81^0 of corresponding inlet and exit configurations (see table 5.1). With inlet 70 mm, the inlet and exit velocities were 0.19 and 0.49 m/s respectively, higher than those of roof 81^0 with inlet 70 mm. This could be attributed to lower pressure resistance at roof angle 64^0, compared to that of angle 81^0. The temperatures above ambient were therefore lower (0.67, 1.33, 1.83, 2.67, 7.00 and 7.33 ^{0}C at heights 6, 16, 26, 49, 84 and 109 cm respectively, as seen in figures 5.3 and 5.4).

The amount of air entering the drying chamber was again restricted in the case of the inlet 50 mm and a lower exit velocity of 0.45 m/s was observed. But this was higher than that of roof angle 81^0 with the same inlet gap (50 mm), due to the lower roof angle with respect to the vertical. The temperatures at various heights were 1.17, 1.83, 2.67, 4.00, 6.83 and 7.67 ^{0}C in that order above ambient (figure 5.3). Thus almost all the temperatures were higher than those of corresponding points in inlet 70 mm (figure 5.3) but lower than those of similar points in roof 81^0 with inlet 50 mm (figure 5.5).

With inlet 30 mm, the exit velocity (0.40 m/s) was higher than for a similar inlet gap of roof 81^0 (table 5.1) due to lower resistance to air flow. This value was however smaller than in roof 64^0 with inlet 50, as the smaller inlet gap further restricted the airflow into the dryer. The temperatures measured above ambient at various points were 2.67, 4.00, 5.17, 8.17, 9.67, 9.67 ^{0}C at heights 6, 16, 26, 49, 84 and 109 cm in that order (see figure 5.3). These values were clearly higher than in inlet 50 and 70 mm but lower than in roof 81^0 of a similar inlet gap (figure 5.6) due to differences in the airflow.

In all the 3 inlets gaps of roof 64^0, the general trends of the air temperature rise were similar to those of roof 81^0, with the temperature dependency on the height reducing

after midway up the chimney. The lowest rise of temperature through the drying chamber (at height 49 cm) was again observed with the inlet gap 70 mm, which was 2.67 ^{0}C. Those of inlet gaps 50 and 30 mm were 4.00 and 8.17 ^{0}C respectively.

5.1.2.3 Roof angle 51^0, with solar chimney

With lowest angle to the vertical and therefore least resistance to airflow, roof 51^0 with inlet 70 mm had highest exit velocity (0.52 m/s) of all the trials. The inlet velocity of 0.20 m/s was also higher than its inlet counterparts of roof 64^0 and roof 81^0, as shown in table 5.1. The high airflow gave rise to lowest temperatures above ambient as 0.67, 1.17, 1.67, 2.67, 7.00 and 7.33 ^{0}C at heights 6, 16, 26, 49, 84 and 109 cm in that order, as seen in figures 5.2 and 5.4. The air temperature remained the same as that of roof 64^0 from the exit of drying chamber to the top of the chimney.

The trial of roof 51^0, inlet 50 mm had 0.47 m/s as exit velocity, which is lower than that of inlet 70 mm due to the air restriction at inlet. But both the inlet and exit velocities were higher than those of the roofs with angle 64^0 and 81^0 of similar inlet gaps, because of the lower pressure resistant to the airflow. The air temperatures at various points were 0.83, 1.50, 2.50, 4.00, 7.33 and 7.67 ^{0}C for this trial, as seen from figure 5.2. These were higher than those at similar points for inlet 70 mm (figure 5.2), but slightly lower than those of most points of roof angle 64^0 and a bit more lower than those of roof angle 81^0 of the same inlet gap (figure 5.5).

The air flow reduced further, with the smaller inlet gap of 30 mm, resulting in an exit velocity of 0.40 m/s. This was not different from that of roof 64^0 of the same inlet gap, but the inlet velocity of 0.37 m/s was higher. The temperatures recorded above ambient at heights 6, 16, 26, 49, 84 and 109 cm were 2.67, 3.83, 5.00, 8.00, 8.83 and 8.83 ^{0}C respectively (figure 5.2). Again, these were higher than those of the trials of higher inlets with the same roof angle (figure 5.2) but lower than those of higher roof angles with similar inlet gaps (figure 5.6). Thus with lower mass flow of air, the temperature rise is higher, for a given heat transfer.

5.1.3 Test-set 3: No load with different angles of incidence

Table 5.2 compares the data obtained at different angles of incidence of the lamps. The maximum exit velocity of 0.52 m/s was measured at angle of incidence $22½^0$. There was a marked airflow reduction at higher angles of incidence.

The whole system could be considered as two chimneys connected in series; performing very well when the two separate ones gave their optimum performance. In the event that one did not perform well, it resisted the performance of the other and, therefore, the whole system. At low angles of incidence, the lamps were directed further towards the drying chamber. The air was then heated much more in the drying chamber and less in the upper main chimney, as compared to that of incidence angle $22½^0$ (see figure 5.7). The drying chamber, with the base absorber then performed as a heated, convergent chimney. For these lower angles of incidence the upper, rectangular chimney then did not receive enough irradiation. It therefore functioned almost like a normal, unheated chimney, so that there was a slight airflow reduction in the structure.

Angle of incidence	15^0	$17½^0$	20^0	$22½^0$	25^0	$27½^0$	30^0
Ambient air temperature (^{0}C)	23.67	23.67	23.17	23.50	22.67	22.67	21.83
Dryer exit air temperature (^{0}C)	30.17	30.33	31.17	30.83	32.17	32.83	33.67
Inlet air relative humidity (%)	42.33	46.17	50.17	42.33	55.17	42.17	53.17
Dryer exit air relative humidity (%)	28.67	31.33	32.83	24.83	33.00	21.50	27.17
Ambient air velocity (m/s)	0.02	0.02	0.02	0.01	0.01	0.02	0.02
Dryer inlet air velocity (m/s)	0.20	0.19	0.19	0.20	0.19	0.18	0.12
Dryer exit air velocity (m/s)	0.47	0.46	0.45	0.52	0.46	0.43	0.41

Table 5. 2 Overview of ambient, inlet and exit conditions of dryer trials with different angles of incidence

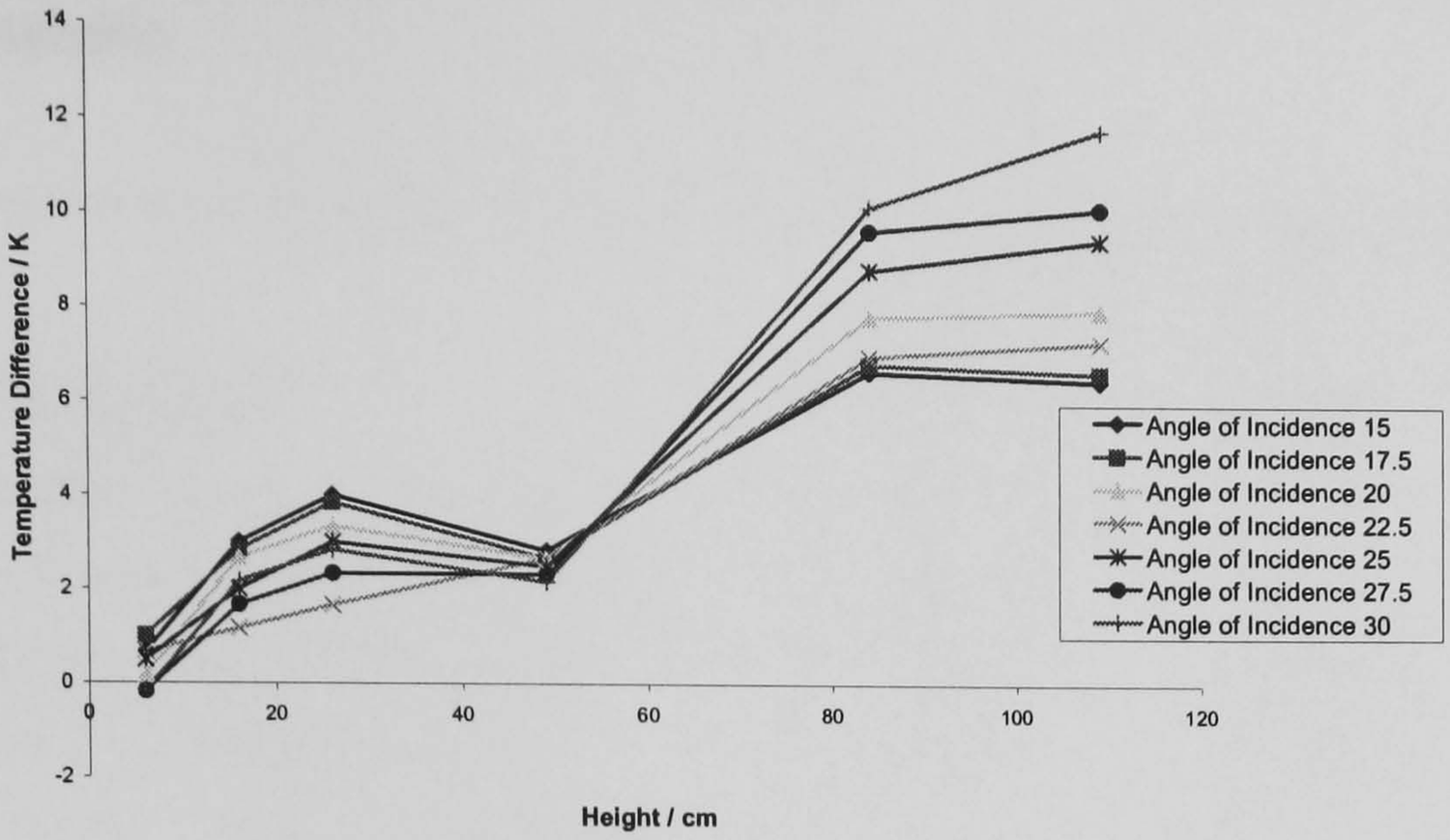

Figure 5.7 Air temperature above ambient vs. Height for different angles of incidence; No Load

With higher angles of incidence, the irradiation was directed more towards the chimney than towards the drying chamber. The drying chamber received less irradiation and the air temperature at the bottom (height 6 cm) fell slightly below ambient (see figure 6). This may be due to the sudden change of air velocity at entry of the chamber, causing a fall of temperature. There was not much heat transfer at this level to keep the temperature above atmospheric. With the drying chamber receiving less heat, it behaved as a massive block of resistance to the airflow at the entry to the main chimney above. This may explain the significant flow reduction when more energy was directed to the main chimney and less to the drying chamber. The flow reduction then caused a temperature rise in the middle part of the chamber, which is visible in figure 5.7. It could then be said that, of all the set angles, the angle $22½^0$ was the angle of incidence from the lamps for best performance of both the chimney and the drying chamber.

5.1.4 Test-set 4: The temperature profile of the drying chamber

The results of test-set 4, indicating the temperature profile of the drying chamber for roof angle 51^0, inlet 70 mm, are given in table 5.3. The upper part of the drying-chamber roof had the highest mean temperature of 38.33 ^{0}C, followed by base of the chamber (28.33 ^{0}C) and the bottom part of the roof (28.33 ^{0}C). The air temperatures at the bottom, middle and top of chamber are those measured at heights 6 and 16 and 26

cm respectively. The temperatures of the side walls of the chamber were only slightly above atmospheric

	Temperature / ^{0}C	Temp. above ambient / K
Ambient air temperature	22.17	0.00
Drying chamber base (floor) temperature	32.50	10.33
Drying chamber air temperature; bottom	22.33	0.17
Drying chamber air temperature; middle	23.33	1.17
Drying chamber air temperature; top	24.00	1.83
Drying chamber roof temperature; bottom	28.33	6.17
Drying chamber roof temperature; top	38.33	16.17
Drying chamber back wall temperature; bottom	23.17	1.00
Drying chamber back wall temperature; top	23.33	1.17
Drying chamber side wall temperature; bottom	22.33	0.17
Drying chamber side wall temperature; top	22.33	0.17

Table 5.3 The temperature profile of the drying chamber

5.2 Under load trials

The results overview of various data obtained from the under-load trials are plotted against the drying time in figure 5.8. to figure 5.26. Figure 5.8 (a to c) compares the dryer inlet velocities of a given inlet gap for different roof angles. Figures 5.9 to 5.14 show the variation of ambient relative humidities (RH), moisture contents, and drying rates in that order. Each graph is plotted first for a given inlet gap and different roof angles, and then for a given roof angle and different inlet gaps. The variations of temperature above ambient with height in the dryer are also compared in figures 5.15 to 5.20, for each drying day. Figures 5.21 to 5.26 compare the performances of different loading arrangements (crop size, crop mass and shelf position) with that of the standard arrangement (defined later in context). The time axis has 0 to 7 hours for the first day of drying, 7 to 14 hours for the second day and 14 to 21 hours for the third day. Each

drying trial ended on the morning of the fourth day. The night performance of the dryer was determined as the difference between the MC at close of the day and that on the following morning (just at the start of the following day's trial). The results of the trials are discussed in the following sections.

5.2.1 Test-set 5: Drying with normal chimney

Each of the two trials performed in test-set 5 (with the normal chimney and inlet gap of 70 mm) are discussed in this section. The first trial had roof angle of 81^0 to the vertical plane (close to that of a cabinet dryer). The other trial was with a lower roof angle of 51^0.

5.2.1.1 The normal chimney with roof angle 81^0

On each day of the drying process, the inlet velocity of dryer with the normal chimney and roof angle 81^0 increased from around the ambient value of 0.01 to 0.02 m/s to stay around an average value of 0.12 m/s, as shown in figure 5.8. The average values fell below that of the no-load trial of the same dryer configuration. This may be due to resistance from the drying shelf, as suggested by Ekechukwu and Norton (1997).

The drying process began with cassava of moisture content (MC) 202 %, dry basis (d.b.), as seen in figures 5.11a and 5.12a. The first day started with an ambient relative humidity (RH) of 47 % (figure 5.9a and 5.10a). The RH then fell steadily in the first five hours to 40 % and rose to 42 % by close of the day. The drying rate stayed around 0.063 $kg_w/(kg_s.h)$ for most of the day (see figures 13a and 14a). Day 1 ended with 161 % (d.b.) MC. The cassava looked very brownish at this time, apparently due to the temperature rise of the crop lowering the crop quality in the high MC range, as explained in the literature review. During the night, the RH increased from 42 % at the end of day 1 to 56 % on the morning of day 2. By the morning of day 2, the MC had dropped to 127 % (d.b.). This drop in MC is attributable to self drying of the system with some extra energy stored during the first day when the lamps were on.

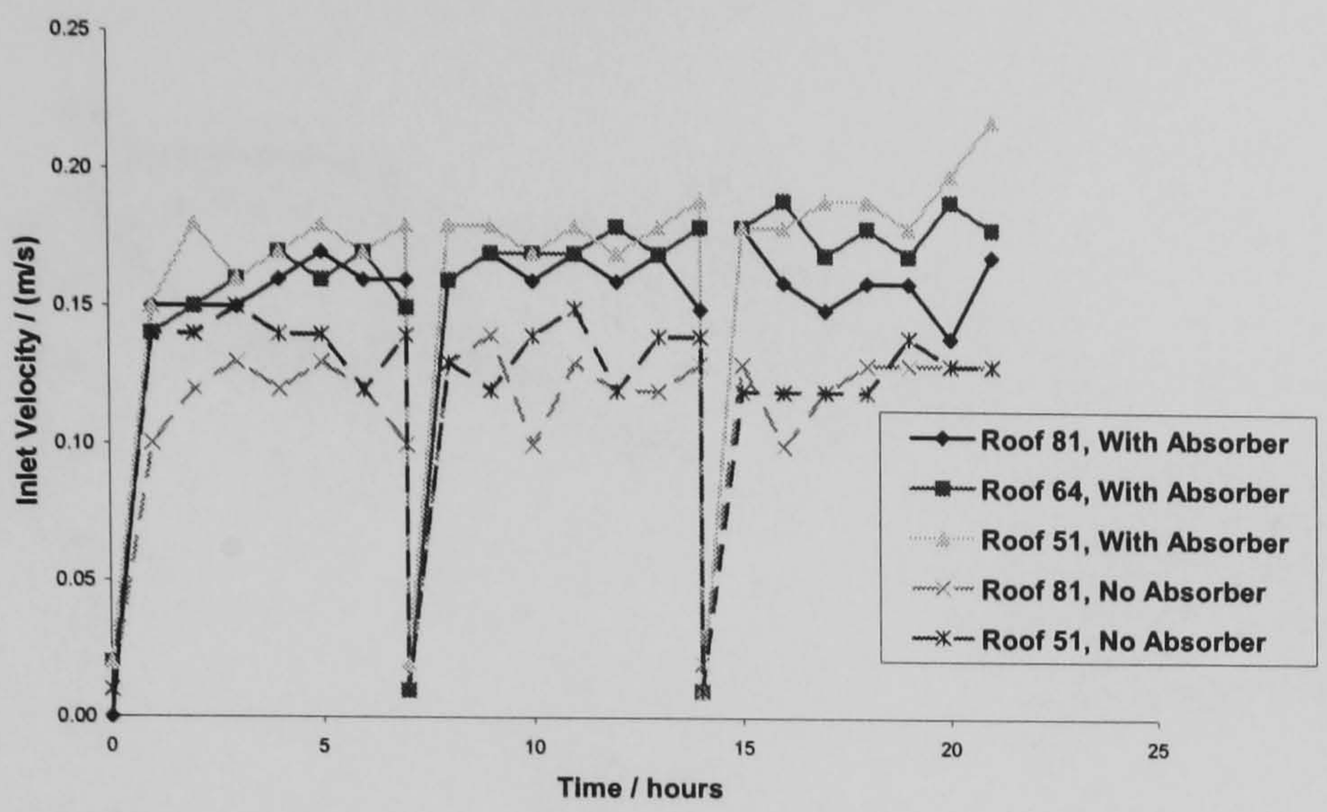

a) Inlet gap 70 mm

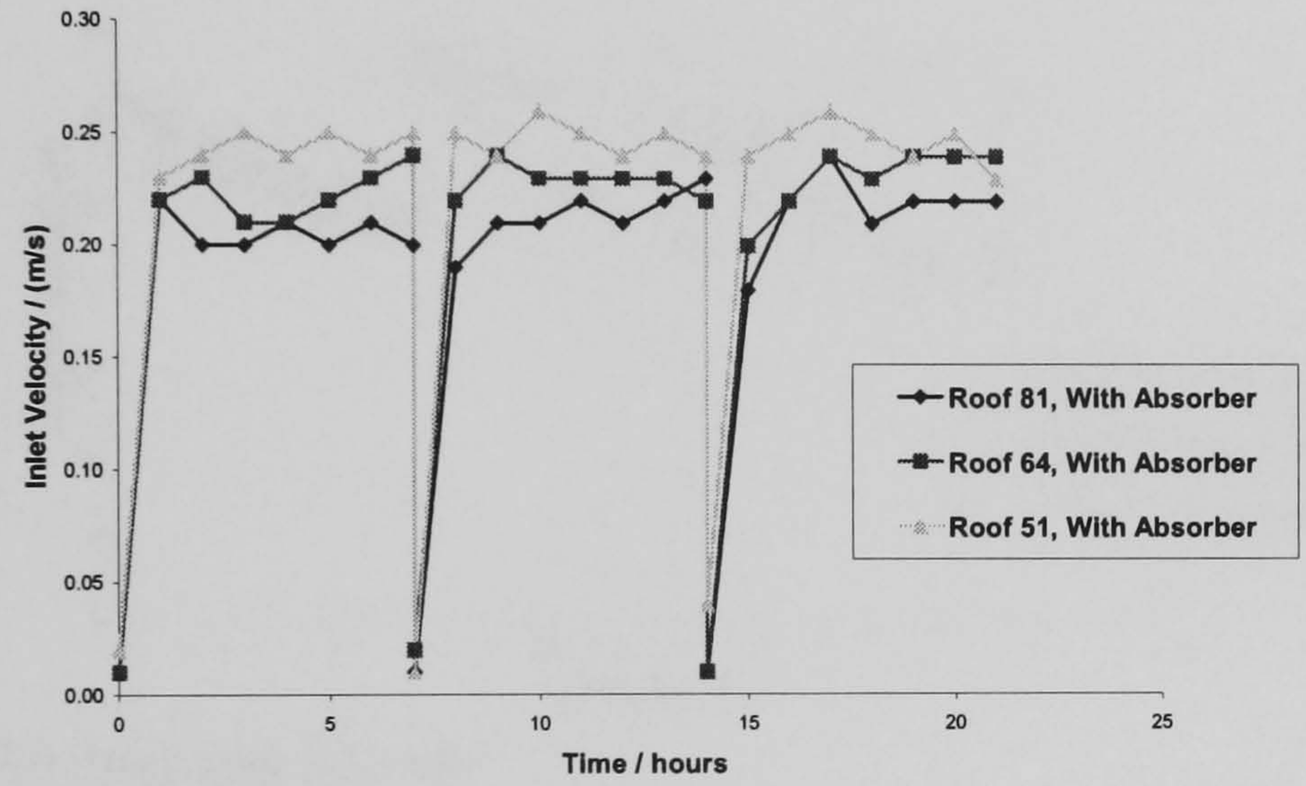

b) Inlet gap 50 mm

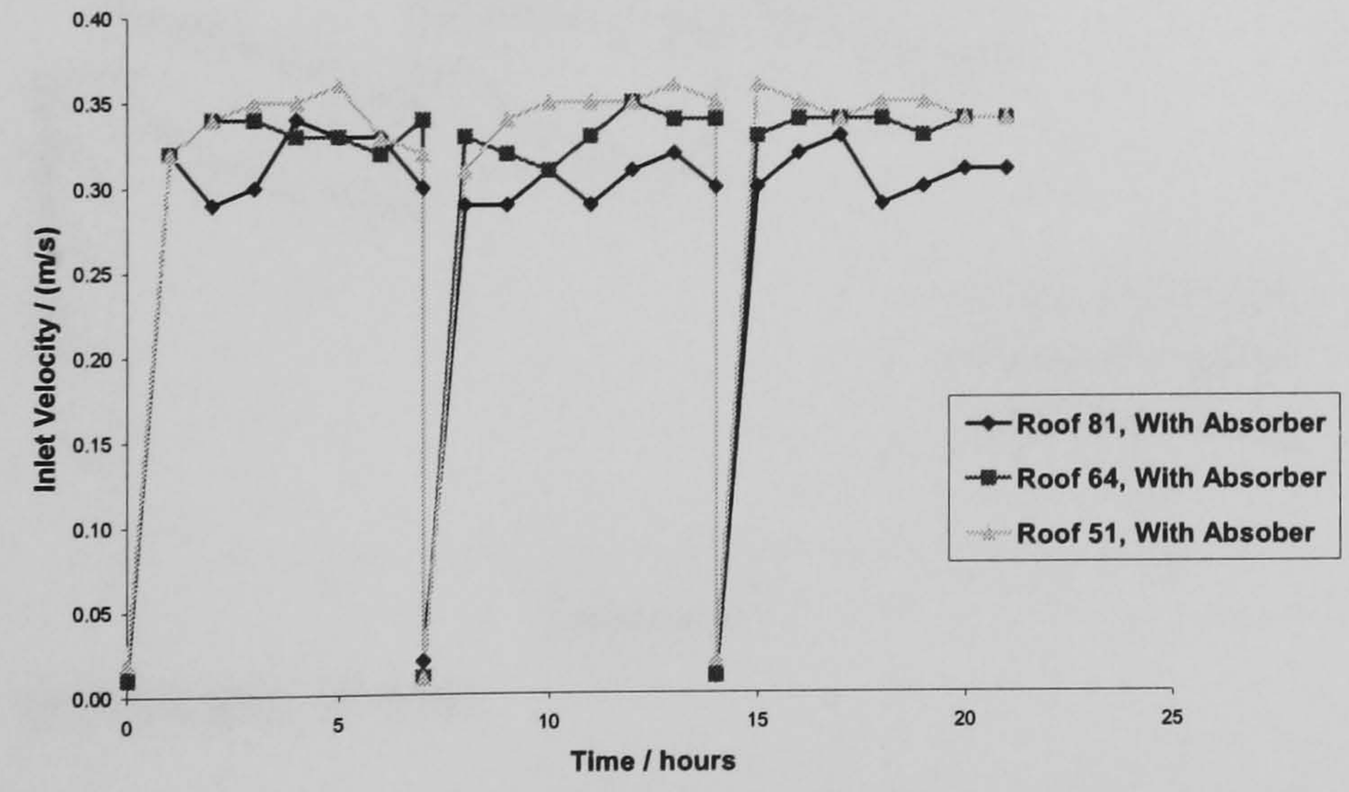

c) Inlet gap 30 mm

Figure 5.8 Inlet velocity vs. drying time, for a given Inlet Gap; Under load

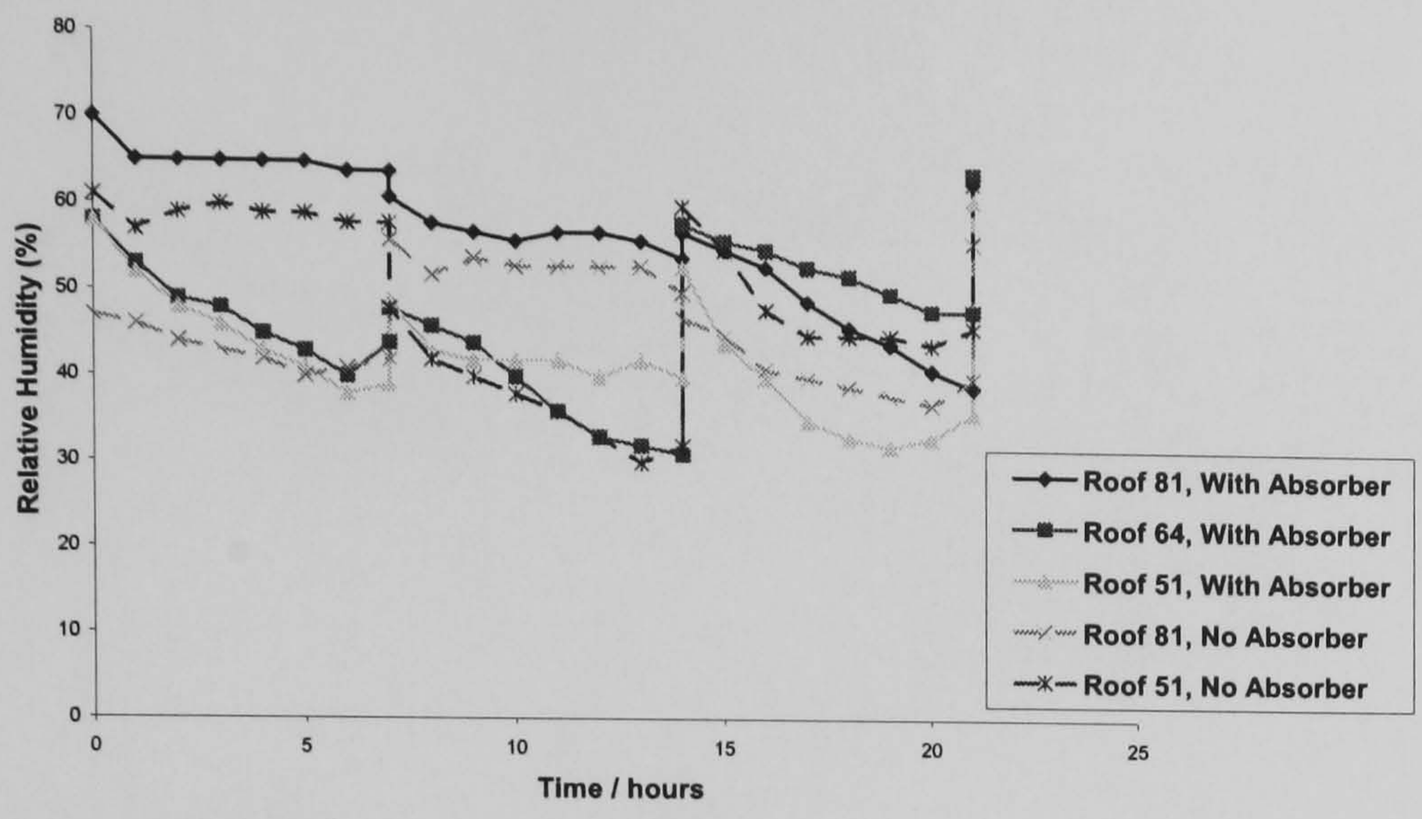

a) Inlet gap 70mm

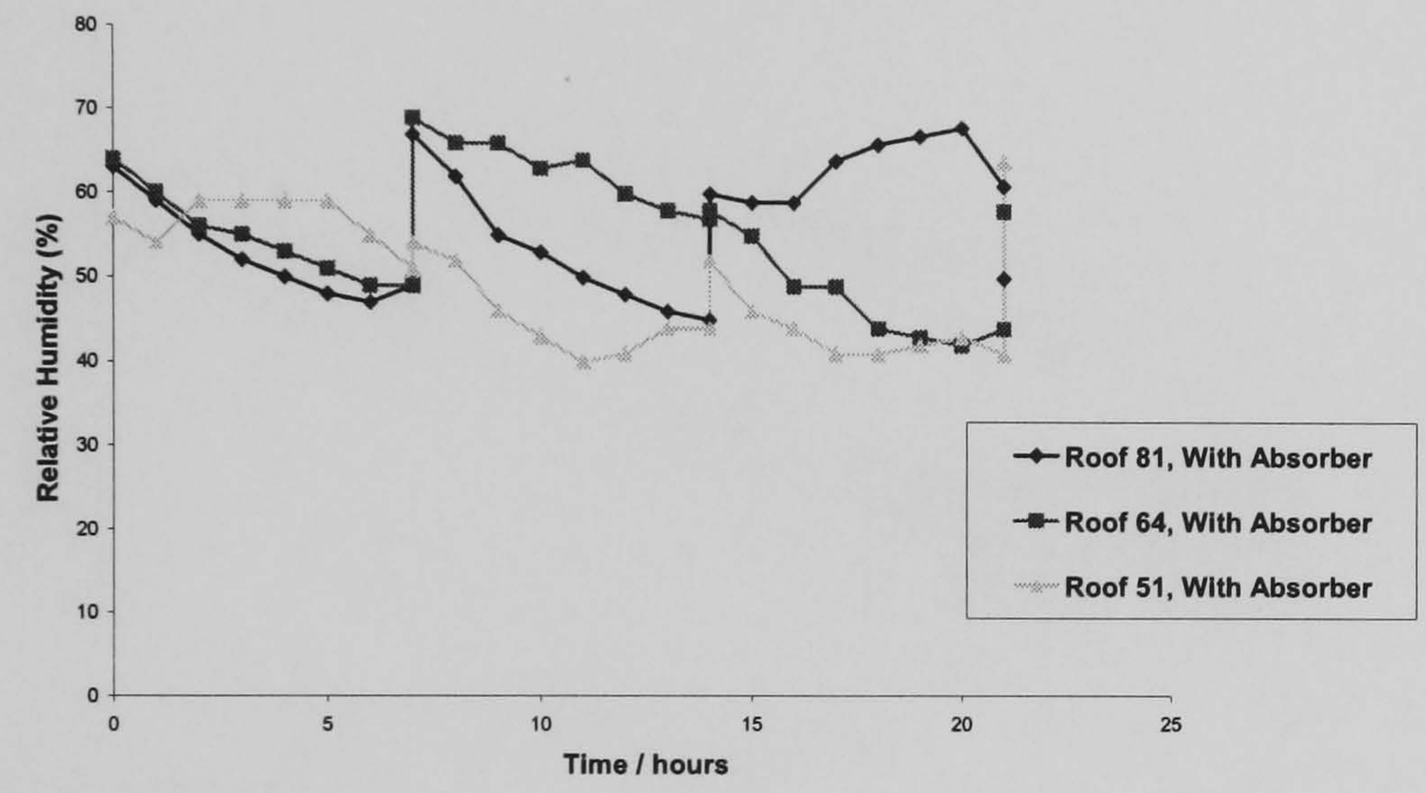

b) Inlet gap 50 mm

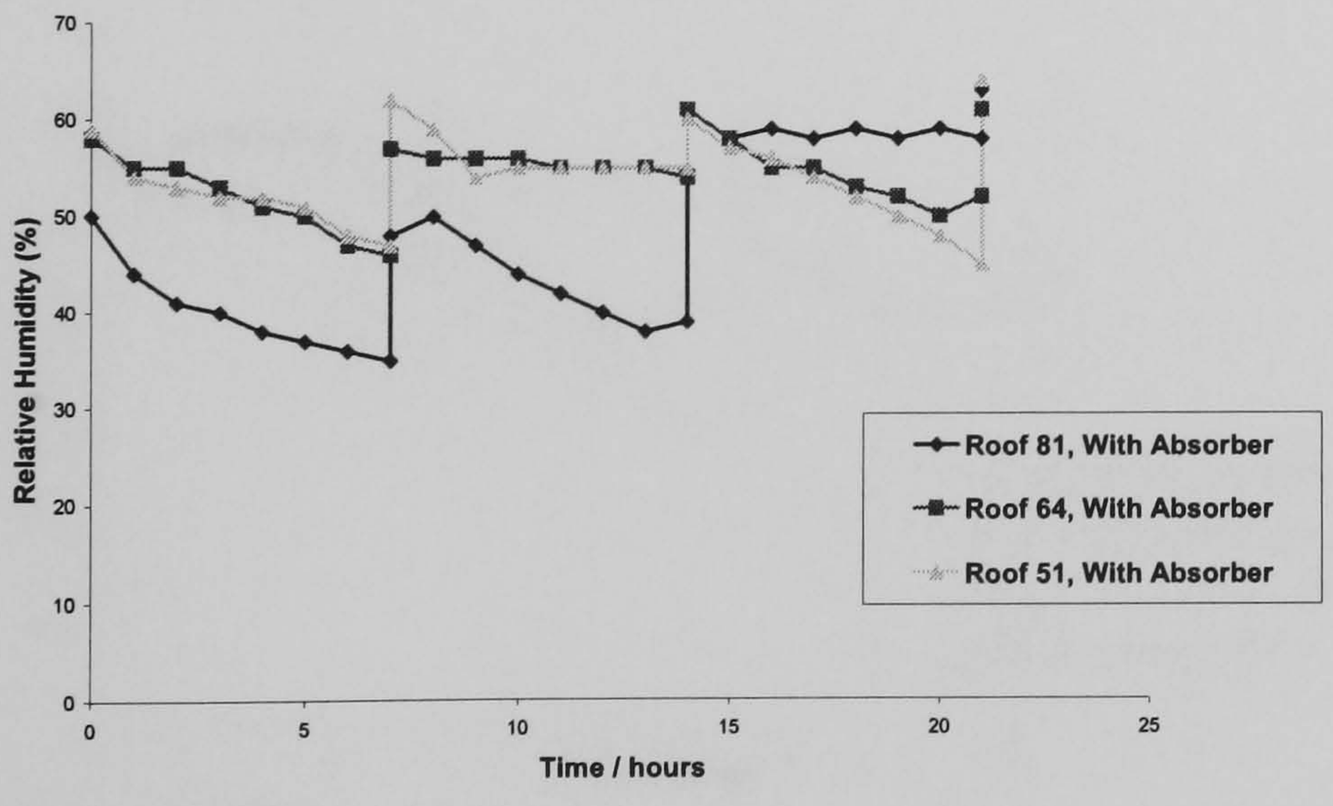

c) Inlet gap 30 mm

Figure 5.9 Ambient RH vs. Drying time for, a given Inlet Gap; Under load

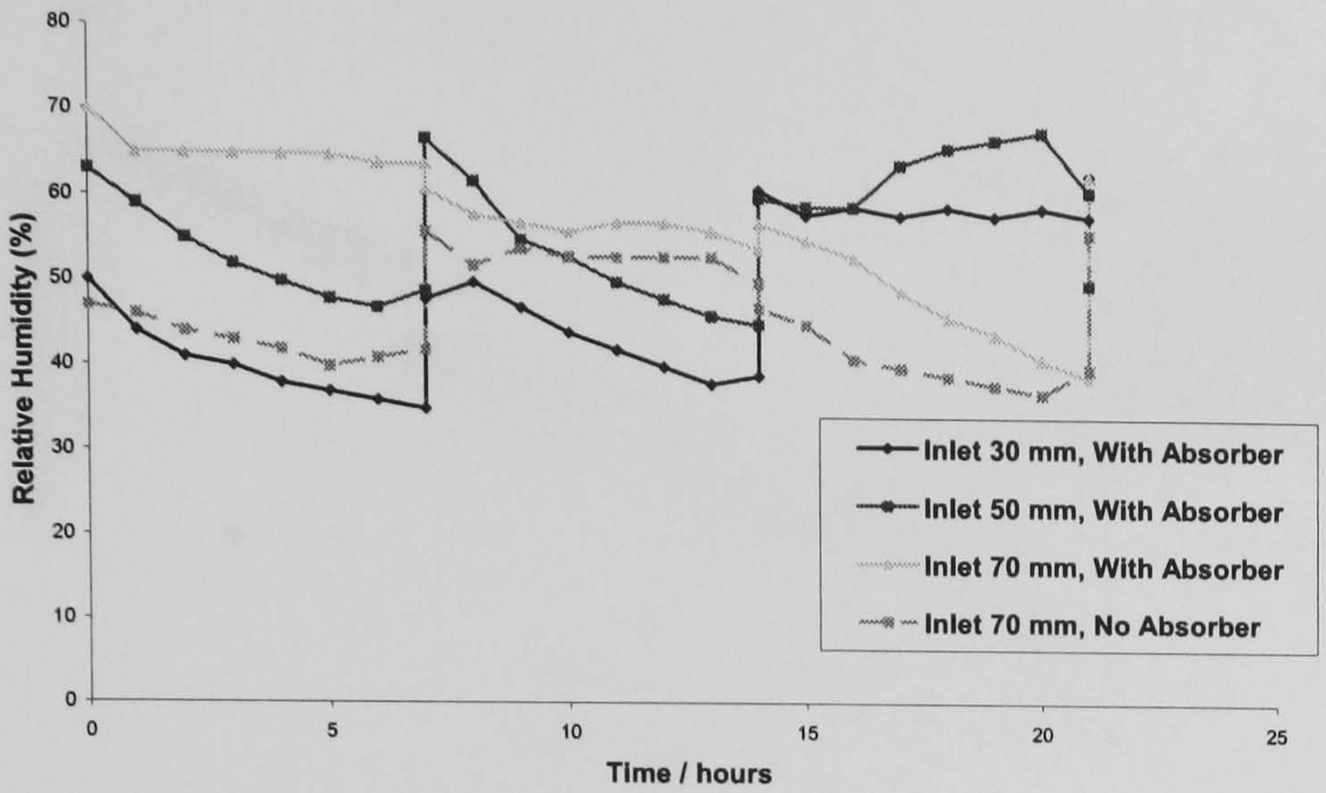

a) Roof 81^0

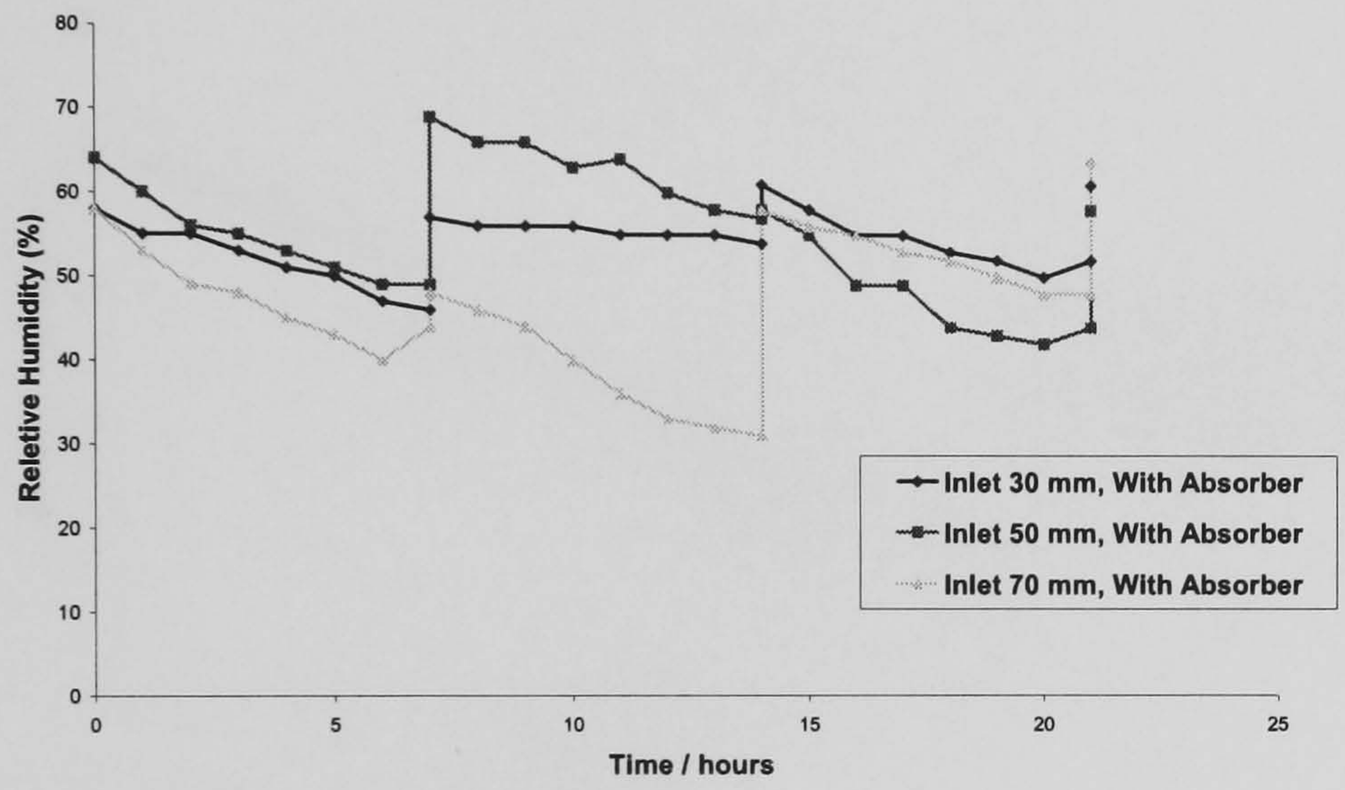

b) Roof 64^0

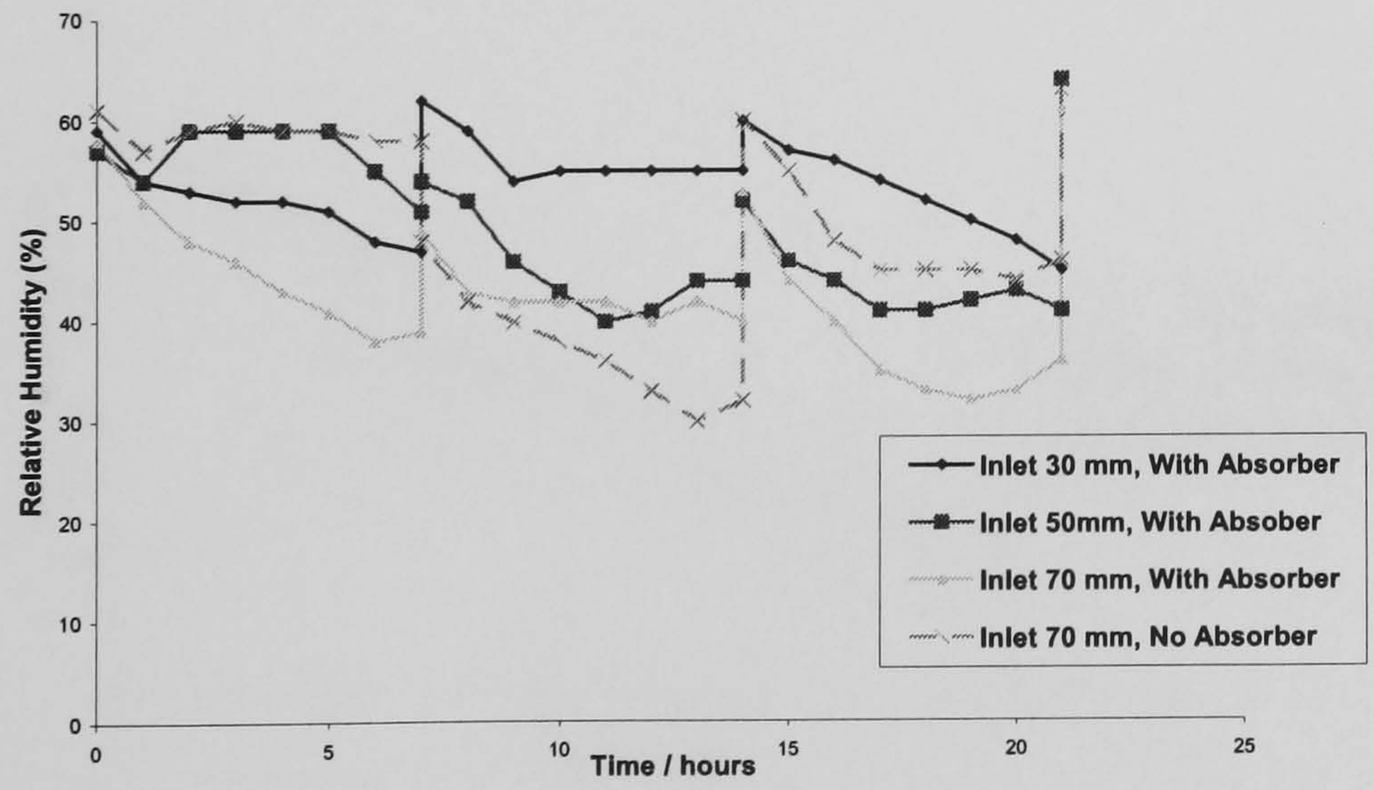

c) Roof 51^0

Figure 5.10 Ambient RH vs. Drying Time, for a given Roof Angle: Under load

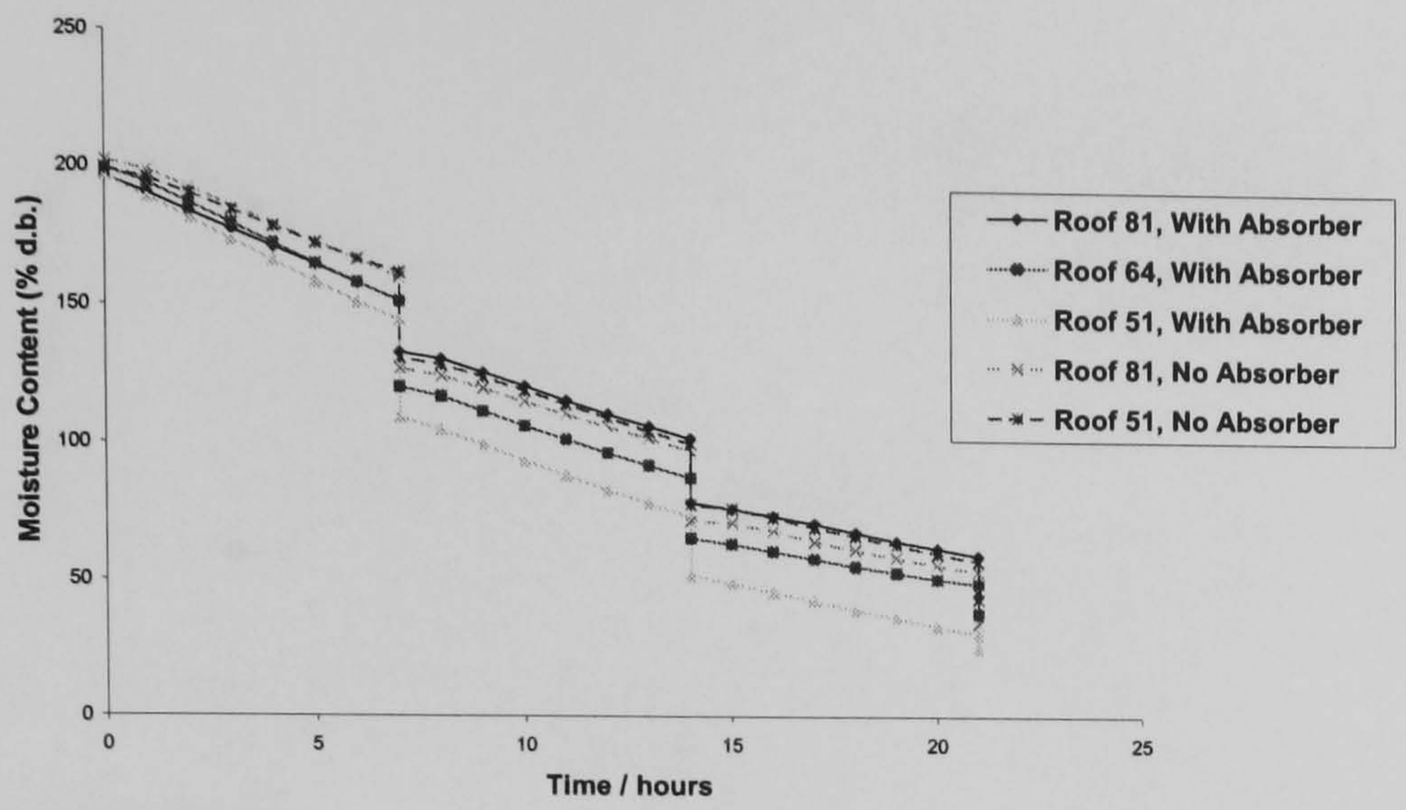

a) Inlet Gap 70 mm

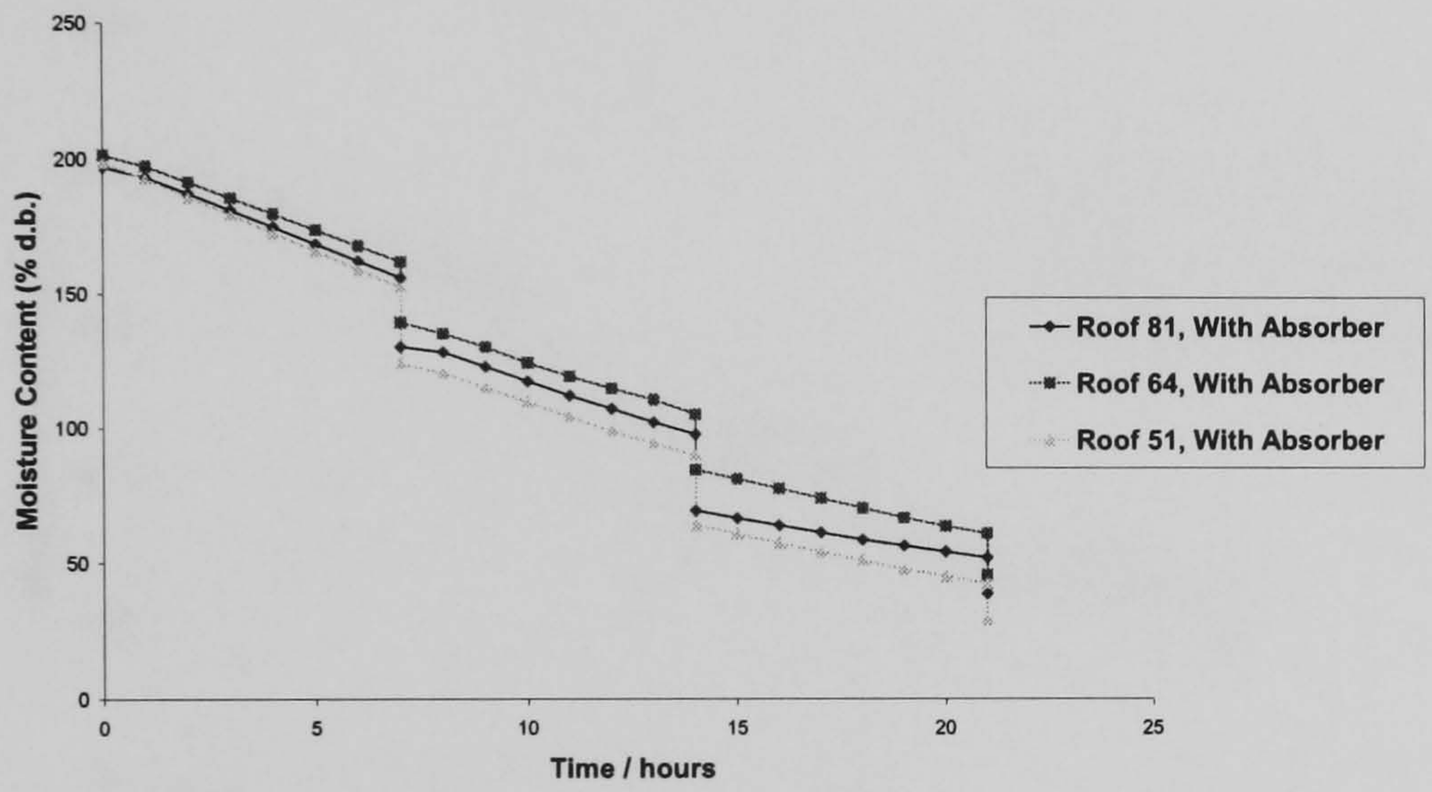

b) Inlet Gap 50 mm

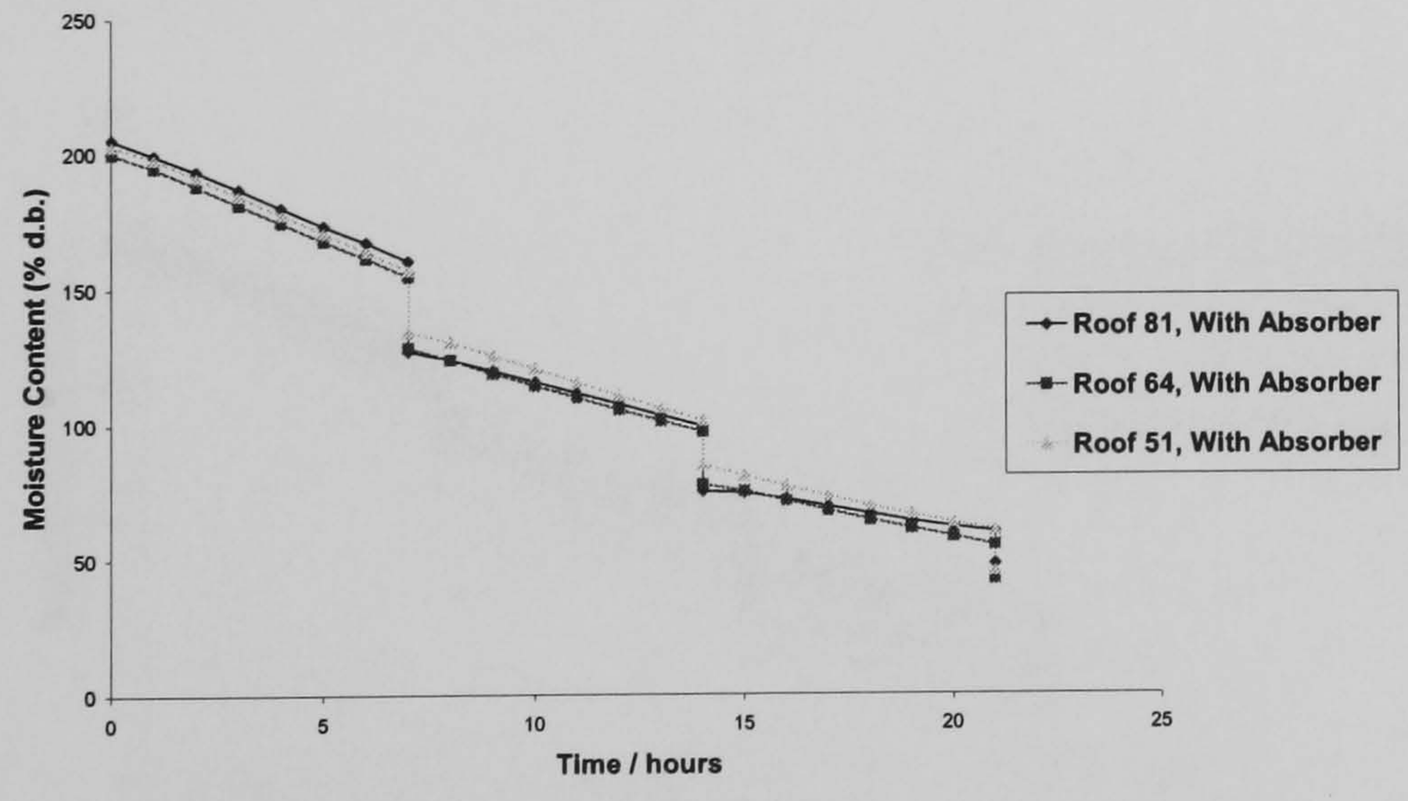

c) Inlet Gap 30 mm

Figure 5.11 Moisture Content vs. Drying Time, for a given Inlet Gap; Under load

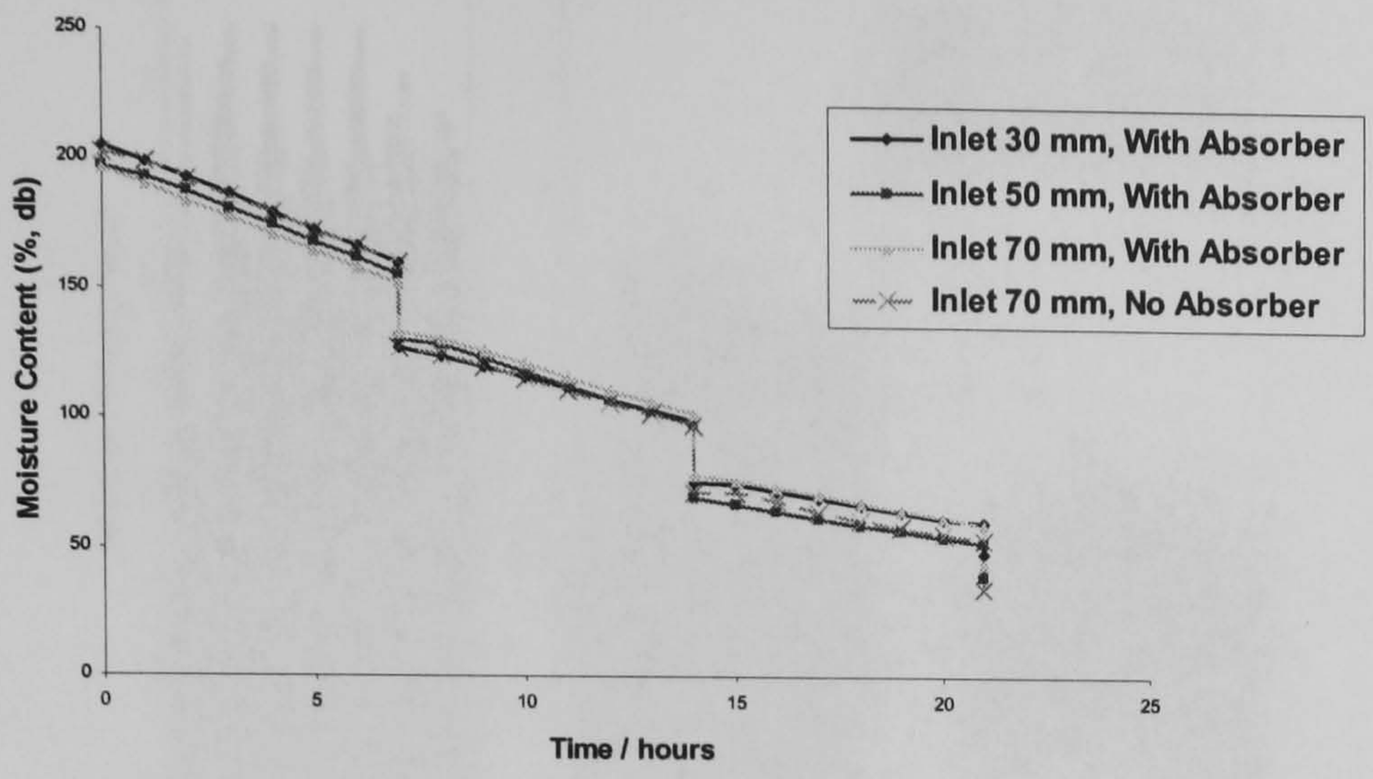

a) Roof 81^0

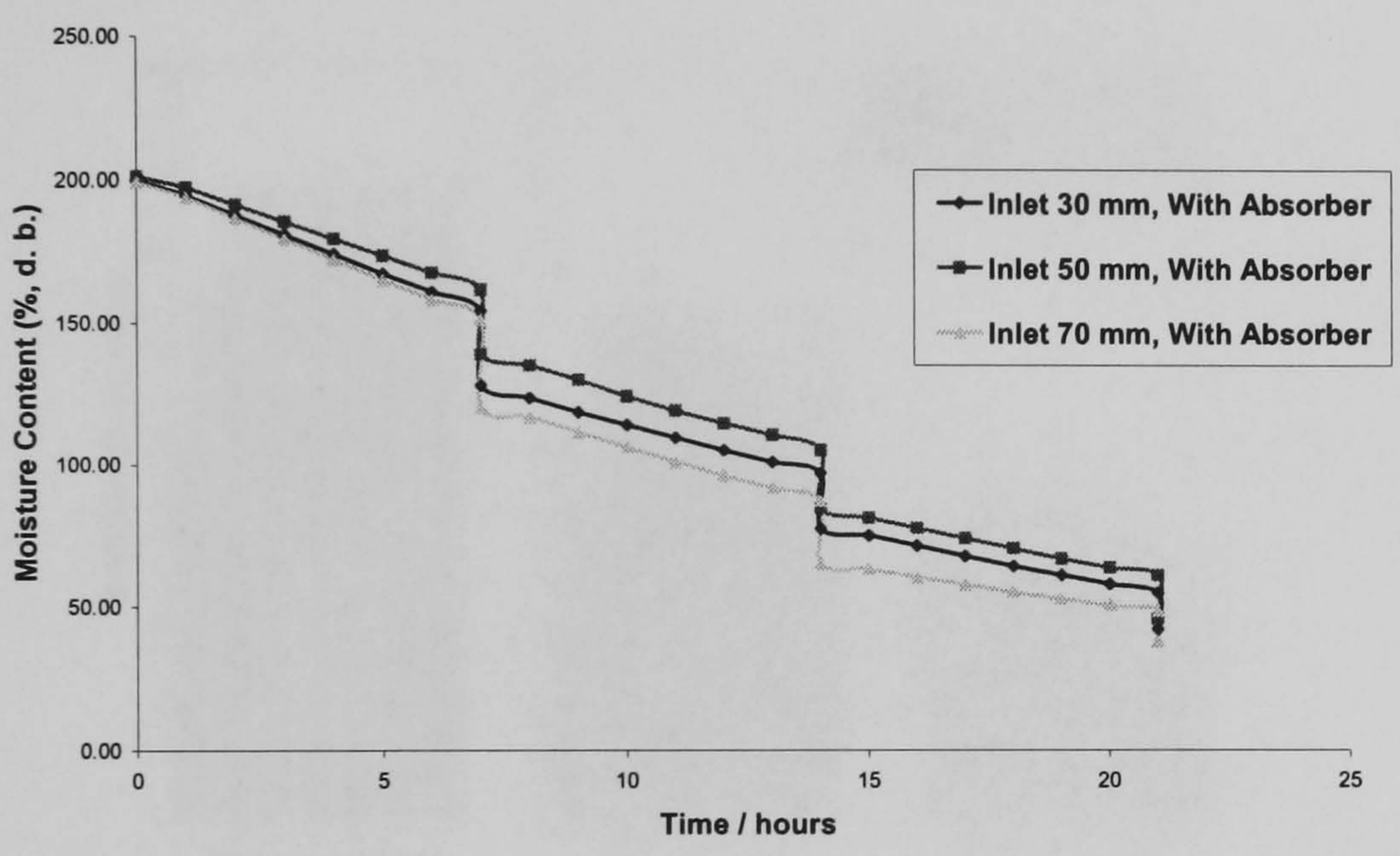

b) Roof 64^0

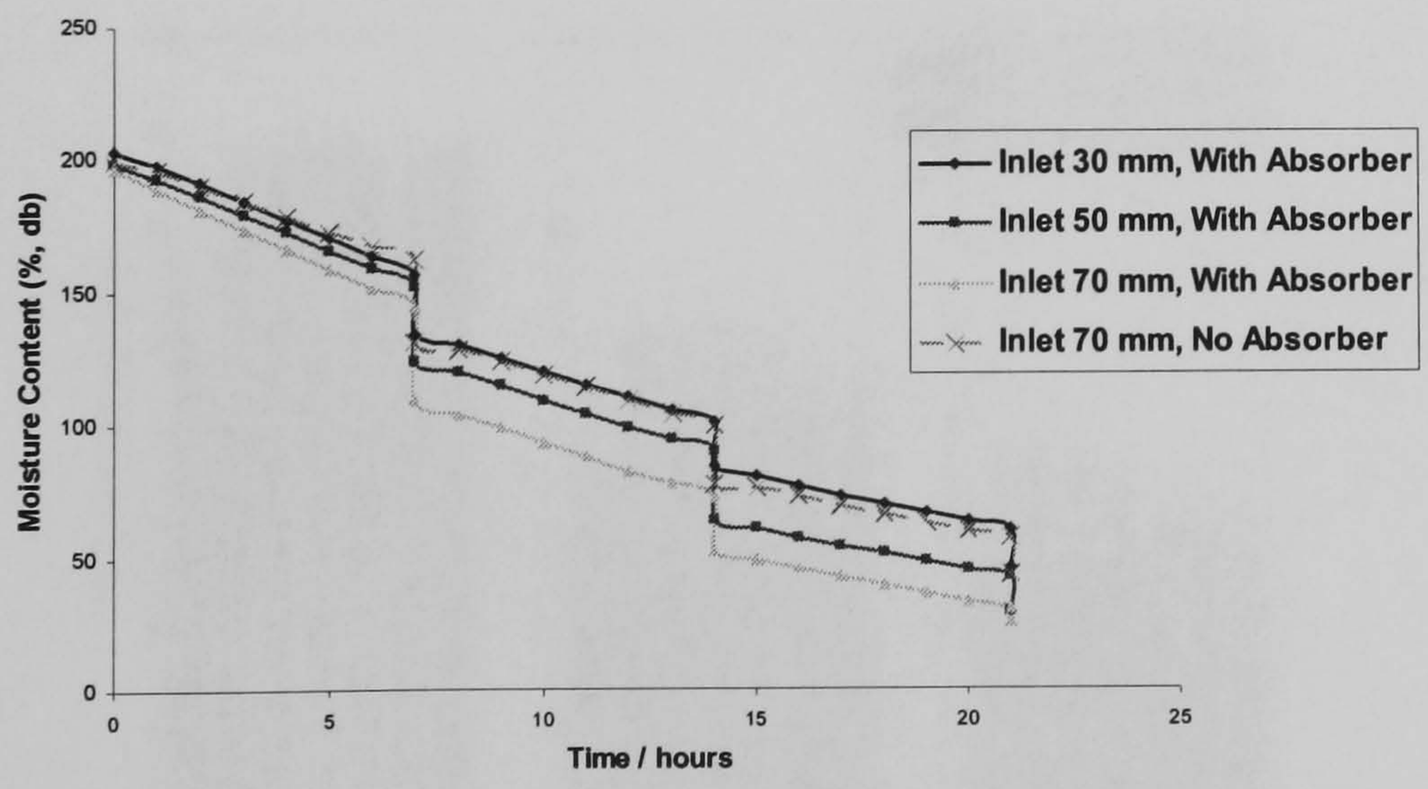

c) Roof 51^0

Figure 5.12 Moisture Content vs. Drying Time, for a given Roof Angle; Under load

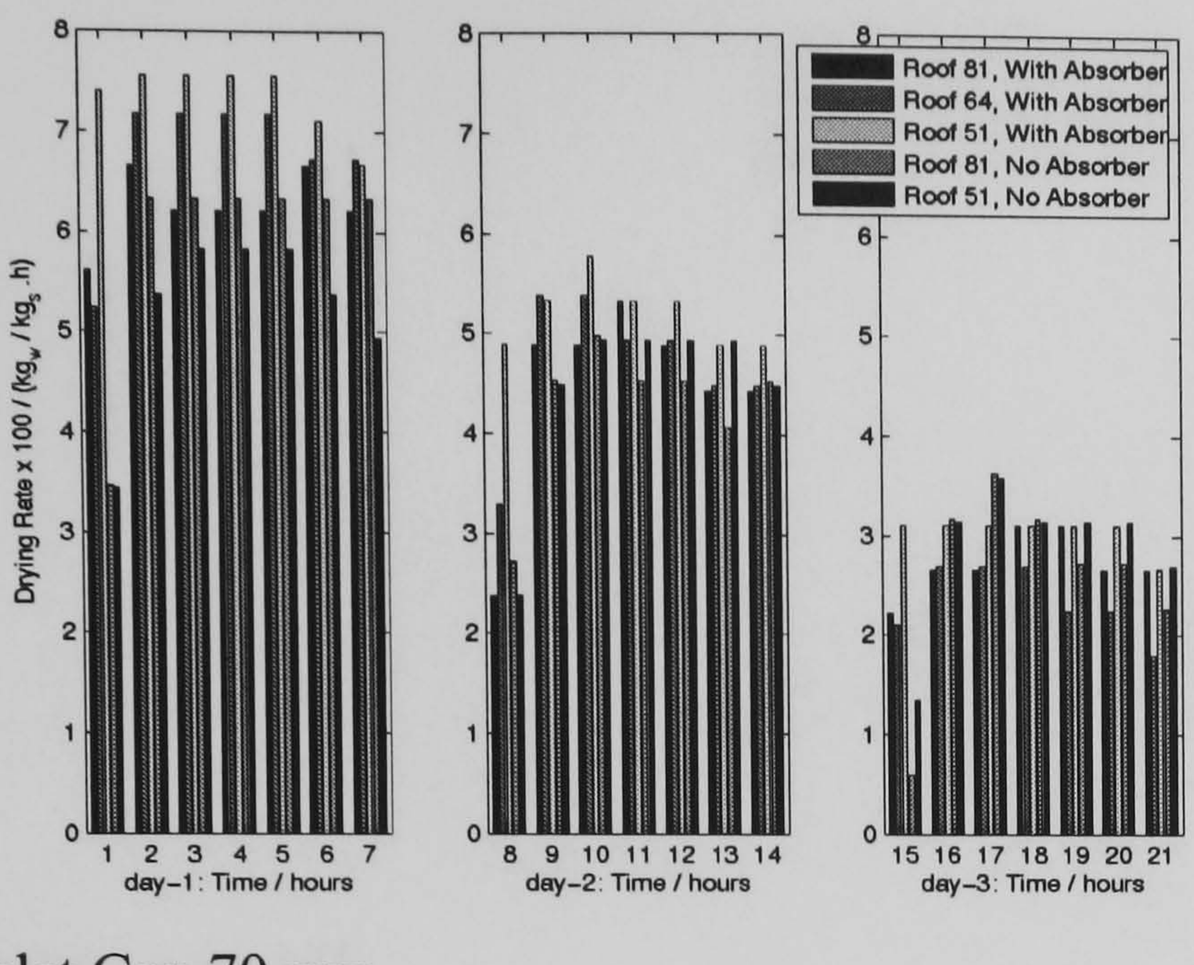

a) Inlet Gap 70 mm

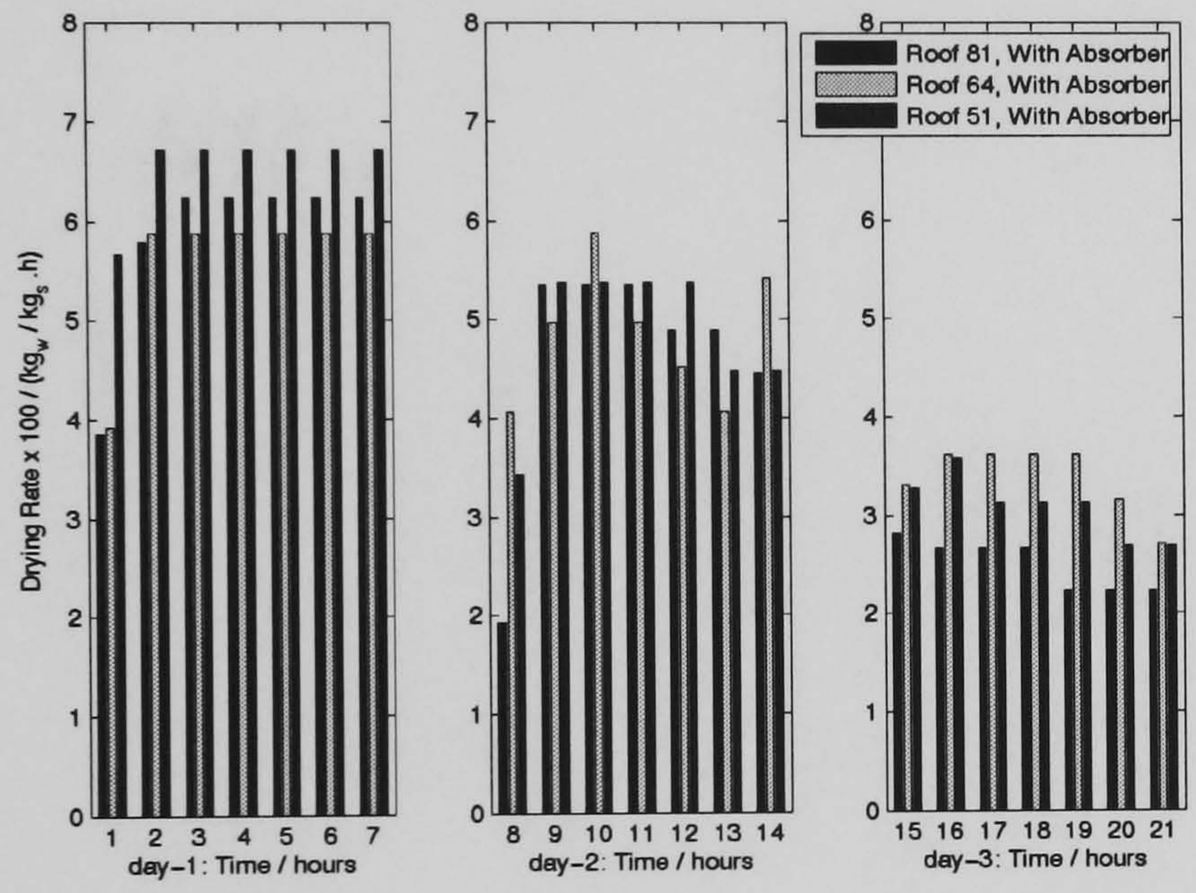

b) Inlet Gap 50 mm

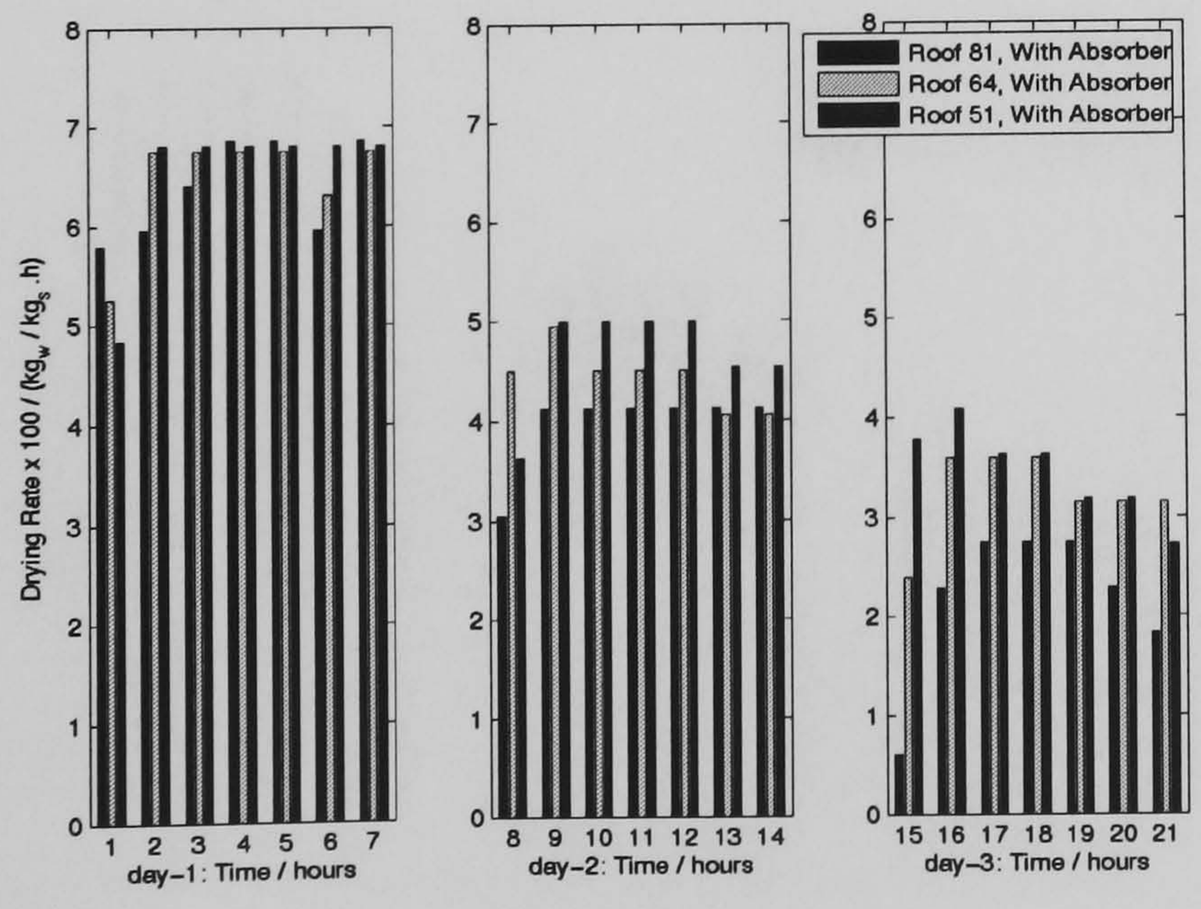

c) Inlet Gap 30 mm

Figure 5.13 Drying Rate vs. Drying Time, for a given Inlet Gap; Under load

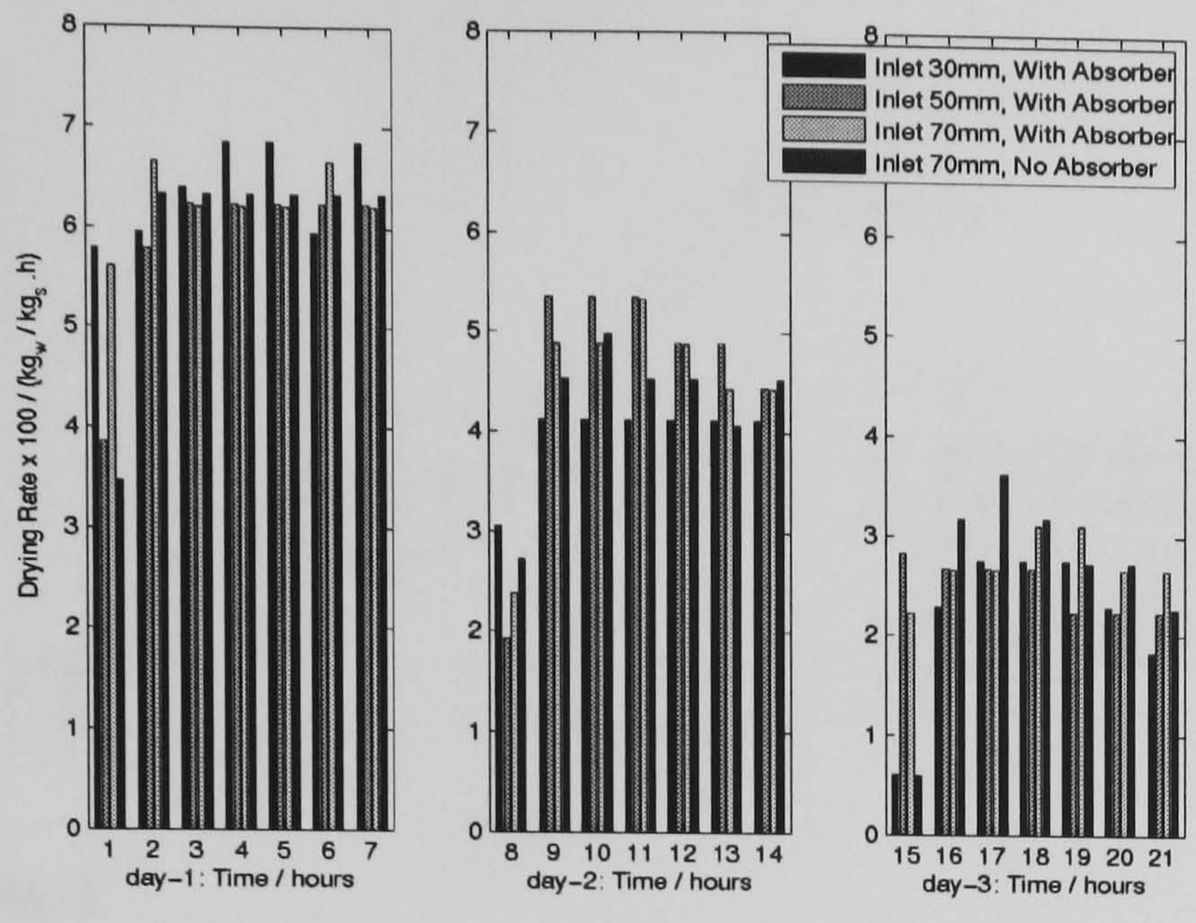

a) Roof Angle 81^0

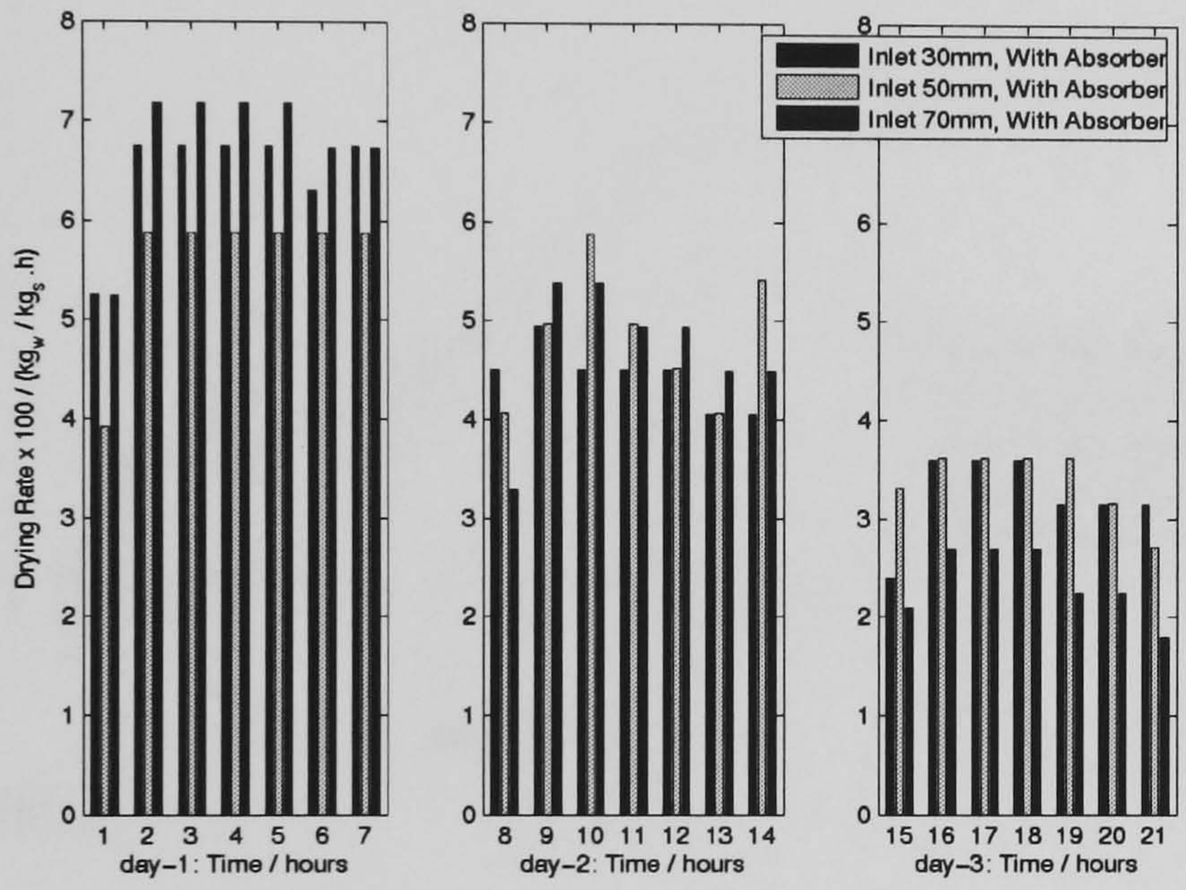

b) Roof Angle 64^0

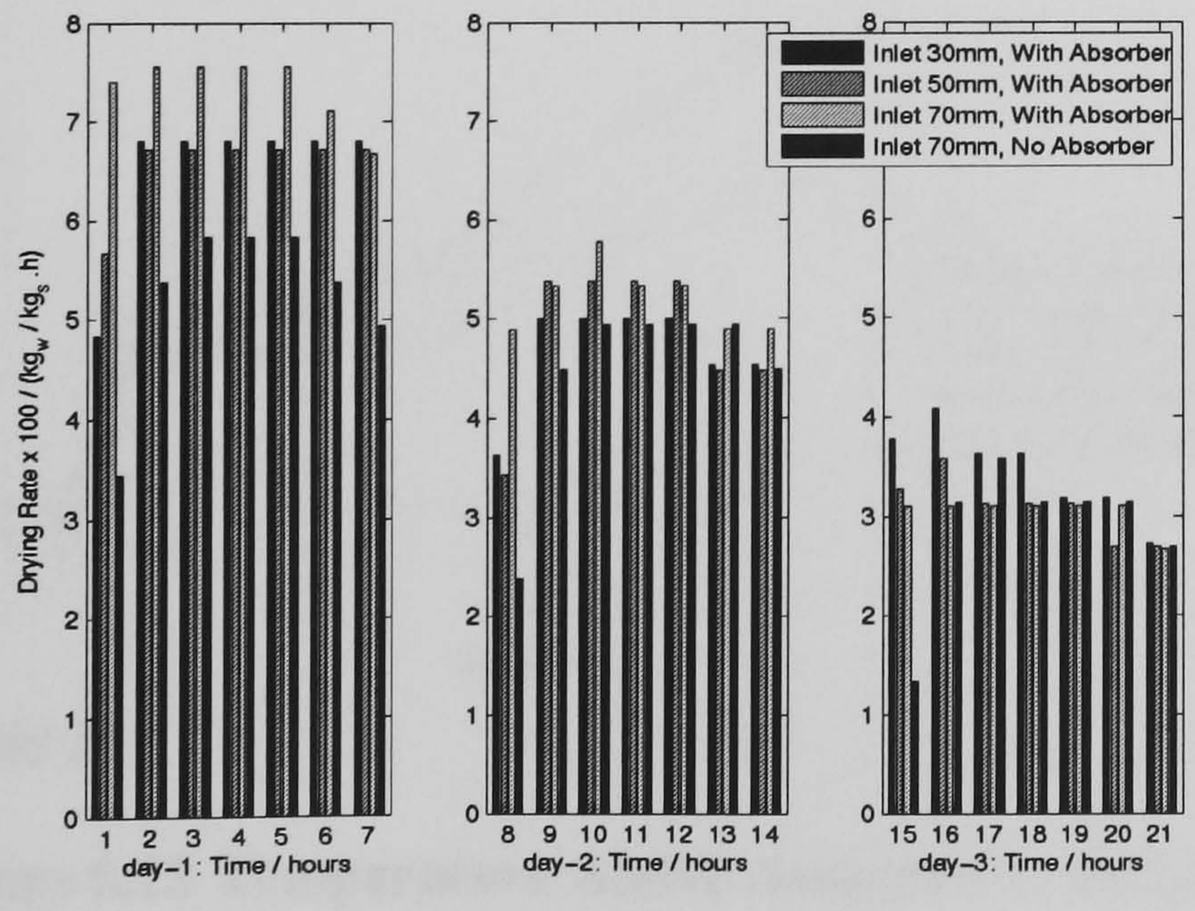

c) Roof Angle 51^0

Figure 5.14 Drying Rate vs. Drying Time, for a given Roof Angle; Under load

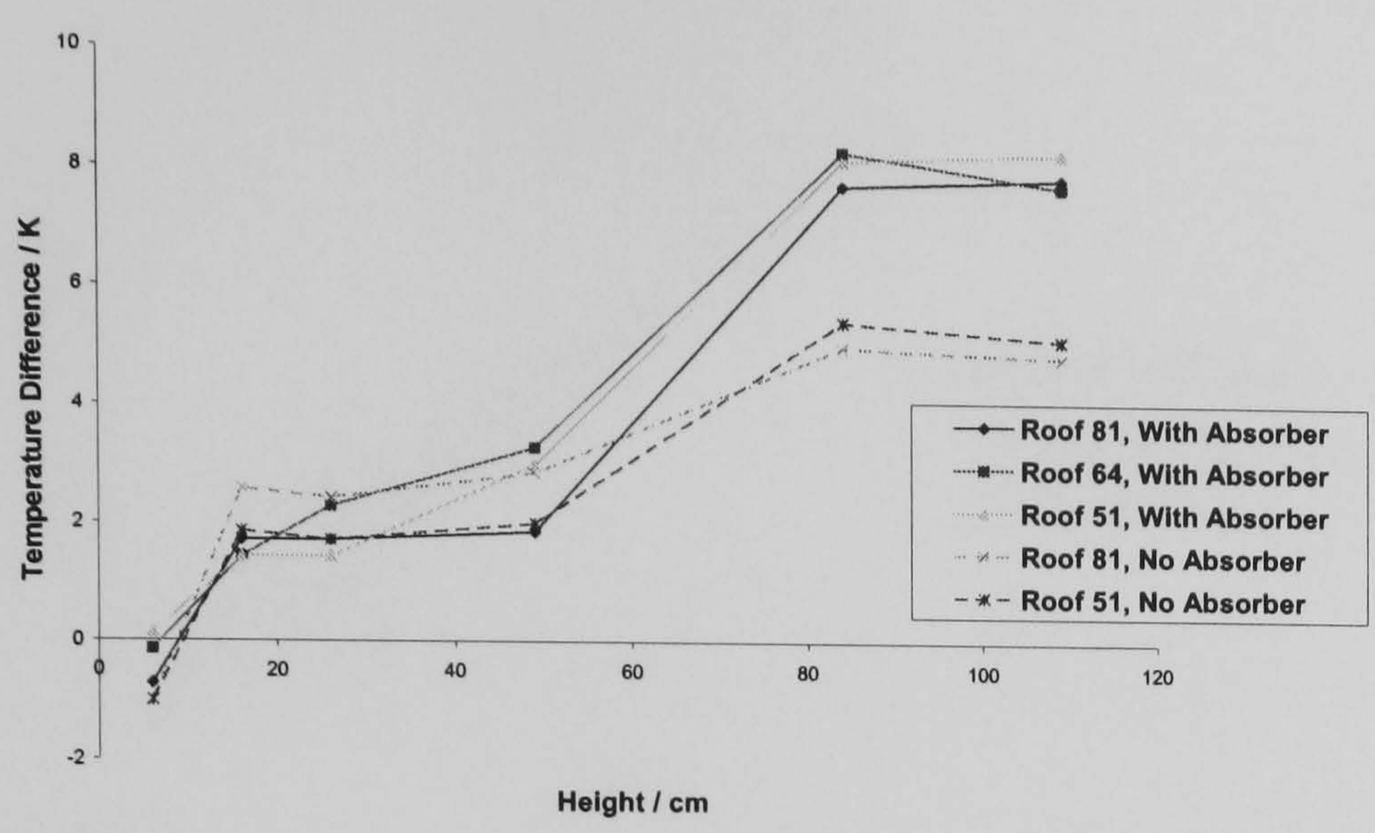

a) Day1

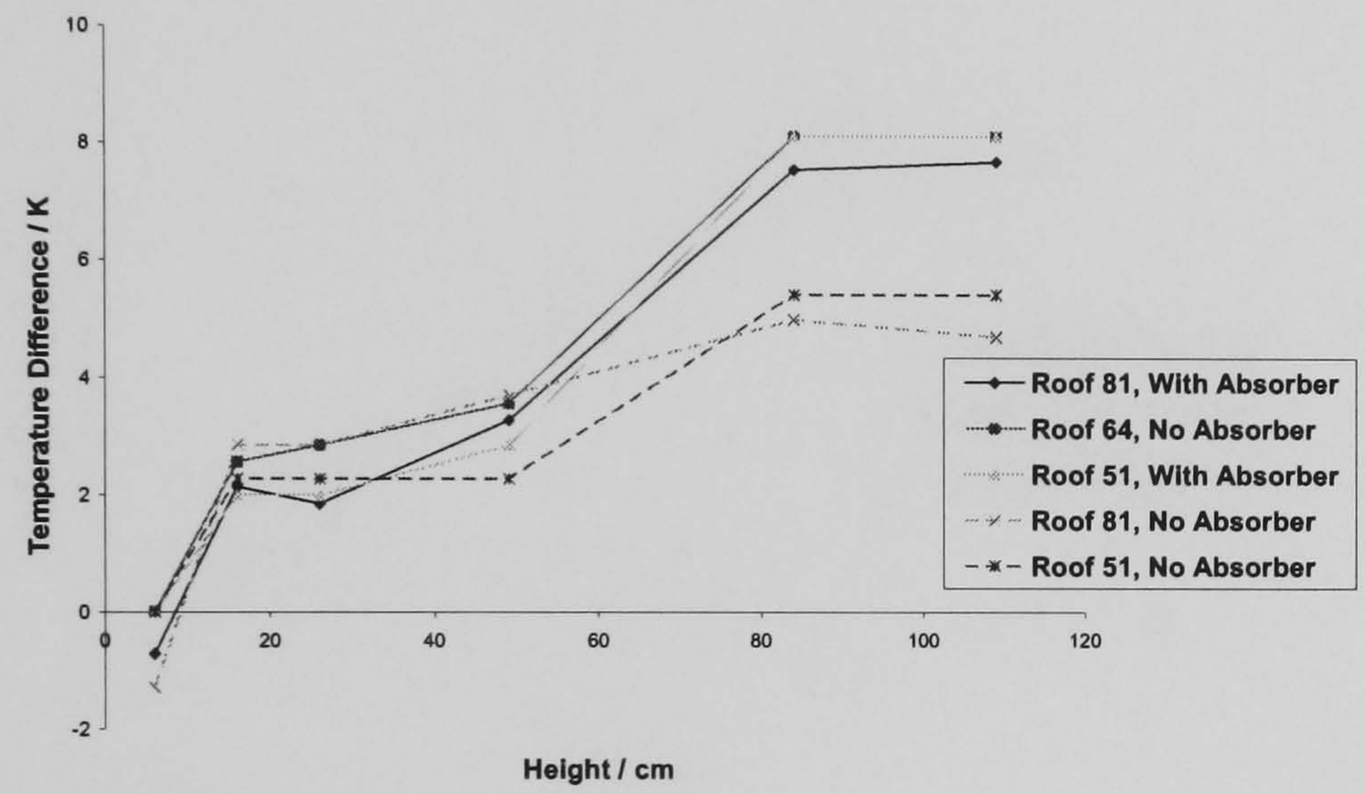

b) Day 2

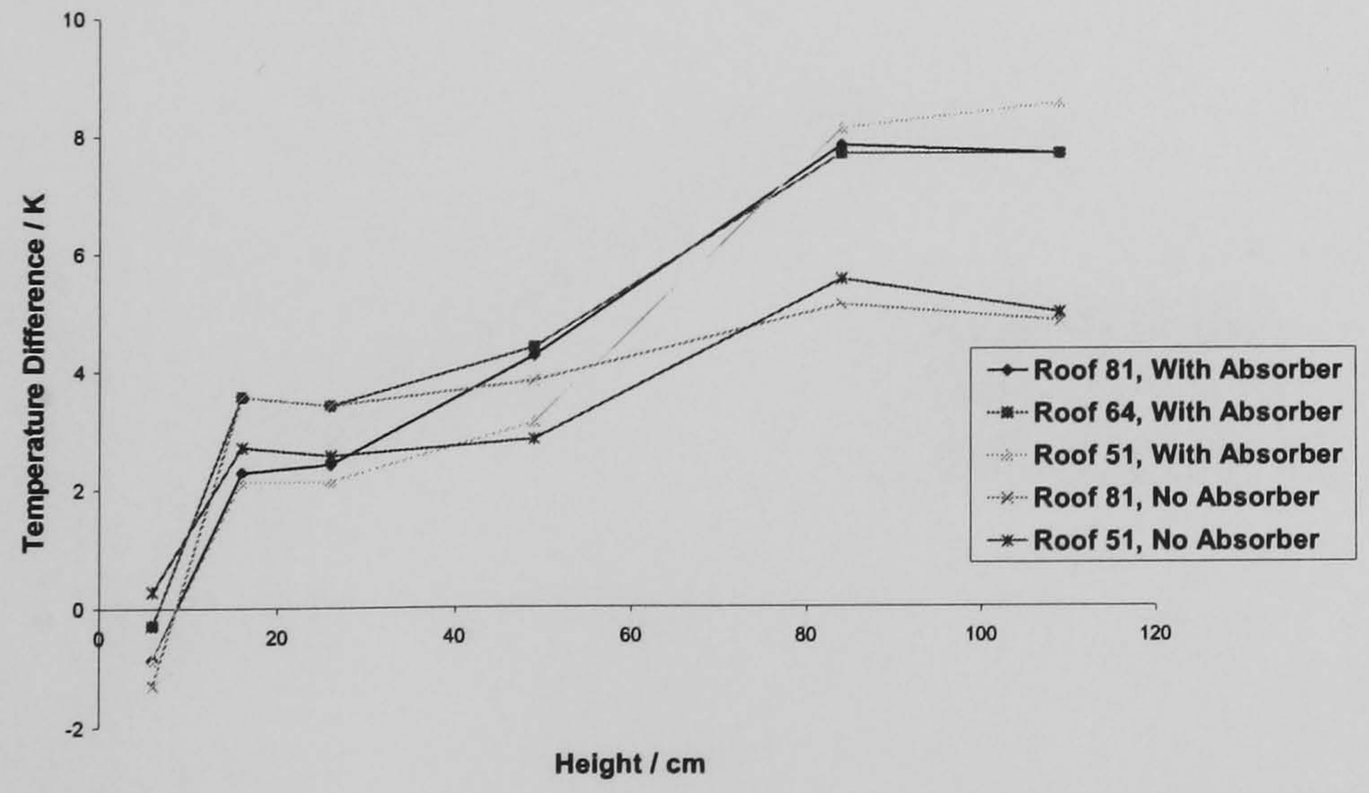

c)Day 3

Figure 5.15 Temperature Above Ambient vs. Height; Under load, Inlet Gap 70 mm

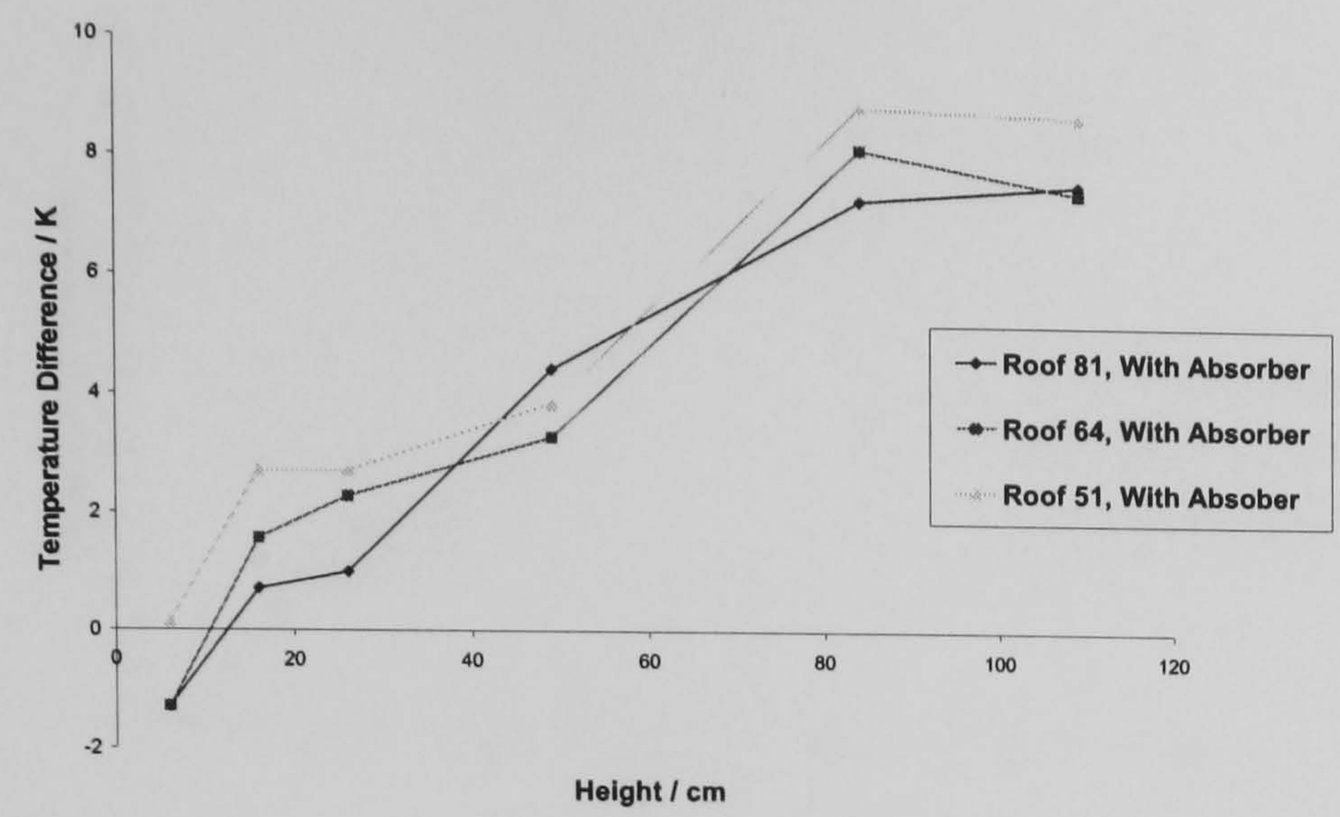

a) Day 1

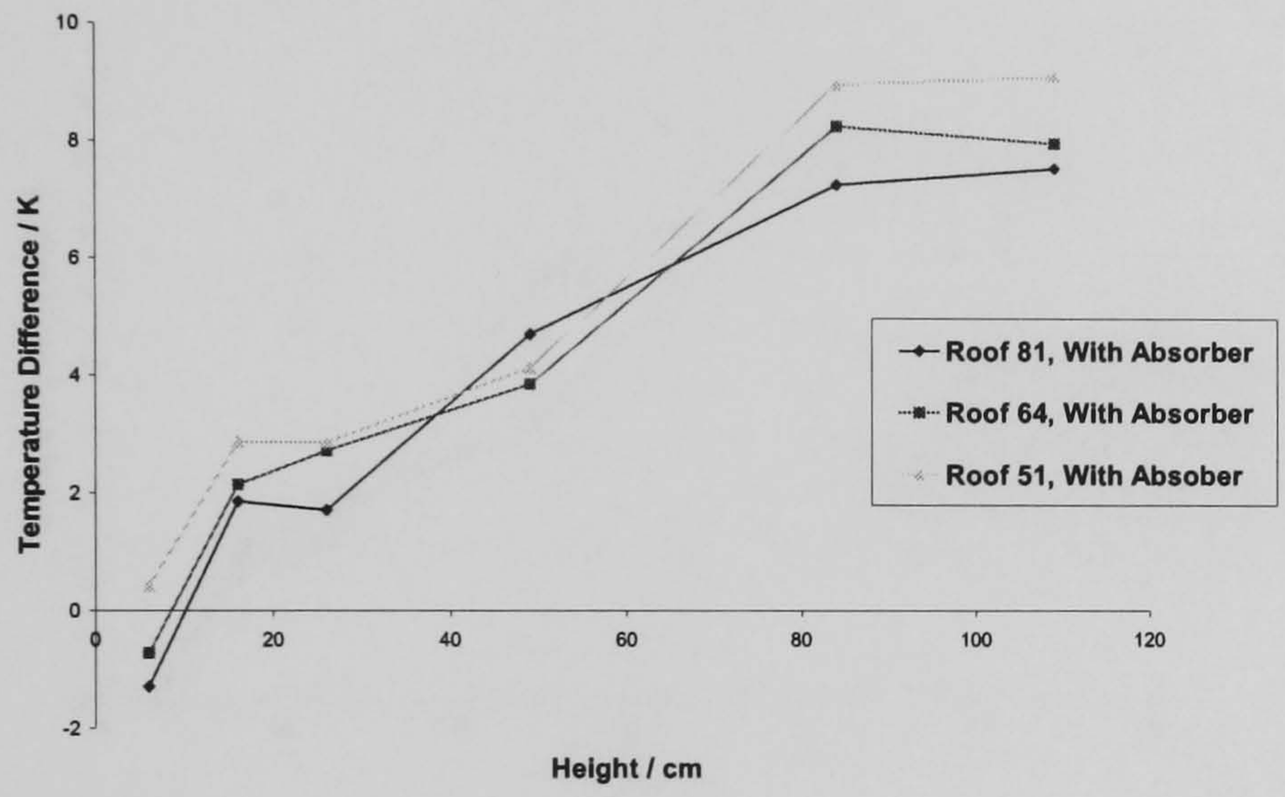

b) Day 2

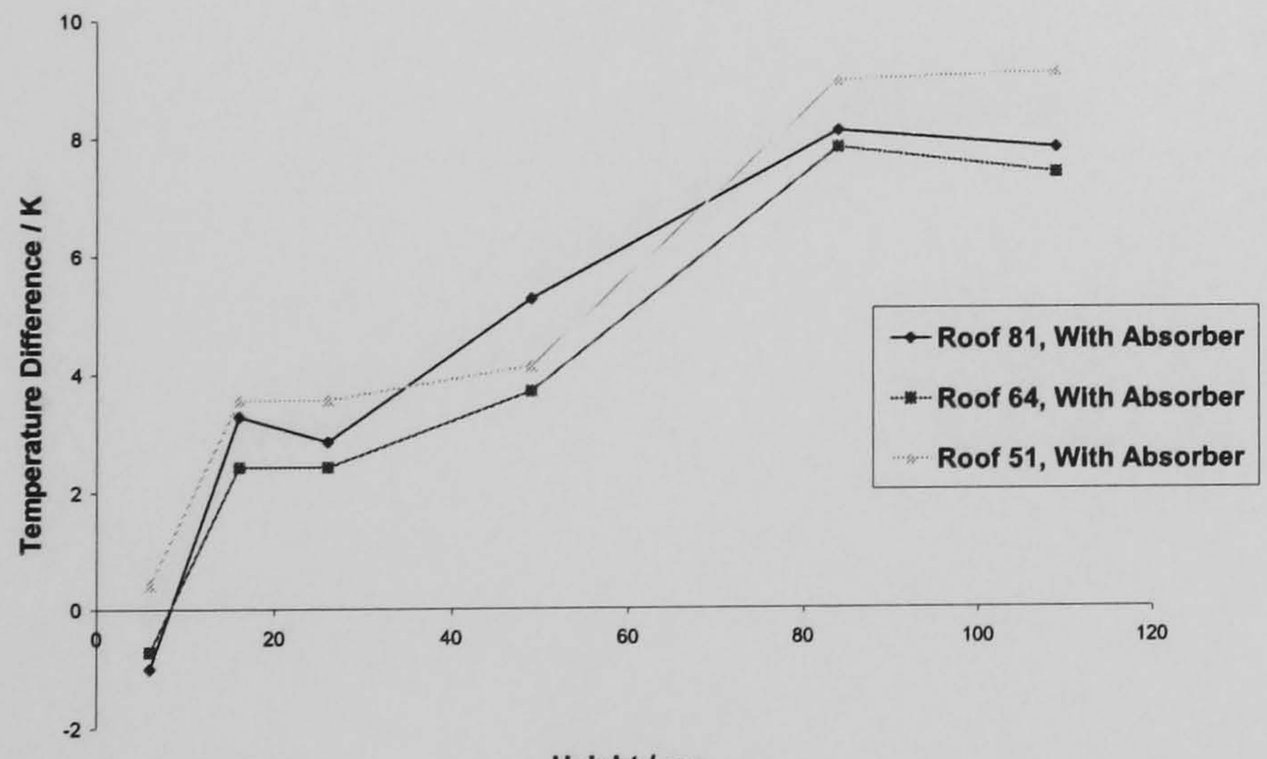

c) Day 3

Figure 5.16 Temperature Above Ambient vs. Height; Under load, Inlet Gap 50 mm

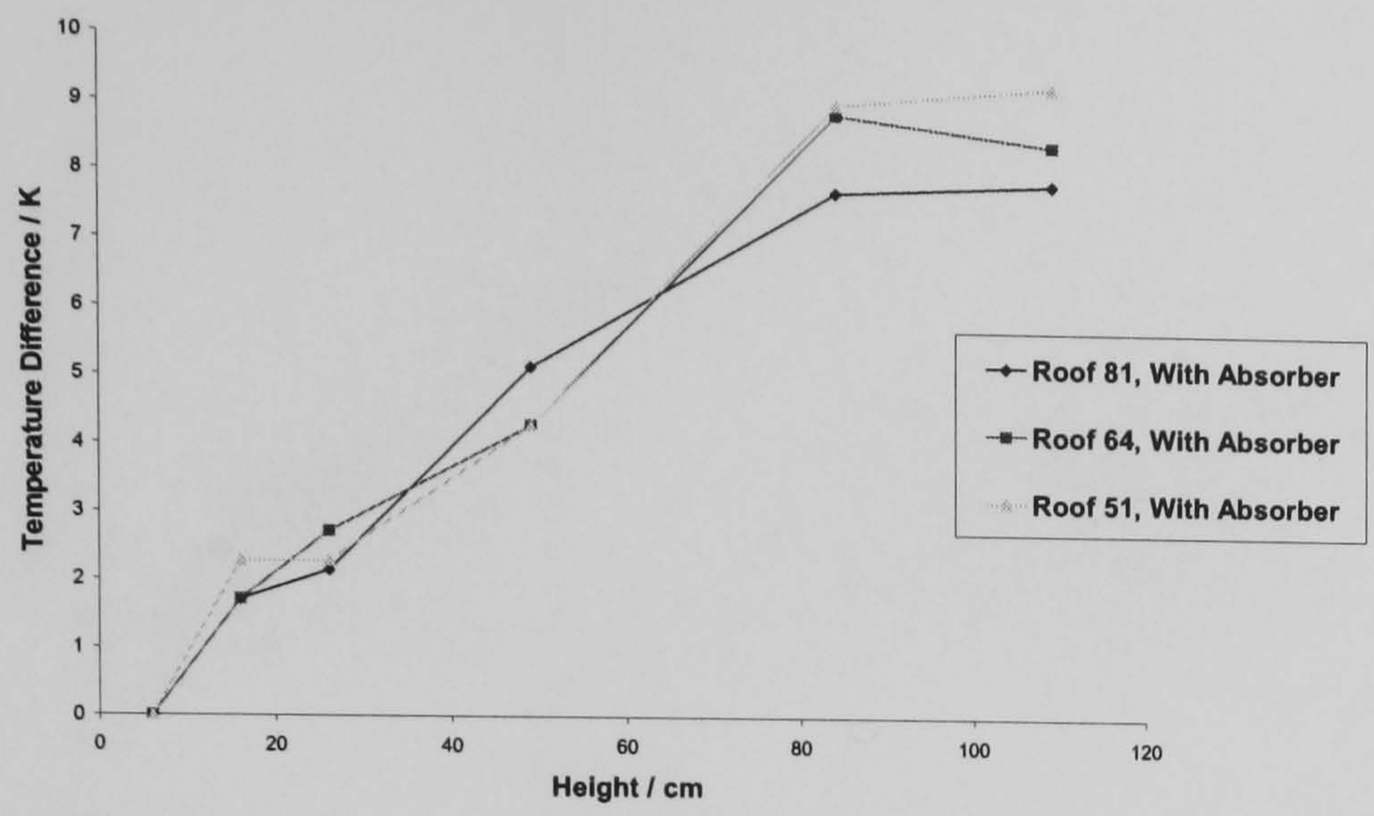

a) Day 1

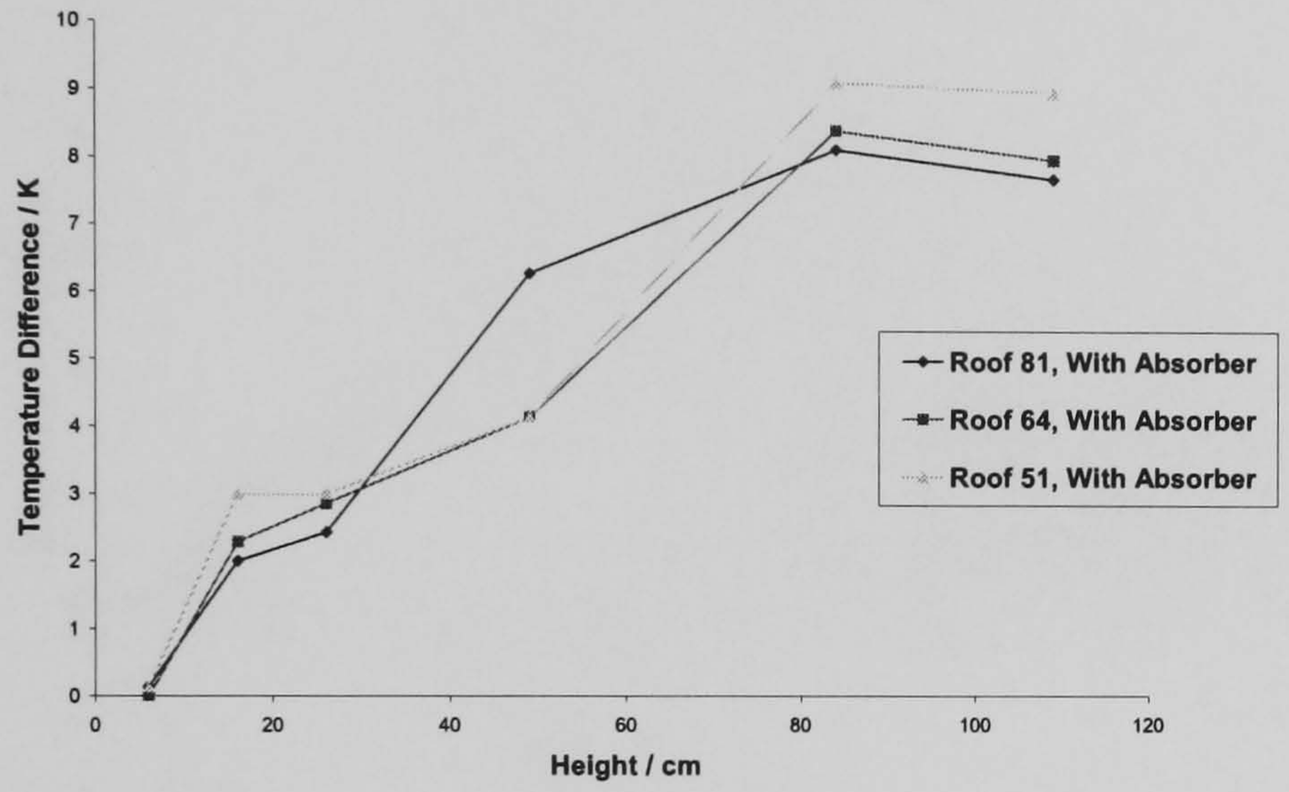

b) Day 2

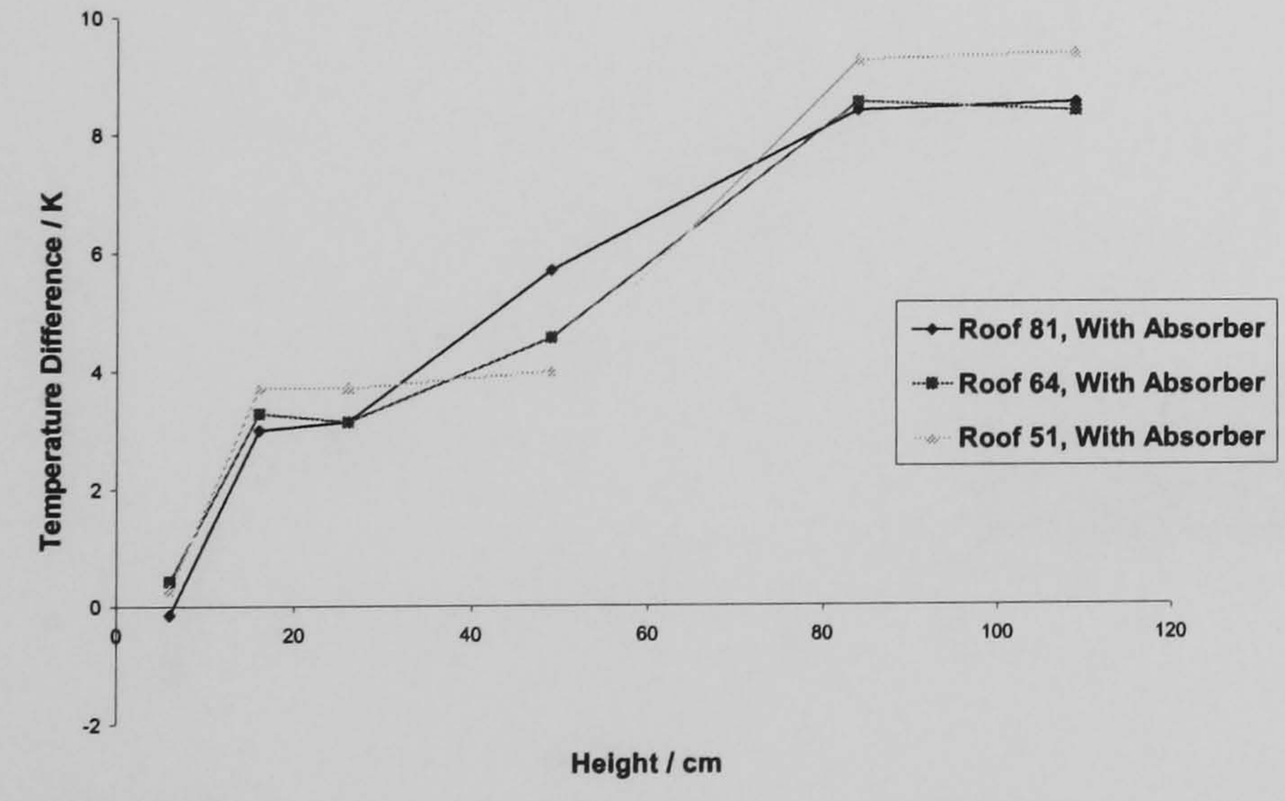

c) Day 3

Figure 5.17 Temperature Above Ambient vs. Height; Under load, Inlet Gap 30 mm

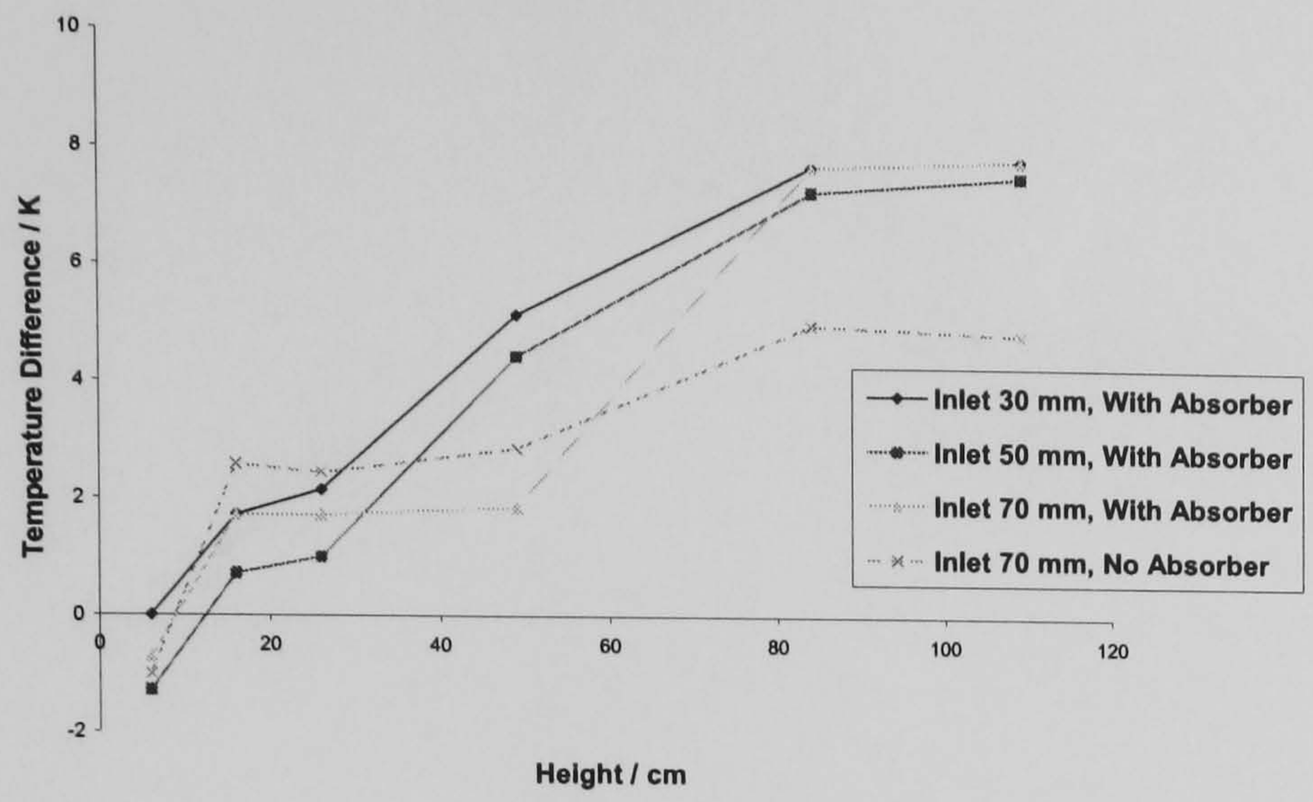

a) Day 1

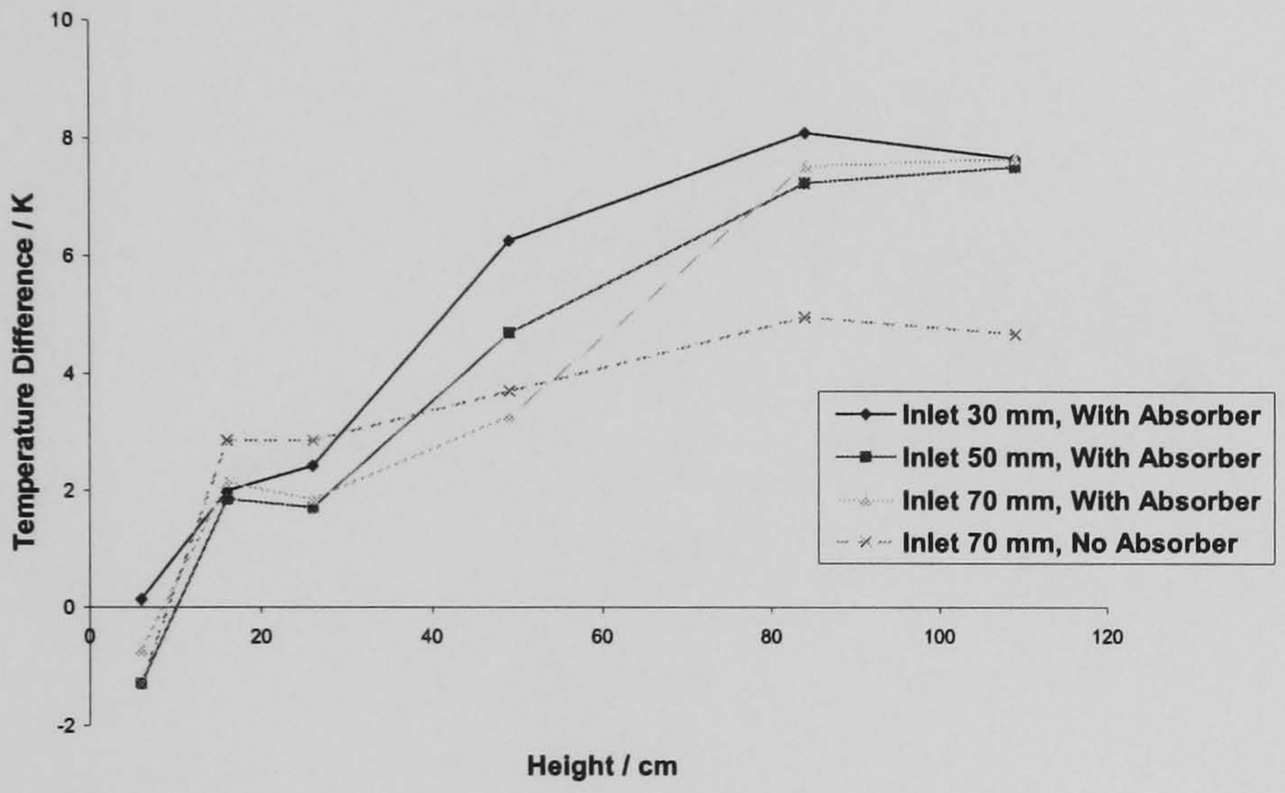

b) Day 2

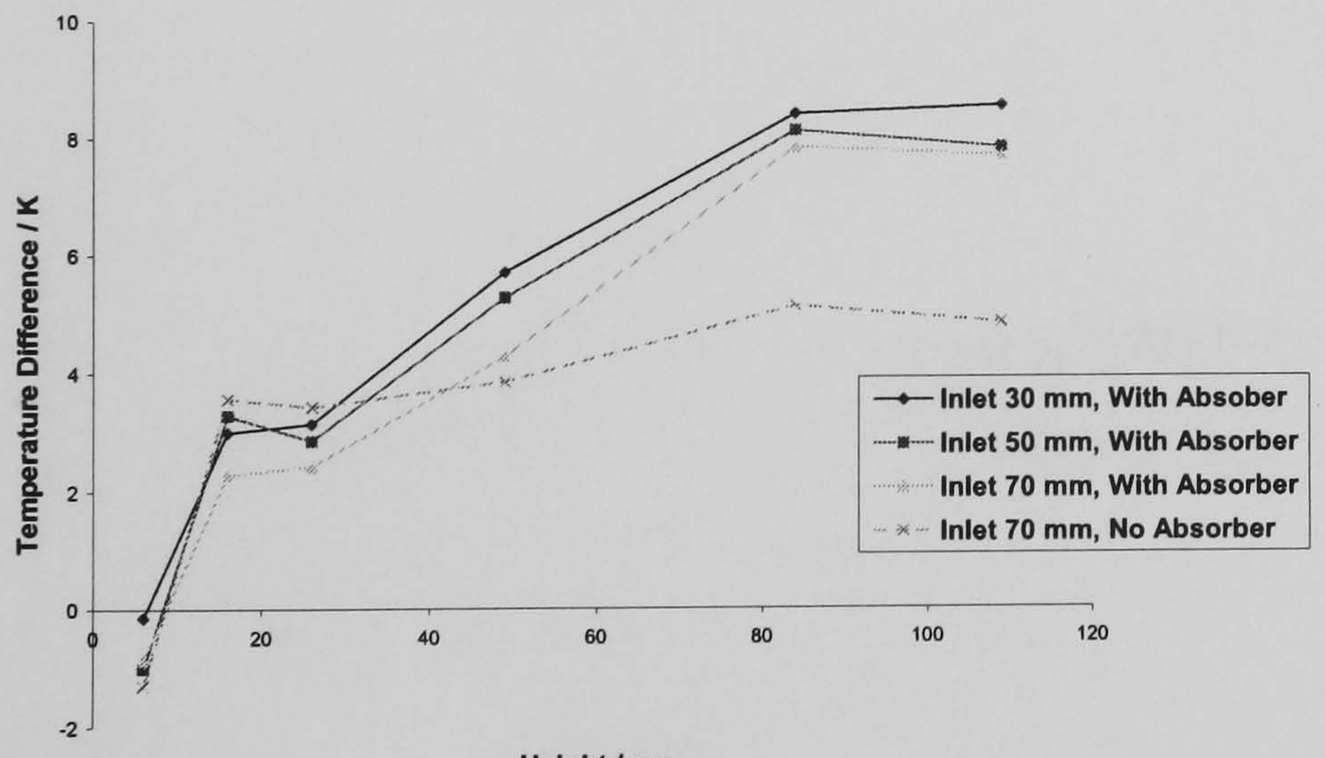

c) Day 3

Figure 5.18 Temperature Above Ambient vs. Height; Under load, Roof Angle 81^0

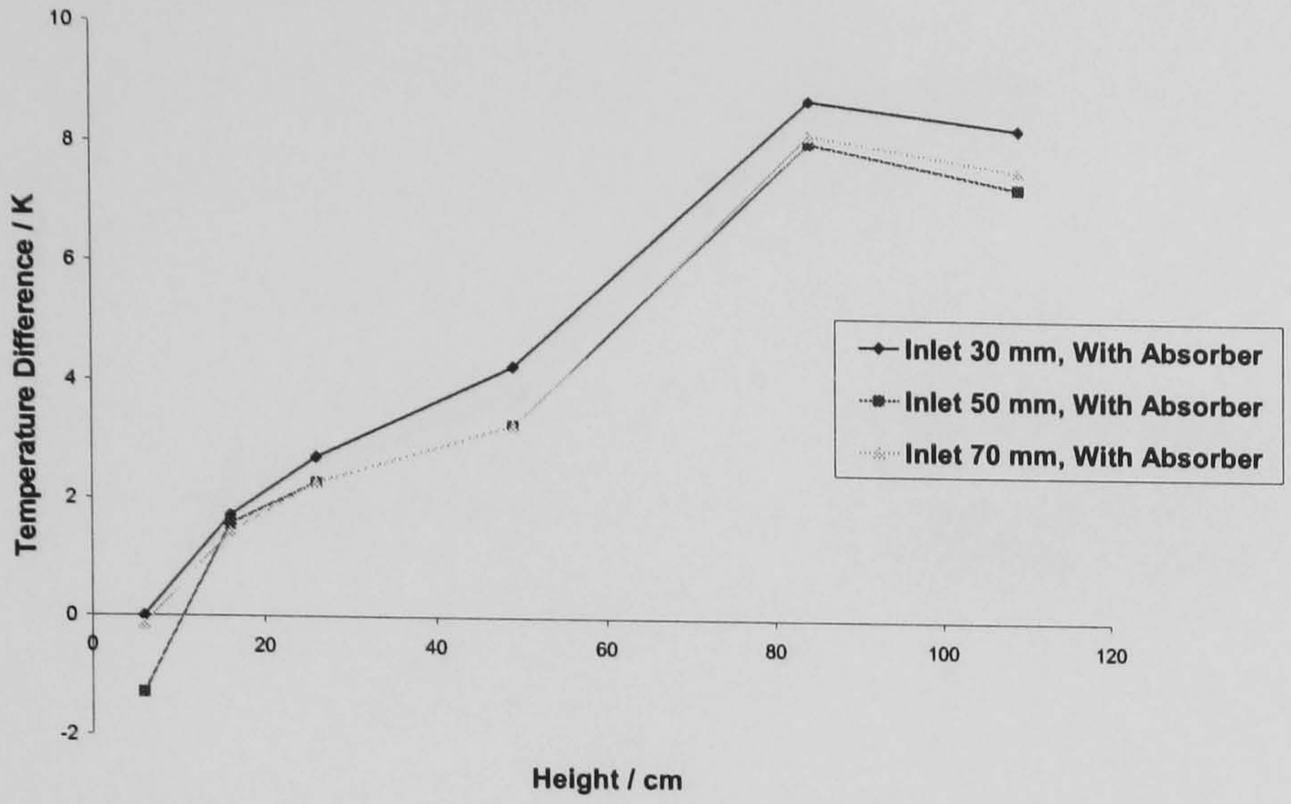

a) Day 1

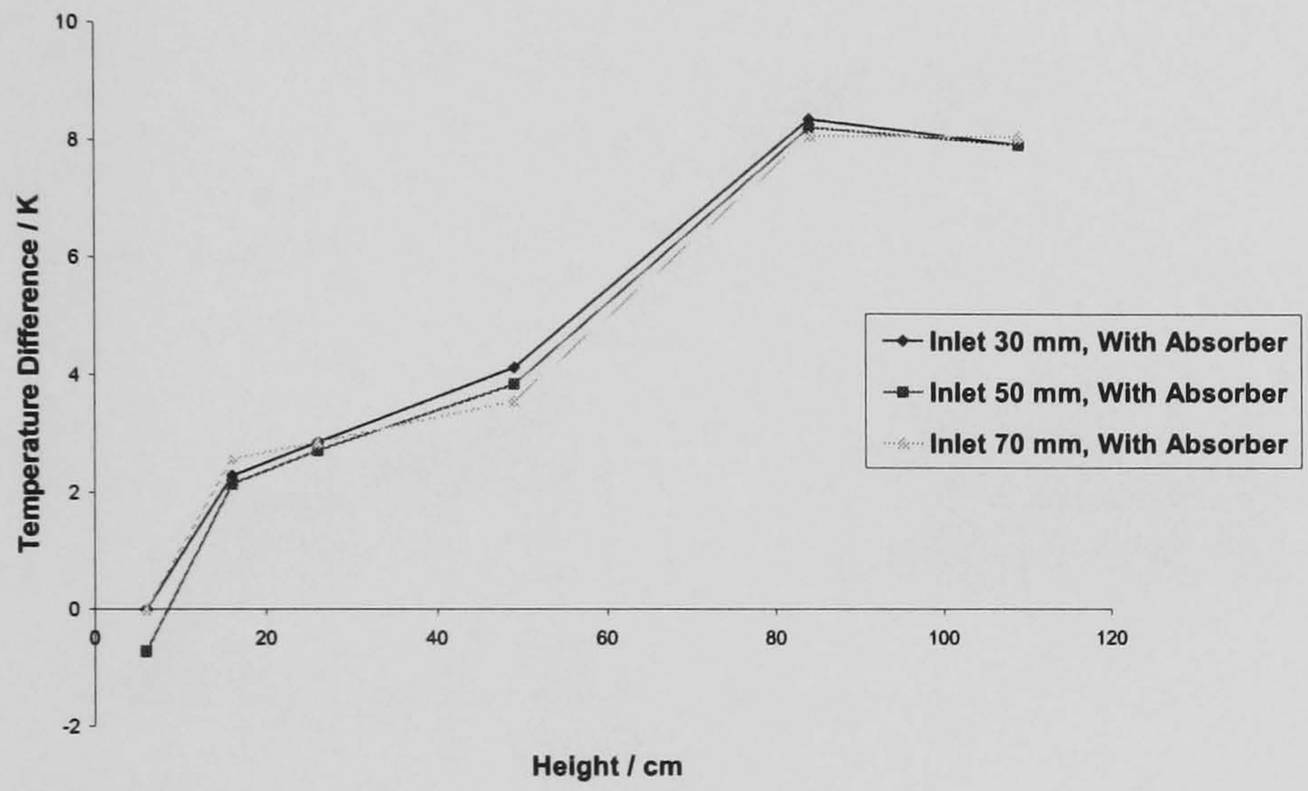

b) Day 2

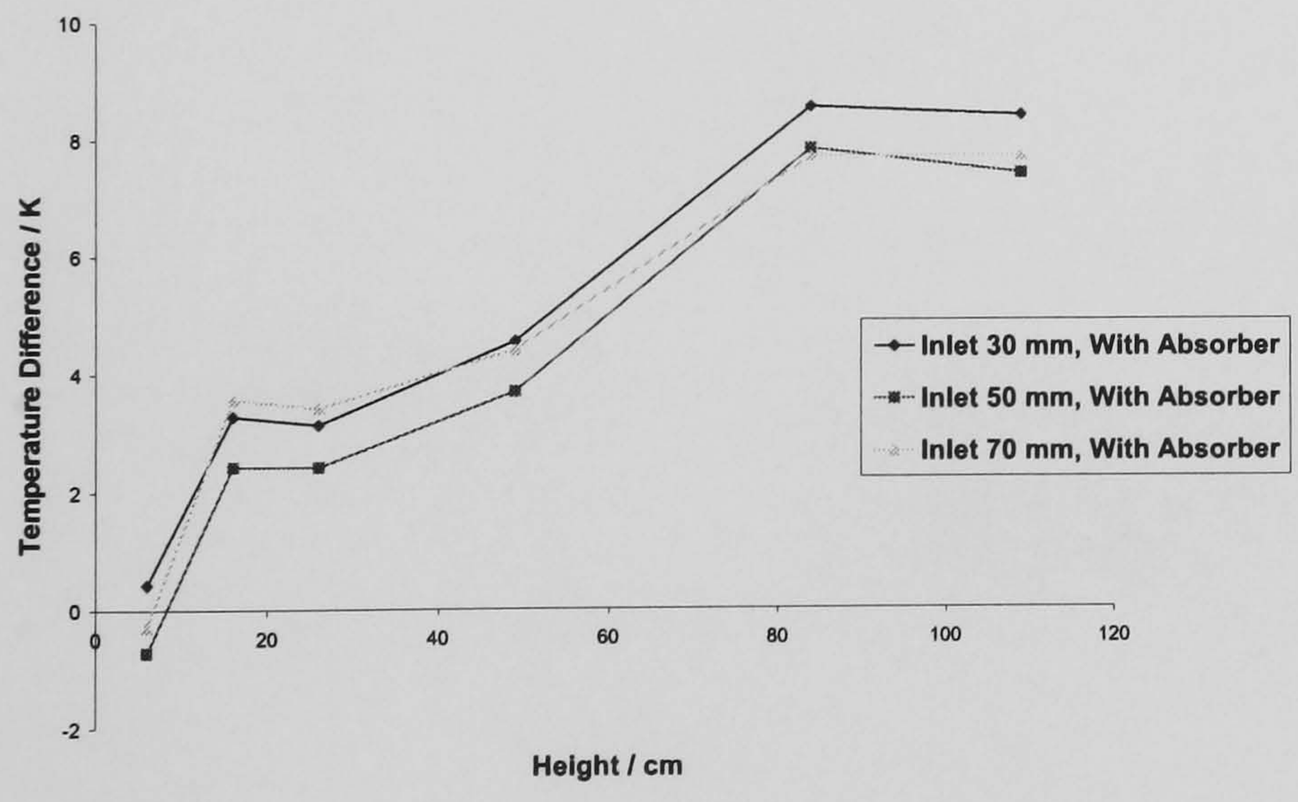

c) Day 3

Figure 5.19 Temperature Above Ambient vs. Height; Under load, Roof Angle 64^0

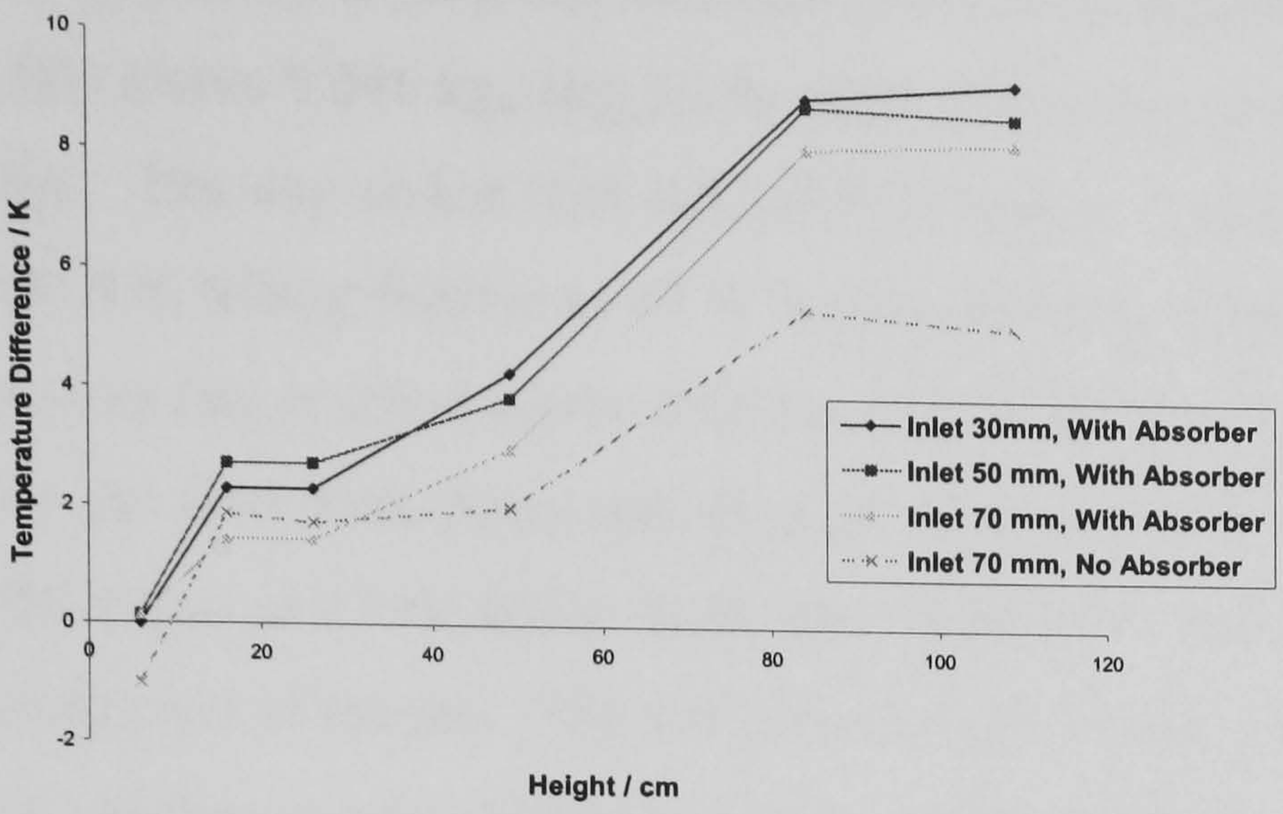

a) Day 1

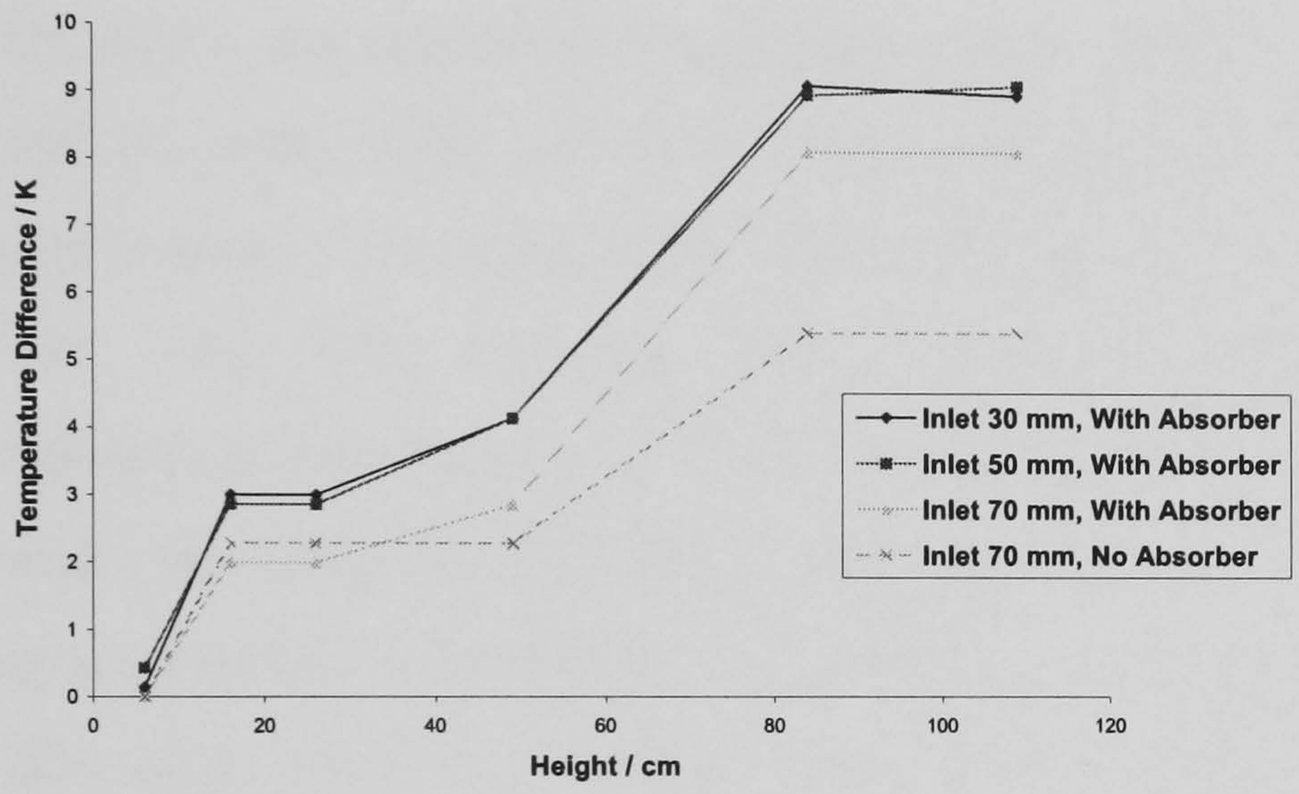

b) Day 2

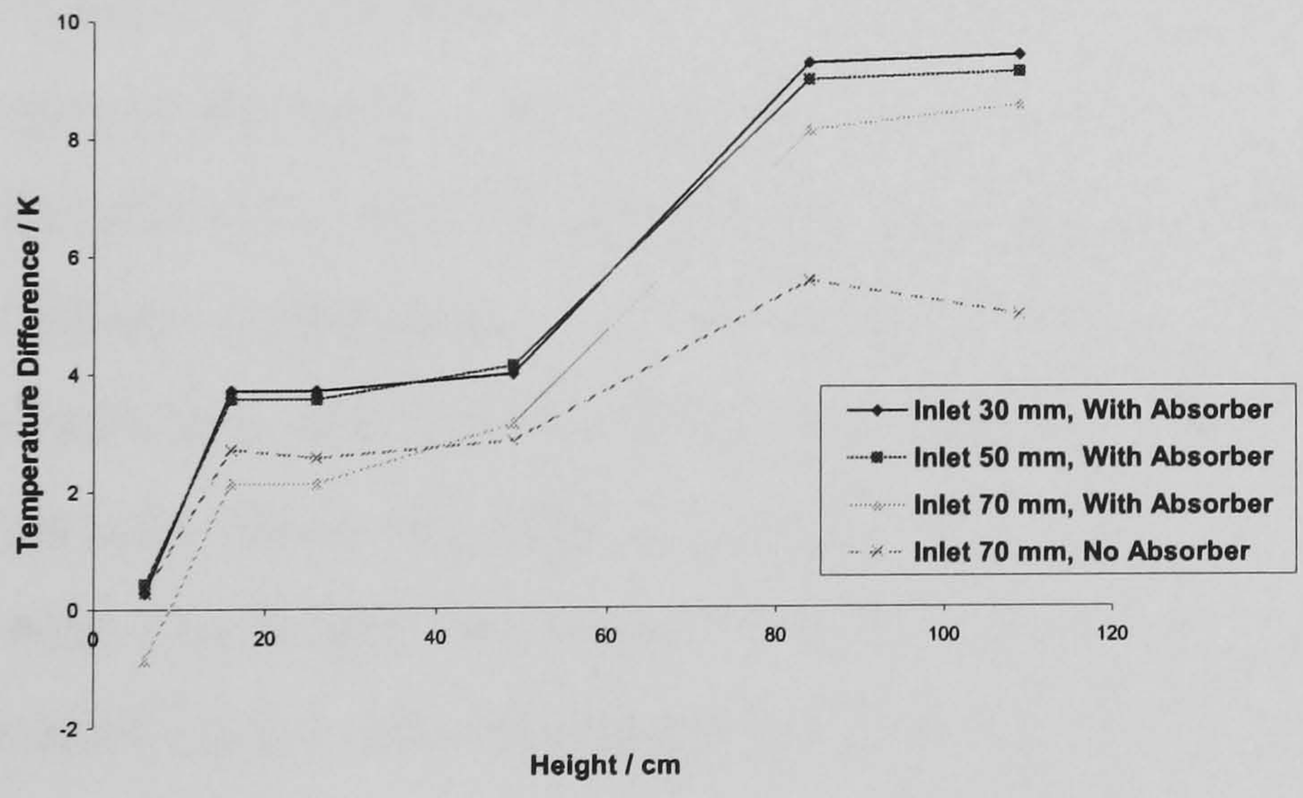

c) Day 3

Figure 5.20 Temperature Above Ambient vs. Height; Under load, Roof Angle 51^0

On day 2, the drying rate increased from 0.027 $kg_w/(kg_s.h)$ in the first hour and stayed a little above 0.045 $kg_w/(kg_s.h)$ for most of the day, as the RH fell to 50 % by close of the day. The day ended with MC of 97.6 % (d.b.), and this reduced to 71.9 % (d.b.) with the RH falling further to 47 % by the morning of the third day. On the third day, the drying rate reached above 0.03 $kg_w/(kg_s.h)$ by the second hour, stayed above this value for the next three hours and dropped to around 0.023 $kg_w/(kg_s.h)$ by the last hour. The RH began at 47 %, fell to 40 % after three hours and remained just below 40 % for most of the rest of the day. The MC then dropped again from 54 % at the close of day 3 to 34 %, on the morning of the fourth day with the RH rising to 56 %.

On day 1, the respective temperatures above ambient at heights 6, 16, 26, 49, 84 and 109 cm were -1.00, 2.57, 2.43, 2.86, 5.00 and 4.86 ^{0}C. Those at the same heights on day 2 were -1.29, 2.86, 2.86, 3.71, 5.00 and 4.71 ^{0}C, and those on day 3 were -1.29, 3.57, 3.43, 3.86, 5.14 and 4.86 ^{0}C, in the corresponding order (figure 5.15). The increase in temperature, as the air moved up the dryer, was generally similar to the no-load trials (compare figures 5.1 and 5.4 to figures 5.15 and 5.18). There were however minor distortions attributable to differences in the RH and drying rates on those days. The crop shelf also caused further differences in the temperature trend. The temperatures under the shelf fell below ambient (indicated on the graphs as negative values over ambient). This may be attributed to the sudden change in velocity as the air entered the dryer. The absorber at the base of the dryer was mostly shaded and was therefore not able to provide enough heating for the incoming air to maintain the ambient temperature. On the other hand, part of the metallic shelf was exposed to irradiation, and this heated the air so that the temperatures above ambient at height 16 cm (just above the shelf) were higher than that at a similar height in the no-load trials. After this height, the temperatures fell lower, compared to the no-load. This could be caused by the relatively higher humidity ratio after moisture removal by the air.

5.2.1.2 The normal chimney with roof angle 51^0

The trial with roof angle 51^0 started in an ambient RH of 61 % and stayed just below 60 % for most of the day (figure 5.9a), which were much higher than those in roof angle

81^0. On day 1, the inlet velocity increased from the ambient to an average value of 0.14 m/s within an hour and prevailed around this value almost the whole day, seen in figure 5.8a. This value was higher than the inlet velocity of roof angle 81^0. However, the drying rates of roof angle 51^0 were lower, changing from zero to around 0.058 $kg_w/(kg_s.h)$ in three hours (figure 5.13a), in spite of the higher airflow. The rate stayed around this value till the fifth hour and then dropped to 0.049 $kg_w/(kg_s.h)$ at the end of the first day. This lower drying rate could be attributed to the much higher RH. Also the starting MC (199 %, d.b.) of roof angle 51^0 was slightly lower than that of roof 81^0 (figure 5.11a), and this could cause a slight different in the drying rate, as reported by Ekechukwu (1991a) and Okos et al. (1992) among others. The MC at the end of day 1 was 162.5 % (d.b.), which was higher than that of roof 81^0, although roof 81^0 began with a higher MC. The colour of the cassava had also become brown, as in the trial with roof 81^0. In the night, the RH decreased from 58 % to 48 % on the morning of the second day (figure 5.9a), and the MC dropped to 131 %, d.b. (figure 5.11a).

During day 2, the RH dropped steadily to 30 % in six hours and then rose to 32 % in the last hour. In this seven-hour period the MC fell to around 100 %, d.b.(figure 5.11a) with drying rates prevailing just below 0.05 $kg_w/(kg_s.h)$ from the third up to the sixth hour (figure 5.13a). Though slightly lower than on the first day, the inlet velocity (changing from the ambient 0.01 m/s to prevail around an average of 0,13 m/s) was still higher than that on day 2 of roof 81^0 (figure 5.8a). The drying rate was also higher than in roof 81^0 for the same drying period. This could be from the combined effect of higher airflow rate, lower RH (figure 5.9a) and slightly higher MC (figure 5.11a).

The MC on the morning of day 3 was 77.68 % (d.b.), and the RH was 60 %. The RH fell to an average of 45 % in three hours and stayed around this value for the rest of the day. The inlet velocity got to around 0.12 m/s from the first to the fourth hour. The value then increased to 0.14 m/s in the fifth hour and reduced to 0.13 m/s for the last two hours (figure 5.8a). As shown in figure 5.13a, the drying rate reached just about 0.036 $kg_w/(kg_s.h)$ in the first three hours. The rate then got to around 0.03 $kg_w/(kg_s.h)$ in hour 4, and remained at this value till the sixth hour before ending the day at around 0.027 $kg_w/(kg_s.h)$. The third day drying ended with an MC of 57.5 %, slightly higher

than for roof 81^0 which had 54 % at the end of day 3 (figure 5.11a). The MC was at 43.5 % (d.b.) while the RH got to 63 % by the morning of day 4.

The temperature trend was again similar to that of the no-load counterpart, but the values were lower due to the shading below the crop shelf and the higher humidity above the crops. At heights 6, 16, 26, 49, 84 and 109 cm, the temperatures above ambient on the first day were -1.00, 1.86, 1.71, 2.00, 5.43 and 5.14 ^{0}C respectively (figure 5.15). Those for day 2 at corresponding heights were 0.00, 2.29, 2.29, 2.29, 5.43 and 5.43 ^{0}C and those for day 3 were 0.29, 2.71, 2.57, 2.86, 5.57 and 5.00 ^{0}C in that order.

5.2.2 Effects of the solar chimney, roof angle and inlet gap on drying; test-set 6

In this section, the results of drying with the solar chimney for the three inlet gaps of each roof angle are presented and discussed. These results are compared with each other and also with those obtained for similar drying-chamber configurations with the normal chimney. Airflow comparisons are also made with the no-load trials of similar dryer configurations. This is required for examining the effect of using the solar chimney in conjunction with a given roof angle and inlet area on crop drying.

5.2.2.1 Drying with the solar chimney and roof angle 81^0

Using the inlet gap 70 mm with roof angle 81^0

With the inlet gap 70 mm, the experiment began in an RH of 70 % which got down to 65 % for the next five hours and then to 64 % for the last two hours (see figures 5.9a and 5.10a). The inlet velocity rose from the ambient to stay at 15 m/s for three hours, increased steadily to 17 m/s on the fifth hour and then fell again to 16 m/s in the remaining two hours. These values were predominantly lower than those of the no-load trial but much higher than the counterpart with normal chimney (see table 5.1 and figure 5.8a).

The first day started with 196 % (d.b.) MC. The drying rate reached around 0.067 $kg_w/(kg_s.h)$ on the second hour. It then reduced to 0.062 $kg_w/(kg_s.h)$ for the next three

hours, and then back to 0.067 $kg_w/(kg_s.h)$ on hour 6 and again to 0.062 $kg_w/(kg_s.h)$ in the end, as shown in figure 5.13a. The drying-rate was slightly less than that with the normal chimney for greater part of the first day, in spite of the higher airflow enhanced by the solar chimney. This is attributable to the slightly lower MC and much higher ambient relative humidity whose effect overrode that of the airflow. The first day ended with an MC of 152 % (figure 5 11a). The relative humidity (RH) remained fairly higher in the night, falling to only around 61 % the next morning. The self drying on the first night was thus lower (with the MC falling only to 133 %, d.b.) than that with normal chimney. Spots of sticky fluids were observed on the surfaces of the crops.

Drying proceeded on day 2 with the RH falling below 60 % within the first hour. The inlet velocity hovered mostly between 0.16 and 0.17 m/s. The drying rate changed from 0.024 $kg_w/(kg_s.h)$ in the first hour through 0.049 $kg_w/(kg_s.h)$ in the second hour to above 0.05 $kg_w/(kg_s.h)$ in the fourth hour. It then dropped continuously to remain at 0.044 $kg_w/(kg_s.h)$ in the sixth and seventh hours. Thus, with the RH below 60 % for most of the day, the higher airflow together with the higher MC caused a slightly higher drying rate than that with the normal chimney. Also, the drying process in the early hours consisted mainly of the evaporation of the fluid that had deposited at the crop surface the previous night, and this was easier than the moisture diffusion from within the crop. But this rate was not enough, and the MC at the end of day 2 was 102.4 %, still higher than that of the normal chimney.

As compared to that with normal chimney, the RH remained relatively higher (rising from 54 % to 57 %) at night, and so was the MC (78.51 %, d.b.) on the morning of day 3. There was however no more sticky fluid on the crop surfaces. The inlet velocity stayed around 0.16 m/s for most of day 3, as the RH fell continuously to 39 % by the last hour and the MC dropped to 59.4 % (d.b.). The moisture reduction on this day was not so different from that with normal chimney in the same period. Thus the difference in their RH (both well below 60 % RH for most of the day) apparently did not cause any significant difference in their drying rates. The higher airflow was not that effective on the third day. By the next morning, the RH had risen again to 63 %, and the MC was 44.8 %.

Comparing figure 5.1 or 5.4 and figure 5.15 or 5.18 respectively, it could be seen that the air temperature rose as the air moved upwards. The temperatures above ambient were though smaller, as compared to the no-load trial of the same roof 81^0 inlet gap 70 mm, apparently due to the shading of the base and the higher humidity ratio, as explained earlier. The temperatures above ambient at heights 6, 16, 26, 49, 84 and 109 cm on the first day were respectively -0.71, 1.71, 1.71, 1.86, 7.71, and 7.86 ^{0}C (figure 5.15). Those at similar heights on day 2 were -0.71, 2.14, 1.86, 3.29, 7.57 and 7.71 ^{0}C, and values of -0.86, 2.29, 2.43, 4.29, 7.86 and 7.71 ^{0}C were recorded in the same order for day 3 (figure 5.15).

Using the inlet gap 50 mm with roof angle 81^0

The RH for the trial with roof angle 81^0 and inlet gap 50 mm was 63 % at start of the experiment. The value then fell steadily down to 47 % in six hours and rose to 49 % (figures 5.9b and 5.10a). The inlet velocity rose from ambient and hovered around an average of 0.21 m/s (see figure 5.8b). This was lower than that observed in the no-load trial (see table 5.1). The MC dropped from 197 % at the start to 156.2 % at the end of day 1 (figure 5.11b). As shown in figure 5.13b, the dominant drying rate was around 0.062 $kg_w/(kg_s.h)$. The performance was not so much below that of inlet gap 70 mm with the solar chimney (figures 5.12a and 5.14a). Thus the effect of poor humidity conditions in the trial with inlet 70 mm appeared to balance the effect of inlet airflow restrictions of the smaller inlet of 50 mm. Again, the crop looked brownish by the evening. In the first night, an MC drop of 25.7 % occurred to an MC of 130.5 %, as the RH varied from 49 to 67 % by the morning of day 2. This drop was better than that of inlet 70 mm whose drop in the same period was around 19 % (figure 5.12a) with RH levels of 64 to 61 % (figure 5.10a). Hence, in an absence of higher airflow, the RH became the dominant determining factor in the night. Spots of fluids were however found on the surfaces of the cassava on the morning of the second day.

On day 2, the RH reduced continually through 50 % around the middle of the day to 45 % at close of the day. The inlet velocity again rose from ambient to hover around an average value of 0.21 m/s (figure 5.8b). Like the case of inlet 70 mm, the early hours of

day 2 consisted mainly of evaporation of fluid from the surface. The drying rate increased from around 0.02 $kg_w/(kg_s.h)$ in the first hour to remain around 0.053 $kg_w/(kg_s.h)$ for the next three hours, dropped just below 0.05 $kg_w/(kg_s.h)$ in the next two hours and then ended the day at around 0.045 $kg_w/(kg_s.h)$ as in figure 5.13b. The MC fell to 98 % (d.b.) by the end of day 2 (figure 5.11b). During the second night, the RH rose from 45 % to 60 %, with the MC dropping by 28 % to around 70 % (d.b.) on the third morning. This was again higher than the MC drop of about 24 % of inlet 70 mm in an RH of 54 to 57 % (figure 5.10a). However, mould had started developing on the surfaces of the crop in this trial (roof 81^0 inlet 50 mm).

On day 3, the RH reduced from 60 to 59 % for two hours, and then increased continuously to 68 % in the sixth hour before dropping to 61 % in the last hour. The inlet velocity rose through 0.18 m/s in the first hour to 24 m/s in the third hour and hovered around an average of 0.22 m/s for the rest of the day (figure 5.8b). The drying rate remained around 0.027 $kg_w/(kg_s.h)$, slightly higher than that for inlet 70 mm of same roof angle for the first half of the day, and then fell lower to 0.022 $kg_w/(kg_s.h)$ for the rest of the day (figure 5.14a). The MC at the end of the day was 52 %, d.b. as compared to that of inlet 70 mm (59 %, d.b., figure 5.12a). The MC dropped to 39 %, d.b with the RH falling to 50 % on the fourth morning. Thus the process ended with a lower MC than that of inlet 70 mm which ended with around 45 %, d.b. The RH effect nullified or overrode the airflow effect throughout the process. In spite of the relatively lower MC, the crops of inlet 50 mm were still mouldy on the day 4. This is attributable to the possible low quality of the cassava. The researcher had not much control of the quality of cassava which was always purchased from the open market in Leicester, England, the day before each drying trial.

The temperatures above ambient corresponding to heights 6, 16, 26, 49, 84 and 109 cm for inlet gap 50 mm with roof angle 81^0 were -1.29, 0.71, 1.00, 4.43, 7.29 and 7.51 ^0C on the first day, -1.29, 1.86, 1.71, 4.71, 7.29 and 7.57 ^0C on day 2 and -1.00, 3.29, 2.86, 5.29, 8.14 and 7.86 ^0C on day 3 (see figure 5.18). This follows the general trend, but the air always left the drying chamber (at height 49 cm) at a higher temperature than in

the trial with inlet gap 70 mm in which the same quantity of irradiation energy has to heat greater mass of air.

Using the inlet gap 30 mm with roof angle 81^0

On the first day of the trial with roof angle 81^0 inlet gap 30 mm, the RH at the beginning was 50 %, which fell continuously to 38 % at the close of the day (figure 5.9c or 5.10a). From the ambient value at the start, the inlet velocity went up to 0.32 m/s in the first hour, fell to 0.29 m/s in the second hour, got to 0.34 m/s in the fourth hour and fell again to 0.32 m/s in the last hour (figure 5.8c). This was again less than that of the no-load trial of the same configuration (compare the value of table 5.1).

Starting with an MC of around 205 % (d.b.) in the morning, the first day ended with around 160 %, d.b. (see figure 5.11c or 5.12a). The drying rate was just below 0.06 $kg_w/(kg_s.h)$ in the first two hours, and this got to around 0.069 $kg_w/(kg_s.h)$ in the fourth and fifth hours, fell to around 0.06 $kg_w/(kg_s.h)$ in the sixth hour and rose again to 0.069 $kg_w/(kg_s.h)$ in the end (figure 5.14a). Thus, the first-day performance was better than those of inlet gaps 50 mm and 70 mm (see also figure 5.12a) as the RH was much lower (figure 5.10a), overriding the effect of airflow restriction at inlet. The smaller amount of air could also be better preheated. But the crop had again turned brownish by close of day 1, as the MC was still high. Also, the RH stayed relatively lower in the night (35 to 48 %), and the MC drop from 160 % to 127 % was the best of all the three inlet gaps. Unlike the case of inlet gaps 50 mm and 70 mm, no fluid was observed at any crop surface the next morning

On day 2, the RH remained the lowest. It rose to 50 % in the first hour, fell steadily to 38 % on the sixth hour and then rose slightly to 39 % in the evening. The inlet velocity rose from the ambient value in the beginning to hover around an average of 0.3 m/s the whole day. The drying rate rose to remain just above 0.04 $kg_w/(kg_s.h)$ from hour 2 to the rest of the day, and this was lower than those of inlet gaps 50 mm and 70 mm (figure5.14a). The moisture had to diffuse from within the crops, unlike the other two where the drying of day 2 consisted mainly of surface fluid evaporation as explained earlier. Also the RH gaps had reduced compared to day 1, with all three operating

below 60 % (see figure 5.10a). Hence the effect of higher mass flow of air and higher MC came into play. So the need for moisture to diffuse to the surface, the lowest mass inlet of air and the lowest MC of the trial with inlet gap 30 mm caused this trial to dry slower than the others on day 2. The day ended with MC of around 99 %, d.b. During the second night, the RH increased from 39 % to 61 %, as the MC dropped to 75 %.

The inlet velocity on the third day was not much different from day 2, staying predominantly around the average of 0.31 m/s (figure 5.8c). The RH started at 61 % and then remained between 58 and 59 % (figure 5.10a). The drying rate increased to 0.027 $kg_w/(kg_s.h)$ by the third hour and remained till the fifth hour and dropped to 0.018 $kg_w/(kg_s.h)$ in the end (figure 5.14a). The MC at the end of day 3 was 60 % (d.b.). With the RH increasing to 63 % by the next morning, the trial of roof angle 81^0 inlet 30 ended with 48 % MC, higher than those of inlet gaps 50 mm and 70 mm.

The following are the temperatures above ambient at heights 6, 16, 26, 49, 84 and 109 cm on various days of drying as shown in figures 5.17 and 5.18. Day 1 had -0.14, 1.71, 2.14, 5.14, 7.71 and 7.86 ^{0}C respectively. The corresponding temperatures for day 2 were 0.14, 2.00, 2.43, 6.29, 8.14 and 7.17 ^{0}C, and those for day 3 were -0.29, 3.00, 3.14, 5.71, 8.43 and 8.57 ^{0}C. With mass flow of air further restricted at the inlet, the air left the drying chamber (height 49 cm) with the highest temperature rise of all trials of roof angle 81^0 with solar chimney. Also, the temperature depression at inlet is reduced as compared to those of higher inlet gaps (figure 5.18a). Hence the small amount of air allowed into the drying chamber experienced higher temperature rise than those with higher inlet gap, which let in higher mass of air in a given time.

5.2.2.2 Drying with the solar chimney and roof angle 64^0

<u>Using the inlet gap 70 mm with roof angle 64^0</u>

The experiment with the inlet gap 70 mm and roof angle 64^0 began in an environment of RH 58 % which then fell continuously to 40 % in six hours and then rose again to 44 % in the last hour (figure 5.9a). The inlet velocity changed from the ambient value to 0.15 m/s in two hours, stayed between 0.16 m/s and 0.17 m/s for the next four hours and fell again to 0.15 m/s in the last hour (figure 5.8a). The MC dropped from 199 % at the

beginning to around 152 % (d.b.) by close of the day (figure 5.11a). The drying rate prevailed around 0.072 $kg_w/(kg_s.h)$ from the second up to the fifth hour and reduced to 0.067 $kg_w/(kg_s.h)$ for the last two hours. These were higher than those of roof 81^0 of the same dying configuration (see figure 5.13a) as a result of the low levels of RH. With this relatively lower MC, the browning of the crop at the end of day 1 was barely noticeable, compared to those of the other trials described earlier. The RH was still lower at night, rising only to 48 % (figure 5.9a). This resulted in a higher drop of MC (from 152 % to 121 %, d.b.) as compared to that of roof 81^0 of the same inlet, which fell from 152 % to 133 %, d.b. on the first night (figure 5.11a).

As shown in figure 5.9a, the RH fell steadily from 48 % to 31 % on day 2. This was still much lower that of roof 81^0 of the same inlet gap, which though had also fallen in this time to below 60 %. The inlet velocity was slightly higher, averaging around 0.17 m/s. These together gave rise to a somewhat higher drying rate for most of day 2. The drying rate started at 0.033 $kg_w/(kg_s.h)$, increased to 0.054 $kg_w/(kg_s.h)$ for the next two hours, fell to around 0.049 $kg_w/(kg_s.h)$ for the following two hours and then reduced again to 0.045 $kg_w/(kg_s.h)$ in the last two hours (figure 5.13a). The MC fell from 121 % to 88 %, d.b. on the second day (figure 5.11a). The MC reduced further in the night to 65.5 % (d.b.), while the RH increased to 58 % (figure 5.9a) by the morning of the third day.

The inlet velocity on the third day averaged around 0.18 m/s (figure 5.8a). The RH decreased steadily to 48 % in the sixth and seventh hours. The drying rate increased to remain around 0.027 $kg_w/(kg_s.h)$ from the second to the fourth hour, dropped to 0.022 $kg_w/(kg_s.h)$ for the next two hours and fell to 0.018 $kg_w/(kg_s.h)$ in the last hour. These rates were mostly lower than those of roof 81 inlet 70 mm on day 3, despite the higher airflow. This may again be attributed to the higher RH values in the same period. The MC dropped from 65.5 % to 49 % (d.b.) by the end of the day. In comparison to that of inlet 70 mm, the night self drying was lower with the MC dropping by 11 % to 38 % (d.b.) on the morning of day 4, as the RH increased to 64 %.

The temperatures above ambient at heights 6, 16, 26, 49, 84 and 109 cm were -0.14, 1.43, 2.29, 3.29, 8.29 and 7.71 ^{0}C respectively on day 1 (figure 5.15). Corresponding values on day 2 were 0.00, 2.57, 2.86, 3.57, 8.14 and 8.14 ^{0}C and those measured above ambient on day 3 were 0.29, 3.57, 3.43, 4.43, 7.71 and 7.71 ^{0}C, in that order. As seen from figure 5.15 (a and b), the temperatures above ambient were higher than in the trial of roof 81^0 (of the same inlet gap) at most of the points in the first two days. The vast difference of RH in these periods could be the cause. On the third day, the effect of the slight difference of RH (figure 5.9a) seemed to have been balanced by differences in the drying rates. The air left the drying chamber around the same temperatures as those of roof 81^0 (figure 5.15c).

Using the inlet gap 50 mm with roof angle 64^0

The inlet velocity of the trial with roof angle 64^0 inlet gap 50 mm prevailed between 0.21 and 0.24 m/s (with average of 0.22 m/s) from the second hour up to the end of day 1 (figure 5.8b), lower than that of the no-load trial of the same dryer configuration (compare the value from table 5.1). The RH started as 64 % and reduced continuously to 49 % in the last two hours. The values were at any point higher than those of roof 81^0 with the same inlet gap of 50 mm (figure 5.9b) and those of inlet gap 70 mm of the same roof angle 64^0 (figure 5.10b). The high RH values led to lower performance than the other two configurations, irrespective of the airflow rate. The drying rate was relatively lower, around 0.059 $kg_w/(kg_s.h)$ from the second hour to the close of the day (see figures 5.13b and 5.14b). The MC dropped from 201 % to 162 %, d.b. (figures 5.11b and 5.12b) with the colour of the crop turned brown by the evening. The RH rose in the night to 69 % the next morning, and the MC dropped to 140 % (d.b.) with some sticky fluids on the crop surfaces.

On the second day, the inlet velocity was most prevalent around 0.23 m/s in a highly humid environment of RH from 69 % in the morning to 57 % in the evening. The high RH again gave rise to lower performance than on the second day of inlet 70 mm and that of roof 81^0 inlet 50 mm. However, the initial evaporation of the surface fluids caused a higher average drying rate in the first three hours before the effect of the higher RH on drying came into play. The drying rate started around 0.04 $kg_w/(kg_s.h)$, peaked

around 0.059 $kg_w/(kg_s.h)$ in the third hour, fell again to 0.04 $kg_w/(kg_s.h)$ on the sixth hour and then rose again to 0.054 $kg_w/(kg_s.h)$ in the last hour (figures 5.13b and 5.14b). The crop dried from the MC of 140 % to 106 %, d.b. (figures 5.11b and 5.12b) on day 2. The second night was still humid (57 to 58 %), and the fluid had again deposited on the crop surfaces by the morning of day 3. The MC at this time was 85 % (d.b.).

On day 3, the inlet velocity rose from the ambient value to remain between 0.20 and 0.24 m/s (figure 5.8b). The RH reduced to 49 % in the second and third hours and then decreased steadily to 42 % on hour 6 before rising again to 44 % in the end. The values were at any point lower than those of roof 81 inlet 50 mm and roof 64^0 inlet 70 mm (figures 5.9b and 5.10b). The drying rate was higher than these other two on this day (figures 5.13b and 5.14b). This could be the result of lower RH and higher MC. The day began with an MC of 85 % (d.b.) and ended with 61 % (figures 5.11b and 5.12b). The RH rose to 58 % while the MC reduced to 46 % (d.b) the next morning. Mould had developed on the surfaces of the crop.

The general curve profile was maintained for the temperature above ambient, increasing with increase in height. Temperatures corresponding to heights 6, 16, 26, 49, 84 and 109 cm were -1.29, 1.57, 2.29, 3.29, 8.14 and 7.43 ^{0}C on the first day, -0.71, 2.14, 2.71, 3.86, 8.29 and 8.00 ^{0}C and -0.71, 2.43, 2.43, 3.71, 7.86 and 7.43 on the second and third days respectively (see figure 5.16 or 5.19). The air left the drying chamber with a lower temperature rise than that with the same inlet of roof 81^0 (figure 5.16). However, in the first two days the temperature was higher inside the drying chamber. This may be attributed to the lower drying rates on those days. On the third day, the drying rate was high and the temperatures were lower. The irradiation energy falling into the drying chamber had to be shared between drying and heating, so that higher drying rate resulted in low temperature rise. In figure 19, the temperature difference with that of the inlet 70 mm of the same roof angle was not much on day 1. The effect of high RH apparently tried to balance that of low drying rate in relation to inlet 70 mm. On day 2, inlet 70 (of same roof angle) had much lower RH (figure 5.10) and so the temperatures of roof angle 64^0 inlet 50 mm were slightly lower in the chamber, in spite of the lower

drying rate. On day 3, the temperatures were clearly lower as the drying rate was much higher.

Using the inlet gap 30 mm with roof angle 64^0

With the inlet gap at 30 mm, the inlet velocity on day 1 hovered between 0.32 and 0.34 m/s, again lower than the no-load counterpart (compare values of table 5.1 and figure 5.8c). Starting with 58 %, the RH reduced and stayed at 55 % for the next two hours and then decreased progressively to 46 % at the close of the day. The values were much higher than those of roof 81^0 of the same inlet gap (figure 5.9c) but slightly lower than those of inlet 50 mm of the same roof angle (figure 5.10 b). The MC of 200 % at the beginning dropped by 45 % to 155 %, d.b. (figure 5.11c) with a predominant drying with of 0.0675 $kg_w/(kg_s.h)$ as shown in figure 5.13c. Thus, despite the much higher RH, the first-day performance was just about that of roof 81^0 inlet 30. The effect of the slightly higher airflow seemed to balance that of the difference in RH both of which were below 60 %. Also in spite of the just slightly lower RH and the airflow restriction at inlet in comparison to inlet 50 mm of the same roof angle, the performance was much better than that of inlet 50 mm whose MC drop for the same period was 39 %. This result could be attributed to the fact that the much lower amount of air that was allowed into the dryer was better heated by that part of the irradiation energy that trickled down to the base of the drying chamber. Hence the air came into contact with the crops with lower RH than ambient. The crops were somewhat brownish in the evening. The RH rose to 57 % and MC reduced to 128.5 % by the morning of day 2 (figure 5.9c or 5.10b).

During day 2, the RH fell to remain at 56 % for the first three hours, and then got to 55 % for the next three hours and then finally to 54 % in the last hour. The inlet velocity remained around an average of 0.33 m/s. The drying rate was most prevalent at 0.045 $kg_w/(kg_s.h)$, higher than that of roof 81^0 of the same inlet gap (figure 5.13c). Again, the RH was higher than in roof 81^0, but both fell below 60 % (figure 5.9c) so that the higher airflow became more effective. But it was lower for most of the day than that of inlet 50 of the same roof angle (figure 5.14b) whose second day consisted mostly of the clearing of deposited fluid from the surface, as already explained. The crop was dried

to 97.5 % (d.b.) on day 2. During the night, the RH rose to 61 %, while the MC fell to 78 %, on the morning of the third day.

The third-day drying of roof 64^0 inlet 30 mm took place with the RH reducing to 55 % in the second and third hours, and then changing further to 50 % on the sixth hour and then back to 52 % in the end. These were generally lower than in the trial of roof 81^0 inlet 30 mm (figure 5.9c) but higher than that of roof 64 inlet 50 mm (figure 5.10b). The inlet velocity averaged around 0.34 m/s (figure 5.8c). The already lower RH of the air together with its added effectiveness of heating caused a much higher drying rate than in roof 81^0 of equal inlet gap (figure 5.13c). Starting at 0.024 $kg_w/(kg_s.h)$ in the first hour, the value changed to 0.036 $kg_w/(kg_s.h)$ for the next three hours and then changed back to 0.031 $kg_w/(kg_s.h)$ in the last three hours. The rate was however comparable on the average to that of inlet 50 mm of equal roof angle, despite the higher RH (figure 5.14b). This is again attributable to an improved heating of smaller amount of air before the air got to the crops, as explained earlier. The crop was dried from MC of 78 % to 55 %, d.b. on day 3. On the morning of day 4, the RH was 61 % and the MC was 42 %.

As shown in figures 5.17 and 5.19, the temperatures recorded above ambient on day 1 at the usual heights 6, 16, 26, 49, 84 and 109 cm were -0.14, 1.71, 2.71, 4.29, 8.86 and 8.43 ^{0}C respectively. The corresponding temperatures above ambient on the second day were 0.00, 2.29, 2.86, 4.14, 8.43 and 8.00 ^{0}C, and those on the third day were 0.43, 3.29, 3.14, 4.57, 8.57 and 8.43 ^{0}C. Like the trial of roof 81^0 inlet 30 mm, the air left the drying chamber with the highest temperature of all those trials with roof 64^0, with least temperature depression at inlet in most cases (figure 5.19).

5.2.2.3 Drying with the solar chimney and roof angle 51^0

<u>Using the inlet gap 70 mm with roof angle 51^0</u>

With the roof angle 51^0 inlet gap 70 mm, the trial began with MC 196 %, d.b. (figure 5.11a) in an ambient RH of 58 %. The RH fell steadily to 38 % on the sixth hour and rose slightly to 39 % at the close of the day (figure 5.9a). The inlet velocity prevailed around an average of 0.17 m/s for most of the day (figure 5.8a); lower than what was

observed in the no-load trial of the same dryer configuration (compare table 5.1). With comparable RH to those of other roof angles with similar inlet gaps, all of which fell below 60 %, the highest airflow in this trial became the deciding factor of the drying rate. The first-day drying rate was therefore the highest of all the trials in test-set 6. As shown in figures 5.13a and 5.14c, the drying rate was most prevalent around 0.075 $kg_w/(kg_s.h)$ up to the fifth hour, and then reduced steadily to 0.067 $kg_w/(kg_s.h)$ in the end. The trial ended the day with MC of 145 % (d.b.), showing the highest MC drop of all the first-day drying processes in test-set 6 (figures 5.11a and 5.12c). Unlike the other results discussed so far, no change was observed in the colour of the crop. This may be due the high moisture drop which was able to match the temperature rise in the drying chamber, as explained in chapter 2. This trial also had the lowest RH values (from 39 % to 49 %) in the first night (figure 5.9a or 5.10c). It therefore had the best night performance with the MC falling from 145 % to 110 % (d.b.) in the night.

Day 2 started in an RH of 49 %. The RH reduced within an hour and stayed between 42 % and 40 % throughout the day (figure 5.9a or 5.10c). From around the third hour onwards, the environment was more humid than those of roof 64^0 inlet 70 mm in a similar period (figure 5.9a). The inlet velocity averaged around 0.18 m/s for most of the day (figure 5.8a). Again, with both RHs much below 60 %, the higher airflow of roof 51^0 inlet 70 mm gave rise to a higher drying rate than in roof 64^0 inlet 70 mm. However, the difference in the drying rates was lower on day 2 than on day 1. This is attributable to the fact that higher airflow did not affect the drying process so much on the second day as on the first day of drying. With average drying rate of around 0.52 $kg_w/(kg_s.h)$, the trial ended the second day with 73.33 % (d.b.) MC. The second night performance was not much different from that in roof angle 64^0 of a similar inlet gap (figure 5.11a); the MC reduced from 73.33 % to 52 % (d.b.) in an RH range of 40 % to 53 %.

On day 3, the RH fell to 32 % in five hours and then rose to 36 % by the end of the day. The inlet velocity rose from ambient to hover between 0.18 m/s and 0.19 m/s in the first five hours, and then rose steadily to 0.24 m/s by the end of the day. This marked increase of velocity may be due to shrinkage of the crop in the drying process, and

therefore the reduction of resistance to the airflow. The shrinkage also caused more exposure of the metallic shelf to the lamps, so that additional heat could be transferred to the air to boost the airflow. With the drying rate prevailing at 0.031 $kg_w/(kg_s.h)$ for six hours and then dropping just to 0.027 $kg_w/(kg_s.h)$ in the last hour, the MC decreased from 52 % in the morning to 30.7 % (d.b.) in the evening. The overnight rise of RH was rather high, rising to 61 % on the morning of day 4. This, together with the already low moisture content at the end of day 3, resulted in the lowest night drying in all the trials in test-set 6. The MC fell from 30.7 % to 25.33 % (d.b.) on the morning of day 4 (figure 5.11a or 5.12c).

The following are the respective temperatures above ambient at heights 6, 16, 26, 49, 84 and 109 cm on various drying days (figure 5.15 or 5.20). The first day had 0.14, 1.43, 1.43, 3.00, 8.14 and 8.29 ^{0}C. The second day had 0.00, 2.00, 2.00, 2.86, 8.14 and 8.14 ^{0}C, whilst -0.86, 2.14, 2.14, 3.14, 8.14 and 8.57 ^{0}C were recorded for the corresponding heights on the third day. These values were generally the lowest, compared to those recorded at similar points in other trials of test-set 6 (figures 5.15 and 5.20). This could have been caused by a combination of low RH, high airflow and high drying rate.

Using the inlet gap 50 mm with roof angle 51^0

This trial started in a fairly humid environment of RH 57 %. The RH then dropped to 54 % the next hour, rose again to remain at 59 % in the next four hours and reduced steadily to 51 % in the last hour. These were quite higher than those of roof 64^0 of the same inlet gap, from the third hour to the end of day 1 (figure 5.9b). The RH values were also much higher than those of inlet 70 mm of the same roof angle, for most of the day (figure 5.10c). The inlet velocity was again lower than that in the no-load, prevailing around an average of 0.24 m/s (see table 5.1 and figure 5.8b). The dryer did not perform so well as in roof 51^0 inlet 70 mm on day 1 (figures 5.12c and 4.14c). This may be due to higher humidity and lower velocity from the airflow restriction at inlet. However, it did better than in the trial with roof 64^0 with the same inlet gap of 50 mm (figures 5.11b and 5.13b), as the effect of higher velocity withstood that of RH (both of which fell mostly around 50 % to 60 %). The drying rate was most prevalent at 0.067 $kg_w/(kg_s.h)$, with the crops being dried from MC of 198.5 % to 152 % (d.b.). The crops

were slightly brownish. The RH increased to 54 %, and the MC reduced to 124 % (d.b.) by the next morning. There were fluid deposits at the crop surfaces.

On the second day, the RH fell steadily for four hours to 40 % and rose to remain at 44 % in the last two hours. Rising from the ambient value as usual in the beginning, the inlet velocity remained around the average value of 0.25 m/s. On the average, the RH was higher with lower airflow, in comparison to those of inlet 70 mm of the same roof angle. However, the rapid evaporation of the fluid from the crop surface resulted in comparable performance to that of inlet 70 mm. The drying rate started at 0.034 $kg_w/(kg_s.h)$, remained at 0.054 $kg_w/(kg_s.h)$ in the next four hours and then reduced to 0.045 $kg_w/(kg_s.h)$ in the last two hours. The MC dropped from 124 % to 90 % (d.b.) on day 2. The RH rose in the night from 44 % to 52 %, and the MC fell to 64.5 % on the third morning. The fluid had by then disappeared from the crop surface.

On day 3, the RH fell progressively to 41 % in the third and fourth hours, got to 43 % in the sixth hour and back to 41 % in the last hour. These were in most cases lower than that of roof 64^0 inlet 50 mm (figure 5.9b) but higher than in roof 51^0 inlet 70 mm (figure 5.10c). Also, at any time of day 3 the MC was lower than in the former (figure 5.11b) but higher than in the latter (figure 5.12c). The effect of MC tended to nullify that of RH. So on the average, the drying rate was not much different from in roof 51^0 inlet 70 mm (figure 5.12c), but it was slightly lower than in roof 64^0 inlet 50 mm (figure 5.13b). The drying rate was at 0.033 $kg_w/(kg_s.h)$ and 0.036 $kg_w/(kg_s.h)$ in the first and second hours respectively, then at 0.031 $kg_w/(kg_s.h)$ for the next three hours and at 0.027 $kg_w/(kg_s.h)$ in the last two hours. In spite of the lower RH values, the drying rate in the evening was lower than in the morning due to the lower MC, hence confirming the strong effect of MC even on day 3. The MC started at 64.5 % (d.b.) in the morning and ended around 43 % in the evening (figures 5.11b and 5.12c). The RH rose to 64 % whilst the MC fell to 29.5 % by the morning of day 4.

On the first day, the temperatures above ambient were 0.14, 2.71, 2.71, 3.86, 8.86 and 8.71 ^{0}C at heights 6, 16, 26, 49, 84 and 109 cm respectively (figures 5.16 or 5.20). Those recorded on day 2 at those heights were 0.43, 2.86, 2.86, 4.14, 9.00 and 9.14 ^{0}C

and those on day 3 were 0.43, 3.57, 3.57, 4.14, 9.00 and 9.14 ^{0}C in the order of those heights. The air left the drying chamber with a higher temperature rise than that of inlet 70 mm of the same roof angle (figure 5.20).

Using the inlet gap 30 mm with roof angle 51^0

On the first day, the RH of this trial was not much different from that of roof 64^0 of the same inlet gap (figure 5.9 c), but quite lower than that of inlet 50 mm of the same roof angle (figure 5.10c). The RH began as 59 % and fell continuously to 52 % in the third and fourth hours and fell again to 47 % in the evening. Though lower than in the no-load trial, the average inlet velocity of 0.34 m/s was higher than that of roof 64^0 inlet 30 (figure 5.8c). This higher air flow caused a slightly better drying performance of the inlet gap 30 mm with roof angle 51^0 than with roof 64^0 (figures 5.11c). Also in spite of airflow restrictions at inlet, the trial with roof angle 51^0 inlet 30 mm performed better (see figures 5.12c and 5.14c) than that of inlet 50 mm whose RH was just below 60 % for most of the first day. The drying rate was around 0.068 $kg_w/(kg_s.h)$ from the second to the seventh hour (figures 5.13c), and the MC dropped from 203 % to 157 % (d.b.) as seen in figure 5.12c. The crop however turned brown, due to the temperature rise and the MC which was still high. On the second morning, the RH was 62 % and the MC was 134 % with sticky fluid on the crop surfaces.

The inlet velocity was most prevalent at 0.35 m/s on day 2, with the RH falling continuously to remain at 55 % in the last five hours. The second-day drying consisted mainly of evaporation of deposited fluid, as in the trial of inlet 50 mm of the same roof angle. As the airflow still had strong effect on the loosely held moisture at the surfaces, the drying rate was lower than that of inlet 50 mm which allowed more air into the dryer. The rate was however higher as compared with roof 64^0 inlet 30 mm in which moisture had to diffuse from within the crops. The drying rate was 0.036 $kg_w/(kg_s.h)$ in the beginning, then it rose and remained just below 0.05 $kg_w/(kg_s.h)$ from hour 2 to hour 5, and then fell to 0.045 $kg_w/(kg_s.h)$ in the last two hours. The crop dried from MC 134 % to 102 % (d.b.). The MC dropped in the night by 17 % to 85 % (d.b.), with the RH rising to 55 %, by the third morning.

During the third day, the inlet velocity remained mostly between 0.34 m/s and 0.36 m/s (figure 5.8c). The RH fell steadily to finish the day at 45 %, marginally lower on average than in roof 64^0 of the same inlet gap (figure 5.9c), but fairly higher than in inlet 50 mm of the same roof angle (figure 5.10c). The drying rate started at 0.038 $kg_w/(kg_s.h)$, got to 0.041 $kg_w/(kg_s.h)$ the next hour, stayed at 0.36 $kg_w/(kg_s.h)$ in the third and fourth hours, fell again to 0.032 $kg_w/(kg_s.h)$ the following two hours and then to 0.027 $kg_w/(kg_s.h)$ in the end. The drying rate was higher in this configuration (roof 51^0 inlet 30 mm) than for the other two configurations, irrespective of the RH. This could again be due to the higher MC effect which was stronger than that of RH on day 3. The crop was dried from 85 % (d.b.) to 61 % on day 3 (figures 5.11c and 5.12c). The RH rose in the night to 64 %, with an MC drop of 15 % to 46 % (d.b.) on the fourth morning.

The temperatures recorded above ambient at various heights, 6, 16, 26, 49, 84 and 109 cm, were respectively 0.00, 2.29, 2.29, 4.29, 9.00 and 9.29 ^{0}C for the first day, 0.14, 3.00, 3.00, 4.14, 9.14 and 9.00 ^{0}C for the second day and 0.29, 3.71, 3.71, 4.00, 9.29 and 9.43 ^{0}C for the third day (figure 5.17 or 5.20). Like other trials of inlet 30 mm, the air left the drying chamber with higher temperature than those of greater inlet gaps of similar roof angles, with a general least temperature reduction at inlet (figure 5.20).

5.2.3 Test-set 7: The mutual effects of crop size and air flow

The results of the two types of drying with half the normal size are presented for comparison with those of the Standard Size (SS) in Figure 5.21. The standard size had a quadrant cross section of average radius 30 mm and a height (or thickness) of 15 mm. In the first trial, the crop used half the cross-section (Half Cross-section or HC) with the height maintained at 15 mm. The other trial used half the height (Half Height or HH) and maintained the cross-section of the standard size. All trials used the same mass of 1 kg and the same dryer configuration of roof angle 51^0 inlet gap 70 mm.

HC started with the lowest MC of 194%, whilst SS and HH had 196% and 200% respectively, at the beginning. Even though HC had a bit lower RH (Figure 5.21a) its performance was lower than that of SS on the first day. The RH of both trials were well

below 60%. With half size, the number of crop pieces was almost doubled. Thus, for the same net airflow cross-sectional area, the number of flow boundaries in the HC was about twice that of SS. This increased the resistance to airflow for the HC, with a resultant decrease in the airflow rate (Figure 5.21b) and therefore lower drying rate (Figure 5.21c). HH also had more crop pieces with more flow boundaries. Also, the larger cross-section of crops, as compared with those of HC, meant additional resistance to airflow. However, the reduced height decreased the resistance to the airflow to balance that of the larger area (Duffie and Beckman, 1991; ASHRAE, 2001), so that the inlet velocity was slightly higher than that of HC. Moreover, the top surface area exposed to the lamps for energy absorption was nearly twice that of the others. These, together with the low RH gave the HH the highest drying rate on the first day. HH dried the crop from MC of 200 % to 143 % (d.b.), SS dried from 196 % to 145 % and HC dried from 194 % to 147 % (d.b.).

HC had higher RH levels in the first night (50 % to 51 %) and those of HH were the lowest, falling from 44 % to 38 %. So HH had the lowest MC of 103 % (d.b.) by the second morning, followed by SS with 110 % and HC with 120 % (d.b.). All the second-day RH of HH values were lower than those of the other two. The inlet velocities followed a similar trend to that of day 1. There was a balance between the airflow and RH so that both HH and SS had not much difference in MC drop. HH dried from an MC of 103 % to 67 % (d.b.), whilst SS dried from 110 % to 73 % (d.b.). HC had a slightly lower drop from 120 % to 87 % (d.b.) on day 2. Thus, the effect of higher MC could not override those of higher airflow and lower RH. The second night of HC was fairly humid, rising from 39 % in the evening to 73 % in the morning (Figure 5.21a). In a similar period, the RH rose from 38 % to 53 % for HH and 40 to 53 % for SS. The MC in on the third morning was 44 % (d.b.) for HH, 52 % (d.b.) for SS and 71 % (d.b.) for HC (Figure 5.21d).

On the third day, the RH of SS was fairly lower than that of HH. The RH of HC was much higher than these two, operating above 70 % the whole day. The RH gap between HC and SS was so much that SS dried fastest on day 3, despite the higher MC of HC. But the effect of this higher MC overcame that of lower RH of HH so that HC was

faster than HH for most of the day (Figure 5.21c). The MC of HC was however still the highest at 56 %, d.b. and those of HH and SS were 51 % each. On the morning of day 4, the RH was 61 % for HC, 61% for SS and 48 % for HH. The performance of HH was the best of all three (in fact, of all the trials), ending with MC of 22 %. This was followed by SS which finished at 25 %, whilst the HC was at 41 % (d.b.). The marginally better performance of HH over SS could be due to better humidity conditions in the last night, rather than the smaller size.

5.2.4 Test-set 8: Drying with higher crop mass (1.4 kg cassava)

Figure 5.22 shows the results overview of the trial with 1.4 kg (referred to as trial-1.4) with that of the trial with 1 kg (trial-1). Both started the drying process with MC 196 % (Figure 5.22a). Despite the much lower RH (Figure 5.22b), the drying with 1.4 kg was very slow on the first day (Figure 5.22c). This is attributable to the reduced velocity with the increased number of boundaries (Figure 5.22d) and also the quantity of cassava which was probably too much for the model (i.e. the model was probably working beyond its capacity, though the loading was nowhere near the maximum loading density of 15 kg/m^2). Trial-1.4 ended the day with MC of 154 %, with browning of the cassava, as against that of trial-1 with 145 % (d.b.). The first-night RH values of trial-1.4 were from 41 % to 55 %, and the MC on the next morning was 129 % (d.b.) with fluid on the crop surface.

On day 2, the inlet velocity remained generally lower for trial-1.4 (figure 5.22d), and the RH was higher (figure 5.22b). So neither the higher MC (figure 5.22a) nor the evaporation of fluid on the surface could help raise the drying rate of trial-1.4 towards that of trial-1 (figure 5.22c). It could be seen from (figure 5.22b) that the atmospheric conditions remained poorer for trial-1.4 through the second day and night. At the end of day 2, the MC of trial-1.4 was around 101 % (d.b.) and that of trial-1 was 73 % (d.b.), as shown in figure 5.22a. The MC of trial-1.4 was 83 % (d.b.) on the third morning, whilst that of trial-1 was 52 % (d.b.).

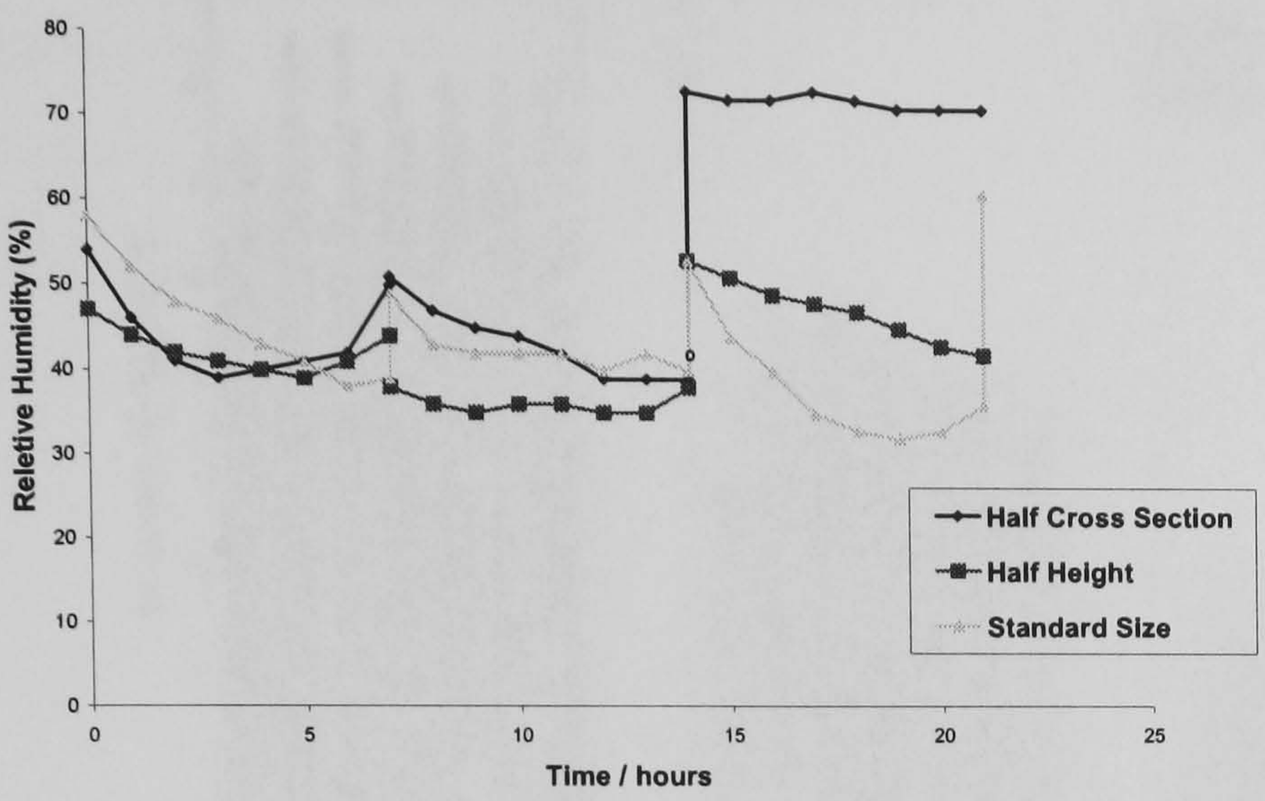

Figure 5.21a Ambient RH vs. Drying Time; Standard and Half Sizes

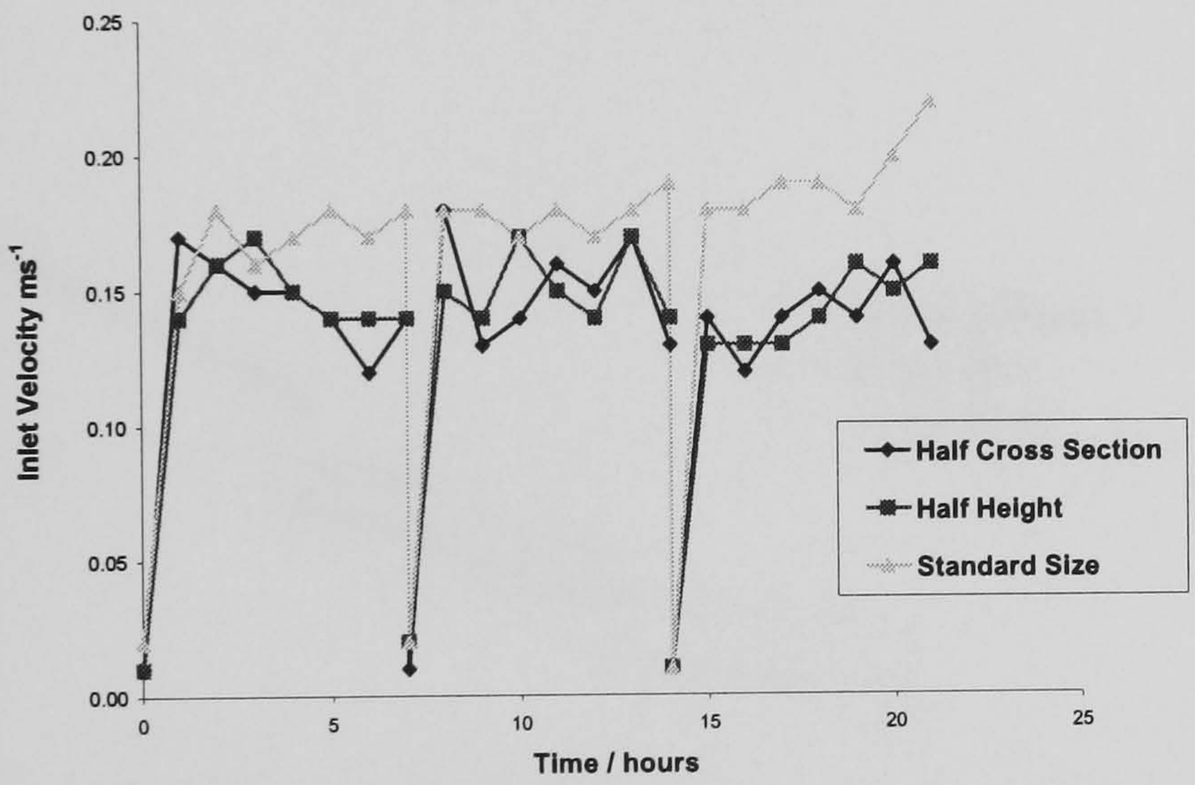

Figure 5.21b Inlet Velocity vs. Drying Time; Standard and Half Sizes

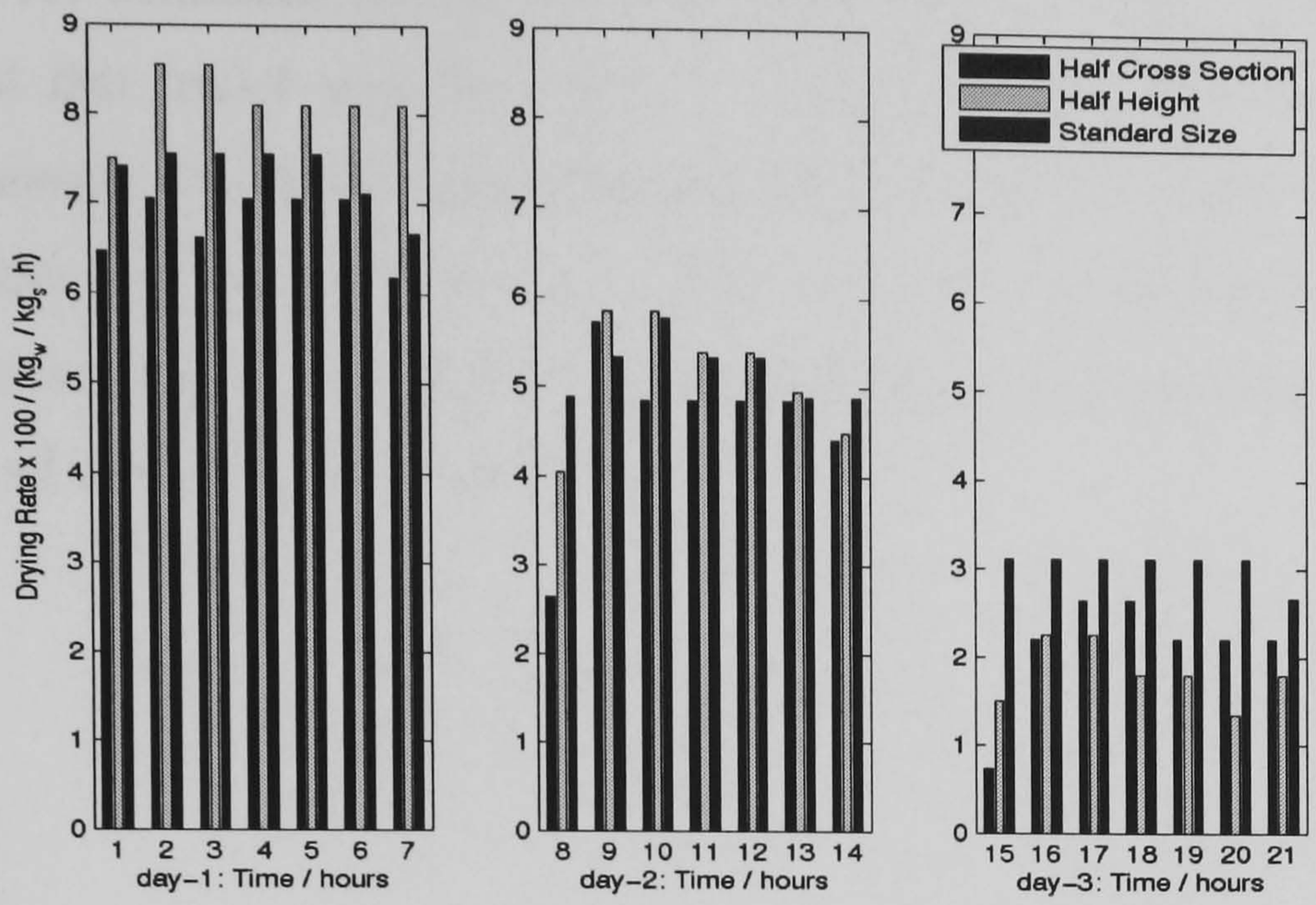

Figure 5.21c Dying Rate vs. Drying Time; Standard and Half Sizes

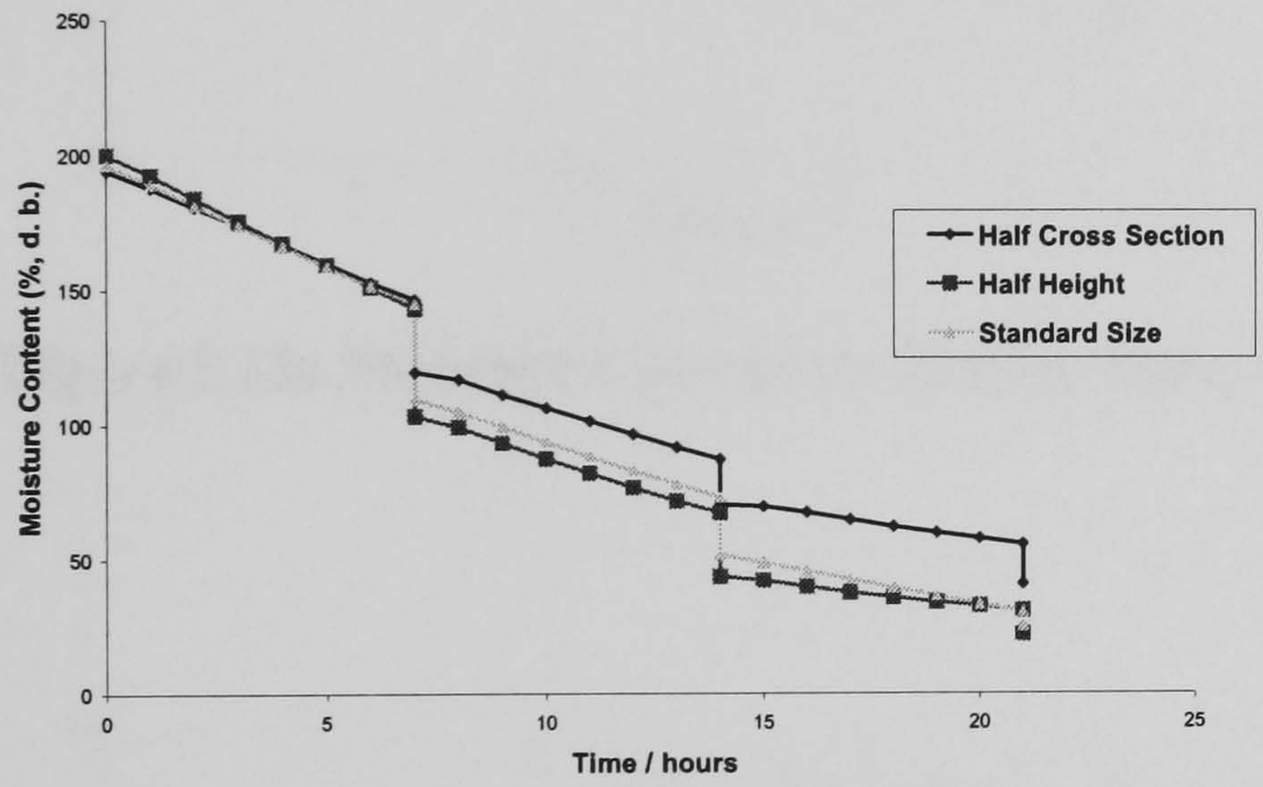

Figure 5.21d Moisture Content vs. Drying Time; Standard and Half Sizes

Trial-1.4 continued on the third day with the RH mostly above 60 % (figure 5.22b), whilst that trial-1 was far lower, yet trial-1.4 started at a faster rate (figure 5.22c). Apparently, the much higher MC had stronger effect than other factors on day 3. There was however not much reduction in MC gap at the end of day 3. Also the RH remained higher in the night for trial-1.4, and so it ended the process with 48% MC, as against the 25% of trial-1 (figure 5.22a).

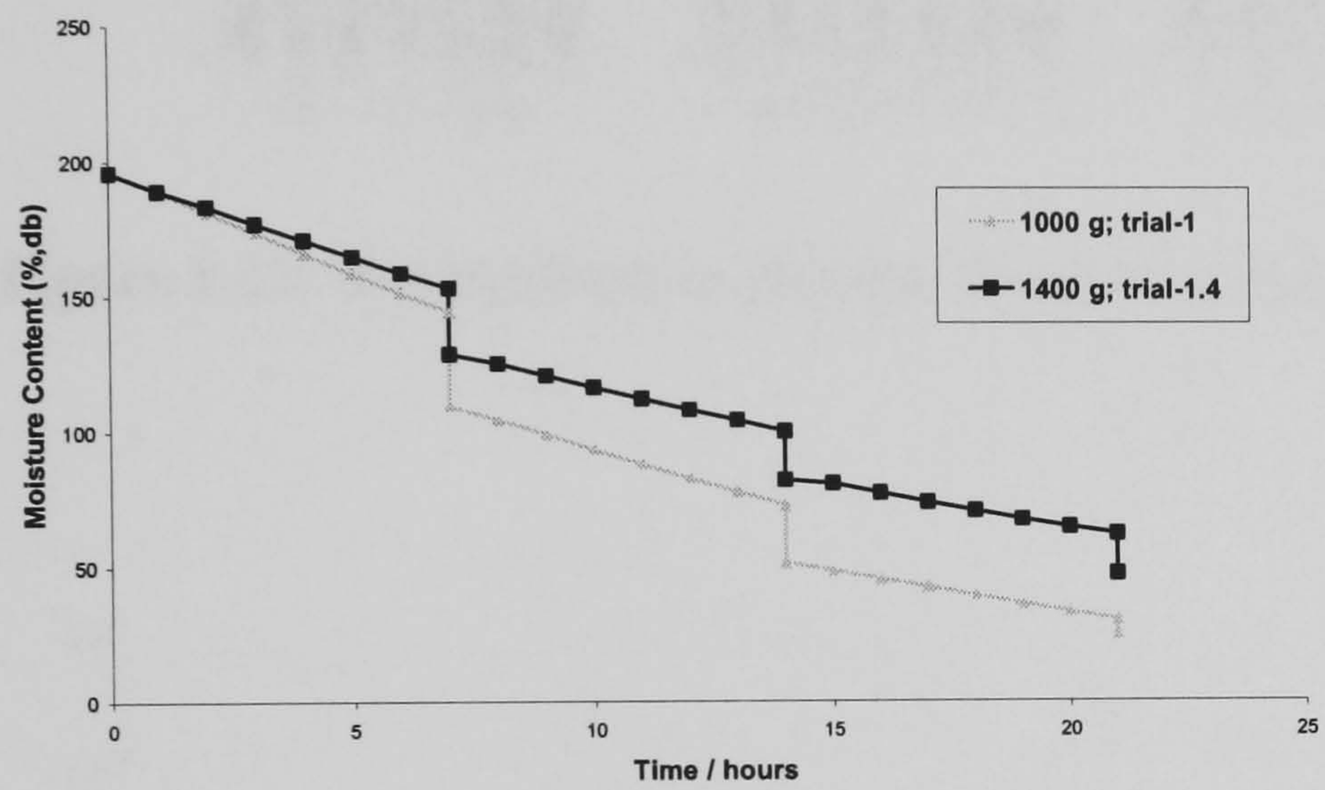

Figure 5.22a Moisture Content vs. Drying Time; crop masses of 1 kg and 1.4 kg

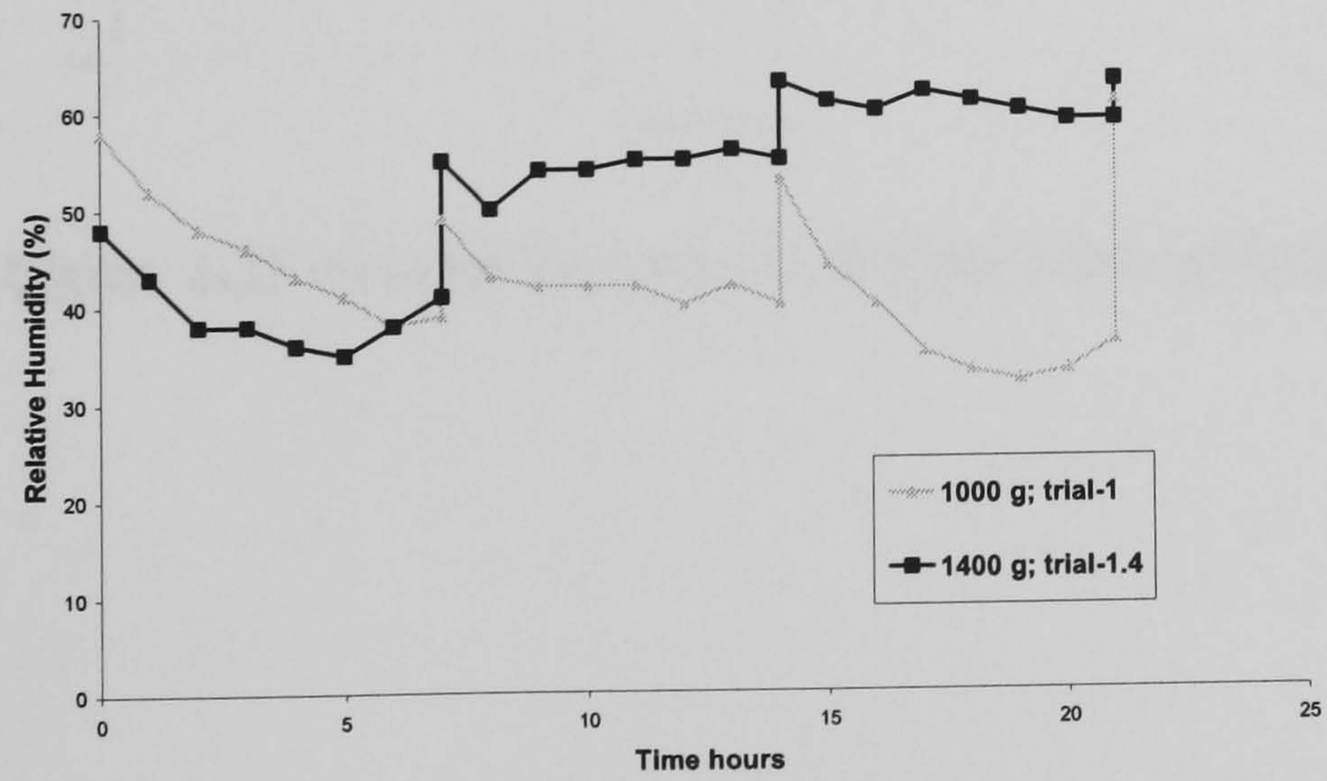

Figure 5.22b Ambient RH vs. Drying Time; crop masses of 1 kg and 1.4 kg

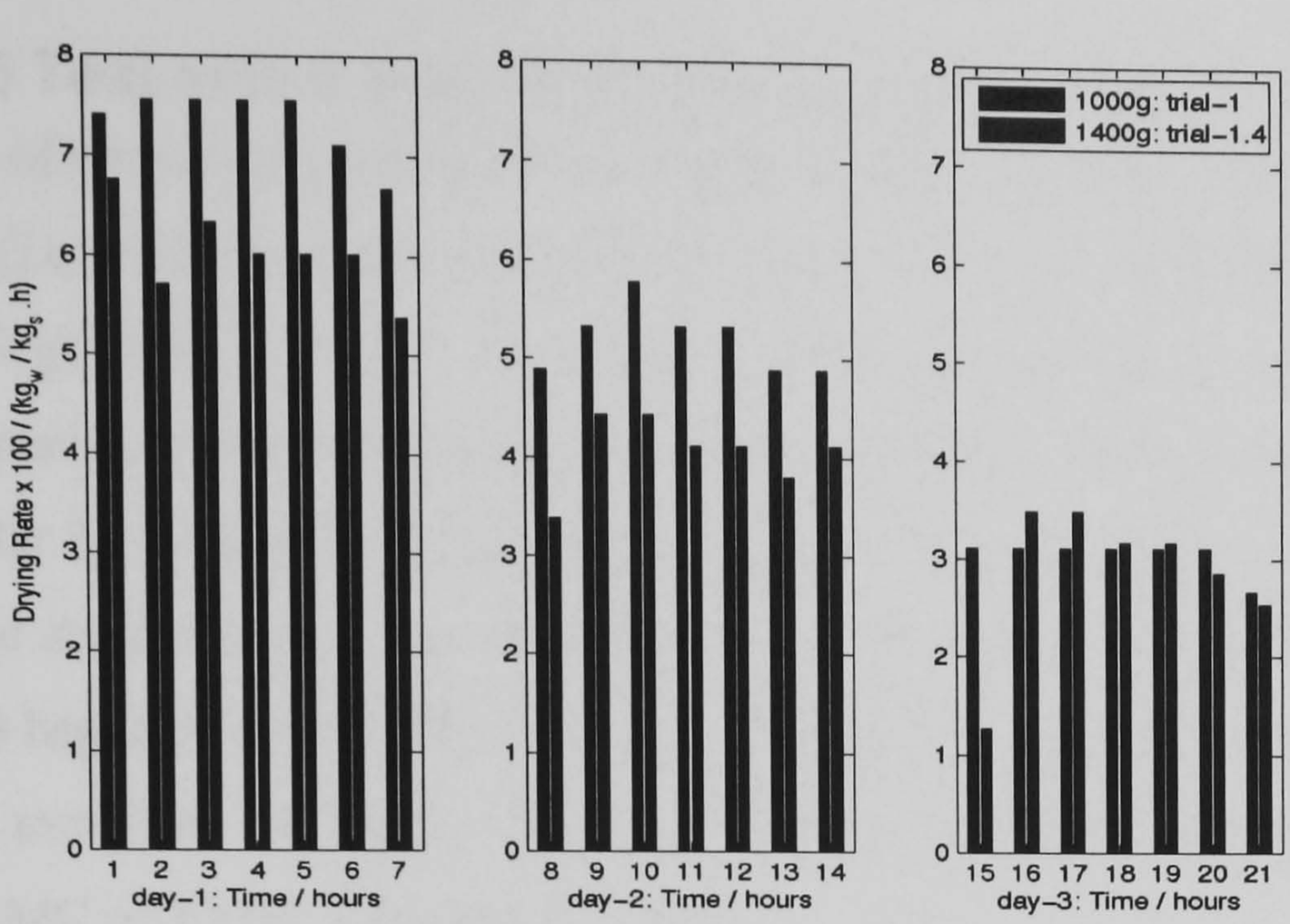

Figure 5.22c Drying Rate vs. Drying Time; crop masses of 1 kg and 1.4 kg

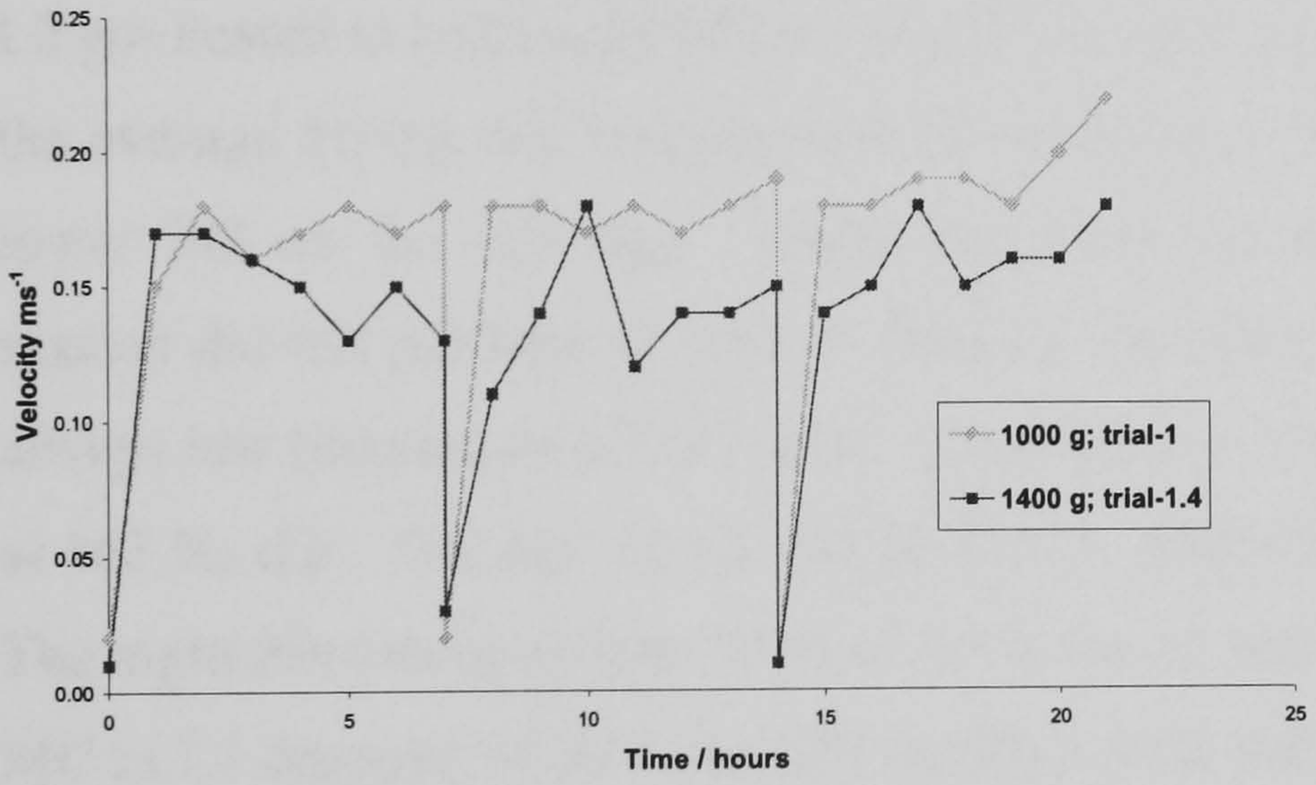

Figure 5.22 d) Inlet Velocity vs. Drying Time; crop masses of 1 kg and 1.4 kg

5.2.5 Test-sets 9 and 10: Lower crop mass and the effect shelf height

Plots of the various results of two separate trials (Test-sets 9 and 10), both with 500 g of crop (i.e. half the standard mass) can be found together with those of the standard mass (1000 g) in Figure 5.23. The results include those of the control trials, where the crop was placed outside to be dried under the conditions of the environment, as explained in chapter 3. Test-set 9 (or L1) had the crop at the same height of 140 mm above the base as the standard mass (i.e. on the lower shelf). The test, together with its control trial (Ct1) began with MC 203 % (d.b.). In test-set 10, the crop was dried on a higher shelf (240 mm from the base). This test-set also had control drying (Ct2), and both began with MC of 200 %, d.b. (figure 5.23a).

As shown in Figure 5.23b, the crop of L1 did not dry fast on day 1, due to the high RH which started at 65 % and reduced to 53 % in the evening (Figure 5.23c). L2 was in a more humid environment, also at 65 % and reducing only to 59 %. However, the air in L2 got heated to reduce the RH before the air got to the crops at the higher position. So the average drying rate was just around that of the standard mass which had relatively lower RH on the first day. Under the same environmental conditions, the control masses did not perform so well as those in the dryer, as the airflow in the room was always low (maximum of 0.02 m/s). L1 ended day 1 with MC of 158 % whilst Ct1 was at 163 %, d.b. The MC of L2 was at 148 %, with Ct2 at 160 % (d.b.) in the evening. The night RH changed from 53 % to 59 % for L1 and from 59 % to 58 % for L2. The MC in L1 dropped by 32 % to 126 % (d.b.), with that of Ct1 dropping by 43 % to 120 % (d.b.) the next morning. The MC L2 dropped by 30 % to 118 % (d.b.), with that of Ct2 dropping by 39 % to fall on 121 % in a similar period. Thus the night performances were better outside the dryer than inside the dryer. The performance outside the dryer was even better in the night than that of the standard trial with a drop of 35 % in a less humid atmosphere.

On day 2, the RH was about the same in the two trials for most of the day, though slightly reduced compared to day 1 (figure 5.23c). The slight preheating of the air in L2 was just as effective as that of the higher MC in L1. Therefore the crops inside the

dryer dried at about the same rate in the two trials, whilst the test with standard mass dried a little faster (figure 5.23b). Again the two controls had the slowest drying rates, as the energy containment inside the dryer was higher than outside, and also the higher airflow inside the dryer was still effective on day 2. L1 dried from 126 % to 90 % (d.b.) inside the dryer, with Ct1 drying from 120 % to 92 % (d.b.), As shown in figure 5.23a, the crop in L2 dried from 118 % to 83 % (d.b.) whilst Ct2 dried from 121 % to 92 % (d.b.). During the second night, the MC of L1 dropped by 25 % inside the dryer to 65 % (d.b.) as Ct1 dropped by 28 % to 64 % (d.b.). Within a similar period, that of L2 dropped by 25 % inside the dryer to 58 % (d.b.), with Ct2 falling by 33 % to 59 % (d.b.). Again the night drying was better outside the dryer than inside the dryer.

On the third day, the standard one still dried fastest and the drying rate in L1 was higher than in L2 (figure 5.23b). The controls still performed relatively poorly. L1 dried from 64 % to 47 % (d.b.) inside the dryer as Ct1 dried from 64 % to 50 % (d.b.). In both trials, the night drying was slightly better outside the dryer than inside. At the end of the trials, the MC of L1 was 38 % (d.b.) in the dryer, and Ct1 had 39 %. L2 ended with MC of 32 % (d.b.), same as Ct2 (figure 5.23a).

The night performance inside the dryer was so poor in comparison with the outside performance that the MC of crops inside the dryer was almost the same as that outside, after drying in the same environmental conditions. In the night, the solar chimney functioned as normal chimney after all the energy stored in the day had been used up. The poor night performance of the dryer could be down to the low temperatures at night in the high chimney (as noted by Ekechukwu, 1997) and the high levels of RH especially during the first two days. As a result, more condensation occurred in the system to slow down the drying process, with rewetting possibilities, at night.

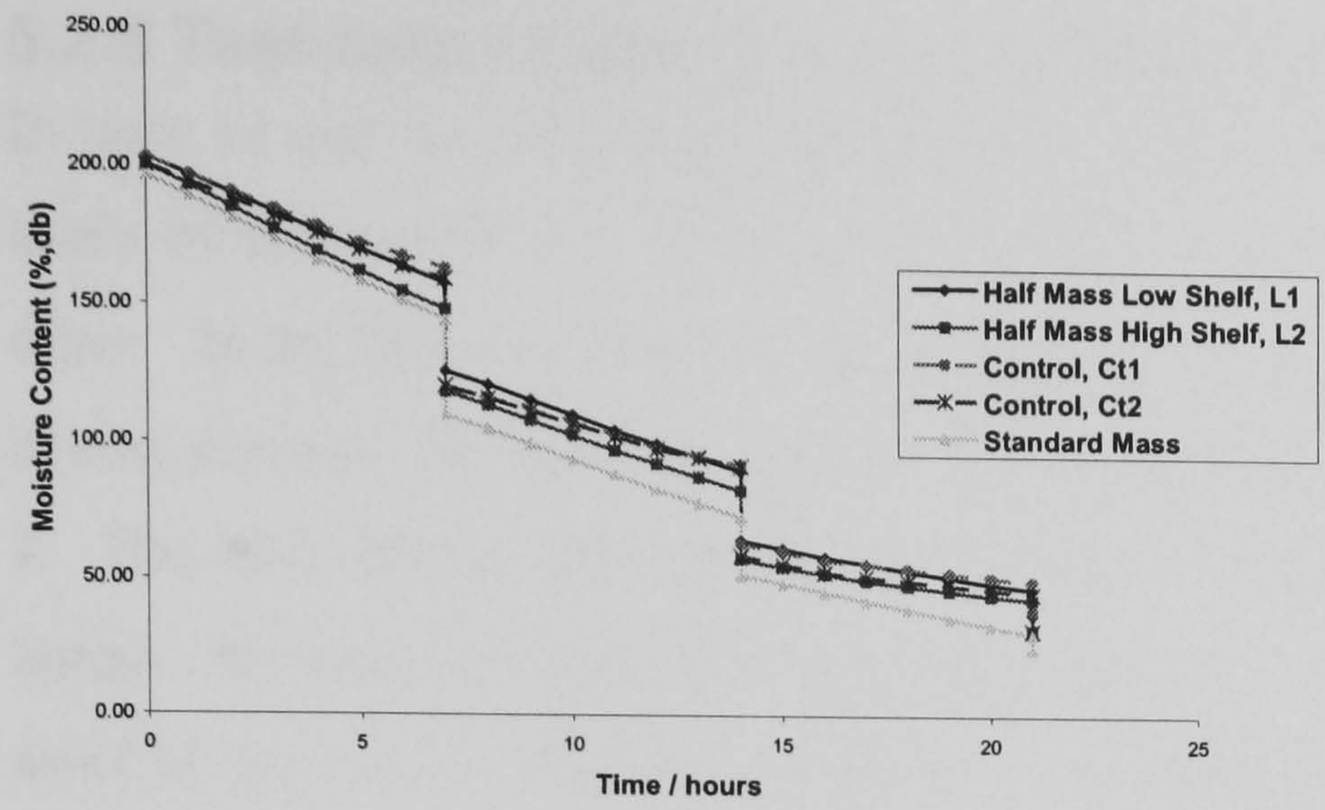

a) Moisture Content vs. Drying Time

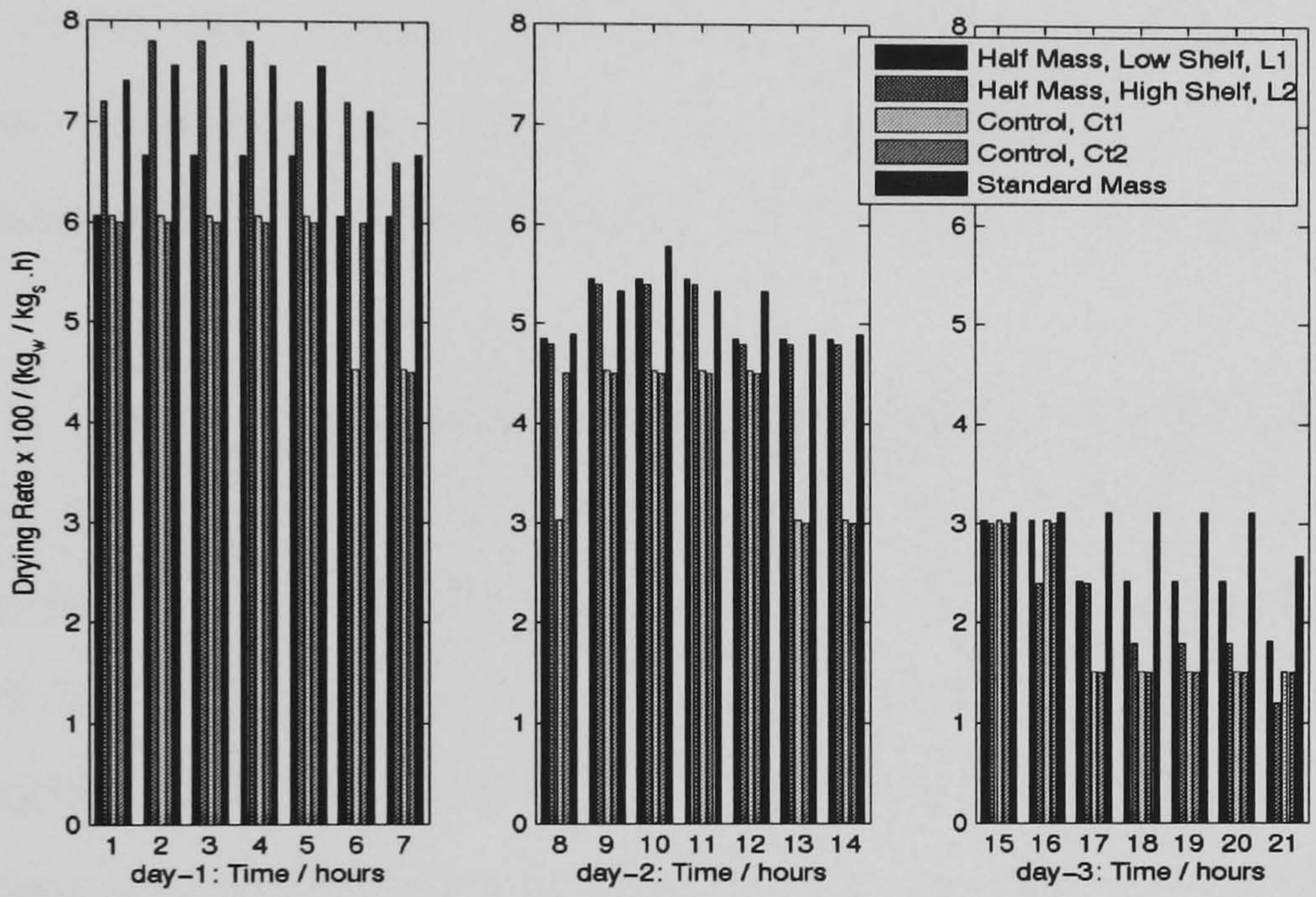

b) Drying Rate vs. Drying Time

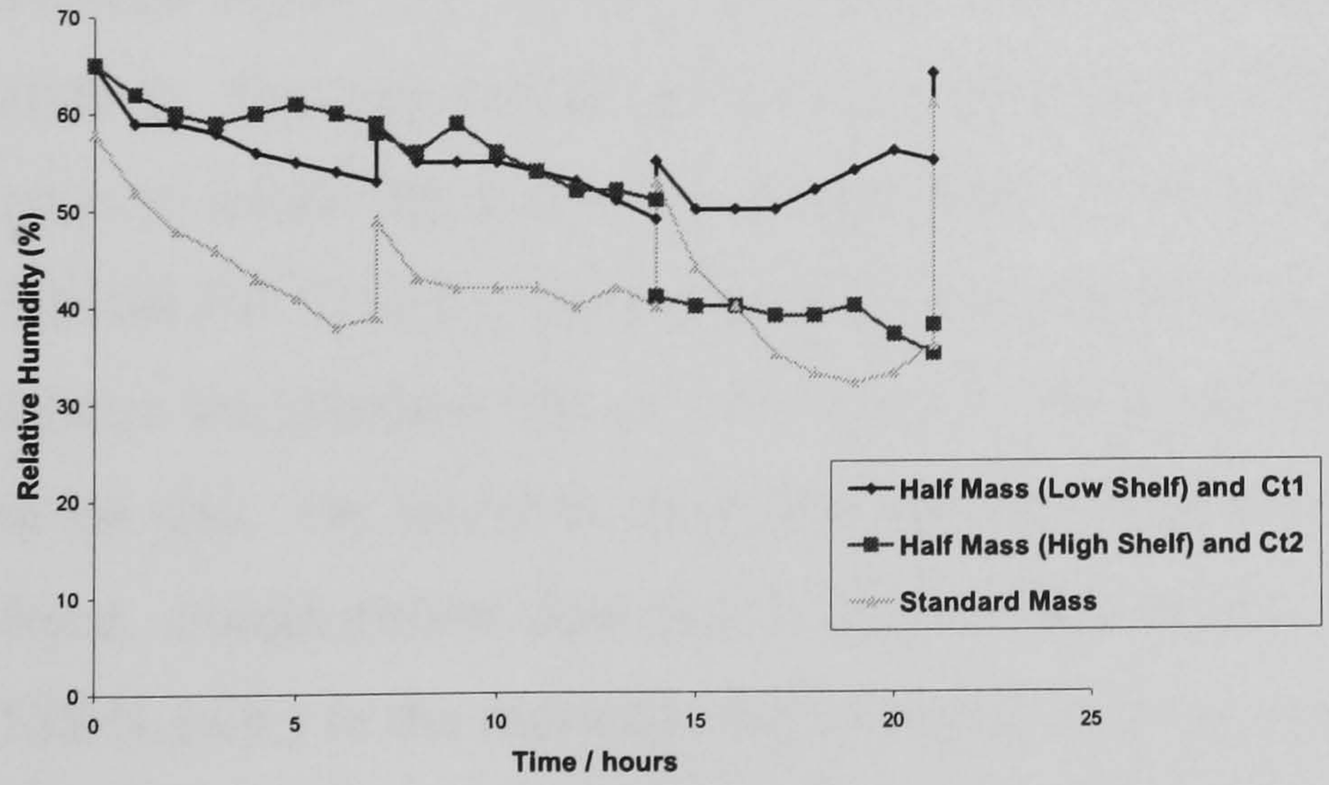

c) Ambient RH vs. Drying Time

Figure 5.23 The performances on Half mass, Standard mass and Control

5.2.6 Test-sets 11 and 12: Using different loading arrangements

In tests 11 and 12, two types of trials were performed. In each of them the separate loads of test-sets 9 and 10 were put together, at their respective shelf heights in the dryer. In the first one (trial-1), the shelves remained at their positions through out the drying process. In the other drying trial (trial-2), the shelves were interchanged on day 2. The two shelves were always placed such that they were equally irradiated by the lamps. As in test-set 9 and 10, there was also control drying in each trial (Ct3 for trial-1 and Ct4 for trial-2). Figure 5.24 shows the variations in MC and drying rates for trial 1, those for trial 2 are shown in Figure 5.25. The variations are shown for the separate loads in the same chamber (X1 for trial-1 and X2 for trial-2), the calculated average of the two values in the chamber, the control load and the standard load. The RH variations of the two trials have been plotted together in Figure 5.26.

Trial-1; test-set 11 Drying the two half loads together without interchange

Trial-1 started day 1 with MC of 203% (Figure 5.24a) and an ambient RH slightly above the 60% mark which soon fell to below the mid-fifties (figure 5.26). As shown in Figure 5.24b, the lower shelf (X1) dried a little slower than the upper shelf (X2). Thus, the ambient RH was fairly high, so that drying was slow and more heat (rather than moisture) was transferred to the air on the lower shelf. The air left the lower shelf hotter and less humid to dry the upper shelf faster. As shown in figure 5.24b, the overall average drying for the day was faster than the standard one, whose MC was lower (196%). Towards the end of the day, the effects of MC and RH tried to counteract each other to reduce the gap in the drying rates. At the end of the day, X1 had 153 % (d.b.), X2 had 147 % (d.b.), the average MC was 150 % (d.b.) and Ct3 was 168.02 % (d.b.), all against the standard MC of 145 % (d.b.). Thus, the control drying was again very poor in the day. On the other hand, the night performance of Ct3 was better than inside the dryer, though poorer than that of the standard drying. Ct3 fell in the night by 30 % to 138 % (d.b.) in the morning, the average MC drop inside the dryer was 25 % (reducing to 125 %, d.b.) and the standard one reduced by 35 %. The high MC of Ct3 at the close of day 1 might have aided the overnight fall in MC to some extent. The RH of trial 1 reduced from 61 % in the evening to 42 % in the morning (Figure 5.26).

On the second day the RH remained low (mostly below 40 %). This facilitated fast drying on the lower shelf, so that the air became more humid on leaving the lower shelf. Drying on the upper shelf slowed down as a result; slower than on the lower shelf from the fourth hour onwards (Figure 5.24b). The higher MC of the lower shelf contributed to this overtaking of the drying rate. Ct3 had lowest drying rate on day 2. On average, the standard one dried the fastest on day 2, despite its slightly higher RH (Figure 5.26). Probably, the slow rate on the upper shelf was impeding the whole drying process in trial 1. On the second day, X1 dropped from 132 % to 94 % (d.b.), X2 from 119 % to 85 % (d.b.) and the average drop was from 125 % to 89 % (d.b.). The standard MC reduced from 110 % to 73 % (d.b.).

In the night from day 2 to the morning of day 3, the MC drop of the control was again the highest. The standard one had lowest drop, apparently due to the low moisture at the end of day 2. On the third day, the sequence in the MC ratings was not so different from those of the previous day. The drying rates became steadier, with that of the standard higher than the rest. The drying rate on the lower shelf again overtook that of the upper shelf which even fell below the control. Yet again, the MC drop in the control was the highest overnight, with the standard one being the lowest. X1 ended the process at 48 % with X2 at 46 %, and the average in the dryer at 47%, as against Ct3 with 59% (d.b.) and the standard with 25% (d.b.). Though the control generally performed better at night, the dryer did much better on the whole, unlike in test-sets 9 and 10. The better performance of the dryer could be due to the much less humid environment of the second drying day. The MC gap between the dryer and control was much more widened on this day.

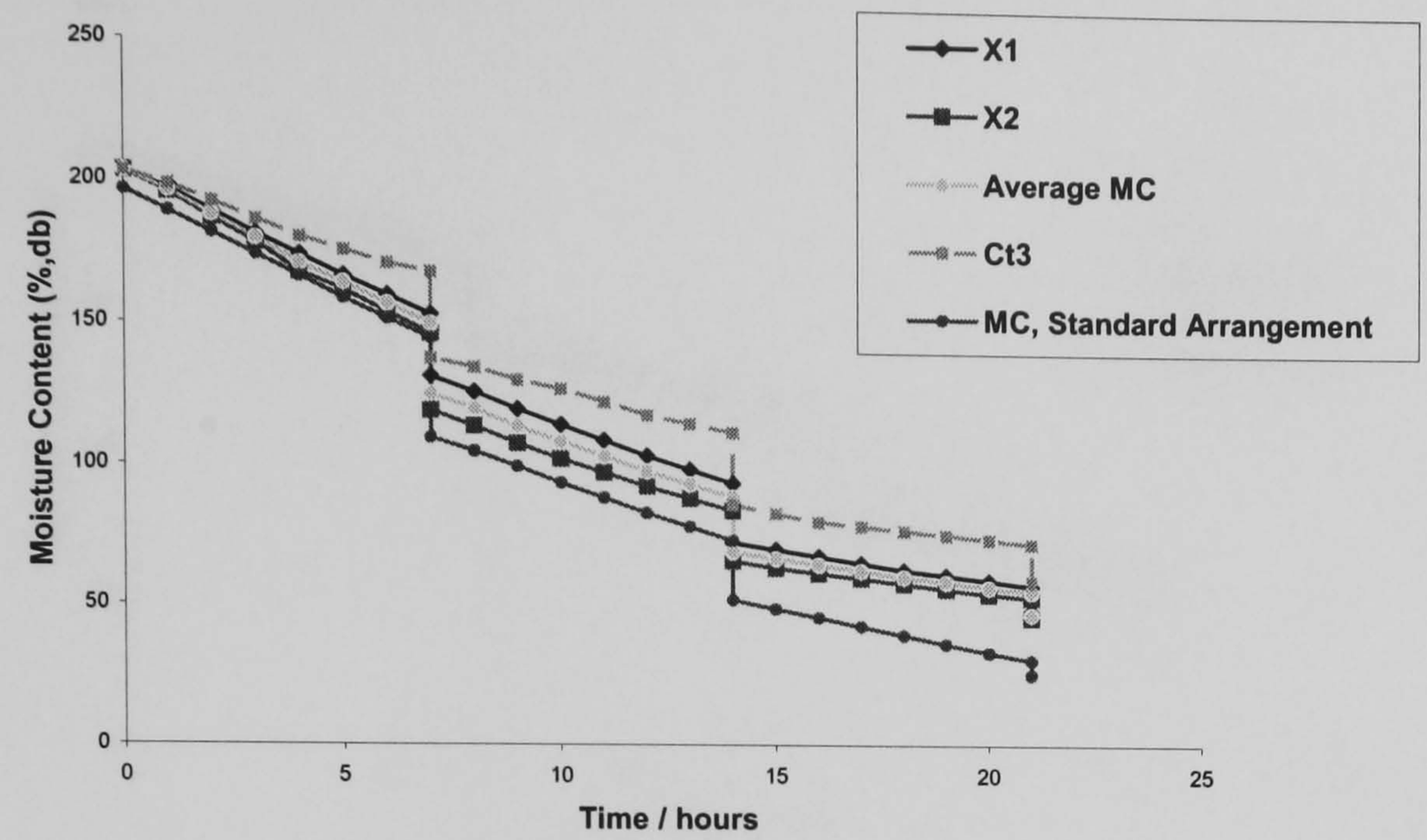

a) Moisture Content vs. Drying Time

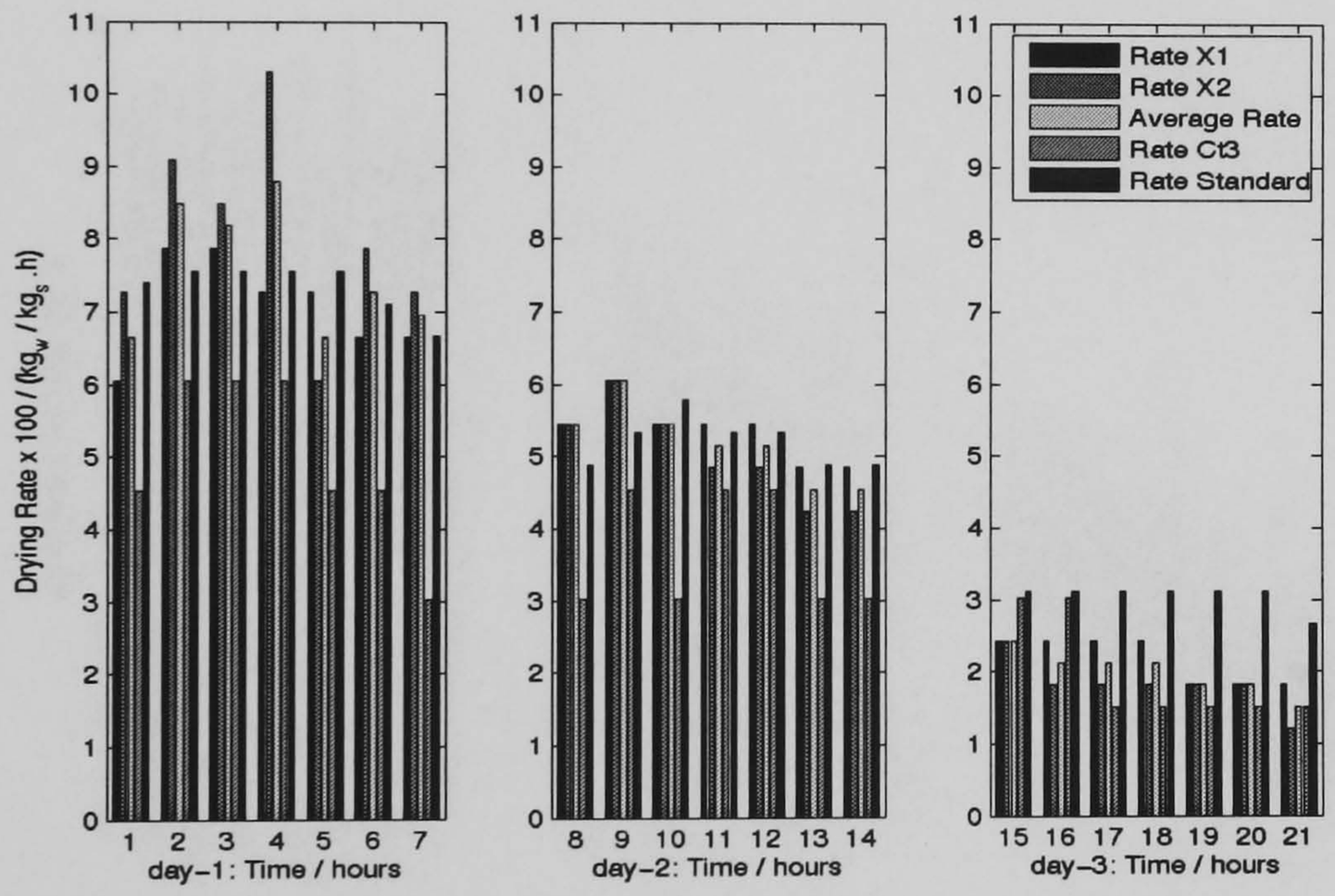

b) Drying Rate vs. Drying Time

Figure 5.24 The performances of the two half loads being dried together at different height (without interchange), with Standard and Control.

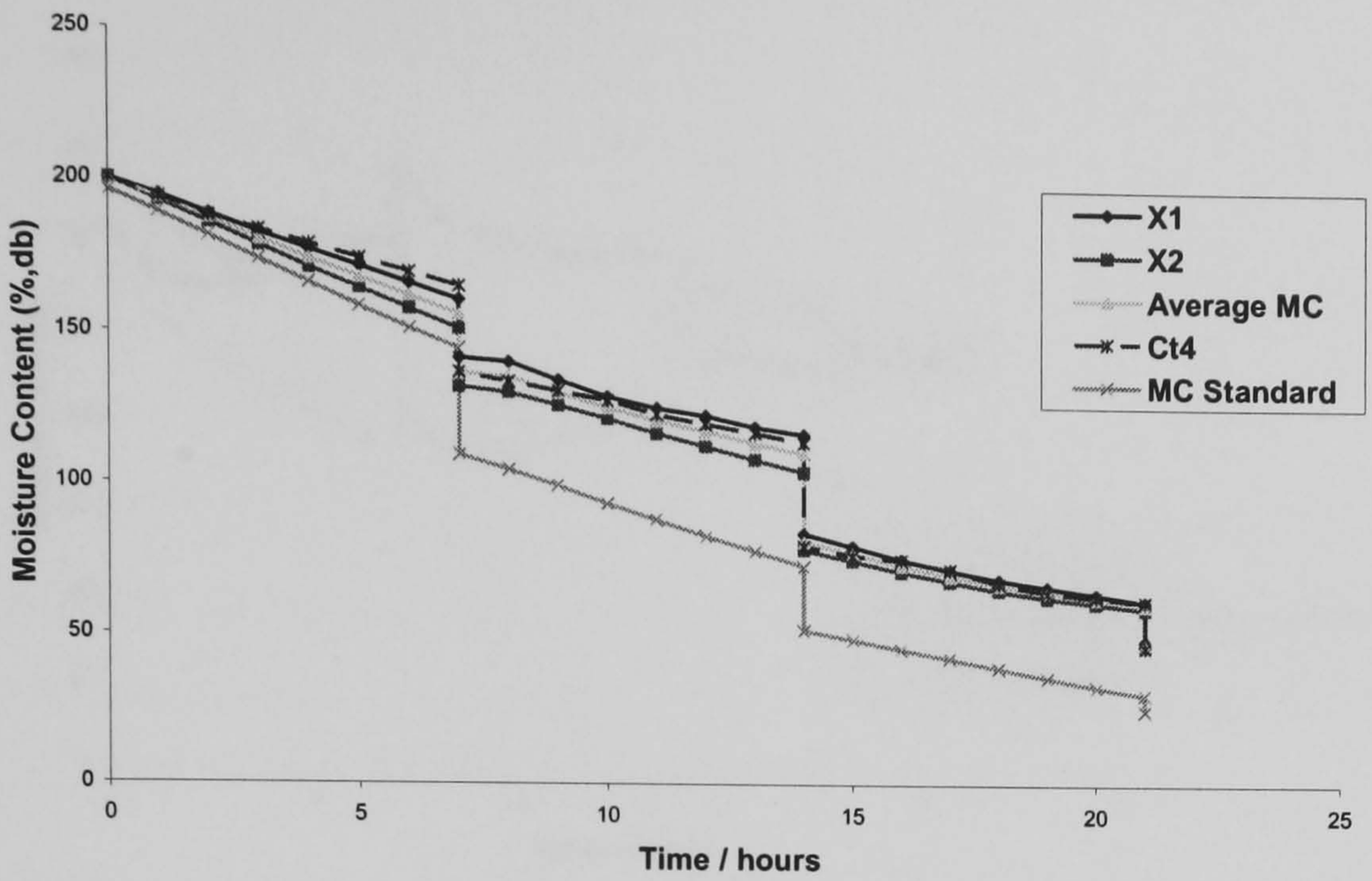

a) Moisture Content vs. Drying Time

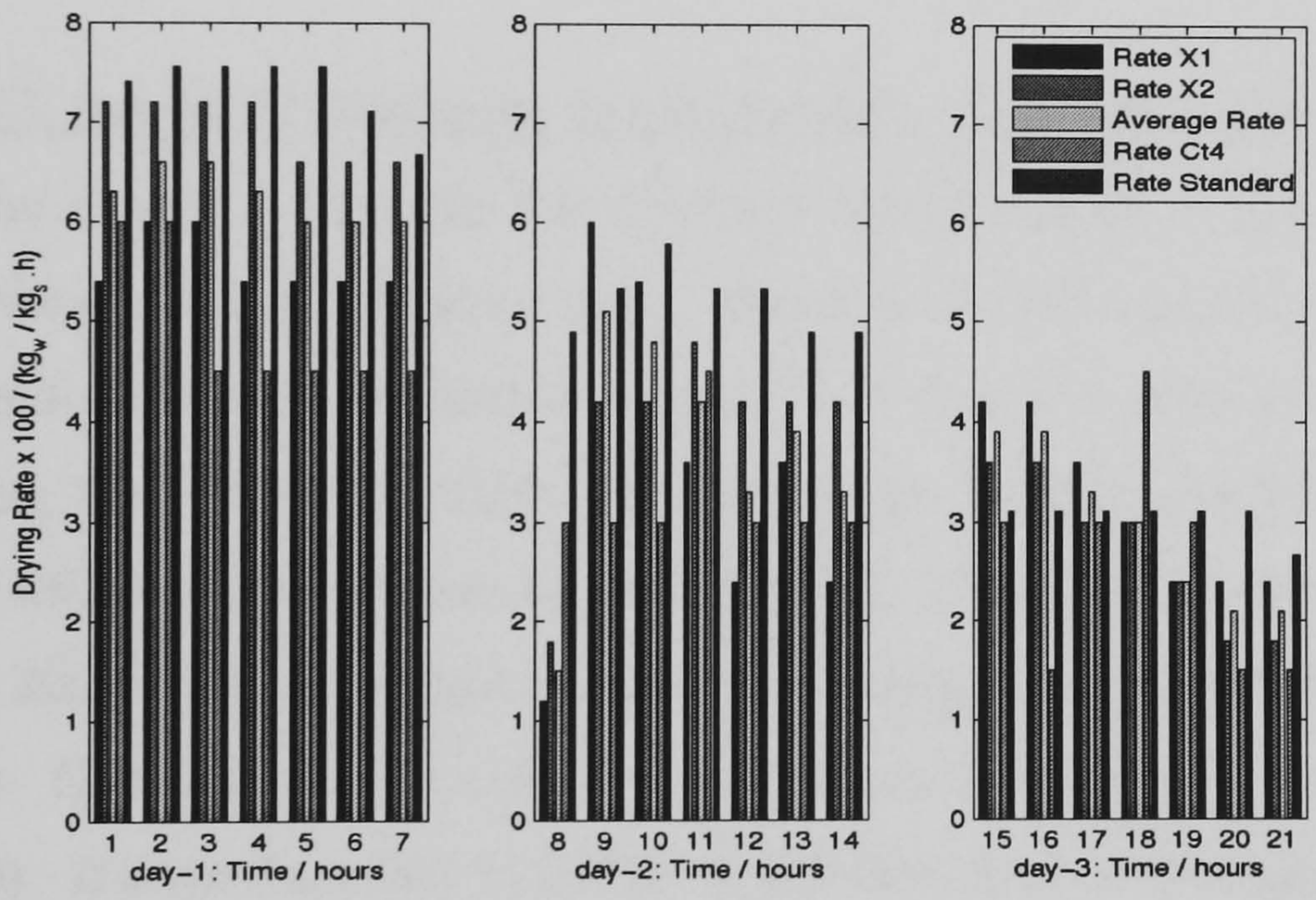

b) Drying Rate vs. Drying Time

Figure 5.25 The performances of the two half loads being dried together at different height (with interchange on Day 2), with Standard and Control.

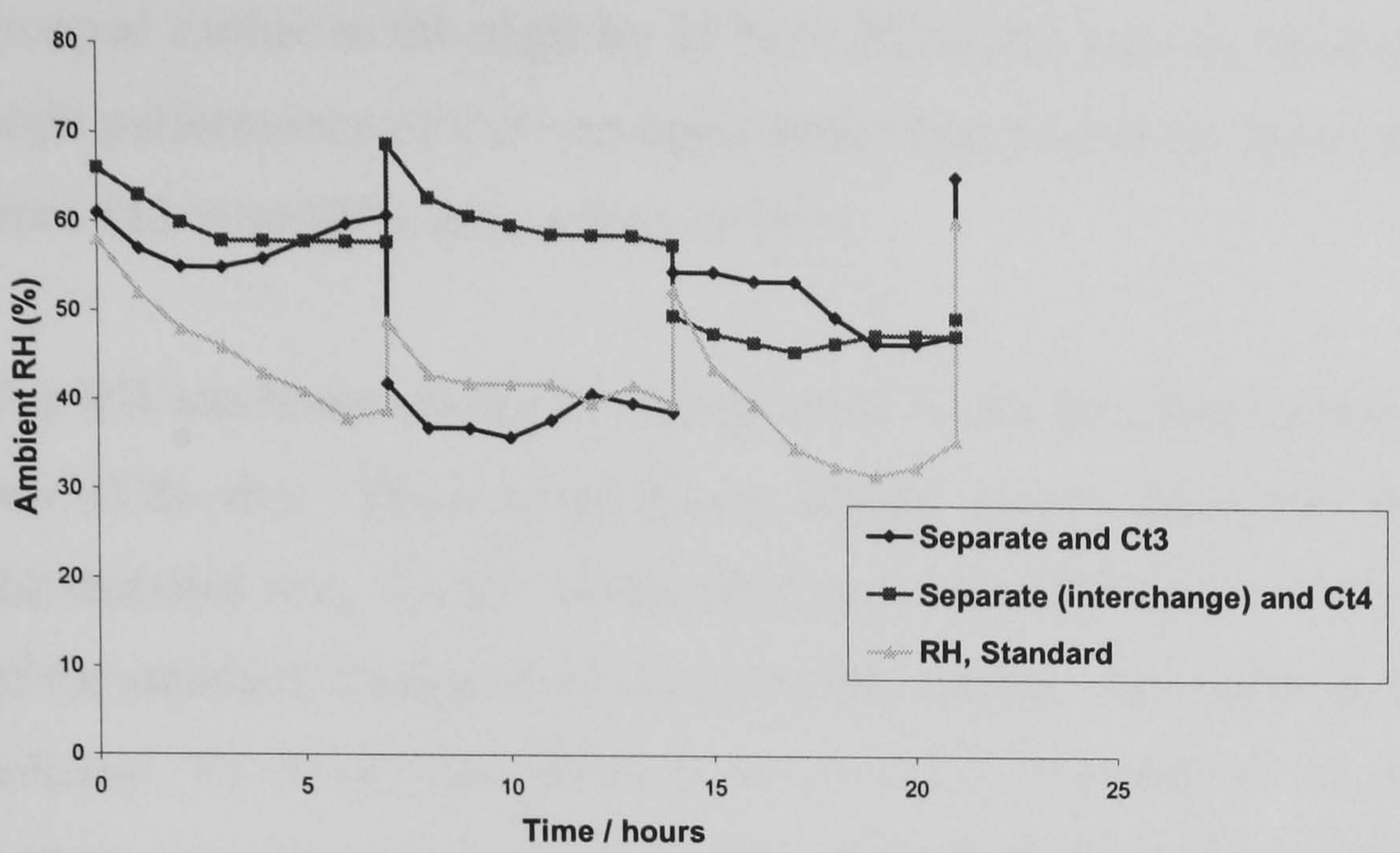

Figure 5.26 Ambient RH vs. Drying Time; The Half Loads together (with and without interchange), Standard and Control Loads

Trial-2; test-set 12 Drying the two half loads together with interchange on Day 2

Similar to trial 1, the high RH (Figure 5.26) caused the lower shelf to perform poorer than the upper shelf (Figure 5.25b). However, the RH was this time too high (starting in the mid-sixties and remaining around 58 % from the third hour onwards. So, as the heating from the lower shelf was not enough to lower the RH adequately, the upper shelf still dried slower than the standard one. X1 dried from 200 % to 161 % (d.b.), X2 from 200 % to 151 % (d.b.) and so the average MC at the end of day 1 was 156 % (d.b.). Once again the control Ct4 was poorer in the day but better in the night (Figure 5.25a). It dried from 200 % to 166 % and then dried in the night to 137 % (d.b.) on the second morning. X1 was 142 % and X2 was 132 %, with the average at 137 % on that morning. The RH increased from 58 % to 69 % that night.

On day 2, the RH fell from 69 % to just around 60 % for the whole day, always higher than the values in day 1 (Figure 5.26). At these high humidity levels, the shelf interchange did not cause any improvement, and X1 (now in the upper position) still performed poorer than X2, as shown in figure 5.25 (a and b). X1 dropped by 25 % to finish the day at 177 % (d.b), and X2 dropped by 27 % to finish at 105 % (d.b.), so that

the average drop was 26 %, resulting in an average MC in the dryer of 111 % (d.b.) in the evening. Ct4 dried from 137 % to 115 % d.b. (a drop of 22 %) in the day. It then dropped further in the night by 35 % to 80 % (d.b.) on the third morning. The second-night performance of Ct3 was again better than that of the dryer whose average MC fell from 111 % to 82 % d.b., a drop of 29 %.

The RH was better on day 3, starting at 50 % and hovering between 48 and 46 % for the rest of the day. The average drying started initially faster, but was soon overtaken by the standard one. On the whole, the third-day performance was slightly lower than that of the standard, though still better than the control. The third-day performances were as follows: X1 dried from 84 % to 62 % (d.b.); X2 from 79 % to 60 %, d.b. (so the average was from 82 % to 61 % (d.b.); the standard dried from 52 % to 31 %; Ct4 from 80 % to 62 % (d.b.). The following were the various MCs in the end. X1 had 49 % and X2 had 47 % (d.b.) with the average at 48 %; Ct4 had 47 %, as against the 25 % (d.b.) of the standard (Figure 5.25a). Thus at end of the process, the MC of the control crop was lower than that of the crop in the dryer, though much higher than that of the standard one.

5.3 Field Work results

This sub section has the presentation and discussion of the results of the five trials conducted on a full-scale model in Ghana. As already indicated in chapter 3, the framework of a tent dryer was divided along the vertical plane through the heights of the side, triangular walls, to get each half similar to that of the laboratory model, and one of them was used for the trials. The dividing wall of the original tent dryer then became the back wall of this modified dryer, which was glazed all-round with a transparent polythene sheet. The sun always started behind the dryer in the morning, came directly overhead around midday and shone at the front of the dryer in the afternoon. The chimney absorber at the top of the dryer cast some shades on the upper trays which in turn had their shadows on the lower trays and the base. There were also some thin shades from the frames. The shades shifted from the front of dryer to the back, during the day. As expected, the control tray was exposed to flies, excreta from birds and other forms of unhygienic conditions during daytime. The weather was very cloudy and windy for almost all the daytime periods. It was later found that the part of the installed system for wind measurement was faulty. There was also no hand-held anemometer to measure the inlet and exit air velocities of the dryer.

Other observations and the results of the various trials are presented and discussed in the following paragraphs. For the sake of the discussions, the period from 8:00 a.m. to 5: 00 p.m. is taken as day time and that from 5:00 p.m. to the next morning (8:00 a.m.) is considered to be night period. As explained in chapter 3, all the first-day drying processes started around midday. So each first-day drying period was about half the normal nine hours set as day-time period. Since the trials took place under different atmospheric conditions, a term 'comparative performance' is used to determine how well the dryer functioned in relation to the control in each trial, defined as

$$\text{Comparative performance} = \text{MC drop in the dryer} - \text{MC drop in the control}$$

The symbols use in the tables for the data overview are explained in table 5.4 below

Symbol	Explanation
T_i	Inlet air temperature (^{0}C)
T_L	Air temperature of lower part of drying chamber (^{0}C)
T_m	Air temperature in the middle of drying chamber (^{0}C)
T_u	Air temperature of upper part of drying chamber (^{0}C)
$T_{ch,i}$	Air temperature at chimney inlet (^{0}C)
T_o	Air temperature at dryer outlet (^{0}C)
T_b	Base (floor) temperature of drying chamber (^{0}C)
T_{sw1}	Side-wall temperature of drying chamber (^{0}C)
T_{sw2}	Side-wall temperature of drying chamber (^{0}C)
T_{BW}	Back-wall temperature of drying chamber (^{0}C)
T_{fW}	Front-wall temperature of drying chamber (^{0}C)
T_{abs}	Chimney absorber temperature (^{0}C)
$T_{ch,g}$	Chimney glazing temperature (^{0}C)
RH_{in}	Relative humidity at dryer inlet (%)
RH_{out}	Relative humidity at dryer outlet (%)
I_G	Global insolation on a horizontal surface(W/m^2)
I_D	Diffuse insolation on a horizontal surface(W/m^2)

Table 5.4 Field-work data symbols and the meanings

5.3.1 Field-trial 1

Table 5.5 shows the moisture content (MC) values determined from the weight of crop at various times of drying. The data of the environment and some points of the dryer can be found from table 5.6. With all the glazing of the other unused half of the dryer then in place, the insolation into the test dryer was reduced significantly. Energy was at the same time stored in that half. The result was that the temperature of the back wall separating the two halves was much higher than the other walls, sometimes even higher than that of the chimney absorber which was also shaded by the additional sheets.

During the first day, the relative humidity of the exit air averaged around 69 %, much higher than that of inlet air of an average of 60.5 %. As shown in table 5.6, the average global insolation was about 462.87 W/m, about half of which was diffuse with 229.41

W/m). The initial MC of the crop was around 181 %, d.b. At the end of day 1 (i.e. after four hours of drying) the cassava on the control tray had lower MC (133 %, d.b.) than the average MC in the dryer (156 %, d.b.). The comparative performance on the first day was -23 %. The cassava in the dryer browned a bit on the first day. The higher performance of the control on the first day may be attributed to the windy conditions which normally facilitates high initial rate of drying cassava (a crop of high initial MC). It rained in the night and, on the morning of day 2, a large amount of water had to be poured away from the sheet used to cover the control crop during the night. The MC reduction of the control in the night was still higher, changing from 133 to 116 %, d.b., whereas the reduction in the dryer was from 156 to 145 %, d.b. Though the top was covered at night, the contact with the air through the mosquito net underneath the control tray allowed self drying of the control crop in the night. On the other hand, the energy stored in the dryer during the day still caused some cold, moist air to be drawn into the dryer in the night. The dryer was at this time not receiving any radiant energy to enhance the escape of humid air through the top vent. These caused fast cooling in the dryer and, at the same time, hindered the moisture evaporation from the crops, and thus slowed down the night self drying (with possible rewetting of the crop).

		Dry wt (g) =	3384.17	3381.33	3380.97	3382.04	3382.39	3381.68					20292.58	1470.9
	Time		A1	A2	A3	A4	A5	A6	B1	B2	B3	B4	Average	Control
Start of Day 1	1300	Wt (g)	9509.00	9501.00	9500.00	9503.00	9504.00	9502.00					57019.00	4133.00
		MC (%, d.b)	**180.98**	**180.98**	**180.98**	**180.98**	**180.98**	**180.98**					**180.98**	**180.98**
End of Day 1	1700	Wt (g)	8578.00	8719.00	8667.00	8586.00	8754.00	8620.00					51924.00	3426.00
		MC (%, d.b)	**153.47**	**157.86**	**156.35**	**153.87**	**158.81**	**154.90**					**155.88**	**132.92**
Start of Day 2	0800	Wt (g)	8235.00	8371.00	8284.00	8248.00	8393.00	8170.00					49701.00	3185.00
		MC (%, d.b)	**143.34**	**147.57**	**145.02**	**143.88**	**148.14**	**141.60**					**144.92**	**116.53**
End of Day 2	1700	Wt (g)	6506.00	6668.00	6519.00	6382.00	6520.00	6225.00					38820.00	2628.00
		MC (%, d.b)	**92.25**	**97.20**	**92.81**	**88.70**	**92.76**	**84.08**					**91.30**	**78.67**
Start of Day 3	0800	Wt (g)	5830.00	5937.00	5849.00	5821.00	5871.00	5600.00					34908.00	2340.00
		MC (%, d.b)	**72.27**	**75.58**	**73.00**	**72.12**	**73.58**	**65.60**					**72.02**	**59.09**
End of Day 3	1700	Wt (g)	4800.00	4960.00	4808.00	4783.00	4892.00	4542.00					28785.00	2040.00
		MC (%, d.b)	**41.84**	**46.69**	**42.21**	**41.42**	**44.63**	**34.31**					**41.85**	**38.69**
Start of Day 4	0800	Wt (g)	4505.00	4630.00	4493.00	4405.00	4560.00	4216.00					26809.00	1951.00
		MC (%, d.b)	**33.12**	**36.93**	**32.89**	**30.25**	**34.82**	**24.67**					**32.11**	**32.64**
End of Day 4	1700	Wt (g)	4143.00	4285.00	4020.00	4048.00	4148.00	3881.00					24525.00	1832.00
		MC (%, d.b)	**22.42**	**26.73**	**18.90**	**19.69**	**22.64**	**14.77**					**20.86**	**24.55**
Start of Day 5	0800	Wt (g)	4075.00	4185.00	3920.00	3958.00	4048.00	3731.00					23917.00	1798.00
		MC (%, d.b)	**20.41**	**23.77**	**15.94**	**17.03**	**19.68**	**10.33**					**17.86**	**22.24**
End of Day 5	1700	Wt (g)	3895.00	3968.00	3769.00	3766.00	3827.00	3655.00					22880.00	1748.00
		MC (%, d.b)	**15.09**	**17.35**	**11.48**	**11.35**	**13.14**	**8.08**					**12.75**	**18.84**

Table 5.5 Field-trial 1; Daily Moisture Contents (Inlet was left open at night)

Drying Day	Period		T_i	T_L	T_m	T_u	$T_{ch,i}$	T_o	T_b	T_{sw1}	T_{sw2}	T_{BW}	T_{fw}	T_{abs}	$T_{ch,g}$	RH_{in}	RH_{out}	I_G	I_D
Day 1	1300 to 1700	Maximum	27.85	41.90	48.25	44.93	46.98	57.21	55.11	45.20	44.77	53.25	49.17	59.74	58.01	65.00	74.00	792.00	359.70
		Average	26.64	38.74	43.54	41.72	43.79	48.84	48.57	43.91	41.34	47.61	43.97	51.23	49.28	60.50	69.50	462.87	229.41
		Minimum	25.57	34.60	37.48	36.79	40.38	41.38	39.71	42.93	36.32	39.43	37.24	43.38	41.38	56.00	65.00	32.83	8.36
Day 2	0800 to 1700	Maximum	28.70	40.91	49.07	46.18	49.37	53.24	58.12	54.51	46.92	56.99	50.49	55.93	54.51	57.00	69.00	863.00	316.40
		Average	27.39	36.45	40.95	35.73	41.10	44.20	44.86	44.57	39.00	50.06	40.58	45.88	45.22	45.17	54.00	539.40	192.69
		Minimum	25.47	26.62	26.27	25.13	24.78	27.83	25.59	25.13	24.79	28.97	25.47	27.34	25.96	30.00	36.00	30.48	16.72
Day 3	0800 to 1700	Maximum	32.82	38.54	44.73	43.22	45.22	48.67	NA	44.07	43.21	54.67	45.32	50.67	49.46	72.00	76.00	513.30	396.70
		Average	28.83	33.87	36.91	37.42	36.80	38.05	NA	37.66	35.75	42.98	36.64	39.71	38.08	57.50	58.83	332.21	242.59
		Minimum	24.94	26.06	25.62	25.68	23.96	25.34	NA	25.68	24.95	26.65	25.47	26.24	25.96	50.00	51.00	7.03	0.00
Day 4	0800 to 1700	Maximum	33.82	42.07	47.59	38.05	47.94	50.47	NA	51.47	45.79	57.01	48.48	51.47	50.46	45.00	43.00	734.00	446.20
		Average	31.57	37.55	40.77	33.76	40.57	44.05	NA	43.61	38.90	49.00	40.15	44.23	43.82	39.83	37.67	461.50	260.55
		Minimum	28.21	27.15	26.56	25.24	25.46	27.11	NA	25.53	25.18	29.37	26.14	25.79	23.24	30.00	29.00	35.16	19.10
Day 5	0800 to 1700	Maximum	33.15	46.89	54.11	49.71	54.89	55.96	NA	51.71	50.48	64.79	54.22	64.20	64.28	63.00	61.00	840.00	499.80
		Average	31.24	40.49	44.29	38.48	43.20	45.28	NA	43.44	41.59	51.44	43.85	47.89	48.46	49.67	48.00	507.45	338.74
		Minimum	28.88	26.77	26.01	26.10	26.10	26.10	NA	26.10	25.00	27.43	25.77	26.10	26.10	39.00	38.00	17.58	9.55

Table 5.6 Field-trial 1; Data Overview

On day 2, drying was a bit faster in the dryer than in the control, as the crops in the dryer had higher MC and the airflow effect waned a bit, whilst the heating effect on the drying process became more prominent. The average global insolation (539.40 W/m) was higher than on day 1 but the diffuse proportion (192.69 W/m) was lower. The RH was lower than on day 1 (45.17 % at inlet and 54 % at exit). The dryer finished day 2 with MC 91 % (d.b.), and that of the control was still lower with about 79 % (d.b.), though the gap had lowered a bit. Similar trends followed throughout day 3 with the MC gap closing up. The RH was higher again, with inlet at 57.5 % and exit at 58.83 %. The browning of the crop in the control became more visible in the course of day 3, and there was no observable colour difference between the crop in the dryer and that outside. The lowest insolation for the whole field-work period was recorded on day 3 with an average of 332.21 W/m^2 (table 5.6). Nonetheless, the rate of moisture reduction in the dryer continued to increase whilst that in the control reduced, for both day and night, apparently due to the increasing effect of heating at later stages. Thus, the dryer was able to retain the energy more effectively than the control. However, it was not until the fourth day that the MC in the dryer fell to that in the control at around 32 % (d.b.), and then overtook it in the cumulative reduction of MC.

By the morning of day 5, the MC in the dryer had fallen below the desired 22 % (d.b), with about 18 % MC. The drying process had to continue on the fifth day before the MC of the control crop fell below the desired level, by which time the cassava in the

dryer had become so brittle with MC around 13 % (d.b). The RH values of the fourth and fifth days of this trial were among the best in the field-work period (table 5.6). This aided the control to dry fast in the last two days. Of the individual trays, A3 and A6 dried the fastest, as they were closest to the constantly-heated back wall (see figure 3.2 of chapter 3). This was followed by those closest to the tilted roof, A1 and A4, which were faster than the middle ones (table 5.5). The exit RH was generally high compared with that of inlet (table 5.6), probably due to ineffective chimney heating.

		Dry wt (g) =	3640.22	3640.22	3640.224	3640.22	3640.22	3640.22					21841.34	3640.224
	Time		A1	A2	A3	A4	A5	A6	B1	B2	B3	B4	Average	Control
Start of Day 1	1200	Wt (g)	10000.00	10000.00	10000.00	10000.00	10000.00	10000.00					60000.00	10000.00
		MC (%, d.b)	**174.71**	**174.71**	**174.71**	**174.71**	**174.71**	**174.71**					**174.71**	**174.71**
End of Day 1	1700	Wt (g)	8294.00	8442.00	8412.00	8474.00	8569.00	8539.00					50730.00	7957.00
		MC (%, d.b)	**127.84**	**131.91**	**131.08**	**132.79**	**135.40**	**134.57**					**132.27**	**118.59**
Start of Day 2	0800	Wt (g)	7654.00	7789.00	7804.00	7818.00	7898.00	7851.00					46814.00	7434.00
		MC (%, d.b)	**110.26**	**113.97**	**114.38**	**114.77**	**116.96**	**115.67**					**114.34**	**104.22**
End of Day 2	1700	Wt (g)	5925.00	6082.00	6089.00	6055.00	6254.00	6149.00					36554.00	5503.00
		MC (%, d.b)	**62.76**	**67.08**	**67.27**	**66.34**	**71.80**	**68.92**					**67.36**	**51.17**
Start of Day 3	0800	Wt (g)												
		MC (%, d.b)												
End of Day 3	1700	Wt (g)	4593.00	4665.00	4660.00	4602.00	4716.00	4711.00					27947.00	4770.00
		MC (%, d.b)	**26.17**	**28.15**	**28.01**	**26.42**	**29.55**	**29.42**					**27.95**	**31.04**
Start of Day 4	0800	Wt (g)	4520.00	4570.00	4565.00	4499.00	4567.00	4566.00					27287.00	4723.00
		MC (%, d.b)	**24.17**	**25.54**	**25.40**	**23.59**	**25.46**	**25.43**					**24.93**	**29.74**
End of Day 4	1700	Wt (g)	4219.00	4289.00	4260.00	4211.00	4267.00	4263.00					25509.00	4643.00
		MC (%, d.b)	**15.90**	**17.82**	**17.03**	**15.68**	**17.22**	**17.11**					**16.79**	**27.55**

Table 5.7 Field-trial 2; Daily Moisture Contents

Drying Day	Period		T_i	T_L	T_m	T_u	$T_{ch,l}$	T_o	T_b	T_{sw1}	T_{sw2}	T_{BW}	T_{fw}	T_{abs}	$T_{ch,g}$	RH_{in}	RH_{out}	I_G	I_D
Day 1	1200 to 1700	Maximum	31.18	41.88	46.61	43.35	48.73	55.21	59.55	40.52	45.13	43.81	47.85	65.33	55.21	56.00	55.00	977.00	924.00
		Average	29.18	40.06	43.12	40.21	44.88	52.63	53.53	37.51	42.42	39.27	44.80	58.10	53.17	54.00	51.50	743.05	683.87
		Minimum	26.92	36.95	39.16	36.72	41.32	51.33	46.40	35.10	38.55	35.67	40.23	51.33	51.33	50.00	48.00	377.30	327.20
Day 2	0800 to 1700	Maximum	27.45	39.71	44.65	39.34	48.19	52.44	56.73	38.67	45.08	39.48	48.29	66.13	53.97	62.00	64.00	834.00	785.00
		Average	26.16	35.26	38.23	36.12	41.79	46.68	43.33	33.67	38.16	35.79	39.61	51.80	48.89	56.67	53.83	574.40	529.74
		Minimum	25.15	28.71	29.71	29.67	34.79	38.36	27.92	25.65	27.88	28.56	28.62	38.64	35.60	53.00	43.00	266.80	239.60
Day 3	0800 to 1700	Maximum	32.78	43.49	45.53	41.98	47.13	53.10	58.44	37.69	45.24	39.97	47.39	64.03	52.83	61.00	62.00	978.00	929.00
		Average	30.56	35.51	37.94	36.60	41.81	47.03	43.24	31.31	37.00	34.59	38.21	51.03	47.10	59.17	58.17	538.68	494.37
		Minimum	27.34	25.80	25.79	27.57	34.74	37.25	24.55	21.92	24.41	25.04	25.07	37.53	35.30	58.00	55.00	50.42	43.00
Day 4	0800 to 1700	Maximum	33.02	54.53	58.16	60.46	61.69	68.72	65.45	42.32	51.30	54.04	52.58	78.50	69.50	58.00	54.00	975.00	928.00
		Average	31.30	42.42	49.17	49.98	52.43	56.47	50.50	35.26	43.26	43.14	43.13	59.16	56.72	52.50	49.00	634.03	603.75
		Minimum	28.73	27.17	28.84	32.39	37.23	39.23	25.80	23.10	25.61	26.83	27.29	39.51	37.00	49.00	46.00	49.22	45.37

Table 5.8 Field-trial 2; Data Overview

5.3.2 Field-trial 2

The MC at various stages of field-trial 2 and the other data could be found from tables 5.7 and 5.8 respectively. The cassava had initial MC of around 175 % (d.b). The first day ended with MC 132 % (d.b.) with crop browning in the dryer and 119 % (d.b.) in

the control. Although the control had lower MC after the first day (ie. after the first five hours), the first-day comparative performance (-14 %) was better than that of field-trial 1. This resulted from the removal of the main glazing of the unused half of the tent dryer which absorbed some of the radiant energy in field-trial 1. The chimney heating was more effective, and this improved the airflow. Also, the average global insolation was higher (743.05 W/m) with a very high diffuse proportion of 683.87 W/m. The inlet RH at 54 % was slightly lower than in field-trial 1. Also unlike in field-trial 1, the exit RH (51.5 %) was lower than that of inlet.

With the dryer inlet covered in this field-trial, the night reduction in the dryer was more than that in the control, unlike in field-trial 1. No cold or moist air was drawn in at night. What happened was just the escape of moisture from the crop and dryer, caused by the energy stored in the dryer during the day. Evidence of this was the moisture deposits at the inner surfaces of the drying-chamber roof and the chimney, on the morning of day 2. This moisture disappeared in the early hours of the day. Insolation was a bit lower on the second day at 574.4 W/m, though with a very high diffuse proportion of 529.74 W/m. The inlet RH was also higher at 56.67 % but again the exit RH was lower at 53.83 % (table 5.8). The control continued drying faster on the second day, though the dryer narrowed the gap a bit. The wind still seemed somehow effective, and the relatively high MC of crops in the dryer could not propel it to dry at the same rate as the control. Day 2 ended with 67 % (d.b.) for the dryer and 51 % for the control (table 5.7).

There was no weighing on the morning of day 3, as power outage prevented the use of the electronic scale. No moisture was found at the inner surfaces, apparently due to the smaller quantity of moisture that had to escape the previous night. In the evening, the cumulative reduction of MC in the dryer had overtaken that of the control whose crop was then as brownish as those in the dryer. The dryer then continued to dry faster till the end of day 4 (table 5.7), when the commodity became brittle dry, with MC around 17 %, d.b. (well below the desired level). The control was still not fully dried with MC around 27 % (d.b.). Unlike those of field-trial 1, the performances of A1 and A4 (closest to the drying-chamber roof) were better than the other trays, followed by A3

and A6 at the back wall, though the differences were only slight. As seen from table 5.8, the back wall received no additional energy as in field-trial 1, and the temperatures were not so high.

In this field-trial the average air temperature at dryer exit was a little higher than at chimney inlet, and the average RH was lower at exit than at the inlet of the dryer. This might be from the more effective chimney heating as a result of the removal of the extra sheets from the unused part of the dryer and the higher insolation as compared with field-trial 1.

5.3.3 Field-trial 3

Field-trial 3 started with an initial MC of about 181 % (d.b.) at midday (table 5.9). The average global irradiation for the day was 711.60 W/m, with diffuse proportion of 660.57 W/m. The inlet RH averaged at 43.75 %, not much lower than that at exit of 45.75 % (table 5.10). By the evening (5:00 p.m.), the average MC in the dryer was around 128 %, with the MC of the control around 124 % (d.b.). This shows a much better first-day comparative performance (-4 %) of the dryer than in field-trial 2, though the control dried faster. This could be due to the much lower RH with comparable insolation and the better arrangement in the dryer. The trays A2, A3, A5 and A6 of field-trial 2 had been moved higher up to B1, B2, B3 and B4 respectively in field-trial 3 (see figure 3.2 of chapter 3). This allowed better irradiation onto the base of the dryer so that the air could be better preheated before contact with the crop. The browning of the crop had reduced in comparison with that in Field-trial 2 after day 1.

The MC in the dryer fell to 110 % (d.b.) by the morning of day 2, lower than that of the control with around 112 % (d.b.). The average global irradiation of 382.36 W/m was lower than on day 1. Also the humidity conditions were poorer with average inlet RH of 51.33 %. The control drying was just a little faster than that in the dryer; apparently the wind still had some strong effect on day 2. The dryer had around 62 % (d.b.), whilst the control had around 63 % (d.b.) in the evening.

The dryer withstood another heavy storm on the second night. The weather was so poor in the night that the control tray was found infested by ants on the morning of the third day. The crop dried much faster in the dryer than in the control, on day 3. The control crop became more brownish than those in the dryer. The dryer ended the third day with average MC around 19 % (d.b.), below the desired 22 % (d.b.), whilst the MC of the control was still above 31 % (d.b.). On the whole, comparative performance of the dryer was better than in field-trial 2. The performances of B1 to B4 were better (table 5.9) than those of A2, A3, A5 and A6 of field-trials 1 and 2 (tables 5.5 and 5.7), which were in the same horizontal position but at a lower height in the dryer. Thus, as the trays were raised, there was more room for air heating and less shading in the lower part of dryer. This enabled much heating of the air before it got to the crop, as suggested in the lab report. B1 and B3, being close to the roof, did better than B2 and B4 which were at the back wall. A1 and A3 had the worst performance in dryer due to their lower level and shading from the upper trays especially during the morning periods. They had to wait in the dryer till the next morning to be completely dried at 19 % (d.b.), though they still did better than the control which was still not fully dry with around 24 % (d.b.) on the morning of day 4.

		Dry wt (g) =	3264.59			3420.12			3418.34	3417.27	3419.05	3419.05	20358.42	2854.962
	Time		A1	A2	A3	A4	A5	A6	B1	B2	B3	B4	Average	Control
Start of Day 1	1200	Wt (g)	9173.00			9610.00			9605.00	9602.00	9607.00	9607.00	57204.00	8022.00
		MC (%, d.b)	**180.98**			**180.98**			**180.98**	**180.98**	**180.98**	**180.98**	**180.98**	**180.98**
End of Day 1	1700	Wt (g)	7503.00			7910.00			7795.00	7696.00	7700.00	7720.00	46324.00	6390.00
		MC (%, d.b)	**129.83**			**131.28**			**128.03**	**125.21**	**125.21**	**125.79**	**127.54**	**123.82**
Start of Day 2	0800	Wt (g)	6948.00			7300.00			7240.00	7061.00	7140.00	7114.00	42803.00	6052.00
		MC (%, d.b)	**112.83**			**113.44**			**111.80**	**106.63**	**108.83**	**108.07**	**110.25**	**111.98**
End of Day 2	1700	Wt (g)	5515.00			5812.00			5552.00	5281.00	5465.00	5367.00	32992.00	4650.00
		MC (%, d.b)	**68.93**			**69.94**			**62.42**	**54.54**	**59.84**	**56.97**	**62.06**	**62.87**
Start of Day 3	0800	Wt (g)	5043.00			5296.00			5089.00	4868.00	5042.00	4940.00	30278.00	4540.00
		MC (%, d.b)	**54.48**			**54.85**			**48.87**	**42.45**	**47.47**	**44.48**	**48.72**	**59.02**
End of Day 3	1700	Wt (g)	4045.00			4201.00			3922.00	4055.00	3995.00	3995.00	24213.00	3749.00
		MC (%, d.b)	**23.91**			**22.83**			**14.73**	**18.66**	**16.85**	**16.85**	**18.93**	**31.32**
Start of Day 4	0800	Wt (g)	3896.00			4099.00								3539.00
		MC (%, d.b)	**19.34**			**19.85**								**23.96**
End of Day 4	1700	Wt (g)												
		MC (%, d.b)												

Table 5.9 Field-trial 3; Daily Moisture Contents

Drying Day	Period		T_i	T_L	T_m	T_u	$T_{ch,i}$	T_o	T_b	T_{sw1}	T_{sw2}	T_{BW}	T_{fw}	T_{abs}	$T_{ch,g}$	RH_{in}	RH_{out}	I_G	I_D
Day 1	1200 to 1700	Maximum	32.82	44.01	43.33	50.23	50.50	53.69	58.11	38.09	41.87	45.35	45.65	67.82	53.42	50.00	52.00	922.00	895.00
		Average	30.18	41.62	39.77	43.96	46.71	52.14	53.18	36.08	39.79	39.56	43.12	59.91	52.18	43.75	45.75	711.60	660.57
		Minimum	25.70	37.93	37.08	38.89	42.66	50.50	47.96	34.22	37.45	37.03	41.01	54.21	50.24	31.00	34.00	460.40	405.90
Day 2	0800 to 1700	Maximum	33.82	41.71	40.36	46.70	46.99	51.80	53.38	36.94	40.82	40.14	44.95	63.06	51.80	72.00	73.00	710.00	608.50
		Average	31.90	35.49	34.41	37.90	39.97	44.66	41.68	32.66	35.50	35.75	37.46	51.00	46.16	51.33	52.50	382.36	337.15
		Minimum	29.56	27.94	27.14	30.40	33.97	35.37	26.56	25.42	26.49	27.41	26.92	36.48	28.46	35.00	37.00	32.80	28.64
Day 3	0800 to 1700	Maximum	31.30	43.00	38.24	42.01	46.68	50.79	52.77	35.10	39.02	37.72	44.59	61.71	51.33	68.00	69.00	748.00	690.70
		Average	29.72	34.75	33.19	35.93	40.81	46.63	41.53	31.09	34.26	34.32	36.75	49.62	46.84	54.50	53.50	433.18	384.91
		Minimum	27.30	27.02	26.62	32.09	36.89	38.47	26.12	23.46	26.15	26.50	26.26	38.75	36.24	42.00	40.00	38.68	19.10

Table 5.10 Field-trial 3; Data Overview

5.3.4 Field-trial 4

Tables 5.11 and 5.12 show the MCs at various stages and the other data, respectively, of field-trial 4. The initial MC was around 175 % (d.b.). The first day was very cloudy, and the sun was not clearly sighted for most of the day. The average global and diffuse insolations were 502.94 W/m and 452.44 W/m respectively. The inlet RH averaged around 53.50 %. These external conditions were poorer than in field-trial 3. On day 1 (i.e. from 11:40 a.m. to 5:00 p.m.), the MC in the dryer fell to around 126 % with very light browning, and the MC of the control reduced to around 124 % (d.b.). Although the control was still a bit faster, this trial had the best comparative performance (-2 %) of all trials on day 1, despite the poor external conditions. B4 even caught up with the control by the end of the day. Unlike field-trial 3, there were no trays at A1 and A2 to somehow increase the relative humidity of the air before it got to the crops on the upper trays.

There was rain on each night of the trial, and a lot of water had to be cleared from the surfaces of both the dryer and control cover each morning. With all the trays in the upper position (B1 to B4), the dryer continued to perform better than the control. However, due to the relatively worse weather conditions (higher relative humidity and sometimes lower insolation, with rain all night), it was not until the third morning that the MC in the dryer fell below the desired level, with about 19 % (d.b.). The MC of the control (still around 34 %, d.b.) is an indication of the poor weather conditions. By evening, the crops in the dryer had become very brittle with an average MC of 14 % (d.b.) and that of control was still around 30 %, no where near the desired level. The crop in the control was very brownish, and that in the dryer had changed only slightly in colour to light brown.

		Dry wt (g) =							3896.495	3898.316	3897.223	3899.044	15591.08	3862.277
	Time		A1	A2	A3	A4	A5	A6	B1	B2	B3	B4	Average	Control
Start of Day 1	1140	Wt (g)							10704.00	10709.00	10706.00	10711.00	42830.00	10610.00
		MC (%, d.b)							**174.71**	**174.71**	**174.71**	**174.71**	**174.71**	**174.71**
End of Day 1	1700	Wt (g)							8850.00	8875.00	8765.00	8725.00	35215.00	8643.00
		MC (%, d.b)							**127.13**	**127.66**	**124.90**	**123.77**	**125.87**	**123.78**
Start of Day 2	0800	Wt (g)							8219.00	8229.00	8144.00	8092.00	32684.00	8285.00
		MC (%, d.b)							**110.93**	**111.09**	**108.97**	**107.54**	**109.63**	**114.51**
End of Day 2	1700	Wt (g)							6123.00	6051.00	5962.00	5855.00	23991.00	6140.00
		MC (%, d.b)							**57.14**	**55.22**	**52.98**	**50.17**	**53.88**	**58.97**
Start of Day 3	0800	Wt (g)							5726.00	5658.00	5598.00	5518.00	22500.00	6007.00
		MC (%, d.b)							**46.95**	**45.14**	**43.64**	**41.52**	**44.31**	**55.53**
End of Day 3	1700	Wt (g)							4847.00	4815.00	4778.00	4759.00	19199.00	5344.00
		MC (%, d.b)							**24.39**	**23.51**	**22.60**	**22.06**	**23.14**	**38.36**
Start of Day 4	0800	Wt (g)							4643.00	4659.00	4599.00	4619.00	18520.00	5182.00
		MC (%, d.b)							**19.16**	**19.51**	**18.01**	**18.46**	**18.79**	**34.17**
End of Day 4	1700	Wt (g)							4437.00	4461.00	4431.00	4470.00	17799.00	5014.00
		MC (%, d.b)							**13.87**	**14.43**	**13.70**	**14.64**	**14.16**	**29.82**

Table 5.11 Field-trial 4; Daily Moisture Contents

Drying Day	Period		T_i	T_L	T_m	T_u	$T_{ch,l}$	T_o	T_b	T_{sw1}	T_{sw2}	T_{BW}	T_{fw}	T_{abs}	$T_{ch,g}$	RH_{in}	RH_{out}	I_G	I_D
Day 1	1130 to 1700	Maximum	32.41	44.93	38.58	40.01	43.81	50.14	51.19	36.38	39.47	38.71	41.83	55.35	52.57	71.00	72.00	720.00	675.10
		Average	31.44	39.00	36.35	37.90	40.84	45.58	43.38	34.67	37.32	36.94	38.33	50.31	48.90	53.50	54.75	502.94	452.44
		Minimum	30.06	34.12	32.54	33.38	33.38	33.38	33.62	31.68	33.18	33.91	33.48	41.24	35.54	44.00	45.00	199.80	171.40
Day 2	0800 to 1700	Maximum	34.17	47.08	41.15	46.49	48.91	53.26	58.12	37.50	41.62	46.62	47.21	64.99	53.26	61.00	60.00	897.00	869.00
		Average	31.49	39.04	36.12	37.73	43.00	47.21	43.62	32.72	36.77	38.67	38.10	51.91	47.97	49.50	49.33	554.01	512.61
		Minimum	27.72	27.18	25.97	30.89	35.17	37.01	25.39	22.24	25.32	25.94	25.31	37.01	33.94	42.00	43.00	37.52	26.28
Day 3	0800 to 1700	Maximum	32.57	49.16	41.16	42.25	49.42	53.22	55.66	38.13	42.28	40.91	45.13	64.79	54.03	64.00	62.00	711.00	644.90
		Average	30.30	39.63	35.78	37.06	44.02	48.02	44.56	33.13	37.26	37.52	38.34	52.74	48.00	55.17	53.00	486.12	442.08
		Minimum	26.09	26.10	25.09	31.29	32.93	34.04	24.44	23.20	24.53	25.74	24.55	36.26	29.02	48.00	46.00	24.61	9.55
Day 4	0800 to 1700	Maximum	30.40	54.60	44.88	46.88	48.69	55.44	60.85	40.86	44.10	44.77	46.22	67.17	56.62	64.00	67.00	711.00	644.90
		Average	26.26	40.05	37.20	36.40	41.71	48.82	44.42	33.89	37.38	38.36	37.92	52.46	49.32	56.83	56.50	486.12	442.08
		Minimum	21.79	26.02	24.67	23.97	35.06	39.01	24.88	22.87	24.63	25.81	25.21	39.00	36.50	52.00	51.00	24.61	9.55

Table 5.12 Field-trial 4; Data Overview

5.3.5 Field-trial 5

Field-Trial 5 had MC of around 181 % (d.b.) in the beginning (see table 5.13). With the dryer at full capacity of nearly 100 kg, the average MC dropped in the dryer to 144 % and in the control to 122 %, showing a comparative performance of -22 % on day 1. The inlet RH was 48.5 % and the average insolation was 600.71 % (see table 5.14). Though still better than that of trial 1, field-trial 5 had the worst first-day comparative performance of all the field-trials after the dryer was modified to improve the night performance and irradiation into the dryer. The two full layers of trays offered more resistance to air flow in the drying chamber.

There were moisture deposits inside the roof and chimney walls on the morning of day 2, from the previous night's self-drying. The night drying was better than control as usual. The comparative performance improved during the second day and night; nonetheless the MC was still higher in the dryer at the beginning of the third day. The third day was a bit hazier with low sunshine, and there was rain towards the end of the day. This rain continued deep into the night and prevented the weighing of the crops in the evening. By the morning of day 4, the dryer's average MC had fallen below that of the control. Furthermore, there were spots of moulds on the surfaces of the control cassava, probably due to the very high humidity from the heavy rain the previous night. The dryer ended the fourth day with an average MC of around 15 % (d.b.) whilst the control still had 23 % (d.b.), though the middle trays at the lower level of dryer still had to wait till the next morning to be completely dried at around 17 %. These trays were shaded most of the day by the upper trays. The control was then just dried with 22 % (d.b.) in the end. As in field-trials 2, 3 and 4, the trays closest to the tilted roof dried fastest than the rest.

	Time		A1	A2	A3	A4	A5	A6	B1	B2	B3	B4	Average	Control
Start of Day 1	1130	Wt (g)	9800.00	9800.00	9800.00	9800.00	9800.00	9800.00	9800.00	9800.00	9800.00	9800.00	98000.00	9800.00
		MC (%, d.b	**180.98**	**180.98**	**180.98**	**180.98**	**180.98**	**180.98**	**180.98**	**180.98**	**180.98**	**180.98**	**180.98**	**180.98**
End of Day 1	1700	Wt (g)	8297.00	8784.00	8695.00	8520.00	8901.00	8709.00	8293.00	8402.00	8299.00	8352.00	85252.00	7743.00
		MC (%, d.b	**137.89**	**151.85**	**149.30**	**144.28**	**155.21**	**149.70**	**137.78**	**140.90**	**137.95**	**139.47**	**144.43**	**122.01**
Start of Day 2	0800	Wt (g)	7853.00	8348.00	8267.00	8051.00	8422.00	8205.00	7932.00	7979.00	7853.00	7851.00	80761.00	7453.00
		MC (%, d.b	**125.16**	**139.35**	**137.03**	**130.84**	**141.47**	**135.25**	**127.43**	**128.77**	**125.16**	**125.10**	**131.56**	**113.69**
End of Day 2	1700	Wt (g)	6174.00	6836.00	6763.00	6285.00	7012.00	6736.00	6005.00	5953.00	5923.00	5750.00	63437.00	5417.00
		MC (%, d.b	**77.02**	**96.00**	**93.91**	**80.20**	**101.05**	**93.13**	**72.17**	**70.68**	**69.82**	**64.86**	**81.89**	**55.32**
Start of Day 3	0800	Wt (g)	5752.00	6375.00	6300.00	5858.00	6474.00	6218.00	5684.00	5600.00	5556.00	5404.00	59221.00	5292.00
		MC (%, d.b	**64.92**	**82.78**	**80.63**	**67.96**	**85.62**	**78.28**	**62.97**	**60.56**	**59.30**	**54.94**	**69.80**	**51.73**
End of Day 3	1700	Wt (g)												
		MC (%, d.b)												
Start of Day 4	0800	Wt (g)	4666.00	5076.00	4992.00	4692.00	5138.00	4856.00	4504.00	4521.00	4446.00	4392.00	47283.00	4675.00
		MC (%, d.b	**33.78**	**45.54**	**43.13**	**34.53**	**47.32**	**39.23**	**29.14**	**29.63**	**27.48**	**25.93**	**35.57**	**34.04**
End of Day 4	1700	Wt (g)	3946.00	4201.00	4167.00	3957.00	4269.00	4088.00	3772.00	3910.00	3837.00	3861.00	40008.00	4299.00
		MC (%, d.b	**13.14**	**20.45**	**19.48**	**13.45**	**22.40**	**17.21**	**8.15**	**12.11**	**10.01**	**10.70**	**14.71**	**23.26**
Start of Day 5	800	Wt (g)		4090.00			4106.00							4259.00
		MC (%, d.b)		**17.27**			**17.73**							**22.11**
End of Day 5	1700	Wt (g)												
		MC (%, d.b)												

Table 5.13 Field-trial 5; Daily Moisture Contents

Drying Day	Period		T_I	T_L	T_m	T_u	$T_{ch,l}$	T_o	T_b	T_{sw1}	T_{sw2}	T_{BW}	T_{fw}	T_{abs}	$T_{ch,g}$	RH_{in}	RH_{out}	I_G	I_D
Day 1	1130 to 1700	Maximum	32.61	40.12	37.55	38.29	45.35	52.87	54.53	38.02	39.36	44.69	44.10	65.95	53.87	60.00	68.00	879.00	738.00
		Average	31.40	36.79	36.61	36.88	43.66	50.63	48.63	35.05	37.57	41.76	40.85	55.84	51.09	48.50	54.00	600.71	492.16
		Minimum	30.31	33.13	34.52	33.52	42.12	46.05	38.19	29.61	35.29	37.80	36.17	46.05	46.05	40.00	45.00	295.10	258.80
Day 2	0800 to 1700	Maximum	31.95	39.83	40.31	43.26	47.83	54.90	57.50	39.48	41.73	41.22	45.14	66.78	53.82	67.00	71.00	812.00	713.00
		Average	29.20	34.08	34.51	36.43	41.02	46.28	42.86	33.64	35.61	35.70	37.41	52.51	46.86	49.33	52.67	498.15	424.82
		Minimum	26.01	26.48	25.65	29.29	33.89	36.38	24.57	23.90	25.01	26.51	25.44	35.27	31.94	41.00	43.00	24.61	13.13
Day 3	0800 to 1700	Maximum	33.34	37.92	38.50	40.22	42.84	50.33	51.03	40.22	41.06	44.57	42.99	59.04	55.32	57.00	60.00	771.00	693.60
		Average	30.40	33.07	33.75	35.72	37.88	41.77	38.82	33.95	34.91	35.99	35.64	47.08	45.01	47.20	50.00	414.03	366.60
		Minimum	25.15	27.26	26.52	28.84	28.84	28.84	25.84	25.20	25.94	26.94	26.26	28.84	27.97	39.00	43.00	1.17	0.00
Day 4	0800 to 1700	Maximum	32.75	41.96	43.51	43.17	48.92	54.83	61.97	41.10	42.93	46.00	48.69	69.81	55.63	65.00	66.00	853.00	815.00
		Average	28.80	35.40	36.88	37.21	41.80	47.70	45.68	34.85	37.12	38.76	39.31	54.87	50.45	51.67	52.83	569.88	522.14
		Minimum	25.28	26.87	26.81	28.20	36.00	38.61	26.05	23.33	25.13	26.93	26.59	39.17	34.98	40.00	41.00	39.85	23.88

Table 5.14 Field-trial 5; Data Overview

5.4 Summary observations, discussions and recommendations

5.4.1 The laboratory model

The observations from the no-load trials showed that the solar chimney was able to heat the air effectively, and this facilitated higher airflow through the CDSCD than using the normal chimney. As the dying-chamber roof became more horizontal, the resistance to airflow at the roof increased, causing airflow reduction. This resulted in high temperature in the drying chamber. When the roof was turned towards the vertical plane, the resistance reduced and the airflow increased, resulting in low temperature in the drying chamber. This may explain why tent dryers perform better than cabinet dryers of the same loading capacity under similar environmental conditions as, previously reported (Ekechukwu, 1999 (I)). The upward-converging tent dryer was a very effective chimney when it was well heated. As in all heat and mass transfer processes, the heat and airflow mutually affected each other in equilibrium. The airflow rate depended also on the amount of air allowed into the dryer at inlet. For a given roof angle, a large inlet gap enhanced higher airflow and lowered the temperature. Furthermore, air that entered the dryer with low humidity was a bit more effectively heated, resulting in higher flow rate, than air of higher humidity.

During the under-load trials, it was observed that obstruction by the drying shelf with crop added to the resistance to the airflow and thus reduced the flow velocity further, as suggested by Ekechukwu, 1997. After moisture absorption from the crop zone, the air temperature reduced further up the chamber, due to the increased absolute humidity from the drying process. The solar chimney was then required to maintain higher air

temperatures up the structure, in order to improve the airflow. High airflow rate did not necessarily bring about high drying rate, unless the relative humidity of the drying air got below 60 %. This result supports the values of Relative Humidity Indicator stated in the literature for fast drying of cassava by which a value of zero is assigned to relative humidity of 60 % or more (Igbeka, 1982). The base absorber of the drying chamber was mostly shielded from the radiant energy and could not transfer much heat to the drying air, except at small inlet gaps. So, with large inlet gaps, the air got to the crop with an RH not much different from that of ambient.

During day time, the well-heated, high chimney improved the air flow to aid the drying process, but at night it functioned just as a normal chimney and impeded the night drying. This made the dryer only effective over open-sun drying in a low-humidity environment. The dryer became ineffective in the long run when the environment became more humid. The air left the exit of the chimney with higher temperature and much lower RH than at inlet; thus the exit air could very much have been used for drying but it was just allowed to go to waste in the atmosphere.

In most trials, the ambient RH started at a high value and reduced in the course of the day. This distorted the usual drying curve described in the literature review. Rather than following the usual decrease in drying rate with time, the drying rate remained at times constant on a particular day, with a stepwise wise decrease from one day to the next. Within the first hour of each day, the drying rate was generally lower than expected. In this period, the system (i.e. the dryer with its contents) normally used most of the supplied energy to heat up to the drying state, leaving just a small fraction to dry the crops. This heating-up energy was stored in the system until the lamps were switched out. The stored energy was then released and most of it was used for self drying in the night, as the system cooled down to atmospheric conditions.

5.4.2 The field model

During the field work, maximum insolation was generally in the afternoon periods, peaking generally between 700 and 1000 W/m^2, apart from the third day of field-trial 3 when a peak of 513 W/m^2 was recorded (see the tables of external data). The

atmosphere was mostly cloudy, with high proportion of diffuse light. The relative humidity of the local environment was a bit high, sometimes around 50 % or more (on average).

The control tray (in the open sun) always dried faster than the dryer on the first day, as the drying site was very windy. Similar results were observed by Jain and Tiwari (2004, I). From the literature review, the energy of moisture removal of a starchy crop like cassava is generally lower than the heat of vaporisation of water, in the initial stages of drying. Also, the diffusion through the crop is mainly liquid diffusion. High winds can therefore do a good job in removing liquid moisture from the crop in the initial stages of drying. The situation could however be different at low wind speeds. Data recorded a few years earlier for February and early March in the periods from 8:00 am to 5:00 pm gave low wind speed values prevailing between 0.5 and 2.5 m/s. Also, with each trial starting around midday on day 1, there was not much time for the drying rate in the dryer to catch up with the control on this day. The situation was however reversed at some point in the drying process when airflow effect waned and the effect of heating became more prominent.

As expected, drying was always fastest within the first two days when the MC was high. Thus due to the short drying periods on day 1, the highest MC drop was at times observed on day 2, unlike during the laboratory trials. Raising the shelves in the dryer created enough room at the lower part of dryer for some air heating before it got to the crops. This phenomenon was aided by the very high proportion of diffuse light, which reduced the shading effect from the upper shelf onto the lower shelf and onto the base of drying chamber.

Table 5.15 summarises the daily average drying efficiency η of the dryer for the various trials, estimated from the relation

$$\eta = \frac{WL}{I_g A}. \tag{5.1}$$

where W is the mass of moisture removed from the crop in a given period, I_g is the irradiation energy in the same period, L is the energy per unit mass of moisture removal and A is the aperture area of the drying chamber

Day		Trial 1	Trial 2	Trial 3	Trial 4	Trial 5
		Dryer	Dryer	Dryer	Dryer	Dryer
1	L	2501000.00	2501000.00	2501000.00	2501000.00	2501000.00
	W	5.10	9.27	10.88	7.62	12.75
	η	**19.13**	**21.68**	**26.57**	**26.31**	**36.87**
2	L	2501000.00	2501000.00	2501000.00	2501000.00	2501000.00
	W	10.88	10.26	9.81	8.69	17.32
	η	**15.58**	**13.79**	**19.81**	**12.12**	**26.86**
3	L	2501000.00	2501000.00	2501000.00	2501000.00	2501000.00
	W	6.12		6.07	3.30	
	η	**14.23**		**10.81**	**5.24**	
4	L	2501000.00	2501000.00	2501000.00	2501000.00	2501000.00
	W	2.28	1.78		0.72	7.28
	η	**3.82**	**2.17**		**1.15**	**9.86**
5	L	2501000.00	2501000.00	2501000.00	2501000.00	2501000.00
	W	1.04				
	η	**1.58**				

Table 5.15 Average Drying Efficiencies of the Field Dryer for various trials

The efficiency is a measure of the utilisation of the radiant energy supplied into the drying chamber. Trial-5 (with full load) had highest efficiency. Trial-1 had lower first-day efficiency than trial 2, due to the slightly less load and the ineffectiveness of energy transmission associated with the too much shading. The efficiency of trial 3 was better than that of trial 2, which had about the same loading. This resulted from the better loading arrangement in trial 3, which allowed more air-preheating. With more load and better humidity conditions, the efficiency of trial 3 was higher than that of trial 4. Thus, the drying efficiency of the dryer improved as the load increased (at least up to full load) and also when the shelves were high up the drying chamber, with the right atmospheric conditions. The first-day efficiency proved very much essential for the overall reduction of the total drying time. For instance, the dryer finished trial 5 (with full load, but highest first-day efficiency) just about a day later than the rest, which had less than two-thirds the full load. This supports the proposal by Leon *et al* (2002) that the first-day drying efficiency be used as an evaluation criterion.

From the very high levels of insolation, the temperatures in the field dryer were much higher in the day than those in the laboratory model. This caused faster quality deterioration in the field dryer. Browning was observed at MC as low as 130 % (d.b.), but the crop in the laboratory model looked unchanged in colour even at around 145 % (d.b.).

Nocturnal drying was very much retarded when the inlet was left open at night, as very cold and humid air was then drawn in. But when the inlet was covered, the energy stored in the system aided the removal of moisture from the crops by the surrounding air, and thus enhanced the night drying to some extent. Also, the short chimney did not pose much hindrance to the exit of moist air. In general, the nocturnal drying accounted for just about one-fifth of the total moisture reduction. Nonetheless its effect, especially during the first night, was essential to enable the cumulative moisture reduction in the dryer to overtake that of the control shelf. Drying then proceeded faster in the dryer than the control, once its MC fell below that of the control, and finished earlier.

The dryer always finished earlier with the crops fully dried rather than partially cooked, even at full load and also when the inlet was open at night. On the other hand, the control crops were not fully dried by the end of the process. In fact the control drying would have been impossible throughout the field-work period, if the top part had not been covered at night or anytime there was rain. Thus personnel had to be constantly alert of the weather to take good care of open-sun drying. One other problem with the control (open-sun) drying was the usual constant exposure of the control to unhygienic conditions during the process.

The dryer was able to withstand heavy storms, as the short chimney did not raise the centre of gravity that much, though the framework of the other half of dryer provided additional support.

5.4.3 Comparing the CDSCD with other natural-convection solar crop dryers

The CDSCD, with the use of a solar chimney and the tent-dryer effect, works with improved ventilation through the drying chamber. However, being a direct-mode dryer, it has no effective means of preheating the drying air to lower the relative humidity before the air comes into contact with the crop. Therefore the dryer does not perform well when the ambient relative humidity remains persistently above the maximum RH value for fast drying of the crop. For instance, the test by Olufayo and Ogunkunle (1996) of a direct-mode solar dryer with cassava yielded no superior results to that of open-sun drying. With their dryer operating constantly in an environment of high relative humidity (76 to 81 %), equipping the dryer with a solar chimney for improved airflow would not offer much help to the drying process.

With an indirect-mode dryer on the other hand, the preheated air always contacts the crop with low relative humidity. However, the crop receives no direct radiant energy and has to depend on the preheated air to raise the vapour pressure of moisture in the crop for drying. Thus, a preheater of large surface area is required for effective performance of the indirect-mode dryer. This makes the dryer much more expensive, although it is better suited to crops which are sensitive to light.

The mixed-mode dryer, like the indirect-mode type, is not so sensitive to the RH of the environment. It also ensures that preheated, drying air gets to the crop at low relative humidity. Unlike the indirect-mode type, the crop does not have to depend on the drying air to raise the vapour pressure of moisture in the crop, due to the direct exposure of the crop to irradiation. This dryer functions much more effectively and has better returns than the direct-mode and indirect-mode dryers. However, like the indirect-mode type, the construction of the mixed-mode dryer is more expensive than the direct-mode type due to the need for an additional preheating device.

5.4.4 Ways of improving the CDSCD

The design can be improved for effective heating in the drying chamber during the day, with the chimney height reduced so that the impedance to night drying would also

reduce. Rather than raising the height of the chimney, the base of dryer can slightly be extended forward (i.e. the upper half of the chimney could instead be used at the inlet to form a short air pre-heater). This would also ensure that less humid air, of high moisture carrying capacity gets to the drying commodity. It would aid the night self drying (even when the inlet is left open) as the preheater could store additional energy for the night. Furthermore, the chimney exit of the field dryer should be changed from facing the back of the dryer to face upwards. This will enable the dryer to make better use of the local wind. Moreover, the net cost would be far less than using the same area to raise the chimney, as no extra structures would be needed to support the dryer against the wind, and also the heated air would be used rather than wasted. The height of the chimney would be just enough to maintain the airflow needed for drying. Also the extended chamber base could be better irradiated. Alternatively, raising the shelves in the dryer can enhance better air preheating and ensure that air of high moisture-carrying capacity contacts the crops. One disadvantage, though, is that the dryer capacity reduces when the shelves are raised for the given tilted roof. Also, drying may be aided by reducing the inlet gap at the final stages. This will reduce airflow and improve the heating in the drying chamber, for efficient drying. This part would depend on the user's culture of following instructions.

Considering the merits and demerits explained above, the use of the Chimney-dependent Direct-mode Solar Crop Dryer is arguably better than open-sun drying, at least for drying cassava. Employing some of the improvement suggestions above would make it even far better.

CHAPTER 6 DEVELOPMENT OF THE SIMULATION CODE

The simulation code is developed from the mathematical model and the results of experimentations of the physical model of the CDSCD. The code is to be used to investigate the behaviour and to refine the design (where necessary) of the dryer, among others. Factors and relations (or models) gathered from the literature are used together with those established experimentally for developing this code. The chapter begins with the empirical determination of the relevant data and additional relations needed for developing the code. This is followed by the description of the components of the simulation code and how they are used in the code. As next comes the validation of the code with the laboratory results, followed by some parametric studies on the no-load process. The field results could not be used for the validation, as information of the magnitude of the wind velocity is lacking. The chapter ends with the summary observations, discussions and recommendations on the simulation code.

6.1 Empirical relations and other data

This section describes the use of the experimental data for finding the air bulk temperatures in the chimney and drying chamber and their mean temperature approximations, in terms of the their inlet and exit temperatures. Also determined empirically were the pressure coefficients K_{in} at the inlet, K_{roof} at the roof and K_{out} at the exit, in relation to the dimensions of the dryer. A program was also written to estimate the irradiation onto the dryer and the absorption and emission properties of the dryer glazing.

6.1.1 The air bulk temperatures and mean temperature approximations

6.1.1.1 Air temperature relations in the chimney

The chimney air temperature T was plotted against the height h, using the 3 air-temperature data recorded inside the chimney, for each of the nine trials in test-set 2 (as described in chapters 3 and 5). The heights were $h = 0$ at the chimney inlet, $h = 35$cm in

the middle (i.e. 35cm above the chimney inlet) and h = 60cm at the top of the chimney. The curves were found to follow closely second-order polynomials of the form

$$T = ah^2 + bh + c \tag{6.1}$$

where a, b and c are coefficients of the equation. Table 6.1 shows an overview of the coefficients and the bulk temperature relations. The bulk temperature $T_{f,chm}$ was calculated from the relation

$$T_{f,chm} = \frac{\int_0^{H_{ch}} T dh}{H_{ch}} = \frac{a}{3} H_{ch}^{\ 2} + \frac{b}{2} H_{ch} + c$$

or

$$T_{f,chm} = \frac{a}{3}(60)^2 + \frac{b}{2}(60) + c \tag{6.2}$$

where H_{ch} is the chimney height = 60 cm.

The mean temperature approximation γ_{chm} is then obtained from equation 4.23b as

$$\gamma_{chm} = \frac{T_{f,chm} - T_{ch,i}}{T_{out} - T_{ch,i}}. \tag{6.3}$$

where $T_{ch,i}$ and T_{out} are air temperatures at chimney inlet and exit respectively.

	Roof Angle 81^0			Roof Angle 64^0			Roof Angle 51^0		
Inlet Gap	30 mm	50 mm	70 mm	30 mm	50 mm	70 mm	30 mm	50 mm	70 mm
a	-0.0013	-0.0015	-0.0021	-0.0007	-0.0008	-0.0018	-0.0004	-0.0014	-0.0018
b	0.1206	0.1581	0.2109	0.0679	0.1087	0.1883	0.0377	0.1430	0.1883
c	29.1667	26.8333	26.1667	29.8333	28.3330	24.8830	30.1670	28.6680	26.1667
$T_{f,chm}$	31.2247	29.7763	29.9737	31.0303	30.6340	28.3720	30.8180	31.2780	29.6557
$T_{ch,i}$	29.16667	26.83333	26.16667	29.83333	27.83333	24.833333	30.16667	28.66667	26.16667
T_{out}	31.83333	30.83333	31.33333	31.33333	31.5	29.5	31	32.33333	30.83333
γ_{chm}	0.7718	0.7358	0.7368	0.7980	0.7638	0.7583	0.7816	0.7122	0.7476
$\gamma_{chm,av}$	0.7562								

Table 6.1 Air bulk temperature relations in the chimney

From table 6.1, γ_{chm} varies between 0.712 and 0.798 with an average, $\gamma_{chm,av}$, of 0.756. This does not differ so much from the 0.74 found experimentally by Ong and Chow (2003) in their study of the performance of a solar chimney, and the 0.75 used by Hirunlabh *et al* (1999) in the modelling and physical testing of the natural ventilation of houses by a metallic solar wall.

6.1.1.2 Air temperature relations in the drying chamber

The plot of air temperature T in the drying chamber against the height h = 6, 16, 26 and 49 cm was also found to follow closely a second-order polynomial. The air bulk temperature $T_{f,dc}$ was determined from the equation

$$T_{f,dc} = \frac{\int_0^{H_{dc}} Tdh}{H_{dc}} = \frac{a}{3} H_{dc}{}^2 + \frac{b}{2} H_{dc} + c$$

or

$$T_{f,dc} = \frac{a}{3}(49)^2 + \frac{b}{2}(49) + c \qquad (6.4)$$

where H_{dc} is the drying chamber height = 49 cm.

It was realised in chapter 4 that the heat transfer coefficient of a film between the air and a wall depends on the inclination of the wall. This meant that the air bulk temperature in the drying chamber could be different for each roof angle. The experimental results have therefore been used to determine the empirical relations between the air bulk temperature $T_{f,dc}$ in the drying chamber in relation to the roof angle of drying chamber. The equation coefficients and the bulk temperature relations for each drying chamber configuration can be found in table 6.2

	Roof Angle 81^0			Roof Angle 64^0			Roof Angle 51^0		
Inlet Gap	30 mm	50 mm	70 mm	30 mm	50 mm	70 mm	30 mm	50 mm	70 mm
a	-0.0009	-0.0016	-0.0012	0.0001	0.0000	-0.0005	0.0003	-0.0003	-0.0001
b	0.1713	0.1655	0.1140	0.1241	0.0863	0.0758	0.1075	0.0899	0.0543
c	23.004	22.525	23.391	23.608	24.481	22.405	24.185	24.923	23.824
$T_{dc,in}$	21	22.33333	23.000	21.66667	23.83333	22.166667	22.16667	24.66667	23.5
$T_{ch,i}$	29.16667	26.83333	26.16667	29.83333	27.83333	24.833333	30.16667	28.66667	26.16667
$T_{f,dc}$	26.4806	25.2992	25.2236	26.6965	26.5713	23.8619	27.0589	26.8855	24.9903
γ_{dc}	0.6711	0.6591	0.7022	0.6159	0.6845	0.6357	0.6115	0.5547	0.5589
$\gamma_{dc,av}$	0.6775			0.6454			0.5750		

Table 6.2 Air bulk temperature relations in the drying chamber

From equation 4.33, the mean temperature approximation γ_{dc} is given as

$$\gamma_{dc} = \frac{T_{f,dc} - T_{dc,in}}{T_{ch,i} - T_{dc,in}} \qquad (6.5)$$

where $T_{dc,in}$ is the drying-chamber inlet air temperature.

The values for roof angle 81 averaged at 0.6775; the average for angle 64 was at 0.6454, with that for angle 51 at 0.575. With these values, a second-other polynomial relationship was developed between the average mean temperature approximation $\gamma_{dc,av}$ and the roof angle θ as

$$\gamma_{dc,av} = -0.3856\theta^2 + 1.084\theta - 0.0844 \qquad (6.6)$$

6.1.2 Determining the Pressure coefficients

The inlet and exit configurations remained unchanged throughout the trials. Therefore, the pressure loss coefficients at these sections were expected to be the same for all the trials. However, the roof loss coefficient was expected to vary in relation to the roof angle. The coefficients were determined by considering the pressure equations of the drying chamber and the chimney separately, with the roof forming the exit and inlet arrangements of the drying chamber and chimney respectively. For the drying chamber,

$$\rho g \beta_{dc} \Delta T_{dc} H_{dc} = K_{in} \rho \frac{v_{in}}{2} + \Delta P_{roof} \tag{6.7}$$

where $\beta_{dc} = \frac{1}{T_{f,dc}}$ (6.8)

and, from equation 4.9,

$$\Delta P_{roof} = \frac{1}{2} \frac{K_{roof}}{\rho A_b A_{ch,i}} \dot{m}^2 = \frac{1}{2} K_{roof} \rho \frac{A_{in}^2}{A_b A_{ch,i}} v_{in}^2 \tag{6.9}$$

ΔP_{roof} of the equation 6.9 was substituted into equation 6.7 to get

$$K_{roof} = \frac{A_b A_{ch,i}}{A_{in}^2} \left(\frac{D_{dc}}{v_{in}^2} - K_{in} \right) \tag{6.10}$$

where

$$D_{dc} = 2 g \beta_{dc} \Delta T_{dc} H_{dc}$$

A method of trial and error was used with assumed values of K_{in}, together with the measured data, in equation 6.10. For each assumed K_{in}, K_{roof} was calculated and checked for consistency with all the inlet areas of each roof angle. The most closely consistent values of K_{roof} were obtained for each roof with $K_{in} = 1.9$. This is just slightly below the approximate value of 2.0 deduced from the results of Flourentzou *et. al* (1998) as explained in sub section 4.1.1 (chapter 4). Table 6.3 shows the values K_{roof} determined with $K_{in} = 1.9$. The roof with angle 51^0 to the vertical had the lowest average coefficient of 0.29. That of angle 64^0 averaged at 0.98 and angle 81^0 had average K_{roof} of 3.62. The plot of K_{roof} versus roof angle θ follows closely the second-order polynomial

$$K_{roof} = 11.233 \cdot \theta^2 - 19.522 \cdot \theta + 8.7662 \tag{6.11}$$

Inlet Gap (m)	Roof Angle 81^0			Roof Angle 64^0			Roof Angle 51^0		
	0.03	0.05	0.07	0.03	0.05	0.07	0.03	0.05	0.07
A_{in}	0.0120	0.0200	0.0280	0.0120	0.0200	0.0280	0.0120	0.0200	0.0280
β_{dc}	0.003339	0.003352	0.003353	0.003337	0.003338	0.003369	0.003333	0.003335	0.003356
ΔT_{dc}	8.17	4.50	3.17	8.17	4.00	2.67	8.00	4.00	2.67
H_{dc}	0.48	0.47	0.46	0.48	0.47	0.46	0.48	0.47	0.46
D_{dc}	0.25	0.14	0.09	0.25	0.12	0.08	0.25	0.12	0.08
v_{in}	0.35	0.23	0.18	0.36	0.24	0.19	0.36	0.25	0.20
v_{in}^2	0.12	0.05	0.03	0.13	0.06	0.04	0.13	0.06	0.04
K_{roof}	3.59	3.78	3.49	0.99	0.95	0.99	0.29	0.28	0.30
$K_{roof,av}$	3.62			0.98			0.29		

Table 6.3 Determining the values of K_{roof} for each roof angle.

The exit coefficient K_{out} was then calculate from the pressure equation for the chimney

$$\rho g \beta_{chm} \Delta T_{r,chm} H_{r,chm} = \Delta P_{roof} + K_{out} \rho \frac{v_{out}^2}{2} \tag{6.12}$$

with $$\beta_{chm} = \frac{1}{T_{f,chm}} \tag{6.13}$$

and

$$\Delta P_{roof} = \frac{1}{2} K_{roof} \rho \frac{A_{out}^2}{A_b A_{ch,i}} v_{out}^2 \tag{6.14}$$

so that equation 6.12 was rearranged together with 6.13 and 6.14 to get

$$K_{out} = \frac{D_{chm}}{v_{out}^2} - K_{roof} \frac{A_{out}^2}{A_b A_{ch,i}} \tag{6.15}$$

where

$$D_{chm} = 2 g \beta_{chm} \Delta T_{r,chm} H_{r,chm} .$$

$\Delta T_{r,chm}$ and $H_{r,chm}$ are the temperature difference and height respectively from the roof to the top of the chimney. As shown in table 6.4, the average value of K_{out} was 1.28.

Inlet Gap	Roof Angle 81^0			Roof Angle 64^0			Roof Angle 51^0		
	30 mm	50 mm	70 mm	30 mm	50 mm	70 mm	30 mm	50 mm	70 mm
T_{roof}	30.50	29.45	29.81	30.17	30.27	28.09	30.01	30.97	29.37
β_{chm}	0.003295	0.003306	0.003302	0.003298	0.003297	0.003321	0.003300	0.003290	0.003307
$\Delta T_{r,chm}$	5.35	5.53	6.11	4.64	4.93	5.64	3.94	5.45	5.84
$H_{r,chm}$	0.68	0.68	0.68	0.79	0.79	0.79	0.90	0.90	0.90
D_{chm}	0.23	0.24	0.27	0.24	0.25	0.29	0.23	0.32	0.34
v_{out}	0.39	0.44	0.45	0.40	0.45	0.49	0.40	0.47	0.52
v_{out}^2	0.15	0.19	0.20	0.16	0.20	0.24	0.16	0.22	0.27
K_{out}	1.37	1.11	1.17	1.41	1.20	1.17	1.43	1.41	1.26
$K_{out,av}$	1.28189								

Table 6.4 Determining the value of K_{out}.

6.1.3 Irradiation

The irradiations onto the chimney and drying chamber were estimated experimentally, using the energy balances of chimney glazing, chimney absorber and drying chamber base (i.e. equations 4.20, 4.22 and 4.36 respectively). The temperatures measured experimentally at various points were used in equations 4.26 and 4.37 to find the convection heat transfer coefficients in the above energy balance equations. In order to use equation 4.36, the drying-chamber walls were transformed into an enclosure of uniform wall temperature T_{dc} over the base via the equation

$$T_{dc} = \frac{2A_{SW}T_{SW} + (A_{BW} + A_{FW})T_{FW} + A_{roof}T_{roof}}{2A_{SW} + A_{BW} + A_{FW} + A_{roof}} \tag{6.16}$$

where A_{BW}, A_{FW}, A_{SW}, A_{roof}, are areas of the back wall, front wall, side wall and roof of the dryer respectively; T_{BW}, T_{FW}, T_{SW}, T_{roof} are temperatures of the respective walls.

An iterative program was developed using FORTRAN for the estimation of irradiation and the radiative properties of the glazing. As in the whole simulation process, the absorptivities of chimney absorber (α_p) and drying chamber base (α_b) were each assumed to be 0.98, from Incropera and Dewitt (1996). The glazing emissivities were guessed initially, and the final values obtained at convergence were adopted. The reflectivity of glazing was assumed negligible, as compared to the absorptivity and transmissivity. The inputs to the program are

- the dryer dimensions and heat transfer properties of the materials
- climatic data of the environment
- the known temperatures at various points measured in the lab

The program for determining the irradiation and radiative properties of glazing is described in the following algorithm (shown graphically in the flow chart in figure 6.1):

1. A glazing transmissivity value τ_c is assumed; $0 < \tau_c > 1$.
2. Absorptivity and emissivity of glazing are calculated; $\alpha_c = 1 - \tau_c$; $\varepsilon_c = \alpha_c$ (for a grey body)
3. Radiation and convection heat coefficients are determined for the chimney (equations 4.26 a to j).

4. Heat absorbed by chimney glazing S_c is calculated, using the known temperatures and heat transfer coefficients (equation 4.20).
5. Irradiation onto chimney I_{chm} is calculated (4.26k)
6. Heat absorbed by chimney absorber S_p is computed, using the known temperatures and heat transfer coefficients (4.22).
7. New glazing transmissivity $\tau_{c,nw}$ is recalculated (4.26*l*).
8. $\tau_{c,nw}$ is compared with τ_c; if the absolute value of the relative difference is greater than 0.001, the process is repeated from step 2, with $\tau_{c,nw}$ in place of τ_c, otherwise the process continues with the next step (i.e. τ_c is confirmed)
9. $\alpha_c = 1 - \tau_c$ and $\varepsilon_c = \alpha_c$ are recalculated, with $\tau_{c,nw}$ in place of τ_c. Also I_{chm} is recalculated from equation 4.26k.
10. Radiation and convection heat coefficients are determined for the drying chamber (equations 4.37 a to *l*).
11. Heat absorbed by drying chamber base S_b is calculated, using the known temperatures and heat transfer coefficients (equation 4.36)
12. Irradiation onto the drying chamber I_{dc} is determined (4.37n), with $\tau_{dc} = \tau_c$.

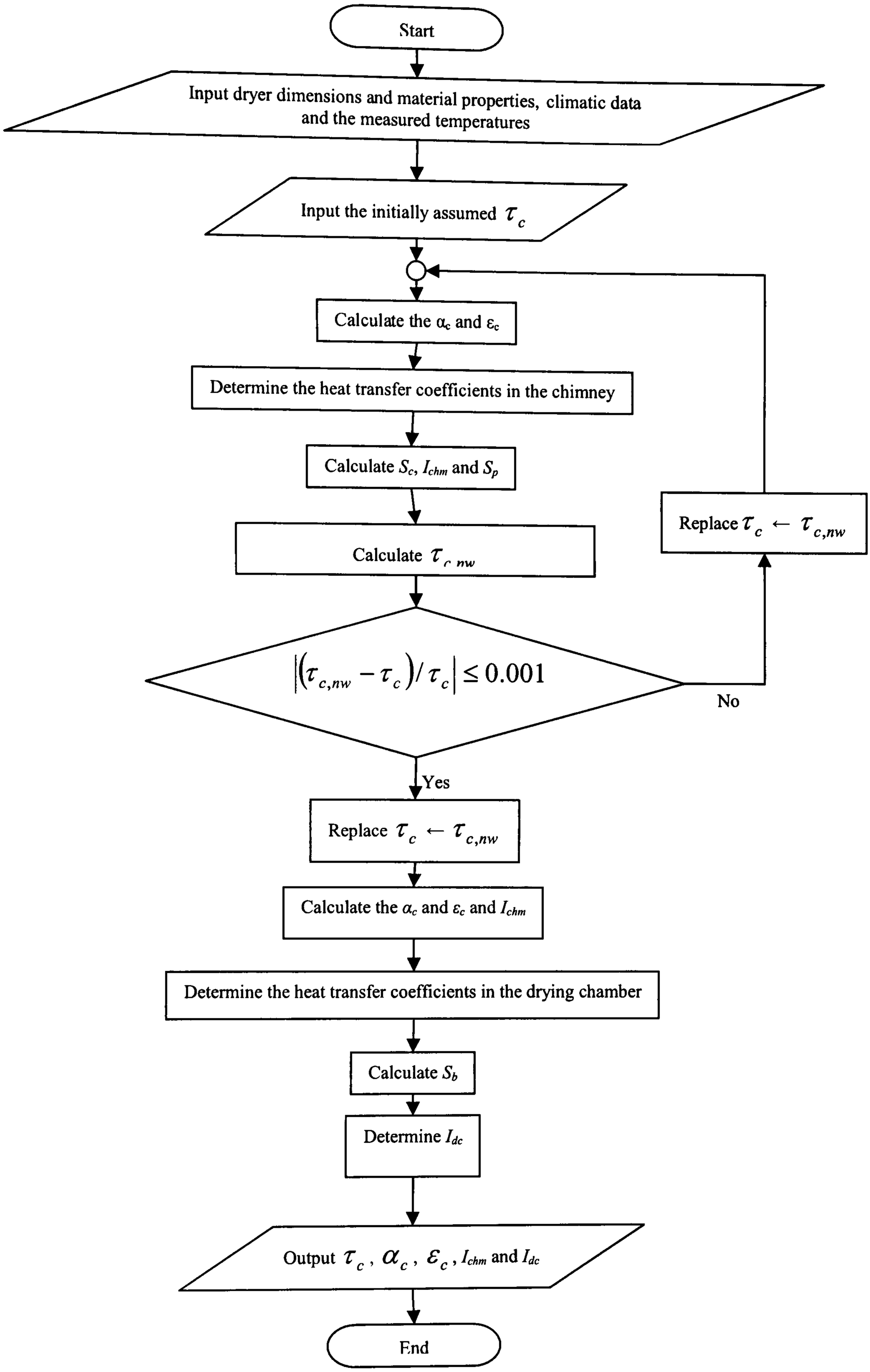

Figure 6.1 Flow chart for determining the Glazing Radiative Properties and the Irradiations into the Chimney and the Drying Chamber of the Laboratory Model

The following results came out of the iteration, and they were used in all the simulations of the laboratory model;

- Transmissivity of chimney and drying chamber glazing 0.3386
- Absorptivity 0.6614
- Emissivity 0.6614
- Irradiation on chimney (W/m^2) 390.78
- Irradiation on drying chamber (W/m^2) 186.60

6.2 Components of the simulation code

The simulation code was developed in FORTRAN from the algorithms described in sub section 4.3 for solving the mathematical models. The code has one main program FLODRY that determines the airflow characteristics of the no-load process and the airflow and the drying characteristics of the under-load process. The program makes use of a number of subroutines to carry out certain specific tasks that have to be performed frequently. Figure 6.2 shows the coordination between the main program and the various subroutines. The main program and subroutines are described in the following sections.

6.2.1 The program FLODRY

The program FLODRY is the main program of the simulation code with interface to the user. FLODRY accepts the following values as inputs for the no-load process:

- Dryer dimensions and material properties
- Atmospheric temperature and air velocity
- Dryer inlet temperature
- Irradiation
- Constants for the drying-chamber mean temperature approximation and the roof coefficient.

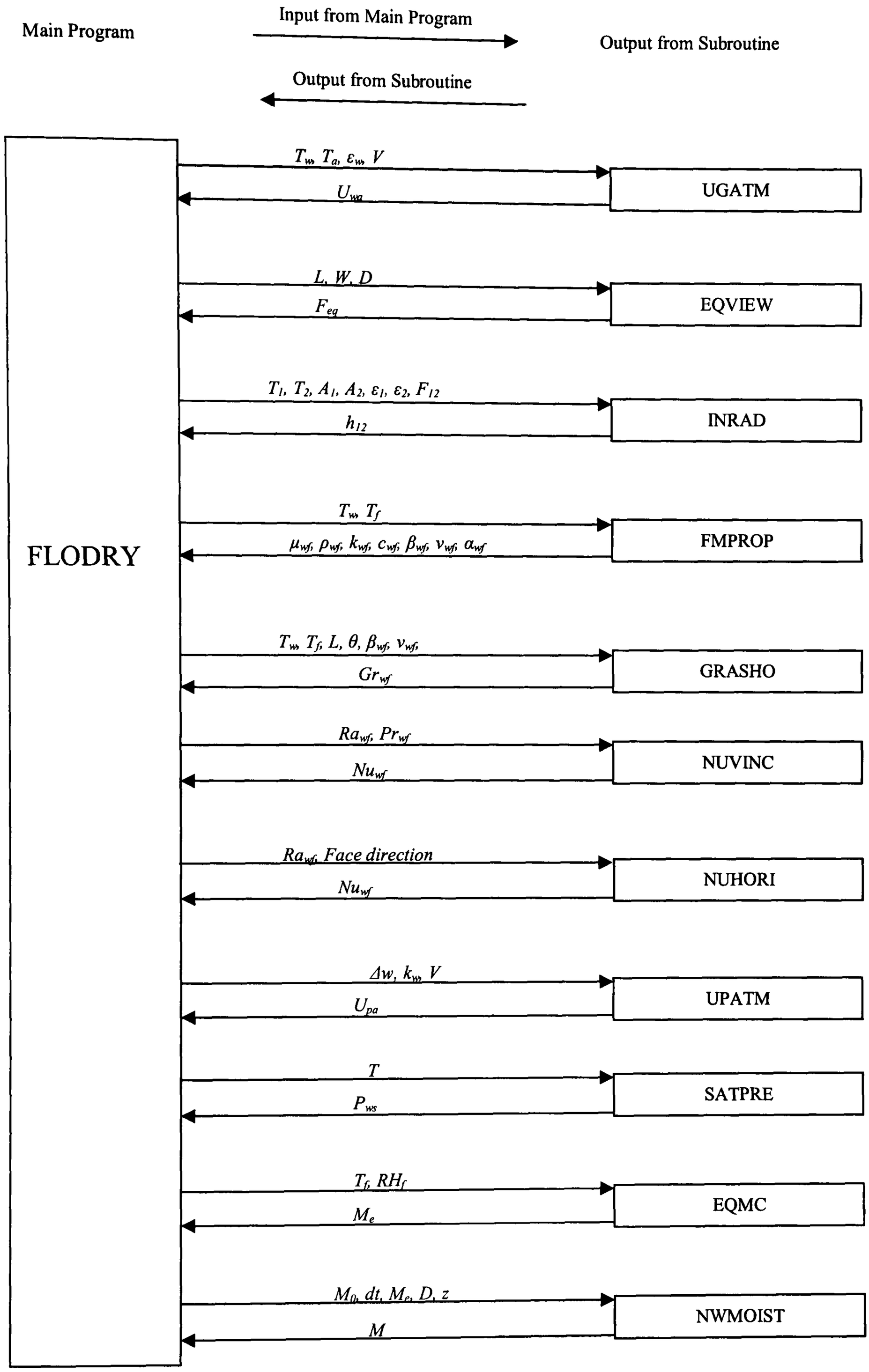

Figure 6.2 Coordination between the main program FLODRY and the various subroutines

The following inputs are also accepted in addition to those indicated above, for the under-load process:

- Crop-bed dimensions and positions (or heights)
- Crop characteristics (specific heat capacity, crop mass, loading density, radiative properties etc.)
- Moisture characteristics (specific and latent heat capacities, etc.)
- Initial and final (desired) moisture contents
- Shelf properties (specific heat capacity, mass, etc.)
- Ambient relative humidity
- Atmospheric Pressure
- Time intervals between outputs points
- The final output point (number of outputs or duration of the day's cycle).

The program automatically determines all the initialised temperatures as functions of the dryer inlet temperature.

All the input data for the no-load process are read from a separate input file. For the under-load data, additional input files are used, depending on whether the dryer has a single layer or two layers of crop beds. However after the first drying day, the program prompts the user for on-screen entries of the climatic and moisture data for the next day. This allows appropriate validation with experimental results based on the drying conditions day concerned.

The airflow rates and the temperatures at various points are given out as output values from the no-load simulation. These values are also given out as output from the under-load simulation, together with the drying time and the moisture contents.

6.2.2 Subroutines

As shown in figure 6.2, the program FLODRY employs 11 subroutines. These subroutines are described in this section.

6.2.2.1 The subroutine UGATM

This subroutine determines the resultant overall heat transfer coefficient U_{wa} from the chimney (or drying-chamber) glazing to the atmosphere, based on equations 4.26 (a to d) and 4.37 (a to c). UGATM is fed by the main program with the wall and atmospheric temperatures T_w and T_a, the wall emissivity ε_w and the atmospheric air velocity V.

6.2.2.2 EQVIEW

EQVIEW calculates the view factor F_{eq} between two parallel plates of equal dimensions that are not long enough or close enough to each other for a view factor of unity to be assumed. This F_{eq} has been used (with its definition) in equation 4.67 (c and d). The main program supplies the subroutine with the plate dimensions L and W and the distance D between them, as inputs for this calculation.

6.2.2.3 INRAD

The subroutine INRAD is for the determination of the radiation heat transfer coefficient h_{12} between any two surfaces *1* and *2* in the CDSCD (e.g. see equation 4.67b). The inputs to this program from FLODRY are the surface temperatures T_1 and T_2, areas A_1 and A_2, and emissitivities ε_1 and ε_2, of the walls as well as the view factor F_{12} between the walls.

6.2.2.4 The subroutine FMPROP

FMPROP is for determining the mean film properties between the fluid (air) and the wall surface, using the wall and fluid temperatures T_w and T_f, as explained after equation 4.26i.

6.2.2.5 GRASHO

This determines the Grashof Number Gr_{wf} of a fluid-wall interface (see equations 4.26 and 4.37). The required inputs are the respective wall and fluid temperatures T_w and T_f, the characteristic length L, the angle of inclination θ of the wall, the film volumetric coefficient of expansion β_{pf} and the film kinematic viscosity v_{pf}.

6.2.2.6 The subroutine NUVINC

This subprogram uses the Rayleigh Number Ra_{wf} and Prandtl Number Pr_{wf} from the main program to calculate the Nusselt Number Nu_{wf} at the inner surface of a vertical or inclined wall as described in equations 4.26 and 4.37. The inclination of the wall is already in the calculation of Gr_{wf} which is used to determine the input Ra_{wf}, as explained in sub-section 4.1.2.2.

6.2.2.7 The subroutine NUHORI

NUHORI is the subprogram for calculating the Nu_{wf} on a horizontal surface. The result depends on two possibilities;

1. whether the heated surface faces upwards or the cooled surface faces downwards
2. whether the heated surface faces downwards or the cooled surface faces upwards

The inputs for this program are the Rayleigh Number Ra_{wf} and the coded direction of the surface.

6.2.2.8 UPATM

This subroutine calculates the overall resultant heat transfer coefficient through the chimney-absorber plate U_{pa} or that through the drying-chamber base U_{ba}, using the wall thickness Δw and thermal conductivity k_w, and the atmospheric air velocity V (see equation 4.26j and 4.37*l*.

6.2.2.9 The subroutine SATPRE

SATPRE determines the saturation pressure p_{ws} of air of a given temperature T as described as part of equation 4.83 for determining the relative humidity RH.

6.2.2.10 The subroutine EQMC

EQMC is for the determination of the equilibrium moisture content M_e from T_f and RH_f, as shown in equation 4.44b or 4.80b.

6.2.2.11 NWMOIST

The final subprogram NWMOIST computes the moisture content M at current time. For this computation, NWMOIST is fed from the main program FLODRY with the last moisture content M_0, the time interval dt from the calculation of M_0, the equilibrium moisture content M_e at current time, the diffusion coefficient D at current time and the thickness of the crop bed z (see equation 4.79). The drying day is also supplied as input, as explained subsequently (in subsection 6.3.2).

6.2.3 The flow chart for the simulation code

The flow chart in figure 6.3 shows the steps in the simulation code and when the main program FLODRY invokes the subroutines to accomplish the necessary tasks. The subroutines are invoked when need, through 'Call Statements'.

The straight course of the chart describes the no-load iteration which proceeds through the page connectors 7, 10 and 13 (ending on the same page with page connector 13). The branch connectors indicate the additional or alternative information for the under-load iteration. The branch connectors 1 and 2 are the link points for extra under-load inputs into the program. The branch connectors 3 and 4 describe the alternative initialization of the drying-chamber air temperatures for the under-load simulation. The chart branches again at 5 to be linked again at 6 with the calculated mass flow and mass flux of the air in the under-load process. The branch connectors 9 and 11 show the calculation of the under-load drying-chamber coefficients. The final branch at 12 shows the calculation of the under-load temperatures. This branch then follows its own path to the end with the simulation of the drying process.

The connectors with whole numbers indicate links to the main-stream program. Those connectors with decimal fractions indicate links to a branch program which is in turn linked to the main program. For example; the connector 12.4 is the fourth link to the branch program which is in turn linked to the main program through the connector 12.

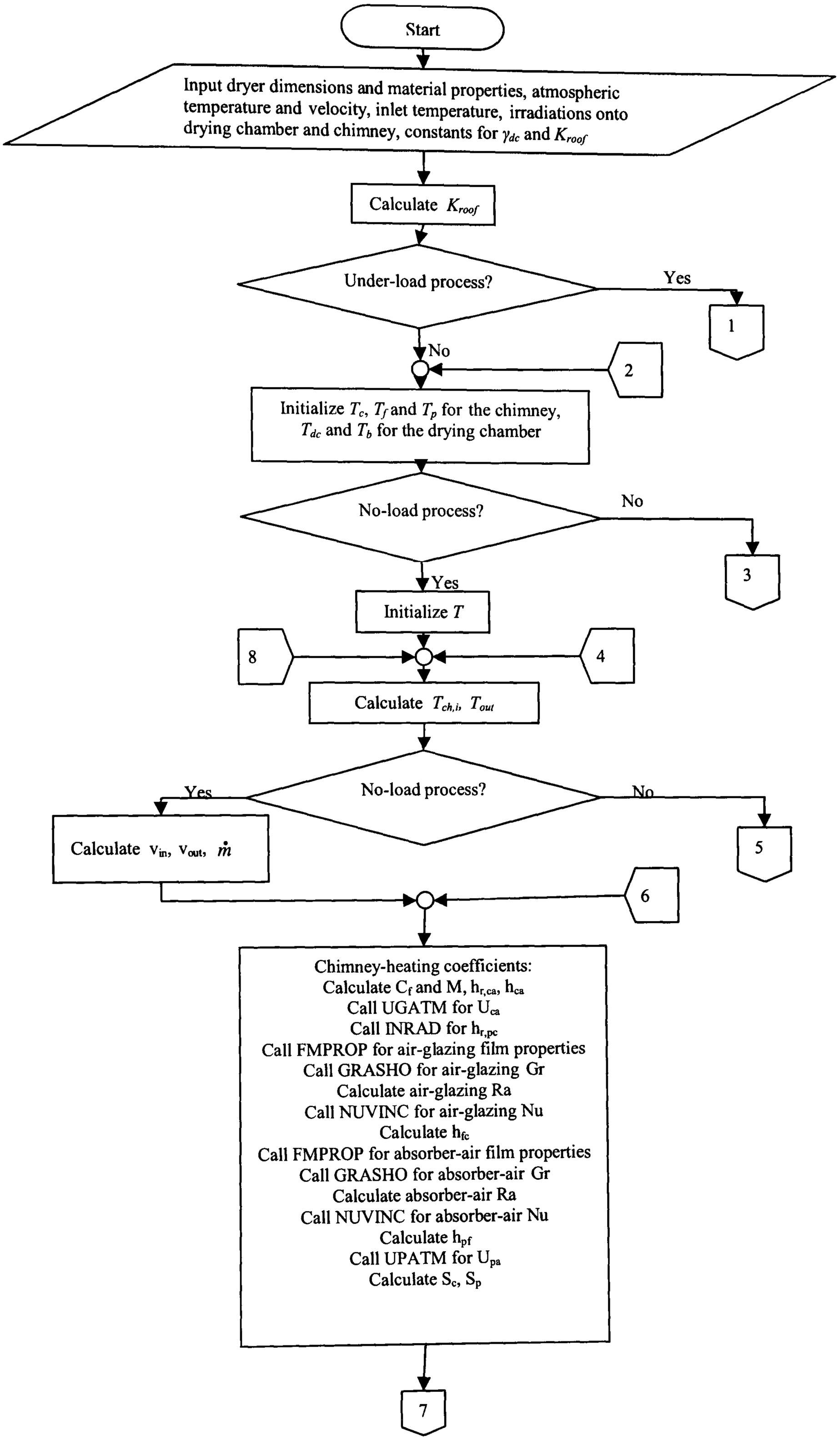

Figure 6.3 Flow chart for the Simulation Code

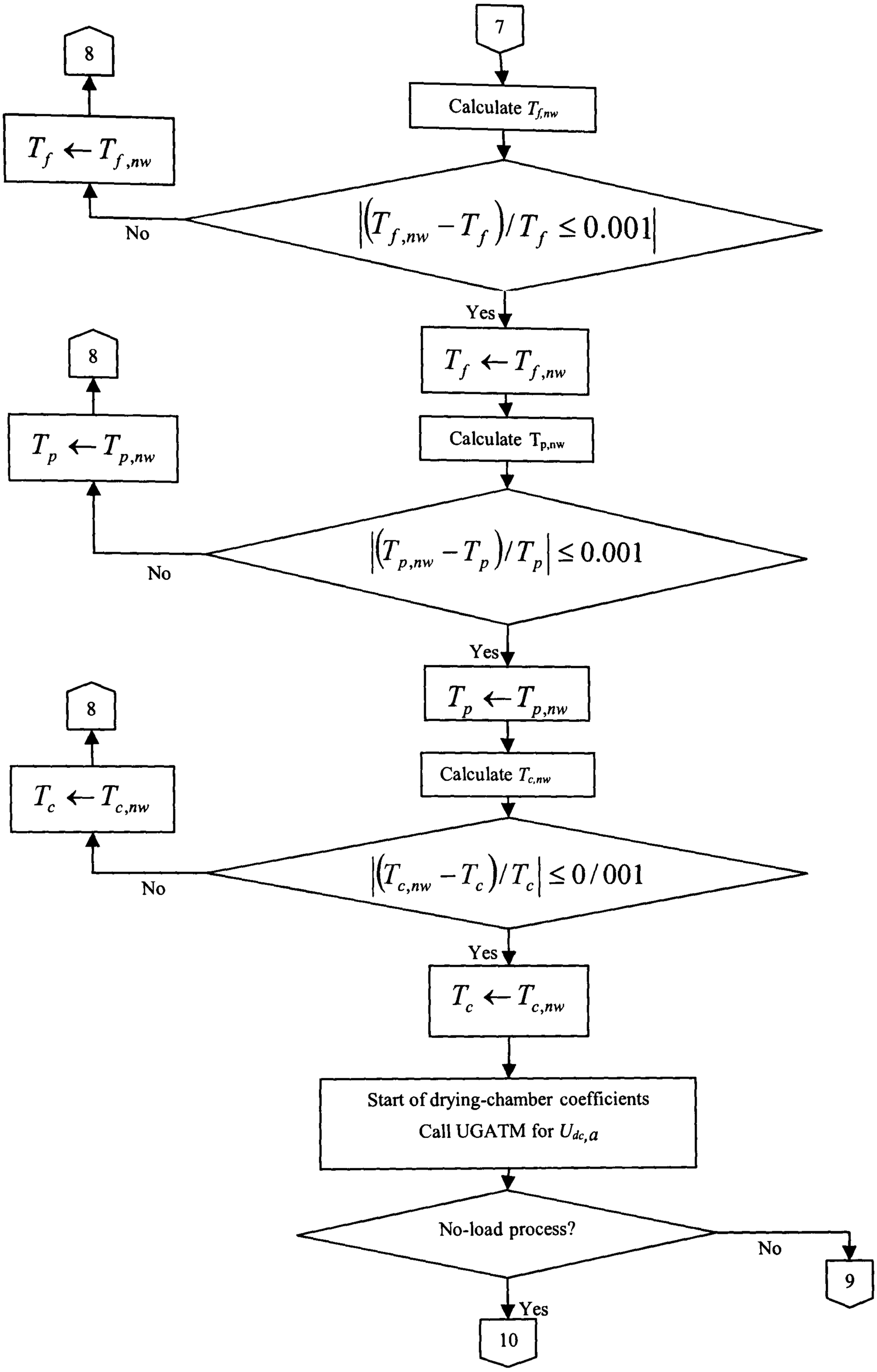

Figure 6.3 Continued

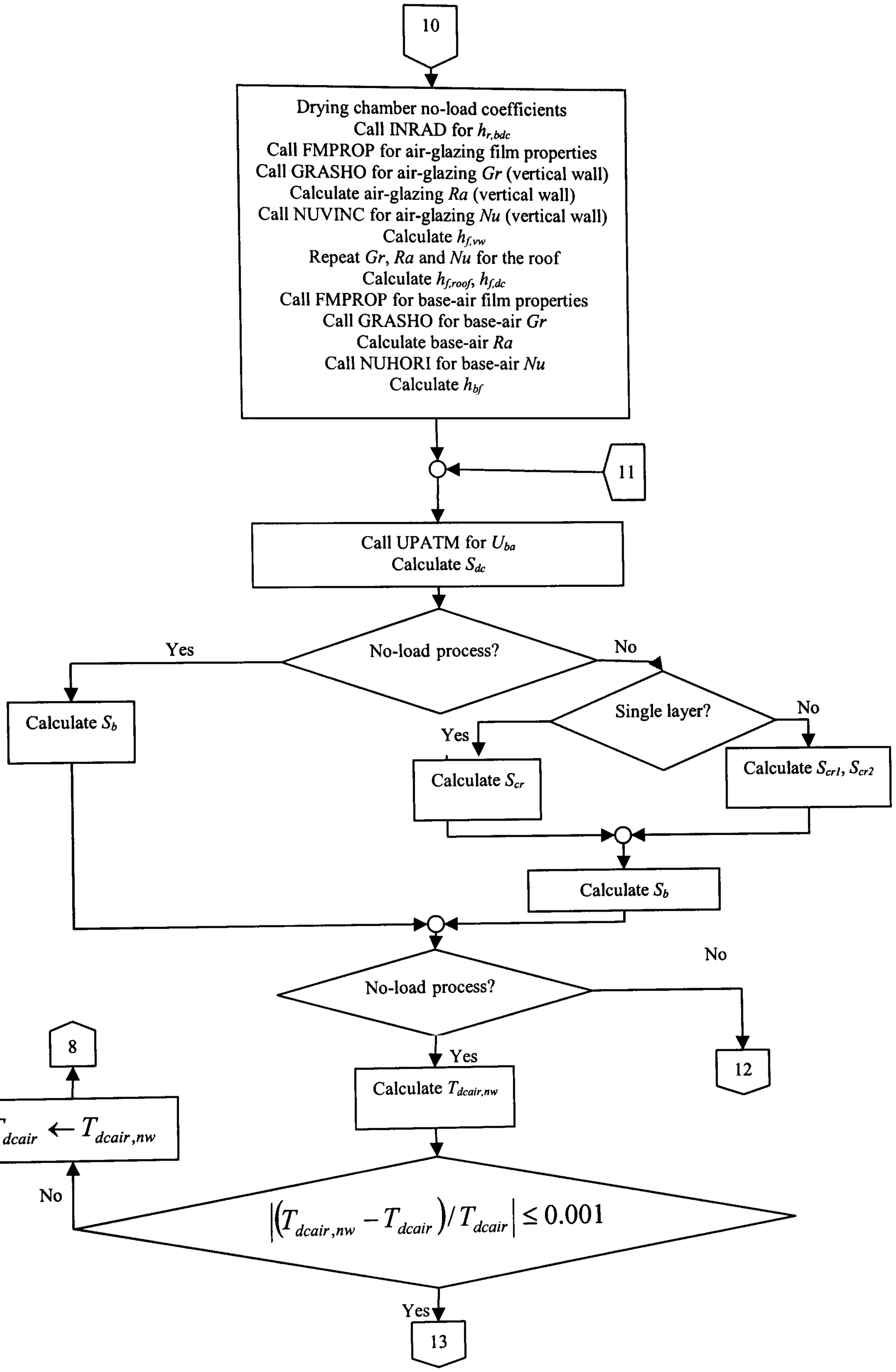

Figure 6.3 Continued

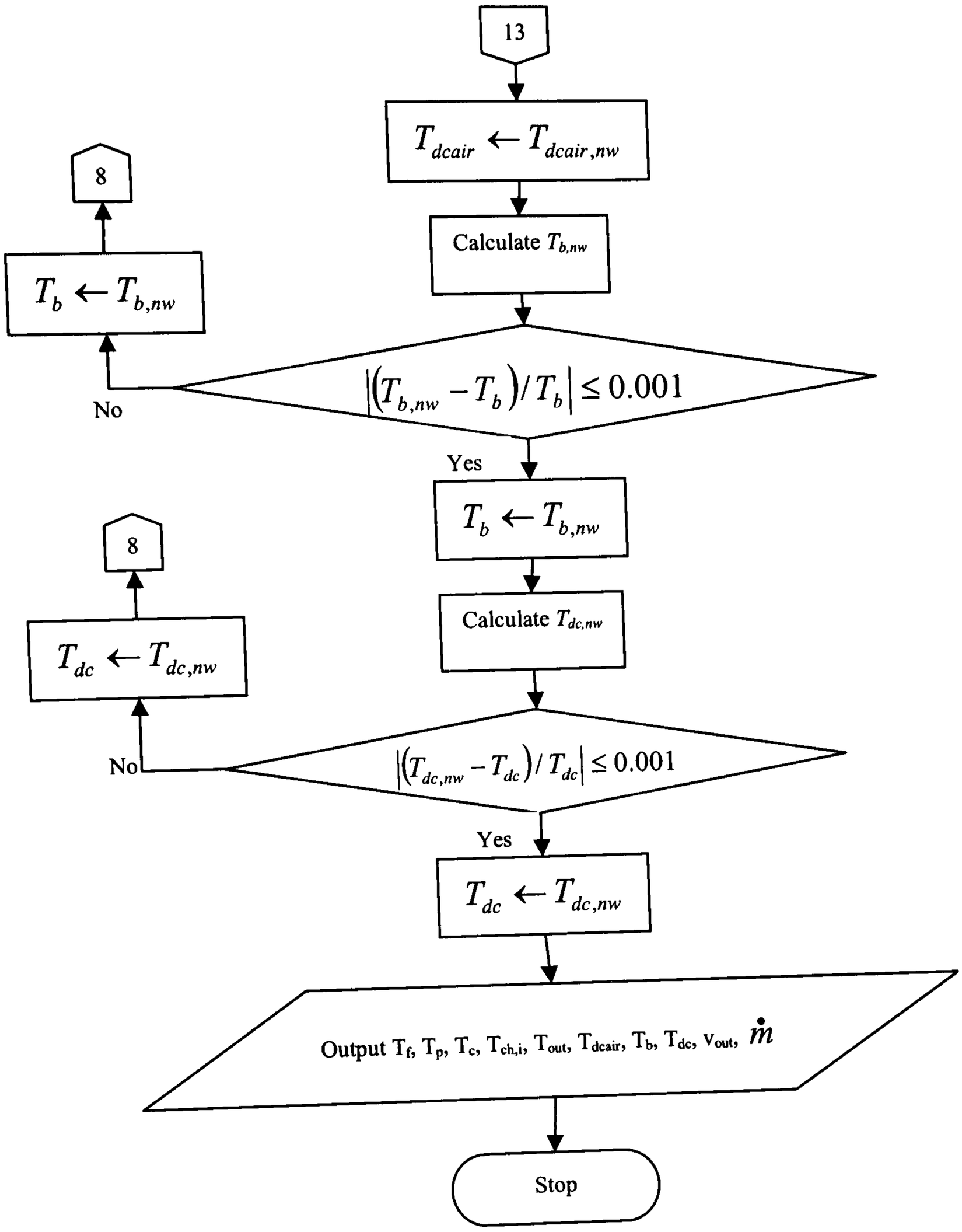

Figure 6.3 Continued

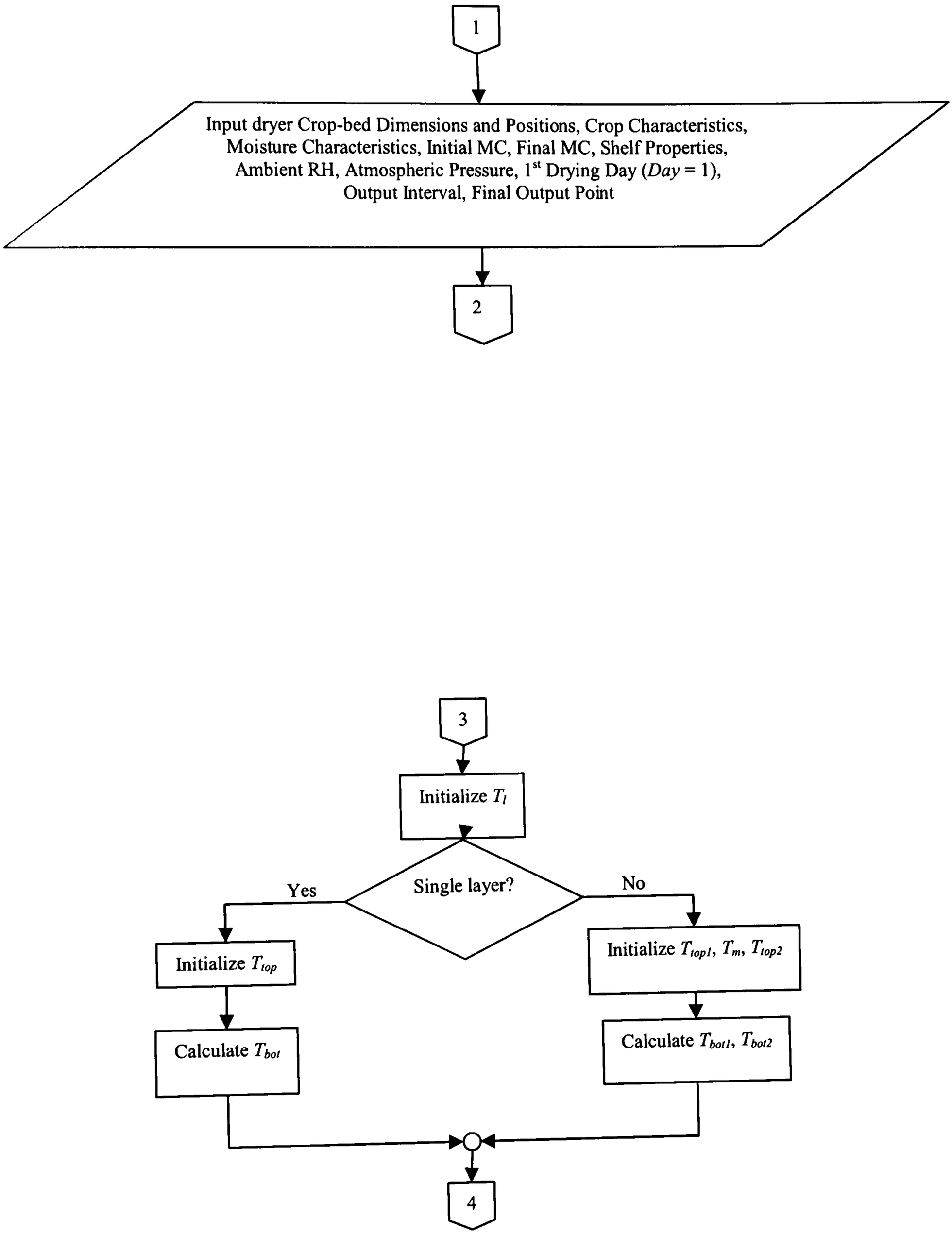

Figure 6.3 Continued

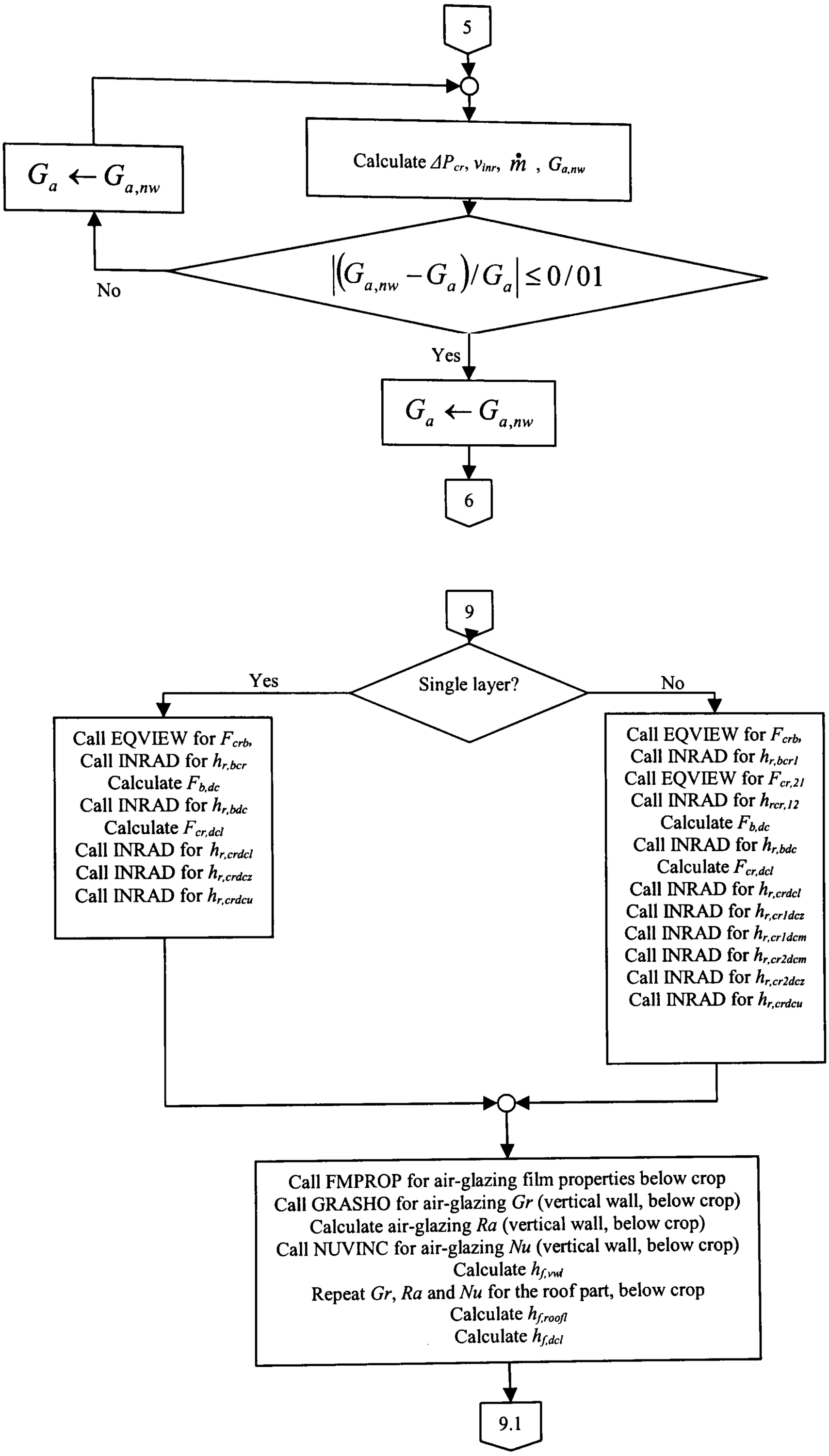

Figure 6.3 Continued

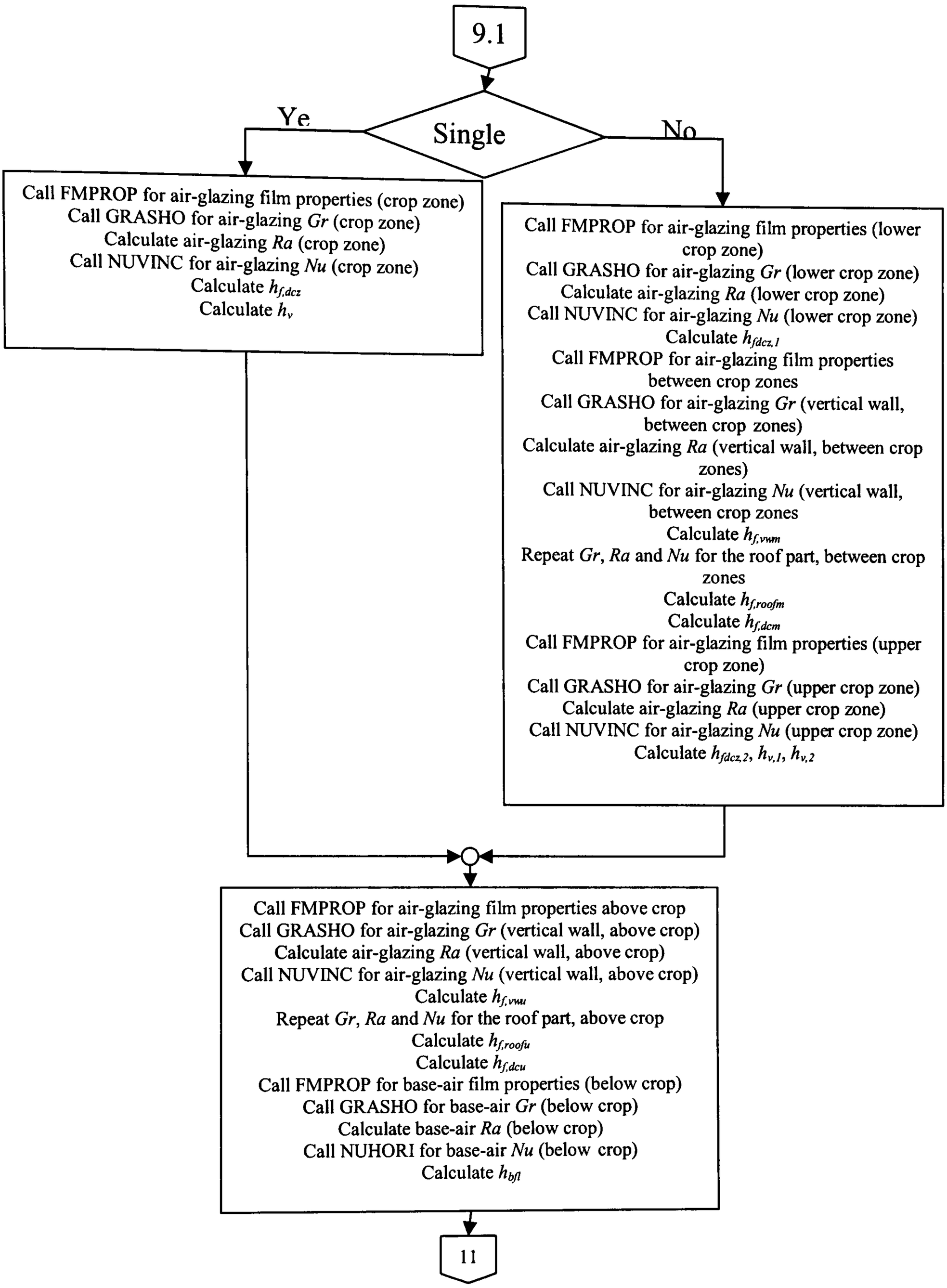

Figure 6.3 Continued

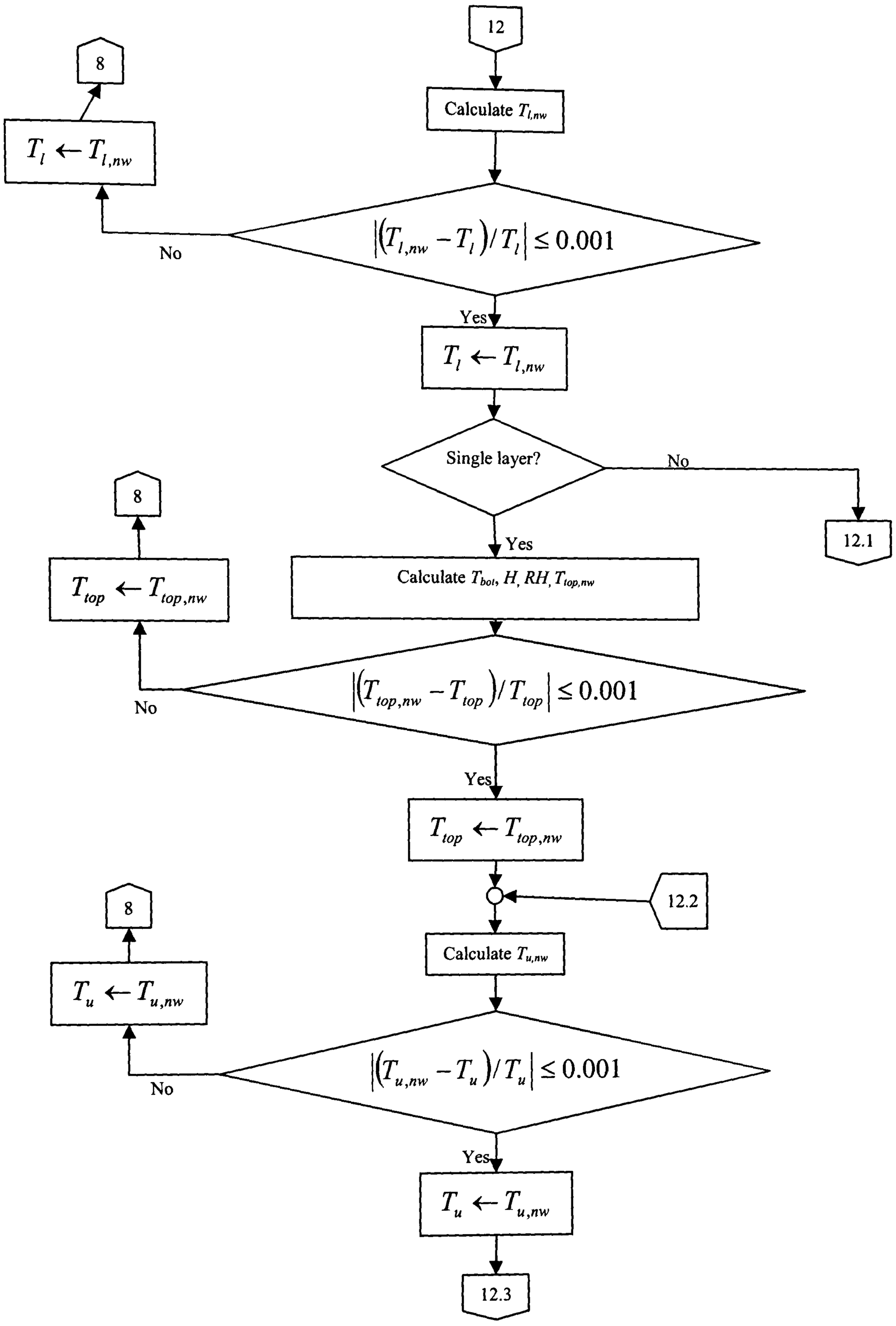

Figure 6.3 Continued

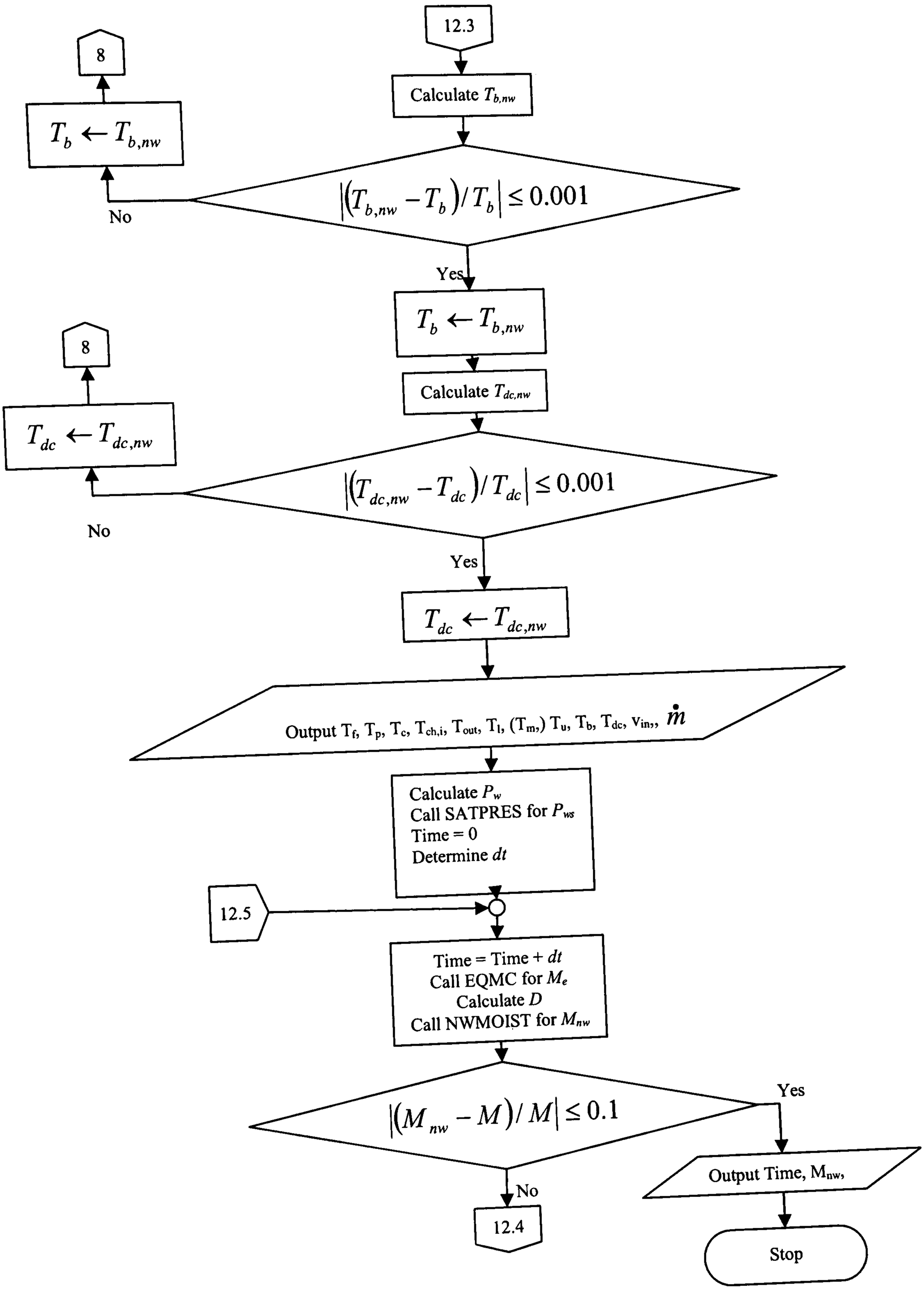

Figure 6.3 Continued

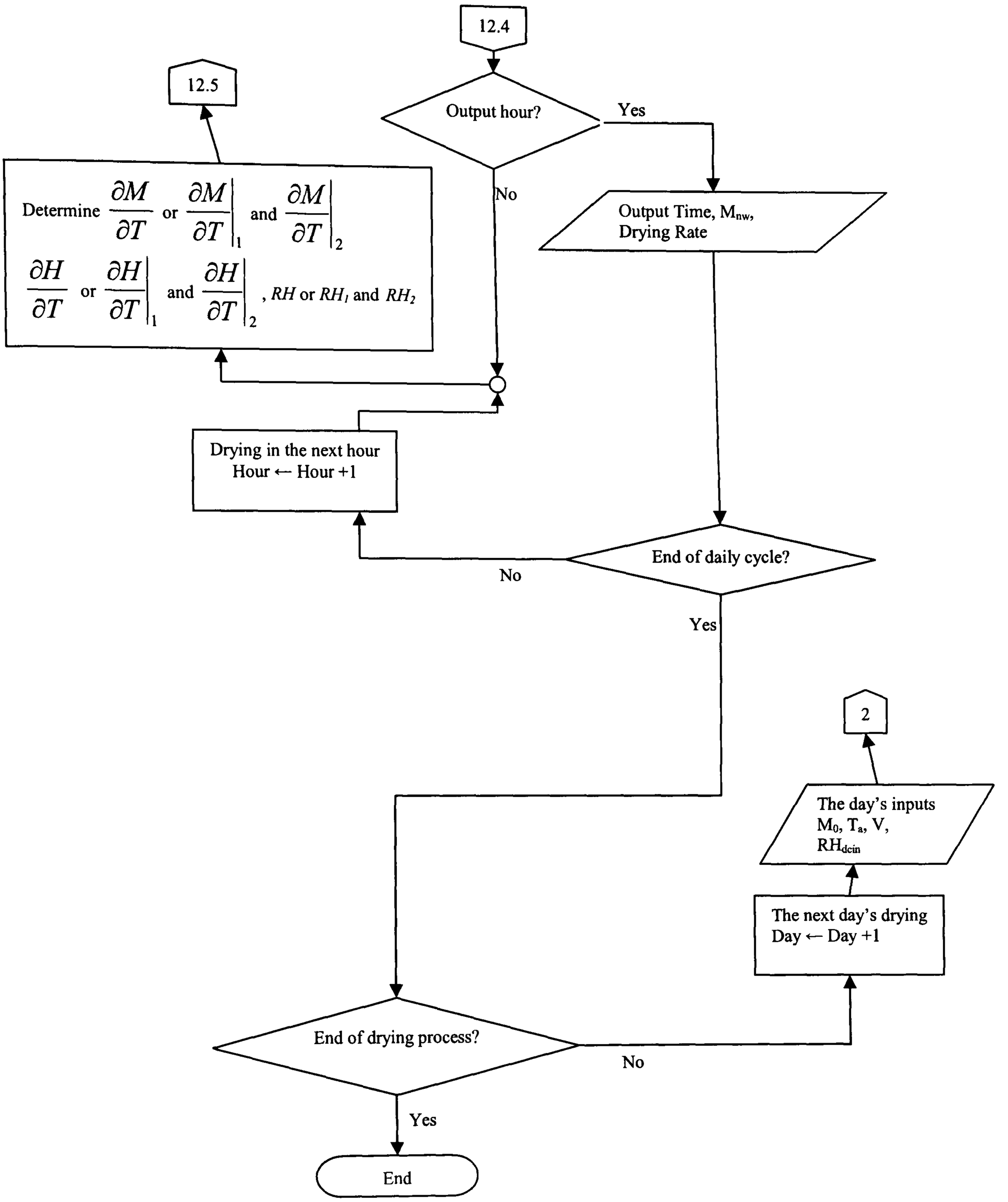

Figure 6.3 Continued

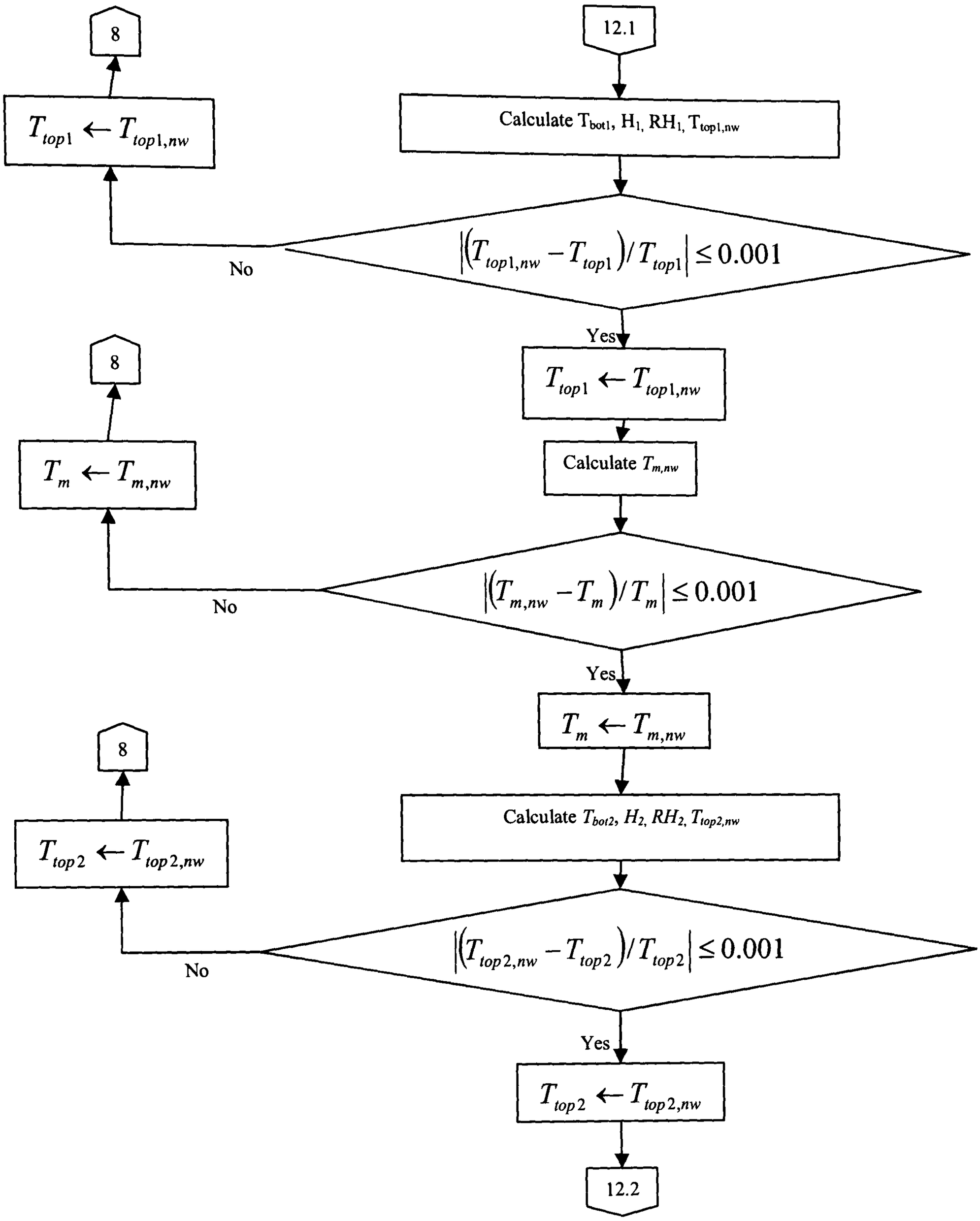

Figure 6.3 Continued

6.3 Validation of the simulation code

In this section, the results of the physical trials are compared with those obtained by running the simulation code on the same configuration of the CDSCD model. The phenomena that underlie any differences between the two results are analysed, and the necessary adjustments are made. The term 'relative' is very often used in this section, with regard to the deviation between the predicted and experimentally measured values. For example; the relative difference (or relative deviation) is defined as the magnitude of the difference (or deviation) between the predicted and measured values divided by the measured value. The smaller the relative difference (or relative deviation), the more accurate the results predicted by the simulation process.

6.3.1 The no-load validation

Figures 6.4 to 6.12 show the results of the no-load trials on the CDSCD model, using the solar chimney with different configurations of the model. The exit velocities for the simulation and laboratory trials are presented in the legends of the graphs. The air temperatures in the dryer are plotted against the heights. The height at inlet is taken as half the inlet gap. So the inlet heights differ from one inlet gap to another. Also, the heights of 26 cm and 84 cm have been selected for the bulk fluid temperatures in the drying chamber and chimney respectively, for the purpose of the graphical presentation, though these may not be the exact heights for the bulk temperatures. Other heights are; 49 cm at chimney inlet and 109 cm at chimney exit. The results are described in the following subsections.

6.3.1.1 Roof angle 81^0, inlet gap 70mm

As shown in figure 6.4, the simulation of this configuration resulted in air temperatures 23^0C at height 3.5cm (inlet), 24.64^0C at the height of 26cm (for the bulk fluid in the drying chamber), 25.42^0C at 49cm (chimney inlet), 27.99^0C at 84cm (bulk fluid in the chimney) and 28.80^0C at 109cm (exit). Temperatures measured in the laboratory for the corresponding heights were 23^0C, 25.22^0C, 26.17^0C, 29.97^0C and 31.33^0C. Thus, apart from the inlet temperature (an atmospheric condition) higher temperatures were measured than those obtained with the simulation code, for the same heights (see figure 6.4). On the other hand, the exit velocity from the simulation was 0.48m/s whilst that

measured in the laboratory was 0.45m/s. Thus there is a small relative difference between the predicted and the recorded velocities, which is 0.067. The differences between the results of simulation and the physical trial could be due to the metallic frames that held the walls of the laboratory model of CDSCD together. The frames transferred some extra heat to the air (and caused high air temperatures with the tendency to increase the airflow) and at the same time offered some extra flow resistance to the air flow. These two phenomena are not accounted for by the simulation code but their effects are significant for the small size of the laboratory model. They however counteract each other so that the predicted airflow does not deviate much from the recorded one.

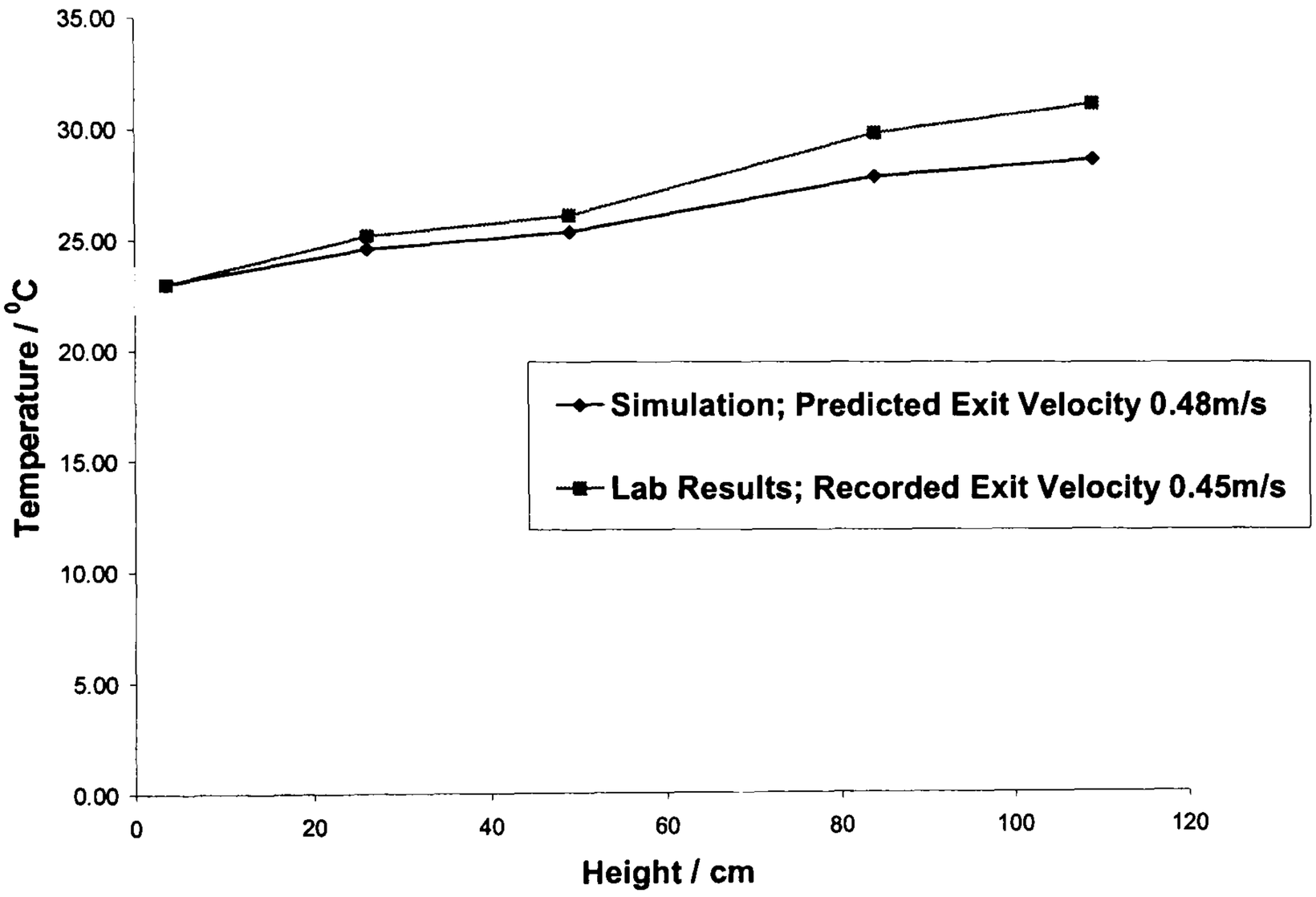

Figure 6.4 Air Temperature vs. Height: Simulation and Lab Results; Roof 81^0 Inlet 70mm, No Load.

6.3.1.2 Roof angle 81^0, inlet gap 50mm

Figure 6.5 shows the graphs of air temperature versus height for both the simulation and the experimental results of roof angle 81^0 inlet 50mm. The simulations resulted in 22.33^0C, 24.04^0C, 24.85^0C, 27.51^0C and 28.35^0C at heights 2.5cm (inlet), 26cm, 49cm, 84cm and 109cm respectively. Again, higher values were measured at the respective heights as 22.33^0C, 25.30^0C, 26.83^0C, 29.78^0C and 30.83^0C (figure 6.5). The temperature differences between the simulation and the experimental results are slightly

higher, as compared with those of inlet 70mm of the same roof angle. Thus as the inlet gap 50mm allowed less amount of air into the dryer, the additional temperature rise in the laboratory trial was higher than in inlet 70mm where the same quantity of extra energy from the metallic frames had to over-heat greater amount of air. Again, the predicted exit velocity is not much different from that measured in the laboratory; the simulation has 0.46m/s and the laboratory result has 0.44m/s, giving a relative difference of 0.045.

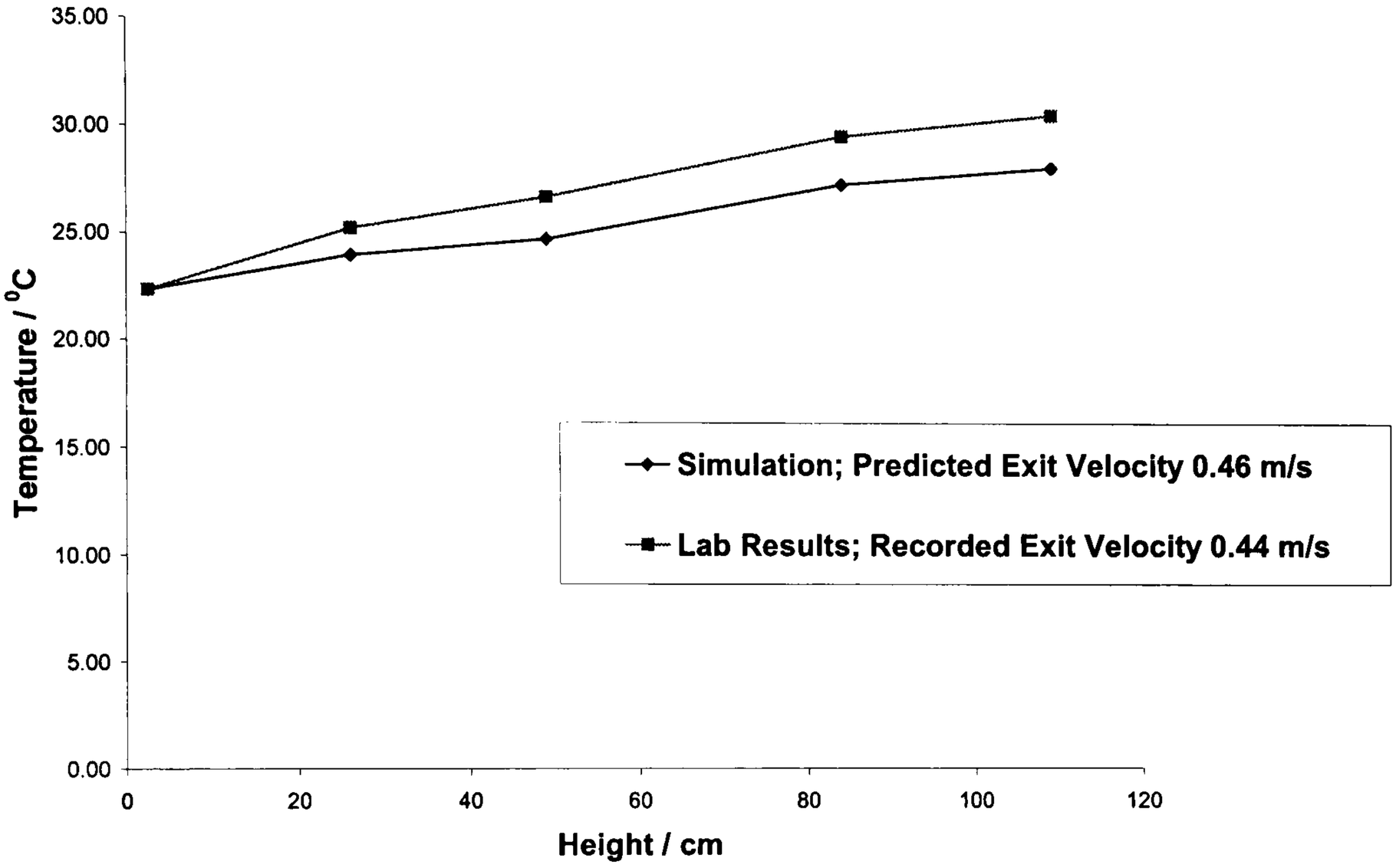

Figure 6.5 Air Temperature vs. Height: Simulation and Lab Results; Roof 81^0 Inlet 50mm, No Load.

6.3.1.4 Roof angle 81^0, inlet gap 30mm

The air temperatures predicted from the simulation of roof 81^0 inlet 30mm are 21^{0}C at dryer inlet (height 1.5cm), 22.89^{0}C at 26cm, 23.79^{0}C at 49cm, 26.74^{0}C at 84cm and 27.67^{0}C at exit (height 109cm), as shown in figure 6.6. The laboratory data for these heights are 21^{0}C, 26.48^{0}C, 29.17^{0}C, 31.22^{0}C and 31.83^{0}C respectively. The gap between the physically measured temperatures and those of simulation are much higher than those of inlet gaps 50mm and 70mm of the same roof angle (compare the diverging curves in figures 6.3, 6.4 and 6.5). Thus the extra heating from the frames was more pronounced in inlet 30mm than those of the other two inlet gaps which let in more air into the CDSCD. Like those of the other two inlet gaps, the difference in the exit

velocities is small, with 0.40m/s from the simulation and 0.39m/s from the laboratory experiment, indicating a low relative difference of 0.025.

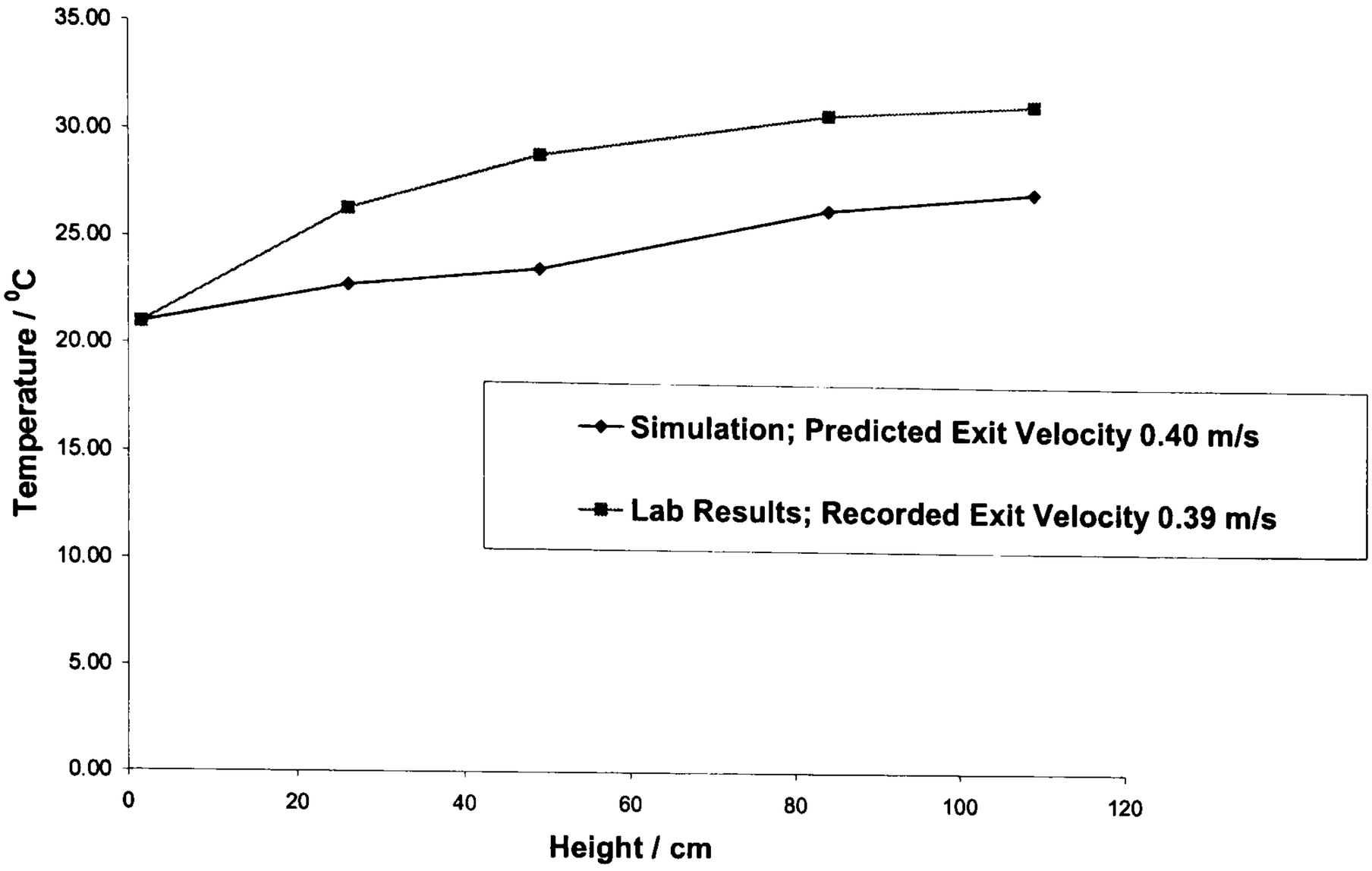

Figure 6.6 Air Temperature vs. Height: Simulation and Lab Results; Roof 81^0 Inlet 30mm, No Load.

6.3.1.5 Roof angle 64^0, inlet gap 70mm

The simulation and laboratory results for roof angle 64^0 and inlet gap 70 are compared in figure 6.7. The respective air temperatures at heights 3.5cm, 26cm, 49cm, 84cm and 109cm are 22.17^0C, 23.64^0C, 24.46^0C, 27^0C and 27.8^0C for the simulation code. Those from the laboratory at the corresponding heights are 22.17^0C, 23.86^0C, 24.83^0C, 28.37^0C and 29.5^0C in that order. Like those of roof 81 of the same inlet, the temperatures recorded in the laboratory are only slightly higher than those predicted by the simulation code. The exit velocities of 0.50m/s predicted by the simulation code and the 0.49 recorded in the laboratory again show a small relative difference of 0.02.

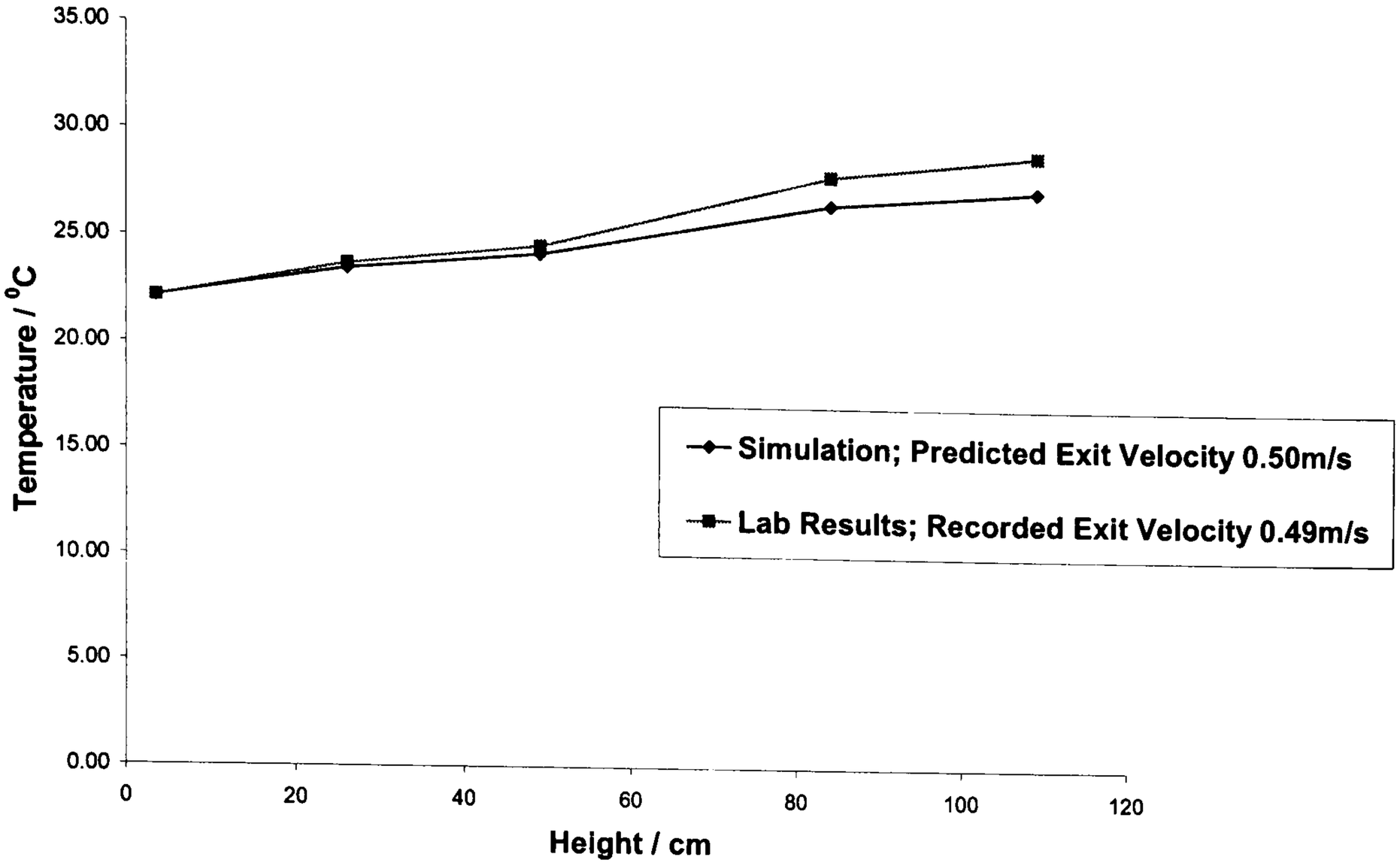

Figure 6.7 Air Temperature vs. Height: Simulation and Lab Results; Roof 64^0 Inlet 70mm, No Load.

6.3.1.6 Roof angle 64^0, inlet gap 50mm

As shown in figure 6.8, the simulation process gives air temperatures of 23.83^0C, 25.40^0C, 26.28^0C, 28.91^0C and 29.74^0C at heights 2.5cm, 26cm, 49cm, 84cm and 109cm respectively. Those obtained in the same order of heights from the laboratory trial are 23.83^0C, 26.57^0C, 27.83^0C, 30.63^0C and 31.50^0C. The temperature gaps between the simulation and the physical trial are higher than those of roof 64^0 inlet 70mm (akin to the gap differences between the same inlets of roof 81^0, due to the influence of the metallic frames). The simulation has an exit velocity of 0.47m/s whilst the physical trial has 0.45m/s (figure 6.8), so that the relative difference is 0.04.

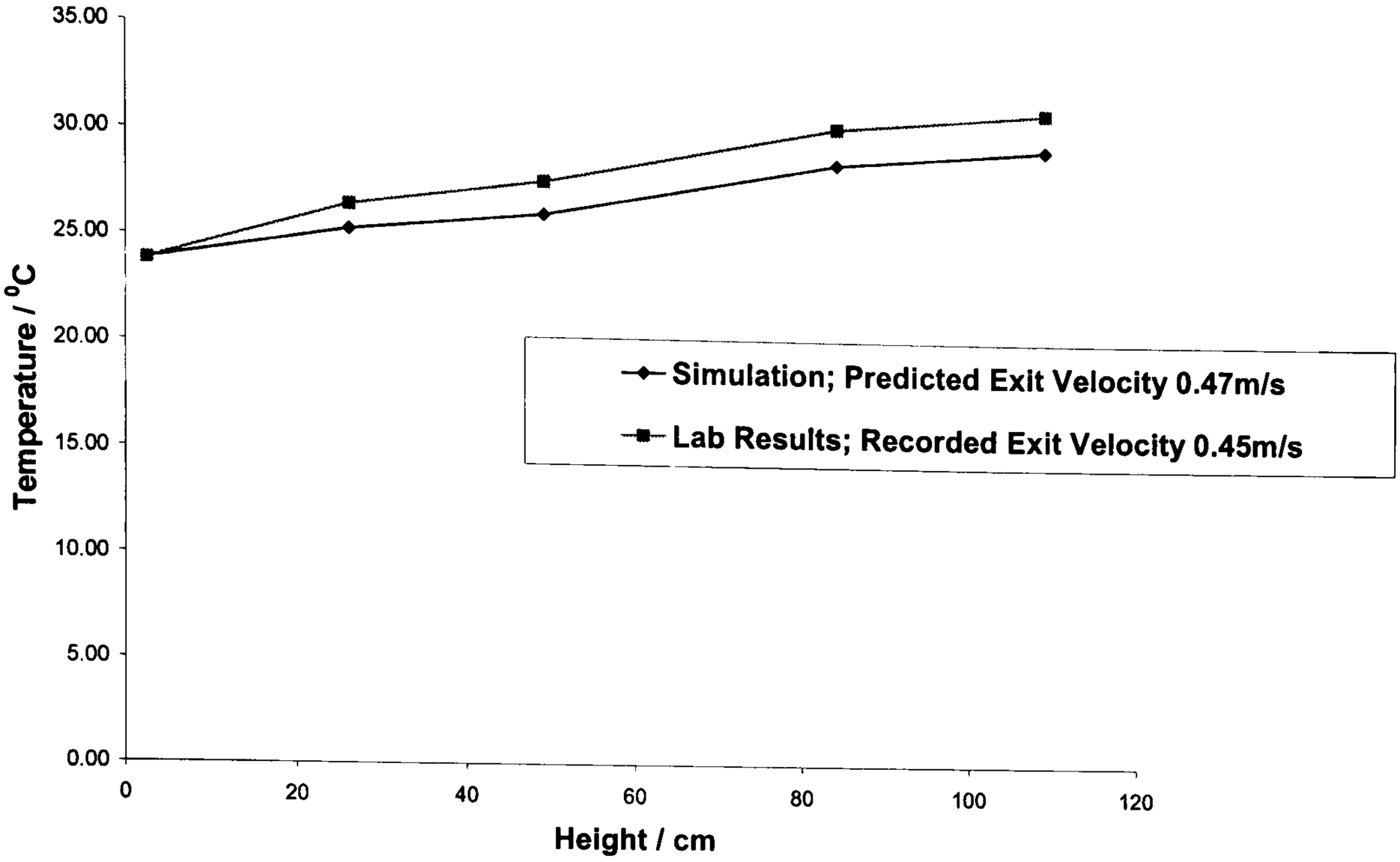

Figure 6.8 Air Temperature vs. Height: Simulation and Lab Results; Roof 64^0 Inlet 50mm, No Load.

6.3.1.7 Roof angle 64^0, inlet gap 30mm

As shown in figure 6.9, the differences in air temperatures between the measured and predicted ones are the highest of those trials with roof angle 64^0. Also, the predicted exit velocity is only 0.01m/s above the measured one, as in roof 81^0 inlet 30mm. This could again be attributed to the small airflow admitted at the inlet, so that the temperature rose higher than those with wider inlet gap. The respective air temperatures predicted by the simulation code at heights 1.5cm, 26cm, 49cm, 84cm and 109cm are 21.67^{0}C, 23.40^{0}C, 24.38^{0}C, 27.32^{0}C and 28.25^{0}C. The data from the laboratory are 21.67^{0}C, 26.70^{0}C, 29.83^{0}C, 31.03^{0}C and 31.03^{0}C. The simulation code predicts an exit velocity of 0.41m/s and that of the laboratory experiment is 0.40m/s. Thus the relative difference remained low (0.025), as in the other comparisons described earlier.

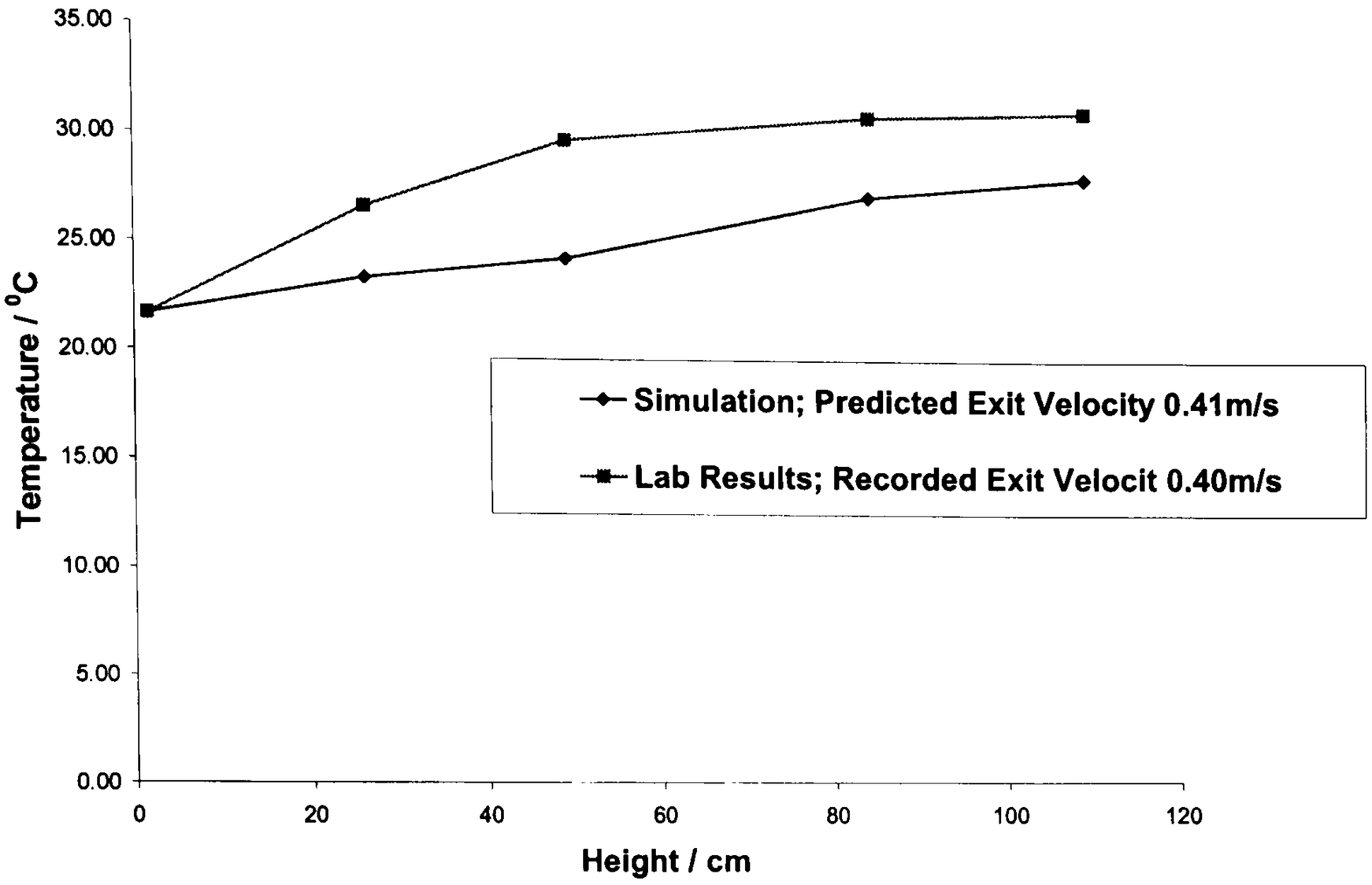

Figure 6.9 Air Temperature vs. Height: Simulation and Lab Results; Roof 64^0 Inlet 30mm, No Load.

6.3.1.8 Roof angle 51^0, inlet gap 70mm

Like the earlier assessments on the other two CDSCD configurations with inlet gap 70mm, the roof angle 51^0 inlet gap 70mm has very small temperature difference between the temperatures predicted by the simulation code and those measured experimentally. The simulation has 23.5^{0}C at 3.5cm (inlet), 24.82^{0}C at 26cm (bulk fluid in drying chamber), 25.79^{0}C at 49cm (chimney inlet), 28.33^{0}C at 84cm (bulk fluid in the chimney) and 29.13^{0}C at 109cm (exit), as shown in figure 6.10. The recorded data from the laboratory are 23.5^{0}C at 3.5cm, 24.99^{0}C at 26cm, 26.17^{0}C at 49cm, 29.66^{0}C at 84cm and 30.83^{0}C at 109cm. The simulation code predicts an inlet velocity of 0.50m/s whilst that from the laboratory is 0.52m/s. The magnitude of the relative difference in inlet velocity is still low at 0.038.

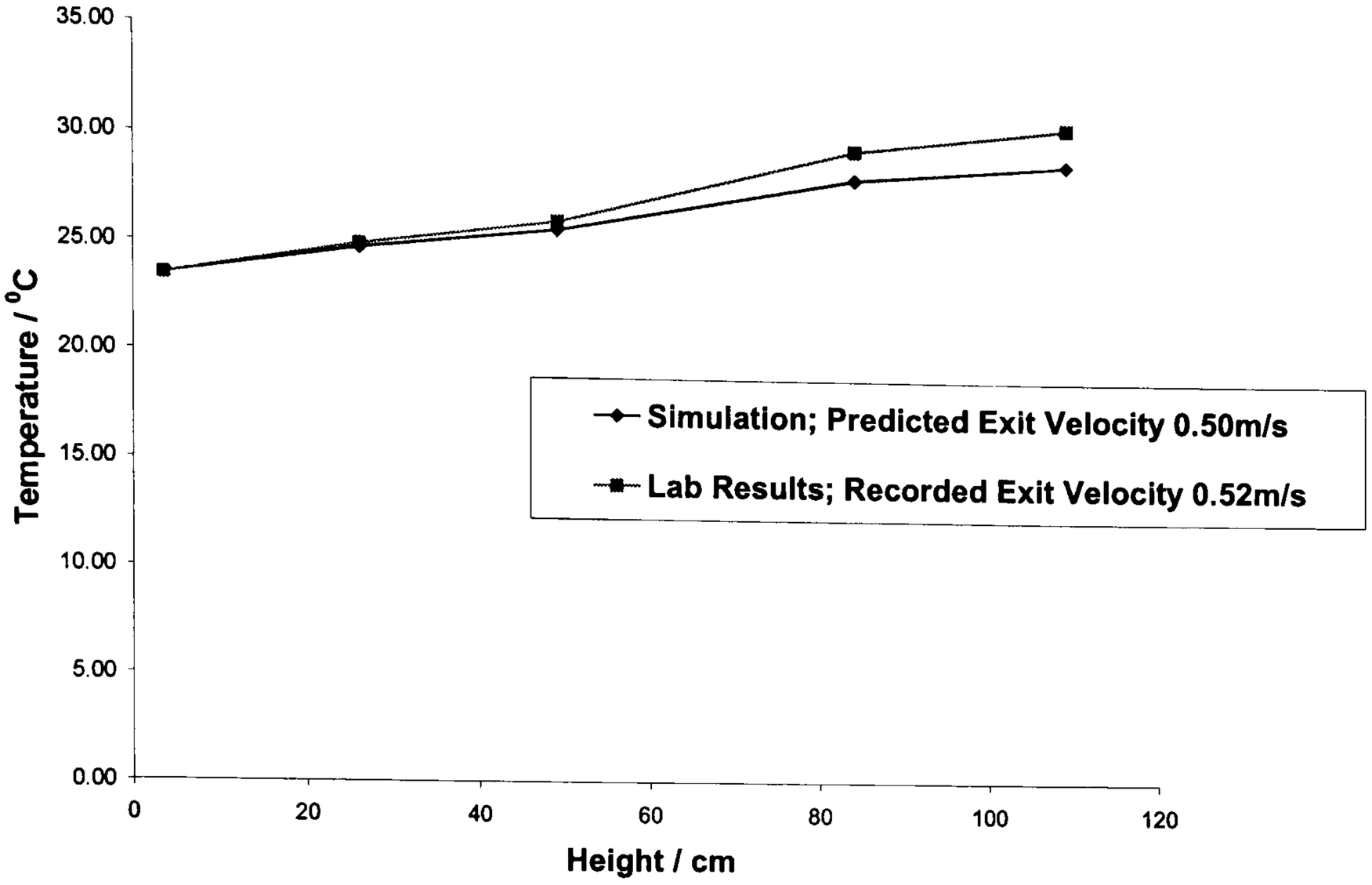

Figure 6.10 Air Temperature vs. Height: Simulation and Lab Results; Roof 51^0 Inlet 70mm, No Load.

6.3.1.9 Roof angle 51^0, inlet gap 50mm

With roof angle 51^0 inlet gap 50mm, the temperature deviations of simulation **from** experimentation are, as usual, somewhat wider than those of inlet gap 70mm with the same roof angle (see figure 6.11). The simulation results in temperatures of 24.67^{0}C, 26.06^{0}C, 27.08^{0}C, 29.72^{0}C and 30.55^{0}C at heights of 2.5cm (inlet), 26cm (bulk fluid in the drying chamber), 49cm (chimney inlet), 84cm (bulk fluid in the chimney) and 109 (exit). Those from the physical trial for the corresponding heights are 24.67^{0}C, 26.89^{0}C, 28.67^{0}C, 31.28^{0}C and 32.33^{0}C. The same exit velocity of 0.47m/s is obtained from both the simulation and the physical trial (i.e. zero relative difference).

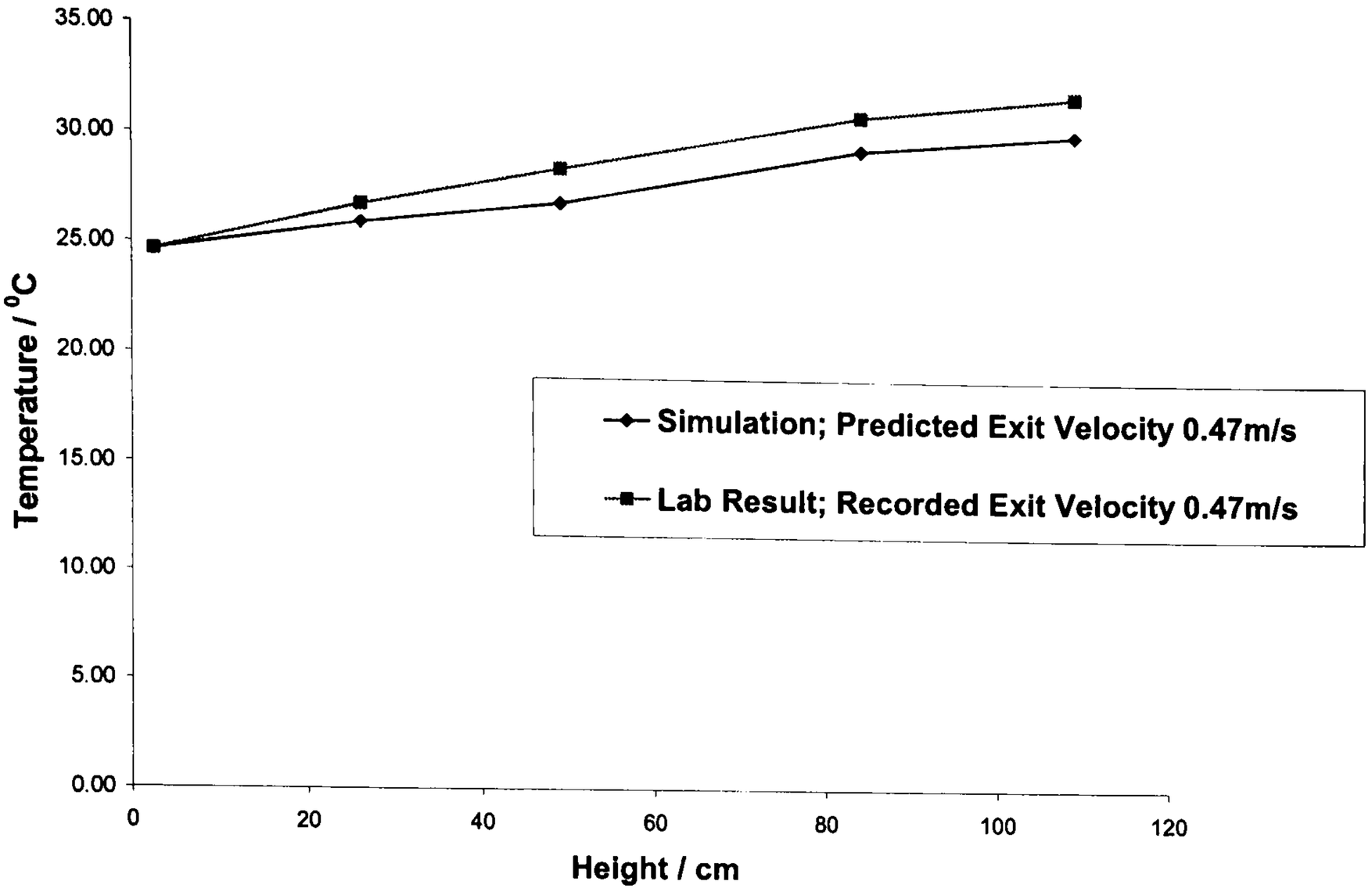

Figure 6.11 Air Temperature vs. Height: Simulation and Lab Results; Roof 51^0 Inlet 50mm, No Load.

6.3.1.10 Roof angle 51^0, inlet gap 30mm

The simulation results of roof angle 51^0 inlet gap 30mm is compared with those of the laboratory trial in figure 6.12. As in the other roof angles, the deviation of simulated temperatures from the measured temperatures was fairly higher than those of the other two inlets of the same roof angle, due to the extra heating effect from the metallic framework of the CDSCD model. The temperatures predicted by the simulation code for heights 1.2cm, 26cm, 49cm, 84cm and 109cm are respectively 22.17^{0}C, 23.71^{0}C, 24.86^{0}C, 27.78^{0}C and 28.70^{0}C. Those measured for the same heights were 22.17^{0}C, 27.06^{0}C, 30.17^{0}C, 30.82^{0}C and 31^{0}C. The exit velocities are 0.41m/s from the simulation code and 0.40m/s from the laboratory experimentation, and the relative difference in velocities is 0.025.

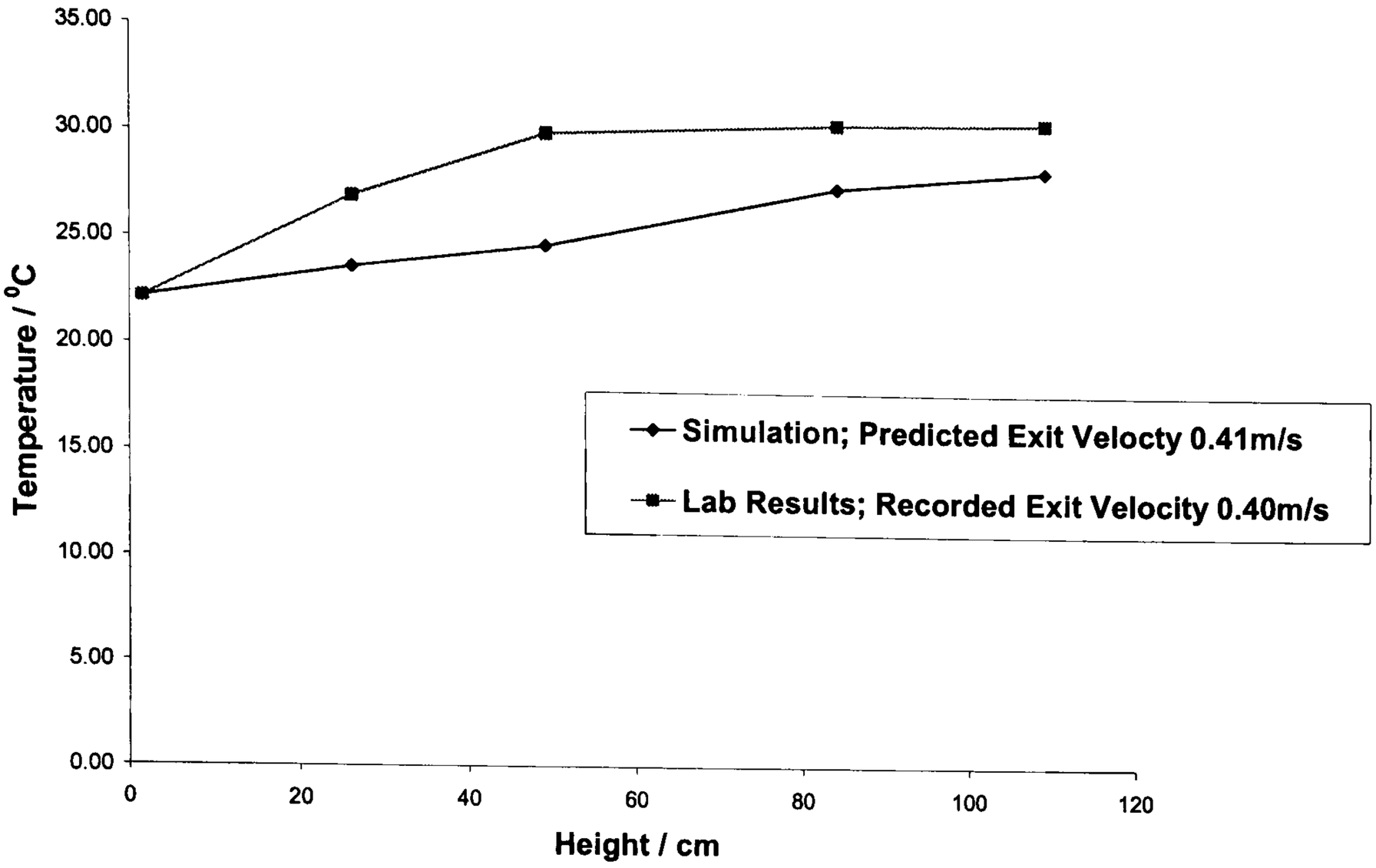

Figure 6.12 Air Temperature vs. Height: Simulation and Lab Results; Roof 51^0 Inlet 30mm, No Load.

6.3.2 The under-load validation

The results of running the simulation code on the drying (under-load) processes are presented together with those from the laboratory in figures 6.13 to 6.30. The inlet velocities are presented in the legends of the graphs. The same drying-chamber configurations of the no-load validations are also used for the under-load validations. Also, the same reference points are used for the chimney air temperatures. However, in the drying chamber, the points below and above the crop beds are considered separately. The height of 26cm represents the air bulk temperature above the crop bed, and that below the crop bed is represented at height of 6cm from the base. All the other points are of the same heights as in the corresponding no-load trials.

As explained in chapter 5, the MC curve of the physical trial did not follow the normal curve described by the general drying relation by which the drying rate falls continuously with time. There was always a transient state where the system had to use some energy to heat up from atmospheric conditions to the drying state. This energy, rather than being used for drying, had to be stored in the system till the evening. The stored energy became available after the supply of irradiation energy ceased in the

evening (i.e. when the lamps were switch out), and this continued the drying process for some into the night. It was also observed that the relative humidity in the laboratory generally started high in the morning and reduced as the day wore on. This prevented the drying rate from falling and at times caused the rate to increase in the course of the day. This phenomenon could be peculiar to the direct-mode dryer due to its sensitivity to the ambient relative humidity. On the other hand, a constant average relative humidity for the drying day is fed into the simulation code as input. Also, the simulation code neglects the transient state, establishes a drying state from time zero and ends the drying process when the lamps are switched out. Thus the simulation curve follows the description of the general drying relations more closely than that of the laboratory experiment. The simulation process ends the drying day in the evening when the lamps are switched out. But the daily drying cycle of the laboratory trial continues till the next morning when all the stored energy is expected to have been used up for drying. Both the simulation and laboratory processes always begin each drying day with the same moisture contents.

As may be seen in the under-load temperature and airflow graphs in the following sections, the airflow rate of a particular drying process barely changes from one day to another. This means that the time interval *dt* which is deduced in relation to the air flux (or air flow) in equation 4.47a (sub-section 4.3.2.1) remains almost constant throughout a given simulation process. Some models (e.g. that of Forson, 1999) are built on time intervals that are moisture content (MC) dependent. For such a model, a larger *dt* is used for higher values of moisture content (MC) than for lower MC values. The *dt* used in the current CDSCD model, which remains almost constant throughout the drying process, happens not to be large enough for the high MC values at the initial stages of the process. According to Okos et al (1992), a high number of series terms are to be used in equation 4.79 for determining the MC when the *dt* is not large enough. Thus, for the CDSCD model, 45 terms are used for the first day, 35 terms for day 2 and 28 terms for day 3. This explains the inclusion of the drying day as input to the module NWMOIST for calculating the MC.

For the calculation of the diffusion coefficient D, the activation energy E_a of 15730.58J/mol was used, but the constant D_0 had to be adjusted to $1.12 \times 10^{-11} m^2/s$ for

the current range of temperatures which are lower than the 328K, as explained in subsection 4.2.1. The following subsections describe the various results.

6.3.2.1 Under-load validation on roof angle 81^0, inlet gap 70mm

The plots of the moisture contents (MC) against the drying time as predicted by the simulation code is presented in figure 6.13 together with those obtained from the physical trial, of the roof angle 81^0 with inlet gap 70mm. Starting with initial MC of $1.96kg_w/kg_s$, the simulation process ends the first drying day with MC of $1.19kg_w/kg_s$, with that of the physical trial still at $1.52kg_w/kg_s$. The physical trial then continues, to complete the daily drying cycle with the MC falling to $1.33kg_w/kg_s$ by the next morning. The relative difference in MC is then 0.105 after the first day. On the second day, both the simulation and laboratory trial start at the same MC of $1.33kg_w/kg_s$. The simulation process ends at $0.69kg_w/kg_s$ at the end of the day's 7 hours of drying, with the MC of the laboratory process still at $1.02kg_w/kg_s$. The laboratory process then reduces to $0.79kg_w/kg_s$ by the end of its daily cycle, showing a relative difference of 0.126 after day 2. The MC drop on the third day is from 0.79 to $38kg_w/kg_s$ for the simulation process and the laboratory experiment ends the third day's cycle with $0.45kg_w/kg_s$. This shows a relative under-prediction of 0.15 by the simulation code at the end of the drying process on day 3.

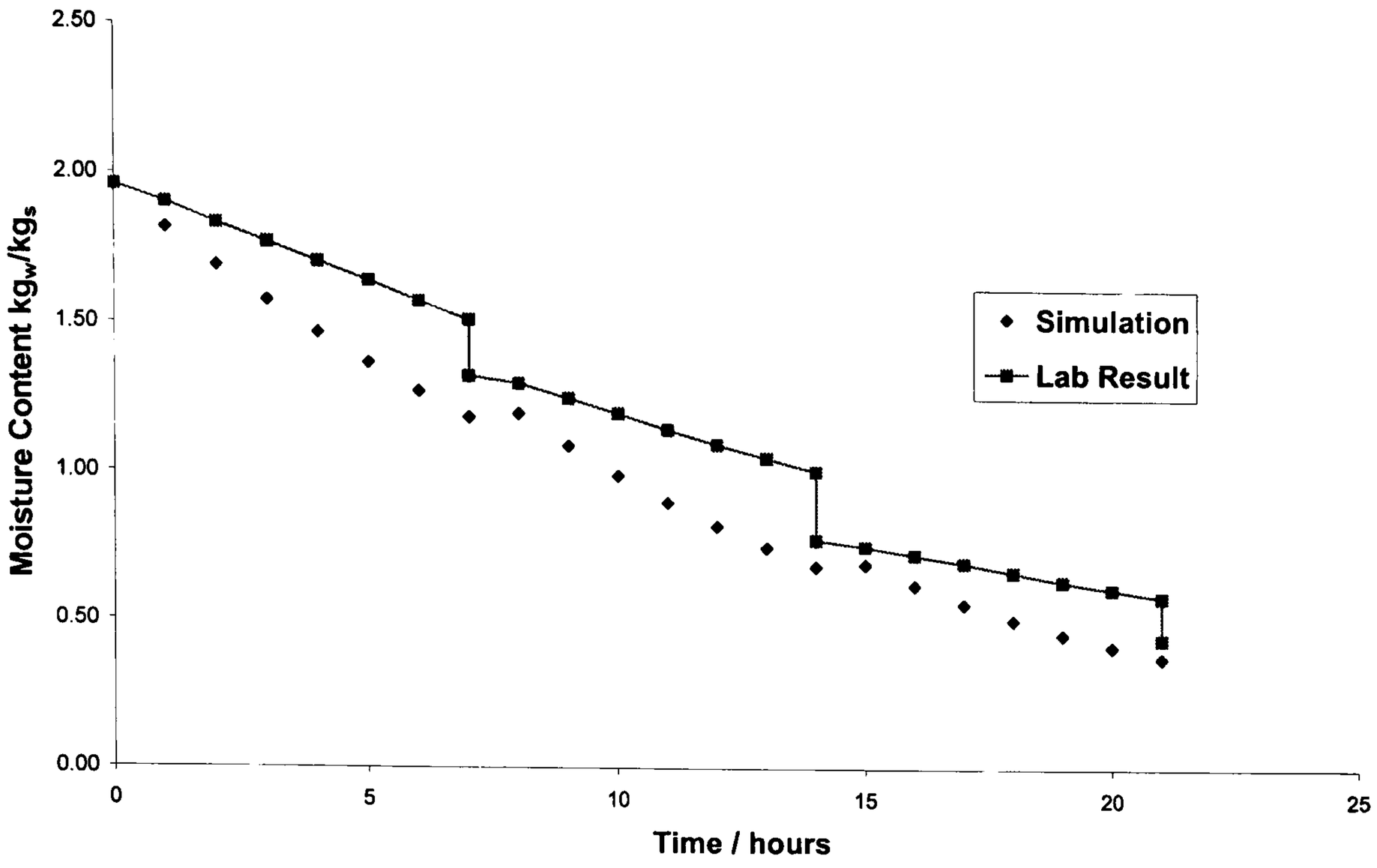

Figure 6.13 Moisture Content vs. Drying Time: Simulation and Lab Results; Roof 81^0 Inlet 70mm

From figure 6.13, the deviation of the simulation curve from the experimental curve is highest on day 1, followed by that on day 2. The curves tend to get close to each other on day 3. This could probably be due to another feature of the simulation code; neglecting the temperature gradient in the cassava crop. In actual fact, the crop has a finite thermal conductivity and therefore a temperature gradient exists within the crop. Hence not all parts of the crop heat up at the same rate as the surface; it takes time for the heat to be transferred from the surface into the crop and back. This phenomenon contributes to the lower drying rate than the predicted rate during the day and a continuation of the drying process in the night. The night performance of the crop outside the dryer (i.e. the control crop described in chapter 5) lends support to this deduction. Apparently the higher deviation between the curves on the first day is due to lower thermal conductivity of the crop, when the crop is more moisture laden, than on subsequent days. The experimental drying curve approaches that of the simulation as the thermal conductivity gets higher, towards the end of the drying process.

The events explained so far seem to suggest the following assertions:

1. The physical drying process would only pass along the curve predicted by the simulation code if
   - the drying process commenced without any transient state at the beginning
   - the crop was of infinity thermal conductivity (i.e. no temperature gradient)
   - the drying process occurred under constant atmospheric conditions

2. There would be no night performance if the physical process could pass along the drying curve predicted by the simulation code.

The first two bullet points of assertion 1 are impossible and the third one is most unlikely in a physical process. Therefore assertion 1 is impossible, and so there will always be night performance after the source of irradiation ceases in the evening. With negligible loss of energy to the surroundings during the transient periods, the MC at the end of the daily physical drying process should not be too different from that predicted at the end of the simulation cycle. This is because the energy stored in the system during the day is released for drying at night, to make up for any slow down that occurs in the day.

Figure 6.14 (a to c) show the temperatures at various heights on each day of the drying process of the CDSCD with roof angle 81^0 and inlet gap 70mm, for both the simulation and laboratory processes. The inlet velocities of each day can be found in the legends of the graphs. The simulation slightly over-predicts the temperature below the crop bed (at height 6cm). This may be due to over-estimation of the energy that trickles down through the crop bed to the base of drying chamber. The simulation however under-predicts the other temperatures, as in the no-load process. From the velocity values shown in the legends, the relative difference in inlet velocity between the simulated and the measured values is 0.125 for all the three days.

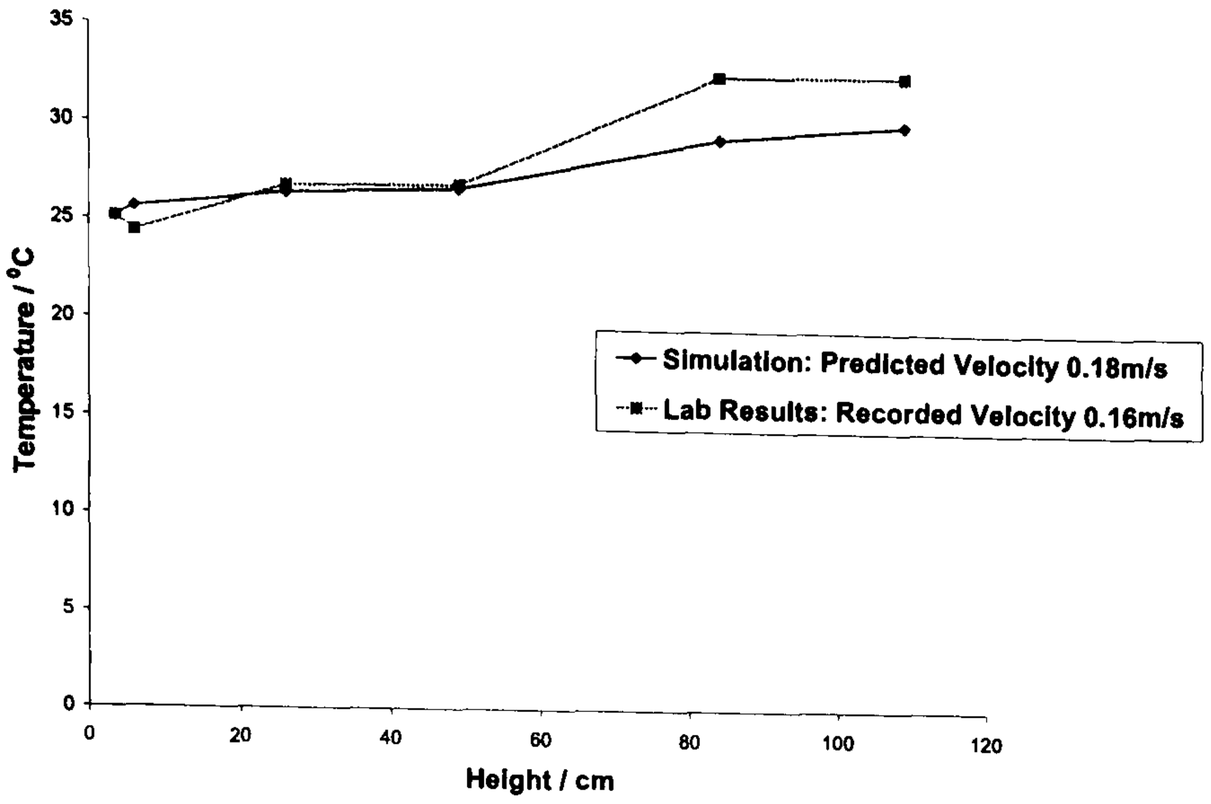

a) Day 1

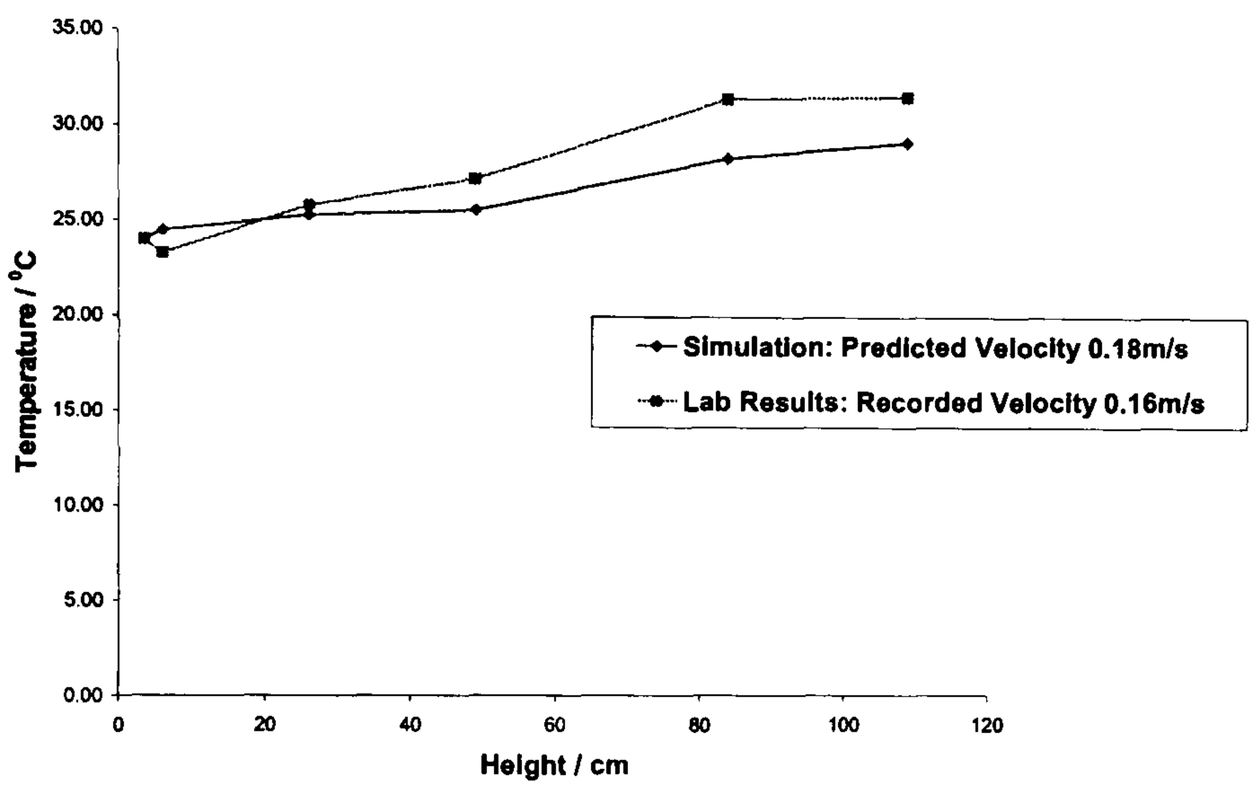

b) Day 2

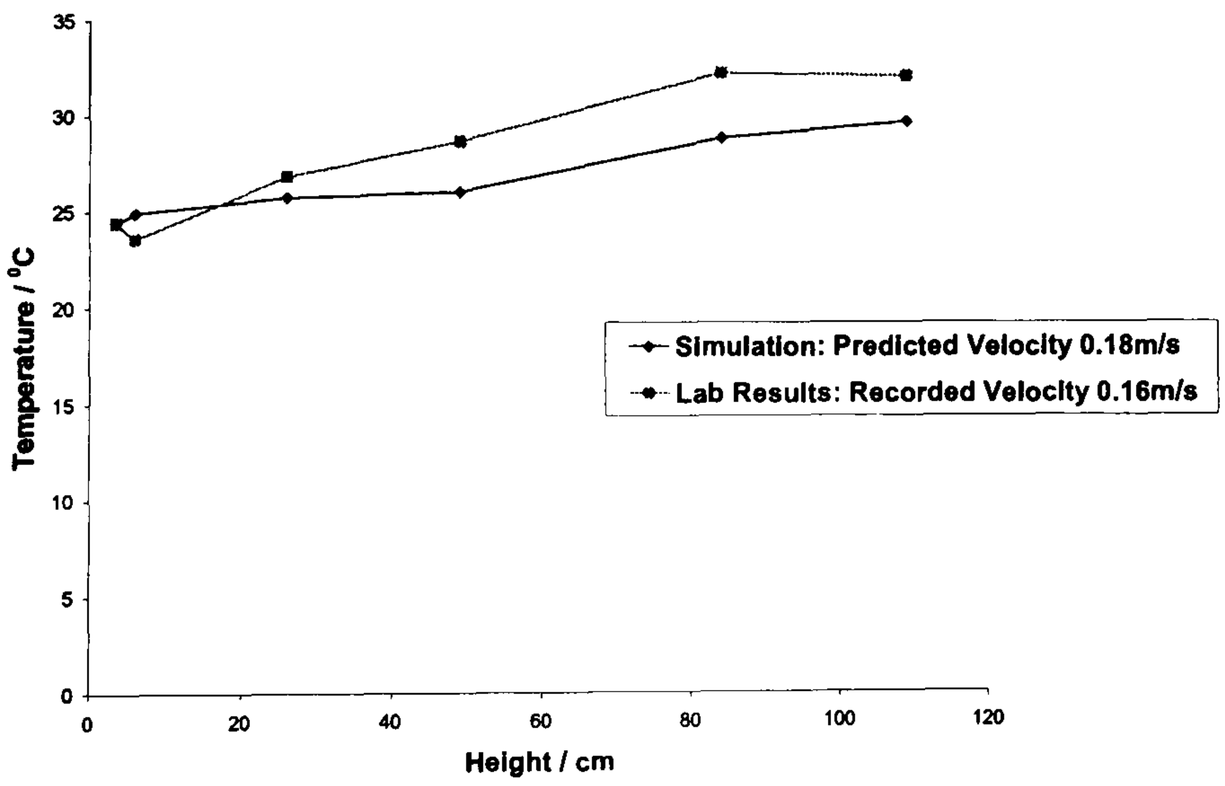

c) Day 3

Figure 6.14 Air Temperature vs. Height: Simulation and Lab Results; Roof 81^0 Inlet 70mm

6.3.2.2 Under-load validation on roof angle 81^0, inlet gap 50mm

Figure 6.15 presents a plot of the MC against drying time for the three days of the drying process of roof 81^0 inlet 50mm. The first-day drying cycle has a predicted MC drop from 1.97 to 1.19kg_w/kg_s from the simulation code and a measured drop from 1.97 to 1.30kg_w/kg_s from the laboratory experimentation. This shows a relative difference of 0.084 after day 1. In the cycle of day 2 the simulation code predicted a drying process in which the MC decreases from 1.30 to 0.69kg_w/kg_s, as against the MCs of 1.30 to 0.70kg_w/kg_s recorded in the laboratory, and therefore with a relative difference of 0.014. The simulation program ends the third cycle at 0.38kg_w/kg_s, whilst the physical drying process ends at 0.39kg_w/kg_s. So there is a relative under-prediction of 0.026 from the simulation code at the end of the drying process.

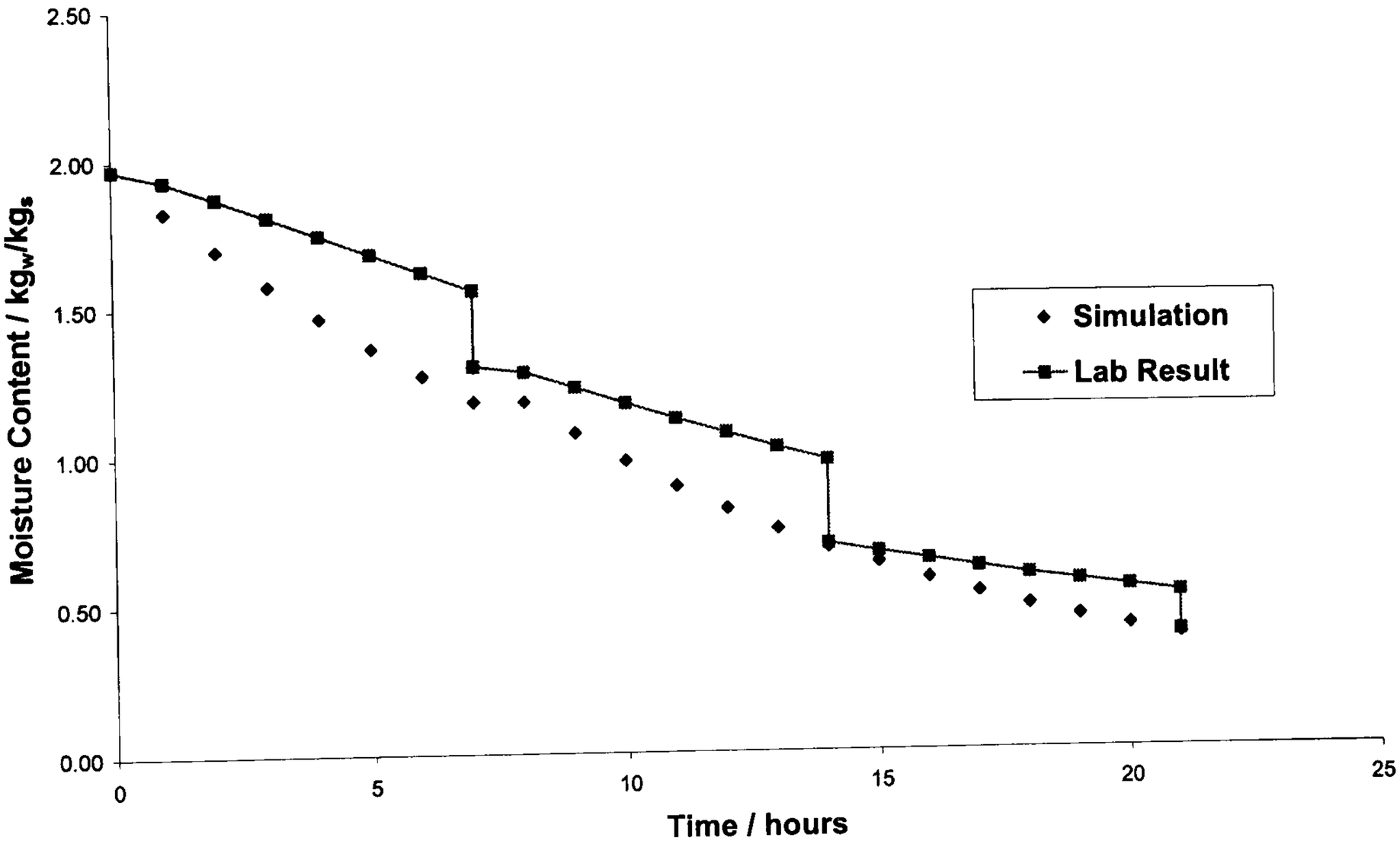

Figure 6.15 Moisture Content vs. Drying Time: Simulation and Lab Results; Roof 81^0 Inlet 50mm

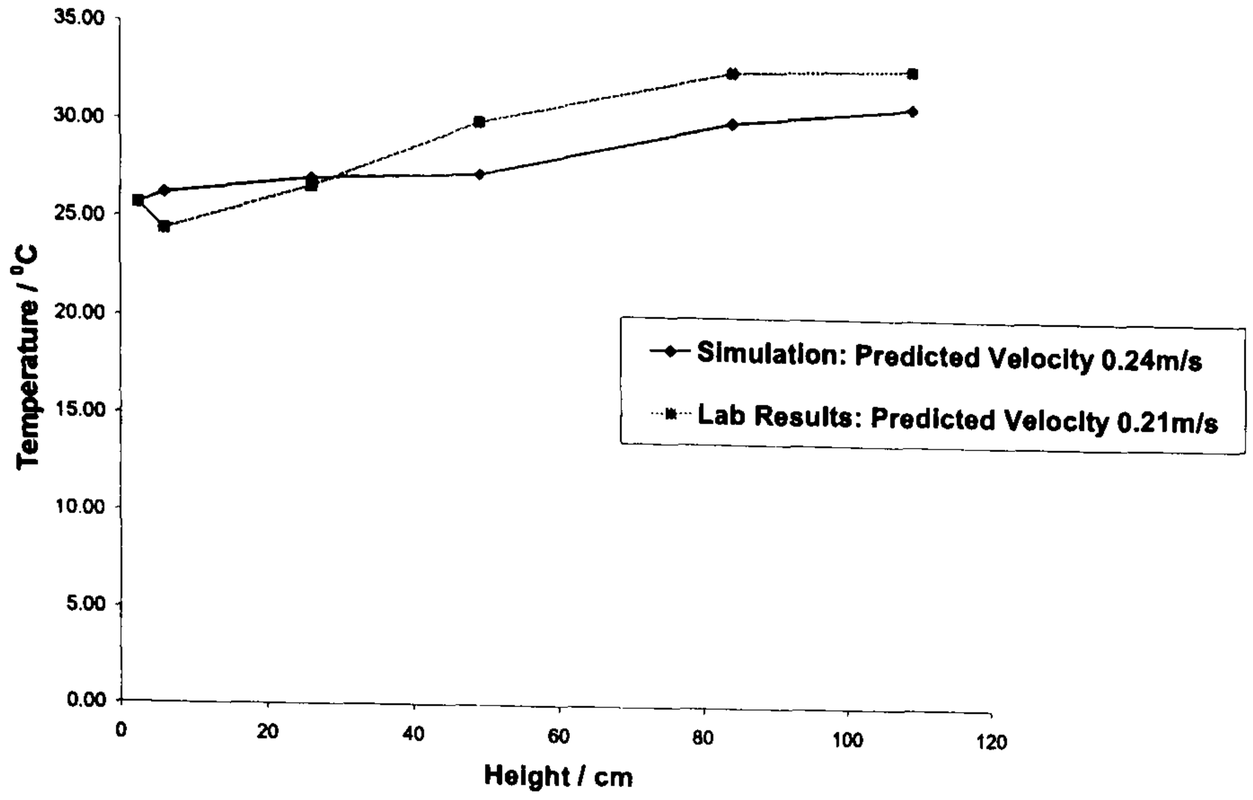

a) Day 1

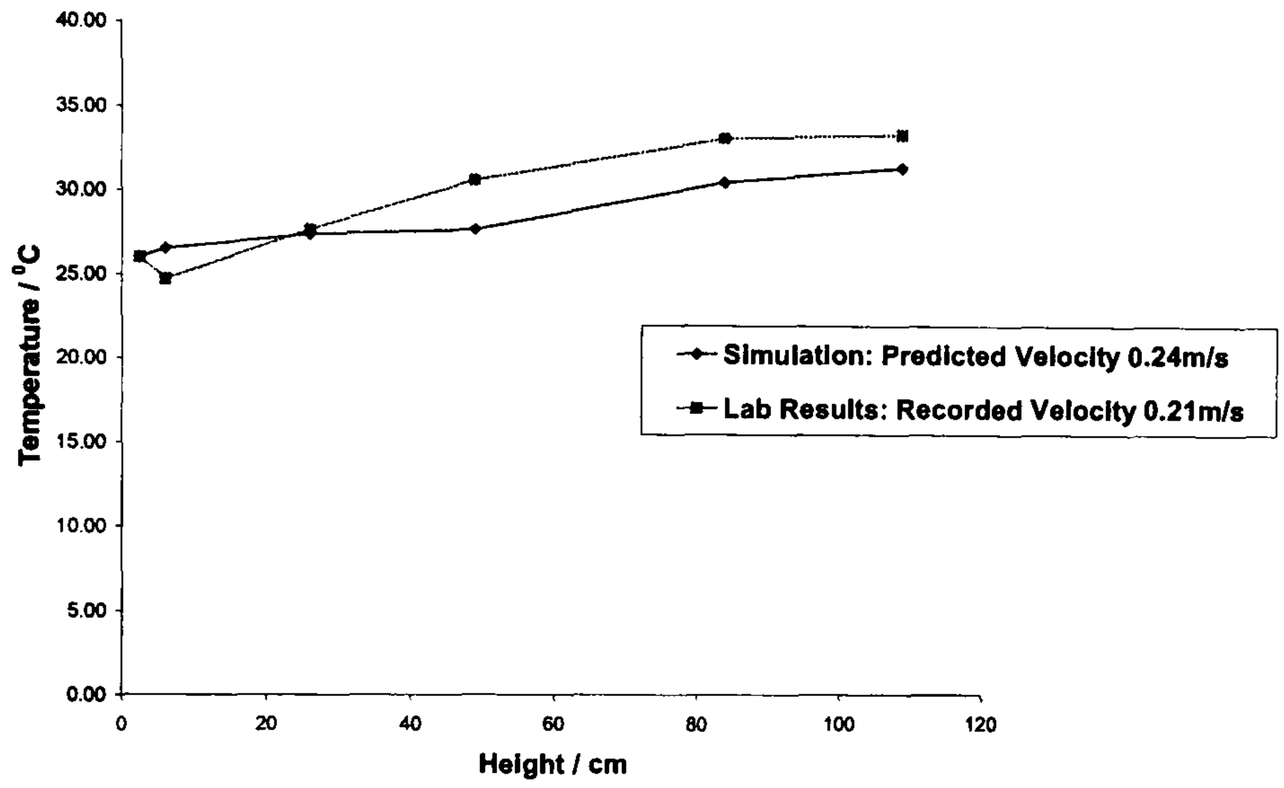

b) Day 2

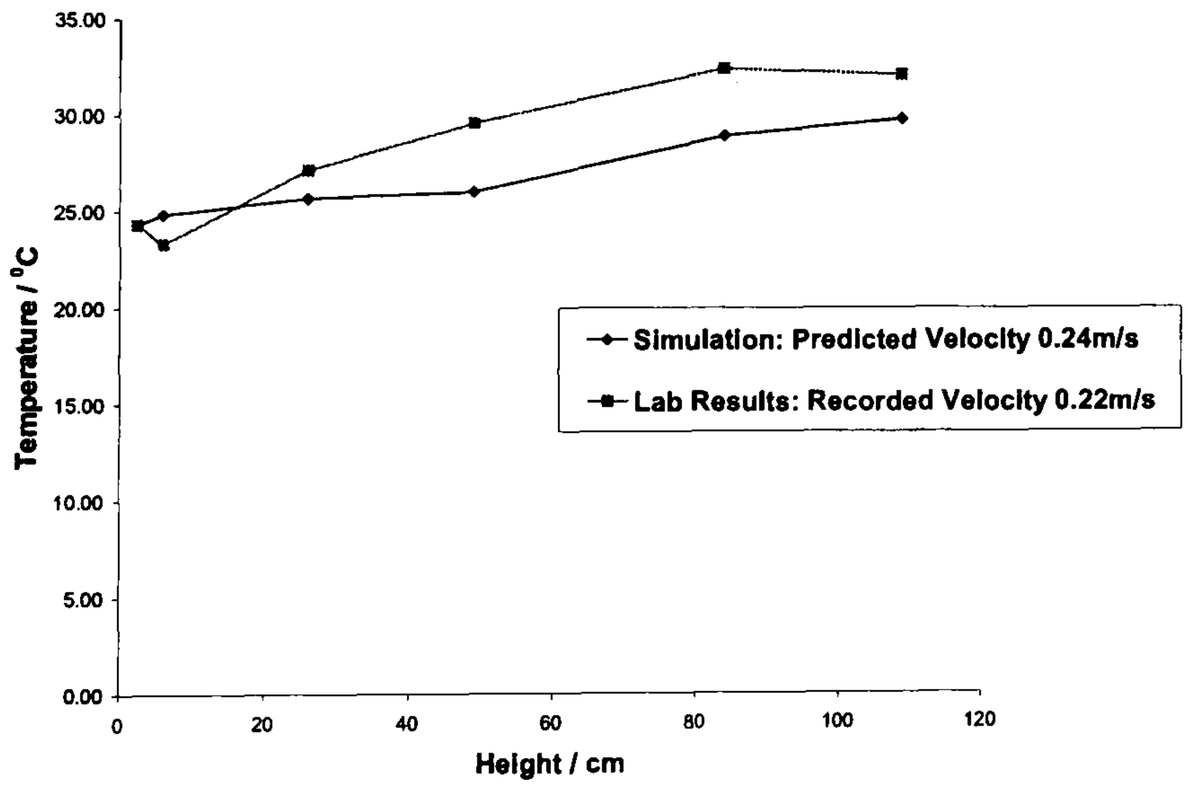

c) Day 3

Figure 6.16 Air Temperature vs. Height: Simulation and Lab Results; Roof 81^0 Inlet 50mm

The air temperatures at various heights in the dryer of roof 81^0 inlet 50mm can be found in figure 6.16 (a to c) for the three days of the simulation and laboratory processes, with the inlet velocities in the legends of the graphs. Again there is over-prediction of the temperature below the crop and under-prediction above the crop bed for the same reasons given in the last section. Also, the values of inlet velocities shown in the graph give relative differences of 0.14 for the first two days and 0.09 for the third day.

6.3.2.3 Under-load validation on roof angle 81^0, inlet gap 30mm

The graph in figure 6.17 show a predicted change in MC from 2.05 to 1.29 kg_w/kg_s by the simulation program whilst that measured from the laboratory is from 2.05 to 1.27kg_w/kg_s, in the first drying cycle. There is a relative difference in MC of 0.015 at the end of the first cycle. The second day shows a drying cycle with MCs of 1.27 to 0.71kg_w/kg_s for the simulation code and 1.27 to 0.75kg_w/kg_s for the physical trial, resulting in the relative difference of 0.05. The third drying ends the whole drying process as usual, with a predicted MC of 0.43kg_w/kg_s from the simulation and a measured 0.48kg_w/kg_s from the laboratory, showing a relative under-prediction of 0.1 by the simulation code.

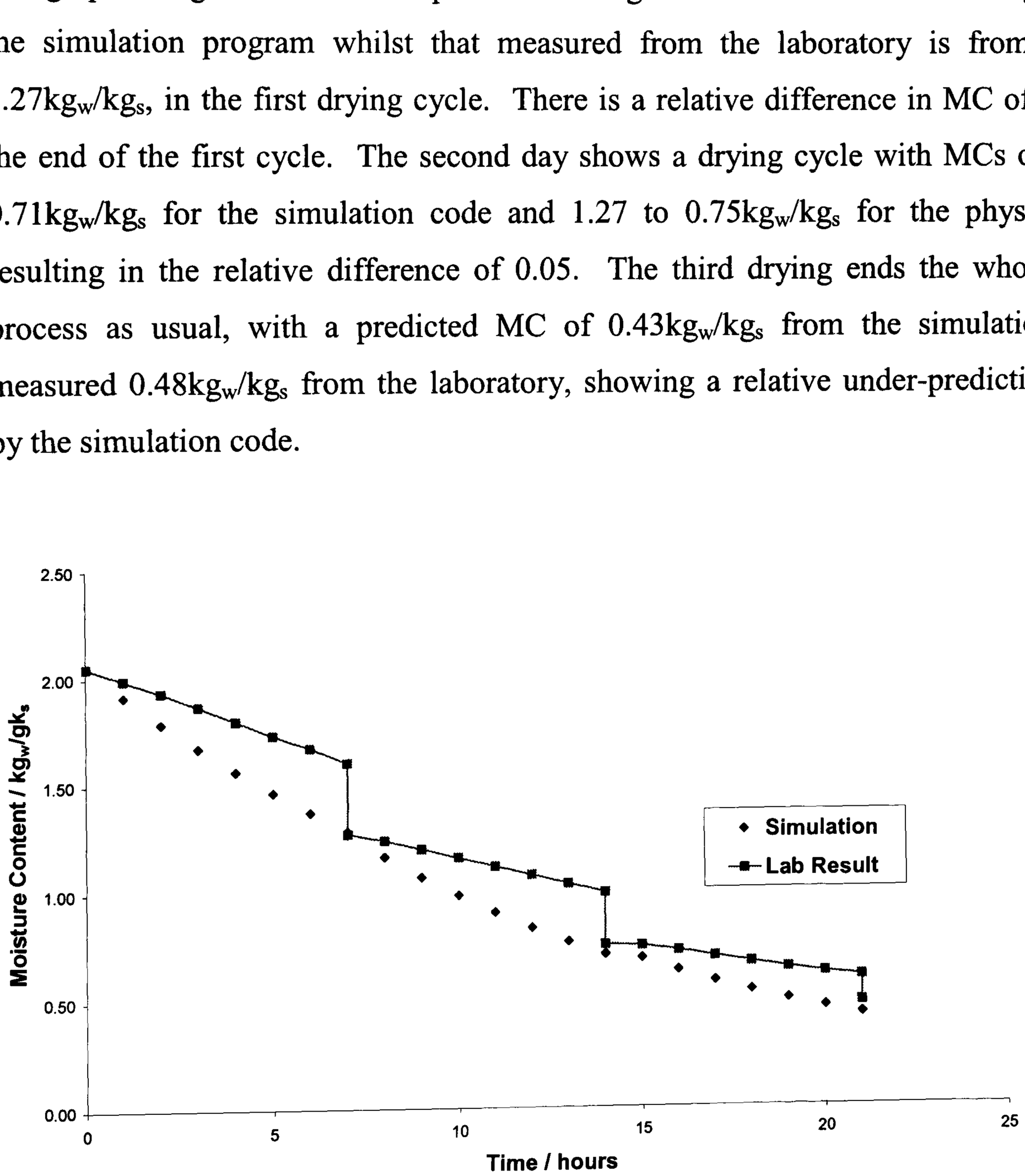

Figure 6.17 Moisture Content vs. Drying Time: Simulation and Lab Results; Roof 81^0 Inlet 30mm

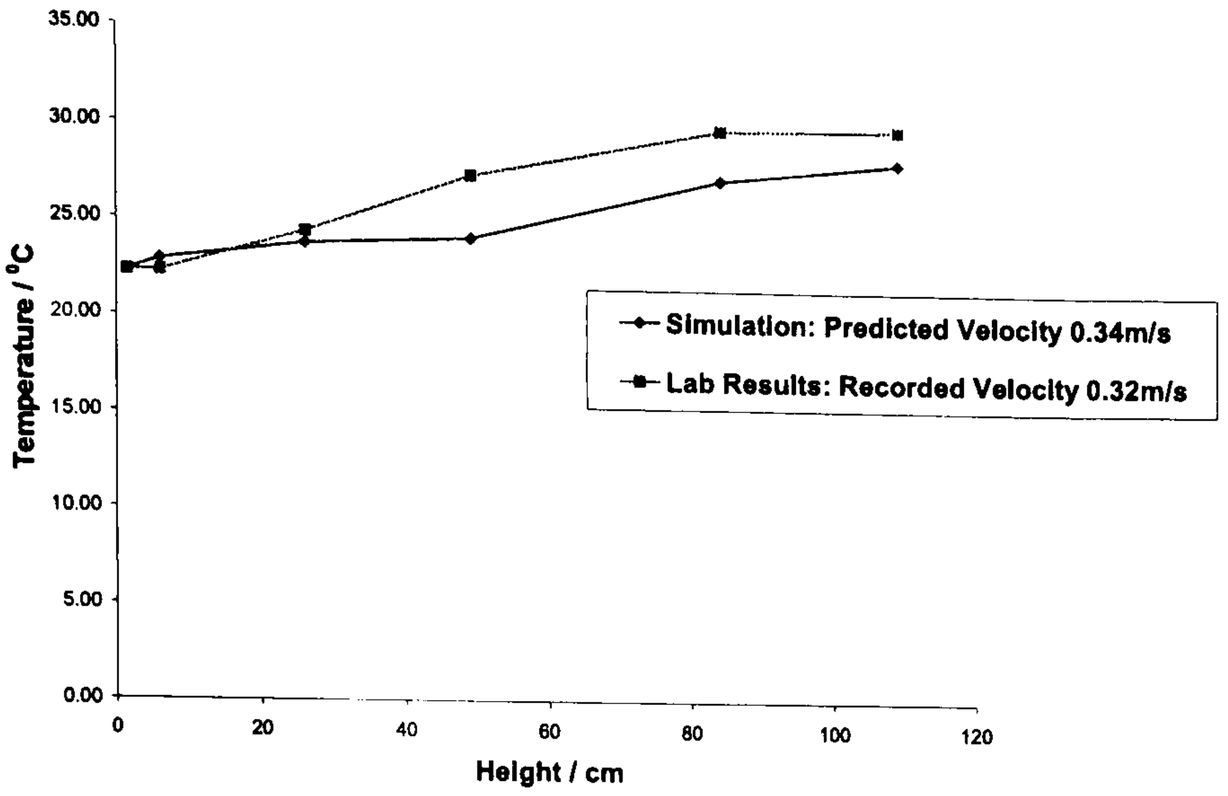

a) Day 1

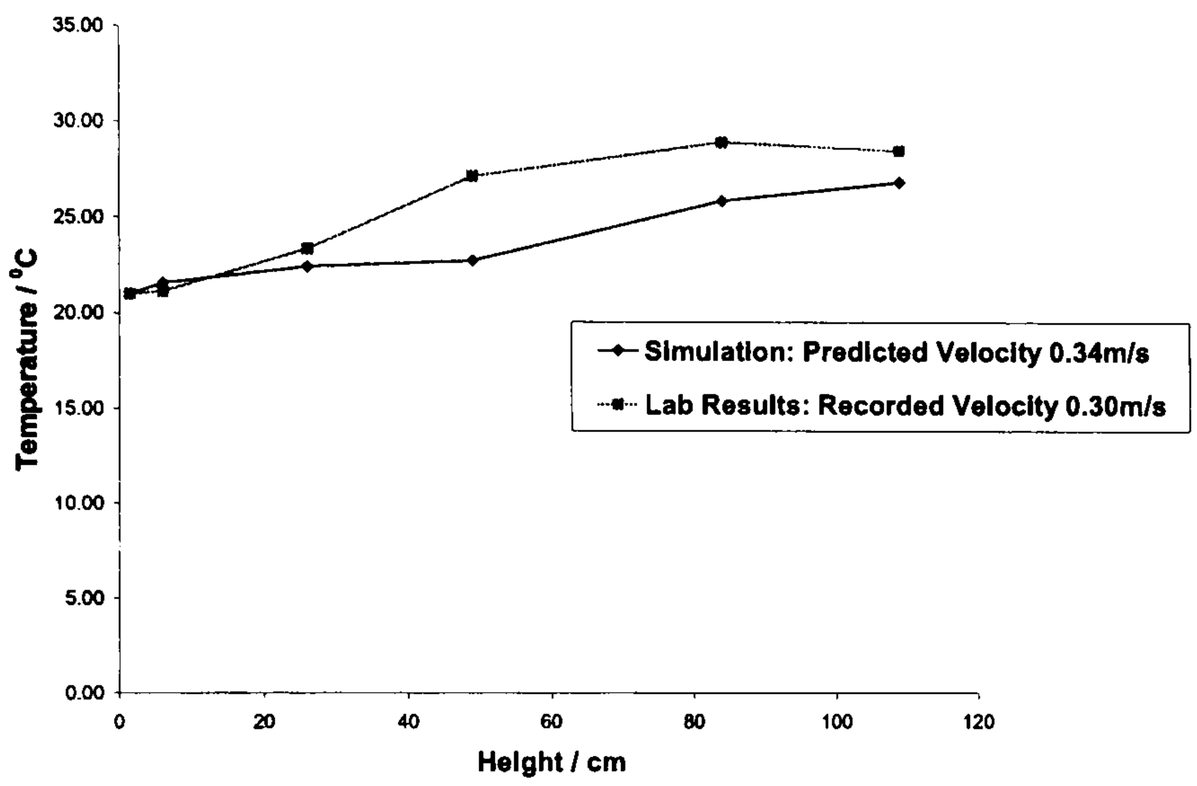

b) Day 2

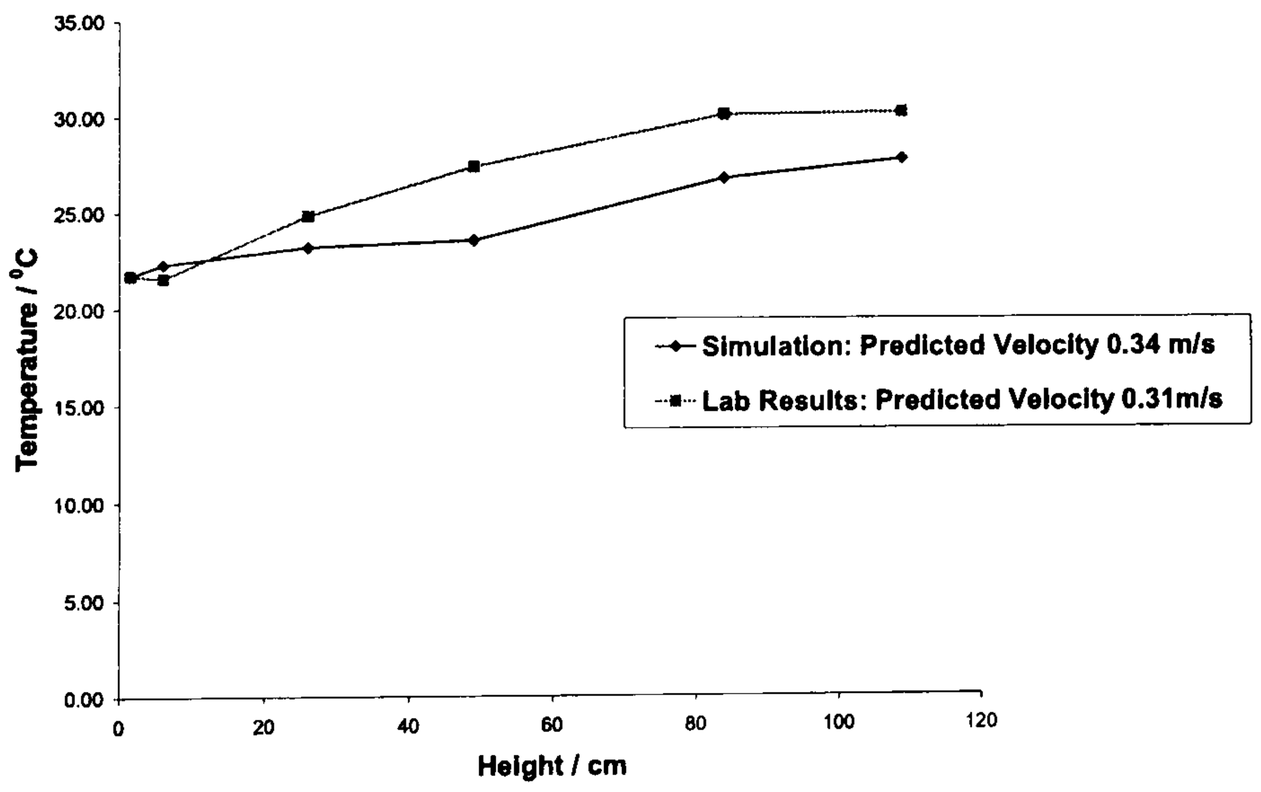

c) Day 3

Figure 6.18 Air Temperature vs. Height: Simulation and Lab Results; Roof 81^0 Inlet 30mm

As indicated in figure 6.18 (a to c) the temperature trends shown for the heights in the CDSCD model with roof 81^0 inlet 30mm are similar to those of the other inlet gaps of the same roof angle; the temperature below the crop is over predicted and those at other points are under predicted. The relative differences in velocity are 0.0625 for day 1, 0.133 for day 2 and 0.096 for day 3.

6.3.2.4 Under-load validation on roof angle 640, inlet gap 70mm

The simulation program of roof 64^0 inlet 70mm shows a drying process from an MC of 1.99 to 1.16kg_w/kg_s whilst the MCs measured from the laboratory are 1.99 to 1.21kg_w/kg_s in the cycle of day 1, as shown in figure 6.19. Thus the simulation code predicts with relative difference of 0.04 after day 1. The values in the second cycle are 1.21 to 0.58kg_w/kg_s for the simulation and 1.21 to 0.66 kg_w/kg_s for the laboratory trial; with a relative of 0.12. The third day's cycle shows predicted values of 0.66 to 0.33kg_w/kg_s and measured values of 0.66 to 0.38kg_w/kg_s, indicating a relative under-prediction of 0.13 at the end of the process on day 3.

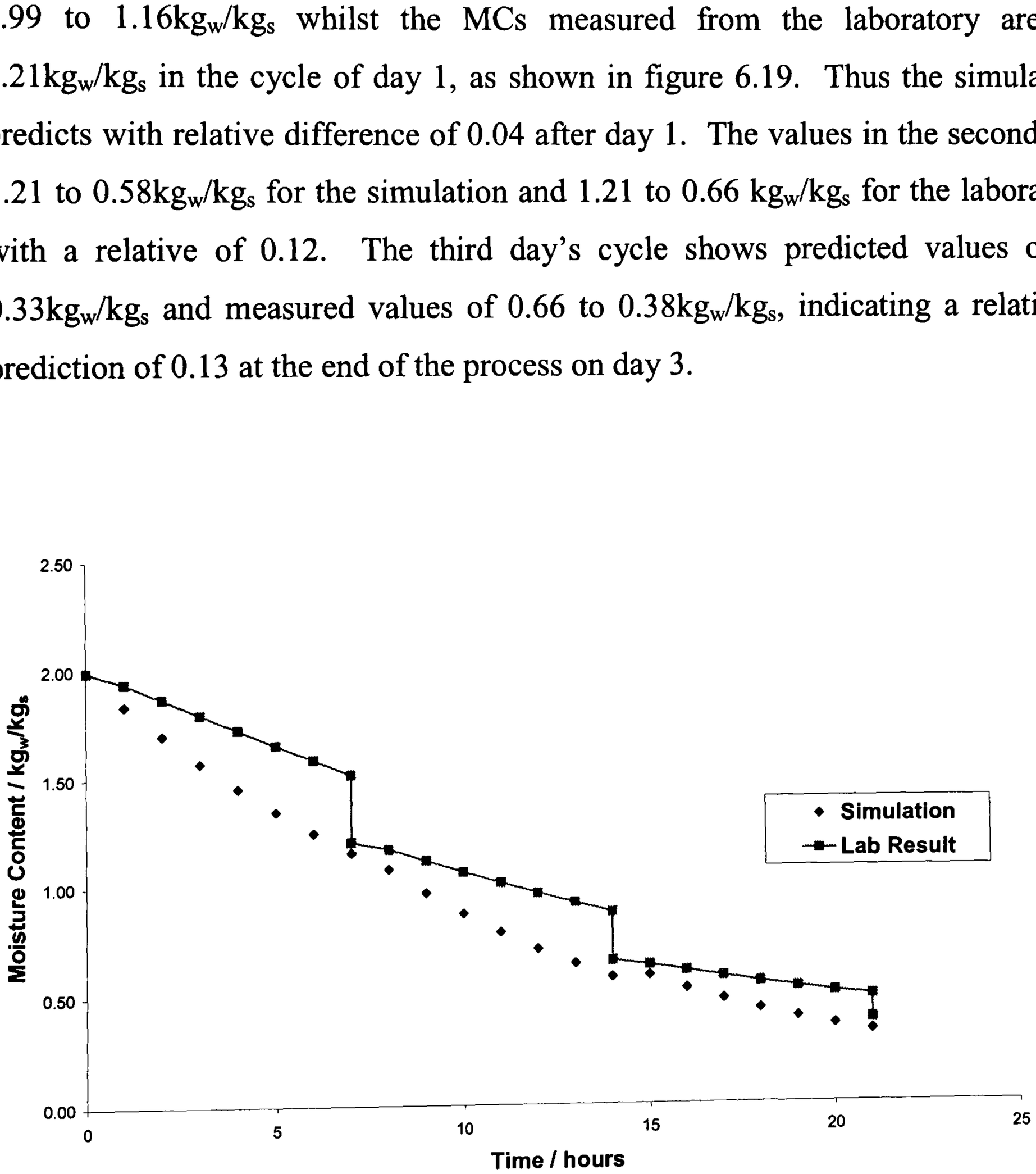

Figure 6.19 Moisture Content vs. Drying Time: Simulation and Lab Results; Roof 64^0 Inlet 70mm

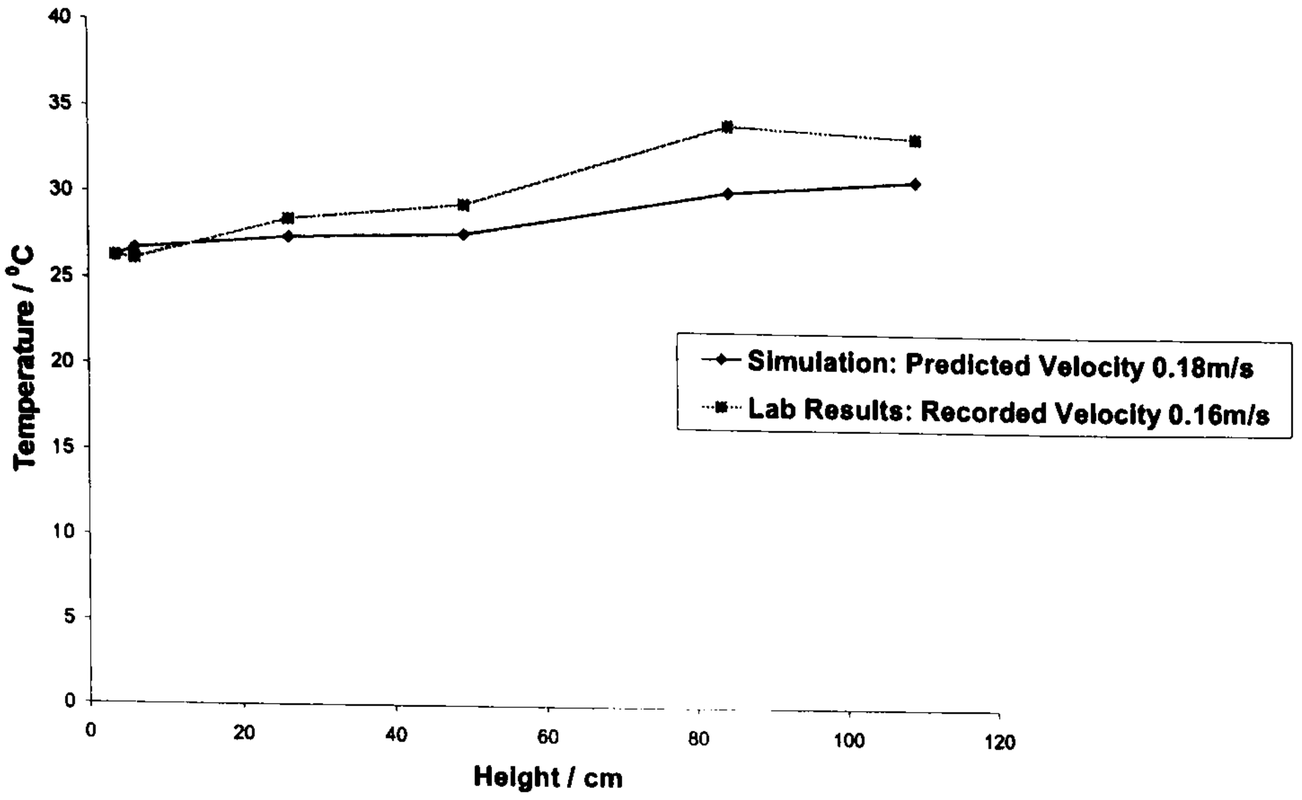

a) Day 1

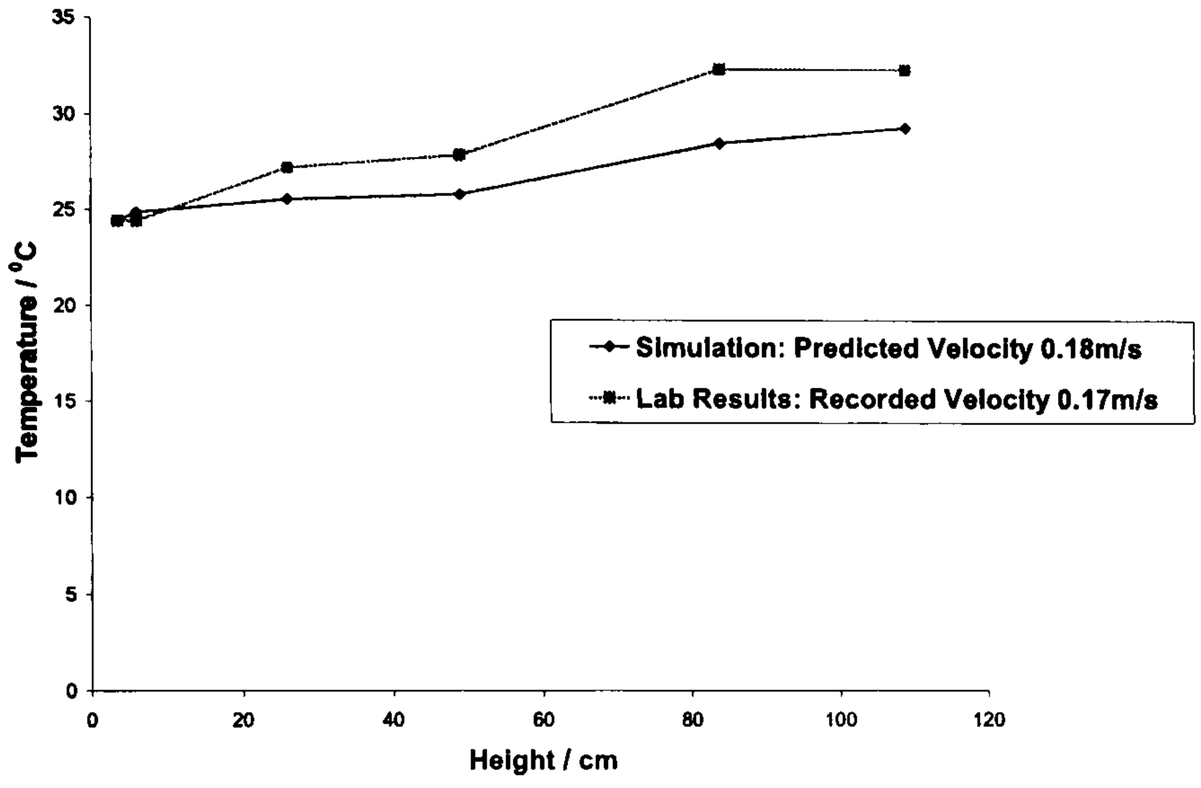

b) Day 2

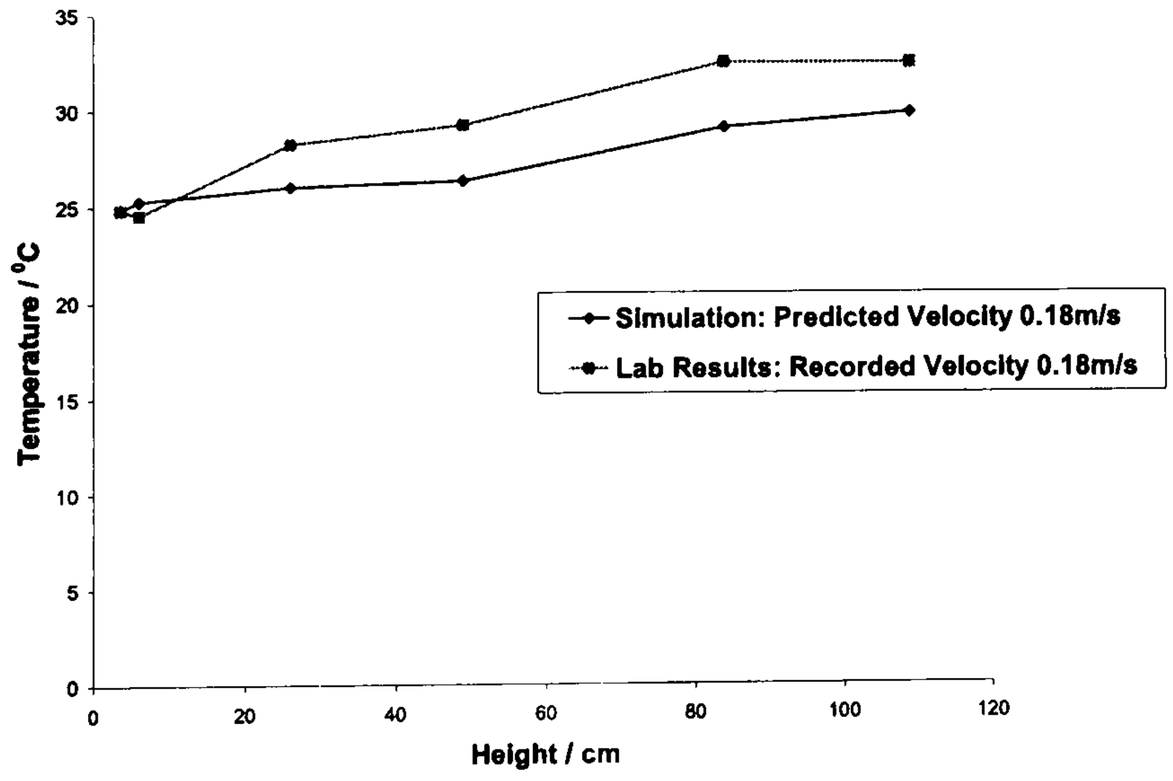

c) Day 3

Figure 6.20 Air Temperature vs. Height: Simulation and Lab Results; Roof 64^0 Inlet 70mm

From figure 6.20, the air temperature is again over-predicted below the crop shelf (i.e. at height 6cm) apparently due to over-estimation of the energy falling on the drying-chamber base. The temperatures at other points in the dryer are under-predicted as the over-heating effects of the metallic frames are not taken into consideration in the simulation code, as already explained previously. The relative differences of velocity are 0.125 for the first day, 0.058 for day 2 and 0 for day 3. Again the over-heating effect is reduced by the effect of extra resistance from the same framework so that the predicted inlet velocities are not much different from the recorded values.

6.3.2.5 Under-load validation on roof angle 640, inlet gap 50mm

Starting with an MC of 2.01kg_w/kg_s, the simulation code predicts an MC of 1.21kg_w/kg_s by the end of the first day and the laboratory trial ends the first-day cycle with 1.40kg_w/kg_s (figure 6.21). The relative difference is 0.136. On day 2, the simulation predicts an MC path of 1.40 to 0.75kg_w/kg_s, whilst the measured values end the cycle at 0.85kg_w/kg_s; showing a relative difference of 0.117. The simulation code completes the third day's process at 0.42kg_w/kg_s and the measured values end the process at 0.46kg_w/kg_s. Thus the relative under prediction is 0.087 at the end of the process.

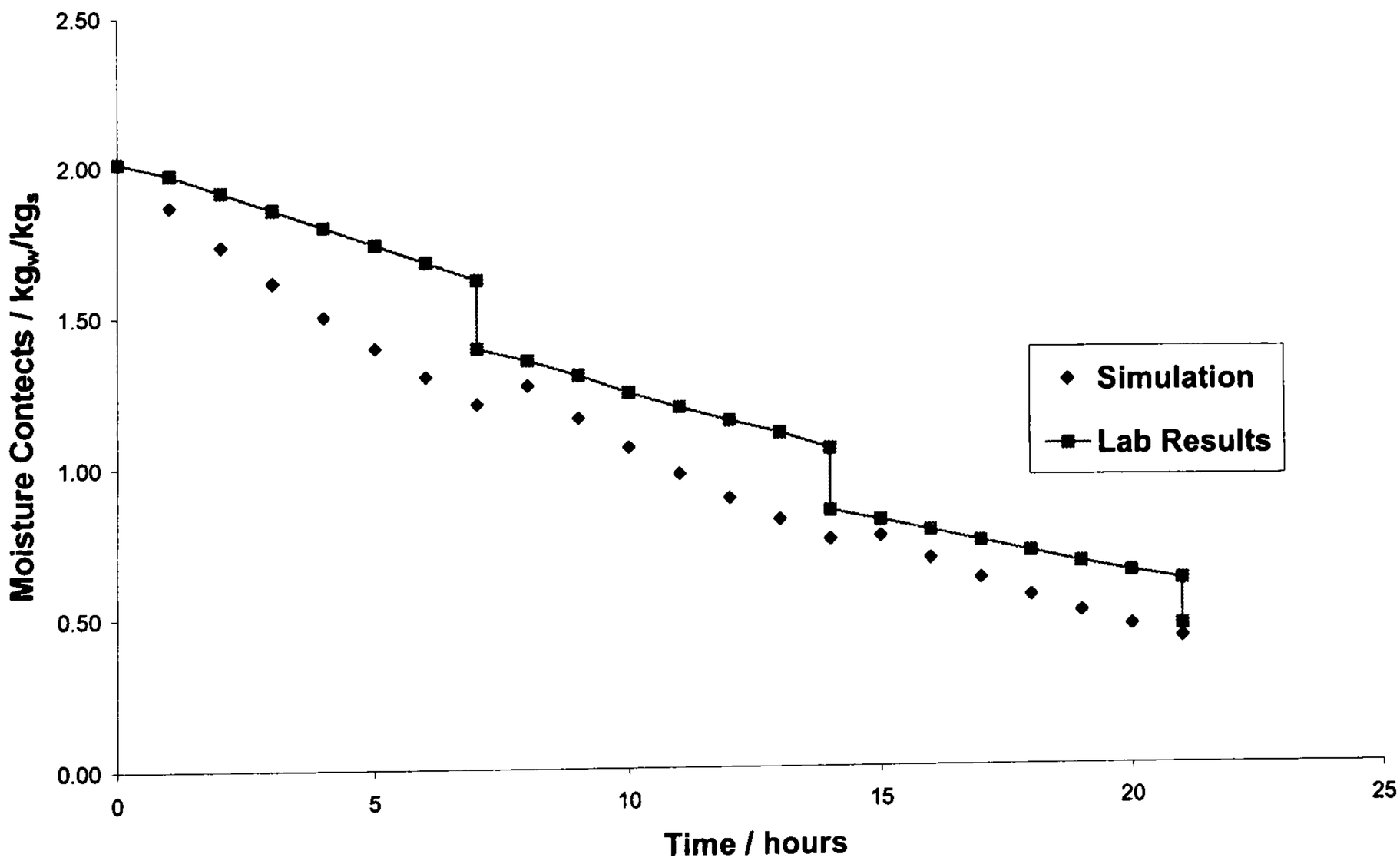

Figure 6.21 Moisture Content vs. Drying Time: Simulation and Lab Results; Roof 64^0 Inlet 50mm

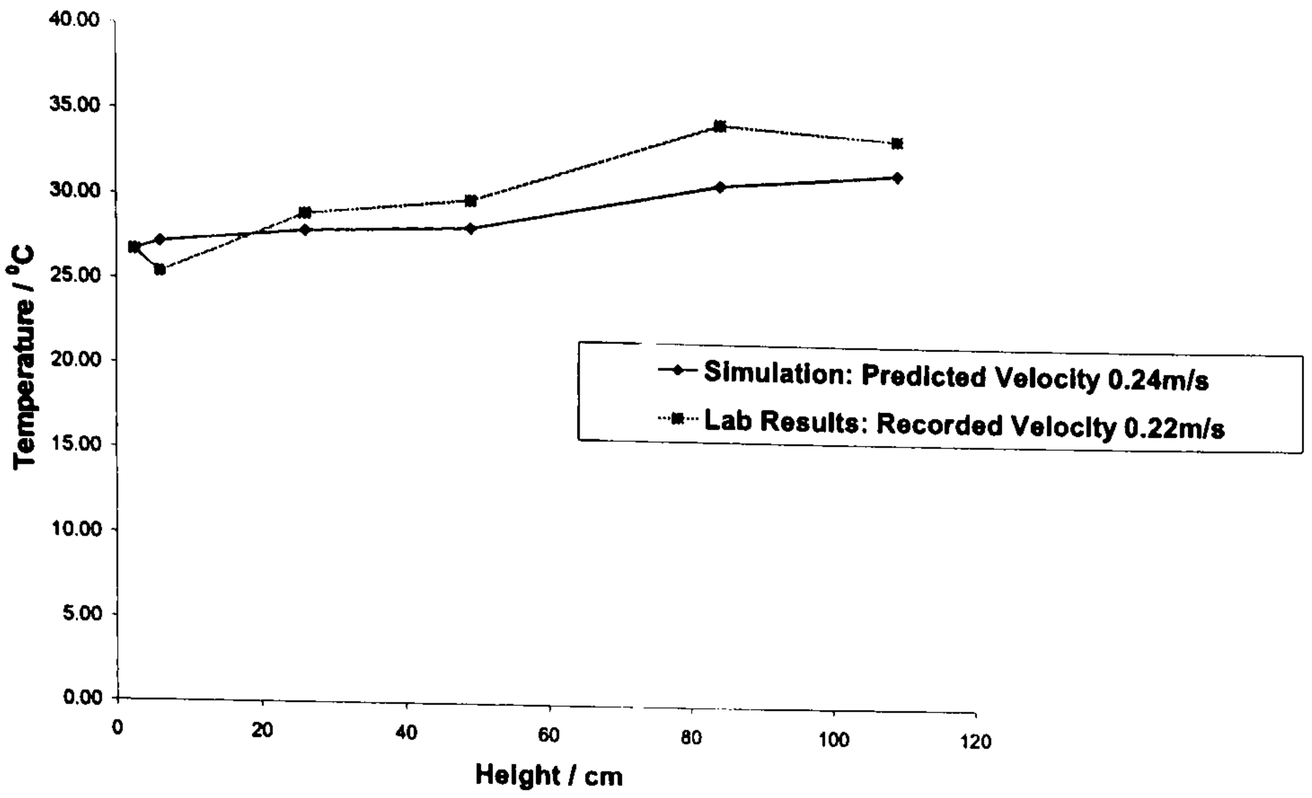

a) Day 1

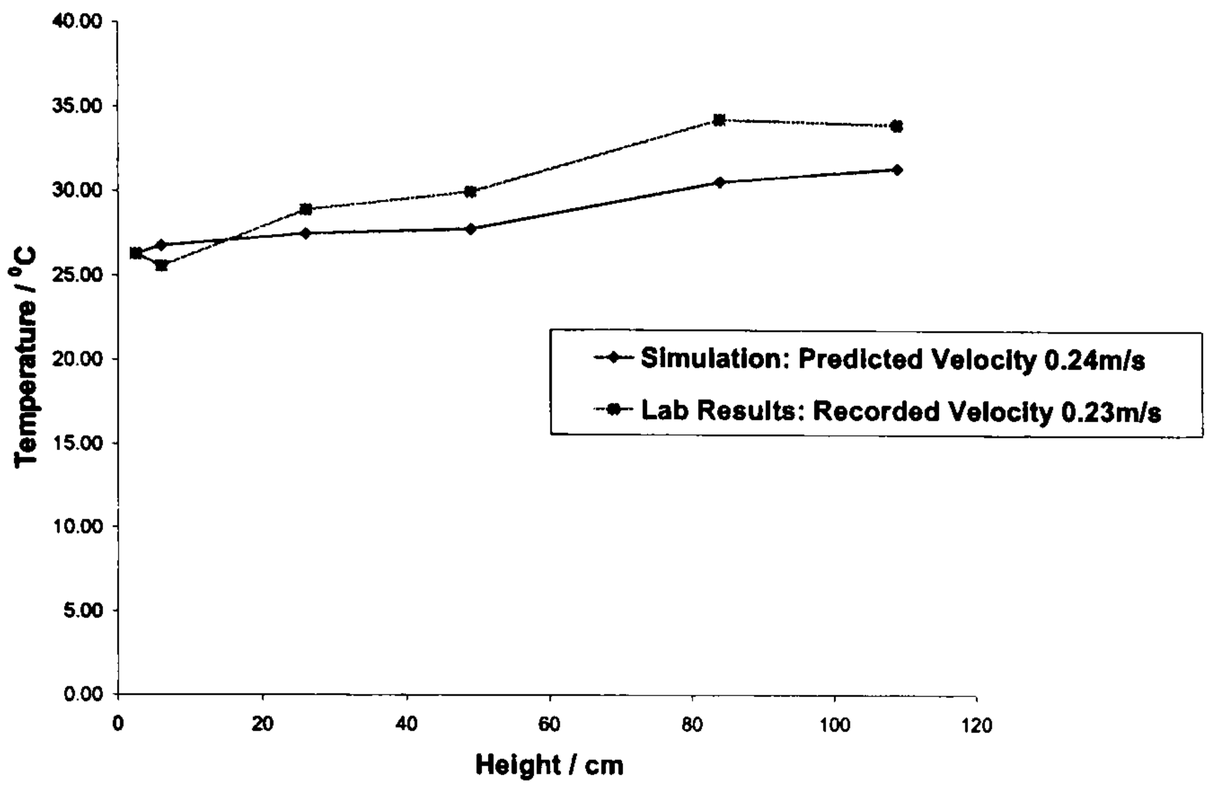

b) Day 2

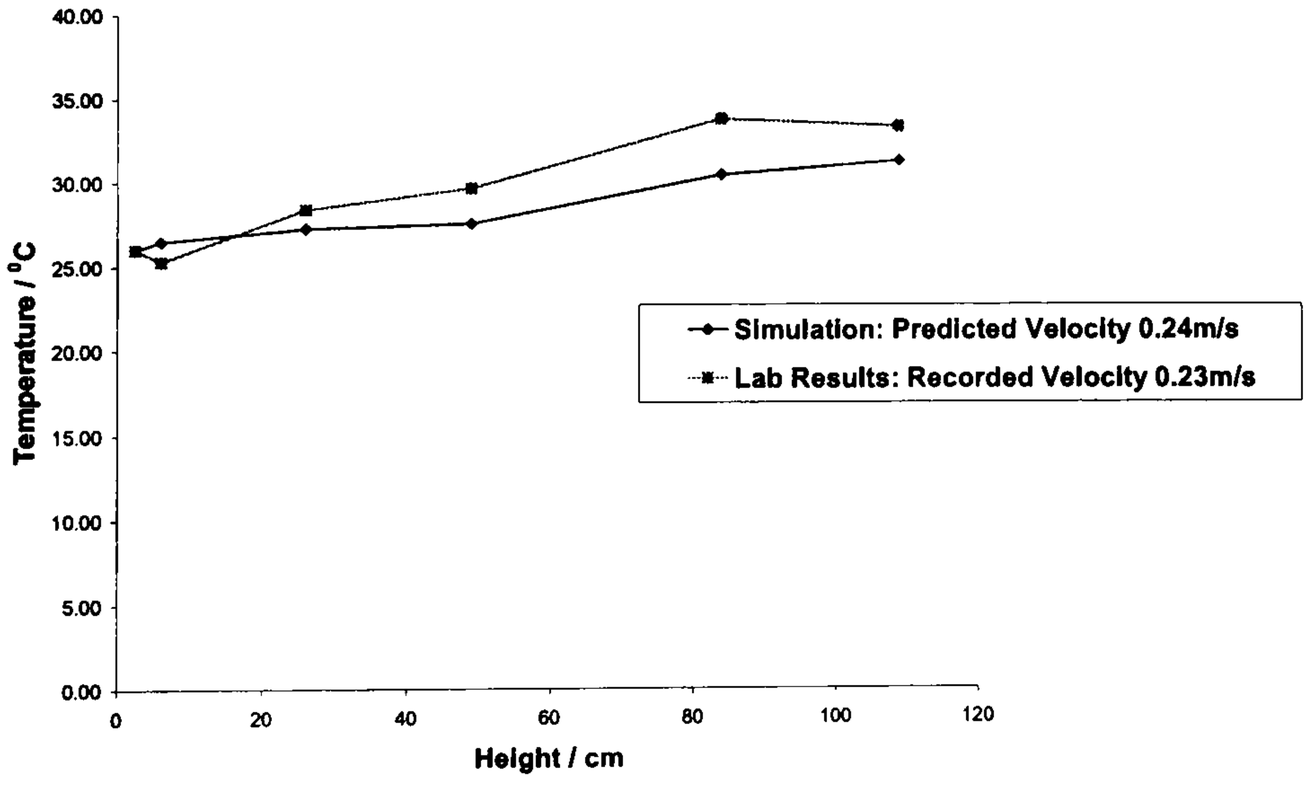

c) Day 3

Figure 6.22 Air Temperature vs. Height: Simulation and Lab Results; Roof 64^0 Inlet 50mm

The usual air-temperature curves are obtained with over-prediction below the crop and under-prediction at other points (see figure 6.22). The relative differences in the inlet velocity, as calculated from the values shown in the legends, are 0.08 for the first day and 0.04 for the second and third days.

6.3.2.6 Under-load validation on roof angle 640, inlet gap 30mm

The graph of MC against the drying time for the simulation and experimental results is presented in figure 6.23, for roof angle 64^0 and inlet gap 30mm. The simulation program shows a drying path with MC from 2.00 to 1.27kg_w/kg_s, and the measured values show a path of 2.00 to 1.28kg_w/kg_s to complete the first cycle, indicating a relative difference of 0.008. The predictions for the second cycle are from 1.28 to 0.73kg_w/kg_s and those measured are from 1.28 to 0.78kg_w/kg_s; so the relative difference is 0.064. On the third day, the simulation code shows a drying process along an MC path of 0.78 to 0.43kg_w/kg_s and those measured follow a path of 0.78 to 0.42kg_w/kg_s. This time, the simulation process over-predicts the measured MC with a relative value of 0.023 at the end of the third day.

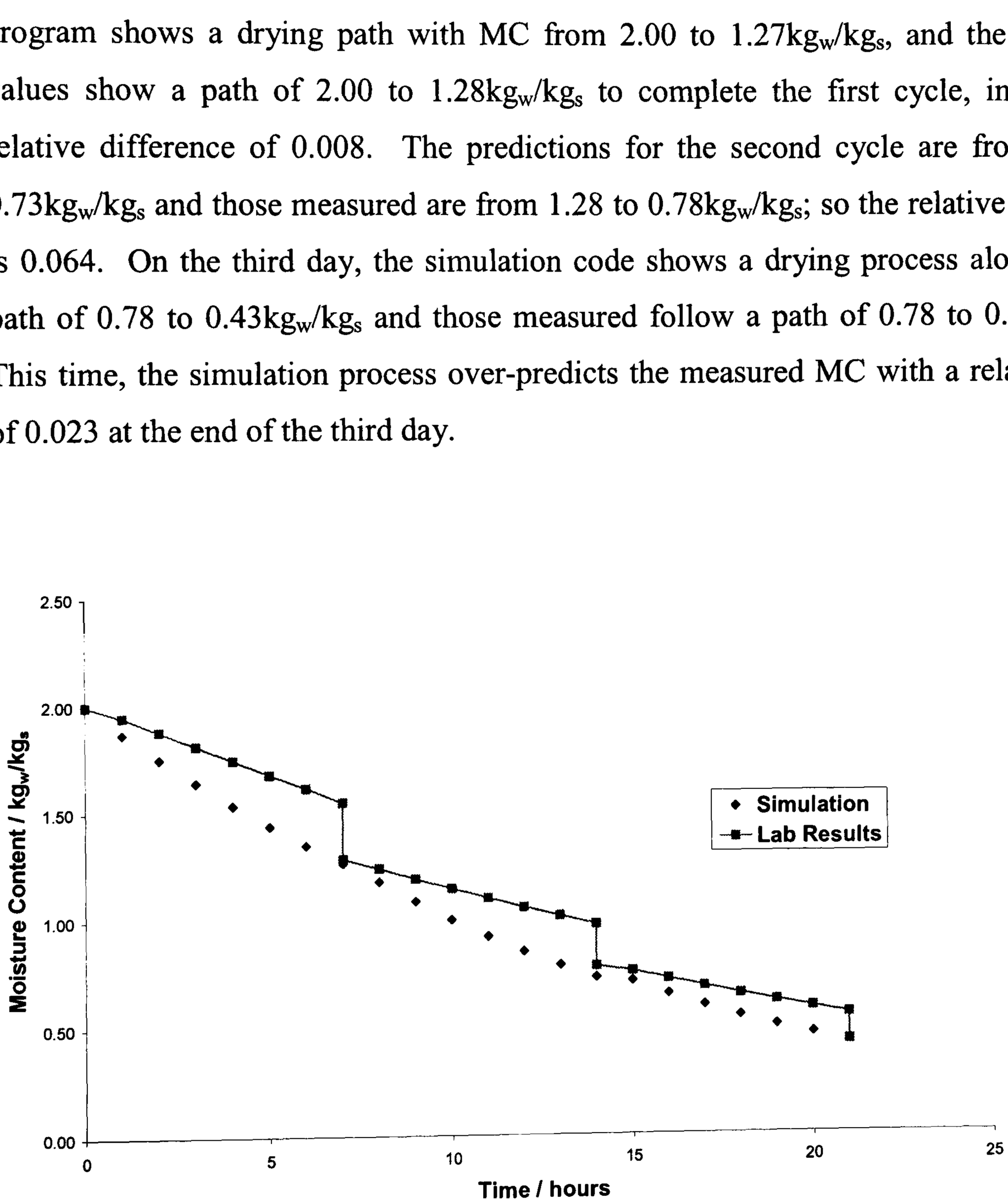

Figure 6.23 Moisture Content vs. Drying Time: Simulation and Lab Results; Roof 64^0 Inlet 30mm

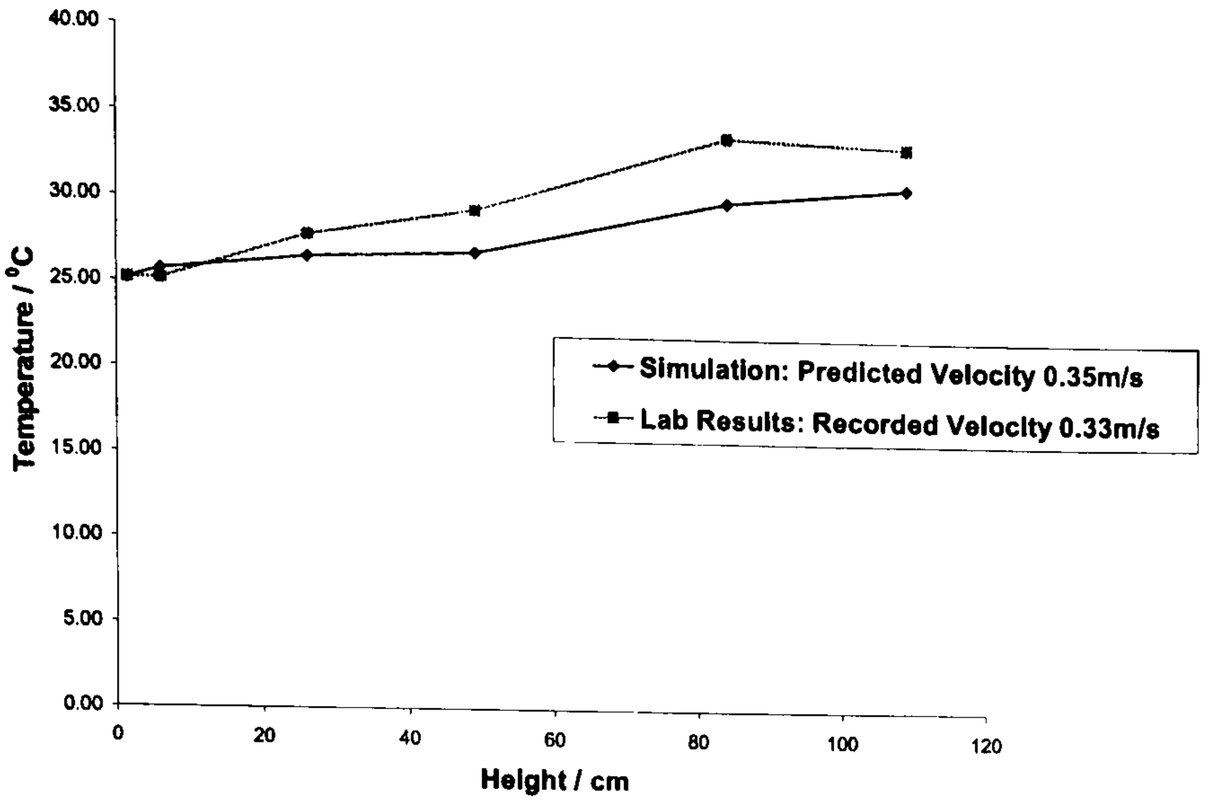

a) Day 1

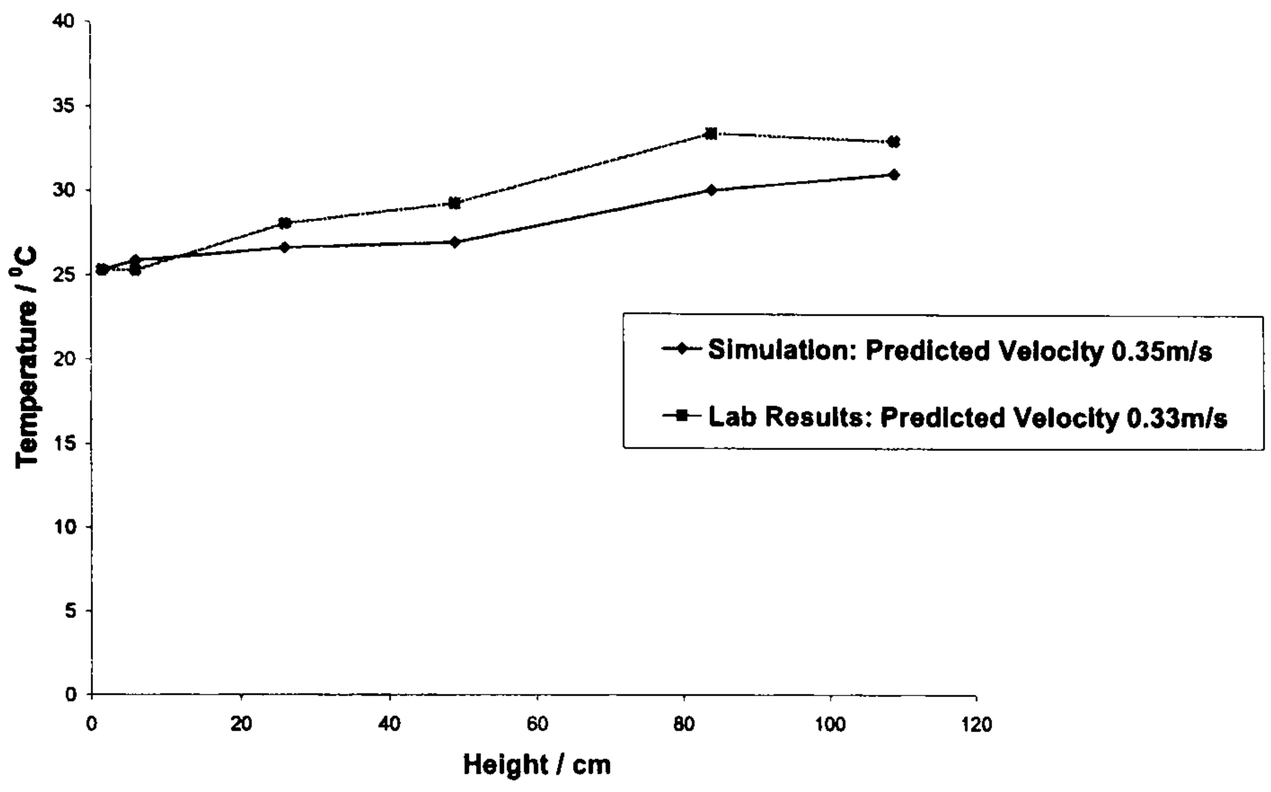

b) Day 2

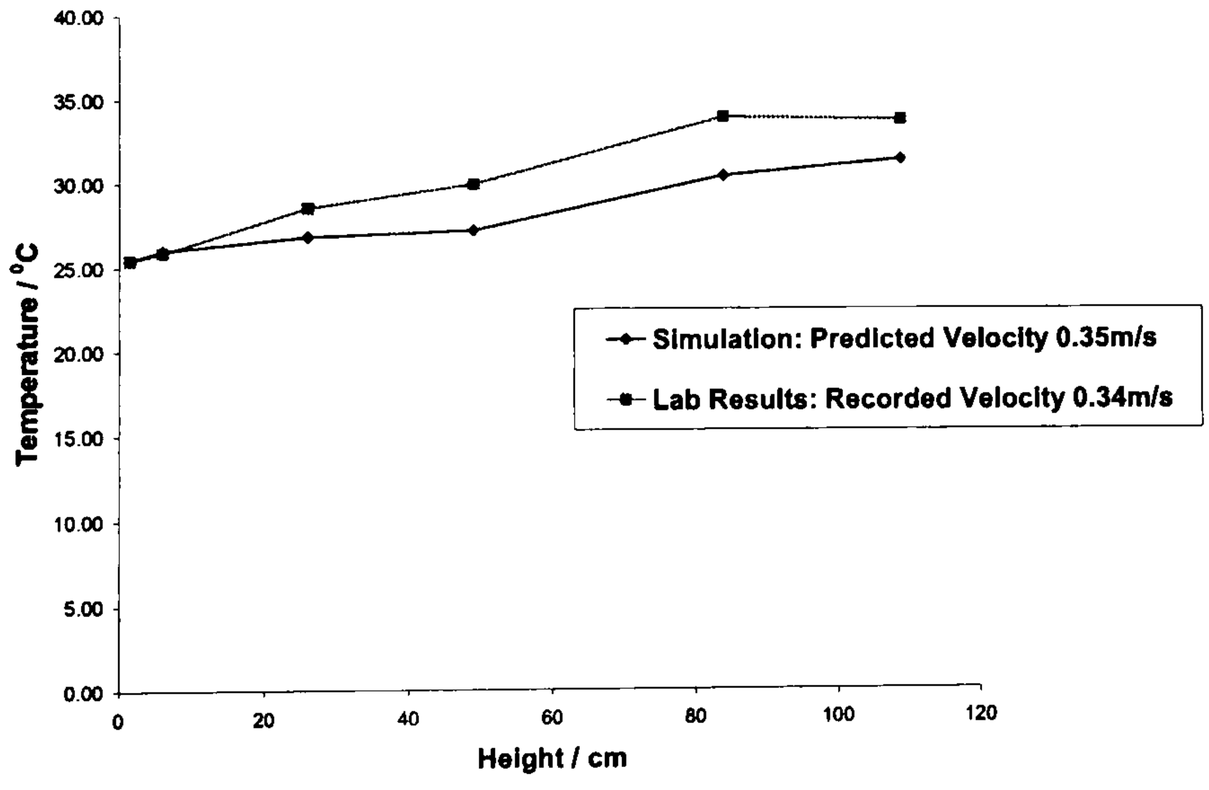

c) Day 3

Figure 6.24 Air Temperature vs. Height: Simulation and Lab Results; Roof 64^0 Inlet 30mm

From figure 6.24, the temperature curves show similar characteristics as those of the other configurations already described, and the relative differences in the inlet velocities are 0.06 for the first and second days and 0.03 for the third day.

6.3.2.7 Under-load validation on roof angle 51^0, inlet gap 70mm

Starting with an MC of 1.96kg_w/kg_s, the simulation code predicts an MC of 1.11kg_w/kg_s after the cycle of day 1, whilst the laboratory gets to 1.10kg_w/kg_s, thus showing a relative over-prediction of just 0.009. From a value of 1.10kg_w/kg_s, the simulation code gives an MC of 0.54kg_w/kg_s and the laboratory process ends at 0.52kg_w/kg_s, showing a relative over-prediction of 0.04, at the end of the second cycle. With MC of 0.52 at the start of the third cycle, the simulation path ends with MC of 0.26kg_w/kg_s, whilst the laboratory path ends with 0.25kg_w/kg_s, so that the simulation code over predicts with just a relative deviation of 0.04.

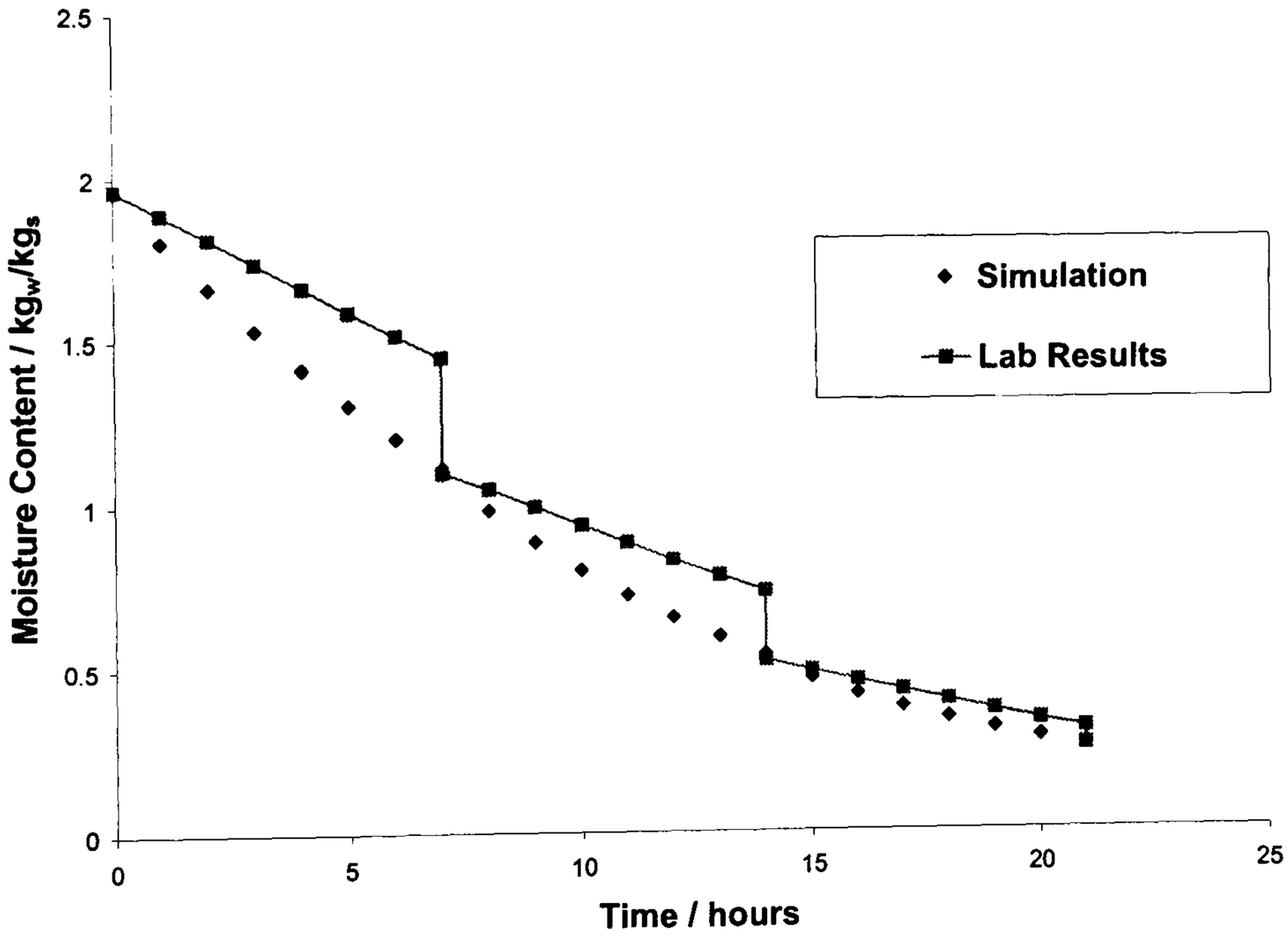

Figure 6.25 Moisture Content vs. Drying Time: Simulation and Lab Results; Roof 51^0 Inlet 70mm

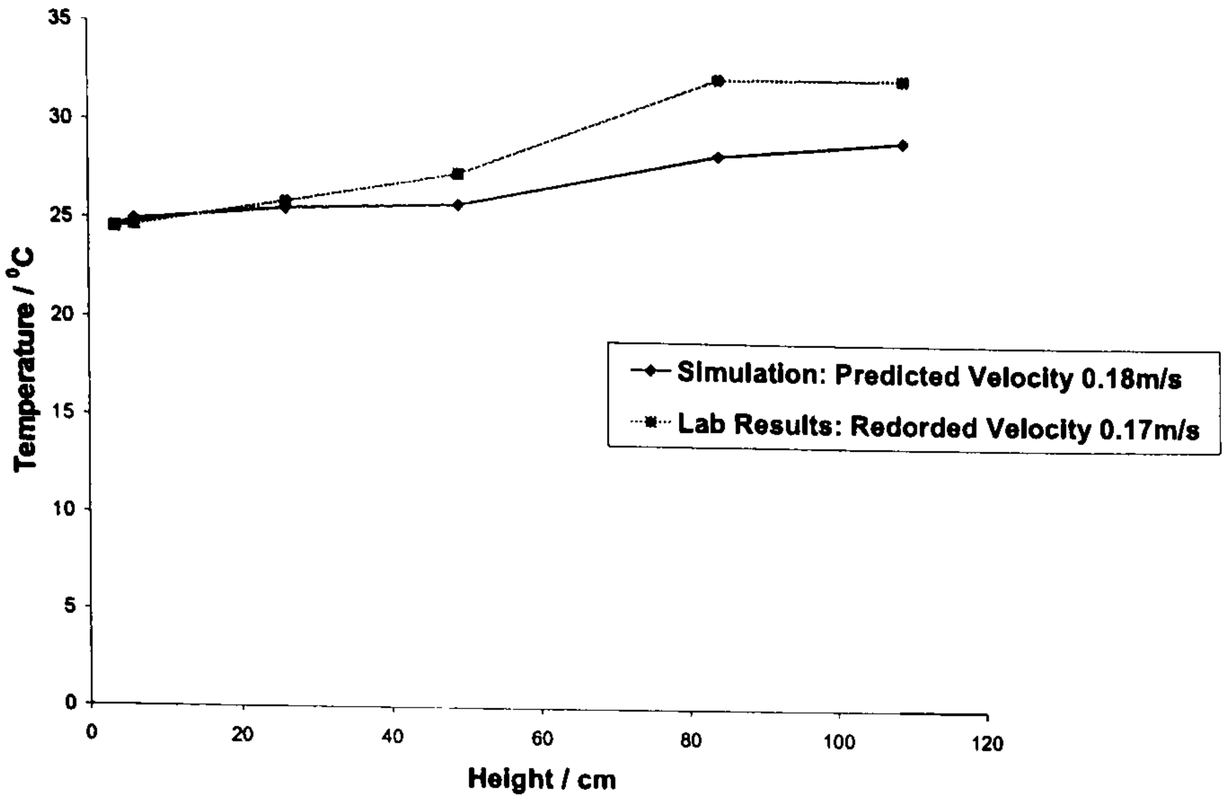

a) Day 1

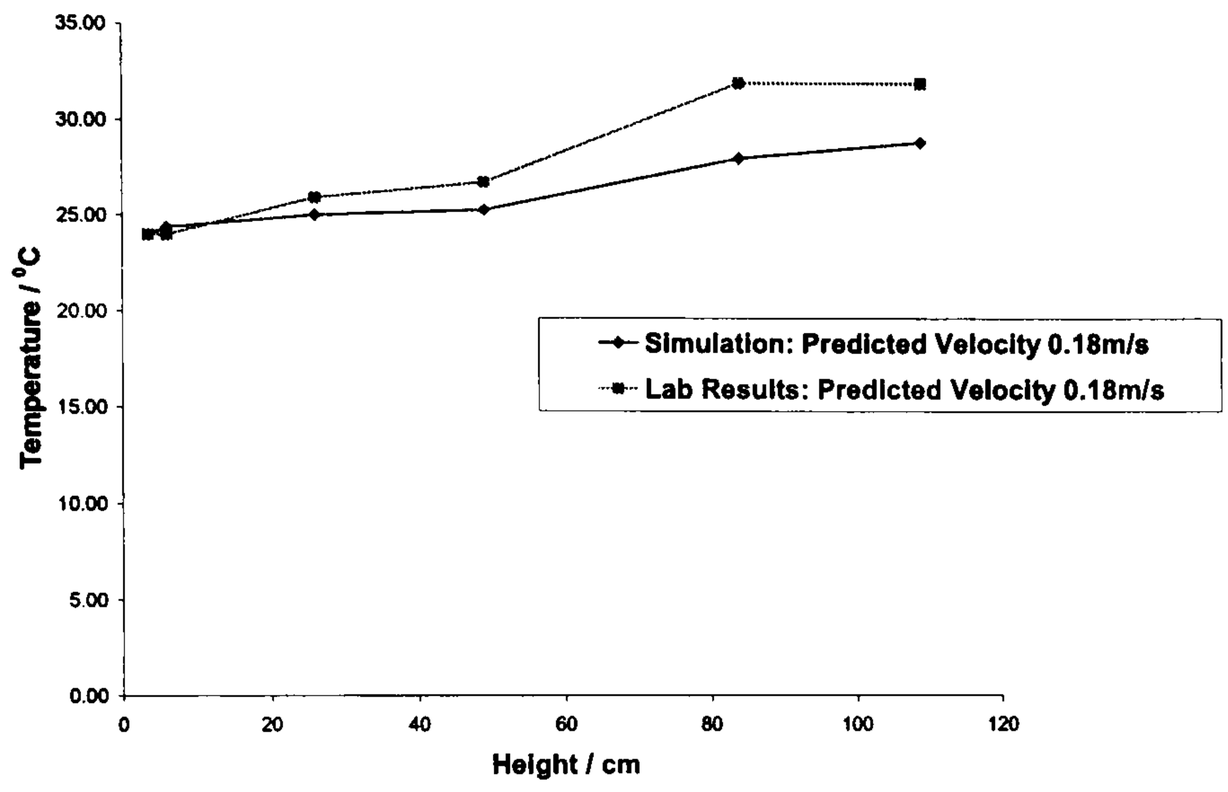

b) Day 2

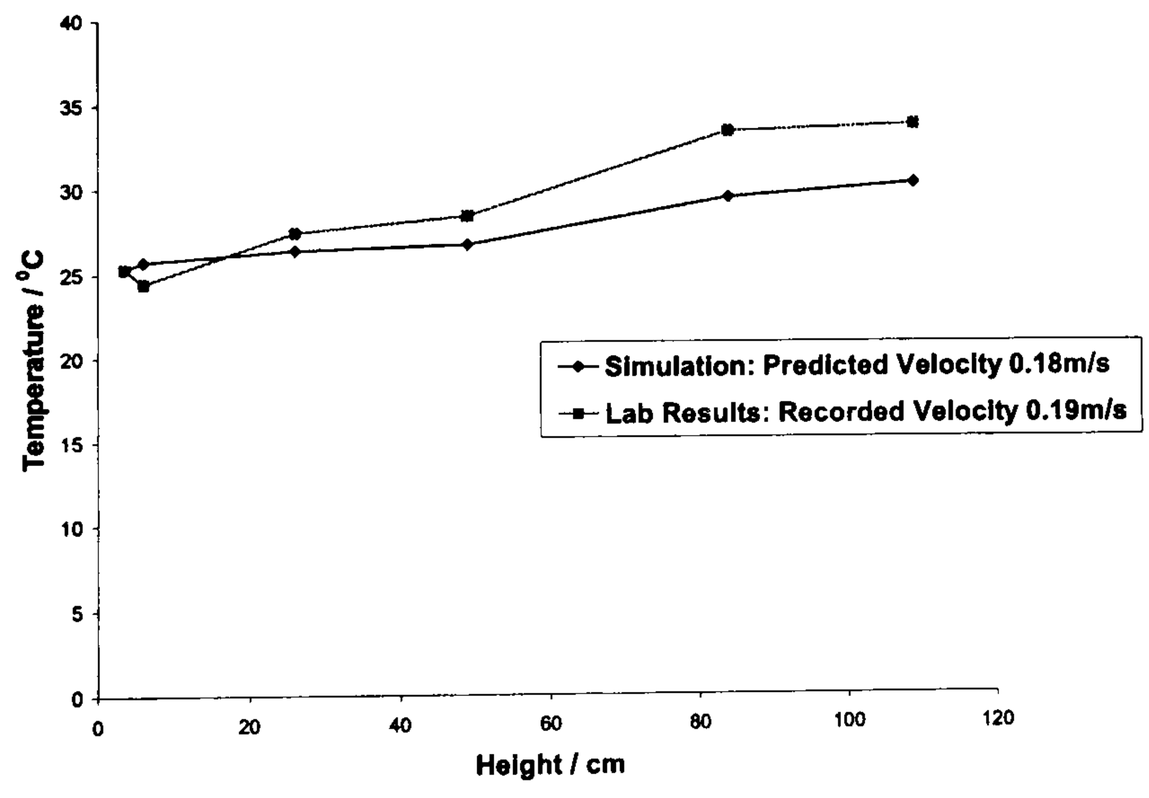

c) Day 3

Figure 6.26 Air Temperature vs. Height: Simulation and Lab Results; Roof 51^0 Inlet 70mm

The temperatures at various points again show the usual trends with that below the crop being slightly over-predicted whilst the others are under-predicted, as shown in figure 6.26. The relative differences in velocity between the simulation and laboratory work are 0.058 for the first day, zero (i.e. exact prediction) for the second day and 0.052 for the third day.

6.3.2.8 Under-load validation on roof angle 510, inlet gap 50mm

Figure 6.27 presents the change in MC with drying time for the simulation process and the physical laboratory trial. From an initial MC of 1.99kg_w/kg_s, the simulation program predicts 1.19kg_w/kg_s after the first day's cycle and the physical trial ends the first cycle at 1.24kg_w/kg_s. This results in a relative under-prediction of just 0.04 after day 1. On the second day, the simulation code predicts a drying path of 1.24kg_w/kg_s to 0.63kg_w/kg_s, whilst the laboratory trial completes the second day's cycle with 0.64kg_w/kg_s. The simulation just slightly under-predicts the measured MC with a relative difference of 0.015 after day 2. The forecast from the simulation code on day 3 is from 0.64kg_w/kg_s to 0.33kg_w/kg_s and the measured path is from 0.64kg_w/kg_s to 0.30kg_w/kg_s, so that the relative difference is 0.1 after the third day.

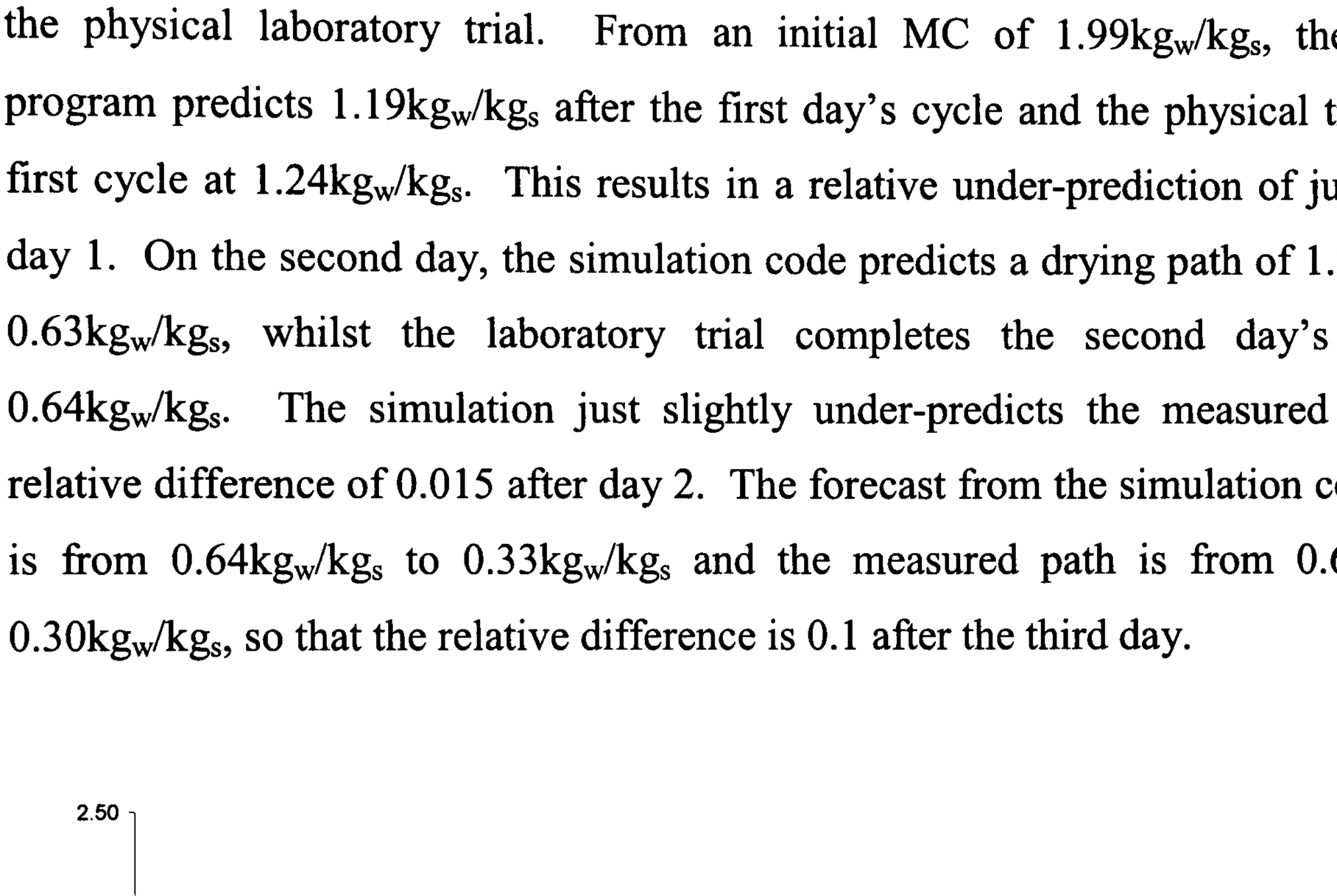

Figure 6.27 Moisture Content vs. Drying Time: Simulation and Lab Results; Roof 51^0 Inlet 50mm

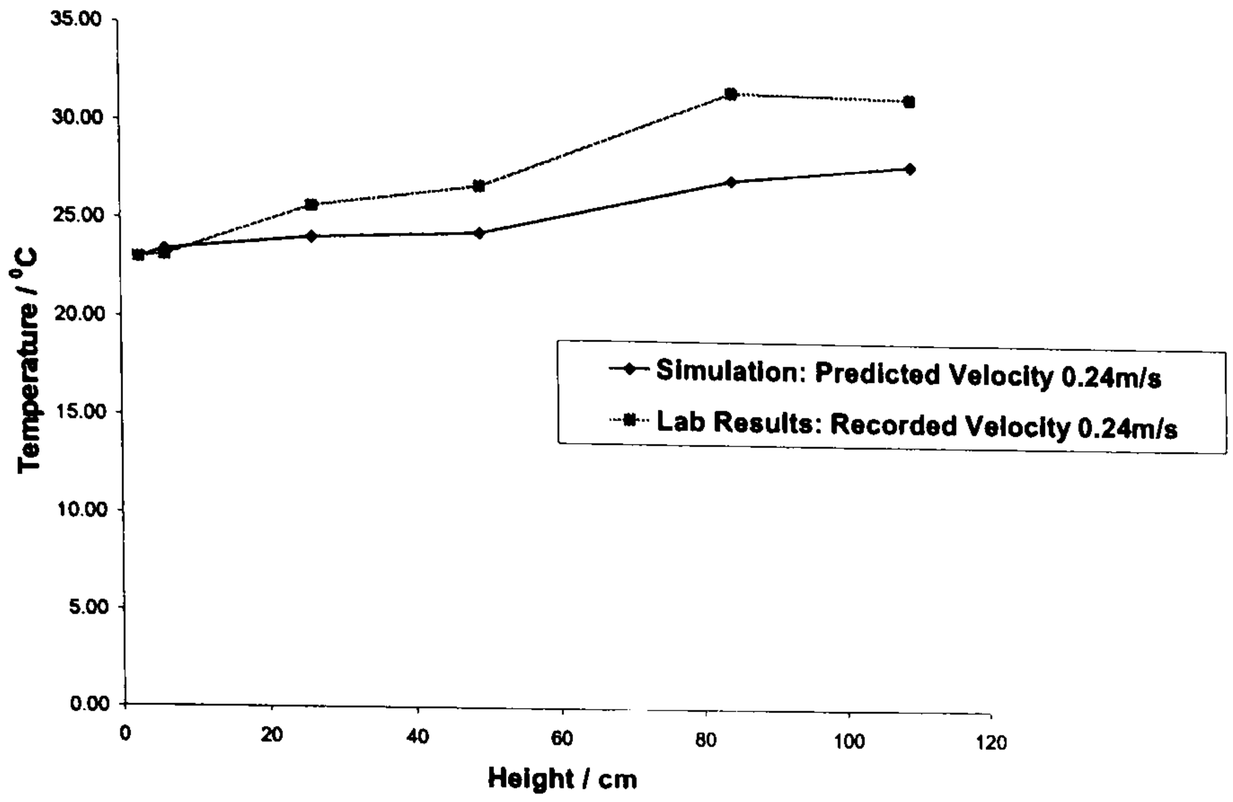

a) Day 1

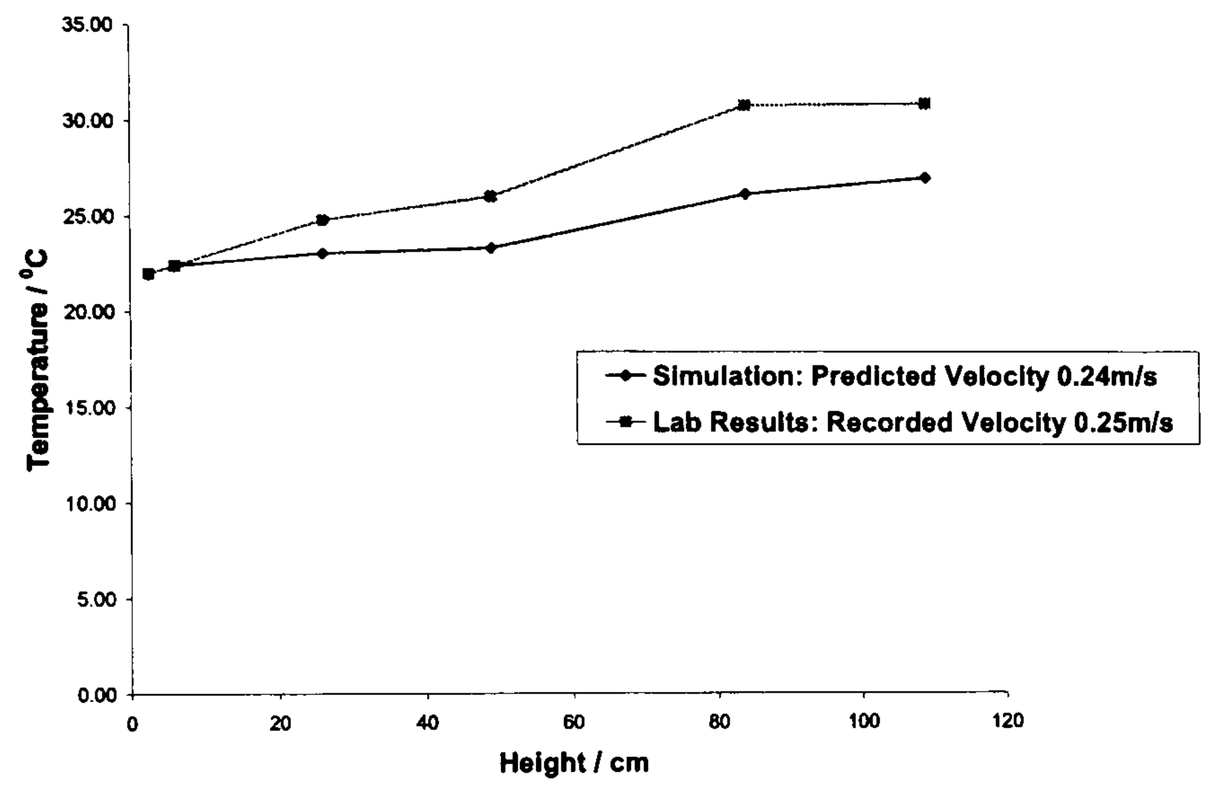

b) Day 2

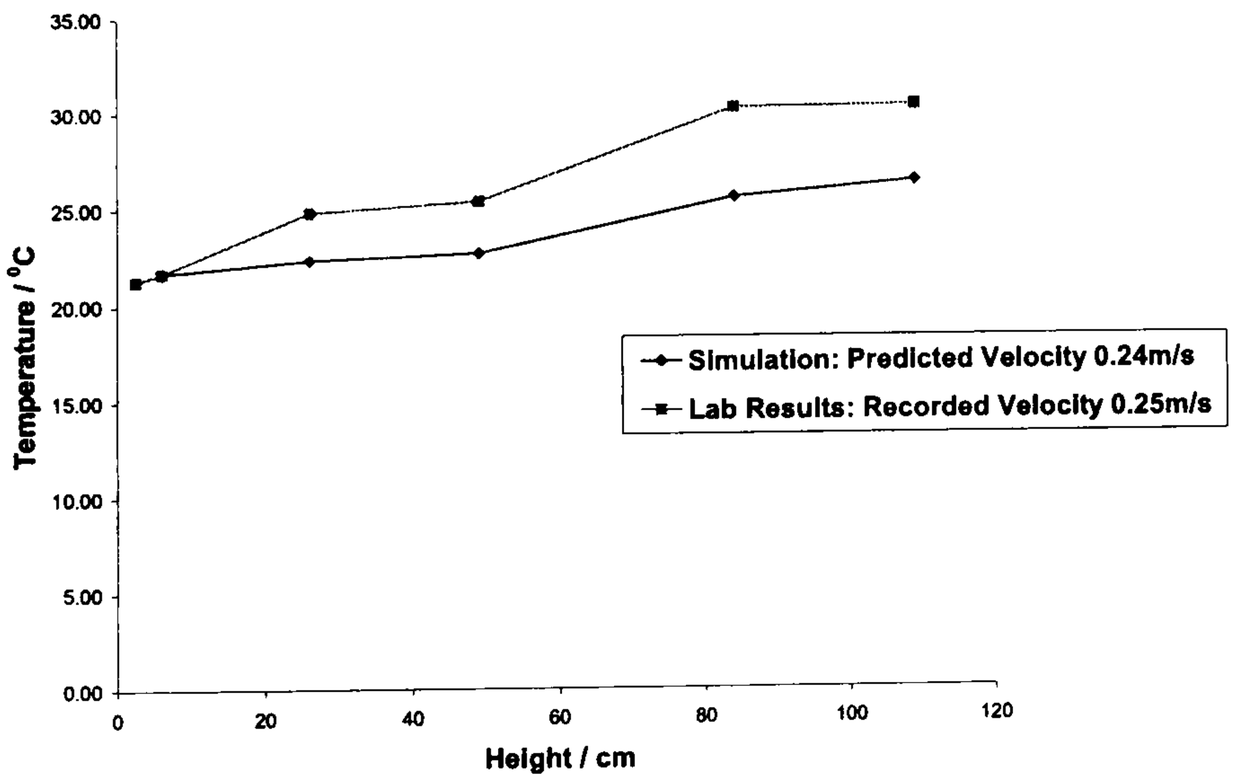

c) Day 3

Figure 6.28 Air Temperature vs. Height: Simulation and Lab Results; Roof 51^0 Inlet 50mm

With this configuration, the over-prediction of air temperature below the crop is reduced. But, just as in the other configurations already described, those at other points in the CDSCD indicate under-prediction of the temperature (see figure 6.28). From the inlet velocities indicated in the various legends, the relative differences in velocities are zero (i.e. exact predictions) for the first day, 0.04 for both day 2 and day 3.

6.3.2.9 Under-load validation on roof angle 51^0, inlet gap 30mm

The drying paths for roof 51^0 inlet 30mm begin with MC of 2.03kg_w/kg_s (figure 6.29). The simulation program ends the first cycle with 1.29kg_w/kg_s whilst the laboratory trial ends with 1.34kg_w/kg_s, so that there is a relative under-prediction of just 0.037 after the first cycle. The second-cycle paths are from 1.34kg_w/kg_s to 0.76kg_w/kg_s for the simulation and from 1.34kg_w/kg_s to 0.85kg_w/kg_s for the physical trial, resulting in a relative difference of 0.105 in the cycle of day 2. Starting the third day with 0.85kg_w/kg_s, both the simulation code and the physical trial end the cycle with 0.46kg_w/kg_s. Thus there is exact prediction (i.e. zero relative difference) by the simulation code at the end of the third day.

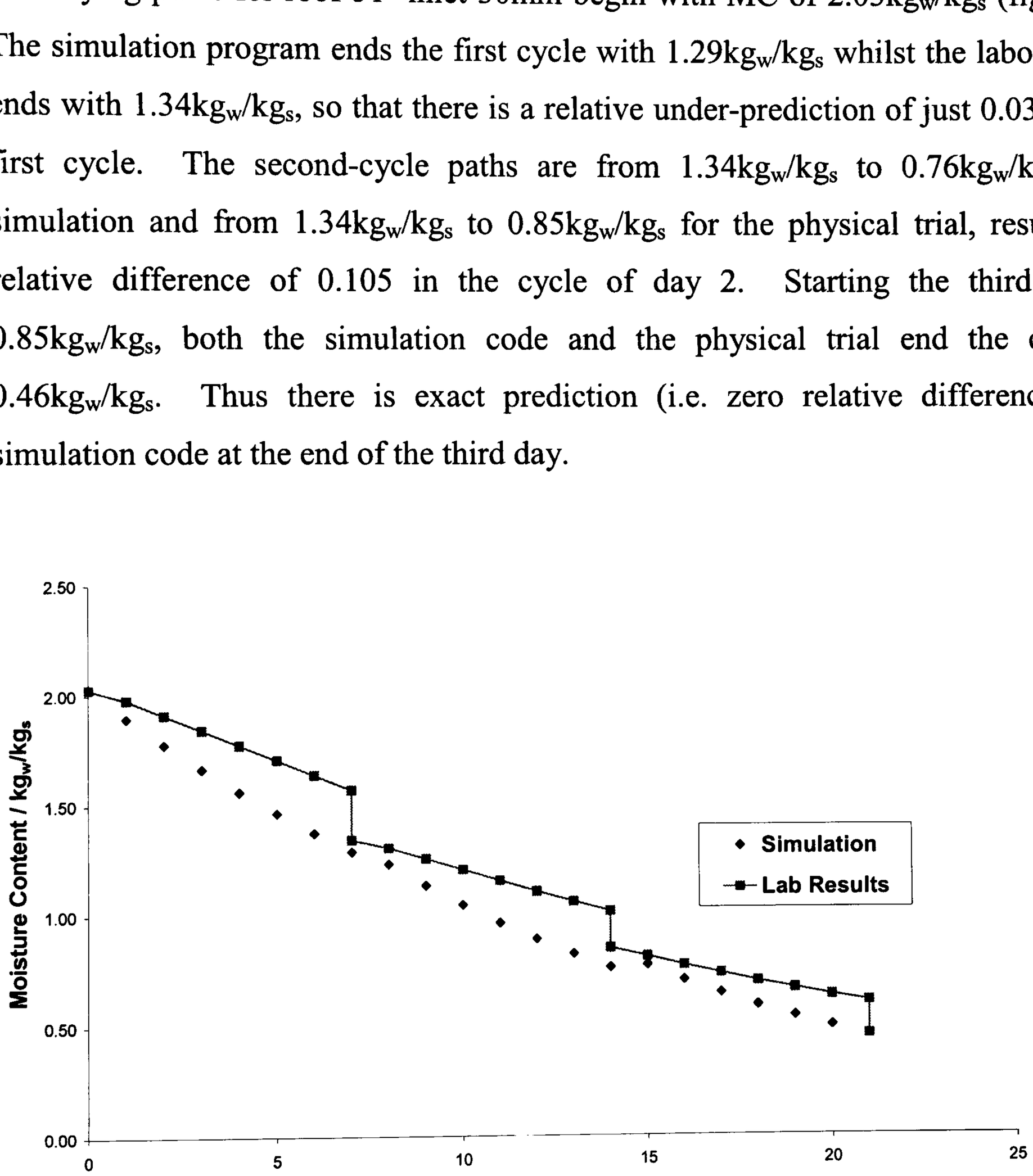

Figure 6.29 Moisture Content vs. Drying Time: Simulation and Lab Results; Roof 51^0 Inlet 30mm

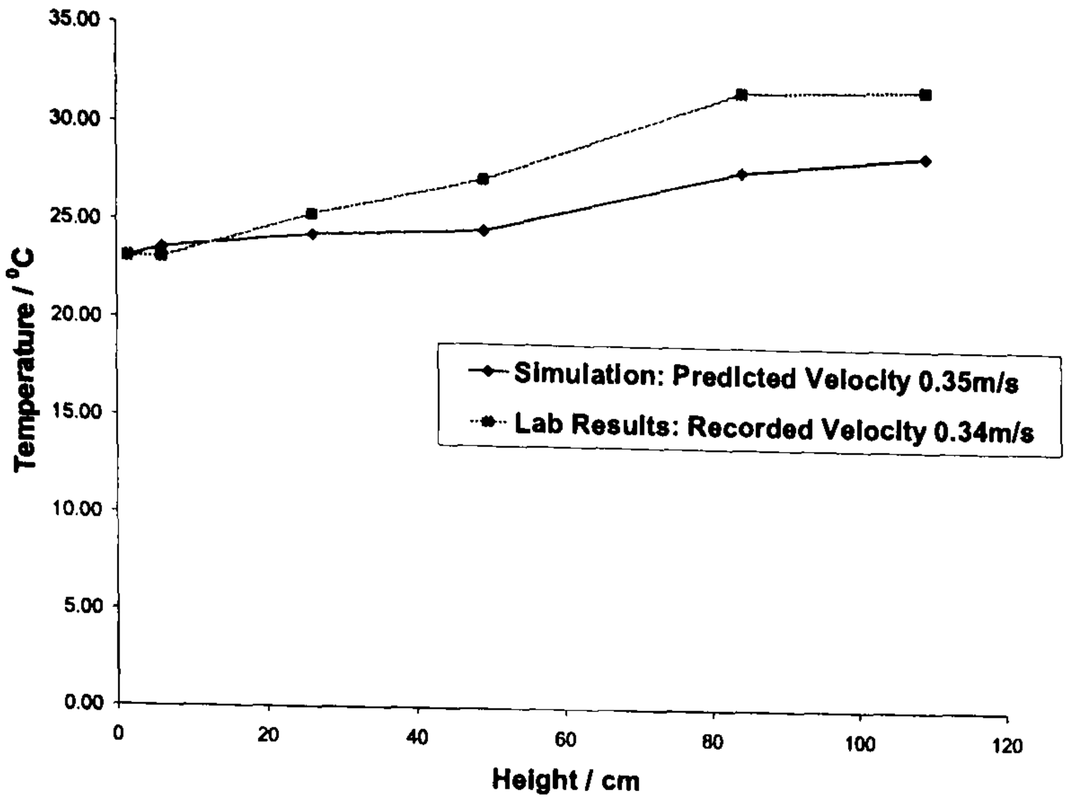

a) Day 1

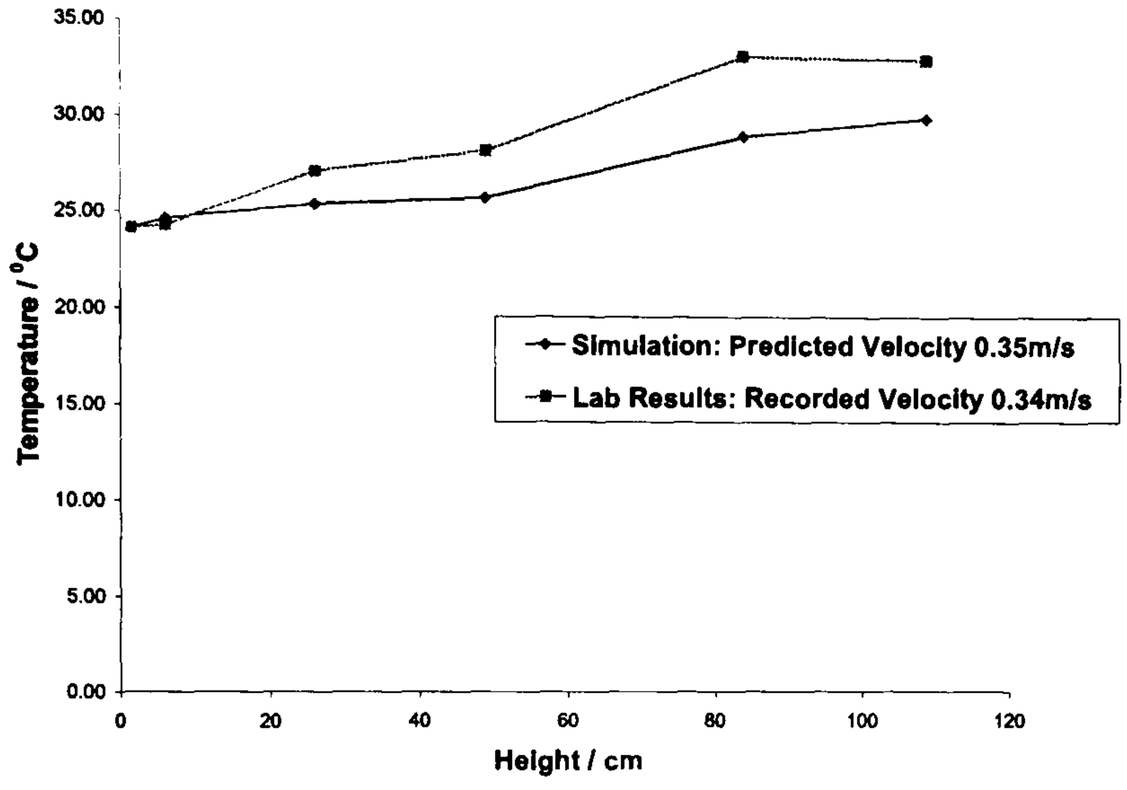

b) Day 2

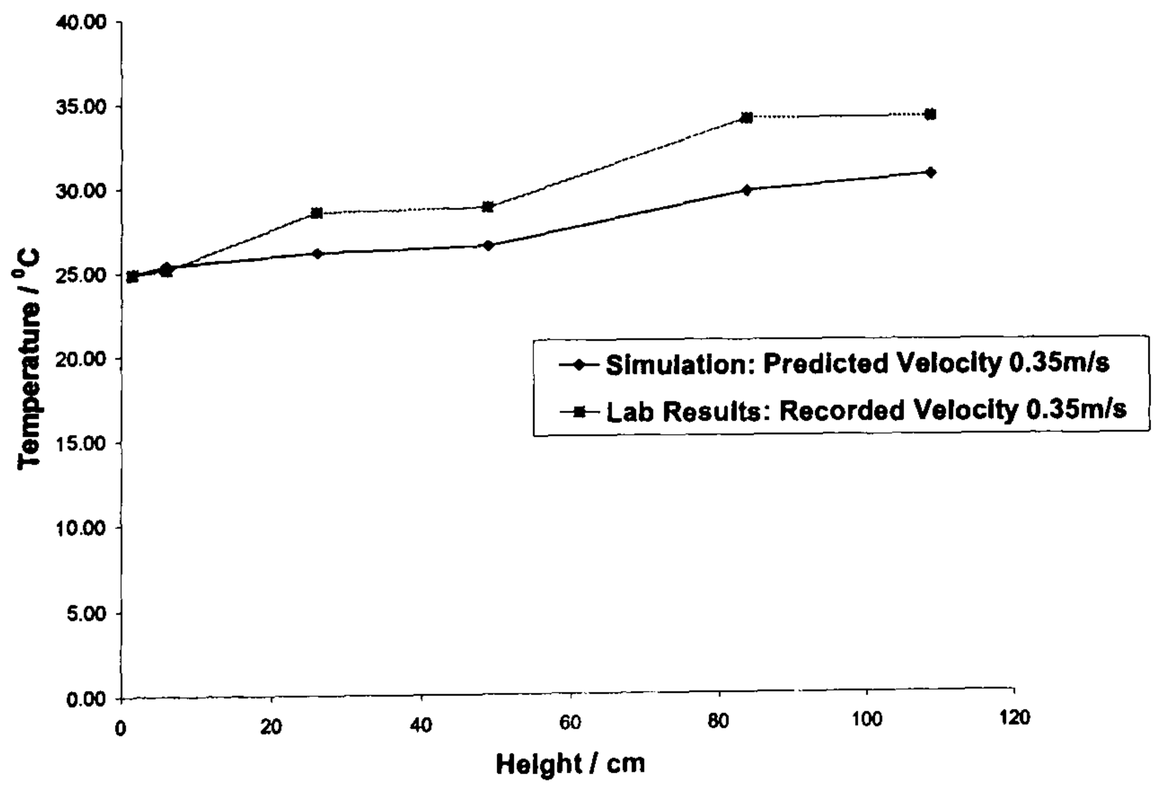

c) Day 3

Figure 6.30 Air Temperature vs. Height: Simulation and Lab Results; Roof 51^0 Inlet 30mm

As shown in figure 6.30, trends similar to the other CDSCD configurations are shown of the air temperatures at various heights of the dryer; the temperature below the crop is slightly over-predicted whilst those at other points are under-predicted. Once again, the relative differences in the inlet velocities are small. The relative difference is 0.029 for the first two days, and there is exact prediction on the third day.

6.4 Parametric studies

The main advantage of the simulation code is that it allows the study of many dimensional and environmental options for investigating the CDSCD, which would be either impossible or too expensive to achieve with the physical trials. The parametric studies involve observing the dependence of the performance of the CDSCD on the dimensional and environmental parameters. The change in performance is examined as the chosen parameters are varied, whilst other parameters remain unchanged. A few studies are described in this section for the no-load trials to investigate the effects of various parameters on the exit velocity. Time limitations do not allow the study of the under-load trials, whose simulation processes take much longer time to converge than the no-load trials.

6.4.1 Varying the drying-chamber roof angles

The trials on various configurations of the physical model took place under different environmental conditions. The simulation code offers an opportunity to examine all of them under the same environmental conditions. Two simulation trials have been performed to examine the effects of the roof angle on the no-load exit velocity of the CDSCD, for the inlet gap of 70mm. In the first trial, the irradiation values are the same as those derived in sub-section 6.1.3 for validating the simulation code, as shown in table 6.5. In the second trial, the irradiation values for the chimney and drying chamber are interchanged as shown in table 6.6.

As expected, the velocity increases as the roof angle decreases with respect to the vertical plane (i.e. as the drying-chamber changes from that of a cabinet dryer to become more of a tent dryer). However, there is a decrease in the margin by which the

velocity increases, as the roof turns more towards the vertical plane. In the first trial (see table 6.5), the increase in exit velocity becomes practically insignificant from the angle 50^0 downwards. In the second trial with high irradiation into the drying chamber, there is a peak value at roof angle 65^0.

Irradiation on chimney I_{chm}=390.78 W/m^2
Irradiation on drying chamber I_{dc}=186.59951 W/m^2
Environment air velocity = 0.01 m/s
Environment temperature = 23.5 ^{0}C
Different roof angles; inlet gap = 70 mm

Roof angle (^{0})	40	45	50	55	60	65	70	75	80	85
Exit air velocity m/s	0.4993	0.4995	0.4994	0.4988	0.4978	0.4953	0.4930	0.4899	0.4858	0.4806

Table 6.5 Exit velocities for different angles of drying chamber roof with respect to the vertical plane (with higher irradiation into the chimney than into the drying chamber)

Irradiation on chimney I_{chm}=186.5995 W/m^2
Irradiation on drying chamber I_{dc}=390.7834 W/m^2
Environment air velocity = 0.01 m/s
Environment temperature = 23.5 ^{0}C
Different roof angles; inlet gap = 70 mm

Roof angle (^{0})	40	45	50	55	60	65	70	75	80	85
Exit air velocity m/s	0.5297	0.5385	0.5388	0.5389	0.5370	0.5455	0.5451	0.5435	0.5394	0.5347

Table 6.6 Exit velocities for different angles of drying chamber roof with respect to the vertical plane (with higher irradiation into the drying chamber than into the chimney)

On the other hand, reducing the roof angle to the vertical can limit the total drying area and therefore the quantity of crops that can be loaded into the dryer for a given height of drying chamber. So it could be uneconomical to use a roof angle of 50^0 or below that. Where necessary, roof angles greater than 50^0 or 60^0 may need to be used, and the other features of the structure (like the height and temperature increase) then have to be considered to contribute for airflow improvement, as shown in equation 4.12.

Comparing the two tables above, it could be seen that for the same roof angle, the CDSCD does better in the second trial (where there is high irradiation into the drying chamber) than in the first trial. The results show how effective the tent dryer can

perform as a chimney, when it is well illuminated. This suggests that the system may perform better in areas near the equator where there is much more radiation onto the horizontal surface than onto the vertical surface.

6.4.2 Effect of inlet-exit area ratio of the CDSCD

The effects of different inlet gaps are studied whilst the other dimensions remain unchanged, under the same environmental conditions. The results of two trials are presented in tables 6.7 and 6.8, using the same irradiation values as in the previous section. Starting from the inlet-exit area ratio of 1.1, the exit velocity increases as the inlet gap gets wider with respect to the exit gap, with peak velocity values obtained within the ratios of 4.8 to 5.9 for both trials. Again, for the same inlet-exit area ratio, higher velocity values are obtained where the drying chamber receives higher irradiation than the chimney (velocities in table 6.8 are higher than those in table 6.7 for each inlet-exit ratio).

Irradiation on chimney I_{chm}=390.78 W/m^2
Irradiation on drying chamber I_{dc}=186.6 W/m^2
Environment air velocity = 0.01 m/s
Environment temperature = 23.5 ^{0}C
Current ratio = 2.6030
Roof angle 51^0; other dimensions and environmental conditions remain unchanged

Inlet gap (m)	0.0300	0.0400	0.0500	0.0600	0.0700	0.0800	0.0900	0.1000	0.1100	0.1200
Inlet area (m^2)	0.0120	0.0160	0.0200	0.0240	0.0280	0.0320	0.0360	0.0400	0.0440	0.0480
Inlet-exit ratio	**1.1156**	**1.4874**	**1.8593**	**2.2311**	**2.6030**	**2.9748**	**3.3467**	**3.7186**	**4.0904**	**4.4623**
Exit air velocity m/s	**0.4082**	**0.4491**	**0.4738**	**0.4893**	**0.4993**	**0.5059**	**0.5104**	**0.5134**	**0.5154**	**0.5167**

Inlet-exit ratios continued

Inlet gap (m)	0.1300	0.1400	0.1500	0.1600	0.1700	0.1800	0.1900	0.2000	0.2100
Inlet area (m^2)	0.0520	0.0560	0.0600	0.0640	0.0680	0.0720	0.0760	0.0800	0.0840
Inlet-exit ratio	**4.8341**	**5.2060**	**5.5778**	**5.9497**	**6.3215**	**6.6934**	**7.0653**	**7.4371**	**7.8090**
Exit air velocity m/s	**0.5175**	**0.5180**	**0.5181**	**0.5180**	**0.5167**	**0.5163**	**0.5158**	**0.5153**	**0.5146**

Table 6.7 Exit velocities for different inlet-exit area ratios of the CDSCD (with higher irradiation into the chimney than into the drying chamber)

Irradiation on chimney I_{chm}=186.5995 W/m^2
Irradiation on drying chamber I_{dc}=390.7834 W/m^2
Environment air velocity = 0.01 m/s
Environment temperature = 23.5 ^{0}C
Current ratio = 2.6030
Roof angle 51^0; other dimensions and environmental conditions remain unchanged

Inlet gap	0.0300	0.0400	0.0500	0.0600	0.0700	0.0800	0.0900	0.1000	0.1100	0.1200
Inlet area	0.0120	0.0160	0.0200	0.0240	0.0280	0.0320	0.0360	0.0400	0.0440	0.0480
Inlet-exit area ratio	1.1156	1.4874	1.8593	2.2311	2.6030	2.9748	3.3467	3.7186	4.0904	4.4623
Exit air velocity m/s	0.4396	0.4847	0.5119	0.5289	0.5397	0.5458	0.5505	0.5535	0.5555	0.5566

Inlet-exit ratios continued

Inlet gap	0.1300	0.1400	0.1500	0.1600	0.1700	0.1800	0.1900	0.2000	0.2100
Inlet area	0.0520	0.0560	0.0600	0.0640	0.0680	0.0720	0.0760	0.0800	0.0840
Inlet-exit area ratio	4.8341	5.2060	5.5778	5.9497	6.3215	6.6934	7.0653	7.4371	7.8090
Exit air velocity m/s	0.5573	0.5575	0.5574	0.5571	0.5565	0.5558	0.5550	0.5541	0.5531

Table 6.8 Exit velocities for different inlet-exit area ratios of the CDSCD (with higher irradiation into the drying chamber than into the chimney)

6.4.3 Varying the chimney height for a given height of drying chamber

Like the previous sections, two simulation runs have been conducted, with the height of the drying chamber maintained at 49cm whilst the height of the chimney varies. Again, the first trial uses the usual irradiation values (390.78 W/m^2 on the chimney, and 186.60 W/m^2 on the drying chamber) used for validating the code as shown in table 6.9, and the values are interchanged for the chimney and drying chamber in the second trial (table 6.10). In both trials, the exit velocity increases as the chimney height increases, for a given height of drying chamber. No peak value is observed. This supports the assertion by Ekechukwu and Norton (1997) that there is no limit to the chimney height for improving the airflow rate. However, like the other features of the CDSCD, there is a reduction in the margin of increase in velocity, as the height increases.

As shown in the two tables, a chimney/drying-chamber height ratio of 0.4 in the second trial performs better than double this ratio in the first trial. Also, the performance of a ratio of 0.8 in the second trial matches that of a ratio of 1.2 in the first trial. Thus once again, the CDSCD performs better with higher irradiation into the drying chamber than into the chimney. This suggests that in the geographical areas near the equator, the chimney height does not have to be as high as in areas far away from the equator.

Irradiation on chimney I_{chm}=390.78 W/m^2
Irradiation on drying chamber I_{dc}=186.60 W/m^2
Drying chamber height (m) = 0.49
Current height ratio = 1.2245
Roof angle 51^0, inlet gap 70mm; other dimensions remain unchanged

Chimney height (m)	0.1000	0.2000	0.3000	0.4000	0.5000	0.6000	0.7000	0.8000	0.9000
Total height (m) =	0.5900	0.6900	0.7900	0.8900	0.9900	1.0900	1.1900	1.2900	1.3900
Chimney/drying-chamber height ratio	**0.2041**	**0.4082**	**0.6122**	**0.8163**	**1.0204**	**1.2245**	**1.4286**	**1.6327**	**1.8367**
Exit air velocity m/s	**0.3258**	**0.3670**	**0.4031**	**0.4375**	**0.4691**	**0.4993**	**0.5280**	**0.5555**	**0.5819**

Table 6.9 Exit velocities for a given height of drying chamber with varying heights of chimney (with higher irradiation into the chimney than into the drying chamber).

Irradiation on chimney I_{chm}=186.5995 W/m^2
Irradiation on drying chamber I_{dc}=390.7834 W/m^2
Drying chamber height (m) = 0.49
Current height ratio = 1.2245
Roof angle 51^0, inlet gap 70mm; other dimensions and environmental conditions remain unchanged

Chimney height (m)	0.1000	0.2000	0.3000	0.4000	0.5000	0.6000	0.7000	0.8000	0.9000
Total height (m) =	0.5900	0.6900	0.7900	0.8900	0.9900	1.0900	1.1900	1.2900	1.3900
Chimney/drying-chamber height ratio	**0.2041**	**0.4082**	**0.6122**	**0.8163**	**1.0204**	**1.2245**	**1.4286**	**1.6327**	**1.8367**
Exit air velocity m/s	**0.4299**	**0.4571**	**0.4820**	**0.5054**	**0.5311**	**0.5517**	**0.5712**	**0.5907**	**0.6082**

Table 6.10 Exit velocities for a given height of drying chamber with varying heights of chimney (with higher irradiation into the drying chamber than into the chimney).

6.4.4 Varying the heights of chimney and the drying chamber for a given total height.

In this section, the heights of chimney and drying chamber vary within the given total height of 109cm. Thus the height of drying chamber reduces as the chimney height increases. Two simulation runs are performed with same values as those in the previous sections, as shown in tables 6.11 and 6.12. In the trial with lower irradiation into the drying chamber (see table 6.11), the exit velocity reduces as the height of drying chamber increases whilst the height of the chimney reduces. But in the second trial where the irradiation into the drying chamber is higher (table 6.12), high drying chambers with short chimneys perform better than short drying chambers with high chimneys. This suggests that a geographical area that is very close to the equator may favour a high drying chamber with a short chimney, whereas an area far away from the equator may favour a short drying chamber with a high chimney.

For the same height ratio, higher values are obtained for the second trial (where the radiation into the drying chamber is high) than the first trial. A height ratio just above 1.79 would perform equally well for both the areas close to the equator and those far away, as the velocities in the two trials tend to converge just beyond this ratio. Thus, for two geographical locations with direct interchange of irradiations onto the chimney and drying chamber, the height ratio that enhances maximum exit velocity in one area (far away from the equator) would give minimum velocity in the other area (nearer to the equator). However, the dimensions of the CDSCD become inconsistent with the next stepwise decrease of the drying chamber beyond this ratio of 1.79 (i.e. for the next drying chamber height of 0.29m, for the laboratory model). This height would require other dimensional changes e.g. the roof angle.

Irradiation on chimney I_{chm}=390.78 W/m^2
Irradiation on drying chamber I_{dc}=186.60 W/m^2
Total height (m) = 1.090
Current height ratio = 1.2245
Roof angle 51^0, inlet gap 70mm; other dimensions remain unchanged

Chimney height	0.1000	0.2000	0.3000	0.4000	0.5000	0.6000	0.7000
Drying chamber height	0.9900	0.8900	0.7900	0.6900	0.5900	0.4900	0.3900
Chimney/drying-chamber height ratio	**0.1010**	**0.2247**	**0.3797**	**0.5797**	**0.8475**	**1.2245**	**1.7949**
Exit air velocity m/s	**0.4398**	**0.4566**	**0.4724**	**0.4809**	**0.4920**	**0.4993**	**0.5056**

Table 6.11 Exit velocities for a given total height with varying heights of chimney and drying chamber (with higher irradiation into the chimney than into the drying chamber).

Irradiation on chimney I_{chm}=186.5995 W/m^2
Irradiation on drying chamber I_{dc}=390.7834 W/m^2
Total height (m) = 1.090
Current height ratio = 1.2245
Roof angle 51^0, inlet gap 70mm; other dimensions remain unchanged

Chimney height	0.1000	0.2000	0.3000	0.4000	0.5000	0.6000	0.7000
Drying chamber height	0.9900	0.8900	0.7900	0.6900	0.5900	0.4900	0.3900
Chimney/drying-chamber height ratio	**0.1010**	**0.2247**	**0.3797**	**0.5797**	**0.8475**	**1.2245**	**1.7949**
Exit air velocity m/s	**0.6161**	**0.6046**	**0.5906**	**0.5748**	**0.5634**	**0.5517**	**0.5320**

Table 6.12 Exit velocities for a given total height with varying heights of chimney and drying chamber (with higher irradiation into the drying chamber than into the chimney).

6.5 Summary observations, discussions and recommendations

The empirical relations and data of the CDSCD have been established. Good agreements between these and the ones mentioned in earlier publications have been demonstrated. The simulation code has finally been developed and sufficiently validated with the experiment results. Although the measured air temperatures are slightly higher than the predicted ones due to over-heating by the metallic framework of the dryer, there is high agreement between the predicted and measured air velocities (with some exact predictions), as the effect of extra heating by the frames is nullified by the extra flow resistance posed by the same frames. Also, almost all the energy stored in the inertia of the system to cause the predicted drying path to differ from the observed path is released in the night to continue the actual drying process, so that the predicted and observed MCs are almost the same after each drying cycle, also with some exact predictions.

Future trials with a large-scale field dryer, with local wind and other climatic data (which are not prevailing this time) should help to strengthen the validity of the simulation code. The effects of extra heating and extra resistance from the framework on the simulation results would be much reduced on a large-scale CDSCD. Therefore, better predictions are expected of air temperatures in a field dryer than the predictions for the laboratory model.

The simulation code is therefore a well-validated tool for optimising the design of the CDSCD in terms of its performance. The few parametric studies carried out indicate that a change in any particular feature offers only a marginal contribution to the airflow improvement. This is attributable to the square-root relations as given by equation (4.12) for determining the velocity. For instance the height must be quadrupled to double its contribution to the velocity improvement. Therefore relying on one particular feature of the CDSCD for airflow improvement may render the structure uneconomical or unstable. Reasonably moderate changes in two or more features may be the best.

However, the following suggestions are derived from the parametric studies:

1 The optimum roof angle for the airflow is between 50^0 and 60^0. The angle depends on the geographical location of the CDSCD. Areas far from the equator may have around 50^0 whilst the areas near the equator may have around 60^0 as the optimum angle.

2 The maximum exit velocity is obtained within the inlet-exit area ratios of 4.8 to 5.9

3 A design with a high drying chamber and a short chimney is favoured in a location near the equator, whereas a location far from the equator favours a short drying chamber with a high chimney

However, a few more physical trials are needed to ascertain these facts.

Time did not allow the parametric studies on the under-load processes. The under-load optimisation would depend on which of the identified inputs need to be fixed or changed. These are based among others on

- the properties, drying time and the desired end-product quality of the crop
- the material properties and space availability, for the dimensions of the dryer
- the climatic conditions of the geographical location of the dryer.

CHAPTER 7 CONCLUSIONS AND SUGGESTIONS FOR FURTHER WORK

A solar crop dryer (especially the direct-mode natural ventilation type) can be very simple and inexpensive to construct. However, the simplicity and low cost of the construction do nothing to reduce the complexity of the drying process in the dryer. Hence modelling and simulation processes are required to optimise the design of the dryer. A solar chimney has been identified as a structure that improves the ventilation through a room. A small-scale laboratory model of a chimney-dependent direct-mode solar crop dryer (CDSCD) was designed and built in the Mechanical Engineering Workshop of De Montfort University. The model had three replaceable roofs of different angles with respect to the vertical plane and three different inlet arrangements of different gaps. A series of laboratory trials were carried out using some lamps to simulate radiation from the sun. Two sets of laboratory trials were performed. The no-load trials were conducted to investigate the effects of roof angle and inlet gap on the air flow through the model with no crops in it. The under-load trials were performed to examine the mutual effects of the airflow rate and the drying process. In some of the under-load trials, some crops were placed outside the dryer at the same level as those in the dryer, so that the results of drying inside the dryer could be compared with that outside the dryer. Also different loading arrangements inside the drying chamber were experimented on. The laboratory experiments were followed by field trials in the Mechanical Engineering Department of Kwame Nkrumah University of Science and Technology in Kumasi-Ghana. Time constrains allowed only the testing of different loading arrangements in the field dryer. A mathematical model was developed to simulate the performance of the CDSCD and the experimental results were used to validate the simulation code. Conclusions can be drawn from the whole work as follows:

1. The solar crop dryer can be well designed to combine the use of a solar chimney together with the tent-dryer effect of appropriate roof angle of the drying chamber and inlet to exit area ratio, to achieve the require airflow needed for effective performance of the dryer.

2. Unlike the indirect or mixed-mode dryer, the direct-mode dryer is very sensitive to the ambient relative humidity. In geographical locations of persistently high ambient relative humidity, the solar chimney does not offer much help to increase the drying rate. Building a CDSCD in a particular geographical area can become a waste of resources if this high sensitivity to the ambient relative humidity is overlooked.
3. Although open sun drying can proceed very well at the initial stages of the drying, the CDSCD always finishes the drying process faster. Nevertheless, there is still more room for improving the field model of the CDSCD, especially on the first-day performance.
4. In spite of the fact that the simulation code under predicts the no-load process due the effects of the metallic framework which the mathematical model does not take into account, the no-load velocities are well predicted to within 5% of those observed in the physical trials, with the exception of the velocity in a single trial which is over predicted by 6.7%. The under-load velocities are predicted to within 10% of the observed values, except for two trials where the deviation is slightly above 10%. The effect of the extra energy from the frames which tends to increase the observed airflow above the predicted airflow is balanced by the extra resistances to the airflow by the same frames
5. Even though the inertia of the CDSCD causes deviation between the predicted drying path and the observed drying path, the simulation code predicts to within 15% of the observed moisture content at the end of each drying cycle. This is because the inertia energy that is stored in the system is released at night to make up for any slow down during the day.
6. From the parametric studies, the optimum roof angle for the airflow lies between 50^0 and 60^0 with respect to the vertical plane. Areas that are far away from the equator may have an optimum angle of around 50^0, and those close to the equator may have around 60^0.
7. Maximum air velocities through the dryer are attained within the inlet-exit area ratios of 4.8:1 to 5.9:1.

8. Relying on one particular feature of the CDSCD for performance improvement may render the dryer uneconomical or unstable. Reasonably moderate changes in two or more features may be the best method of improvement.
9. A high drying chamber with a short solar chimney is favoured in areas close to the equator, whereas a short drying chamber with a high solar chimney is suitable for areas far away from the equator.

A lot more parametric studies may be performed to aid the refinement of the design, with input parameters such as

- the area ratio of the drying-chamber base to the chimney inlet
- the base to height ratio of the drying chamber
- the gap to height ratio of the chimney.

The studies should be extended to cover the under-load processes, as the optimum parameters for airflow may not necessarily provide the optimum conditions for the drying process. Additional parameters for the under-load processes may include

- the properties, drying time, moisture content and end-product quality of the crop
- material properties of the dryer, space availability and dryer dimensions
- climatic conditions of the geographical area

As a further step to the modelling process would be the adjustment of the predicted drying paths to those obtained from the physical trials. The transient stages at the beginning and end of the daily drying processes then have to be considered. This would depend on the mass and thermal properties of materials used for constructing the dryer.

The validation process was limited to the laboratory model, due to lack of velocity data on the field. However in light of the good prediction on the laboratory model, the simulation code is expected to predict the airflow and drying performance equally well for the field dryer. On a field dryer, the large scale of the dryer will reduce the effects of extra heating and extra resistance from the framework. So the prediction of the air temperatures is expected to be better for the field dryer than for the laboratory model. Trials are required on the field model to ascertain the above expectations.

LIST OF REFERENCES

ABOULNAGA, M. M. 1998. A roof solar chimney assisted by cavity for natural ventilation in buildings in hot arid climates: and energy conservation approach in Al-Ain city. *Renewable Energy,* 14 pp 357-363.

ABOULNAGA, M. M; ABDRABBOH, S. N. 2000. Improving night ventilation into low-rise buildings in hot-arid climates exploring a combined wall-roof solar chimney. *Renewable Energy,* 19, pp 47-54

AFONSO, C; OLIVEIRA, A. 2000. Solar chimneys: simulation and experiment. *Energy and Buildings,* 32, pp 71-79.

ALEXANDER, G; BOYLE, G. 2004. Introducing renewable energy. In BOYLE G. Renewable Energy: Power For A Sustainable Future. 2nd Edition. ISBN 0-19-926178-4

ASHRAE HANDBOOK. 2001. FUNDAMENTALS. SI Edition.

AWBI, H. B. 1994. Design considerations for natural ventilated buildings. *Renewable Energy,* 5 pp 1081-1090.

AWBI, H. B; Gan G. 1992. Simulation of solar-induced ventilation. *Renewable Energy Technology and the Environment,* 4, pp 2016-2030.

AYENSU, A. 1997. Dehydration of food crops using solar dryer with convective heat flow. *Solar Energy* vol. 59, Nos. 4-6, pp. 121-126.

BAKER, C. G. J. 1997. Dryer selection. In BAKER, C. G. J. Industrial drying of foods. Blackie Academy and Professional. ISBN 0-7514-0384-9

BALA, B. K; WOODS, J. L. 1994. Simulation of the indirect natural convection solar drying of rough rice. *Solar Energy,* vol. 53, pp 259-266.

BALA, B. K; WOODS, J. L. 1995. Optimisation of natural convection, solar drying systems. *Energy*, vol. 20 (4) pp 285-294.

BANSAL, N. K. 1993. Solar chimney for enhanced stack ventilation. *Building and Environment,* 28, No. 3, pp 373-377

BANSAL, N. K; MATHUR, R; BAHANDARI, M.S. 1994. A study of the solar chimney assisted wind tower system for natural ventilation in Buildings. *Building and Environment,* 29 No. 4, 495-500

BANSAL, N. K; MATHUR, J; MATHUR, S; MEENASKI, J. 2004. Modelling of window-sized solar chimneys for ventilation. *Accepted for publication in Building and Environment (Available on line at www.sciencedirect.com).*

BASSEY, M. W; OOTHUIZEN, P. H; SARR, J. 1994. Using heated chimneys and reduced collector air gap height to improve the performance of indirect passive solar dryers. *Renewable Energy,* Vol. 4 (2) pp 169-178.

BERNARDES, M. A. dos S; VOSS, A; WEINREBE, G. 2003. Thermal and technical analyses of solar chimneys. *Solar Energy,* 75, pp 511-524

BENGTSSON, L. P; WHITAKER, J. H. 1986. Farm structures in tropical climates. A Textbook for Structural Engineering Design. FAO/SIDA Cooperative Programme. Rural Structures in East and South-East Africa. Food and Agriculture Organisation of the United Nations).

BOUCHAIR, A. 1994. A solar chimney for promoting cooling ventilation in southern Algeria. *Building Service Engineering, Research and Technology,* 15, No. 2, pp 81-93.
BOUCHAIR, A. 1988. Moving air using stored solar energy. *Proceedings of 13th National Passive Solar Conference, Cambridge, Massachusetts.* pp 33-38.

CHAPRA, S. C; CANALE, R. P. 1994. Introduction to Computing for Engineers. McGraw-Hill Inc. 2nd edition.

CHEN, C. 2002. Sorption Isotherms of Sweet Potato Slices, *Biosysterms Engineering* 83 (1), 85-95.

CHEN, Z. D; BANDOPADHAYAY, P; HALLDORSSON, J; BYRJALSEN, C; HEISELBERG, P; LI, Y. 2003. An experimental investigation of a solar chimney model with uniform wall heat flux. *Building and Environment,* vol. 38 pp 893-906.

COOK, M. 1998 An evaluation of computational fluid dynamics for modelling buoyancy-driven displacement ventilation. *PhD thesis,* De Montfort University, Leicester, England.

COOK, M. 2002. Validation of computational fluid dynamics programs for modelling natural ventilation. *Annual Research Report, De Montfort University, Leicester, England.* pp 30.

CRANK, J. 1975. *The mathematics of diffusion,* 2nd Ed., Oxford University Press, Oxford.

DALLY, J. W; RILEY, W. F; McCONNELL, K. G. 1993. *Instrumentation for Engineering Measurements,* 2nd Edition.

DIAMANTE, L. M; MUNRO, P. A. 1993. Mathematical modelling of the thin layer solar drying of sweet potato slices. *Solar Energy*, vol. 51, No. 4, pp. 271-276.

DUFFIE, J. A; BECKMAN, W. A. 1991. *Solar Engineering of Thermal Processes.* 2nd Edition. ISBN 0-471-51056-4. Wiley Interscience.

EKECHUKWU, O. V. 1997. Design and measured performance of a solar chimney for natural circulation solar energy dryers. *Renewable Energy,* 10 (1) 81-90.

EKECHUKWU, O. V. 1999. Review of solar-energy drying systems I: an overview of drying principles and theory. *Energy Conversion and Management,* vol. 40, pp 593-613.

EKECHUKWU, O. V; NORTON, B. 1999. Review of solar-energy drying systems II: an overview of drying technology. *Energy Conversion and Management,* vol. 40, pp 615-655.

EXELL, R.H.B. 1980. Basic design theory for a simple solar rice dryer. *Renewable Energy Review Journal* 1, 2, 1-4.

FINK, A. 1998. *Conducting research literature reviews: From paper to the internet.* SAGE Publications, London. ISBN 0-761-90-9044

FLOURENTZOU, F; VAN DER MAAS, J; ROULET, C. A. 1998. Natural ventilation for passive cooling: measurement of discharge coefficients. *Energy and Buildings,* vol. 27 pp 283-292.

FORSON, F. K. 1999. Modelling and experimental investigation of a mixed-mode natural convection solar crop dryer. *PhD thesis,* De Montfort University, Leicester, England.

FORSON, F. K; NAZHA, M. A. A; RAJAKARUNA, H. 2003. Experimental and simulation studies on a single pass, double duct solar air heater. *Energy Conversion and Management,* vol. 44 pp 1209-1227.

GAN, G. 1998. A numerical study of solar chimney for natural ventilation of buildings with heat recovery. *Applied Thermal Engineering,* vol. 18 pp 1171-1187.

GAN, G. 1998. A parametric study of Trombe walls for passive cooling of Buildings. *Energy and Buildings,* vol. 27 37-43.

GARG, H. P: KUMAR, R. 2000. Studies on semi-cylindrical solar tunnel dryers: thermal performance of collector. *Applied Thermal Engineering,* vol. 20, pp 115-131

GREEN, M. G. SCHWARZ, D. July 2001. Solar Drying Technology for food preservation. *Infogate (GTZ–GATE).*

GREEN, M. G. SCHWARZ, D. August 2001. Solar Drying Technology for food preservation. *Infogate (GTZ–GATE).*

HALLAK, H; HILAL, J; HILAL, F; RAHHAL, R. 1996. The staircase solar dryer: Design and Characteristics. *Renewable Energy*, Vol. 7, No. 2, pp 177-183.

HAMDY, I. F; FIKRY, A. 1998. Passive solar ventilation. *Renewable Energy,* vol. 14, Nos. 1-4, pp. 381-386.

HIRUNLABH, J; KONGDUANG, W; NAMPRAKAI, P; KHEDARI, J. 1999. Study of natural ventilation of houses by a metallic solar wall under tropical climate. *Renewable energy,* vol. 18 pp 109-119.

HOCEVAR, C. J; CASPERSON, R. L. 1979. Thermocirculation data and instantaneous efficiencies for Trombe walls. *Proceedings of 4th National Passive Solar Conference, Kansas City, Missouri, USA,* pp 163-167.

IGBEKA, J.C. 1982. Simulation of moisture movement during drying a starchy food product-cassava. *J. Fd Technol.* 17, 27-36.

INCROPERA, F. P; DE WITT, D. P. 1990. *Fundamentals of Heat and Mass Transfer.* 3rd Edition. John Wiley & Sons.

INCROPERA, F. P; DE WITT, D. P. 1996. *Introduction to Heat Transfer.* 3rd Edition. John Wiley & Sons.

JAIN, D; TIWARI, G. N. 2004. Effect of greenhouse on crop drying under natural and forced convection I: Evaluation of convective mass transfer coefficient. *Energy Conversion and Management,* vol. 45 pp 765-783.

JAIN, D; TIWARI, G. N. 2004. Effect of greenhouse on crop drying under natural and forced convection II: Thermal modelling and experimental validation. *Energy Conversion and Management,* vol. 45 pp 2777-2793.

KHEDARI, J; BOONSRI, B; HIRUNLABH, J. 2000. *Energy and Building,* vol. 32, pp 89-93.

LAHSASNI, S; KOUHILA, M; MAHROUZ, M; IDLIMAM; JAMILI, A. 2004. Thin layer convective solar drying and mathematical modelling of prickly pear peel (Opuntia ficus indica). *Energy*, 29, pp 211-224.

LEON, M. A; KUMAR, S; BHATTACHARYA, S. C. 2002. A comprehensive procedure for performance evaluation of solar crop dryers. *Renewable and Sustainable Energy Reviews,* vol. 6 pp 367-393.

Li, H; MOREY, R. V. 1984. Thin-layer drying of yellow dent corn. *Transactions of ASAE* 27 (2), 581-85.

LOWNDES S. Optimising natural ventilation using a solar chimney. *Website* http://www.buildenergy.com/solarchimney.htm (accessed; 04/03/2004).

Malik, M.A.S; Tiwari, G. N; Kumar, A; Sodha, M. S. 1982. Solar distillation. Oxford; Pergamon Press.

MISRA, M. K; BROOKER. 1980. Thin-layer drying and rewetting equations for shelled yellow corn. *Transactions of ASAE* 23 (5), 1254-60.

MUJUMDAR, A. S. 1997. Drying fundamentals. In: BAKER, C. G. J. Industrial Drying of foods. Blackie Academy and Professional. ISBN 0-7514-0384-9. pp. 7-30

OKOS, M; NARSIMHAN, G; SINGH, R. K; WEITNAUER, A. C. (1992) Food dehydration, in *Handbook of Food Engineering* (eds D.R.Heldman and D.B. Lund), Marcel Dekker, NY, pp. 437-562.

OLUFAYO, A. A; OGUNKUNLE, O. J. 1996. Natural drying of cassava chips in the humid zone of Nigeria. *Bioresource Technology* 58, 89-91.

ONG, K. S. 2003. A mathematical model of a solar chimney. *Renewable Energy* 28, 1047-1060

ONG, K. S; CHOW, C. C. 2003. Performance of a solar chimney. *Solar Energy,* vol. 74 pp 1-17.

PADKI, M. M; SHERIF, S. A. 1999. On a simple analytical model for solar chimneys. *International Journal of Energy Research,* vol. 23, No. 4 pp 345-349.

REUSS, M; BENKERT, S.T; AEBERHARD, A; MARTINA, P; RAUSH, G. 1997. Modelling and experimental investigation of a pilot plant for solar wood drying. *Solar Energy,* vol. 59, Nos. 4-6, pp 259-270.

ROBERSON, J. A; CROWE, C. T. 1997. ENGINEERING FLUID MECHANICS (6TH EDITION). John Wiley & Sons, Inc. ISBN 0-471-14735-4.

ROBERTS, S. 1991. *Solar Electricity; A Practical guide to Designing and Installing Small Photovoltaic Systems.* Prentice Hall Europe. ISBN 0-13-825068-5

ROGERS, G. F. C; MAYHEW, Y. R. 1992. *Engineering Thermodynamics, Work and Heat Transfer.* 4th Edition ISBN 0-582-04566-5

SANDBERG, M; MOSHFEH, B. 1996. Investigation of fluid flow and heat transfer in a vertical chimney heated from one side by PV elements. Part I – Numerical study. *Renewable Energy,* vol. 8, pp 248-253

SANDBERG, M; MOSHFEH, B. 1996. Investigation of fluid flow and heat transfer in a vertical chimney heated from one side by PV elements. Part II – Experimental study. *Renewable Energy,* vol. 8, pp 254-258.

SANDBERG, M; MOSHFEH, B. 1998. Ventilated solar roof and heat transfer investigation. *Renewable Energy,* vol. 15. pp 287-292.

SCHOENAU, G. J; ARINZE, E,A; SOKHANSAN J. 1995. *Energy Conversion and Management,* vol. 36. No. 1 pp. 41-59.

SHARMA, K. V; COLANGELO, A; SPAGNA, G. 1995. Experimental investigation of different solar dryers suitable for fruit and vegetable drying. *Renewable Energy,* vol. 6, No. 4, pp 413-424.

SHARMA, P. K; TIWARI, G. N; SORAYAN, V. P. S. 1999. Temperature distribution in different zones of the micro-climate of a greenhouse: a dynamic model. *Energy Conversion and Management,* vol. 40 pp 335-348.

SHERWOOD, T. K. (1936). Air Drying of Solids. *Trans. Amer. Inst. Chem. Engrs.* 12, 150-168.

SINGH, S; SINGH, P. P; DHALIWAL, S. S. 2004. Multi-shelf portable dryer. *Renewable Energy,* vol. 29. pp 753-765.

THOMPSON, T. L; PEART, R. M; FOSTER, G. H. 1968. Mathematical simulation of corn drying – a new model. *Transactions of* ASAE 11 (4), 582-86.

TOGRUL, I. T; PEHLIVAN, D. 2004. Modelling of thin layer drying kinetics of some fruits under open-air sun drying process. *Journal of Food Engineering*, 65. pp 413-425.

ULRICH, K. T; EPPINGER, S. D. 1995. Product Design and Development. ISBN 0-07-065811-0.

WIDDEN, M. 1996. Fluid Mechanics (Foundations of Engineering Series). ISBN 0-333-51799-7

YALDIZ, O; ERTEKIN C; UZUN, H. I. 2001. Mathematical modelling of thin layer solar drying of sultana grapes. *Energy,* vol. 26, pp 457-65.

YOUNG, F. Y; BRUCE, R. M; OKIISHI T. H. 1997 *A brief Introduction to Fluid Mechanics.* ISBN 0-471-13771-5

ZAMAN, M. A; BALA, B. K. 1989. Thin layer drying of rough rice. *Solar Energy,* vol. 42, No. 2, pp 167-171

ZAMBRANO, W; ALVARADO, S. 1984. Design, construction and testing of a chimney that reduces dangerous temperatures in a radiative convective solar dryer. *Solar Energy,* vol. 32, No. 5, pp. 581-584.